PCA R/D Ser. 1629
PB80-132418

Report to

NATIONAL SCIENCE FOUNDATION
Washington, D.C.
Grant No. ENV77-15333

EARTHQUAKE RESISTANT STRUCTURAL WALLS - TESTS OF ISOLATED WALLS - PHASE II

by

R.G. Oesterle
J.D. Aristizabal-Ochoa
A.E. Fiorato
H.G. Russell
W.G. Corley

Submitted by
CONSTRUCTION TECHNOLOGY LABORATORIES
A Division of Portland Cement Association
5420 Old Orchard Road
Skokie, Illinois 60077

October 1979

50272-101

REPORT DOCUMENTATION PAGE	1. REPORT NO. NSF/RA-790275	Recipient's Accession No. PB80-132418
4. Title and Subtitle: Earthquake Resistant Structural Walls - Tests of Isolated Walls-Phase II, Final Report		5. Report Date: October 1979 6.
7. Author(s): R. G. Osterle, J. D. Aristizabal-Ochoa, A. E. Fiorato, et al.		8. Performing Organization Rept. No. PCA R/D Ser. 1629
9. Performing Organization Name and Address: Construction Technology Laboratories A Division of Portland Cement Association 5420 Old Orchard Road Skokie, Illinois 60077		10. Project/Task/Work Unit No. CR4267-4321 11. Contract(C) or Grant(G) No. (C) (G) ENV7715333
12. Sponsoring Organization Name and Address: Engineering and Applied Science (EAS) National Science Foundation 1800 G Street, N.W. Washington, D.C. 20550		13. Type of Report & Period Covered: Final 1977 - 1979 14.

15. Supplementary Notes

16. Abstract (Limit: 200 words)

Behavior of structural walls for use in earthquake resistant buildings is studied. Included is a presentation of results from sixteen tests on isolated walls. The tests were conducted in an attempt to develop design criteria for reinforced concrete structural walls in earthquake resistant buildings. The objective is to determine ductility, energy dissipation capacity, and strength of a wide variety of walls. Isolated walls representing those found in structural wall systems were tested. Controlled variables included shape of the wall cross-section, amount of main flexural reinforcement, amount of hoop reinforcement around the main flexural reinforcement, amount of horizontal shear reinforcement, axial compressive load, concrete strength, and load history. Two walls were repaired and retested. The following observations were based on test results: (1) Structural walls designed according to the 1971 American Concrete Institute Building Code will attain their design strength in both flexure and shear; (2) Properly detailed structural walls will behave in a ductile manner; (3) Maximum shear stress that can be developed in a wall is limited by web crushing capacity; (4) Presence of confined boundary elements significantly improves inelastic behavior; (5) Construction joints in structural walls will perform adequately if made following standard practice of roughening and cleaning the surface to remove laitance and loose particles; (6) Displacements caused by shear distortions are a significant portion of the total lateral inelastic displacements in structural walls subjected to reversing loads; and (7) Structural wall performance under load reversals is a function of load history.

17. Document Analysis a. Descriptors

Earthquakes
Earthquake resistant structures
Dynamic structural analysis
Shear Properties
Concrete structures
Walls
Bend properties
Yield strength
Plastic deformation
Ductility

b. Identifiers/Open-Ended Terms

Structural walls
Shear walls

c. COSATI Field/Group

18. Availability Statement: NTIS	19. Security Class (This Report)	21. No. of Pages: 335
	20. Security Class (This Page)	22. Price: A15-A01

(See ANSI-Z39.18) See Instructions on Reverse

OPTIONAL FORM 272 (4-77)
(Formerly NTIS-35)
Department of Commerce

TABLE OF CONTENTS

EARTHQUAKE RESISTANT STRUCTURAL WALLS -

TESTS OF ISOLATED WALLS - PHASE II

by

R. G. Oesterle, J. D. Aristizabal-Ochoa, A. E. Fiorato,
H. G. Russell, and W. G. Corley*

HIGHLIGHTS

This report presents results of reversing load tests on reinforced concrete structural walls. Sixteen tests on isolated walls have been carried out. The first phase of the experimental program consisted of nine tests. The second phase consisted of seven.

The first nine tests were previously described in detail.[1] This report includes a general presentation of results from all sixteen tests. In addition, a detailed description of the seven tests from Phase II is given in Appendices A and B.

The tests were part of a combined analytical and experimental investigation to develop design criteria for reinforced concrete structural walls in earthquake resistant buildings. The objective of the experiments is to determine ductility, energy dissipation capacity and strength of a wide variety of walls.

Isolated walls representing those found in structural wall systems were tested. Test specimens were approximately 1/3-scale, although no specific prototype walls were modeled. Controlled variables included shape of the wall cross-section, amount of main flexural reinforcement, amount of hoop

*Respectively, Structural Engineer, Structural Development Department; Structural Engineer, Structural Development Department; Manager, Construction Methods Section; Director, Structural Development Department; and Divisional Director, Engineering Development Division, Portland Cement Association, Skokie, Illinois.

reinforcement around the main flexural reinforcement, amount of horizontal shear reinforcement, axial compressive load, concrete strength, and load history. Two walls were repaired and retested.

The following observations are based on test results:

1. Structural walls designed according to the 1971 American Concrete Institute Building Code[2] will attain their design strength in both flexure and shear. However, the designer must be aware that present provisions underestimate flexural capacity because strain hardening of reinforcement is neglected. For inertia loadings, shear forces developed are related to actual flexural capacity, not design flexural capacity. Thus, the level of shear can be significantly higher than anticipated if inelastic response occurs.
2. Properly detailed structural walls will behave in a ductile manner. Ductility achieved is dependent on the level of shear stress applied to the wall. For lower levels of shear, higher ductilities are attainable. Maximum nominal shear stresses on walls tested ranged from $1.4\sqrt{f'_c}$ to $13.8\sqrt{f'_c}$ psi ($0.1\sqrt{f'_c}$ to $1.1\sqrt{f'_c}$ MPa). Maximum ductilities, as determined from measured rotations, ranged from approximately three to eight.
3. Maximum shear stress that can be developed in a wall is limited by web crushing capacity. Addition of horizontal shear reinforcement beyond present code provisions does not significantly improve strength or ductility for this mode of failure.
4. Presence of confined boundary elements significantly improves inelastic behavior. The confinement reinforcement is only necessary in anticipated hinging regions. Stiff boundary elements help to limit shear distortions and construction joint slip.

5. Construction joints in structural walls will perform adequately if made following standard practice of roughening and cleaning the surface to remove laitance and loose particles.
6. Displacements caused by shear distortions are a significant portion of the total lateral inelastic displacements in structural walls subjected to reversing loads. This fact should be considered in dynamic inelastic analysis of structural wall systems. Loss of shear stiffness with load reversals is primarily dependent on the magnitude of inelastic tensile strains in the reinforcement caused by previous loading. Abrasion and loss of material from grinding also affect stiffness.
7. Structural wall performance under load reversals is a function of load history. The previous level of maximum deformation is critical.

OBJECTIVES

Objectives of the experimental investigation are:

1. To determine flexural and shear strengths of walls subjected to reversing loads, and to compare these with strengths under monotonic loading.
2. To determine load-deformation characteristics for a wide range of configurations of wall specimens. This information can be used in inelastic dynamic analysis.
3. To determine ductilities and energy dissipation capacities of walls subjected to reversing loads.
4. To determine means of increasing energy dissipation capacity of walls where required.
5. To develop design procedures to insure adequate strength and energy dissipation capacity in reinforced concrete structural walls used in earthquake resistant buildings.

OUTLINE OF EXPERIMENTAL PROGRAM

A summary of the experimental program is presented in this section. Further details are included in Appendix A of this report and in the earlier report on the first phase of the program.[1]

Program Variables

All walls tested are listed in Table 1. Controlled variables included shape of the wall cross-section, amount of main flexural reinforcement, amount of hoop reinforcement around the main flexural reinforcement, amount of horizontal shear reinforcement, axial compressive load, concrete strength, and load history. Two walls were repaired and retested.

Test Specimens

Dimensions of the test specimens are shown in Fig. 1. Rectangular, barbell and flanged cross sections were tested. Nominal cross-sectional dimensions of these sections are shown in Fig. 2. A cross section showing locations of the types of reinforcement used is shown in Fig. 3.

The design moment for each wall was calculated following the 1971 ACI Building Code.[2] Design yield stress of the flexural reinforcement was 60 ksi (414 MPa). In proportioning the steel, strain hardening was neglected. Design concrete strength was 3000 psi (20.7 MPa) for Specimen B6 and 6000 psi (41.4 MPa) for all other specimens.

Several criteria were used to select horizontal shear reinforcement. Minimum requirements of the 1971 ACI Building Code[2] governed for the first five specimens in Table 1. For B2, B5, B10 and F1 horizontal reinforcement was designed using a shear force corresponding to the calculated design moment. Shear reinforcement was provided in accordance with the 1971 ACI Building Code.[2] Specimens B6, B7, B9, and F2 were provided with the same amount of shear reinforcement as B2 and B5.

TABLE 1 - PROPERTIES OF TEST SPECIMENS

Specimen	Shape	Axial Load psi	f'_c psi	f_y for ρ_f (ksi)	Reinforcement (%)			
					ρ_f	ρ_h	ρ_n	ρ_s
R1	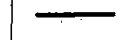	--	6490	74.2	1.47	0.31	0.25	--
R2		--	6735	65.3	4.00	0.31	0.25	2.07
B1		--	7685	65.2	1.11	0.31	0.29	--
B3		--	6860	63.5	1.11	0.31	0.29	1.28
B4(1)	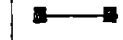	--	6530	65.3	1.11	0.31	0.29	1.28
B2		--	7775	59.5	3.67	0.63	0.29	--
B5		--	6570	64.4	3.67	0.63	0.29	1.35
B5R(2)		--	6205	--	3.67	0.63	0.29	1.35
B6		425	3165	63.9	3.67	0.63	0.29	0.81
B7		545	7155	66.4	3.67	0.63	0.29	1.35
B8		545	6085	64.9	3.67	1.38	0.29	1.35
B9(3)		545	6395	62.3	3.67	0.63	0.29	1.35
B9R(2,3)		450	7510	62.3	3.67	0.42	0.20	1.35
B10(3)		545	6615	64.9	1.97	0.63	0.29	1.35
F1		--	5575	64.5	3.89	0.71	0.30	--
F2		480	6610	62.4	4.35	0.63	0.31	1.43

(1) Monotonic loading
(2) Repaired specimen
(3) Modified reversing load history (MR Loading)
(4) 1000 psi = 1.0 ksi = 6.895 MPa

ρ_f = ratio of main flexural reinforcement area to gross concrete area of boundary element

ρ_h = ratio of horizontal shear reinforcement area to gross concrete area of a vertical section of wall web

ρ_n = ratio of vertical web reinforcement area to gross concrete area of a horizontal section of wall web

ρ_s = ratio of effective volume of confinement reinforcement to the volume of core in accordance with Eq. A.4 of ACI 318-71.

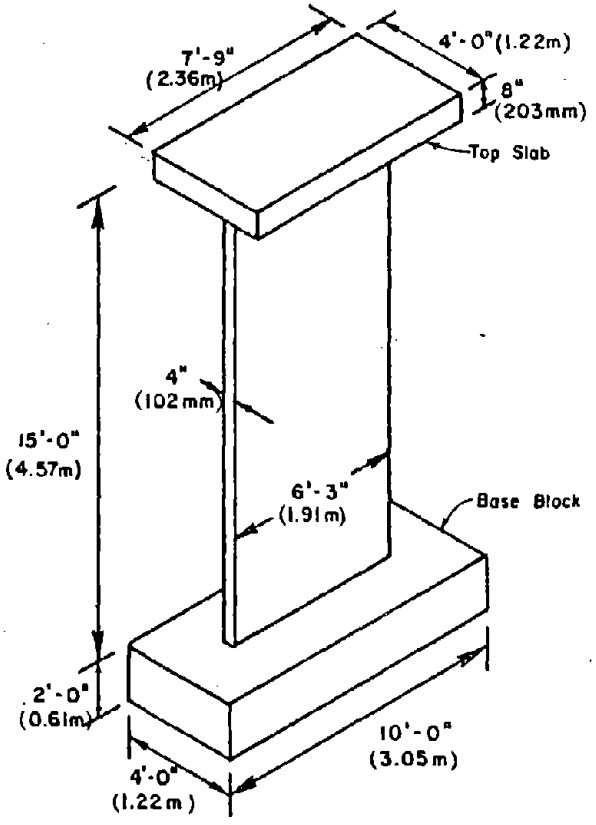

Fig. 1 Nominal Dimensions of Test Specimen with Rectangular Cross Section

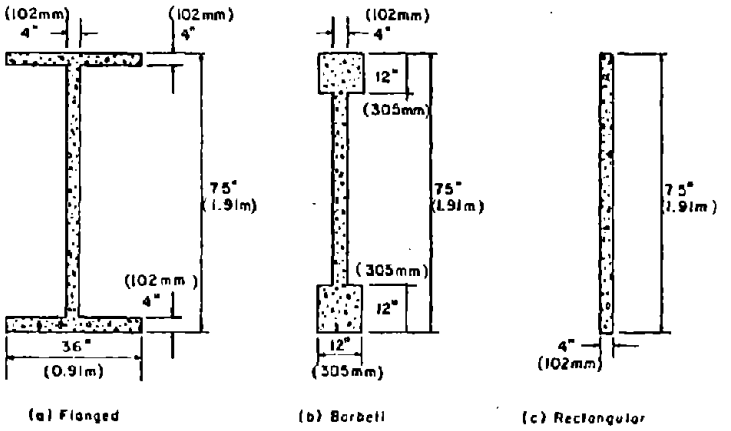

Fig. 2 Nominal Cross-Sectional Dimensions

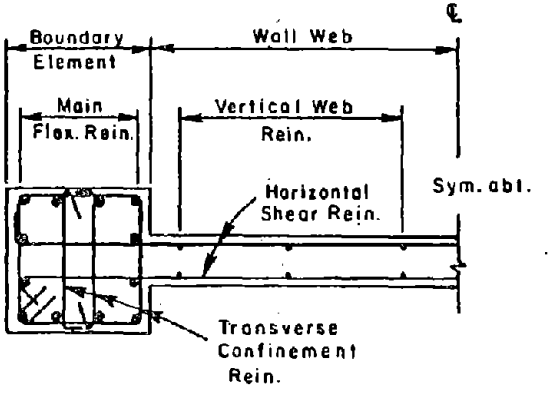

Fig. 3 Types of Wall Reinforcement

To determine the influence of shear reinforcement, a different design procedure was used for Specimen B8. Shear force corresponding to the calculated maximum moment capacity of the wall including strain hardening of the vertical reinforcement was used. Horizontal shear reinforcement was selected to carry this entire shear force at a design yield stress of 60 ksi (414 MPa).

Transverse reinforcement around vertical reinforcement in the boundary elements was designed either as ordinary column ties (unconfined) or as special confinement reinforcement (confined). For rectangular sections, the "boundary element" was taken to extend 7.5 in. (190 mm) from each end of the wall.

Specimens R1, B1, B2, and F1 had ordinary ties as required by Section 7.12 of the 1971 ACI Building Code.[2]

All other specimens had rectangular hoop and supplementary cross-tie reinforcement in accordandance with Appendix A of the 1971 ACI Building Code.[2] This design resulted in a hoop spacing of 1.33 in. (34 mm).

Confinement was used only over the first 6 ft (1.83 m) above the base of the wall. Ordinary column ties were used over the remaining height. Specimen F2 had a special "boundary element" within the intersection of the web and the flange at each end of the wall. The confined zone extended into the web 12 in. (305 mm) from the end of the wall and into the flange 6 in. (152 mm) on either side of the centerline of the web.

Specimens B5R and B9R were retests of B5 and B9, respectively. Following the initial tests, damaged web concrete was removed up to a height of about 9 ft (2.74 mm). New web concrete was cast in three lifts. For Specimen B9R, the new web was cast to a thickness of 6 in. Columns were repaired with a surface coating of neat cement paste.

Test Procedure

The test setup for the walls is shown in Fig. 4. Each specimen was loaded as a vertical cantilever with forces applied through the top slab. The shear span was 2.4 times the

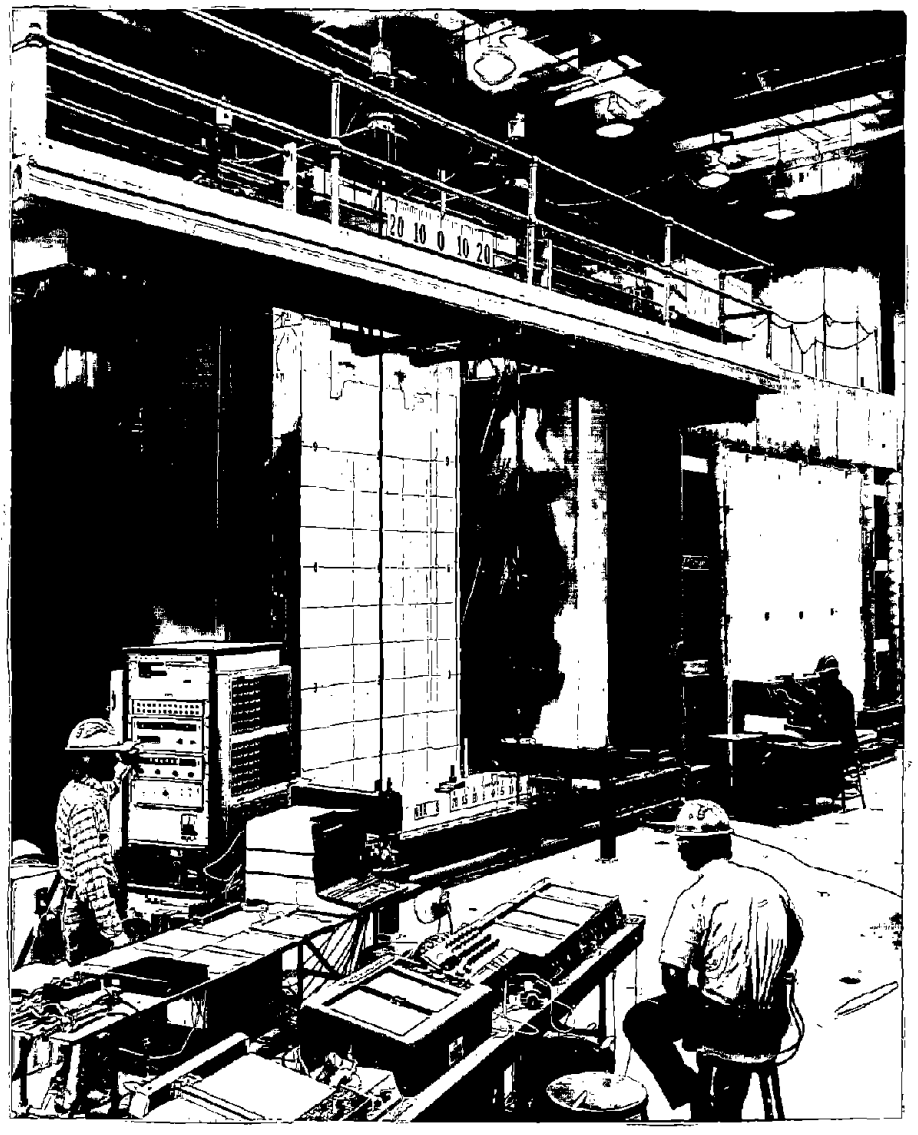

Fig. 4 Test Setup

horizontal length of the wall. For all specimens, except B4, B9, B9R, and B10, reversing horizontal loads were applied in a series of increasing increments (IR loading). Each increment consisted of three completely reversed cycles. About three increments of force were applied prior to initial yielding. Subsequent to initial yielding, loading was controlled by deflections in 1.0 in. (25 mm) increments.

Specimen B4 was subjected to a monotonically increasing load.

Specimens B9, B9R, and B10 were subjected to a modified reversing load history (MR Loading) determined from a statistical investigation of the dynamic response of isolated walls to various earthquake motions.

Typical load histories are shown in Fig. 5. A detailed description of the load histories considered is given in Appendix A.

Constant axial compressive loads were maintained on Specimens B6, B7, B8, B9, B9R, B10 and F2. These loads were applied such that the resultant axial force remained vertical throughout the horizontal load cycles.

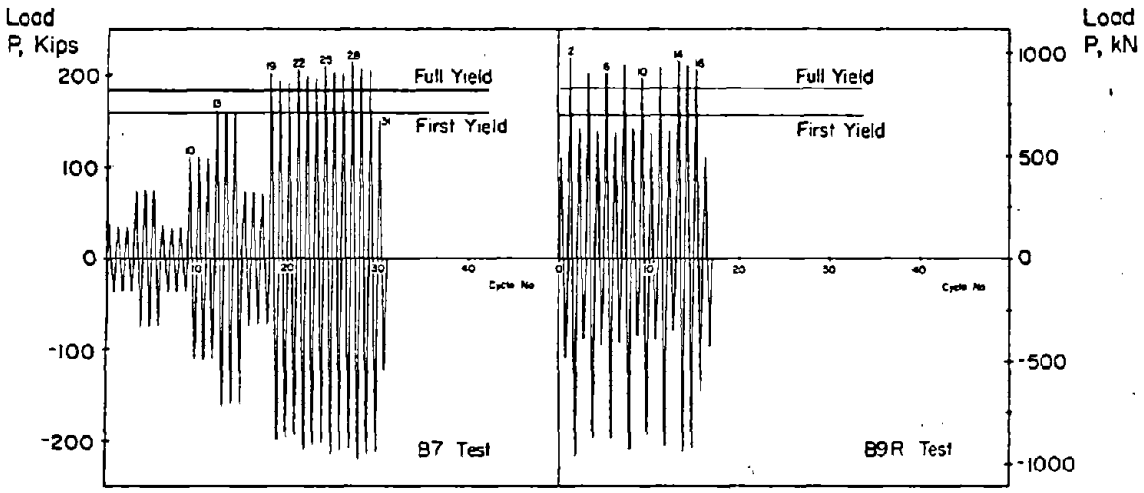

(a) IR Loading (b) MR Loading

Fig. 5 Typical Loading Histories

OBSERVED BEHAVIOR

In this section general observations of specimen behavior are discussed.

General Observations

Behavior of specimens subjected to load reversals was divided into two types distinguished by the magnitude of applied shear stresses. The first type was observed in walls subjected to low nominal shear stresses of $3.1\sqrt{f'_c}$ ($0.26\sqrt{f'_c}$ MPa) or less. The second type was observed in walls subjected to high shear stresses of $7.0\sqrt{f'_c}$ ($0.58\sqrt{f'_c}$ MPa) or greater.

Walls Subjected to Low Nominal Shear Stress

Specimens B1, B3, R1, and R2 were subjected to low nominal shear stress. Their behavior was characterized by the formation of a predominantly horizontal crack pattern in the lower 3 ft (0.91m) of the wall after a few inelastic reversals. This pattern is shown in Fig. 6(a). Therefore, after yield, stresses was predominantly transferred by interface stresses across horizontal cracks and dowel action. The capacity of this shear transfer mechanism was adequate to develop a flexural failure mode. Bar fracture, precipitated by either "inelastic" bar buckling or instability in the compression zone, was the final failure mode in these specimens.

Walls Subjected to High Nominal Shear Stress

Behavior of walls subjected to high nominal shear stress was characterized by the development of inclined cracks crisscrossing the web to form relatively symmetrical compression strut systems for each direction of loading. This pattern is shown in Fig. 6(b). A major portion of the shear transfer mechanism was truss action. Truss action provided a stiffer system than that in specimens exhibiting the first type of behavior. In all but Specimen B10, web crushing occurred at the end of the test.

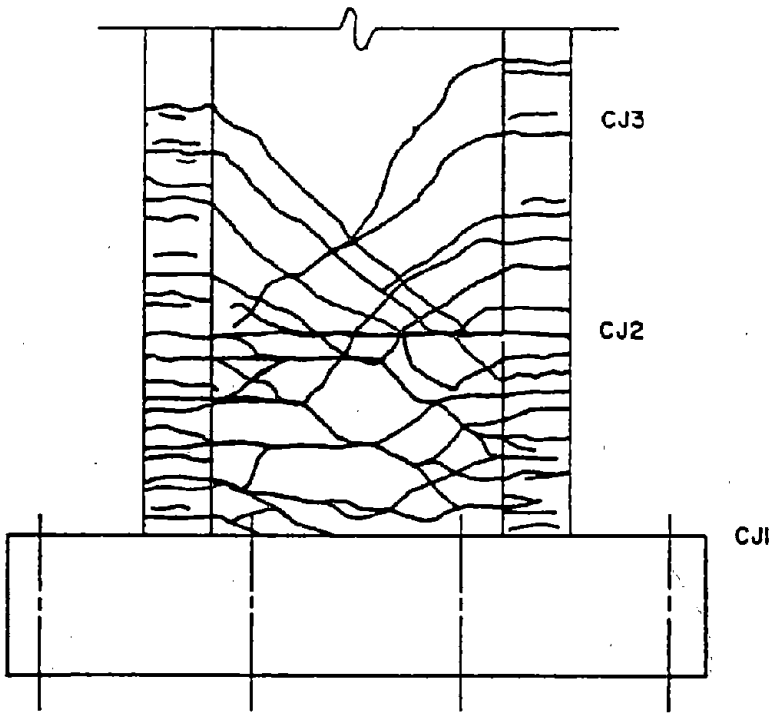

a) Specimen B3

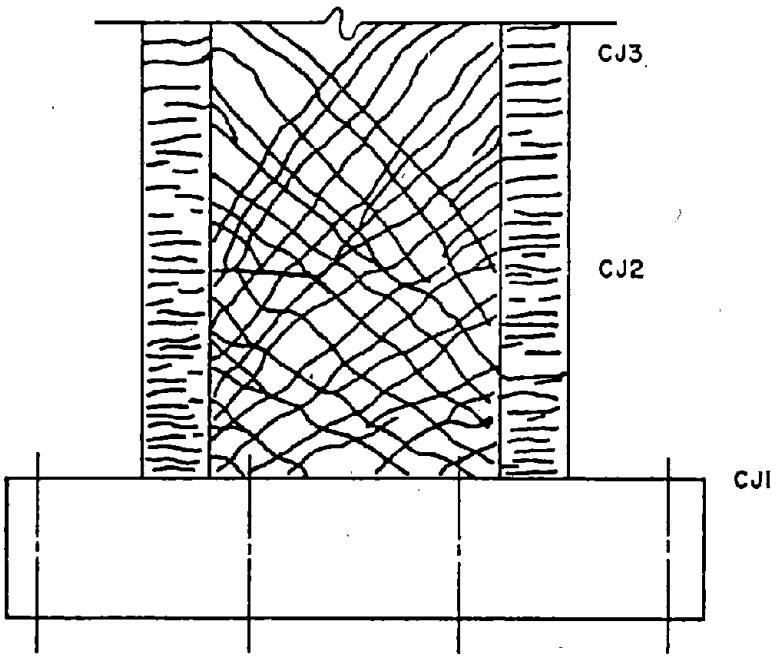

b) Specimen B5

Fig. 6 Crack Patterns in Lower Portions of Walls

The crisscross pattern of cracks that formed was such that the pattern along any horizontal plane was sawtooth shaped. However, in several tests it was noted that as higher rotational ductilities were approached, the diagonal cracks near the base tended to realign and become more horizontal with increasing rotation. The transition is illustrated in Fig. 7(a) and 7(b). The behavior is attributed to loss of interface shear transfer over an increasing portion of the length of the wall. With larger rotations, lower struts became less effective. Shear stiffness near the base became increasingly dependent on shear transfer in the compression zone. Shear transfer from the upper compression struts was focused in a small zone in the lower 3 ft of the web. This concentration of shear eventually resulted in web crushing.

Discussion of Failure Modes

The manner in which the specimens lost load carrying capacity at the end of the test can be divided into five modes.

1. Bar Fracture
2. "Inelastic" Bar Buckling
3. Instability of the Compression Zone
4. Web Crushing
5. Boundary Element Crushing

Bar Fracture

The capacity of one specimen, B4, was limited by fracture of the main tensile reinforcement. Specimen B4 was subjected to monotonic loading. Bar fracture was anticipated because analysis of the wall as a flexural member indicated response as an under-reinforced beam.

"Inelastic" Bar Buckling

The mode denoted as "inelastic" bar buckling was observed in Specimens R1, B1, and B3. These specimens were subjected to low nominal shear stresses. Compressive buckling of the main reinforcement occurred within the lower part of the boundary

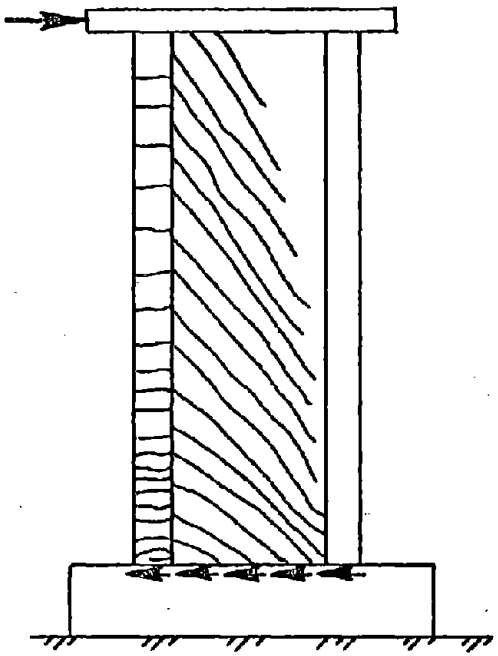

(c) Initial Cracking Pattern
(For One Direction of Loading)

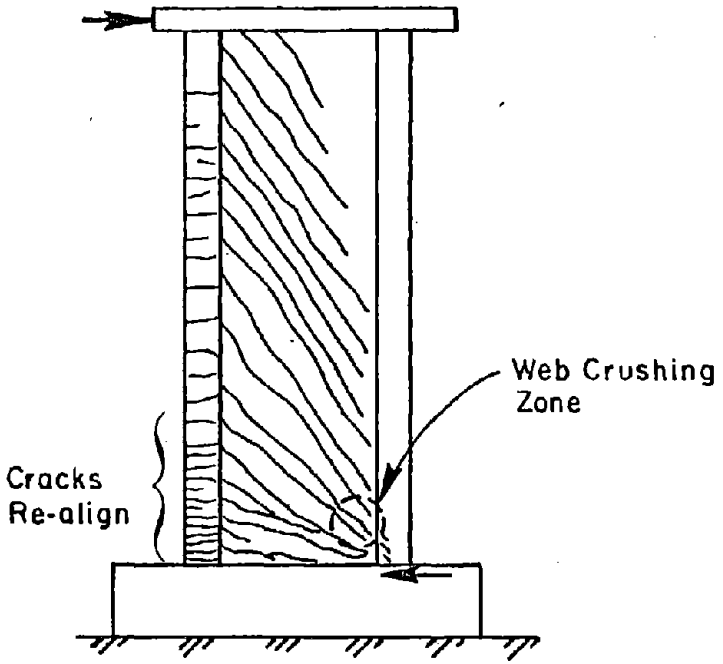

(d) Cracking Pattern After
Several Large Reversals
(For One Direction of Loading)

Fig. 7 Transition of Shear Transfer from Realignment of Cracks with Increasing Rotation

elements as shown in Fig. 8. This buckling is termed "inelastic" because it resulted from cycles of inelastic deformation within the hinging region. Buckling of bars was caused by alternate tensile and compressive yielding. As inelastic cycles progressed, concrete not contained by reinforcement was lost. This reduced the amount of lateral support for the bars. In addition, increasing shear distortions caused eccentric compressive forces on the bars. All of these factors influenced buckling.

Buckling was followed, after several cycles, by bar fracture. One or two bars fractured at a time. Closely spaced confinement hoops delayed but did not prevent "inelastic" bar buckling.

Instability of the Compression Zone

The third mode consisted of an out-of-plane instability of the compression zone of the wall. It was only observed in Specimen R2, a rectangular wall. A large out-of-plane displacement occurred in the lower 3 ft of the compression zone as shown in Fig. 9. Bar fracture followed with subsequent load reversals because of the previous kinking of the bars at the base. This instability was the product of large inelastic load reversals as described in the previous report.[1]

Web Crushing

The fourth mode is denoted as web crushing. This mode is common in beams or girders with large flanges and relatively thin webs subjected to high shear stresses. It was observed in all but one of the specimens subjected to maximum nominal shear stresses greater than $7.0\sqrt{f'_c}$ ($0.58\sqrt{f'_c}$ MPa).

Web crushing was associated with formation of a relatively small zone of high compressive stresses in the web. This zone was located in the lower 3 ft of the web near the interface of the web and boundary element where the compression strut system converged. As lateral load was increased at large inelastic deformations, one or several of the struts crushed. Struts

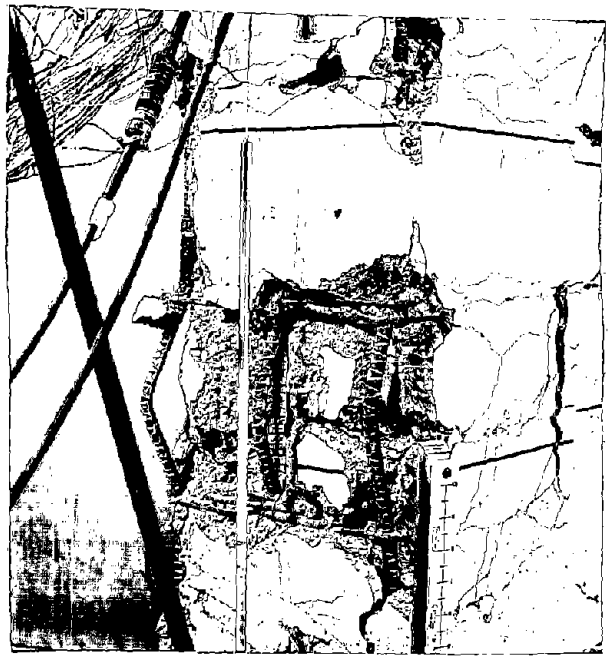

Fig. 8 Buckling of Reinforcement in Specimen 31

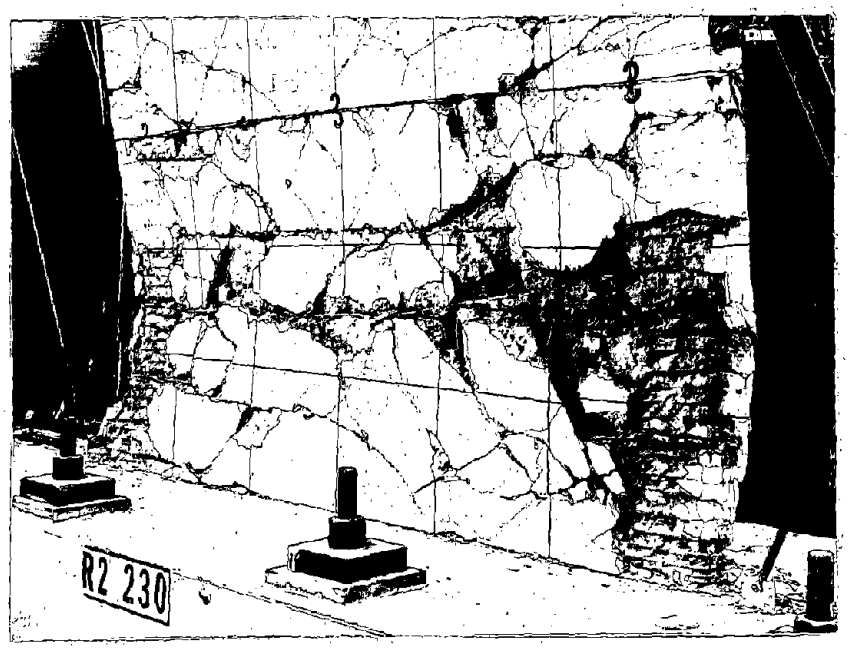

Fig. 9 Out-of-Plane Displacement of Comparison Zone in Specimen R2

that crushed were usually the highest struts in the web that intersected the interface of the wall and base block. Load that had been carried by the crushed struts was transferred to higher or lower struts depending on the stiffness of the compression boundary element. These struts would then progressively shear through forming either a horizontal or vertical failure plane as shown in Figs. 10 and 11.

Loss of load capacity associated with web crushing was sudden. As the web started to crush during the test, a control valve in the hydraulic system was closed manually. This enabled the specimens to be "caught" during failure. In the time taken to close the valve, the applied load dropped from approximately 20% to 70% of the maximum measured load capacity of each specimen.

Since web crushing strength was found to be the limiting factor in inelastic performance, it was considered desirable to develop a method to predict web crushing strength and its relationship to attainable ductility. A detailed discussion of the relationship between web crushing strength and rotational ductility is presented in a separate report.[3]

Boundary Element Crushing

Complete crushing of the boundary element concrete was observed in Specimen B10. This is shown in Fig. 12. Crushing was accompanied by buckling of vertical reinforcement. With subsequent load reversals vertical reinforcement fractured. This crushing was precipitated by honeycombed concrete in the boundary element. Honeycombing resulted from inadequate consolidation of concrete within the conjested boundary element reinforcement cage.

Several other specimens were designed such that compressive stresses in the boundary elements were significantly higher than those in Specimen B10. Evidence of compressive distress was not observed in the confined cores of the boundary elements in any of these specimens.

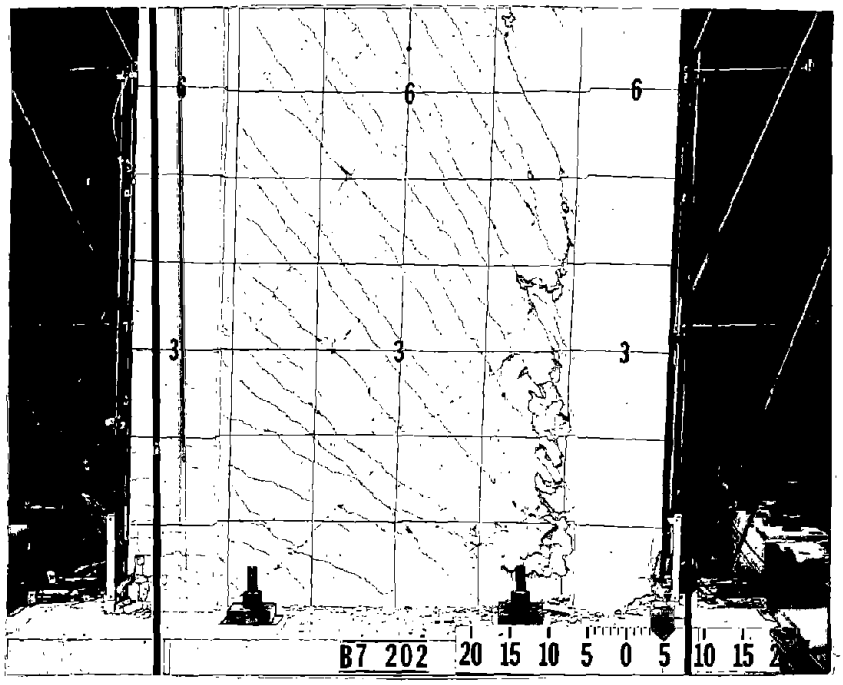

Fig. 10 Specimen B7 After Web Crushing

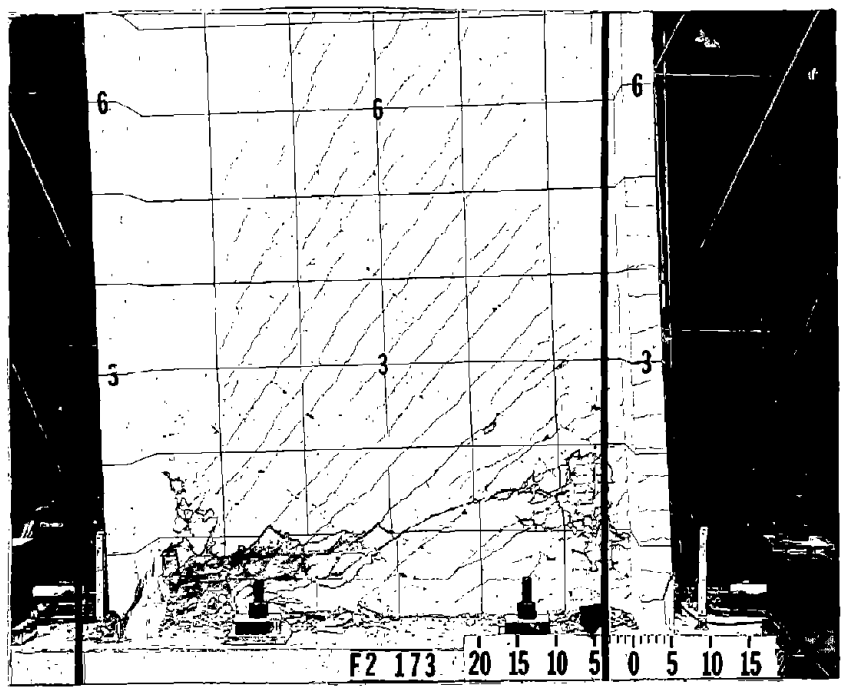

Fig. 11 Specimen F2 After Web Crushing

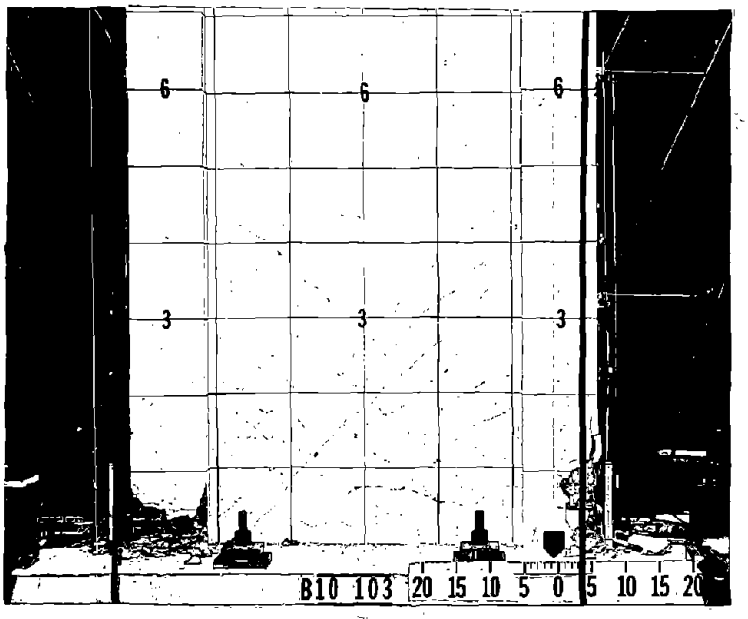

a) Hinging Region

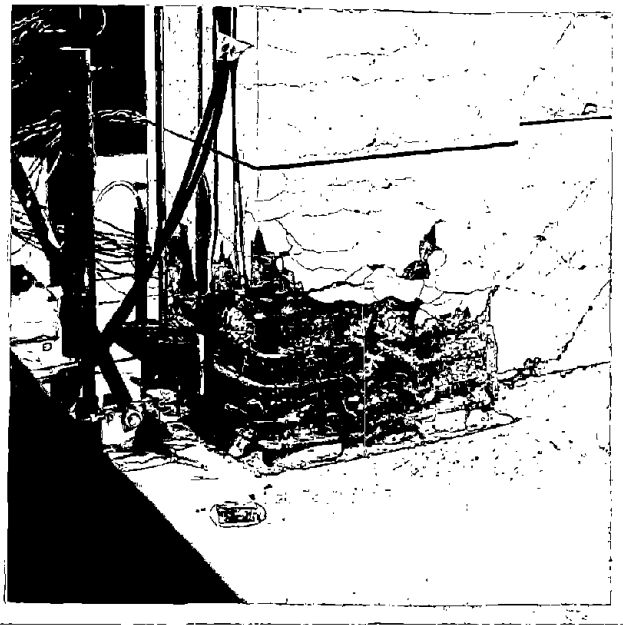

b) Base of Left Column

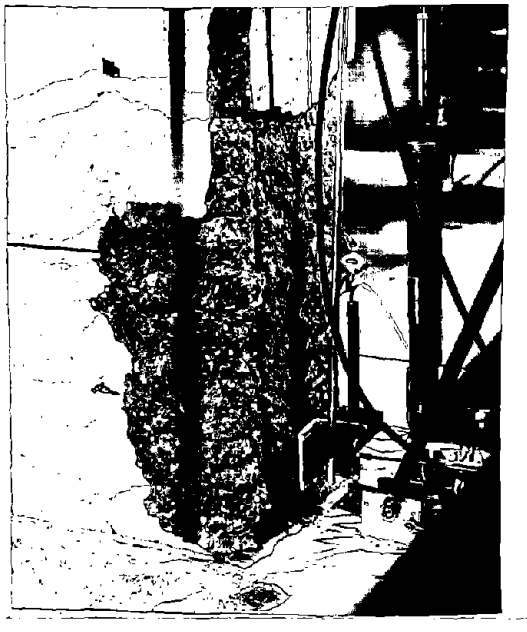

c) Base of Right Column

Fig. 12 Specimen B10 After Boundary Element Crushing

SUMMARY OF TEST RESULTS

A summary of test results is presented in this section. More detailed information is given in Appendix B

Specimen Strengths

Table 2 summarizes observed and calculated strengths for all specimens. Values are given for full yield and maximum load. Full yield loads correspond to the stage when all main vertical reinforcement in the boundary element reached yield. Also shown in Table 2 are design strengths calculated using the 1971 ACI Building Code.[2] As can be seen in Fig. 13, the maximum observed load in all specimens exceeded the ACI design strength for either flexure or shear.

Maximum observed strengths are plotted versus calculated monotonic flexural strengths in Fig. 14. Observed strengths ranged from 77 to 97% of calculated flexural strengths for specimens subjected to load reversals. Calculated strength of Specimen B4, which was monotonically loaded, was in excellent agreement with observed strength.

Deformation Characteristics

Table 3 is a summary of deformation results for all specimens. The deformations are maximum values measured during the last stable load cycle. Stable cycles were defined as those in which the specimen sustained at least 80% of the previous maximum observed load at the peak deformations.

In Table 3, an inelastic cycle is defined as a complete reversed load cycle in which both load and top deflection exceeded the first yield level. First yield level is the first load and deflection at which a yield strain was measured in the boundary element tensile reinforcement. Full yield level is the load and deflection at which all of the main tensile reinforcement in the boundary element yielded.

Load versus deformation relationships observed in the tests are given in the following sections. The general nature of these relationships was discussed in the previous report on the

TABLE 2 - SPECIMEN STRENGTHS

Specimen	Confined Boundary Element	Axial Load	ACI Design				Full Yield Load					Maximum Load						Failure Mode[5]
			Flexure		Shear		Calculated[3]		Observed		Obs.	Calculated[3]		Observed		Obs.	Obs.	
		psi	kips	$\sqrt{f'_c}$[1]	kips	$\sqrt{f'_c}$	kips	$\sqrt{f'_c}$	kips	$\sqrt{f'_c}$	Calc.	kips	$\sqrt{f'_c}$	kips	$\sqrt{f'_c}$	Calc.	ACI[4]	
R1	No	—	18	0.9	82[2]	4.2	17.7	0.9	21.8	1.1	1.23	29.1	1.5	26.6	1.4	0.91	1.48	IB
R2	Yes	—	35	1.8	82[2]	4.2	33.2	1.7	41.8	2.1	1.26	57.3	2.9	48.7	2.5	0.85	1.39	IC
B1	No	—	46	2.2	82[2]	3.9	42.9	2.0	51.0	2.4	1.19	72.1	3.4	61.0	2.9	0.85	1.33	IB
B3	Yes	—	46	2.3	82[2]	4.1	41.9	2.1	51.5	2.6	1.23	73.4	3.7	62.0	3.1	0.84	1.35	IB
B4	Yes	—	46	2.4	82[2]	4.2	43.1	2.2	54.6	2.8	1.27	74.3	3.8	75.3	3.9	1.01	1.64	F
B2	No	—	129	6.1	127	6.0	115.6	5.5	128.0	6.0	1.11	170.9	8.1	152.8	7.2	0.89	1.18	WC
B5	Yes	—	129	6.6	127	6.5	123.1	6.3	138.0	7.1	1.12	213.7	11.0	171.3	8.8	0.80	1.33	WC
B5R	Yes	—	129	6.8	127	6.7	123.1	6.5	—	--	--	213.7	11.5	167.8	8.9	0.79	1.30	WC
B6	Yes	423	157	11.6	132	9.7	154.5	11.4	173.9	12.9	1.13	190.5	14.1	185.5	13.8	0.97	1.41	WC
B7	Yes	545	173	8.5	148	7.3	174.0	8.6	187.5	9.2	1.08	256.2	12.6	220.4	10.9	0.86	1.49	WC
B8	Yes	545	173	9.3	186[6]	9.9	171.6	9.2	189.0	10.1	1.10	241.4	12.9	219.8	11.7	0.91	1.27	WC
B9	Yes	545	173	9.0	148	7.7	165.6	8.6	186.4	9.7	1.13	241.6	12.6	219.6	11.4	0.91	1.48	WC
B9R	Yes	451	173	5.6	162	5.2	165.6	5.3	—	--	--	241.6	7.7	218.7	7.0	0.91	1.35	WC
B10	Yes	575	121	6.2	148	7.6	116.1	5.9	139.7	7.2	1.20	168.0	8.7	159.0	8.2	0.95	1.32	BC
F1	No	—	145	8.1	140	7.8	148.1	8.3	150.6	8.4	1.02	242.6	13.5	187.9	10.5	0.77	1.30	WC
F2	Yes	482	170	8.7	148	7.6	164.4	8.4	180.3	9.2	1.10	240.8	12.3	199.5	10.2	0.82	1.34	WC

(1) Lateral load in terms of nominal shear stress $v = \dfrac{V}{0.8\,\ell_w\, b\sqrt{f'_c}}$ (psi)

(2) Shear reinforcement governed by maximum bar spacing.

(3) Calculated monotonic flexural strength from analysis based on strain compatibility using measured material properties including strain hardening of reinforcement.

(4) ACI taken as the lower of flexure or shear design strength with capacity reduction factor $\Phi = 1.0$.

(5) IB = "Inelastic" Bar Buckling, IC = Instability of Compression Zone, F = Flexural Bar Fracture, WC = Web Crushing, BC = Boundary Elements Crushing.

(6) Maximum $v = 10\sqrt{f'_c}$ governs, ACI Design Shear for B8 would be 256 kips = $13.7\sqrt{f'_c}$ disregarding the maximum allowable.

1 kip = 4.448 kN, $10\sqrt{f'_c}$ (psi) = $0.08304\sqrt{f'_c}$ (MPa)

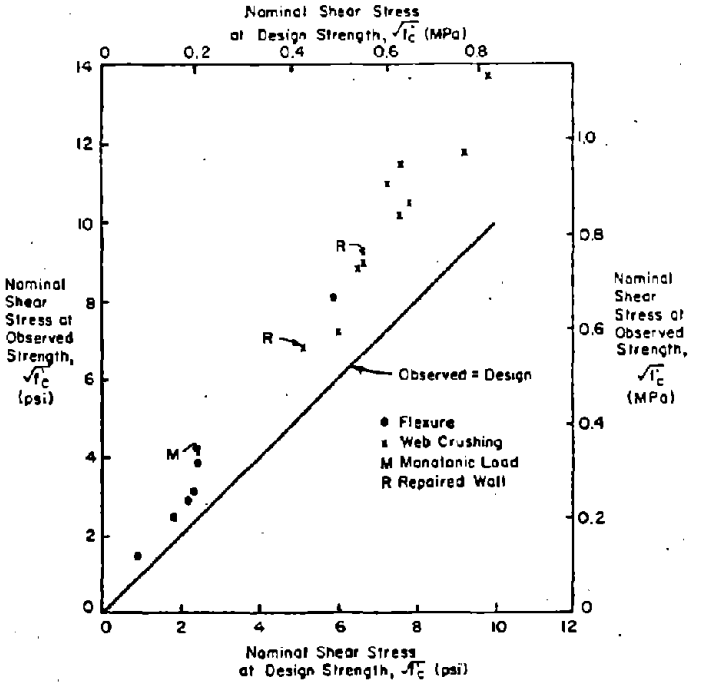

Fig. 13 Observed Strength versus Design Strength

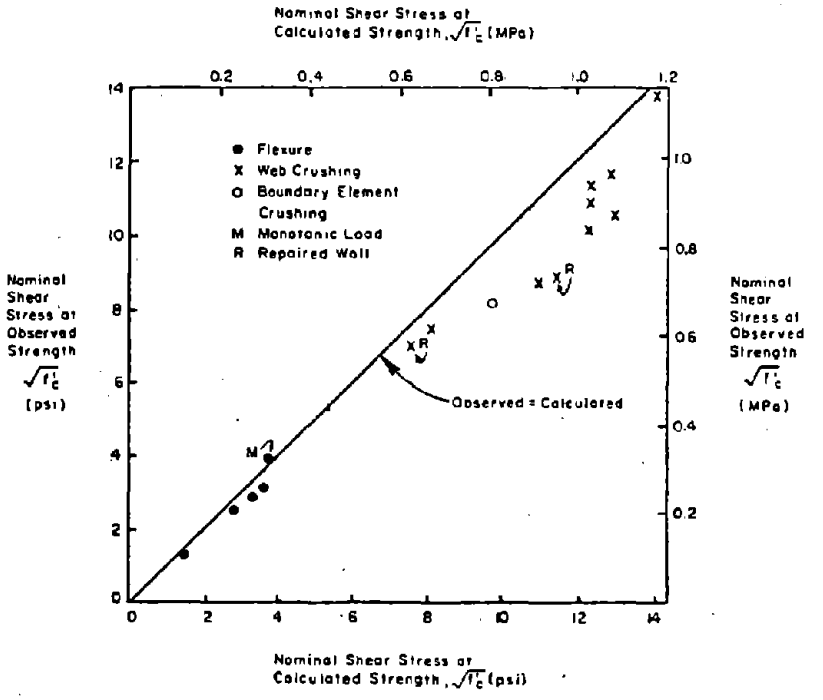

Fig. 14 Comparison of Observed and Calculated Flexural Strengths for Isolated Wall Specimens

TABLE 3 - DEFORMATION RESULTS

Specimen	Top Deflection At Full Yield (in.)	Rotation at Full Yield Θ_3 [2] (Rad.)	No. of Stable Inelastic Cycles	Last Stable Cycle No.	Max. Observed Top Defl. [1] (in.)	Max. Observed Rotation [1] Θ_3 [2] (rad.)	Max Observed Shear Distort. [1] γ_3 [3] (Rad.)	Max Slip At CJI [1] (in.) [4]
R1	0.53	0.0030	13	25	- 4.06	- 0.0240	- 0.0130	- 0.193
R2	0.85	0.0046	14	35	+ 5.25	+ 0.0212	- 0.0300	- 0.380
B1	0.70	0.0042	14	32	- 5.21	- 0.0269	- 0.0235	- 0.258
B3	0.70	0.0090	21	39	- 7.07	+ 0.0276	- 0.0481	+ 0.100 [8]
B4 [5]	0.80	0.0047	-	-	+12.50	+ 0.0630	+ 0.0340	+ 0.145
B2	1.00	0.0052	9	27	- 4.09	+ 0.0161	- 0.0224	+ 0.170
B5	1.10	0.0065	10	28	+ 4.99	- 0.0197	- 0.0237	- 0.134
B5R	2.50 [6]	0.0119 [6]	9	27	+ 4.93	+ 0.0204	- 0.0237	+ 0.192
B6	1.31	0.0049	4	25	+ 3.08	- 0.0136	- 0.0085	- 0.034
B7	1.38	0.0047	12	30	- 5.20	- 0.0242	- 0.0141	- 0.106
B8	1.23	0.0049	12	30	+ 5.14	- 0.0255	- 0.01229	- 0.101
B9 [7]	1.36	0.0048	1	3	- 5.43	+ 0.0238	- 0.0137	- 0.073
B9R [7]	2.99 [6]	0.0125 [6]	8	16	+ 6.88	- 0.0287	- 0.0197	- 0.095
B10 [7]	1.17	0.0048	5	11	+ 4.99	- 0.0243	- 0.0112	- 0.129
F1	1.00	0.0034	6	21	+ 1.99	- 0.0093	- 0.0080	- 0.103
F2	1.13	0.0037	9	27	- 4.00	- 0.0179	- 0.0124	- 0.062

(1) Maximum measured during last stable cycle.

(2) Θ_3 = Rotation of the horizontal section approximately 74 in. (1.88m) above the base block.

(3) γ_3 = Average shear distortion in zone from base to approximately 74 in. (1.08m) above the base block.

(4) CJ1 = Construction joint at the base of the wall.

(5) Monotonic Test.

(6) Measured deformation at yield load level of original specimen.

(7) Modified reversing load history.

(8) Gage failed in cycle 31 at $\pm$ 5 in. defl.

1 in. = 25.4 mm.

first phase of the program.[1] This discussion is valid for tests made in the second phase. Appendix B includes more detailed information for second phase tests.

Load-Top Deflection Relationships

Load versus deflection envelopes for all specimens are shown in Fig. 15. Reported deflection is that at the top of the specimen. The envelope for each curve was obtained by passing lines through the peak points of each new maximum loading cycle.

Moment-Rotation Relationships

Moment versus rotation envelopes for all specimens are shown in Fig. 16. Rotations shown are those measured over a height approximately equivalent to the horizontal length of the wall. This was the region of primary damage observed in the tests.

Shear-Distortion Relationships

Load versus shear distortion envelopes for all specimens are shown in Fig. 17. A key characteristic of this relationship is the shear "yielding" that occurred in each specimen during the same load stage that flexural yielding occurred. Shear "yielding" is defined as a large increase in shear distortion corresponding to a small increase in load. This behavior is used to relate web crushing strength to rotational ductility.[3,4]

Shear-Construction Joint Slip Relationship

Load versus base construction joint slip envelopes for all specimens are shown in Fig. 18. As in the shear distortion data, a key characteristic is the "yielding" exhibited by the envelopes. This "yielding" of slip measured along a horizontal crack verifies that "yielding" observed in the shear distortion data was not caused solely by of rotation across diagonal cracks.

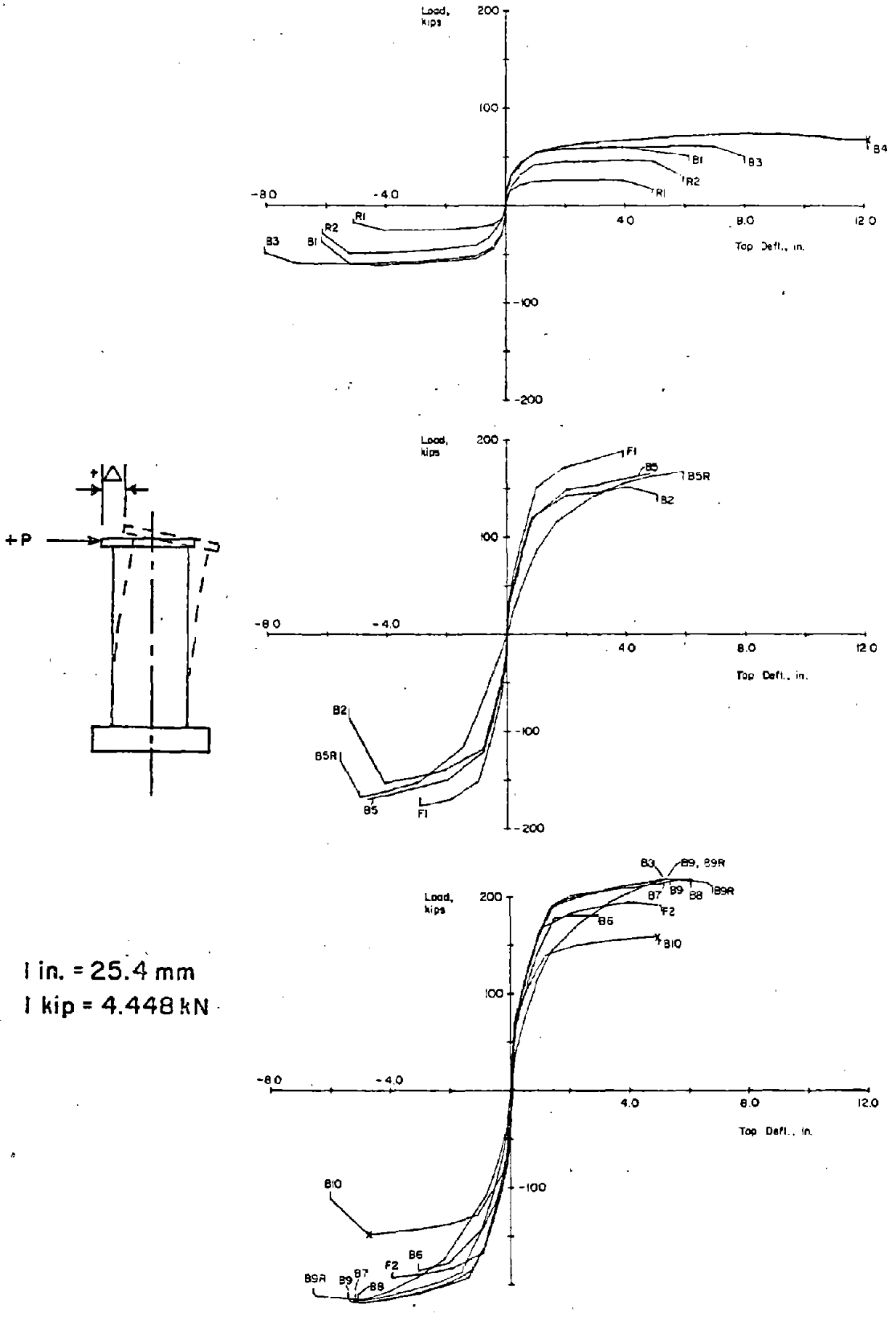

Fig. 15 Load versus Top Deflection Envelopes

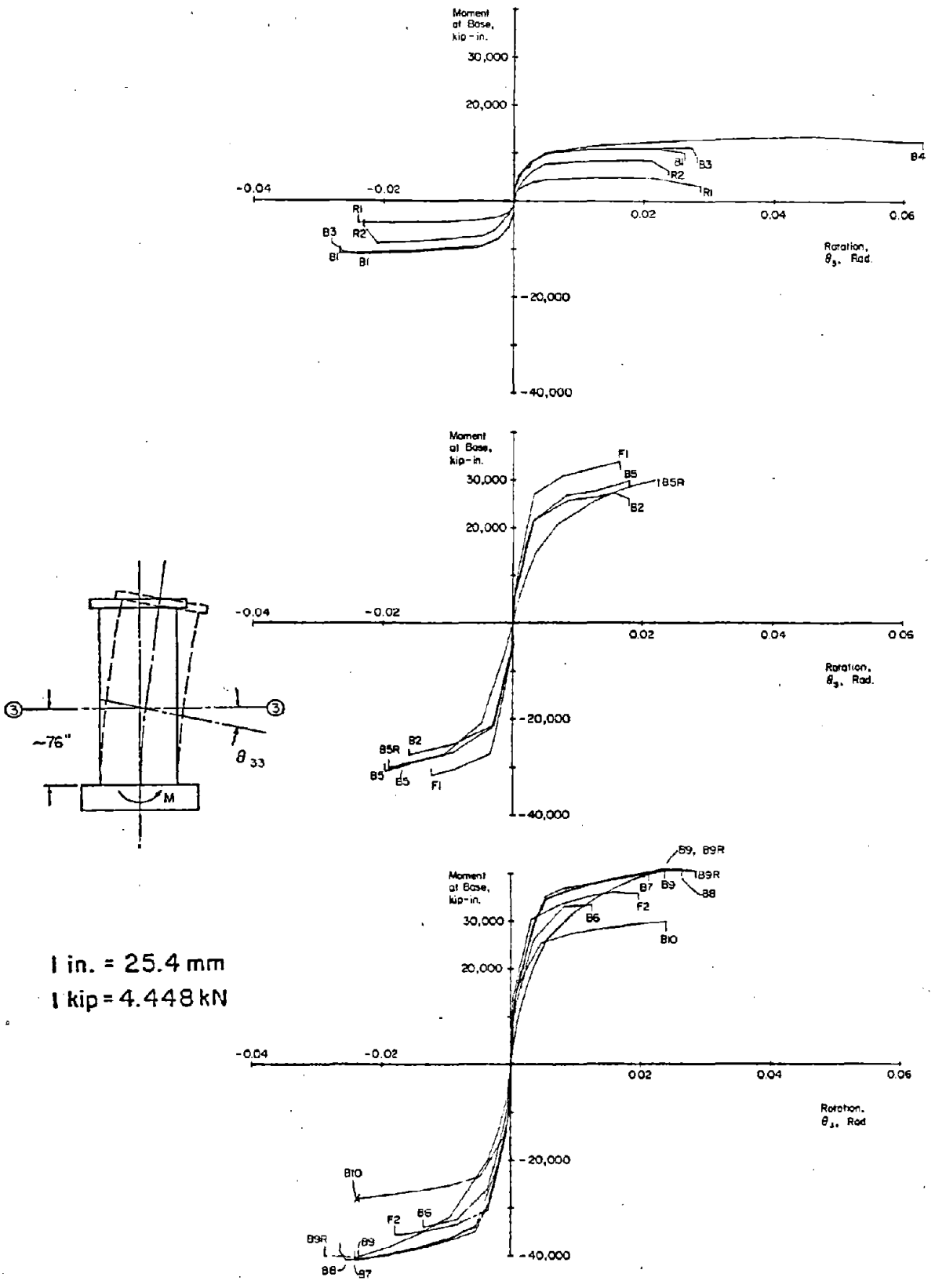

Fig. 16 Moment versus Rotation Envelopes

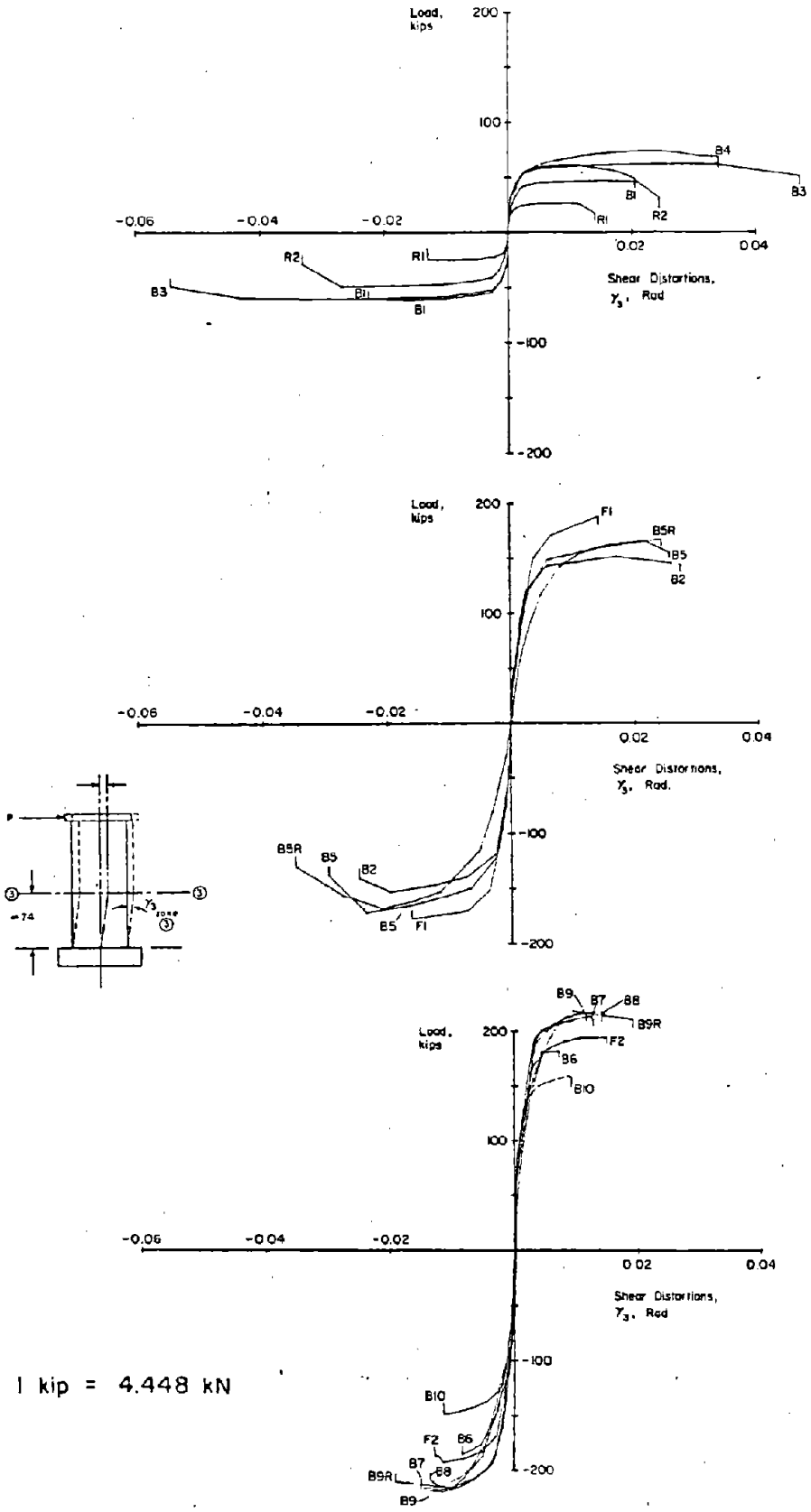

Fig. 17 Shear-Distortion Envelopes

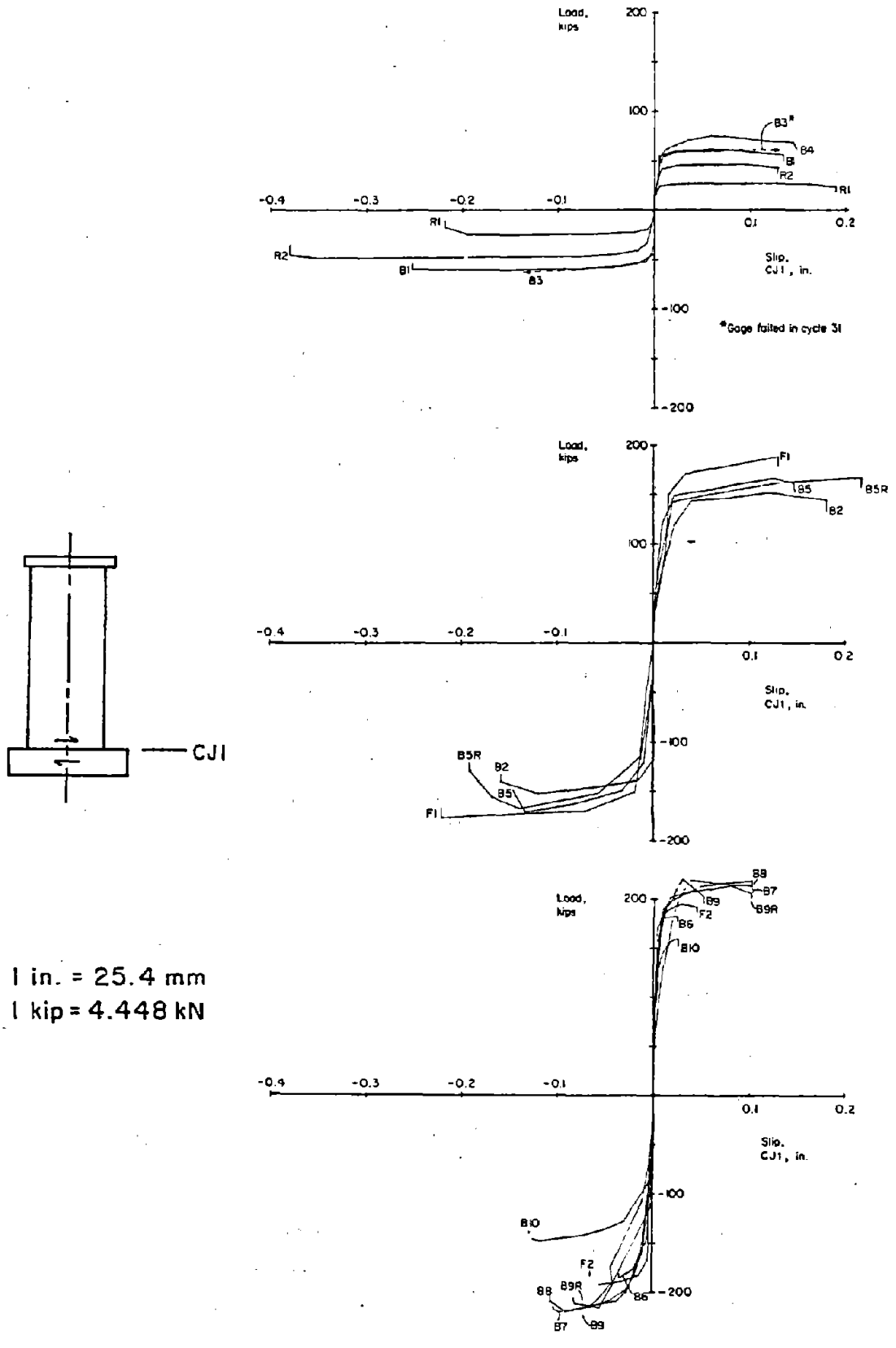

Fig. 18 Load versus Base Construction Joint Slip Envelopes

Ductility

Ductility is commonly used as a measure of inelastic deformation and energy dissipation capacity. Ductility is often defined as the ratio of a specified deformation at a particular load to that at yield. The use of ductility ratios in seismic design implies certain limitations that are discussed by Paulay and Uzumeri.[5]

Inelastic behavior of the specimens was compared using rotational ductility of the hinging region. Rotational ductility, was taken as the ratio of total rotation over the 6-ft (1.83 m) region to the rotation measured at full yield of the flexural reinforcement in the boundary element. Data from all specimens are shown in Fig. 19. Maximum measured ductilities were taken from the last cycle in which the load carrying capacity was sustained throughout the complete cycle.

All specimens tested possessed substantial inelastic rotational capacity under reversing load. Ductility decreased as the maximum level of shear stress increased. The presence of axial load, indicated by the open symbols in Fig. 19, increased ductility in specimens subjected to high shear stress. A comparison of Specimens B7 and B8 indicates that the addition of a large amount of horizontal steel had little effect on the maximum measured ductility.

Energy Dissipation

Energy dissipation capacity may also be used to evaluate inelastic performance under reversing loads. For walls with the same yield load and deflection, optimum performance would be indicated by load-deformation loops that are as open or as full as possible. A measure of energy dissipation capacity should not only relate the amount of energy dissipated to the amount of energy input, but should also relate the energy dissipated to the level of deformations. If the general shape load versus deformation curves was invariant, then ductility would be a sufficient measure for evaluating energy dissipation.

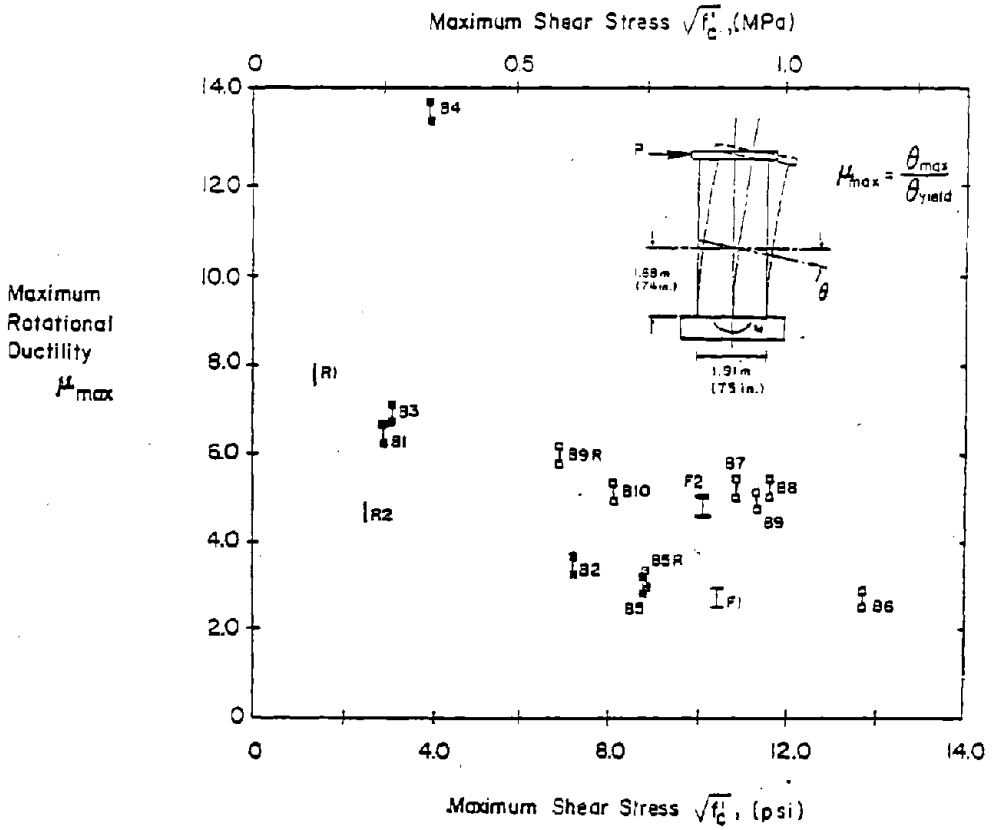

Fig. 19 Observed Rotational Ductilities vs. Maximum Nominal Shear Stress

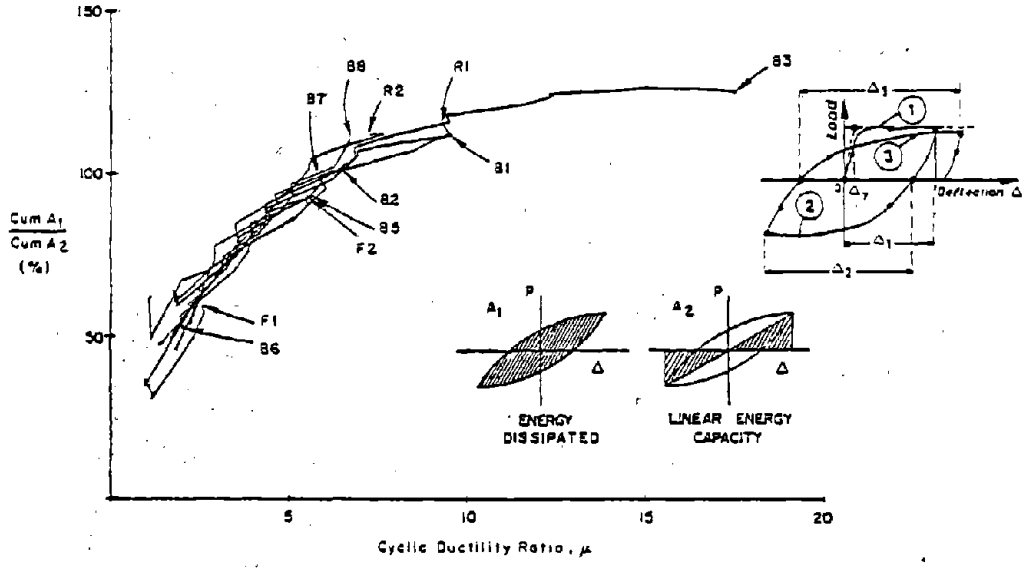

Fig. 20 Ratio of Dissipated Energy to Linear Energy Capacity versus Cyclic Deflection Ductility Ratio

For this report dissipated energy, A_1, and linear energy capacity, A_2, are used to evaluate energy dissipation. These are defined in Fig. 20. For a particular load cycle a larger ratio of A_1/A_2 would indicate a hysteretic loop with less pinching and greater energy dissipation.

In Fig. 20, the ratio of cumulative A_1 to cumulative A_2 for specimens subjected to incrementally increasing load history is plotted as a function of cyclic top deflection ductility. Cyclic deflection ductility is defined in Fig. 20. This relates the energy dissipated to the level of deformations normalized by the yield level. Load versus top deflection data was used because it includes the total energy input and dissipated. Cyclic ductility was used because it represents total deformations sustained by the walls.

Figure 20 indicates that, for equal ductility ratios, the percentage of energy dissipated was essentially the same for all specimens. The general shapes of the load-deformation curves and therefore the energy dissipation capacities were not significantly affected by the variables considered.

Web Crushing

As stated previously in this report, web crushing is the primary factor limiting inelastic performance of walls subjected to high nominal shear stresses. A detailed analysis of the web crushing strength as it relates to rotational ductility is presented in a separate report.[3] Conclusions resulting from this analysis are:

1. Web crushing may limit the shear capacity of structural walls.
2. The present code recommendation that limits allowable shear stress to $10\sqrt{f'_c}$ does not eliminate web crushing in walls subjected to <u>inelastic</u> flexural hinging.
3. Web crushing is dependent on both stress and deformation levels. Reducing the maximum allowable shear stress will not eliminate web crushing in some walls and may be overly conservative in others.

Maximum allowable shear stress should be a function of desired ductility.

4. The truss analogy model can be used, with empirical modifications, to calculate web crushing strengths. The modifications are a function of the rotational ductility desired in the hinging region. They are based on the relationship between rotations and shear distortions in the hinging region. A procedure for calculating web crushing strength is given in Reference 3.
5. The primary variables affecting web crushing strength are the level of axial load and the concrete strength.

DISCUSSION OF PROGRAM VARIABLES

In this section effects of program variables on behavior of structural walls tested are presented.

Wall Versus Beam Behavior

Wall specimens tested behaved basically as cantilevered beams. However, there is a difference in behavior that results from differences in relative proportions of wall sections and beam sections. Several previous studies[6,7,8,9,10] have reported on the behavior of beams under reversing loads. The following should be considered in extrapolating results of beam tests to walls.

1. Loss of cover on the compression face during reversals is a significant factor in loss of shear stiffness and strength in beams.[10] However, in walls, the cover is a considerably smaller portion of the compression zone and loss of this cover does not affect shear stiffness or strength as significantly.
2. Flexural steel in walls is more uniformly distributed over the section than in beams. Also, the ratio of the diameter of the reinforcing bars to cross-sectional dimensions is generally smaller in walls. Therefore, for equivalent ratios of steel to concrete area, the ratio of surface area to cross-sectional area of reinforcement is usually higher in walls. This results in more uniformly distributed cracking in walls than in beams. This is shown in Figs 21 and 22. A more uniform crack distribution improves inelastic deformation capacity by distributing tensile steel strains more uniformly. This increases rotational ductility. In addition, for high shear stresses, a large number of uniformly distributed cracks results in smaller crack widths and less slip along each crack at equivalent deflections. This tends to reduce abrasion and grinding in any one crack.

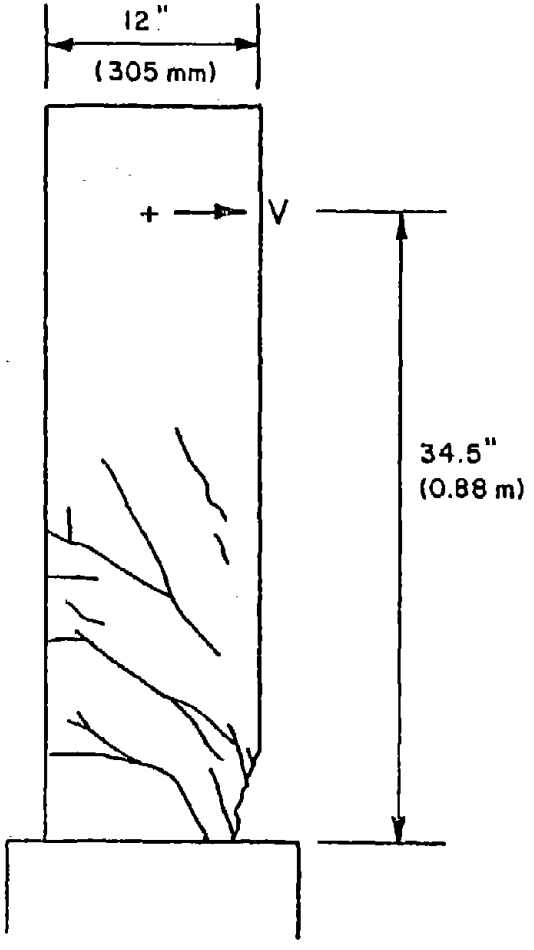

Fig. 21 Crack Pattern in Beam, Ref. (9)

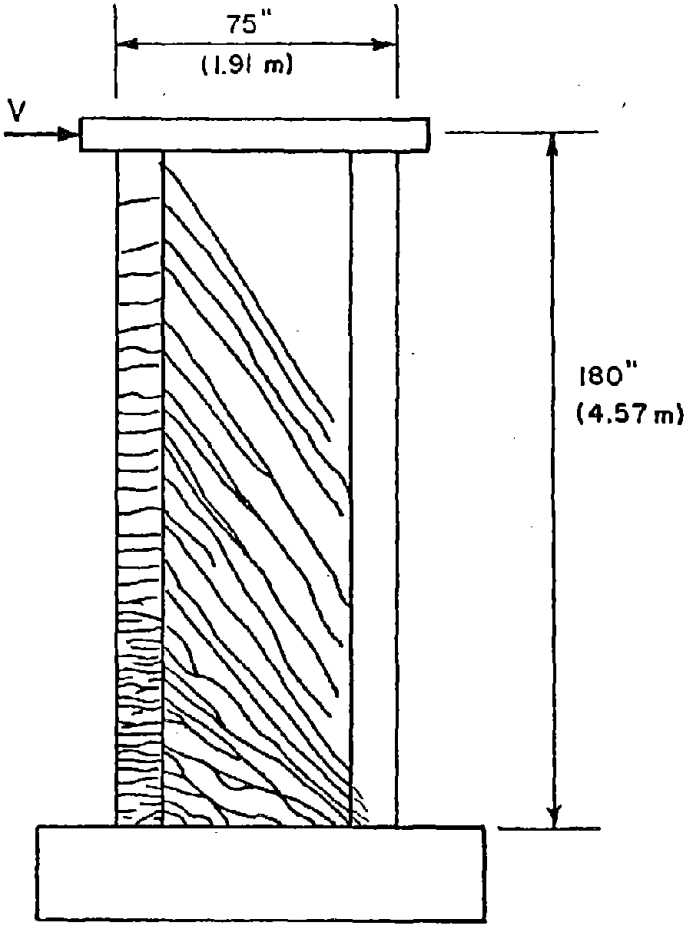

Fig. 22 Crack Pattern for One Direction of Loading in Specimen B7

3. Walls can be more easily provided with confined boundary elements than beams. Confinement steel in boundary elements provides a strong, ductile compression zone and delays inelastic bar buckling. Also, the boundary elements act as large dowels to limit the "sliding shear" mode of failure observed in tests of beams under reversing load.[7]

Shape

Walls tested in this program included three basic shapes: rectangular, barbell and flanged. Each of these shapes were associated with specific behavior patterns as described below.

Rectangular Shape

A rectangular shaped wall is the most functional shape architecturally. However, the relative out-of-plane stiffness of the boundary element is limited by the width of the wall. Therefore, this shape of wall may be susceptible to a lateral instability of the compression zone under severe load reversals. Instability was observed in the test of Specimen R2 as discussed previously.

A rectangular shape also limits flexural capacity for equivalent wall proportions. There is a limit to the amount of reinforcement that can be physically fit into the end regions. Therefore, maximum flexural capacity is low relative to the maximum attainable in a barbell or flanged section of equal horizontal length and web width. Also, for equivalent moment-to-shear ratios the level of shear stresses in rectangular wall webs will generally be lower than in barbell or flanged sections.

Barbell Shape

The barbell section represents a wall between two column lines and can be detailed as a beam with boundary elements. The boundary elements have a relatively large in plane and out of plane stiffness. These elements limit shear sliding at the

base by acting as large dowels. Also, they limit out-of-plane instability. With large areas to place reinforcement in the end regions, relatively high flexual capacities can be developed with this shape. Therefore, this shape can lead to a design with high shear stresses. With the stress concentrations that develop in the hinging region of the web, the barbell is susceptible to the web crushing type of failure.

Flanged Shape

The flanged shape represents a section resulting from intersecting walls. The large out of plane stiffness of the boundary elements prevents instability problems. However, as with the barbell, the flanged shape may lead to a design with high shear stresses. Without the large in-plane stiffness of the barbell boundary elements, the flanged section would be suspected of being susceptible to a sliding shear type of failure. However, this type of failure was not observed in either flanged wall test.

Figures 23 and 24 shows measured deformations within the hinging region of Specimen B7, a barbell wall and Specimen F2, a flanged wall. These specimens were designed with similar flexural capacities and concrete strengths. They were tested under a similar lateral load history and applied axial load. A confined boundary element was included in the intersection region of the web and flange in Specimen F2.

Figure 23 shows measured rotations and shear distortions. These two modes of deformation combine to produce deflections shown in Fig. 24. Inelastic behavior can be evaluated by comparing the maximum measured rotational ductility, the number of inelastic cycles sustained, and the amount of shear distortions and pinching in the shear distortion loops at equivalent rotational ductility.

As shown in Table 3, Specimen B7 sustained 12 inelastic cycles. The maximum rotational ductility was 5.2 and web crusing occurred in Cycle 31.

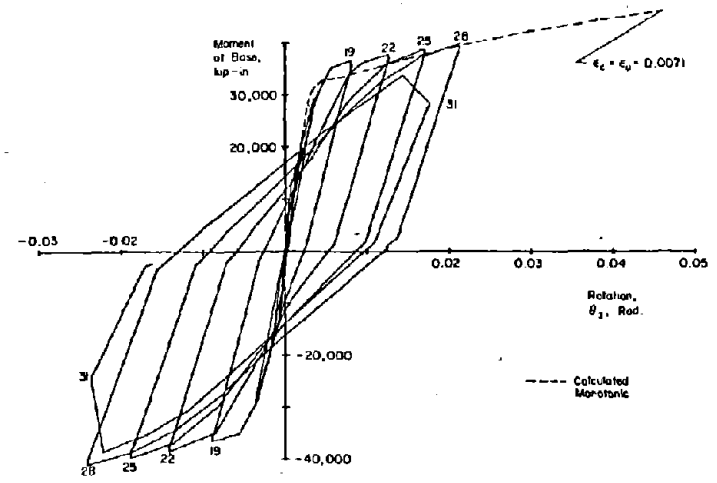

a) Rotation at 6 ft Level, Specimen B7

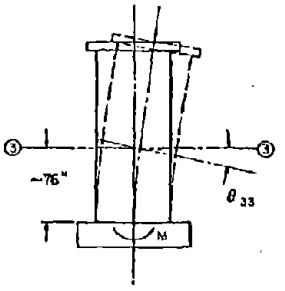

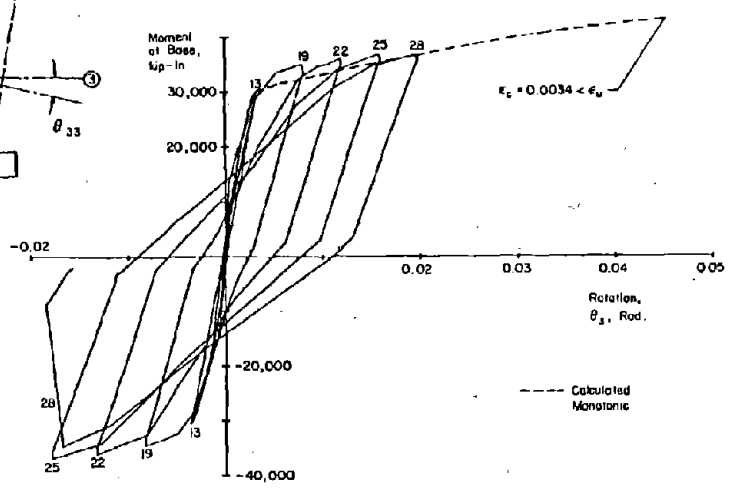

c) Rotation at 6 ft Level, Specimen F2

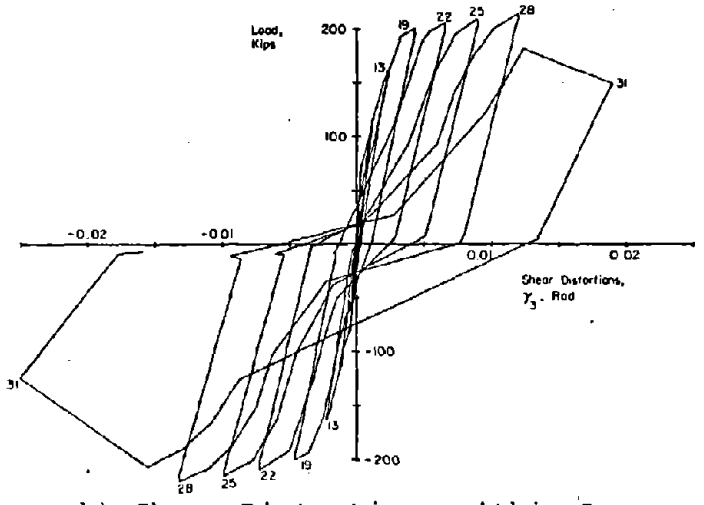

b) Shear Distortions within Lower 6 ft, Specimen B7

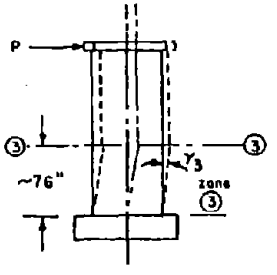

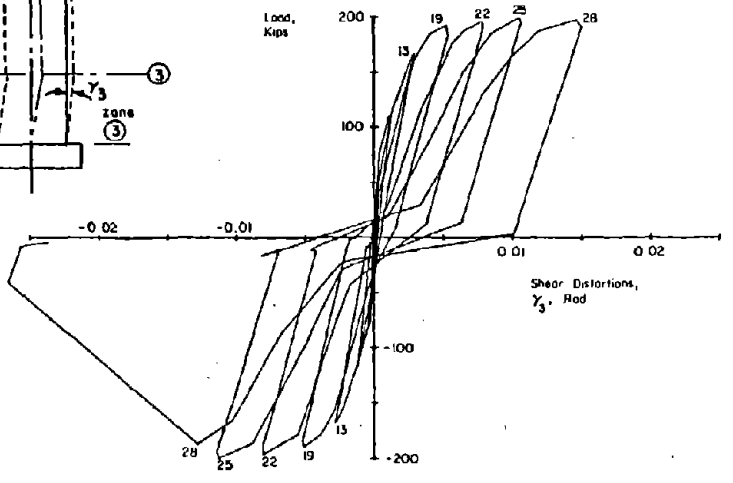

d) Shear Distortions within Lower 6 ft, Specimen F2

Fig. 23 Comparison of Deformations within a Barbell and Flanged Shaped Wall with Similar Design Parameters and Load Histories

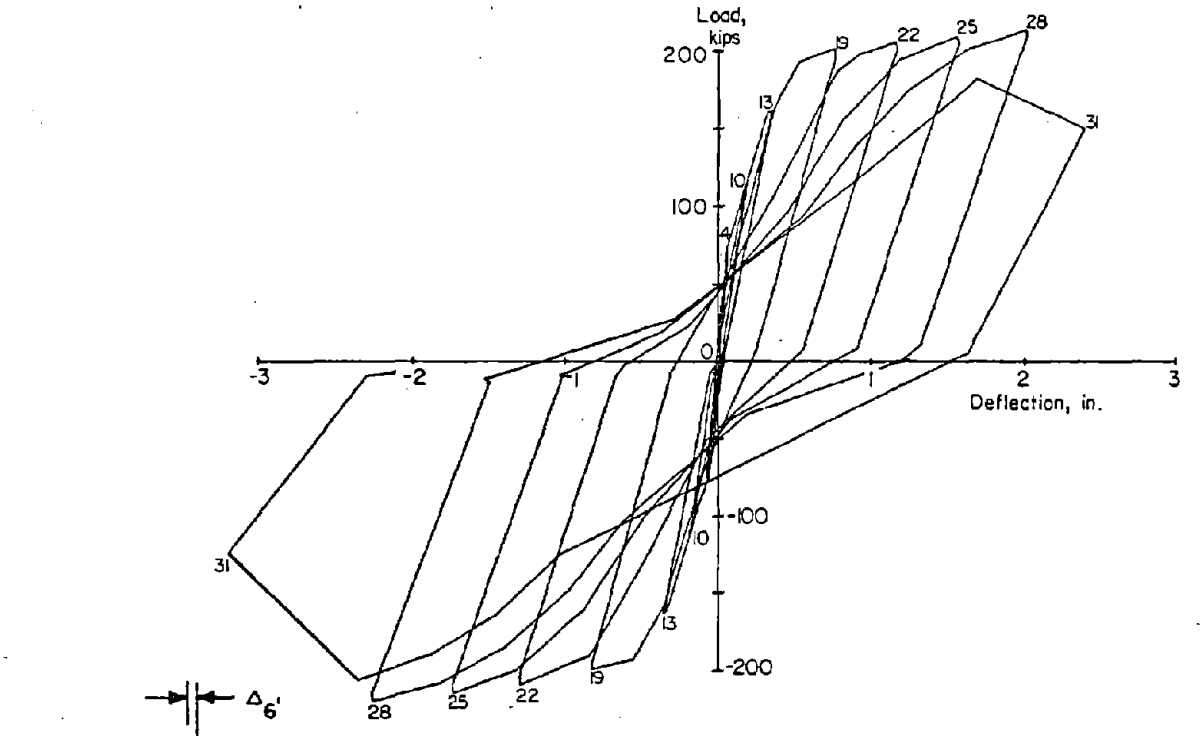

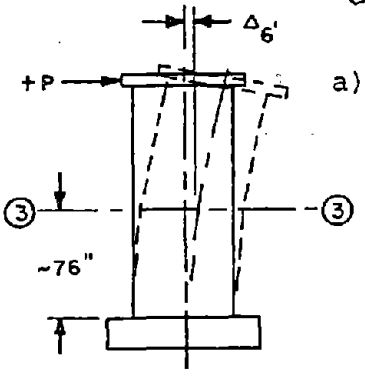

a) Specimen B7

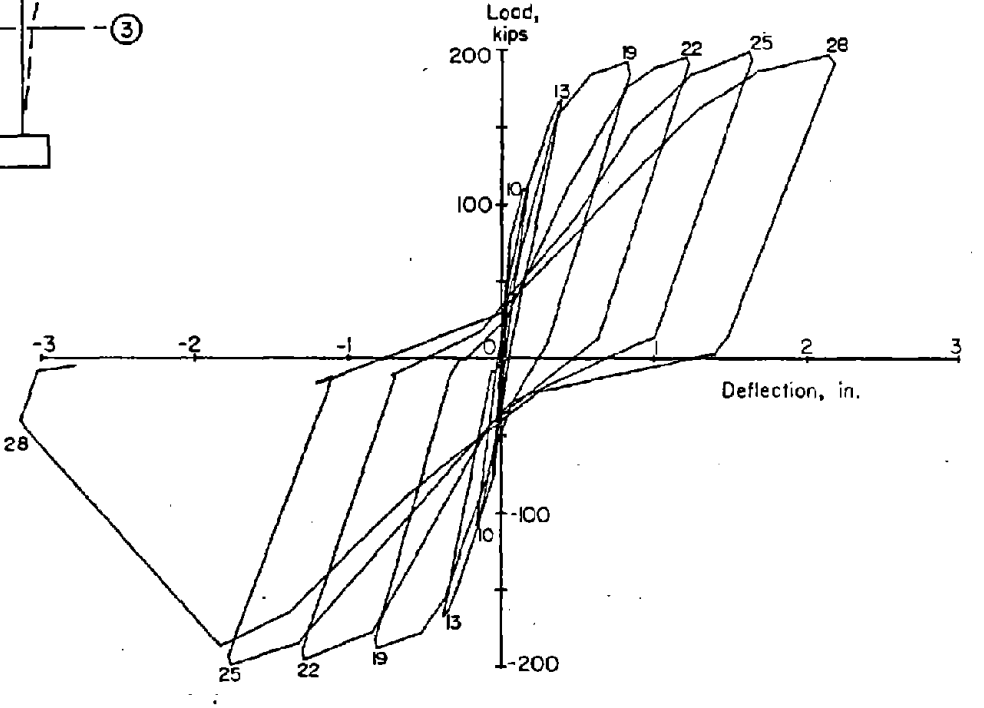

b) Specimen F2

Fig. 24 Comparison of Deflections at the 6 ft Level in Specimens B7 and F2

Specimen F2 sustained 9 inelastic cycles. The maximum rotational ductility was 4.9 and web crushing occurred in Cycle 28.

Figure 23 indicates the shear distortions in F2 were larger than those in B7 at equivalent rotations. However, because the yield rotation was smaller in F2, the shear distortions in the two walls at equivalent rotations ductilities were approximately equal.

Comparing the results of F2 and B7 tests shows that similar performance was obtained. Loss of load capacity was due to web crushing in both specimens.

Amount Of Flexural Reinforcement

Walls in this program were tested under a constant moment-to-shear ratio. The amount of flexural reinforcement was varied to control the moment capacity of the wall sections and, thereby, the maximum level of applied shear. Effects of the level of shear stress were discussed previously in the summary of test results.

The amount of flexural reinforcement determines the maximum level of stress in the compression zone. Since symmetrical wall sections have an equal amount of reinforcement in both boundary elements, they may appear to be under-reinforced and significantly below the balanced condition as defined by the ACI Building Code.[2] However, the depth to the neutral axis of the section is usually significantly less than the boundary element depth. Therefore, a large portion of the reinforcement in the "compression" boundary element may actually be in tension. Considering this additional tension plus tension resulting from strain hardening, crushing of the compression zone may be a possible failure mode in specimens with large amount of flexural steel and relatively low concrete strength.

This failure mode was only observed in Specimen B10 which had inadequately consolidated concrete.

Amount Of Shear Reinforcement

Results of reversing load test on beams have demonstrated that, because of strain hardening the actual moment capacity of a section is considerably higher than the design moment capacity computed using the ACI Building Code.[2] Because of this, several investigators[11,12] have recommended that shear reinforcement be designed to cover the total shear corresponding to the maximum moment capacity including strain hardening.

Also, because of large horizontal cracks crossing the section in beam tests under reversals, the presence of the "concrete contribution" has been questioned.

The results shown in Table 2 indicate that, as with beams, the maximum moment capacity of the walls is significantly higher than the design moment. This should definitely be considered in the design process. However, the test results also show that the diagonal tension shear capacity is also significantly higher than the design capacity. Several of the wall specimens carried maximum shears such that, considering the horizontal reinforcement to take the v_s according to the ACI Building Code, the "concrete contribution" was from $3.2\sqrt{f'_c}$ ($0.26\sqrt{f'_c}$, MPa) in B2 to $6.5\sqrt{f'_c}$ ($0.54\sqrt{f'_c}$, MPa) in B9. Although yield strains were measured in horizontal bars in many of the specimens, there were no horizontal bar fractures associated with diagonal tension.

The test results suggested that additional horizontal reinforcement beyond that required by the ACI Building Code[2] was not necessary for strength purposes. However it was hypothesized that additional horizontal steel might improve inelastic performance in the specimens subjected to high shears by reducing shear deformations.

To investigate this hypothesis, Specimen B8 was constructed similar to B7 except that B8 contained 2.2 times the horizontal reinforcement in B7. Horizontal steel in B8 was designed to remain elastic at a shear corresponding to the maximum calculated moment capacity of the wall.

Specimens B7 and B8 were tested with similar load histories. Measured rotations and shear distortions for these specimens are shown in Fig. 25. Deflections at the 6 ft level are shown in Fig. 26.

Maximum measured rotations were nearly identical in B7 and B8. Shear distortions were only slightly smaller in Specimen B8. Web crushing occurred in B8 only one-half cycle after that in B7.

This indicated that shear stiffness was predominantly dependent on the level of previous maximum deformations and inelastic tensile strain in the flexural steel. The amount of horizontal reinforcement did not have a significant effect on the behavior.

Confinement Reinforcement

Present building codes[2,13] require structural walls to be detailed with confined boundary elements over the entire wall height.

To investigate the effect of confinement steel, several specimens were constructed and tested with ordinary ties. Similar walls were then tested with confinement hoops. Specimens B1 and B3, and Specimens B2 and B5 are comparable specimens with and without confinement reinforcement. Comparison of results from these tests show that confinement increases inelastic performance by performing four primary functions.

1. It increases limiting strain capacity of the concrete core;
2. It supports vertical reinforcement against inelastic buckling;
3. Along with the vertical bars, it forms a "basket" to contain concrete within the core;
4. It increases the shear capacity and stiffness of the boundary elements.

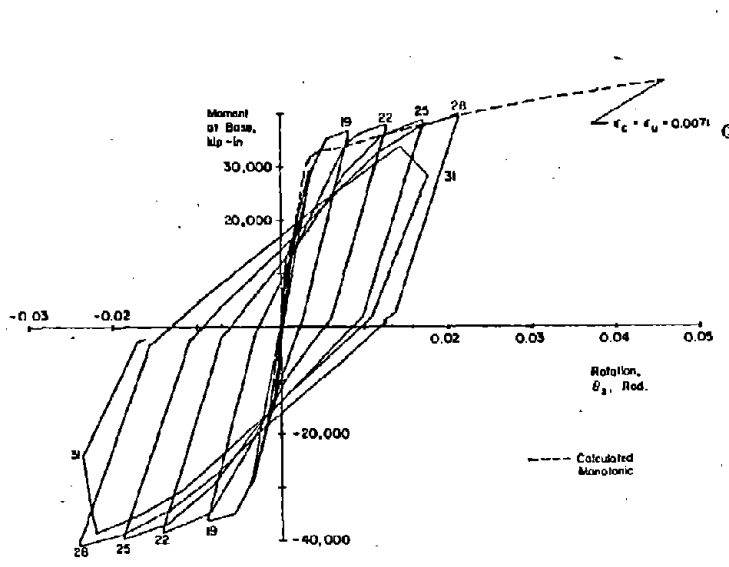

a) Rotation at 6 ft Level, Specimen B7

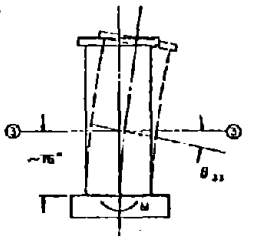

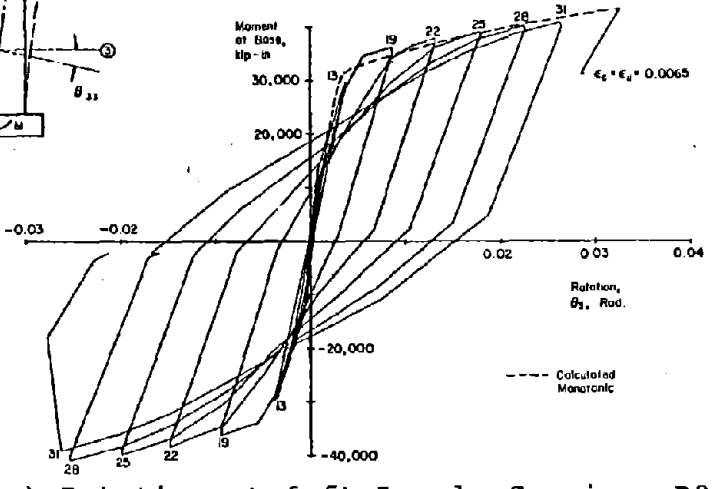

c) Rotation at 6 ft Level, Specimen B8

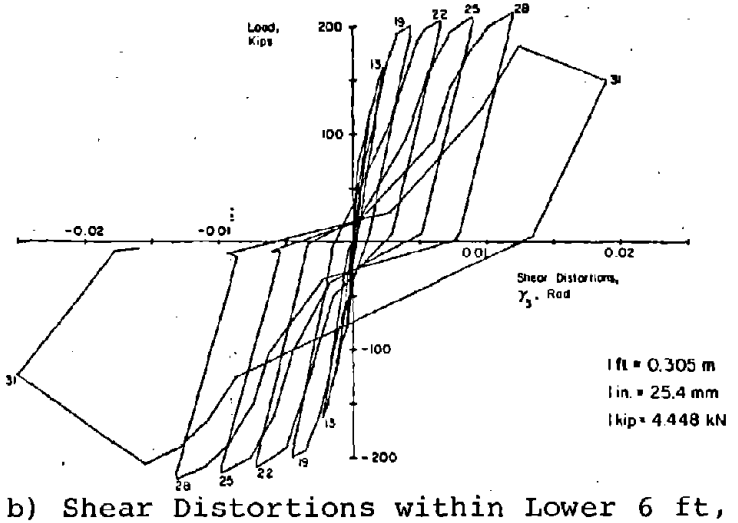

b) Shear Distortions within Lower 6 ft, Specimen B7

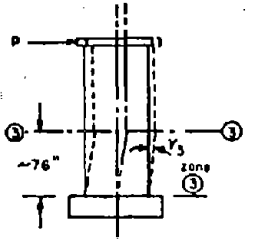

d) Shear Distortions within Lower 6 ft, Specimen B8

Fig. 25 Comparison of Deformations within Barbell Shaped Walls with Different Amounts of Shear Reinforcement

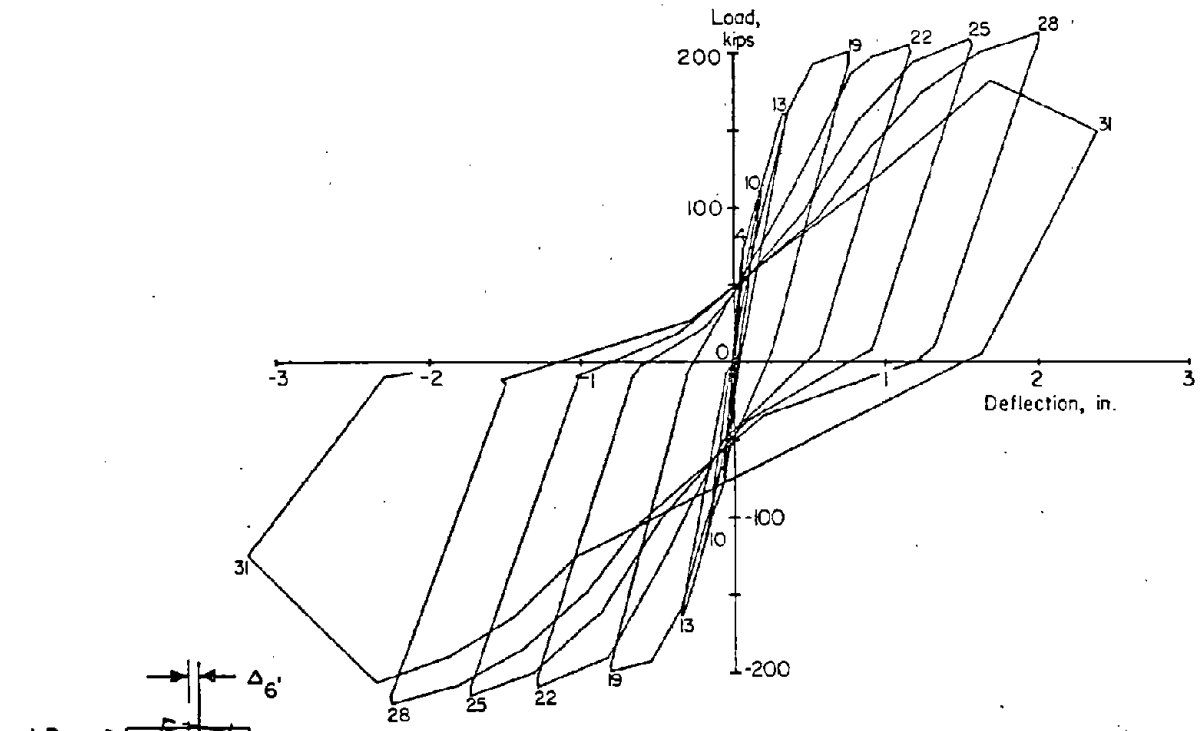

a) Specimen B7

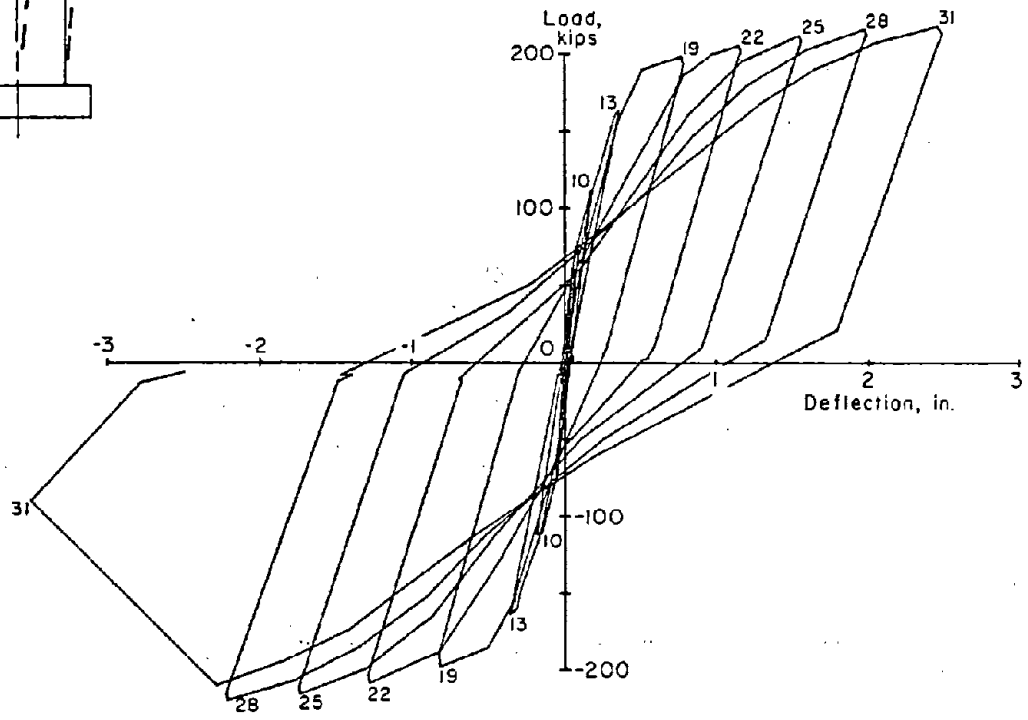

b) Specimen B8

Fig. 26 Comparison of Deflections at the 6 ft Level in Specimens B7 and B8

Confinement to Increase Limiting Concrete Strains

Confinement reinforcement provided in accordance with the 1971 ACI Building Code[2], or the 1976 Uniform Building Code[13] was adequate to maintain the compressive strength of boundary elements under large rotational strains.

Crushing of the boundary element concrete was only observed in Specimen B10 as described previously. This crushing resulted from inadequate consolidation of concrete. It should be noted that the extensive amount of confinement hoops and crossties were the cause of the unconsolidated concrete.

Design of confinement reinforcement according to a limiting strain criteria is not always necessary for structural walls. In many cases, the geometry of walls is such that they are considerably under-reinforced in flexure.

Confinement to Support Vertical Reinforcement and Contain Concrete Core

The functions of transverse reinforcement to restrain vertical bars against inelastic buckling and to contain the concrete core are of considerable importance. Comparison of two tests of isolated structural walls clearly illustrates this function.

Reinforcement details for two of the specimens, B1 and B3, are shown in Figs. 27 and 28, respectively. Specimen B1, the unconfined wall, contained ordinary column ties at a spacing of 8 in. (203 mm) or 16 vertical bar diameters. Specimen B3, the confined wall, had special transverse reinforcement at a spacing of 1.33 in. (34 mm) over the first 6 ft (1.83 m) of the wall. This spacing corresponded to 2.7 vertical bar diameters.

Hysteretic response of Specimens B1 and B3 is illustrated in Fig. 29 and 30. The maximum loads sustained by these walls corresponded to a nominal shear stress of $3\sqrt{f'_c}$ psi ($0.3\sqrt{f'_c}$ MPa).

As shown in Fig. 29 and 30, the behavior of the walls was very similar through Cycle 28. However, deterioration in strength and stiffness of Specimen B1 started in Cycle 31. This deterioration resulted from damage to the boundary

Fig. 27 Reinforcement for Specimen B1

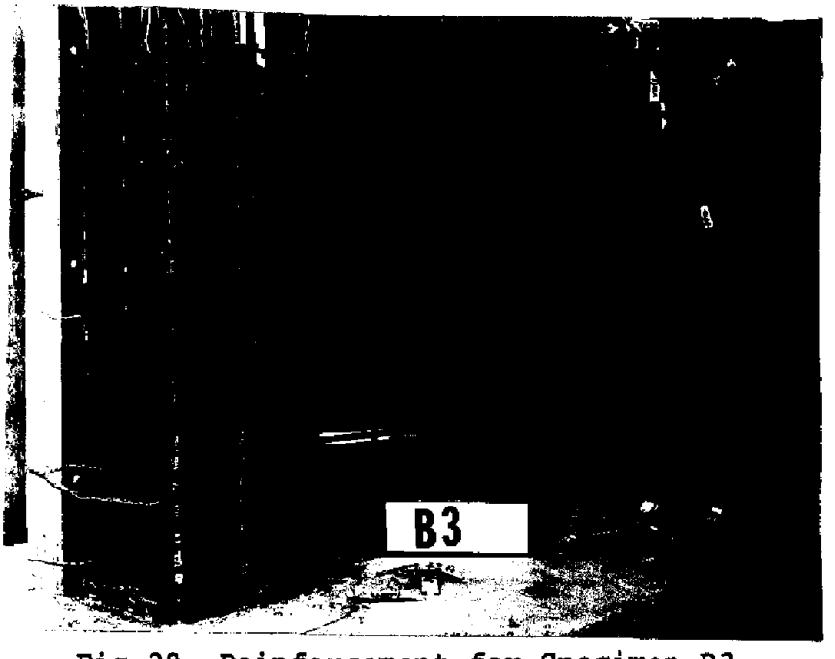

Fig 28 Reinforcement for Specimen B3

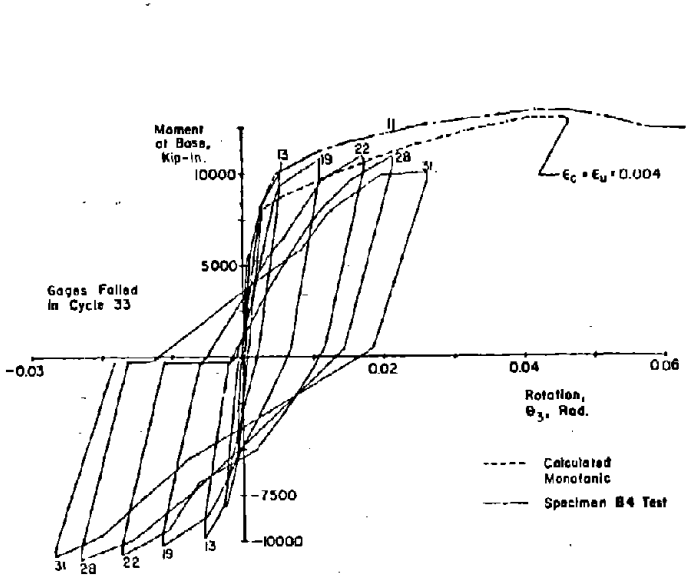

a) Rotation at 6 ft Level, Specimen B1

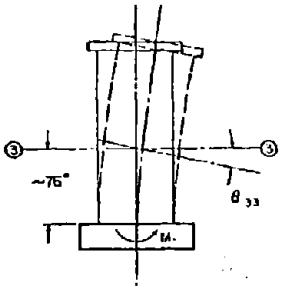

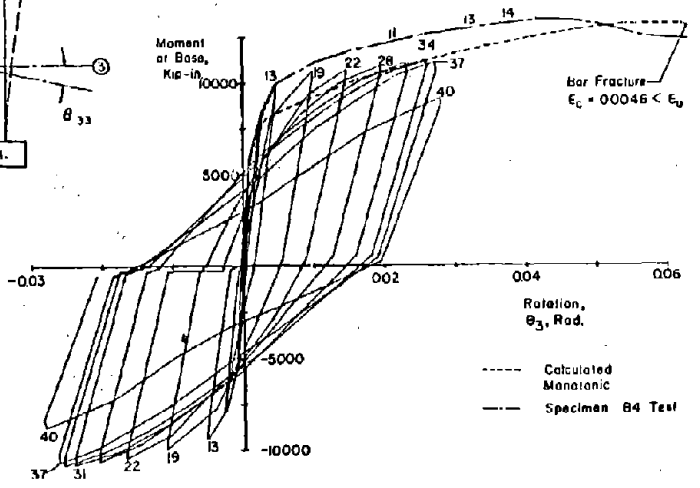

c) Rotation at 6 ft Level, Specimen B3

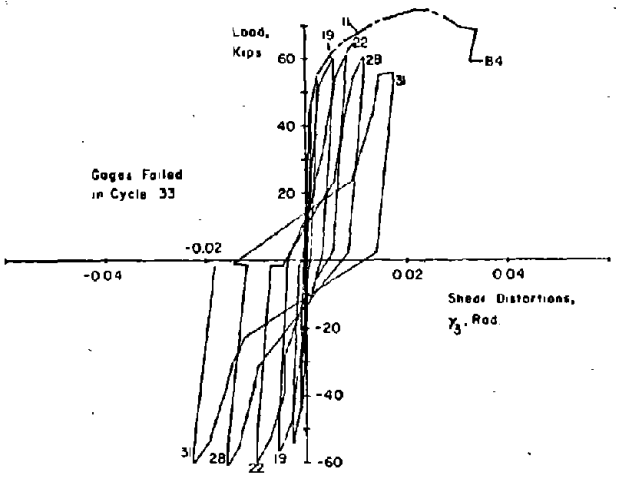

b) Shear Distortions within Lower 6 ft, Specimen B1

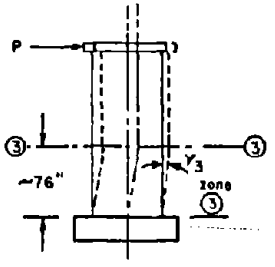

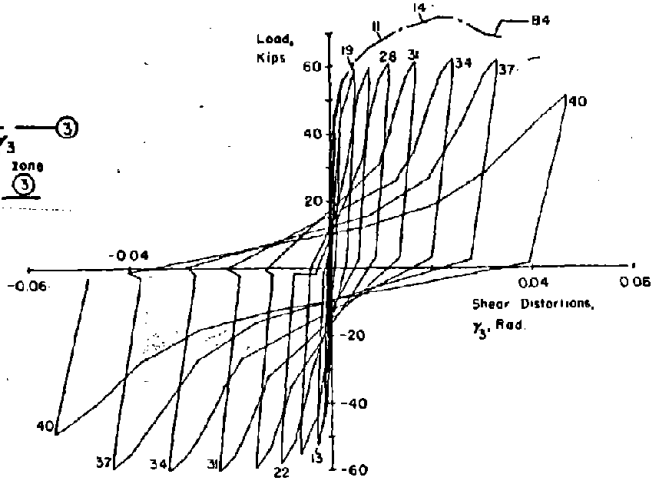

d) Shear Distortions within Lower 6 ft, Specimen B3

Fig. 29 Comparison of Deformations within Barbell Shaped Walls with and without Confinement Reinforcement

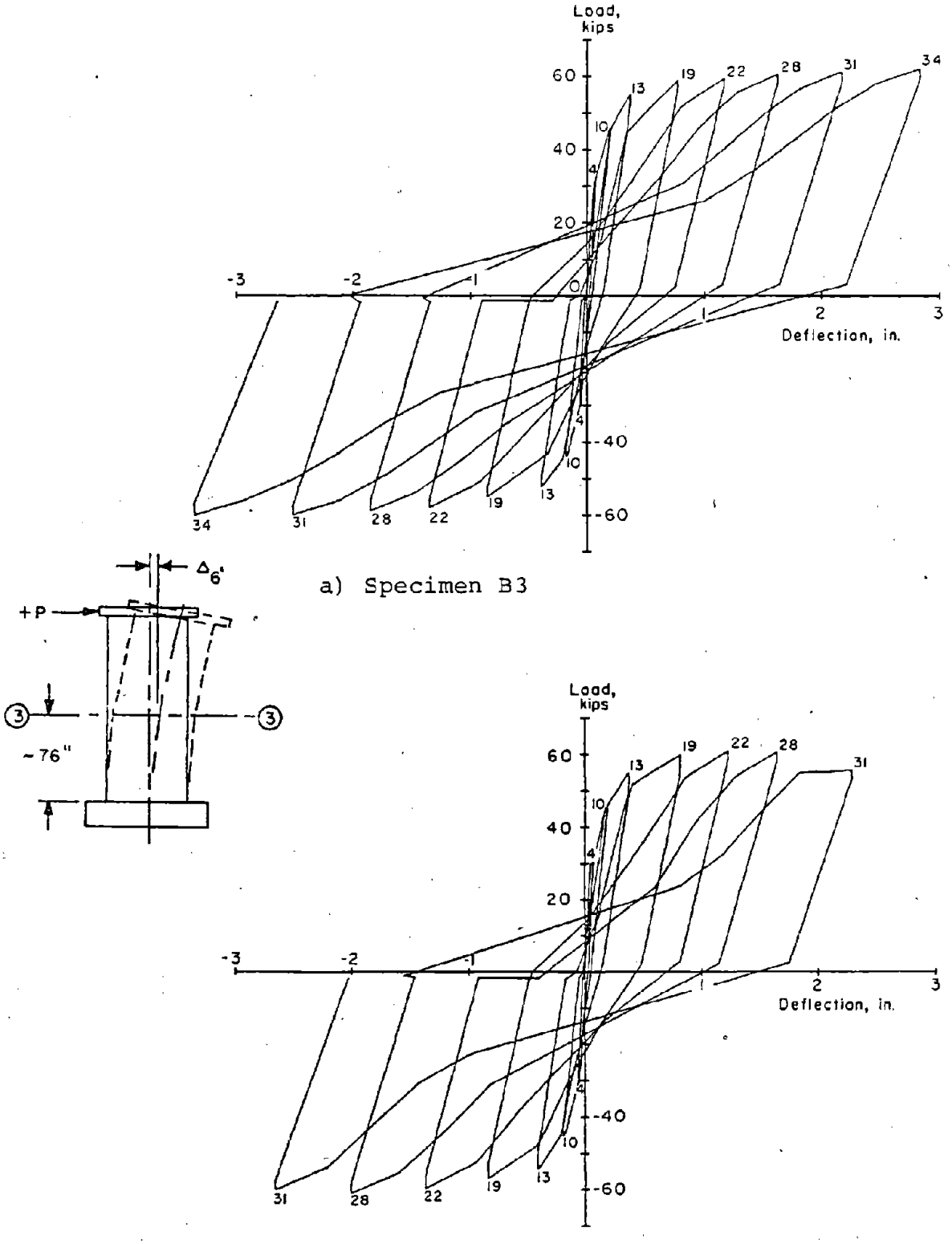

a) Specimen B3

b) Specimen B1

Fig. 30 Comparison of Deflections at the 6 ft Level in Specimens B7 and B8

elements by alternate tensile and compressive yielding. This led to inelastic buckling of the main vertical reinforcement. Buckling was accompanied by loss of concrete not contained by the vertical and transverse reinforcement when the boundary element was in tension.

The confinement hoops in Specimen B3 did not significantly increase strength or maximum rotation as compared to Specimen B1. However, the hoops maintained the integrity of the boundary elements by delaying bar buckling and containing the concrete core. Photographs of the two walls at the same load increment in Figs. 31 and 32 clearly show the effectiveness of the confinement. For equivalent levels of load, the confined wall suffered less damage. Also, the confined wall sustain several more inelastic cycles which included significantly larger shear distortions.

Confinement to Provide Shear Capacity

Tests of isolated walls have indicated that transverse hoop reinforcement in vertical boundary elements improves shear capacity and stiffness. The transverse reinforcement ties each boundary element together to act as a large, ductile dowel on each end of a wall. This is shown by comparison of two isolated wall tests.

Two specimens, B2 and B5, were constructed with nominally identical reinforcement except for the transverse confinement. Both walls had barbell cross-sections with vertical reinforcement in the boundary elements of about 3.7% of the column area. Photographs of the reinforcement are shown in Figs. 33 and 34.

The unconfined wall, Specimen B2, had ordinary column ties at a spacing of 8 in. (203 mm) or 10.7 vertical bar diameters. The confined wall, B5, had hoops spaced at 1.33 in. (34 mm) or 1.8 bar diameters over the first 6 ft (1.83 m) of the wall. Ordinary column ties were used over the remaining height of the wall.

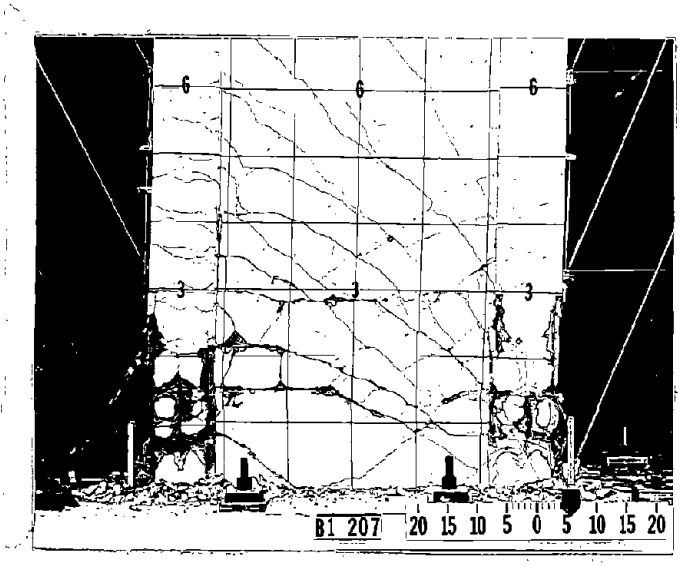

Fig. 31 Specimen B1 During Load Cycle 34

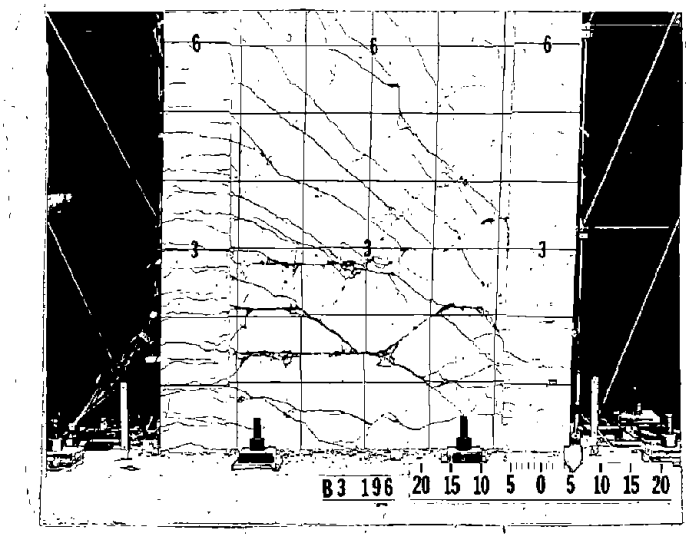

Fig. 32 Specimen B3 During Load Cycle 34

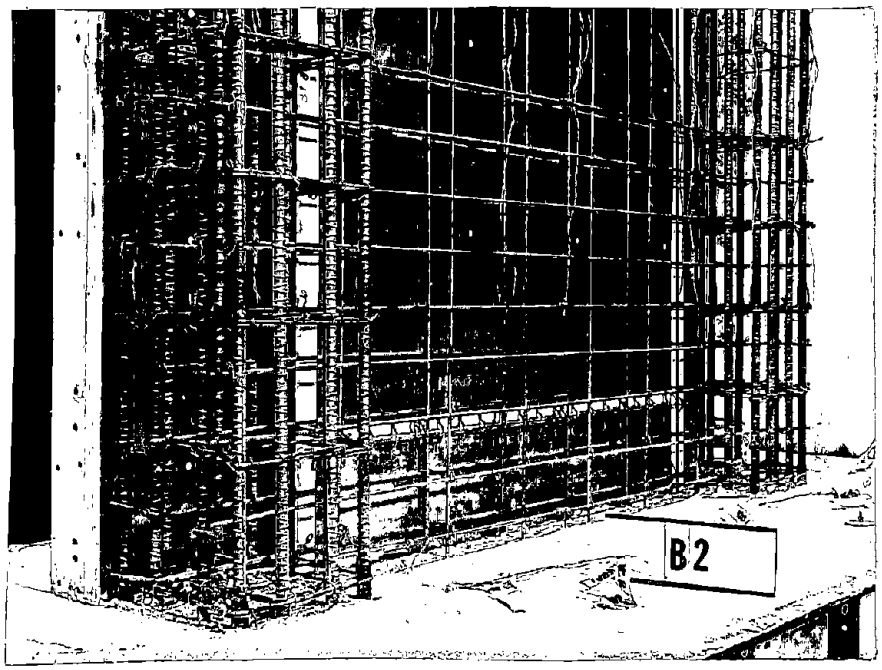

Fig. 33 Reinforcement for Specimen B2

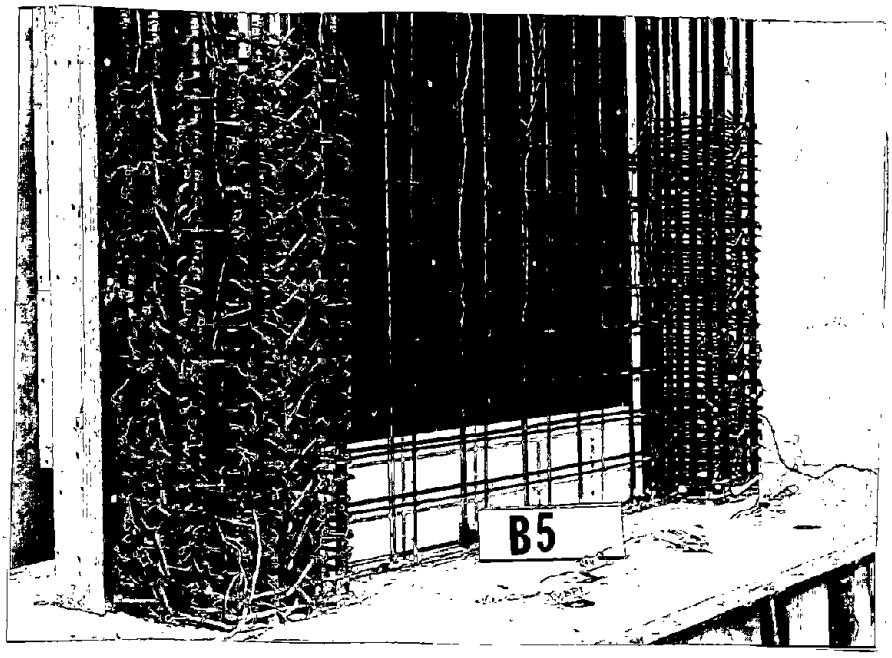

Fig. 34 Reinforcement for Specimen B5

Hysteretic response for the two specimens is illustrated in Figs. 35 and 36. The capacity of both walls was limited by web crushing. Specimen B2 reached a capacity corresponding to a nominal shear stress of 7.2 $\sqrt{f'_c}$ psi (0.60 $\sqrt{f'_c}$ MPa). Specimen B5 reached 8.8 $\sqrt{f'_c}$ psi (0.73 $\sqrt{f'_c}$ MPa).

Comparison of observed deformations in Specimens B2 with those of B5 indicated that confinement reinforcement did not significantly affect the moment rotation relationship. However, shear distortions were decreased by approximately 15% for equivalent rotations. The improvement in shear stiffness was attributed to the confined boundary elements acting as stiff dowels.

In Specimen B2, without confinement, the boundary elements deteriorated prior to web crushing. Several bars buckled and concrete was lost from the core of the columns as loads were reversed. In the last load cycle, the boundary elements were badly damaged near the base. The column was destroyed by combined shear and compression when web crushing occurred. Specimen B2 after web crushing is shown in Fig. 37.

In Specimen B5, confinement hoops prevented bar buckling and loss of concrete from the core of the boundary elements. They also reinforced the boundary elements for shear as can be seen in Fig. 38. The boundary element was capable of deforming to accommodate the large distortions occurring with web crushing while retaining its structural integrity. Because of the confinement, Specimen B5 could be repaired by replacing damaged web concrete.

Location of Confinement Reinforcement

Although present codes[2,13] require confinement reinforcement over the entire wall height, only the lower 6 ft. (1.83 m) of the boundary elements of the test specimens was confined. This is a height equal to the horizontal length of the wall. The primary zone of damage in all walls tested did not extend above this level. Typical strain gage data shown in Fig. 39 indicated that the only hoops stressed significantly were in the lower 3 ft. (0.91 m).

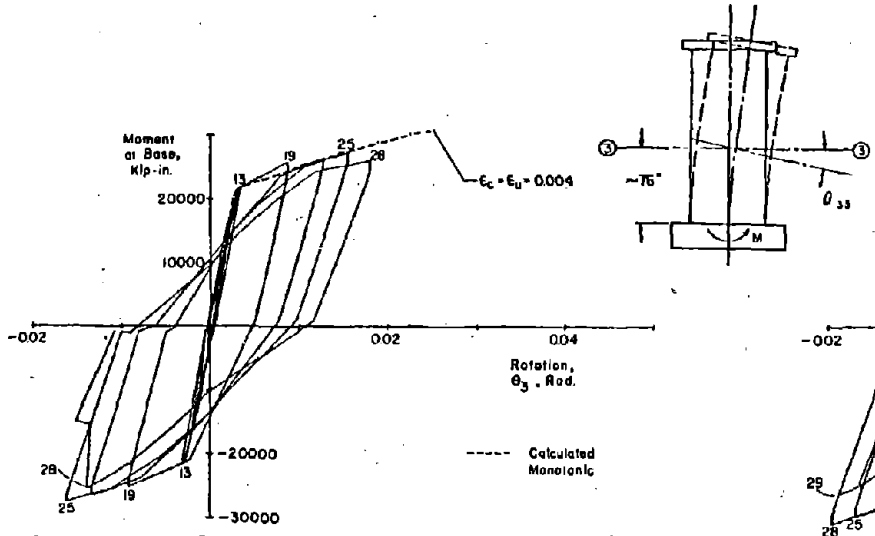

a) Rotation at 6 ft Level, Specimen B2 without Confinement

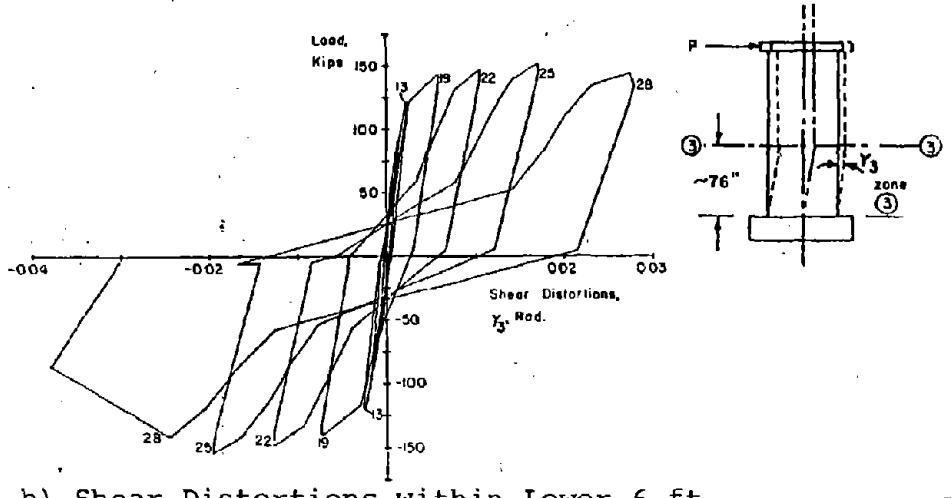

b) Shear Distortions within Lower 6 ft, Specimen B2 without Confinement

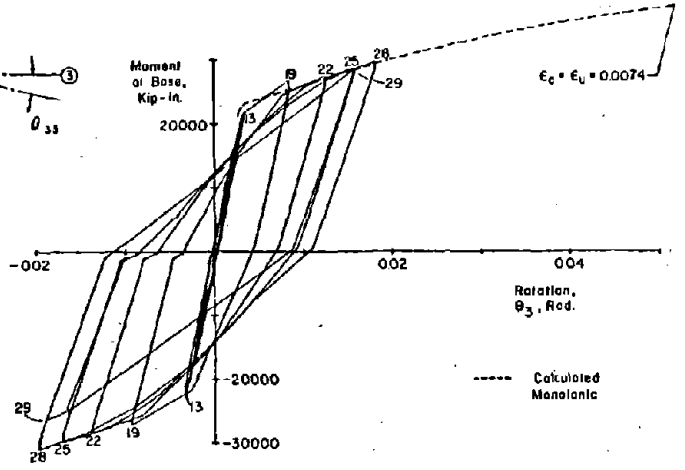

c) Rotations at 6 ft Level, Specimen B5 with Confinement

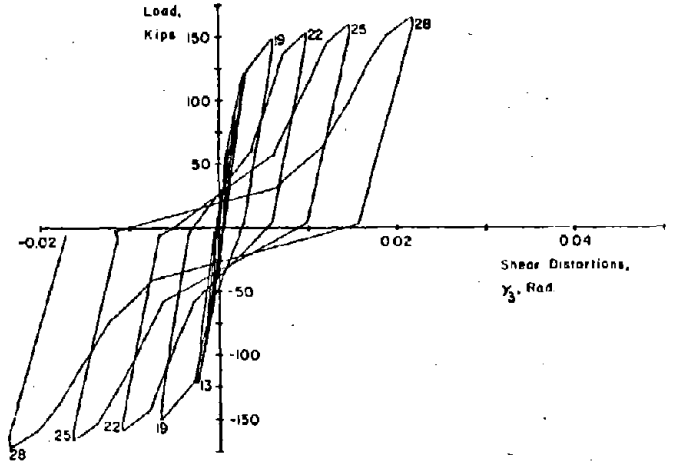

d) Shear Distortions within Lower 6 ft. Specimen B5 with Confinement

Fig. 35 Comparison of Deformations within Barbell shaped Walls with and without Confinement Reinforcement

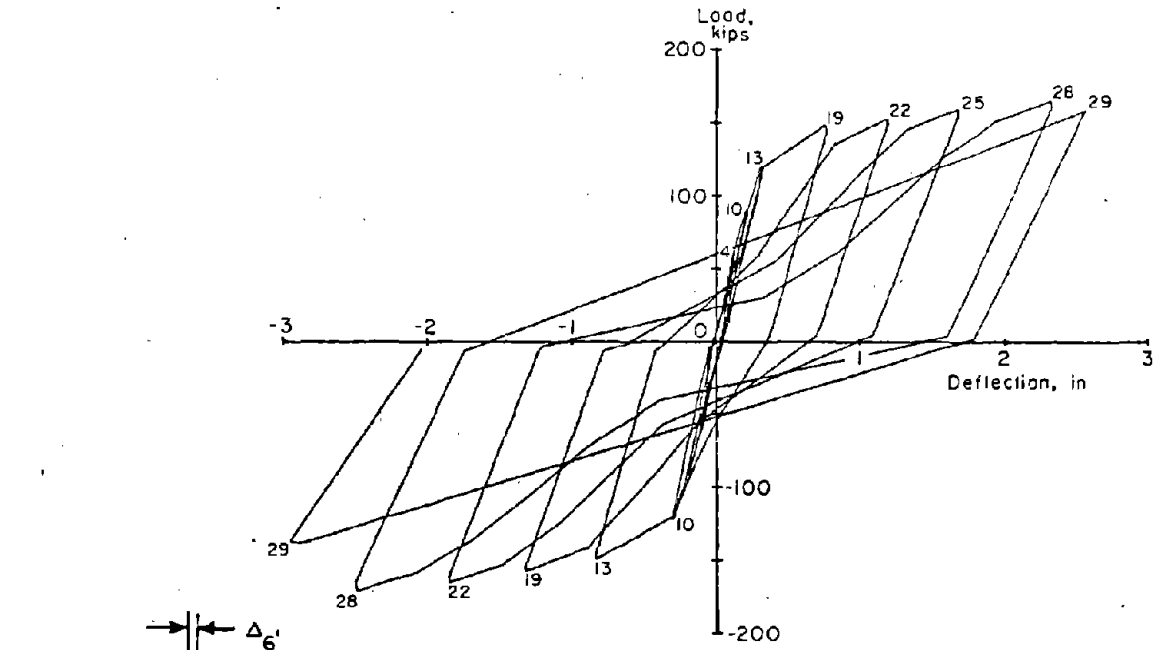

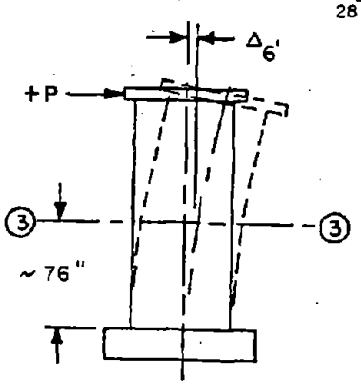

a) Specimen B5

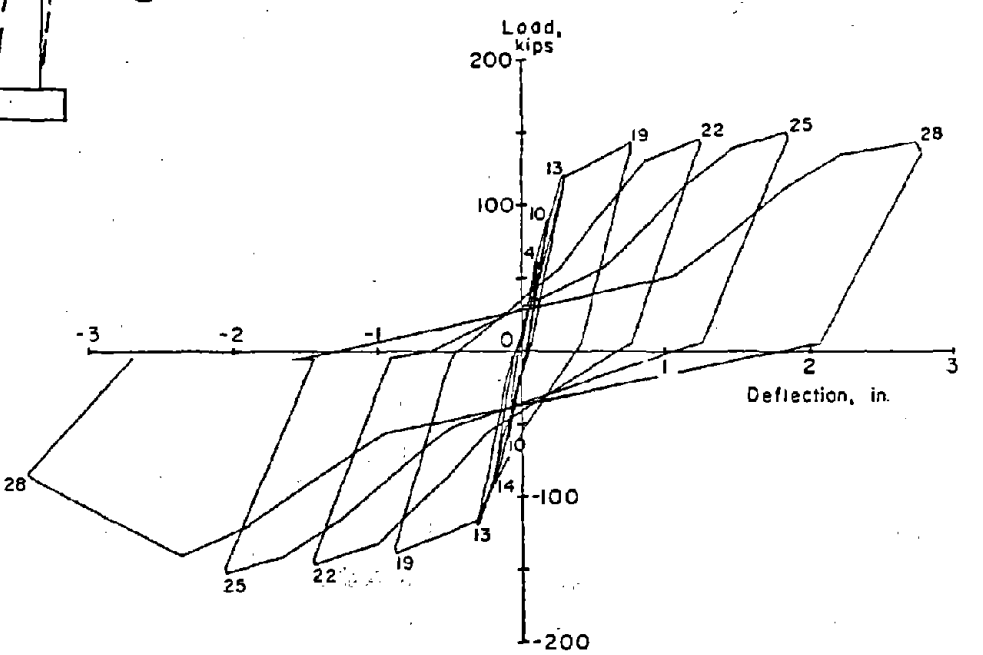

b) Specimen B2

Fig. 36 Comparison of Deflections at the 6 ft Level in Specimens B2 and B5

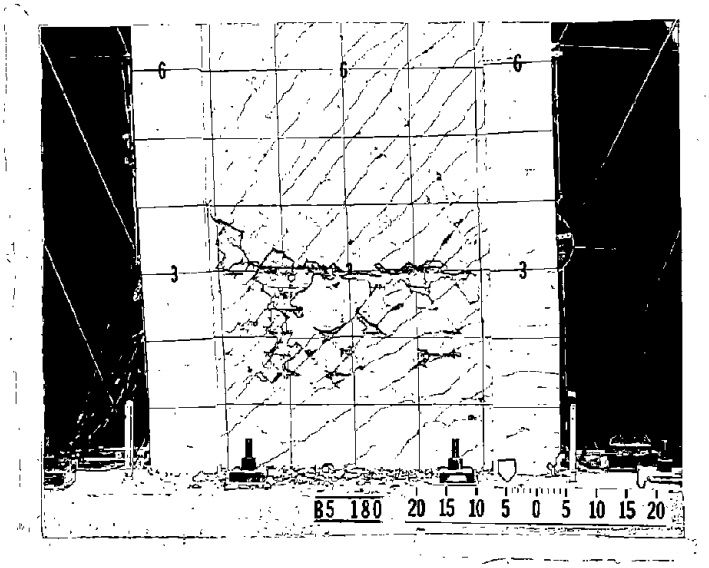

Fig. 37 Specimen B2 After Web Crushing

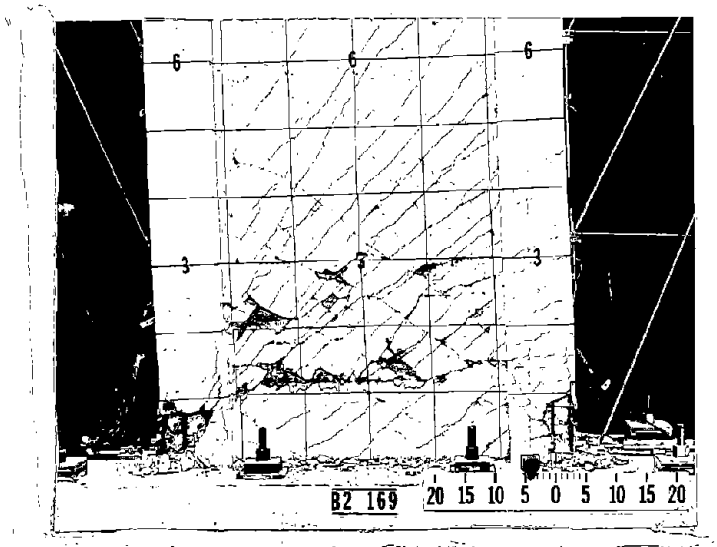

Fig. 38 Specimen B5 After Web Crushing

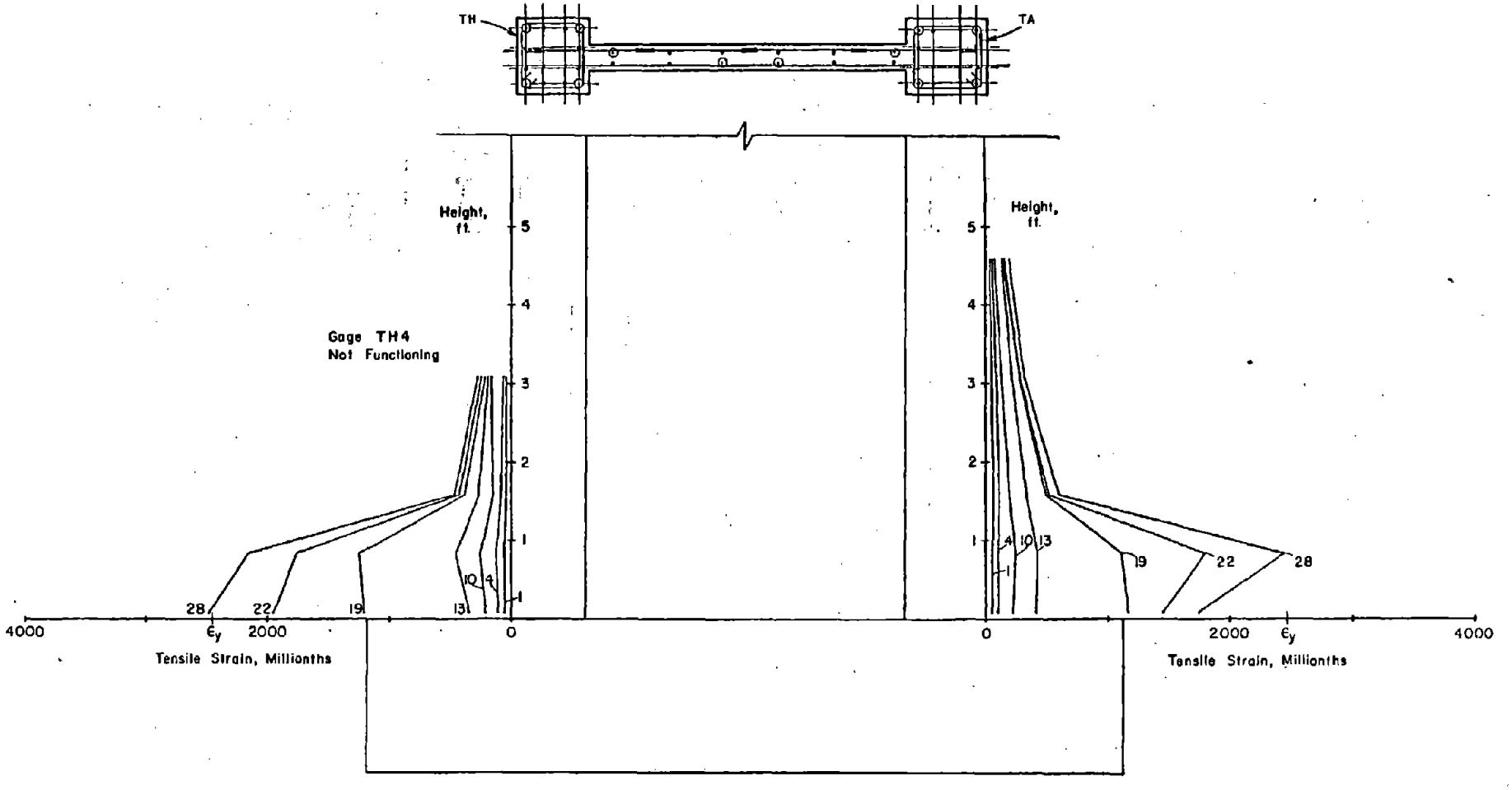

Fig. 39 Confinement Hoop Reinforcement Strains at Maximum Loads for Specimen B7

Vertical Load

It is generally considered that the effect of axial compressive load on the monotonic behavior of reinforced concrete flexural elements is to increase moment and shear capacity (with the axial load lower than the balanced condition) but to decrease ductility.[14] To investigate the effect of axial on wall specimens subjected to reversing load, Phase I tests were performed without axial load and Phase II tests were performed with axial load. Specimen B5 in Phase I and Specimen B7 in Phase II are directly comparable. The level of axial load on B7 was 7% of the ultimate axial load capacity.

Figures 40 and 41 shows the hysteretic response of Specimens B5 and B7. Both specimens lost load capacity through web crushing. A comparison of Figs. 36a and c show that, as expected, axial load increased moment and shear capacity. However, it also increase maximum measured rotation prior to web crushing. This is attributed to a considerable increase in shear stiffness with axial load as shown by comparing Figs. 36b and d.

Web crushing was found to be dependent on both stress and deformation levels.[3] Since axial load decreased shear distortions at equivalent rotations, the specimen with axial load could sustain more cycles at larger rotations prior to web crushing.

Concrete Strength

Concrete strength can have several effects on performance of walls. It was expected to affect column crushing strength, web crushing strength and abrasion resistance along crack interfaces. Of these, web crushing strength is the most critical and the least understood.

To investigate the relationship between web crushing strength and concrete strength, Specimens B6 and B7 were constructed and tested. Measured concrete strengths for B6 and B7 were 3165 psi and 7155 psi (21.8 MPa and 49.3 MPa) respectively.

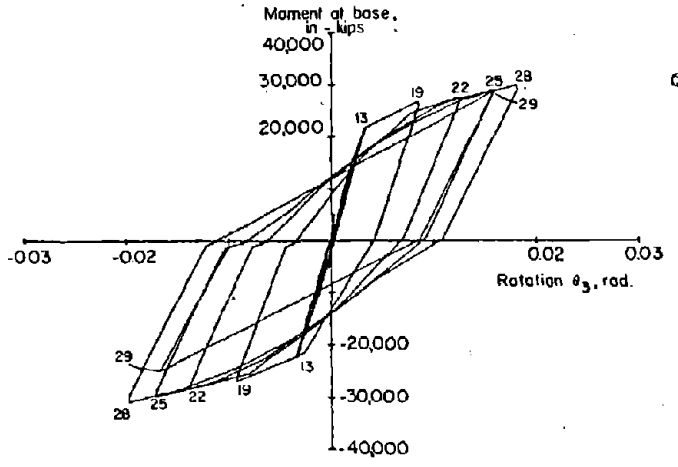

a) Rotation at 6 ft Level, Specimen B5 without Axial Load

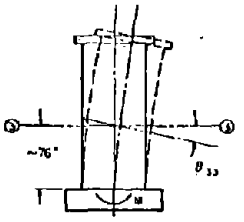

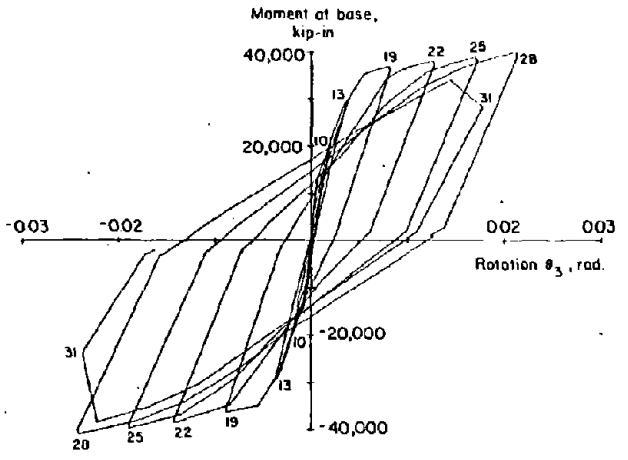

c) Rotation at 6 ft Level, Specimen B7 with Axial Load

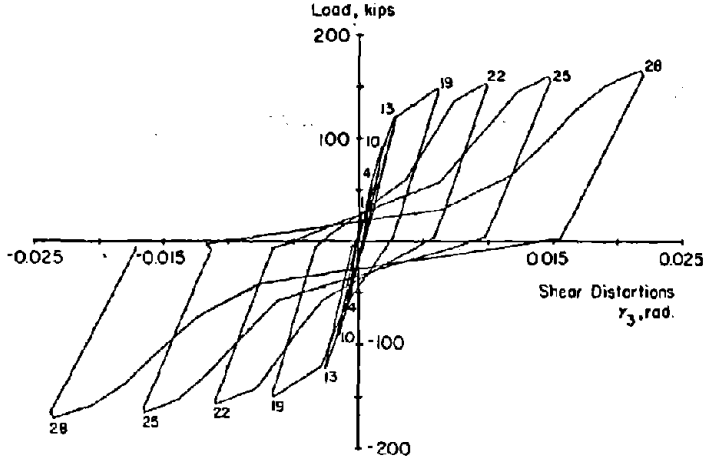

b) Shear Distortions within Lower 6 ft Specimen B5 without Axial Load

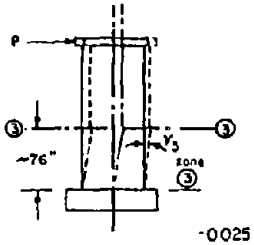

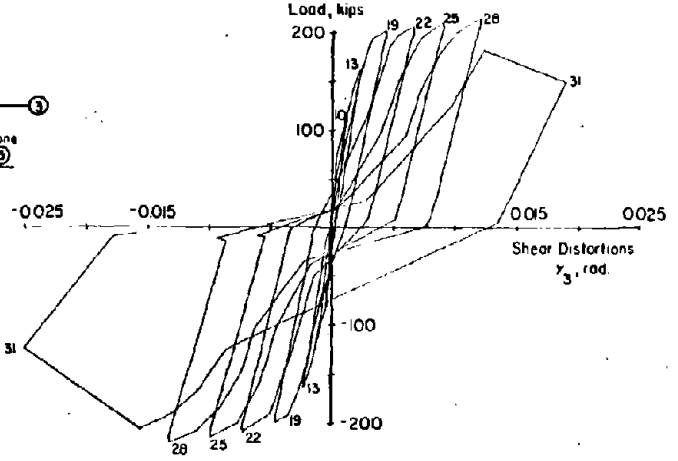

d) Specimen B7 with Axial Load

Fig. 40 Comparison of Deformations within Barbell Shaped Wall with and without Axial Load

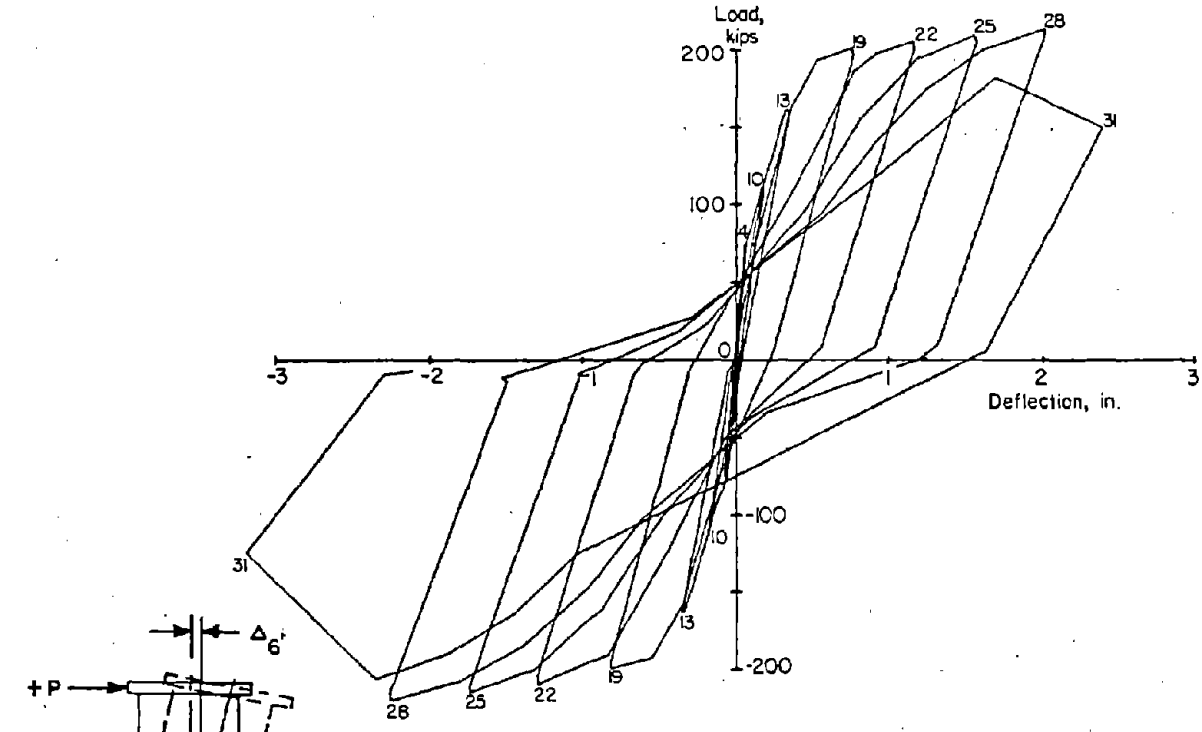

a) Specimen B7

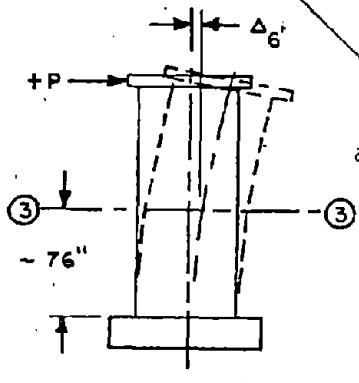

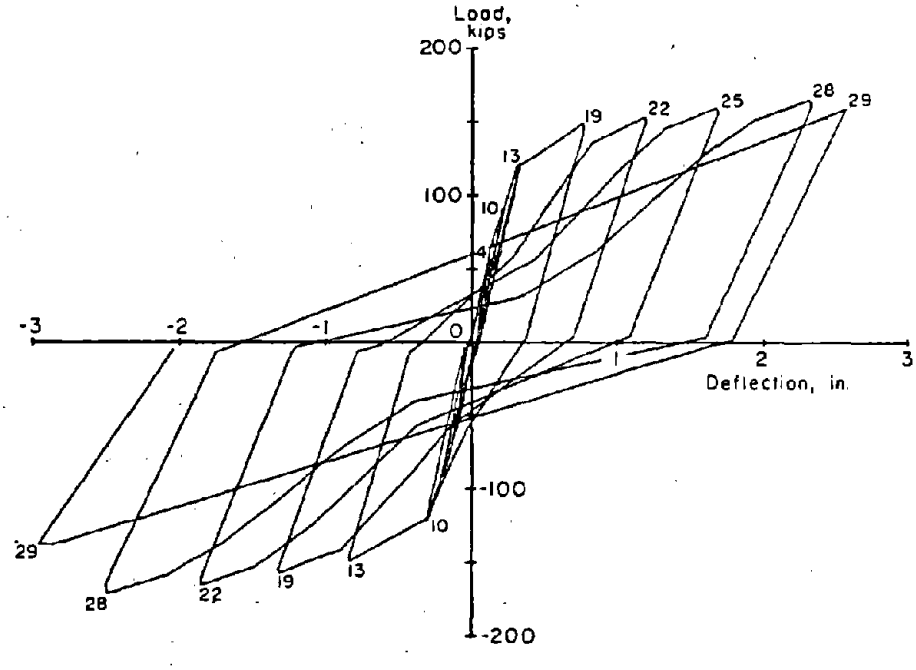

b) Specimen B5

Fig. 41 Comparison of Deflections at the 6 ft Level in Specimens B5 and B7

Figure 42 and 43 shows the hysteretic response for Specimens B6 and B7. Specimen B6 reached a maximum load corresponding to a shear stress of 13.8 $\sqrt{f'_c}$ (1.15 $\sqrt{f'_c}$, MPa). The comparable stress in B7 was 10.9 $\sqrt{f'_c}$ (0.91 $\sqrt{f'_c}$ MPa). The maximum measured deformations prior to web crushing were considerably smaller in Specimen B6.

The results of Specimen B6 test tend to verify the conclusion that web crushing is dependent on both stress and deformation levels. Web crushing strength is commonly considered a function of concrete strength alone.[3] However, Specimen B6 sustained approximately the same level of shear load that crushed the web of B7 even though the concrete strength in B6 was less than half that in B7. Specimen B6 was capable of sustaining this load through yield. However, lower concrete strength in B6 resulted in significantly lower deformation capacity.

Load History

Three load histories were used in the tests: monotonic, incrementally reversing (IR), and modified reversing (MR). The IR and MR load histories are illustrated in Fig. 5.

Monotonic Versus Reversing

Reversing loads affected strength and ductility, and precipitated different failure modes in specimens subjected to low shear. Specimen B3 and B4 demonstrate this. Figure 44 shows the measured rotations and shear distortions for Specimens B3 and B4. Figure 45 shows the deflection at the 6 ft (1.83m) level. Specimen B3 was subjected to an IR load history. Specimen B4 was loaded monotonically to flexural bar fracture. Figure 46 shows the specimens at the end of the tests.

Figure 45 indicates that maximum deflections measured at the 6 ft (1.83m) level were approximately equal in B3 and B4. However, as shown in Fig. 44, the rotation was significantly smaller and shear distortions larger in the reverse loaded Specimen B3.

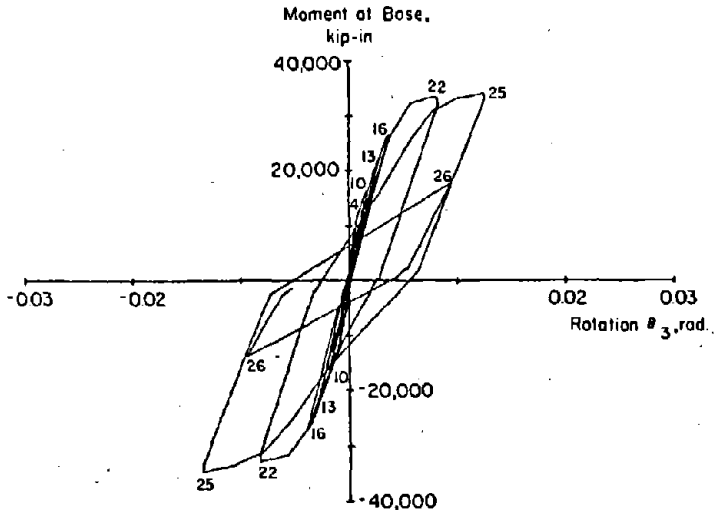

a) Rotation at 6 ft Level, Specimen B6 with f'_c = 3165 psi

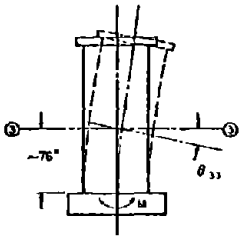

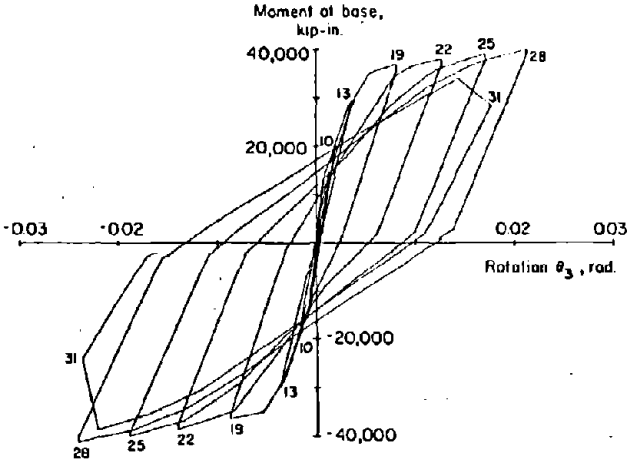

c) Rotation at 6 ft Level, Specimen B7 with f'_c = 7155 psi

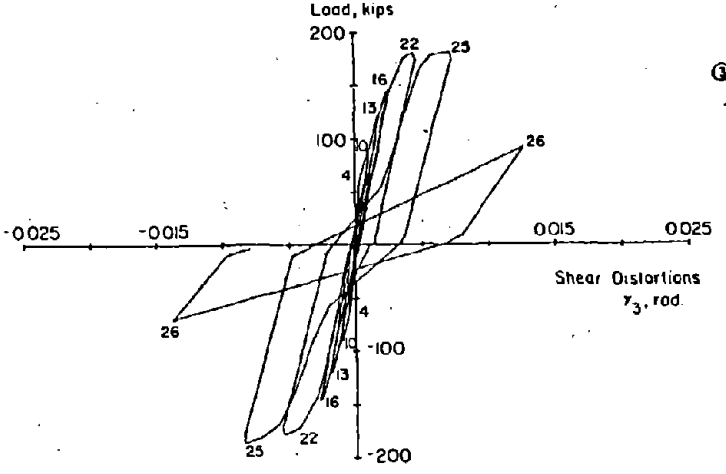

b) Shear Distortions within Lower 6 ft, Specimen B6 with f'_c = 3165 psi

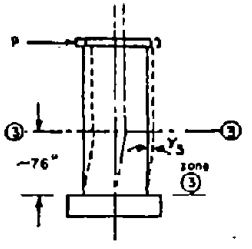

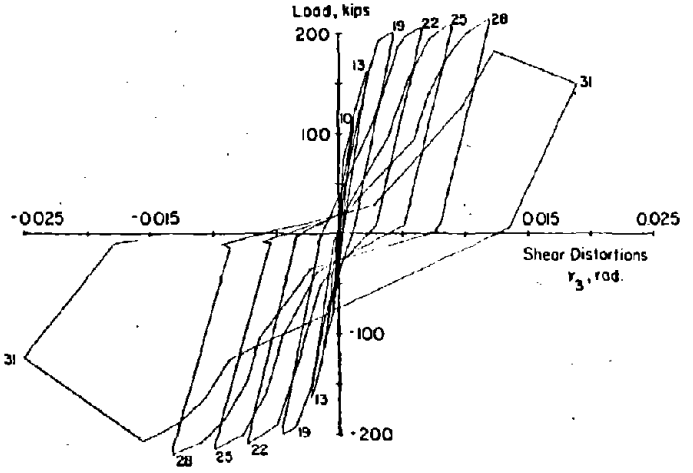

d) Shear Distortions within Lower 6 ft. Specimen B7 with f'_c = 7155 psi

Fig. 42 Comparison of Deformations within Barbell Shaped Wall with Different Concrete Strengths

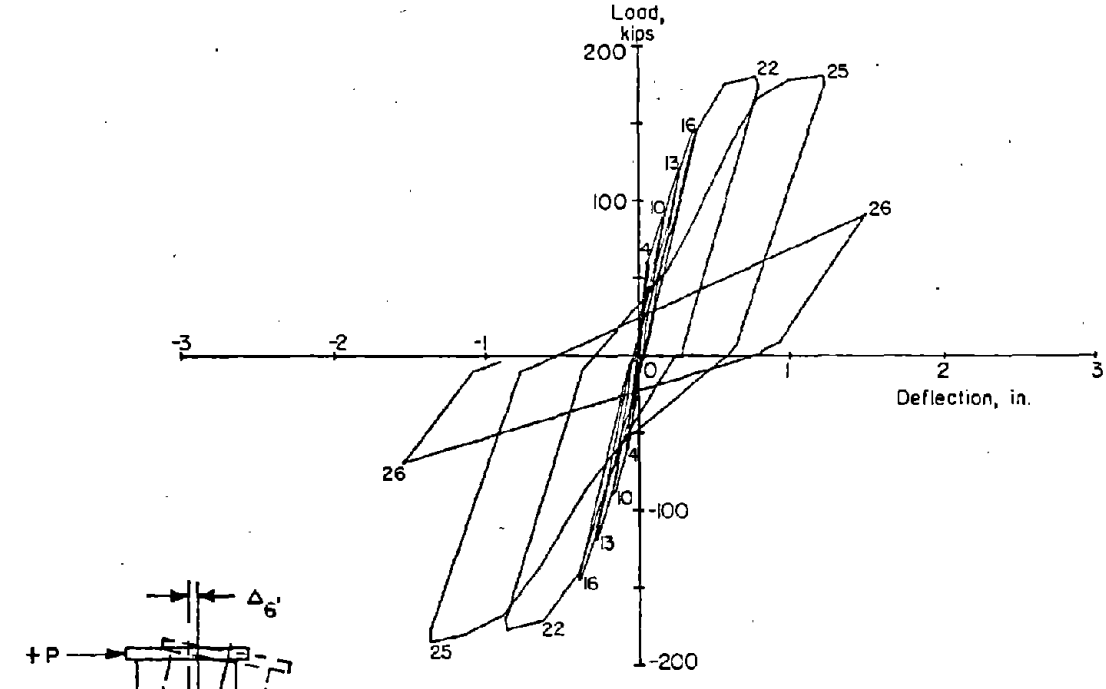

a) Specimen B6

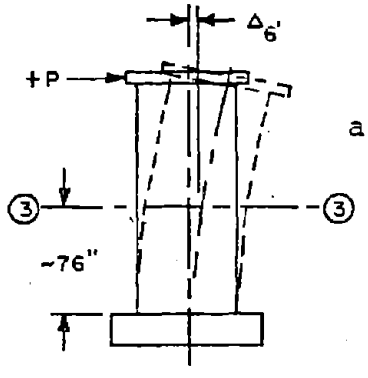

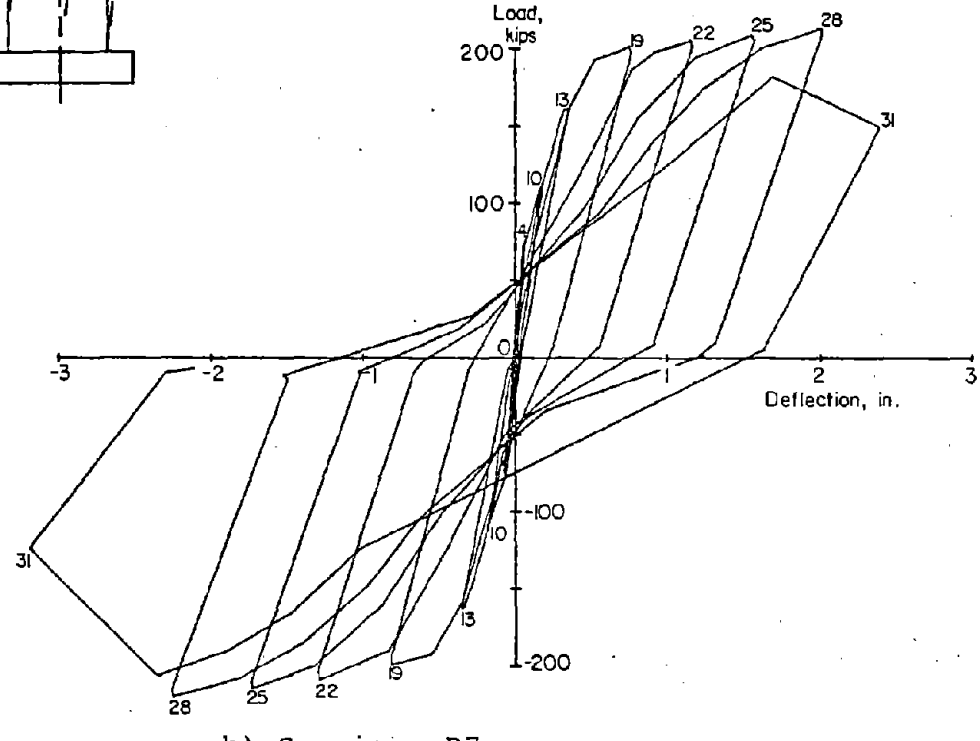

b) Specimen B7

Fig. 43 Comparison of Deflections at the 6 ft Level in Specimens B6 and B7

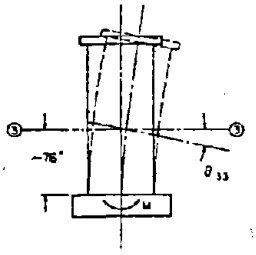

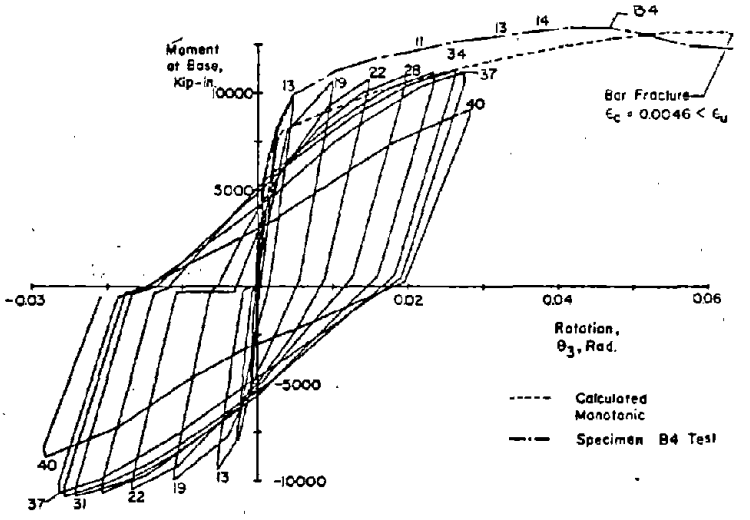

a) Rotations at 6 ft Level, Specimens B3 and B4

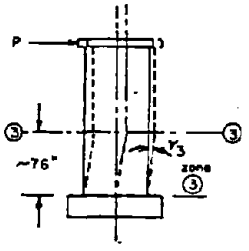

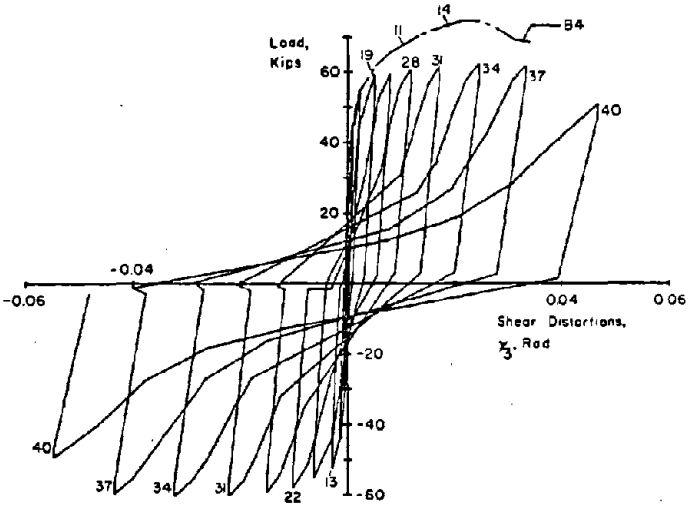

b) Shear Distortions within Lower 6 ft, Specimens B3 and B4

Fig. 44 Comparison of Deformations within Barbell Shaped Walls subjected to Low Shear Stresses for Monotonic versus Reversing Load

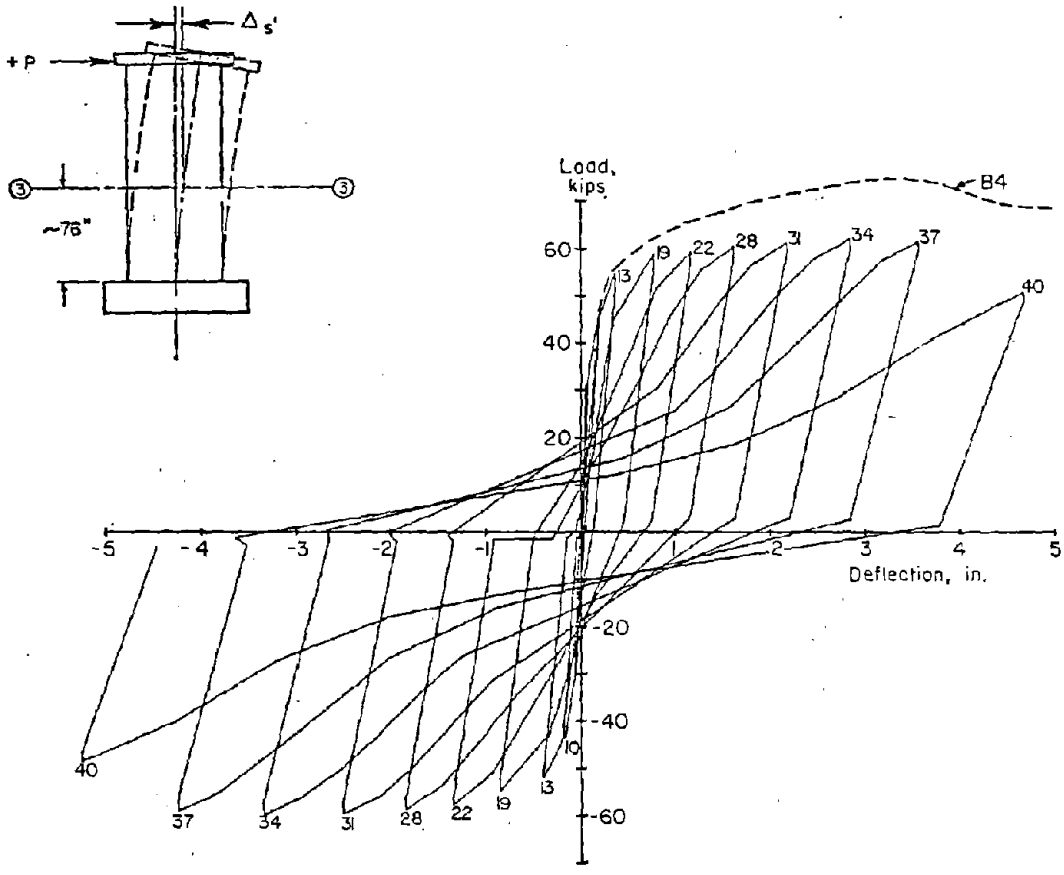

Fig. 45 Comparison of Deflections at the 6 ft Level in Specimens B3 and B4

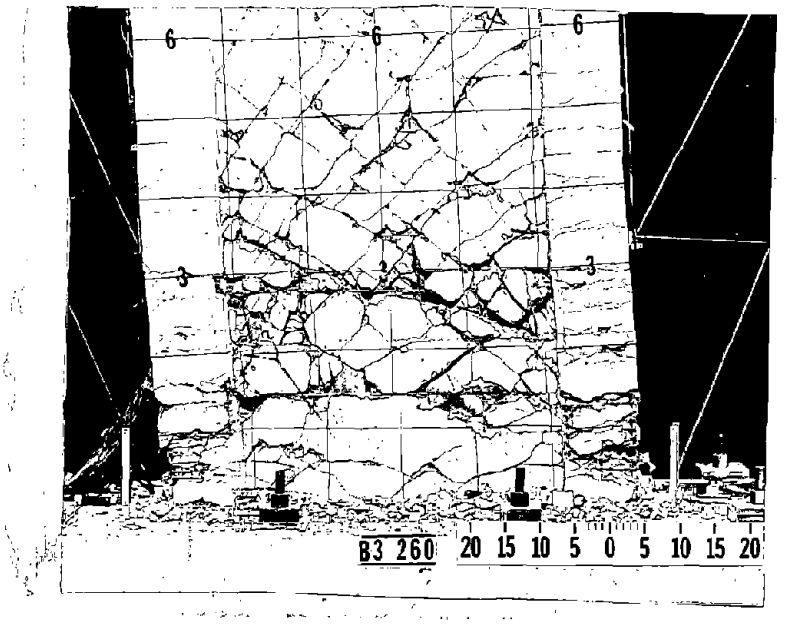

Fig. 46a Specimen B3 at End of Test

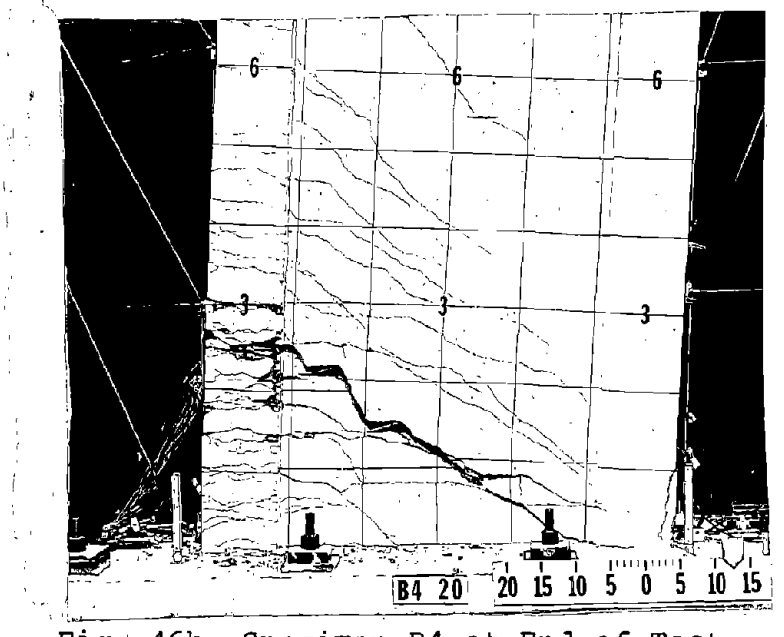

Fig. 46b Specimen B4 at End of Test

Shear stiffness degredation, abrasion of concrete, and inelastic buckling and fracture of bars in B3 were all a function of reversing loads. Specimen B3 attained 82% of the maximum load measured in B4.

No monotonic tests to failure were performed on walls subjected to high shear stresses. However, the positive half of Cycle 2 in the test of Specimen B9 is essentially a monotonic test up to a rotational ductility of 5. Specimen B9 was constructed similar to B7. Figures 47 and 48 show the load-deformation characteristics for Specimen B7 and for the first half of Cycle 2 in Specimen B9. Comparison of the positive envelopes for B7 under cyclic load with that of the "monotonic" portion of Cycle 2 for B9 shows only a slight difference in load deformation characteristic up to the level of failure in B7. For equivalent levels of rotation, Specimen B9 had only slightly lower shear distortions in the first half of Cycle 2 than those measured in Specimen B7.

As opposed to the difference in behavior between B3 and B4, the results of B7 and B9 indicated reversing loads had only a small effect. Specimens B7 and B9 were subjected to a constant axial stress of 545 psi (3.76 MPa) during the lateral load test. As discussed previously comparing B5 and B7, loss of shear stiffness with reversing loads was significantly reduced when axial stress was present. The discussion in the following section will show that shear stiffness degradation was primarily a function of previous maximum deformations.

Reversing Load Histories

It was expected that performance of walls under reversing loads would vary considerably with respect to the sequence of application of large reversals. To investigate this, companion Specimens B7 and B9 were constructed. Figures 49 and 50 shows load-deformation characteristics for these specimens. Specimen B7, was tested with the incrementally increasing reversing (IR) load history. Specimen B9 was tested with the modified reversing (MR) load history as described in detail in Appendix A.

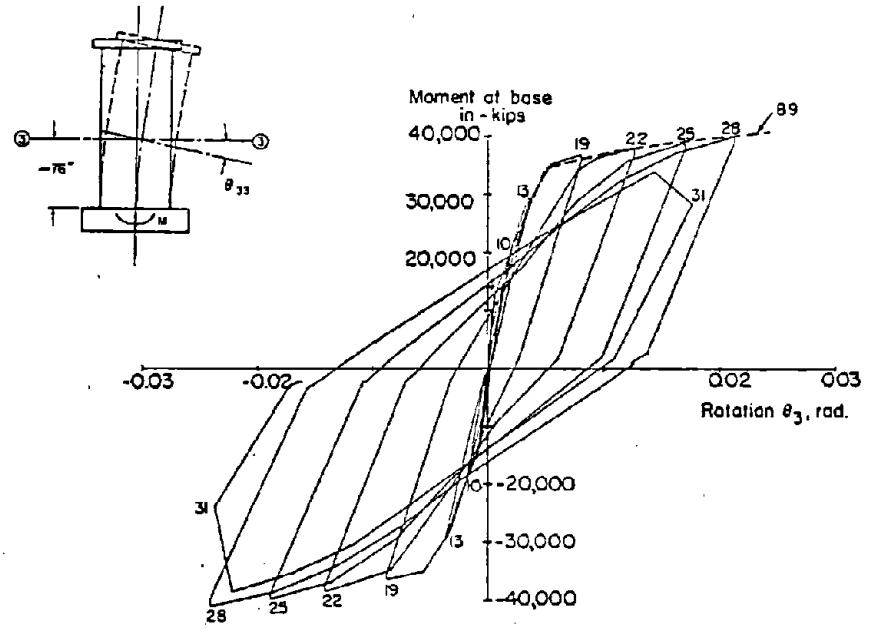

a) Rotations at the 6 ft Level, Specimens B7 and B9

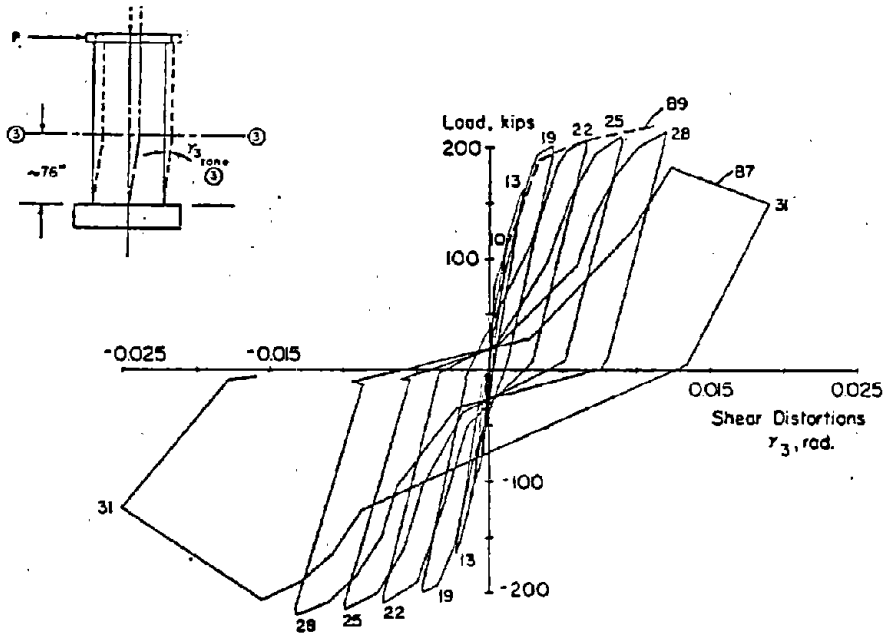

b) Shear Distorions within Lower 6 ft, Specimens B7 and B9

Fig. 47 Comparison of Deformations within Barbell Shaped Walls Subjected to High Shear Stresses for Monotonic versus Reversing Load

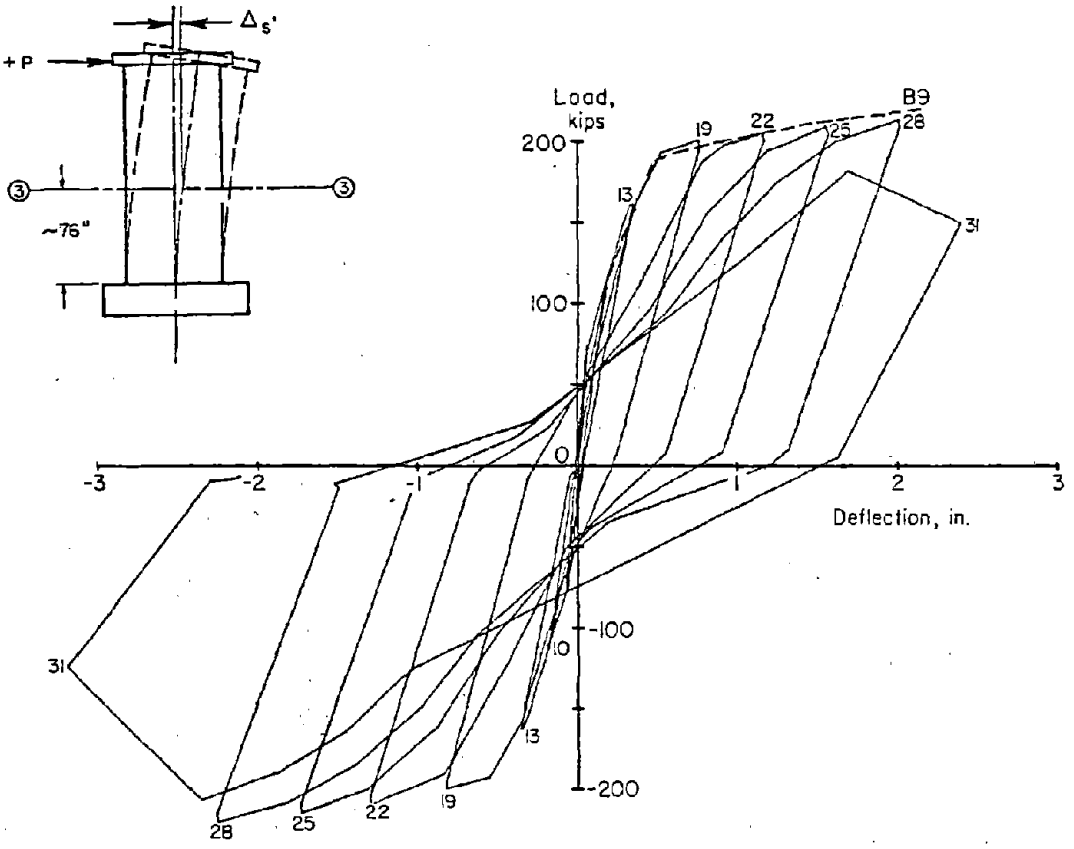

Fig. 48 Comparison of Deflections at the 6 ft Level in Specimens B7 and B9

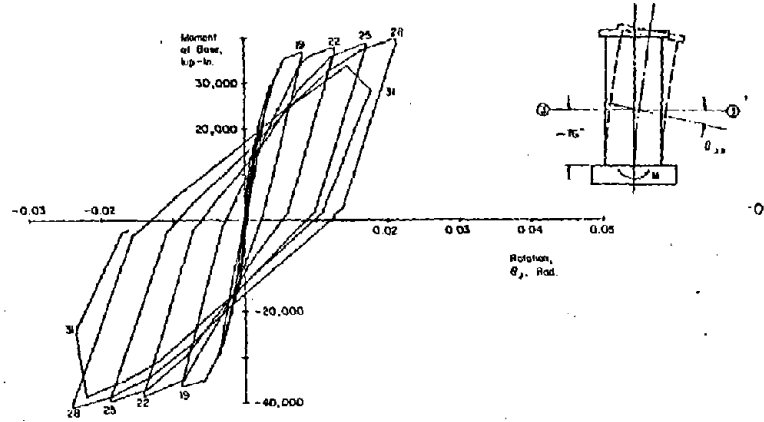

a) Rotation at 6 ft Level, Specimen B7 with IR Load History

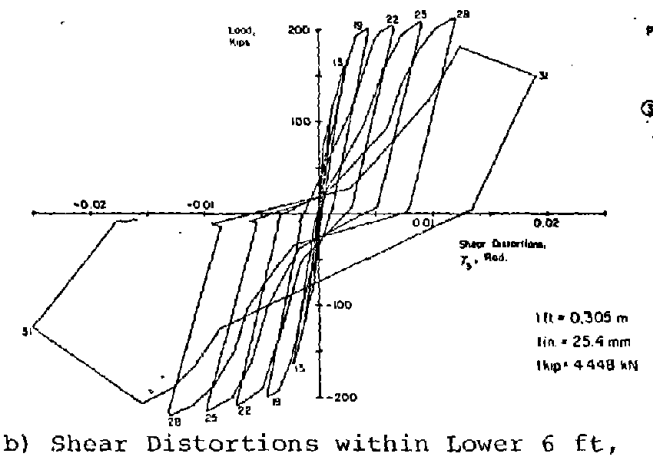

b) Shear Distortions within Lower 6 ft, Specimen B7 with IR Load History

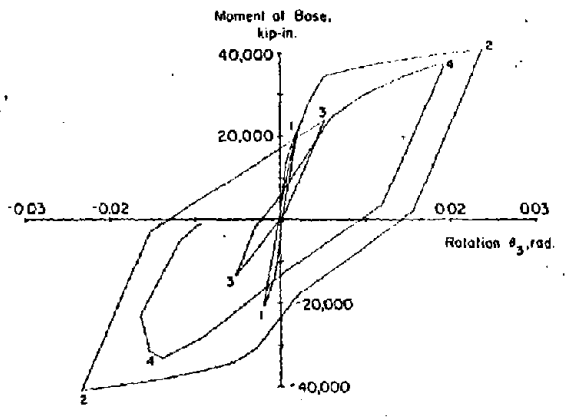

c) Rotation at 6 ft Level, Specimen B9 with MR Load History

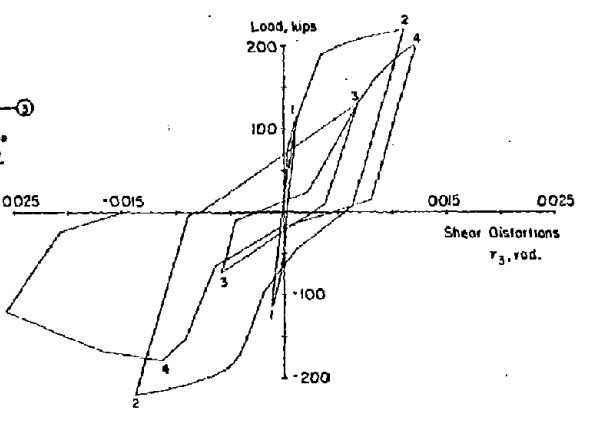

d) Shear Distortions within Lower 6 ft, Specimen B9 with MR Load History

Fib. 49 Comparison of Deformations within Barbell Shaped Walls with Different Load

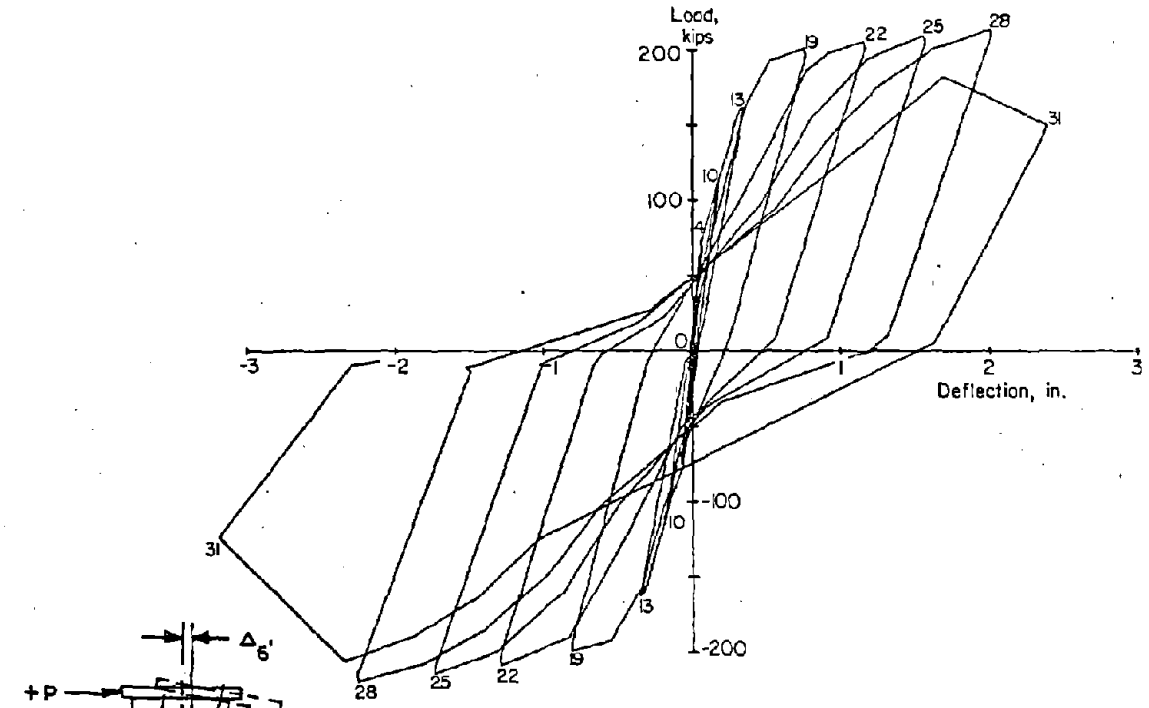

a) Specimen B7

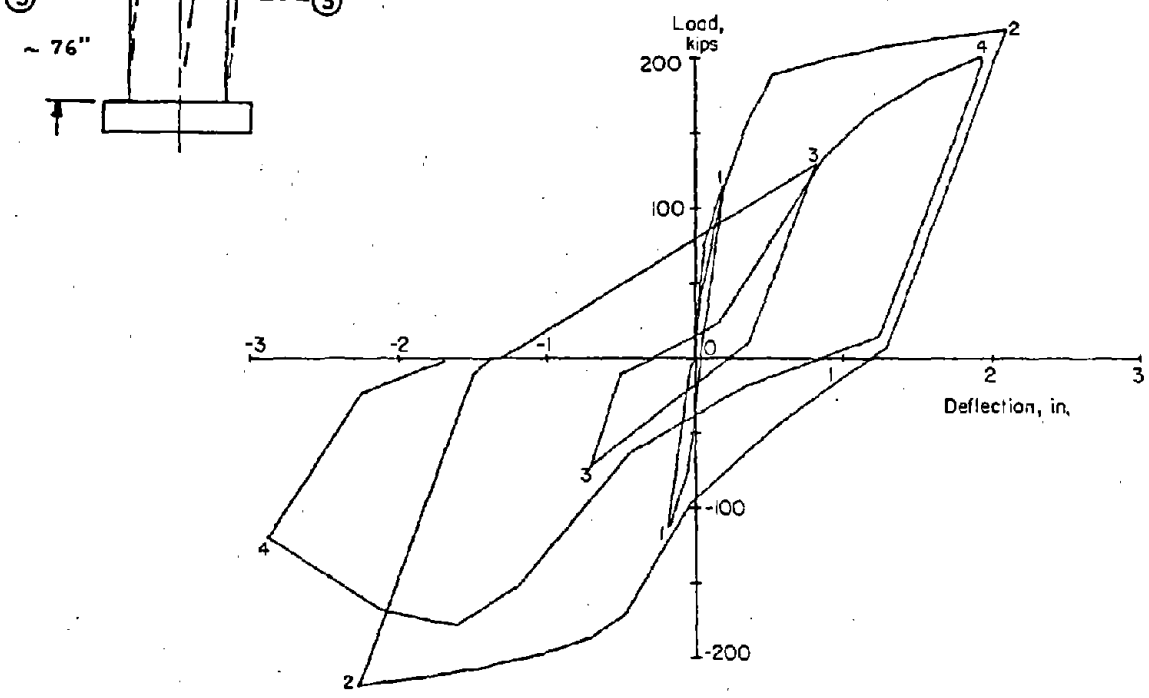

b) Specimen B9

Fig. 50 Comparison of Deflections at the 6 ft Level in Specimens B7 and B9

Using deformation data shown in Table 3, B7 sustained a maximum rotational ductility of 5.2. It was the intent of the test of Specimen B9 to verify that this level of ductility was attainable with a load history representative of what could be induced in an earthquake.

Prior to testing B9, loss of shear stiffness was thought to be strongly depended on the cumulative deformations sustained by the specimen under reversing load. Therefore, it was hypothesized that B9 would sustain the modified load history because the cumulative shear degradation would not be as great as in B7. However, as seen by comparing the shear distortions in Cycle 31 for B7 and Cycle 4 for B9, the loss of shear stiffness from one large reversal at a rotational ductility of 5 was equivalent to that produced by 12 reversals at ductitilties from 2 to 5.

The results showed that a ductility of 5 was not an attainable level for the modified load history. Specimen B9 was loaded to a rotational ductility of 5 in Cycle 2. Web crushing occurred in the second large inelastic cycle. Analysis later showed that maximum shear distortions in both B7 and B9 were very close to limiting values for web crushing.[3] Although Specimen B7 sustained 3 cycles at a ductility of 5, web crushing occurred in the very next cycle. As shown in Fig. 41c, web crushing occurred in Cycle 31 prior to reaching the previous peak rotation. Specimen B9 was loaded too close to this limiting ductility in the first larger cycle.

The results of Specimen B7 and B9 tests do not show that one type of loading is <u>more</u> severe than the other. What the results indicate is that the MR load history was <u>as</u> severe as the IR load history with axial load present. The fact that B7 sustained three cycles and B9 sustained only one cycle at a rotational ductility of 5 may be atrributed to the statistical variation in specimen properties. The concrete strength in B7 and B9 was f'_c = 7155 psi (49.3 MPa) and f'_c = 6395 psi (44.1 MPa) respectively.

Repaired Specimens

Two barbell shaped specimens, B5 and B9, were repaired after the original tests. At the end of the original tests the lower portion of the webs were considerably damaged in each specimen. However the confined boundary elements were in very good condition. To investigate the effect of a simple repair, damaged webs in Specimens B5 and B9 were replaced with new concrete and the walls were tested as Specimens B5R and B9R.

The original 4 in. (102 mm) web was replaced with a new 4 in. (102 mm) web in Specimen B5. The load-deformation characteristics for Specimens B5 and B5R are shown in Figs. 51 and 52.

Although the initial stiffness of Specimen B5R was approximately one-half of that in the original wall, it had a strength and deformation capability similar to Specimen B5.

To investigate the possibility of increasing the repaired specimen stiffness and deformation capabilities, the damaged 4-in. thick web in Specimen B9 was replaced with a 6-in. thick web and tested as Specimen B9R. This reduced nominal shear stress for equivalent loads by 33%.

Figures 53 and 54 shows the load-deformation characteristics for Specimens B9 and B9R.

The additional thickness in the repaired web did not significantly affect initial stiffness. As in B5R, the initial stiffness in Specimen B9R was approximately one-half that of the original wall. However, the strength of B9R was equivalent to that of B9. In addition, deformation capacity for B9R was improved over that for B9. Specimen B9 sustained only 1-1/2 large inelastic cycles with a maximum rotation corresponding to five times yield. Specimen B9R sustained 8-1/2 large inelastic cycles with a maximum rotation corresponding to six times the yield rotation in Specimen B9.

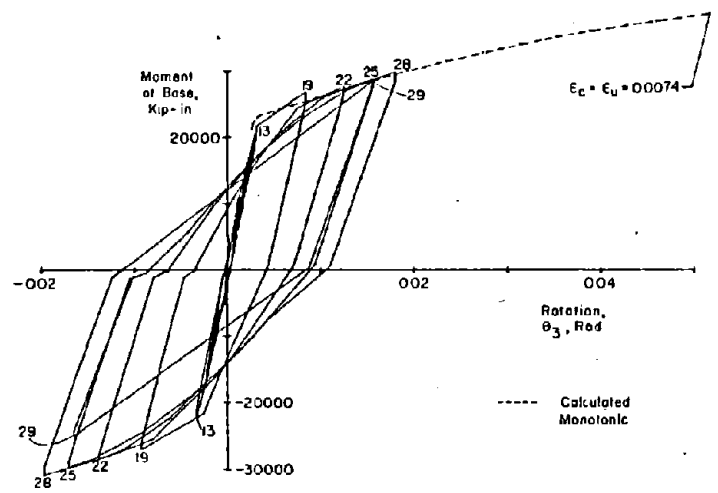

a) Rotations at 6 ft Level, Specimen B5

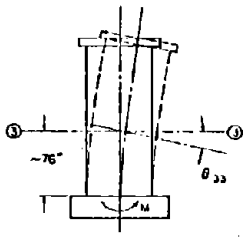

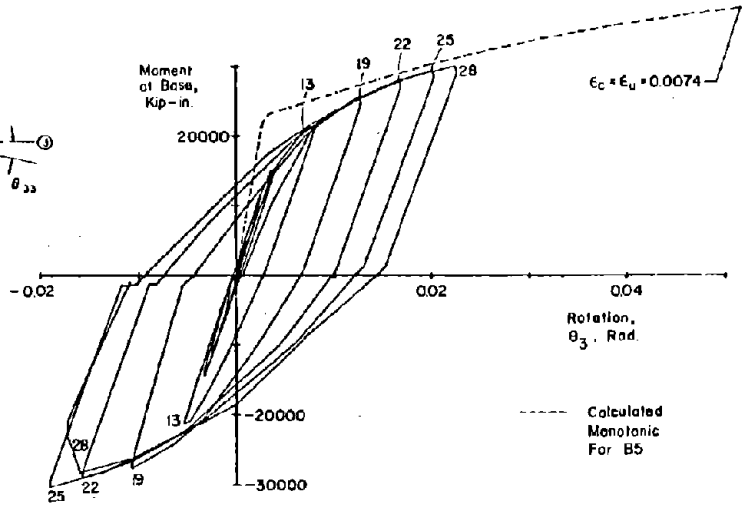

c) Rotations at 6 ft Level, Specimen B5R

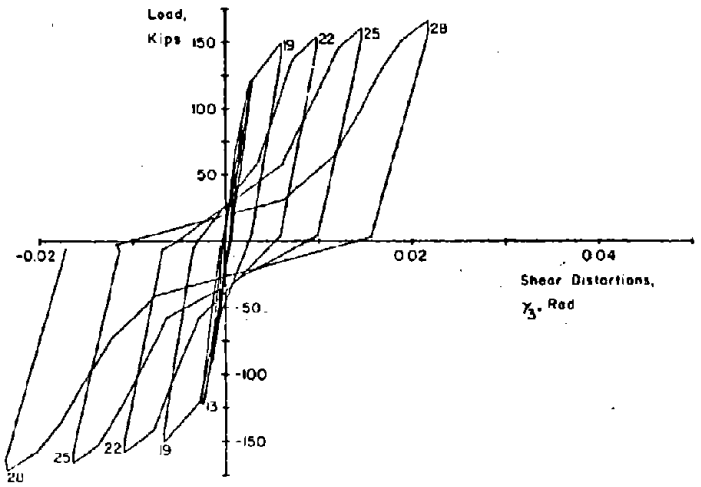

b) Shear Distortions within Lower 6 ft, Specimen B5

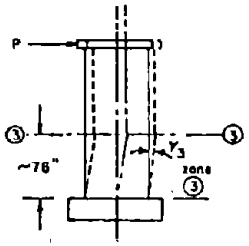

d) Shear Distortions within Lower 6 ft. Specimen B5R

Fig. 51 Comparison of Deformations within the Original Specimen B5 and Repaired Specimen B5R

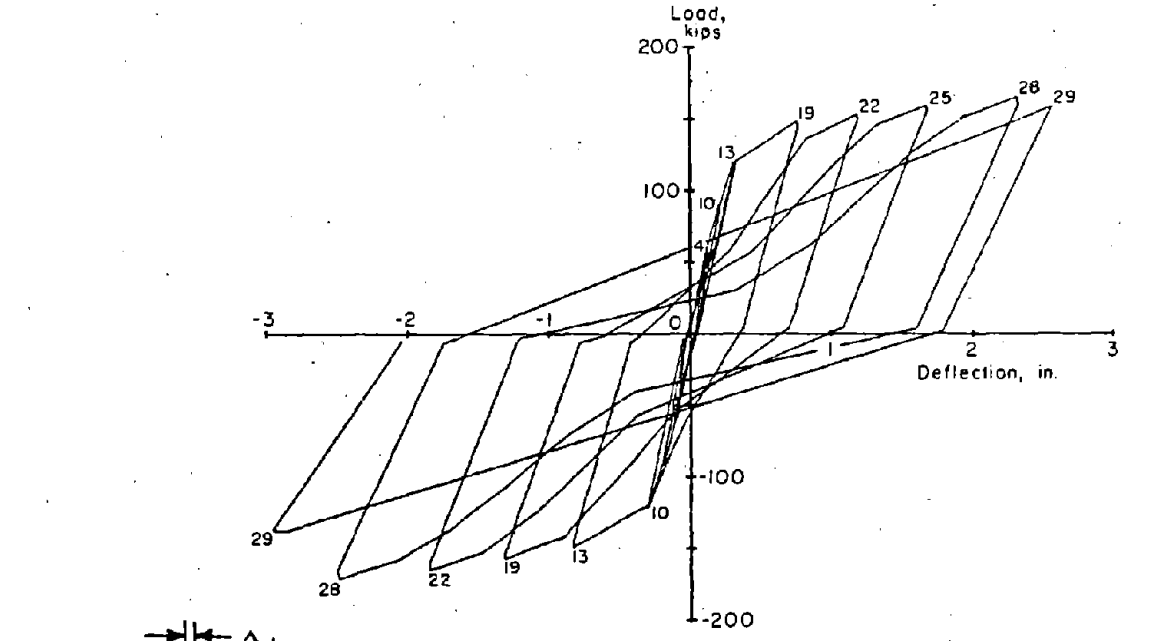

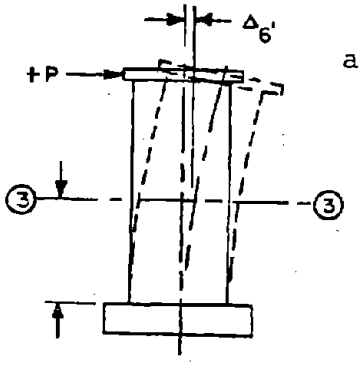

a) Specimen B5

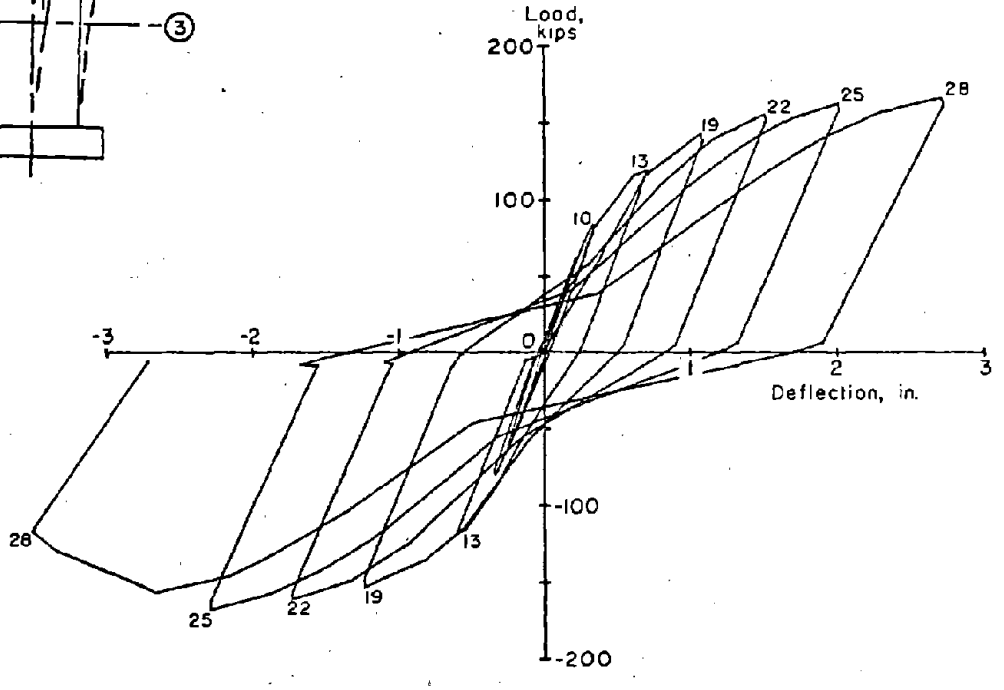

b) Specimen B5R

Fig. 52 Comparison of Deflections at the 6 ft Level in Specimens B5 and B5R

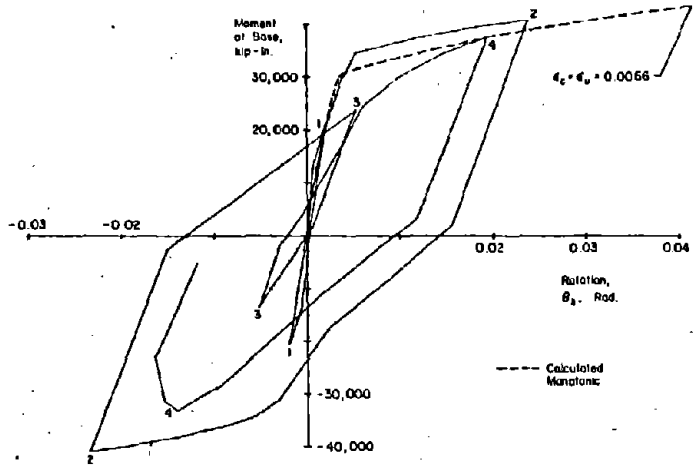

a) Rotation at 6 ft Level, Specimen B9

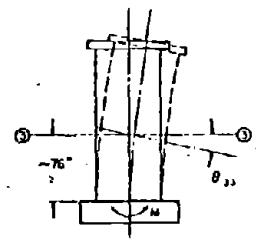

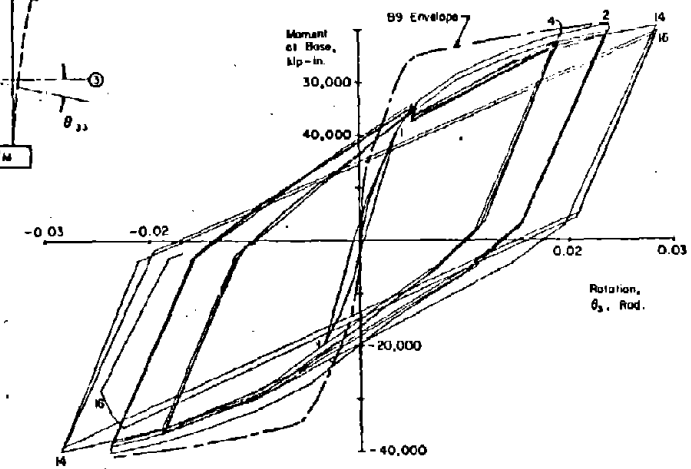

c) Rotation at 6 ft Level, Specimen B9R

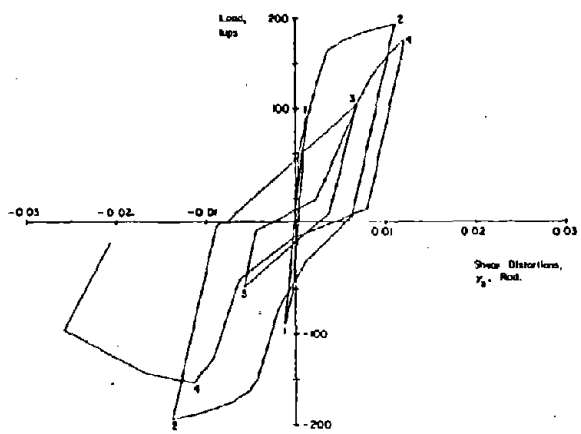

b) Shear Distortions within Lower 6 ft, Specimen B9

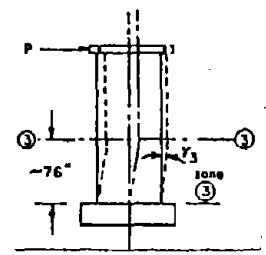

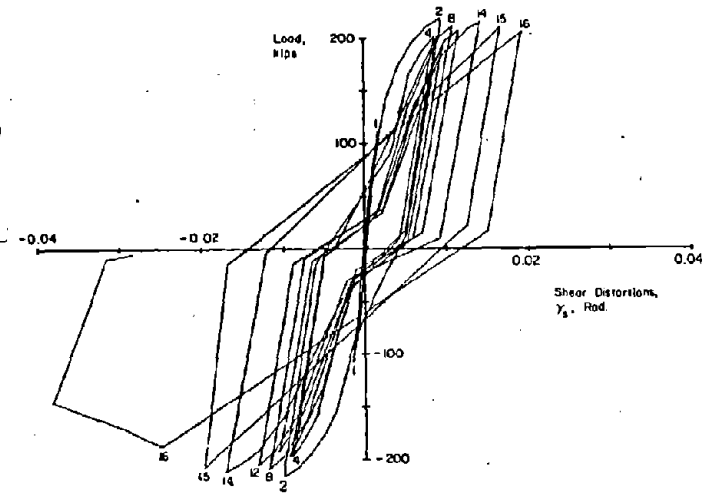

d) Shear Distortions within Lower 6 ft, Specimen B9R

Fig. 53 Comparison of Deformations within the Original Specimen B9 and Repaired Specimen B9R

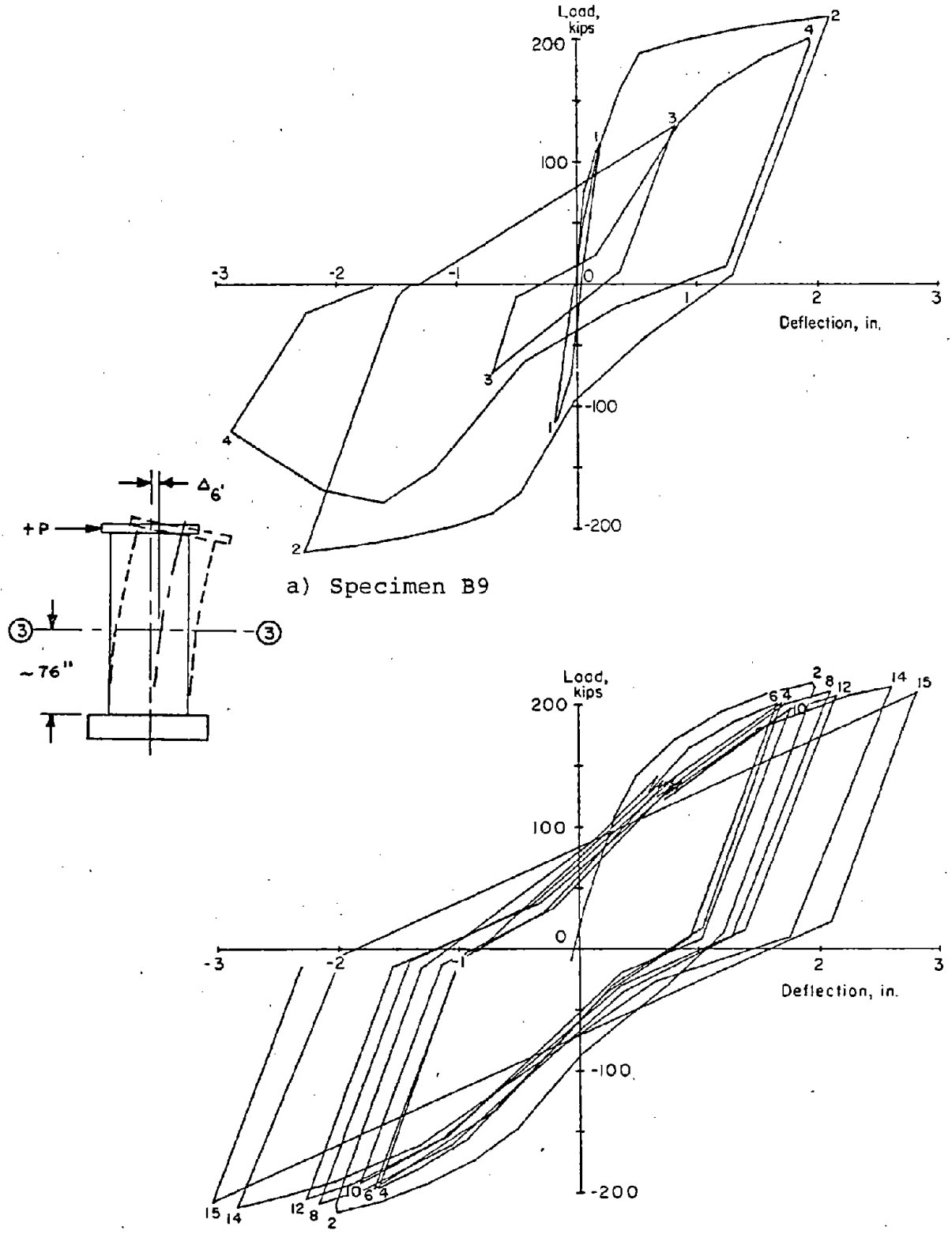

Fig. 54 Comparison of Deflections at the 6 ft Level in Specimens B9 and B9R

CONCLUSIONS

The following conclusions are based on the results of the experimental program:

1. All specimens had a capacity greater than indicated by the 1971 ACI Building Code.[2]
2. Two types of behavior were observed in the walls. Behavior was dependent on the level of shear stress and the resulting crack pattern. For walls subjected to maximum shear stresses less than $3\sqrt{f'_c}$ psi ($0.25\sqrt{f'_c}$ MPa), inelastic performance was limited by flexural bar buckling and loss of core concrete. These walls had capacities ranging from 84% to 91% of the calculated monotonic flexural strength. For walls subjected to maximum shear stresses greater than $7\sqrt{f'_c}$ psi ($0.64\sqrt{f'_c}$ MPa), inelastic performance was limited by web crushing. The walls did sustain a significant number of inelastic cycles. Capacities ranged from 77% to 97% of the calculated monotonic flexural strength.
3. Structural walls behaved in a ductile manner under reversing load within limits dependent on the level of shear stress. Ductility increased with decreasing levels of nominal shear stress.
4. Shear deformations in the hinging region contributed significantly to the total deformation. Loss of shear stiffness with reversals was primarily dependent on the magnitude of inelastic tensile set in the reinforcement from previous loading. Abrasion and loss of material from grinding played a secondary role.
5. Construction joints performed adequately when made following minimum standard practice of roughening and cleaning the surface to remove laitance and loose particles.
6. Web crushing limited ductility under high shear stresses. Web crushing is dependent on both stress and deformation levels.

7. Confinement reinforcement in the boundary elements significantly improved inelastic performance of the walls. Confinement hoops delayed bar buckling and contained the concrete core. The confinement was only necessary in anticipated hinging regions. If first mode effects dominate the response of a structure, significant savings in reinforcement could result from limiting use of confinement to lower floors.
8. Use of horizontal shear reinforcement beyond that required by the 1971 ACI Building Code did not significantly improve strength or ductility where web crushing occurred.
9. Present design criteria for confinement reinforcement are primarily related to requirements to increase strain capacity and to retain the compressive strength of the core. Appropriate design criteria for use in boundary elements of structural walls should be related to delaying inelastic bar buckling and to retaining shear strength.
10. For specimens subjected to high shear stresses, with capacities limited by web crushing, uniform axial compressive load corresponding to approximately 0.1 f'_c increased ductility.
11. Measured strengths and ductilities under reversing loads were lower than those calculated for monotonic load.
12. Structural wall behavior under load reversals was not as dependent on the entire previous load history as it was on the previous maximum level of deformations. One reversal at a rotational ductility of five resulted in a wall equivalent to one which had sustained three complete reversals at ductilities of 1, 2, 3, 4 and 5. Therefore, the concept of cumulative ductility is only valid for comparison of specimens with similar load histories.

13. Walls with confined boundary elements intact after testing were simply repaired by replacing web concrete. While this did not restore the original initial stiffness, inelastic performance of the repaired walls was equivalent to that of the original walls.
14. Test data indicate that the deformation mode usually associated with shear distortions within the hinging region of a wall is coupled to flexural rotations. The effect of this coupling is that large "effective" shear distortions accompany flexural hinging. This deformation mode should be considered in structures designed to utilize the inelastic capacity of structural walls.
15. For one rectangular test wall, out-of-plane instability of the compressive zone limited inelastic performance.

ACKNOWLEDGMENTS

This investigation was carried out in the Structural Development Section of the Portland Cement Association. Fabrication and testing of the specimens were performed by the Technical Staff of this Section under the direction of B. W. Fullhart, Laboratory Foreman. Specimen construction and instrumentation was the responsibility of Senior Technicians, R. K. Richter and W. Hummerich Jr., respectively.

The work formed part of a combined experimental and analytical investigation sponsored by the National Science Foundation through Grant Nos. ENV74-14766 and ENV77-15333 and by the Portland Cement Association.

Advice and suggestions by M. Fintel, Director, Advanced Engineering Services, are appreciated.

Any opinions, findings, and conclusions expressed in this publication are those of the authors and do not necessarily reflect the views of the National Science Foundation.

REFERENCES

1. Oesterle, R.G., Fiorato, A.E., Johal, L.S., Carpenter, J.E., Russell, H.G., and Corley, W.G., "Earthquake Resistant Structural Walls - Tests of Isolated Walls," Report to National Science Foundation, Portland Cement Association, Skokie, Nov. 1976, 315 pp. (Available through National Technical Information Service, U.S. Department of Commerce, 5285 Port Royal Rd., Springfield, Va., 22161, NTIS Accession No. PB271467.)

2. ACI Committee 318, Building Code Requirements For Reinforced Concrete, ACI Standard 318-71, American Concrete Institute, Detroit, 1971 78 pp.

3. Aristizabal-Ochoa, J.D., and Oesterle, R.G., "Earthquake Resistant Structural Walls - Web Crushing Analysis" Report to National Science Foundation, Portland Cement Association, Skokie, (to be published).

4. Oesterle, R.G., Fiorato, A.E., Aristizabal-Ochoa, J.D. and Corley, W.G., "Hysteretic Response of Reinforced Concrete Structural Walls," submitted for publication in the ACI Symposium Vol. on Mathematical Modeling of Reinforced Concrete Structures, Toronto, 1978.

5. Paulay, T. and Uzumeri, M., "A Critical Review of the Seismic Design Provisions for Ductile Shear Walls of the Canadian Code and Commentary," Canadian Journal of Civil Engineering, Vol. 2, No. 4, 1975, pp. 592-601.

6. Brown, R.H. and Jirsa, J.O., "Shear Transfer of Reinforced Concrete Beams Under Reversed Loading," Shear in Reinforced Concrete, Vol. 1, Publication SP-42, American Concrete Institute, Detroit, 1974, pp. 347-357.

7. Paulay, T. and Binney, J.R., "Diagonally Reinforced Coupling Beams of Shear Walls," Shear in Reinforced Concrete, Vol. 2, Publication SP-42, American Concrete Institute, Detroit, 1974, pp. 579-598.

8. Bertero, V.V.,; Popov, E.P. and Wang T.Y., "Hysteretic Behavior of Reinforced Concrete Flexural Members with Special Web Reinforcement," EERC Report No. 74-9, University of California, Berkeley, August 1974, 126 pp.

9. Wight, J.K., and Sozen, M.A., Shear Strength Decay in Reinforced Concrete Columns Subjected to Large Deflection Reversals, Civil Engineering Studies, Structural Research Series No. 403, University of Illinois, Urbana, August 1973.

10. Shui, K.N., Barney, G.B., Fiorato, A.E., and Corley, W.G., "Reversing Load Tests of Reinforced Concrete Coupling Beams," Proceedings Central American Conference on Earthquake Engineering, El Salvador, January 1978. (to be published).

11. Paulay, T., "Design Aspects of Shear Walls For Seismic Areas," Research Report 74-11, Dept. of Civil Engineering, University of Canterbury, Christ Church, New Zealand, Oct. 1974.

12. Bertero, V.V., and Popov, E.P., "Hysteretic Behavior Of Reinforced Concrete Flexural Members With Special Web Reinforcement," U.S. National Conference On Earthquake Engineering, Ann Arbor, Mich., June 1975 pp. 316-326.

13. International Conference of Building Officials, Uniform Building Code, 1976 Edition, Whittier, California, 1976, pp. 2626.

14. Cardenas, A.E. and Magura, D.D., "Strength of High-Rise Shear Walls--Rectangular Cross Section," ACI Special Publication SP-36, American Concrete Institute, Detroit, Mich., 1973, pp. 119-150. Also, PCA Research & Development Bulletin RO 029.01D.

15. ACI Committee 301, Specifications for Structural Concrete for Buildings, ACI Standard 301-72, American Concrete Institute, Detroit, 1972, 36 pp.

16. Bertero, V.V., "Experimental Studies Concerning Concrete Structures," Proceedings of Symposium on Resistance and Ultimate Deformability of Structures Acted On By Well Defined Repeated Loads, International Association For Bridge And Structural Engineering, LISBA, 1973.

17. Derecho, A.T., Iqbal, M., Ghosh, S.K., Fintel, M., and Corley, W.G., "Structural Walls In Earthquake-Resistant Buildings, Dynamic Analysis of Isolated Structural Walls, - Representative Loading History," Report to National Science Foundation, Portland Cement Association, Skokie, August 1978.

18. Kent, D.C. and Park, R., "Flexural Members with Confined Concrete," Proc. of ASCE, Journal of Structural Division, ST&, July 1971, pp. 1969-1990.

19. Corley, W.G., "Rotational Capacity of Reinforced Concrete Beams," Journal of the Structural Division, ASCE, Vol. 92, ST5, October 1966, pp. 121-146.

20. Bachmann, H., "Influence of Shear and Bond on Rotational Capacity of Reinforced Concrete Beams," Publications, International Association for Bridge and Structural Engineering, Vol. 30, Part II, Zurich, 1970, pp. 11-28.

21. Park, R. and Paulay, T., "Reinforced Concrete Structures," John Wiley and Sons, Inc. New York, 1975, pp. 307-309.

NOTATIONS

A_{sh} = Area of transverse hoop bar (one leg)

E_c = Modulus of elasticity of concrete

f'_c = Compressive strength of standard 6x12-in. (152x305 mm) concrete cylinders

f_r = Modulus of rupture of concrete

f_y = Yield strength of reinforcement

f_{su} = Tensile strength of reinforcement

h = Wall thickness

ℓ_h = Maximum unsupported length of rectangular hoop

ℓ_w = Horizontal length of wall

s_h = Center-to-center spacing of hoops

V = Shear force

v = Nominal shear stress = $\frac{V}{0.8\ell_w h}$

v_{max} = Maximum nominal shear stress

Δ_{CJ1} = Slip at the base construction joint

$\Delta\gamma 1$ = Shear deflection at the 3-ft level

γ_1 = Average shear distortion in Zone 1, from 0 to 3-ft (0.91 m) level

γ_2 = Average shear distortion in Zone 2, from 3-ft to 6-ft (0.91 m to 1.83 m) level

γ_3 = Average shear distortion in Zone 3, from 0 to 6-ft (1.83 m) level

ε_c = Strain in concrete at the outer compression faces at the base of the wall

ε_u = Ultimate compressive strain for concrete

θ_1 = Rotational of the horizontal section approximately 3 in. (76.2 mm) above the base block

θ_2 = Rotation of the horizontal section approximately 38 in. (0.97 m) above the base block

θ_3 = Rotation of the horizontal section approximately 74 in. (1.88 m) above the base block

ρ_f = Ratio of main flexural reinforcement area to the gross concrete area of the boundary element. For rectangular sections, the boundary element was taken to extend 0.1 ℓ_w from each end of the wall

ρ_h = Ratio of horizontal shear reinforcement area to the gross concrete area of a vertical section of the wall web

ρ_n = Ratio of vertical reinforcement area to the gross concrete area of a horizontal section of the wall web

ρ_s = Ratio of effective volume of confinement reinforcement to total volume of core $= \frac{2A_{sh}}{\ell_h s_h}$

APPENDIX A - EXPERIMENTAL PROGRAM

TABLE OF CONTENTS

APPENDIX A - EXPERIMENTAL PROGRAM

Tests were carried out in two phases. Phase I included nine tests. Axial load was not applied. A detailed description of these specimens and their behavior is contained in a previous report.[1]

Phase II included seven tests. Axial load was applied during testing of these specimens.

Table A-1 is a summary of Phase I and Phase II test specimens. Phase II specimens are those with axial load listed. Figure A-1 defines the types of reinforcement used in the specimens.

This appendix presents a detailed description of program variables, test specimens, test apparatus, and test procedure for Phase II tests.

Test Specimens

Description

The isolated walls represent an element of a structural wall system. Test specimens are approximately 1/3-scale representations of full scale walls, although no specific prototype walls were modeled.

Overall dimensions of the test specimens are shown in Figs. A-2 and A-3. Height of the wall, from the top of the base block to the center of the top slab, is 15 ft (4.57 m). The horizontal length of the wall is 6 ft 3 in. (1.91 m) and its web thickness is 4 in. (102 mm).

Three different wall cross-sections have been tested. These are flanged, barbell and rectangular sections. The nominal cross-sectional dimensions of the three sections are shown in Fig. A-3.

The 2x4x10-ft base block shown in Fig. A-2 was used to secure the specimens to the laboratory floor during testing. The slab on top of the wall, also shown in Fig. A-2, was used to transfer loads to the test specimen. Both the base block and

TABLE A1 - PROPERTIES OF TEST SPECIMENS

Specimen	Shape	Axial Load psi	f'_c psi	f_y for ρ_E (ksi)	Reinforcement (%)			
					ρ_f	ρ_h	ρ_n	ρ_s
R1		--	6490	74.2	1.47	0.31	0.25	--
R2		--	6735	65.3	4.00	0.31	0.25	2.07
B1		--	7685	65.2	1.11	0.31	0.29	--
B3		--	6860	63.5	1.11	0.31	0.29	1.28
B4(1)		--	6530	65.3	1.11	0.31	0.29	1.28
B2		--	7775	59.5	3.67	0.63	0.29	--
B5		--	6570	64.4	3.67	0.63	0.29	1.35
B5R(2)		--	6205	--	3.67	0.63	0.29	1.35
B6		425	3165	63.9	3.67	0.63	0.29	0.81
B7		545	7155	66.4	3.67	0.63	0.29	1.35
B8		545	6085	64.9	3.67	1.38	0.29	1.35
B9(3)		545	6395	62.3	3.67	0.63	0.29	1.35
B9R(2,3)		450	7510	62.3	3.67	0.42	0.20	1.35
B10(3)		545	6615	64.9	1.97	0.63	0.29	1.35
F1		--	5575	64.5	3.89	0.71	0.30	--
F2		480	6610	62.4	4.35	0.63	0.31	1.43

(1) Monotonic loading
(2) Repaired specimen
(3) Modified reversing load history (MR Loading)
(4) 1000 psi = 1.0 ksi = 6.895 MPa

ρ_f = ratio of main flexural reinforcement area to gross concrete area of boundary element

ρ_h = ratio of horizontal shear reinforcement area to gross concrete area of a vertical section of wall web

ρ_n = ratio of vertical web reinforcement area to gross concrete area of a horizontal section of wall web

ρ_s = ratio of effective volume of confinement reinforcement to the volume of core in accordance with Eq. A.4 of ACI 318-71.

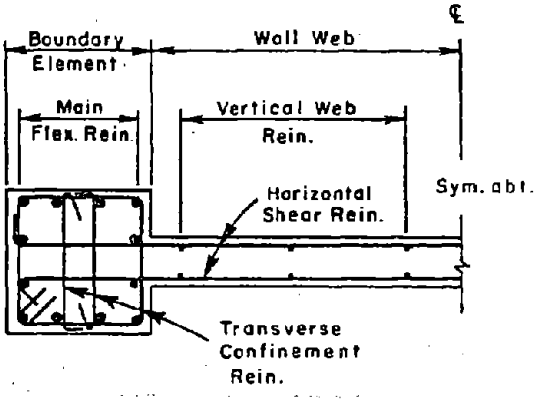

Fig. A-1 Wall Section

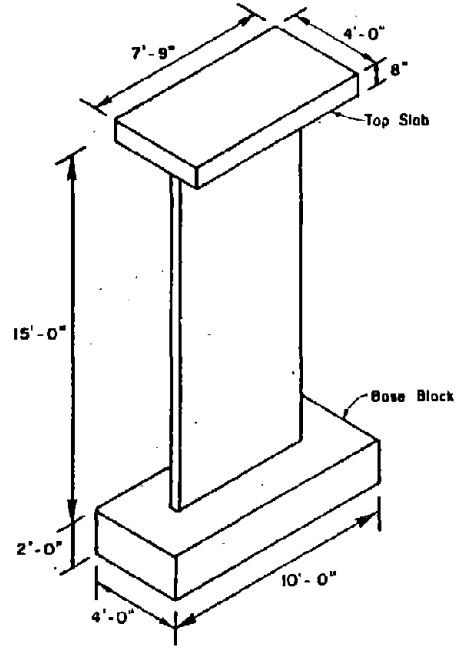

Fig. A-2 Nominal Dimensions of Test Specimens

(1 in. = 25.4 mm)

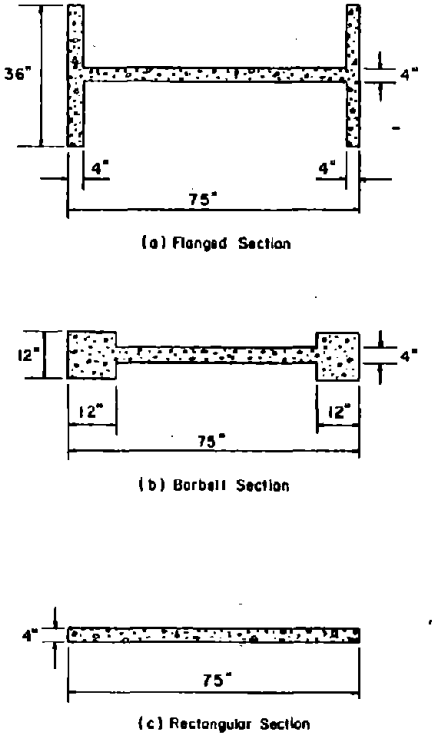

Fig. A-3 Nominal Cross-Sectional Dimensions of Test Specimens

(1 in. = 25.4mm)

the top slab were designed to ensure that no premature termination of the test would occur because of the failure of the loading or supporting elements.

Design

Design criteria used for proportioning reinforcements in Phase I specimens is discussed in the previous report.[1] In general, Phase II specimens were proportioned following the same criteria except as discussed below.

The design moment for each wall was calculated following the 1971 ACI Building Code.[2] Design yield stress of the flexural reinforcement was 60 ksi (414 MPa). In proportioning the steel, strain hardening was neglected. Design concrete strength was 3000 psi (20.7 MPa) for Specimen B6 and 6000 psi (41.4 MPa) for all other specimens.

Several criteria were used to select horizontal shear reinforcement. Minimum requirements of the 1971 ACI Building Code[2] governed for the first five specimens in Table A-1. For B2, B5 and F1 horizontal reinforcement was designed using a shear force corresponding to the calculated design moment. Shear reinforcement was provided in accordance with the 1971 ACI Building Code.[2] Specimens B6, B7, B9, B10 and F2 were provided with the same amount of shear reinforcement as B2 and B5.

To determine the influence of shear reinforcement, a different design procedure was used for Specimen B8. A shear force corresponding to the calculated maximum moment capacity of the wall including strain hardening of the vertical reinforcement was used. The horizontal shear reinforcement was selected to carry this entire shear force at a design yield stress of 60 ksi (414 MPa).

Transverse reinforcement around vertical reinforcement in the boundary elements was designed either as ordinary column ties (unconfined) or as special confinement reinforcement (confined). For rectangular sections, the "boundary element" was taken to extend 7.5 in. (190 mm) from each end of the wall.

Specimens R1, B1, B2, and F1 had ordinary ties as required by Section 7.12 of the 1971 ACI Building Code.[2]

All other specimens had rectangular hoop and supplementary cross-tie reinforcement in accordance with Appendix A of the 1971 ACI Building Code.[2] This design resulted in a hoop spacing of 1.33 in. (34 mm).

Confinement was used only over the first 6 ft (1.83 m) above the base of the wall. Ordinary column ties were used over the remaining height. Specimen F2 and a special "boundary element" within the intersection of the web and the flange at each end of the wall. The confined zone extended into the web 12 in. (305 mm) from the end of the wall and into the flange 6 in. (152 mm) on either side of the centerline of the web.

Reinforcement details for Phase II specimens are shown in Fig. A-4 through Fig. A-15.

Material Properties

Concrete. A concrete mix using a maximum aggregate size of 3/8 in. (9.5 mm) was selected for the walls. Type I cement, sand, and coarse aggregate were combined to provide concrete with a slump of 3 $\pm$ 1/2 in. (76 $\pm$ 13 mm). Aggregate gradation curves for the sand and coarse aggregate are given in Fig. A-16.

The 2x4x10-ft base block shown in Fig. A-2 was used to secure the specimens to the laboratory floor during testing. The slab on top of the wall, also shown in Fig. A-2, was used to transfer loads to the test specimen. Both the base block and the top slab were designed to ensure that no premature termination of the test wold occur because of failure of the loading or supporting elements.

Physical properties of the concrete used in Phase II specimens are given in Table A-2. Compressive strength and modulus of elasticity of the concrete were determined from compressive tests on 6x12-in. (152x305 mm) cylinders. The modulus of rupture was determined from tests on 6x6x30-in. (152x152x762 mm) beams. A representative stress-strain relationship for the concrete is shown in Fig. A-17.

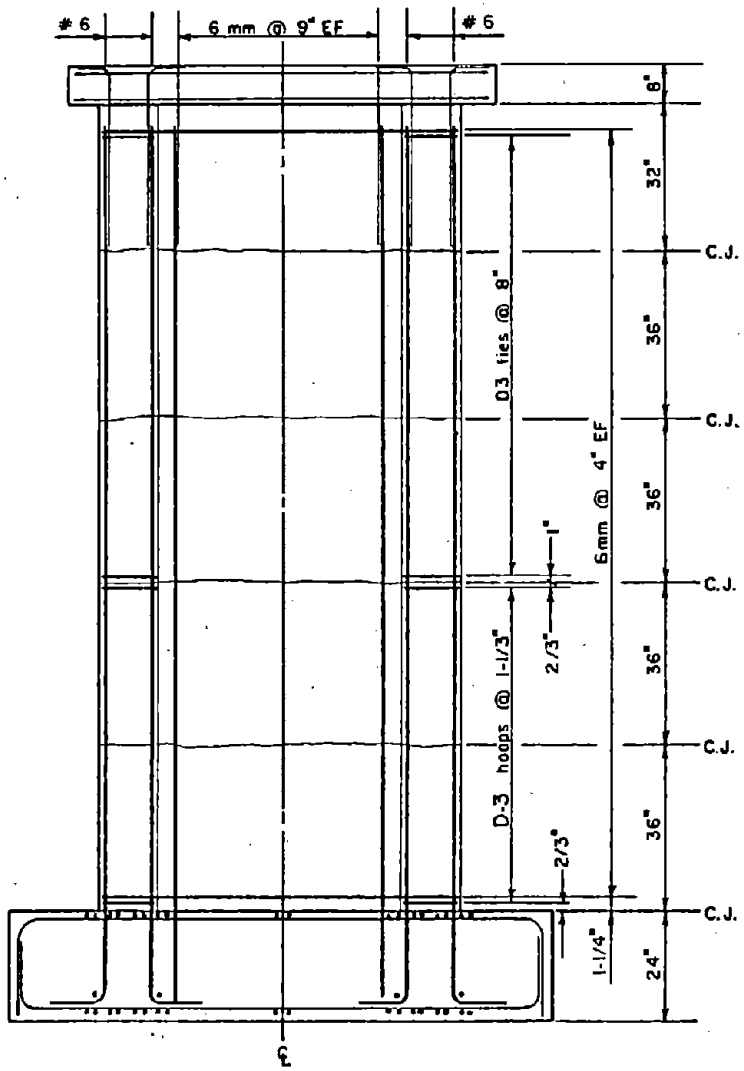

a) Elevation

1 in. = 25.4 mm

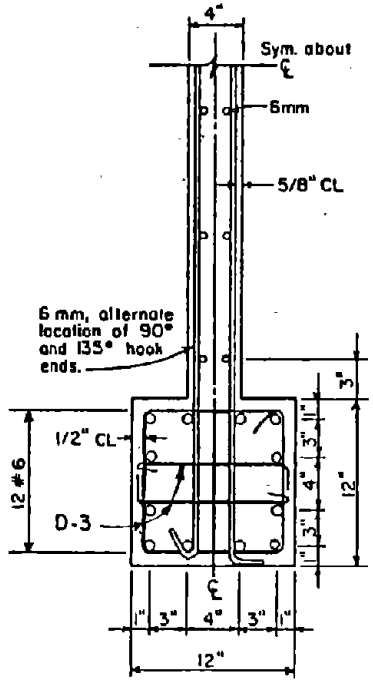

b) CROSS SECTION AT LEVEL OF 6 mm HORIZONTAL BARS

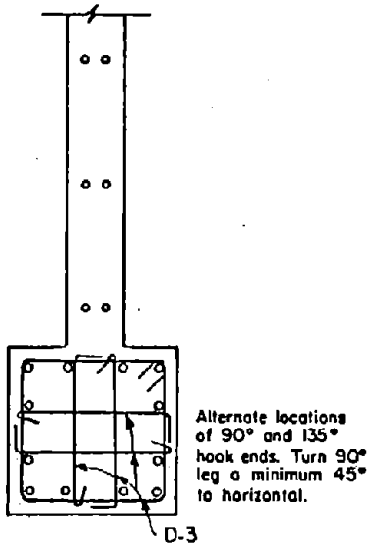

c) CROSS SECTION AT LEVEL BETWEEN 6 mm HORIZONTAL BARS.

Fig. A-4 Reinforcement for Specimen B6

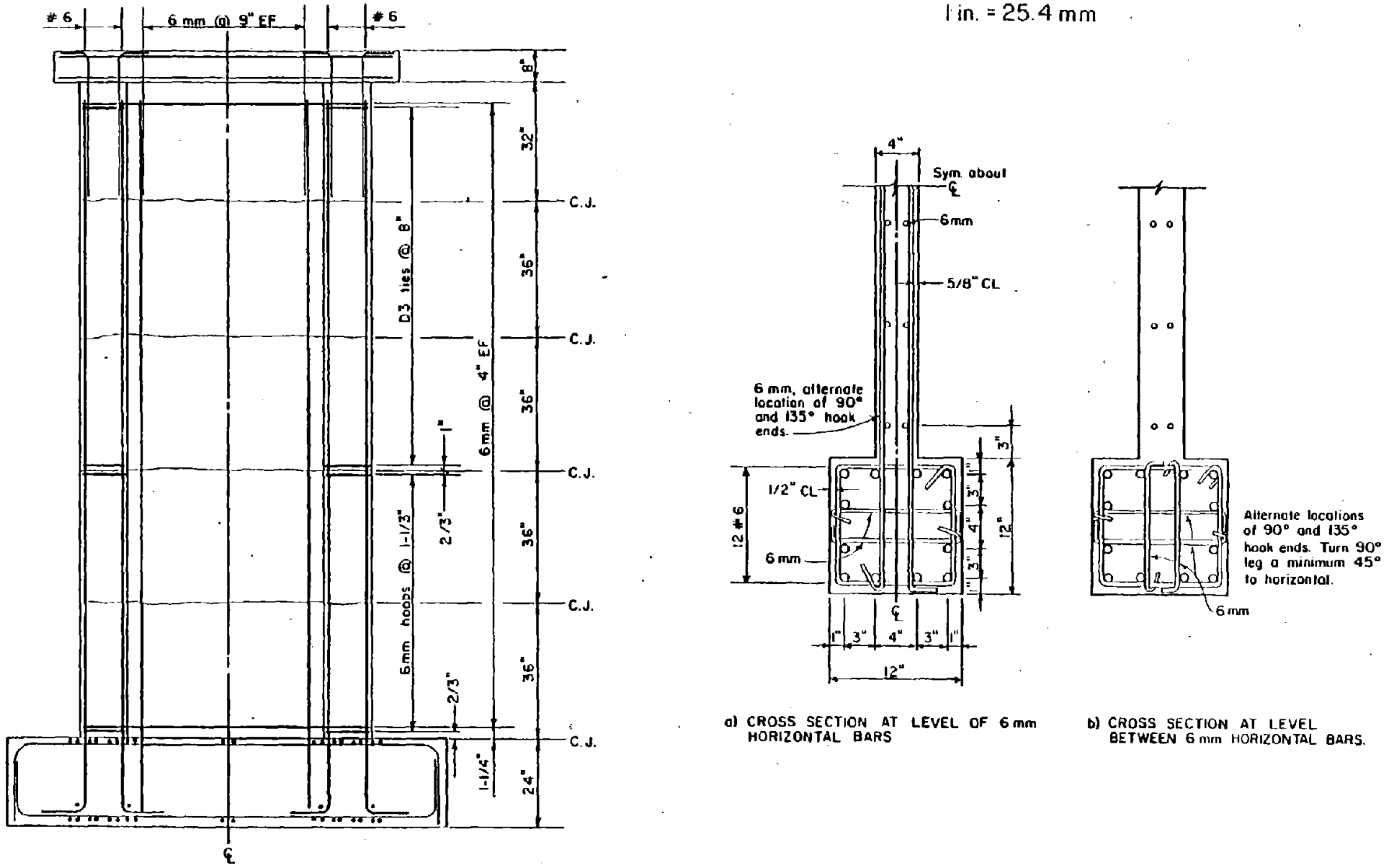

a) Elevation

Fig. A-5 Reinforcement for Specimens B7 and B9

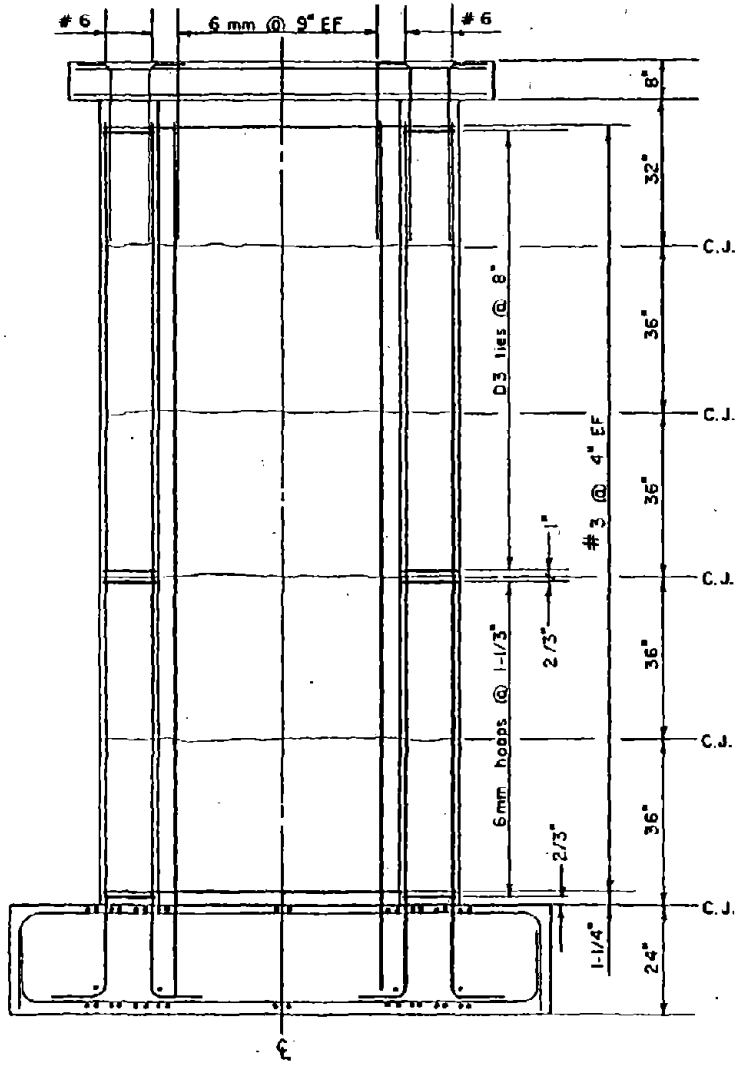

a) Elevation

1 in. = 25.4 mm

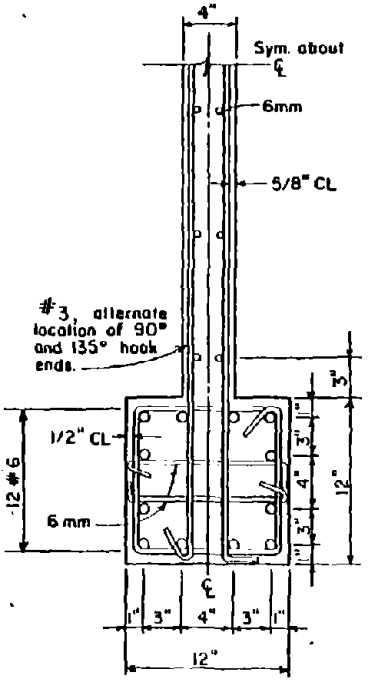

a) CROSS SECTION AT LEVEL OF #3 HORIZONTAL BARS

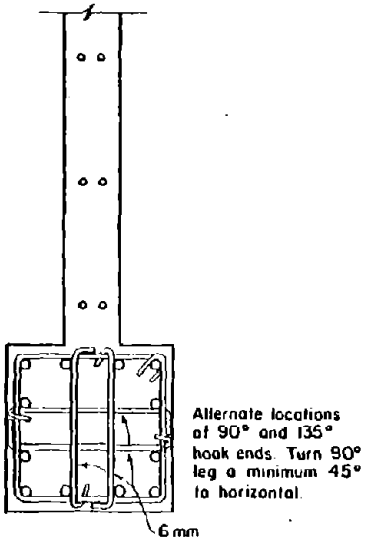

b) CROSS SECTION AT LEVEL BETWEEN #3 HORIZONTAL BARS.

Fig. A-6 Reinforcement for Specimens B8

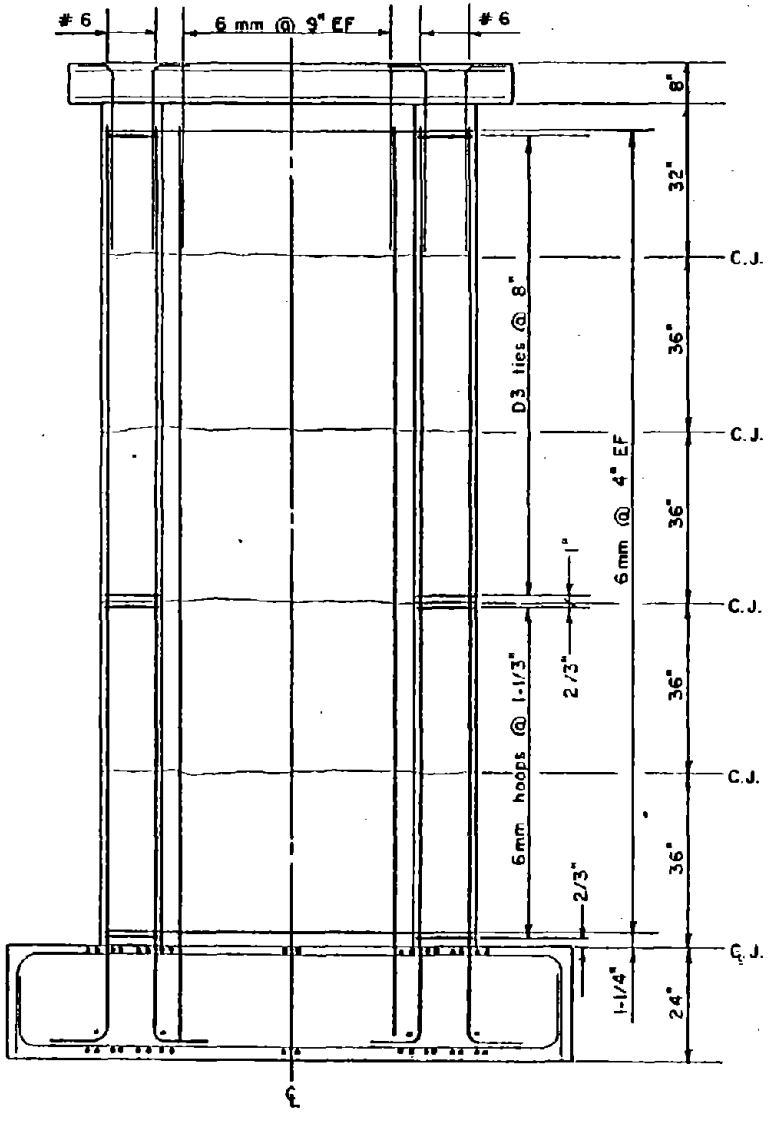

a) Elevation

1 in. = 25.4 mm

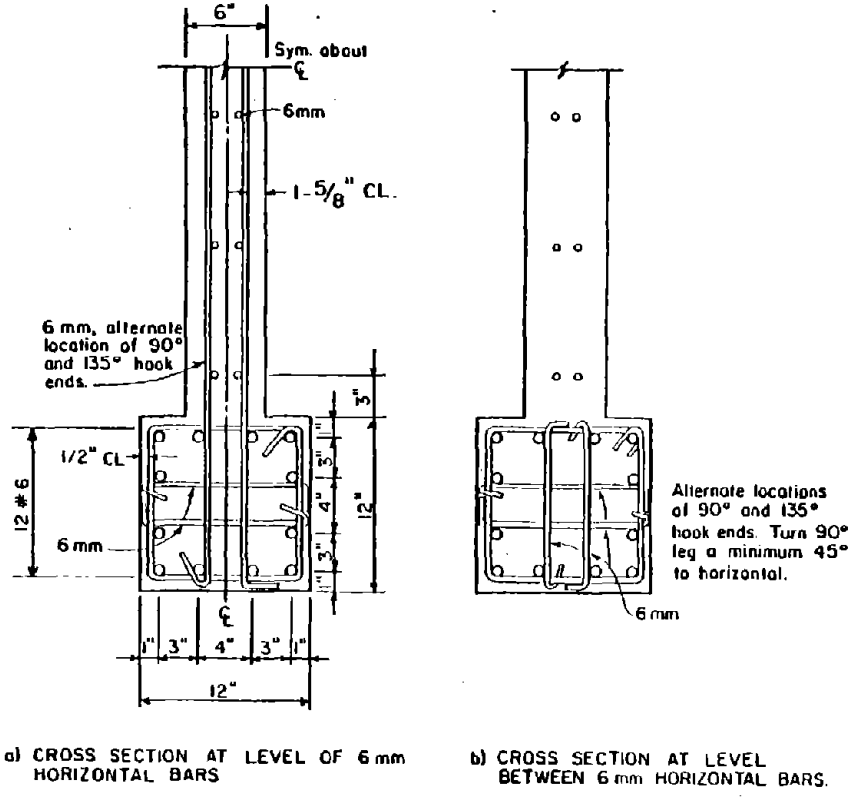

a) CROSS SECTION AT LEVEL OF 6 mm HORIZONTAL BARS

b) CROSS SECTION AT LEVEL BETWEEN 6 mm HORIZONTAL BARS.

Fig. A-7 Reinforcement for Specimen B9R

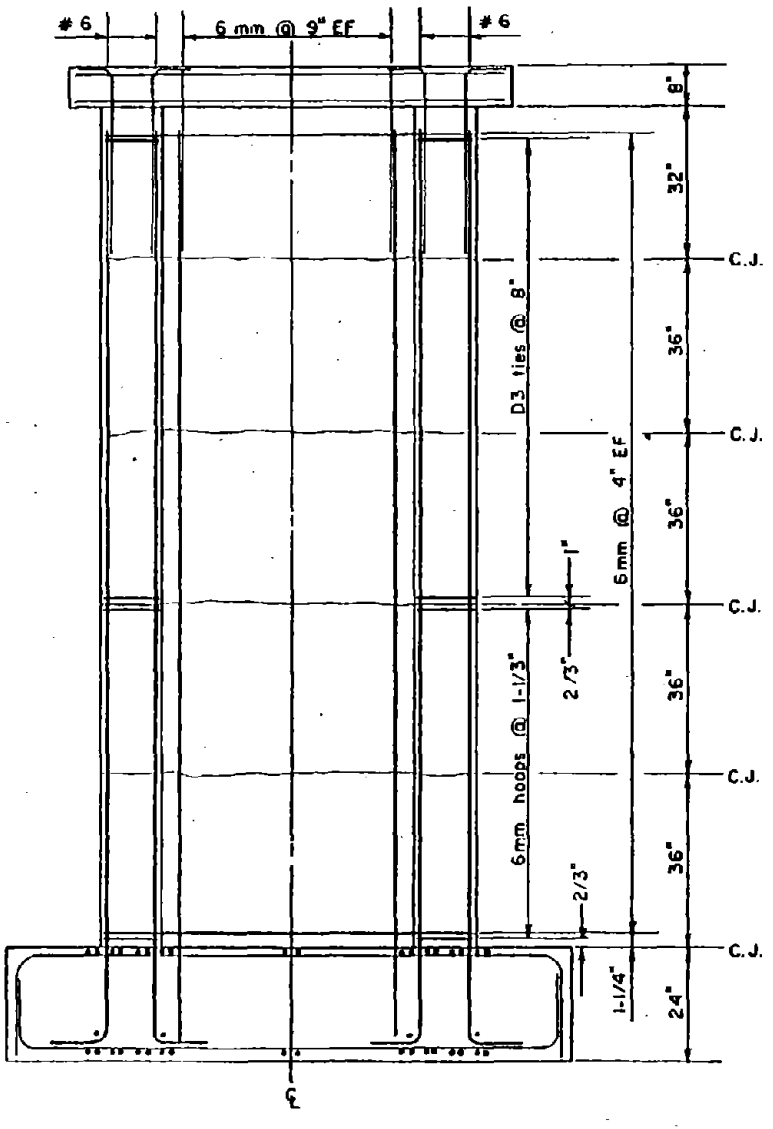

a) Elevation

1 in. = 25.4 mm

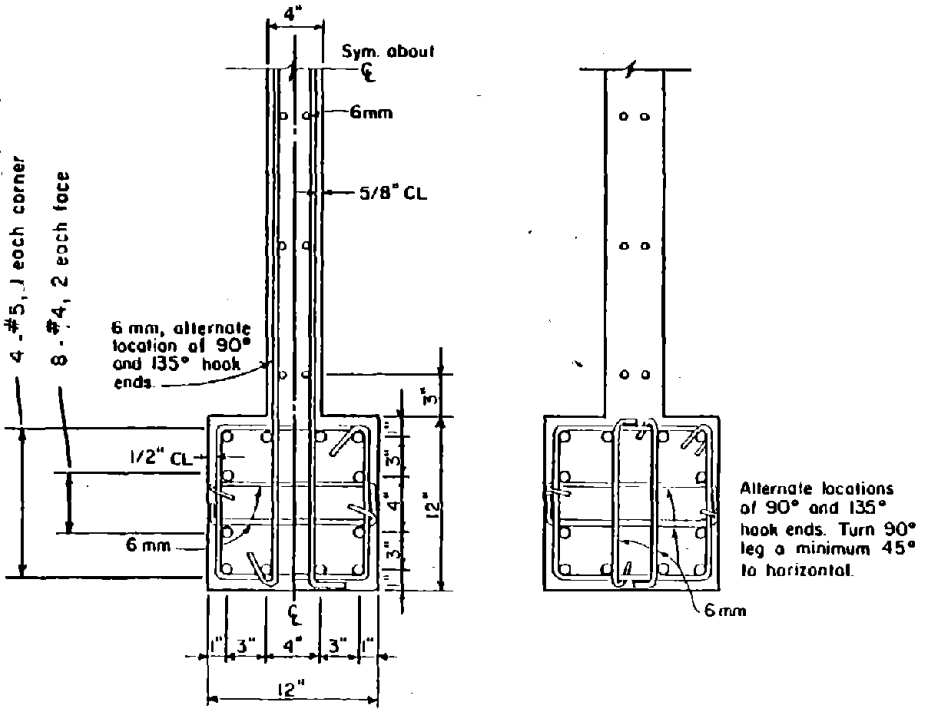

a) CROSS SECTION AT LEVEL OF 6 mm HORIZONTAL BARS

b) CROSS SECTION AT LEVEL BETWEEN 6 mm HORIZONTAL BARS.

Fig. A-8 Reinforcement for Specimen B10

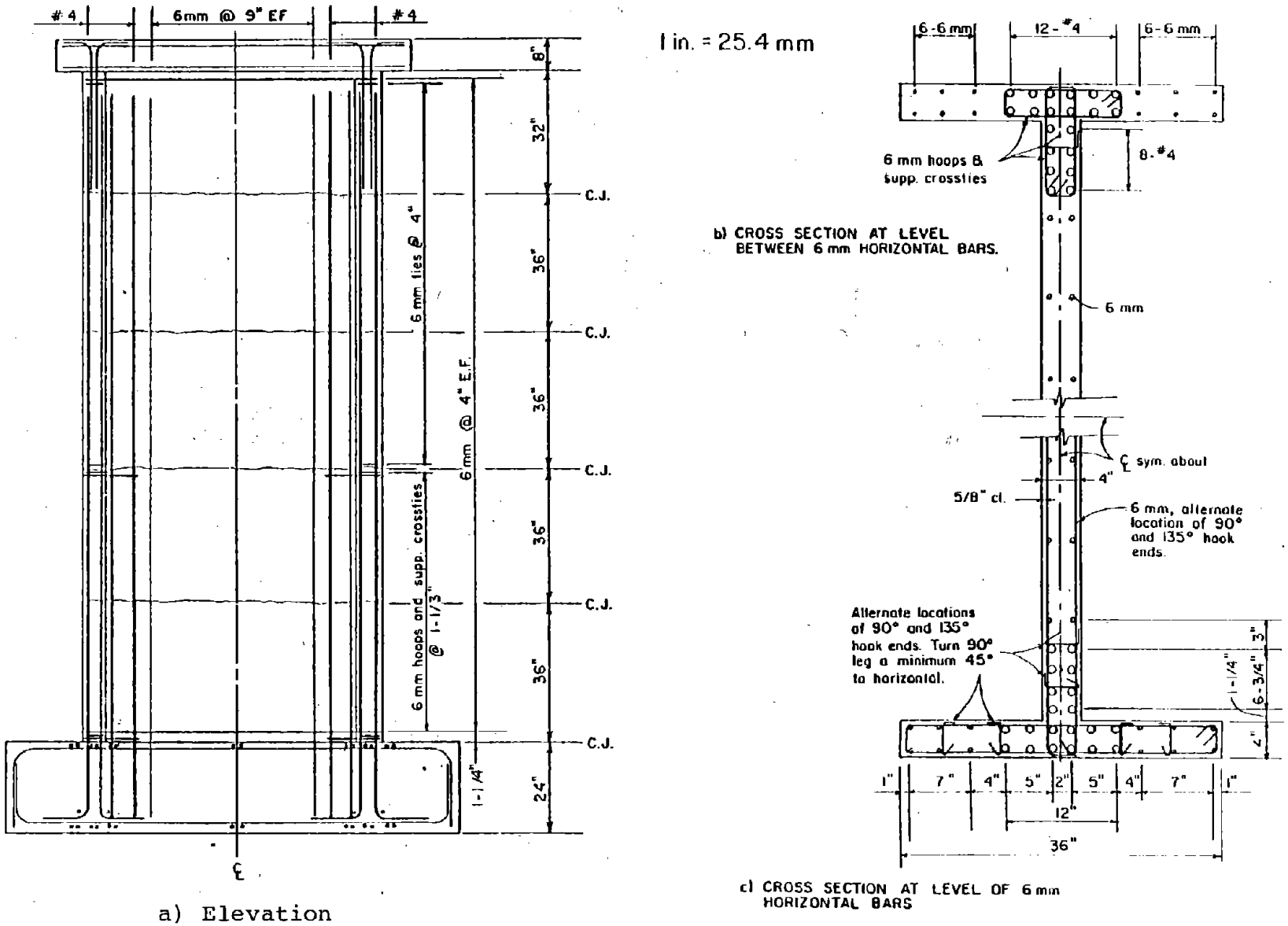

Fig. A-9 Reinforcement for Specimen F2

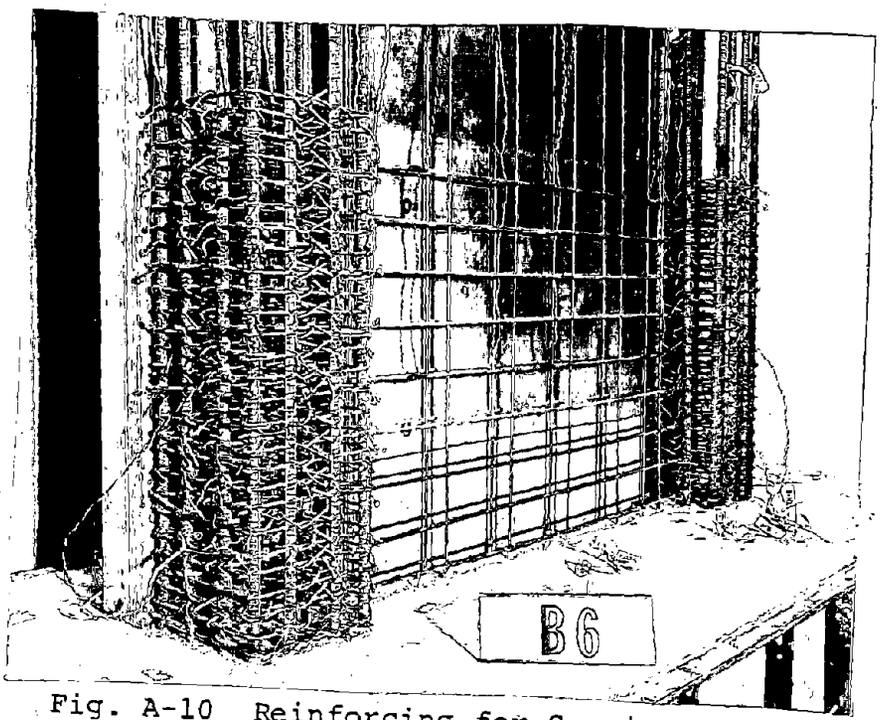

Fig. A-10 Reinforcing for Specimen B6

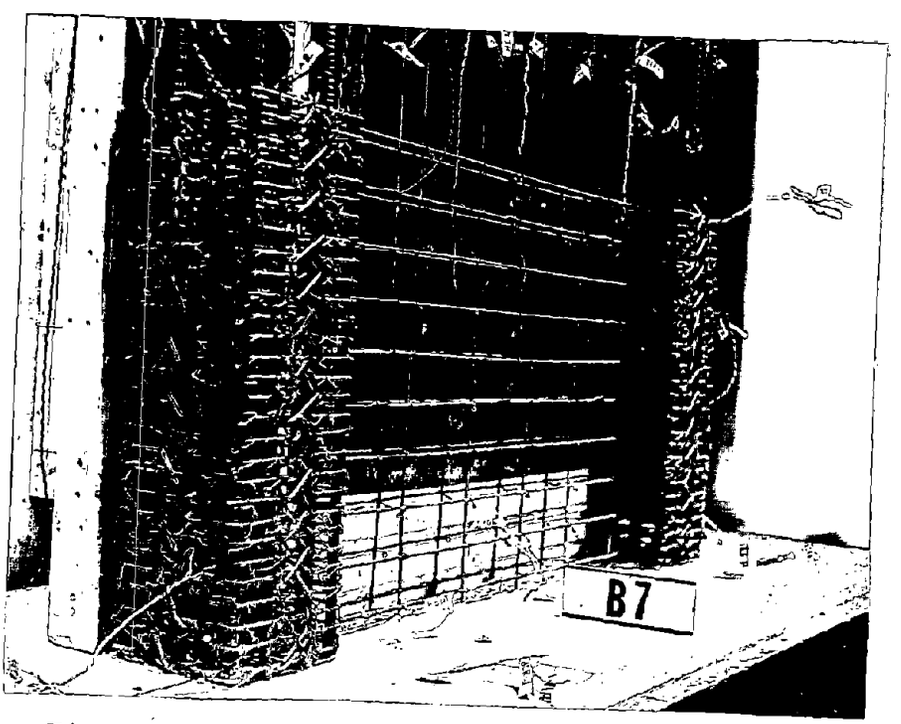

Fig. A-11 Reinforcing for Specimen B7

Fig. A-12 Reinforcing for Specimen B8

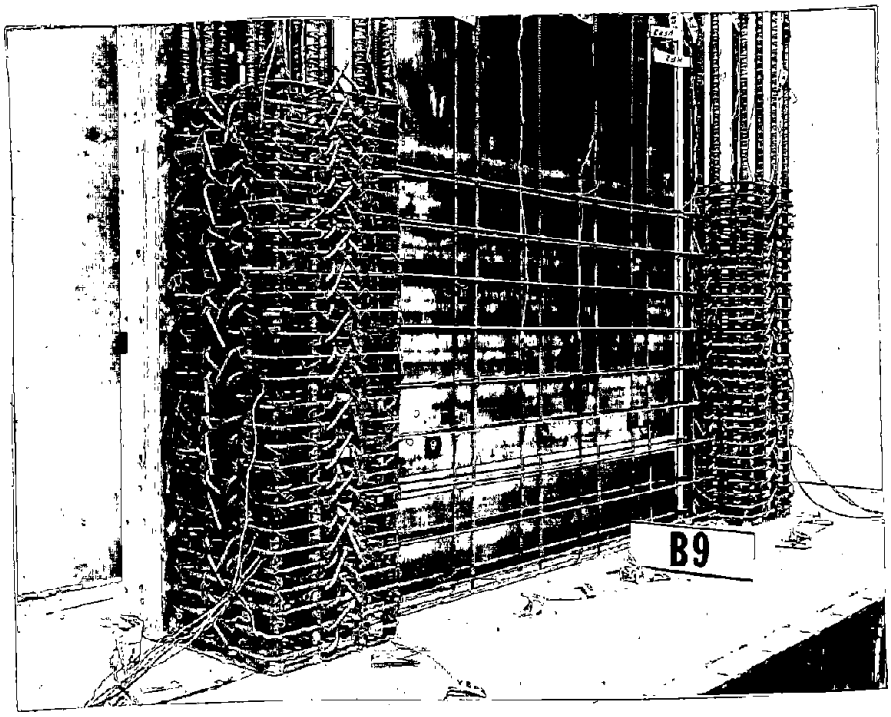

Fig. A-13 Reinforcing for Specimen B9

Fig. A-14 Reinforcing for Specimen B10

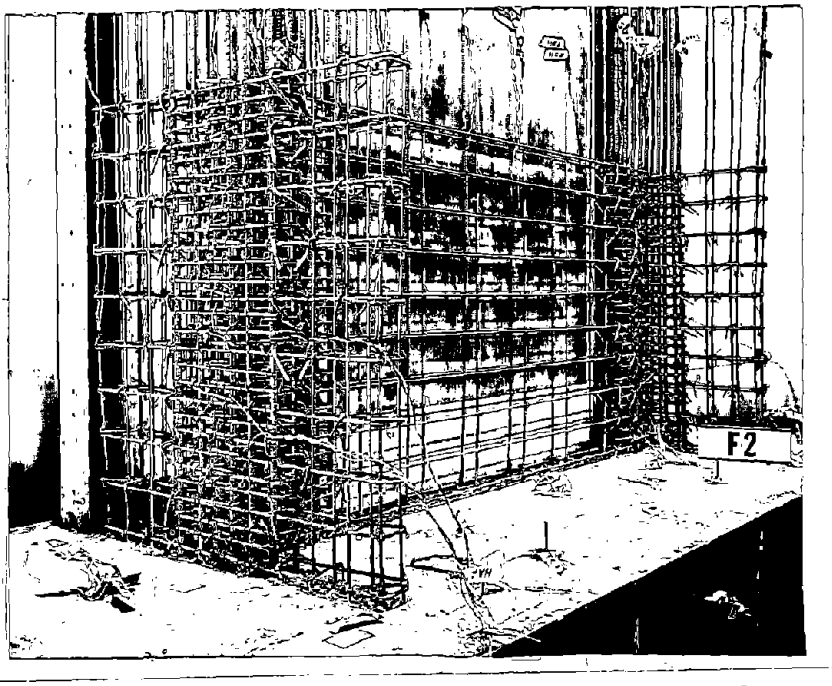

Fig. A-15 Reinforcing for Specimen F2

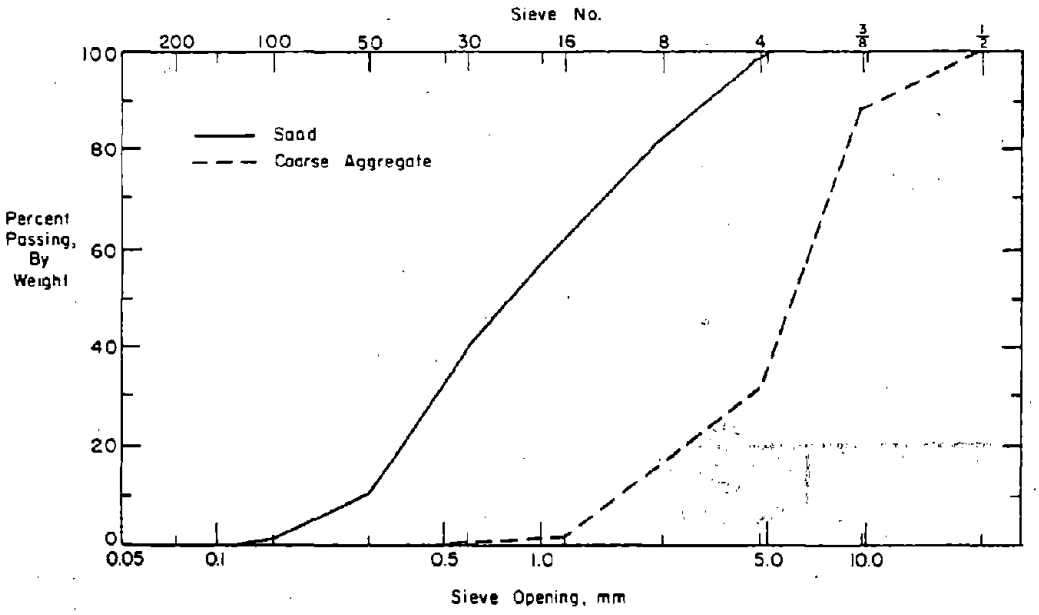

Fig. A-16 Aggregate Gradation Curve

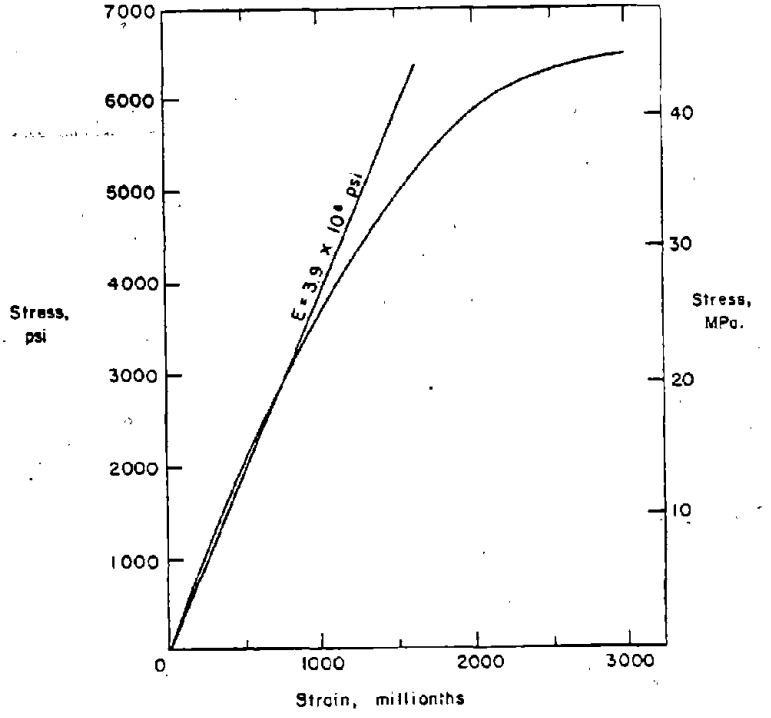

Fig. A-17 Stress versus Strain Relationship for Concrete

TABLE A-2 CONCRETE PROPERTIES FOR PHASE II TEST SPECIMENS[1]

Specimen	Age At Test (days)	Compressive Strength f'_c (psi)[2]	Modulus of Rupture f_r (psi)	Modulus of Elasticity E_c (psi x 10^6)
B6	208	3164	657	3.35
B7	189	7155	873	4.31
B8	77	6085	614	3.90
B9	51	6396	633	3.94
B9R[3]	48	7510	692	4.19
B10	63	6615	611	4.08
F2	60	6610	677	4.20

(1) Average properties for lower 6 ft (1.83 m) of wall
(2) 1000 psi = 1.0 ksi = 6.895 MPa
(3) Average properties for replaced web concrete

Reinforcement. In the specimens, No. 3, No. 4, No. 5 and No. 6 bars conforming to ASTM Designation A615 Grade 60 were used as reinforcement. Deformed 6 mm hot rolled bars with properties similar to Grade 60 were also used. Deformed wire, size D-3, was used to represent smaller bar sizes. This wire was heat-treated to obtain stress-strain characteristics similar to those of Grade 60 bars.

The physical properties of the reinforcement used in Phase II test specimens are summarized in Table A-3. Representative stress-strain relationships for the reinforcement are shown in Fig. A-18.

Construction

Test specimens were constructed in the vertical position. Figure A-19 shows a barbell specimen during construction. The formwork system shown in Fig. A-20 was designed to facilitate construction. Stationary formwork served to maintain the vertical position of the specimen. Each wall was cast in six lifts as shown in Fig. A-21.

At the start of construction, a heavy reinforcing cage for the base block was constructed. This cage was placed on the level base platform of the formwork. Vertical wall reinforcement was then placed in the base cage and supported against the stationary formwork. After vertical reinforcement was secured, the base block was cast. This casting was designated Lift 1.

Following casting of the base block, the construction joint was prepared and the horizontal reinforcement for Lift 2 was placed. Then the removable formwork for Lift 2 was set, and Lift 2 was cast. Subsequent wall lifts were constructed in the same manner. The wall lifts were 36 in. (0.91 m) in height.

Construction joints between lifts were made following standard practice.[15] The surface of the concrete was roughened with a cold chisel, and cleaned of laitance and loose particles prior to placing adjoining concrete. The construction joints are designated CJ1 thrugh CJ5 as shown in Fig. A-21.

TABLE A-3 REINFORCING BAR PROPERTIES FOR PHASE II TEST SPECIMENS

Size	Properties	Specimen					
		B6	B7	B8	B9	B10	F2
D3*	f_y (ksi)	70.7	--	--	--	--	--
	f_{su} (ksi)	74.0	--	--	--	--	--
	E_s (psi x 10^6)	30.0	--	--	--	--	--
	Elong. (%)	13.0	--	--	--	--	--
6mm**	f_y (ksi)	74.2	71.0	65.8	66.9	68.9	67.3
	f_{su} (ksi)	98.0	101.0	89.3	88.9	91.7	88.1
	E_s (psi x 10^6)	30.4	28.5	28.2	28.6	31.3	29.4
	Elong. (%)	9.2	10.4	10.9	10.3	11.1	11.2
No. 3	f_y (ksi)	--	--	69.9	--	--	--
	f_{su} (ksi)	--	--	105.6	--	--	--
	E_s (psi x 10^6)	--	--	25.0	--	--	--
	Elong. (%)	--	--	9.1	--	--	--
No. 4	f_y (ksi)	--	--	--	--	63.5	62.4
	f_{su} (ksi)	--	--	--	--	102.4	104.8
	E_s (psi x 10^6)	--	--	--	--	27.0	27.7
	Elong. (%)	--	--	--	--	12.1	10.7
No. 5	f_y (ksi)	--	--	--	--	64.9	--
	f_{su} (ksi)	--	--	--	--	108.3	--
	E_s (psi x 10^6)	--	--	--	--	27.1	--
	Elong. (%)	--	--	--	--	11.4	--
No. 6	f_y (ksi)	63.9	66.4	64.9	62.3	--	--
	f_{su} (ksi)	106.3	108.8	108.2	106.5	--	--
	E_s (psi x 10^6)	28.5	28.4	27.5	27.6	--	--
	Elong. (%)	11.3	10.8	10.8	10.9	--	--

*A = 0.03 sq. in. d_b = 0.195
**A = 0.05 sq. in. d_b = 0.25 in.
1000 psi = 1.0 ksi = 6.895 MPa

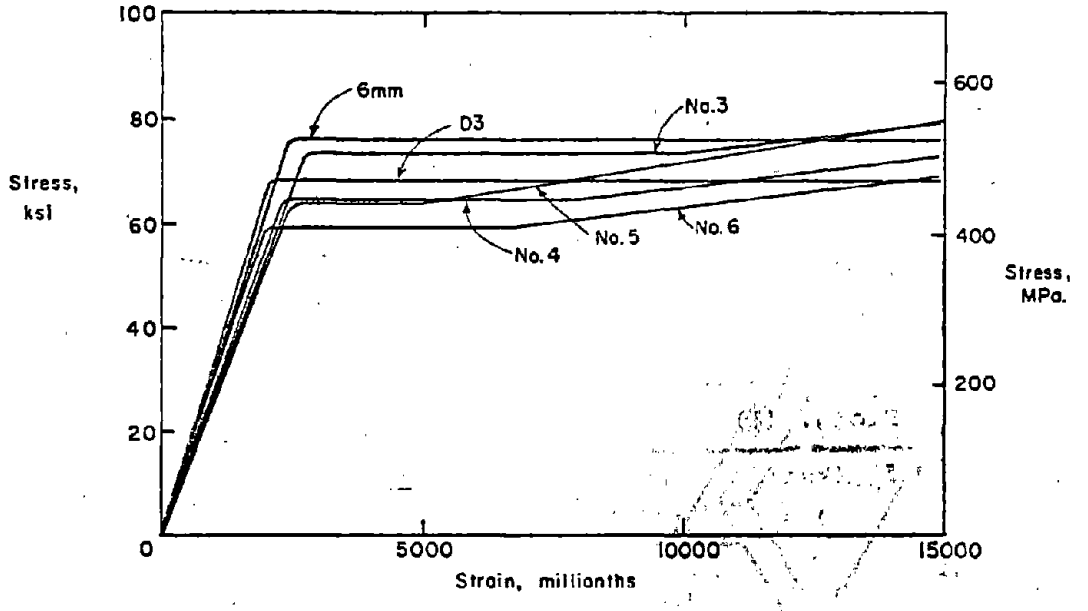

Fig. A-18 Stress versus Strain Relationship for Reinforcement

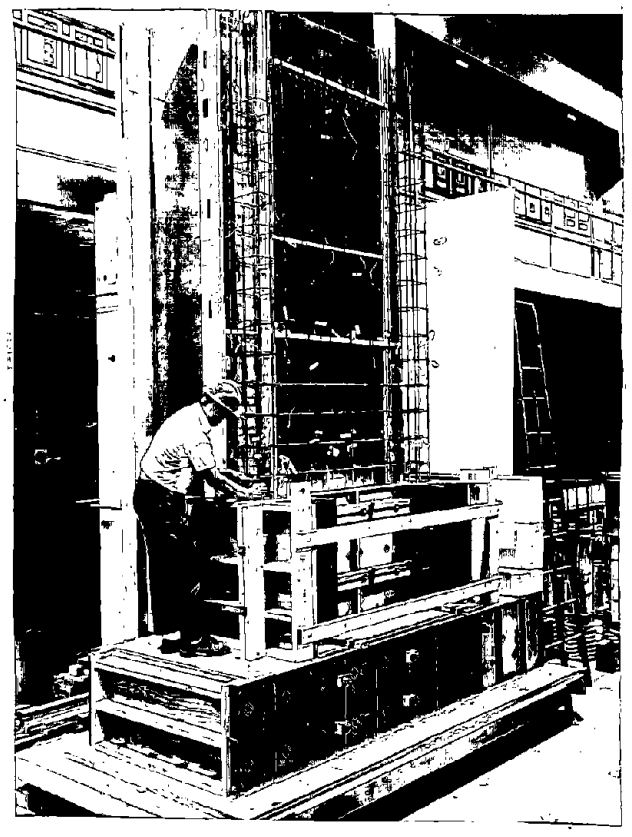

Fig. A-19 Specimen B1 During Construction

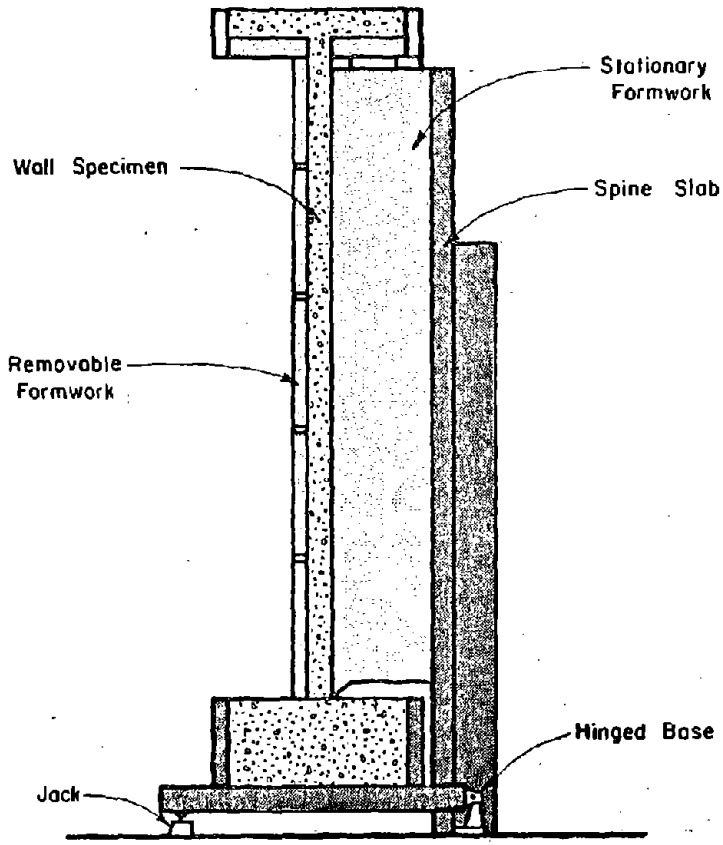

Fig. A-20 Formwork System for Casting Test Specimens

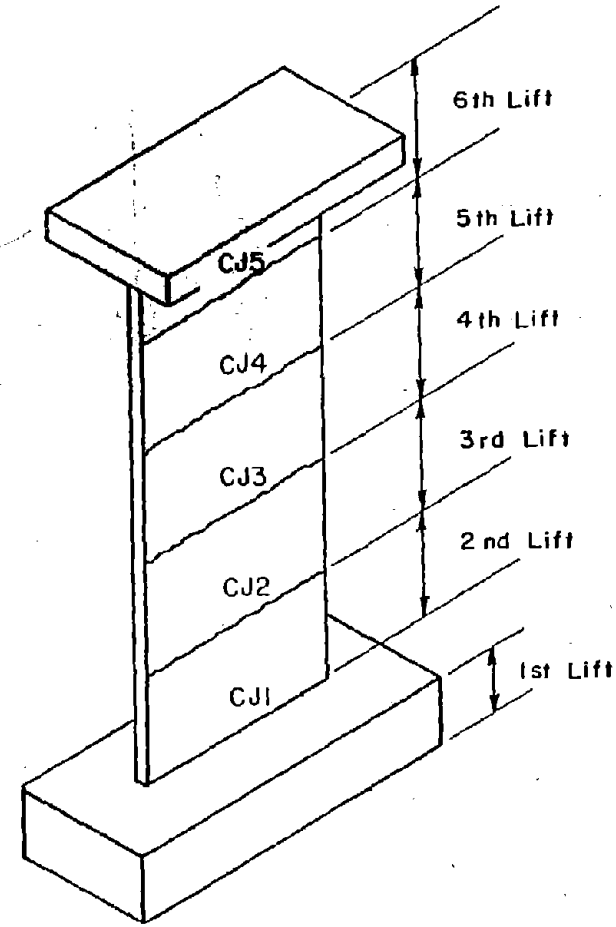

Fig. A-21 Lift Designations for Casting Test Specimens

The sixth lift was cast in two segments. First, the wall segment was cast in the morning, then the slab segment was cast in the afternoon. The delay between segments was to avoid problems caused by plastic shrinkage.

Approximately two days after casting the sixth lift, the removable formwork was stripped. Following this operation, a special lifting rig was placed on the specimen. This rig allowed the specimen to be lifted through rods attached to the base block. Prior to lifting, the base platform of the formwork was rotated to tilt the specimen away from the stationary formwork; thus essentially stripping the specimen from the stationary form. The specimen could then be lifted away from the stationary formwork and placed in position on the test floor.

Repaired Specimen

As shown in Fig. A-22, the web of Specimen B9 was considerably damaged after completion of testing. However, the columns were in very good condition. The outer shell had spalled off the lower 3 to 6 in. (76.2 to 152.4 mm) of the compression face of the columns, but the confined cores were intact. The maximum measured crack widths in the columns during testing were 0.056 in. (1.42 mm) on the tension side and 0.004 in. (0.20 mm) on the compression side at peak lateral load. After completion of the test, the average increase in vertical length of the lower 3 ft of wall was 0.10 (2.5 mm). The average increase in vertical length of the second 3 ft (0.91 m) of wall was 0.18 in. (4.6 mm). No reinforcing steel had fractured or buckled. It was decided that this specimen could be repaired and retested.

Repair procedures were chosen to provide the simplest and least expensive repair that would restore reasonable strength and ductility to the wall.

As shown in Fig. A-23, the web concrete was removed up to the 12 ft (3.7 m) level. The reinforcing steel was left intact. No new steel was added. The columns were rubbed with a soap stone to remove loose particles. The web to base block

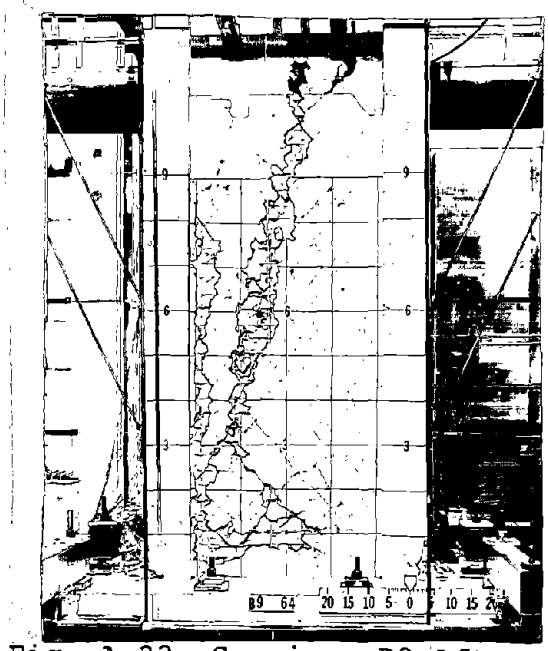

Fig. A-22 Specimen B9 After Lateral Load Test

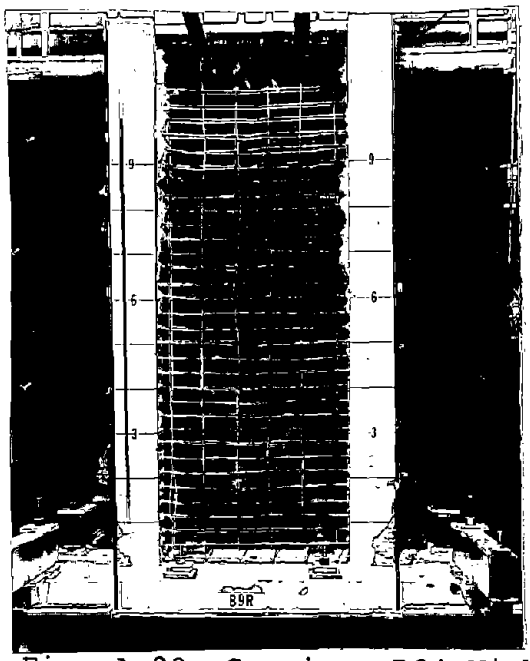

Fig. A-23 Specimen B94 With Web Concrete Removed

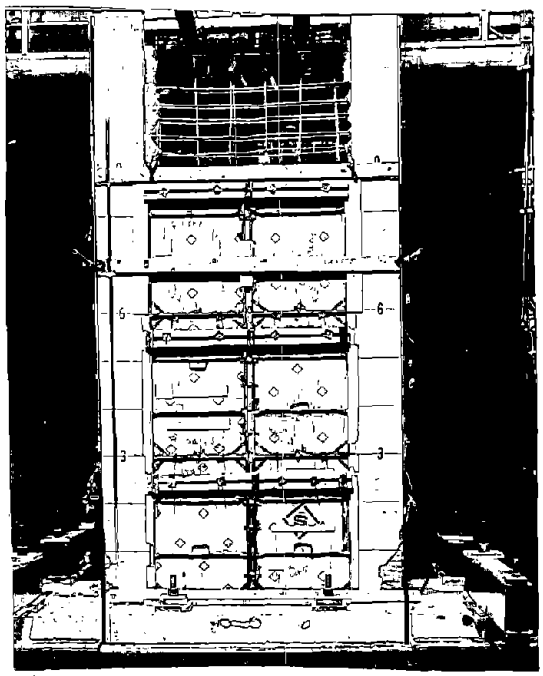

Fig. A-24 Formwork for New Web Concrete

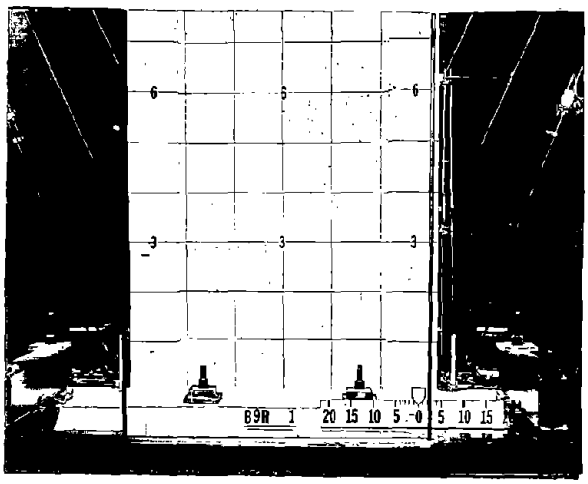

Fig. A-25 Specimen B9R at Start of Test

and web to column joint surfaces were roughened to remove any loose material.

New web concrete was cast in 3 ft (0.91 m) lifts. For Specimen B9, the 4 in. 102mm) thick web was replaced with a 6 in. (152 mm) thick web. This reduced nominal shear stresses by 33%. The formwork for the web is shown in Fig. A-24. The last several inches near the top joint were hand packed with a stiff mix from one side of the wall. After the forms were stripped, this joint was hand rubbed with a sand-cement mortar.

The columns were given a cosmetic repair by hand rubbing a neat cement paste over the surface of the cracks.

Figure A-25 shows the Specimen B9R after completion of the repairs.

Test Setup

Specimens in Phase I were tested under lateral load only. For Phase II tests vertical load capability was added to the test setup.

Lateral Load System

The apparatus for testing the walls is shown in Fig. A-26. Each test specimen was post-tensioned to the floor using eight 1-3/8 in. (34.9 mm) diameter Stressteel bars.

Loads were applied to the specimen as a vertical cantilever with concentrated forces at the top. Hydraulic rams on each side of the specimen alternately applied force to first one side then the other side of the the top slab. Reactions from the applied loads were transferred to the test floor through a large infilled reaction frame. This load transfer occurred directly when the rams closest to the reaction frame were activated, and indirectly through the remote support column and tie rods, when the rams farthest from the reaction frame were activated. A system of one or two rams on each side of the specimen was used depending on the anticipated capacity of each specimen. The hydraulic rams have a capacity of 200 kips (890 kN)

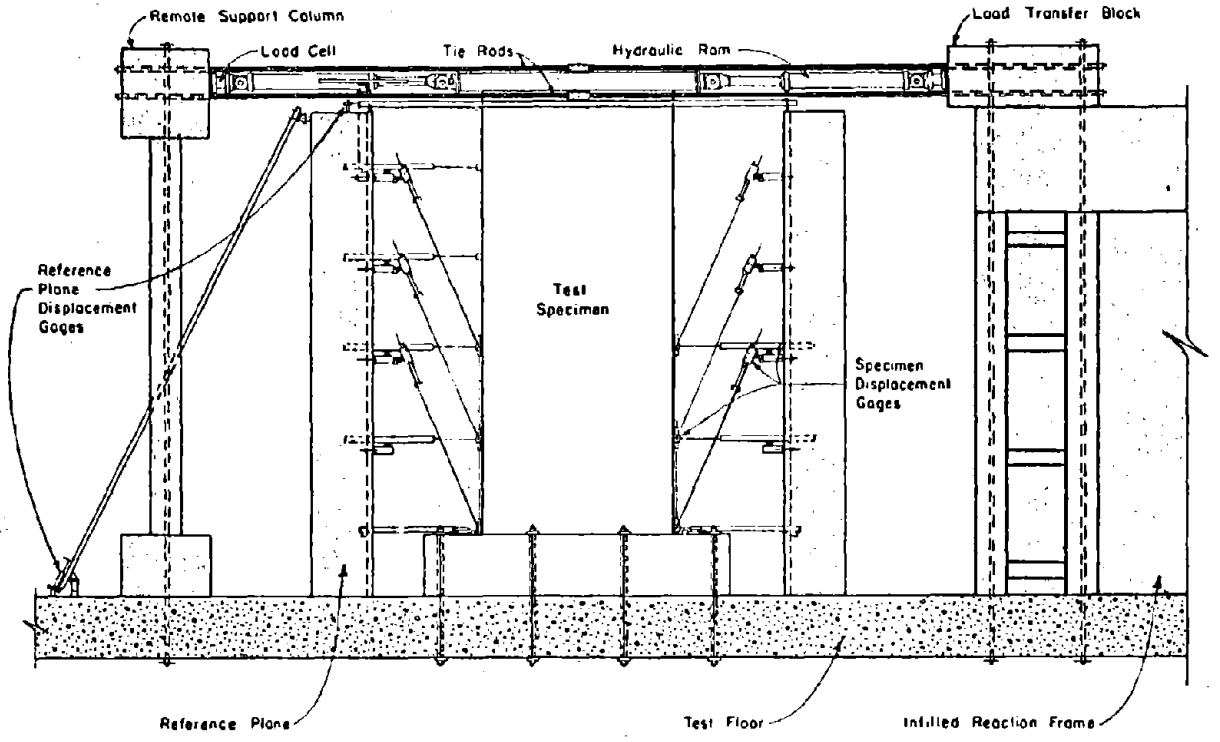

Fig. A-26 Lateral Load Test Setup

and a stroke of 36 in. (0.91 m). At each end of the ram, a clevis bracket and pin arrangement formed a link assembly.

Axial Load System

Axial load was applied only to Phase II specimens. A photograph of the test setup including the axial load system is shown in Fig. 27. The apparatus used to apply the axial load is illustrated in Fig. A-28.

Hydraulic rams at each end of steel loading beams on the top slab were used to apply axial load. The axial load was kept vertical using a movable reaction beam on each side of the wall as shown in Fig. A-28. The movable reaction beams were driven by a hydraulic ram anchored to the floor. Movement of the beam matched the top deflection of the test wall. The applied axial loads were finally transferred from the test specimen to the floor by steel beams attached to the floor.

Axial load was applied before the start of lateral load testing. It was monitored and maintained constant throughout the test.

Instrumentation

Loads

During each test, the applied lateral load was measured and recorded by two methods. In the first method, a load cell was attached to one end of each ram. The load cell readings were recorded as discrete points at each load state during testing. In the second method, pressure cells were attached to the two hydraulic pressure lines for each set of rams. A continuous plot of the pressure cell readings versus the top wall deflection was made during testing.

External Instrumentation

A system of external gages as shown in Fig. A-29 was attached to each specimen.

These gages were mounted on independent reference planes on each side of the specimen. They were used to determine deflections, rotations, shear distortions, and reference plane move-

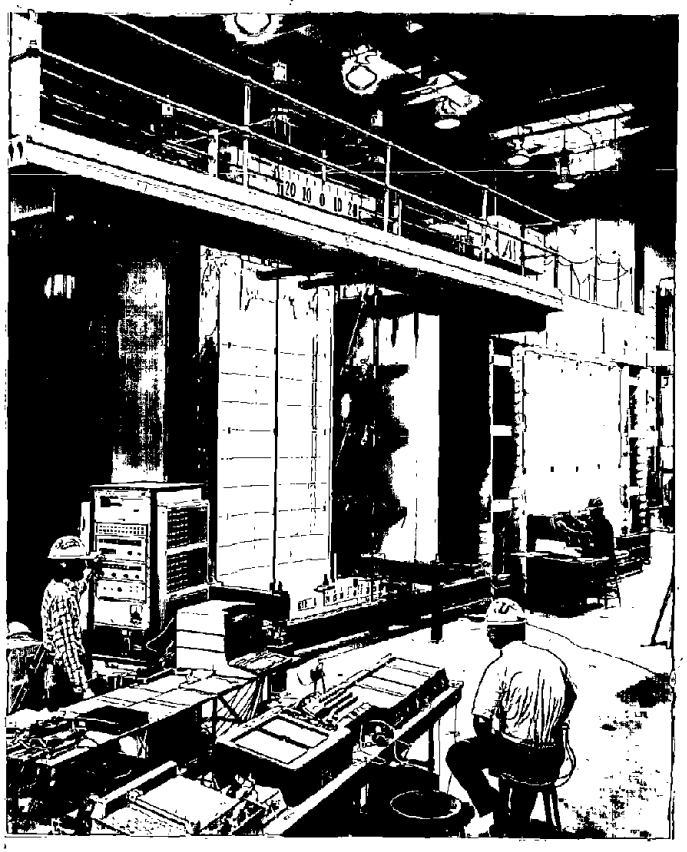

Fig. A-27 Test Setup

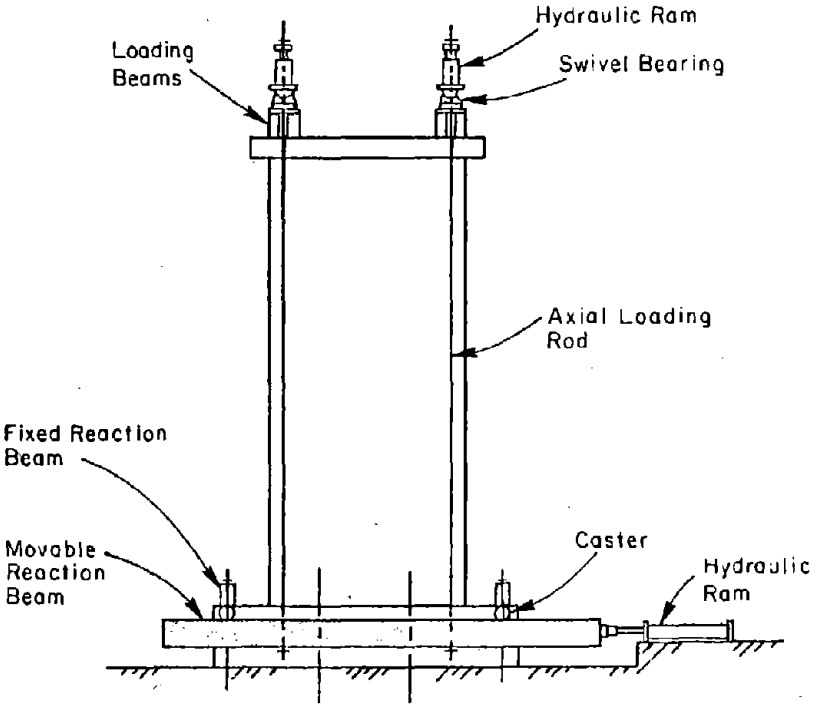

Fig. A-28 Axial Loading System

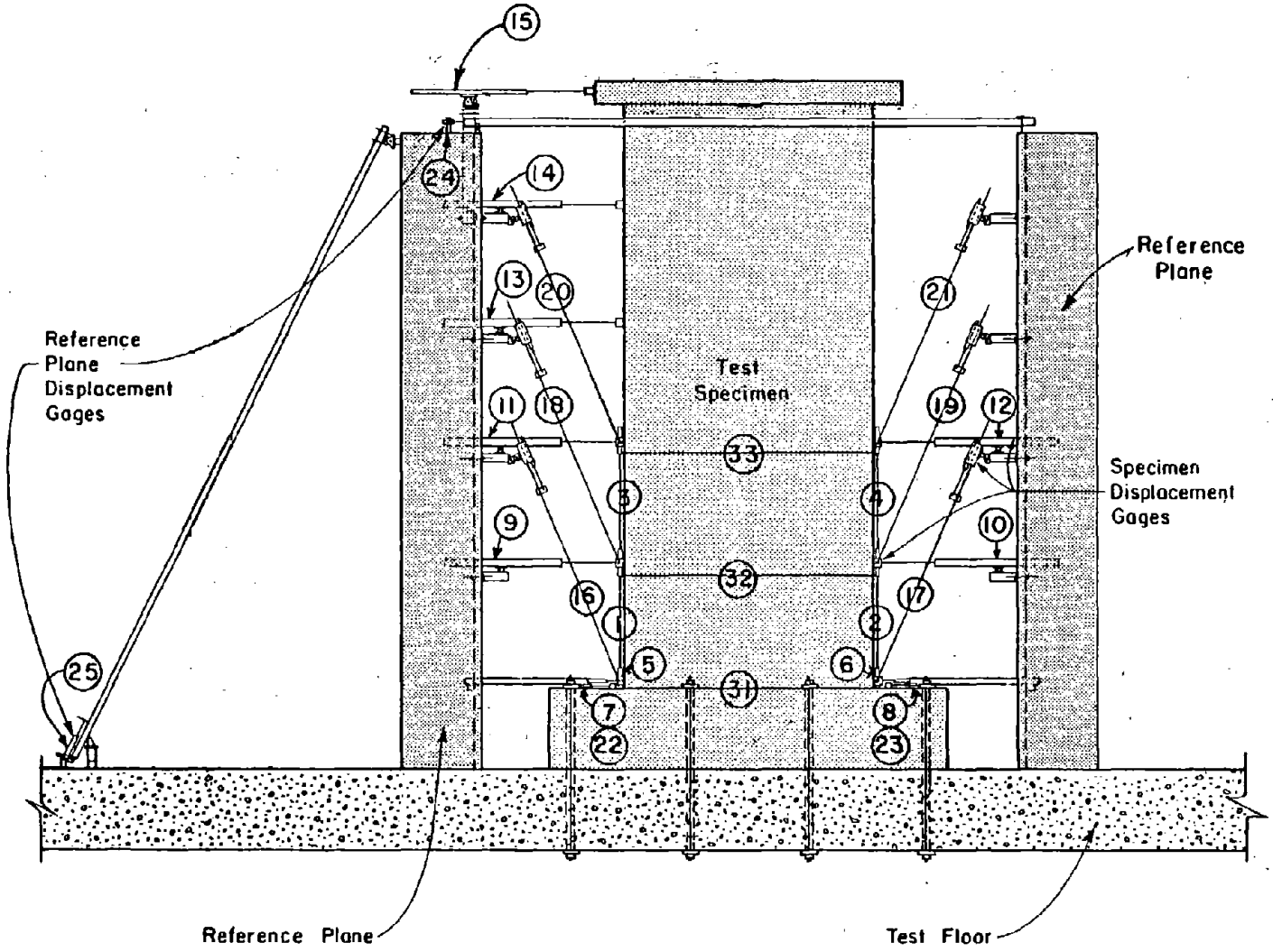

Fig. A-29 External Gages

ment. In addition three dial gages were mounted on the specimen to determine slip at construction joints.

All horizontal and vertical displacement measurements were made using linear potentiometers and direct current differential transducers (DCDT's). These gages have resolutions from 0.001 in. to 0.003 in. (0.025 mm to 0.076 mm).

Horizontal Displacements. Horizontal displacements are measured at seven levels as shown on Fig. A-29. Gages 7 and 8 measured horizontal movement of the base block. Gages 22, 23, and 9 through 15 measured horizontal movement of the wall. For the lower three levels, measurements were made at each end of the wall.

Rotations. Rotations were measured at four levels on the specimen. The first was the rotation of the top of the base block. This rotation was obtained using triangulation calculations from the output of Gages 7 and 16, and Gages 8 and 17.

Rotations in the lower 6 ft (1.83 m) of the wall were obtained by measuring vertical displacements along each end of the wall. Three sets of measurements were made. The first set was made using Gages 5 and 6 between the top of the base block and the bottom of the wall over a nominal gage length of 3 in. (76.2 mm). The other two sets of measurements were made over nominal gage lengths of 36 in. (0.91 m) using Gages 1 and 2, and Gages 3 and 4. An independent check on the output of Gages 9 and 18, 10 and 19, 11 and 20, and Gages 12 and 21.

For Phase II tests, two additional extensometers were used to determine relative vertical displacements between the base block and the six-foot level. Output from these gages were used to plot a continuous load versus rotation curve during the test.

Movement of the reference planes was monitored using Gages 24 and 25 as shown in Fig. A-29. Gage 24 measured the relative horizontal movement between the tops of the reference planes.

Shear Distortions. An indication of shear distortions was obtained over two zones in the lower 6 ft (1.83 m) of the wall. The first zone was from the top of the base block to the

3 ft (0.91 m) level. The second zone was from the 3 ft level to the 6 ft level.

The horizontal and vertical movement of Points A through F in Fig. A-30 were determined from the displacement gages previously described. From this data, the changes in length of the diagonals d_1 through d_4 were calculated.

It can be seen in Fig. A-31a that the length of the diagonals does not change in an element subjected to pure flexure. Also, as shown in Fig. A-31b, the length change of diagonals is equal and in the same direction for each diagonal in vertical or lateral expansion. For shear distortions, however, the change in length of the diagonals is in opposite directions. As shown in Fig. A-32, their change in length can be related to shear distortions by:

$$\gamma_{avg} = \frac{\gamma_R + \gamma_L}{2} \qquad \frac{\delta_1 d_1 \quad - \delta_2 d_2}{2hl} \qquad (A\text{-}1)$$

Shear distortions calculated as described above cannot be considered exact values in a reinforced concrete element. Because of cracking, plane sections not remaining plane, and the existence of a moment gradient across the element, these shear distortions can only be considered as approximate values.

As can be seen in Fig. A-30, the shear distortions measured in the lower 3 ft (0.91 m) zone include the slip at construction joints CJ1 and CJ2. The shear distortions in the upper 3 ft zone include the slip at construction joint CJ3.

Slip at Construction Joints. Dial gages 31, 32 and 33 as shown in Fig. A-29 were used to measure relative slip at construction joints CJ1, CJ2 and CJ3. These gages have a sensitivity of 0.001 in. (.025 mm).

Crack Widths. Crack widths were measured during testing across selected cracks in the lower 6 ft (1.83 m) of the web and boundary elements. These measurements were obtained using a

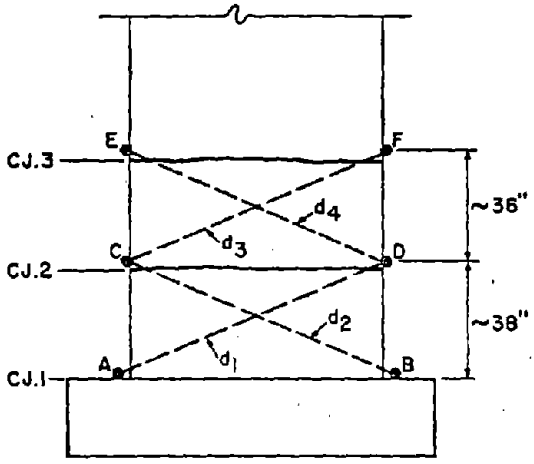

Fig. A-30 Points Measured for Shear Distortions

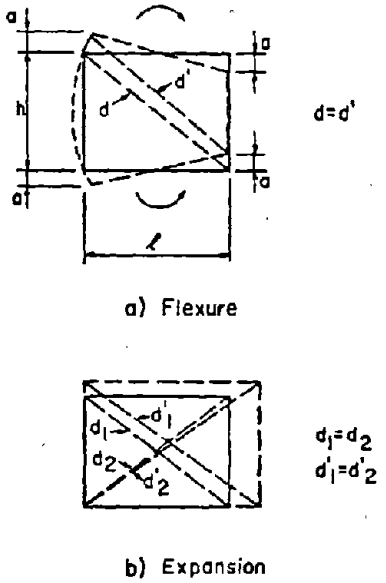

Fig. A-31 Length of Diagonal in Element

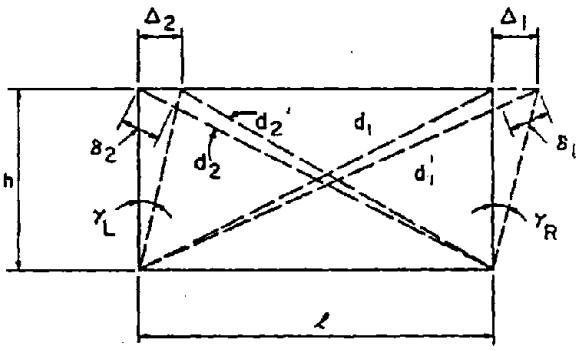

$$\gamma_R = \frac{\Delta_1}{h} \quad , \quad \gamma_L = \frac{\Delta_2}{h}$$

$$\gamma_{Avg.} = \frac{\Delta_1 + \Delta_2}{2h}$$

$$\frac{\Delta_1}{\delta_1} = \frac{d_1}{\ell} \quad , \quad \frac{\Delta_2}{-\delta_2} = \frac{d_2}{\ell}$$

$$\therefore \gamma_{Avg.} = \frac{\delta_1 d_1 - \delta_2 d_2}{2h\ell}$$

Fig. A-32 Calculation of Shear Distortions

hand microscope containing a scale with gradations of 0.001 in. (0.025 mm).

Internal Instrumentation

Strain gages were placed on both vertical and horizontal reinforcement. The basic strain gage layout is shown in Figs. A-33 and A-34. In addition, strains were measured on several of the hoops and supplementary crossties of the confinement reinforcement.

Recording Equipment

Output from load cells, potentiometers, DCDT's and strain gages was recorded as discrete points at each load stage using a VIDAR Digital Data Acquisition System.

Raw test data was stored on printed tape and transferred from the VIDAR directly into an HP9830 calculator for immediate reduction. Reduced data was then stored on magnetic tape cassettes for later analysis.

Data from the construction joint slip gages and crack width measurements were hand recorded.

Photographic Equipment

A complete photographic record was kept for each test. Color slides and black and white photographs were taken at selected load stages throughout the testing. In addition, three time-lapse movie cameras running at one frame per second recorded each cycle of loading.

Load History

Three load histories were used to test the specimens under lateral forces. These were termed monotonic, incrementally increasing reversed (IR), and modified reversed (MR). For all Phase II tests, vertical load was held constant while lateral loads were applied.

Montonic

A monotonic load history consisted of incrementally increasing load or deflection in one direction until a complete loss of load carrying capacity was obtained. Only one specimen, B4, was

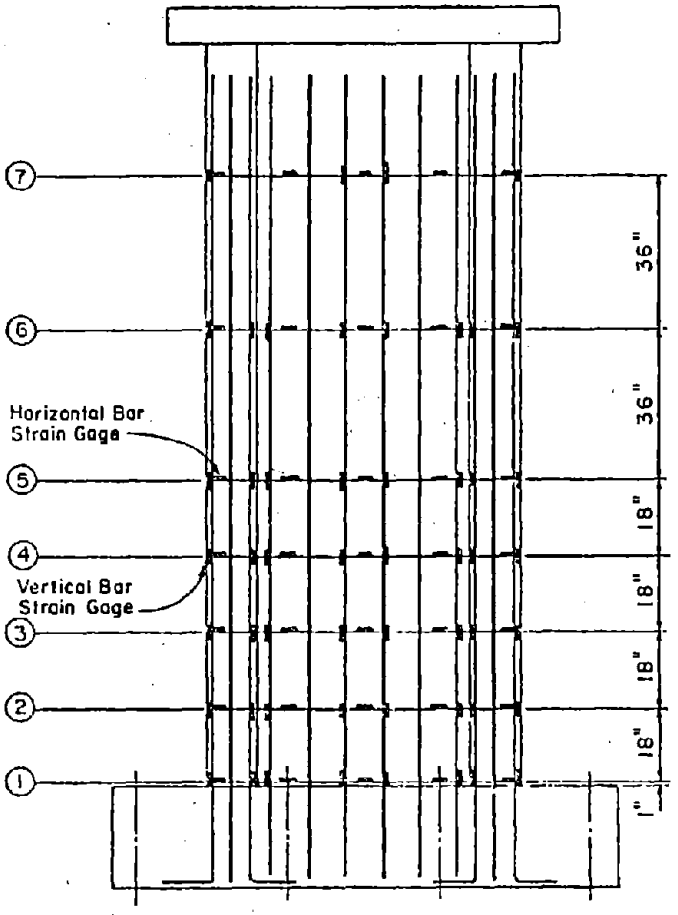

Fig. A-33 Strain Gage Locations in Elevation of Test Specimens

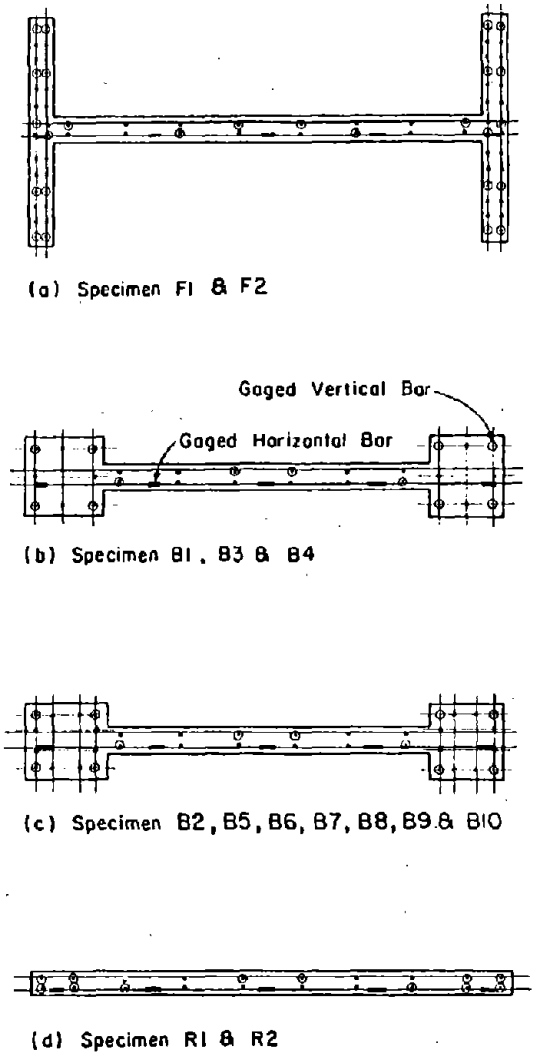

Fig. A-34 Strain Gage Locations in Cross Section of Test Specimens

tested using monotonic loading. This loading was used to establish a base of comparison to evaluate the effects of reversing loads on specimens subjected to low nominal shear stress.

No complete monotonic load test was performed on a specimen subjected to high shear. However, the modified reversing load history discussed below includes a large initial inelastic cycle. The first half of this cycle is representative of a monotonic test up to the point where the load is reversed the first time. Specimens B9, B9R and B10 were subjected to this "monotonic" half-cycle.

Incrementally Increasing Reversing

An incrementally increasing reversing load history consisted of a series loading increments applied at increasing maximum lateral forces or deflections. Each loading increment consisted of three complete reversed cycles at a specific maximum load or deflection. The specimens were initially loaded in equally increasing force increments up to the first yield load. Subsequent to yielding, loading was controlled by equally increasing deflection increments. Deflection increments were increased until a significant loss of load capacity was obtained. An example of an incrementally increasing reversing load history is shown in Fig. A-35.

The incrementally increasing load history is commonly used in experimental investigations. It is used to determine an unknown limiting value of load or deformation. This unknown value is approached within small steps or increments. The stability at each step is checked by applying several cycles at each step.

Modified Reversing

The incrementally increasing load history described above determines a limiting value of load or deformation under one type of reversing load history. However, it was expected that the limiting value is dependent on the load history used to approach it. Bertero[16] has suggested that repeated reversing load cycles gradually approaching a limiting value

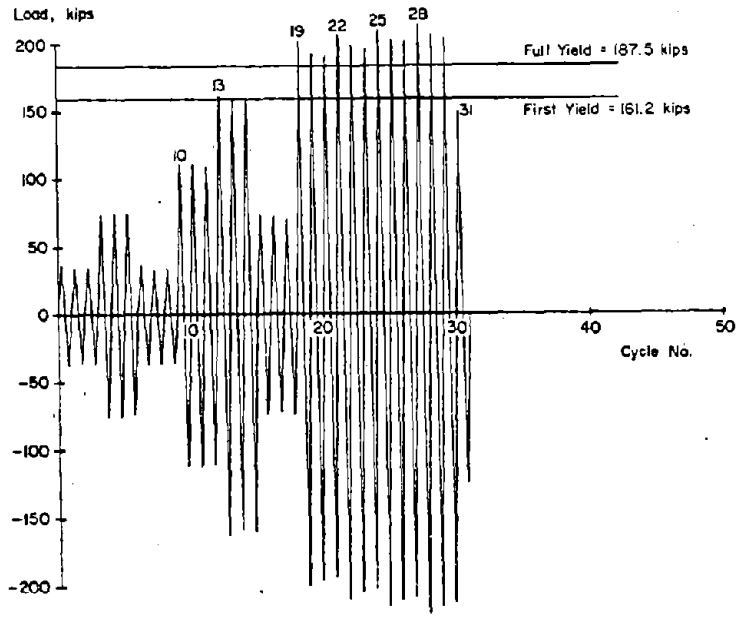

Fig. A-35 Incrementally Increasing Load History

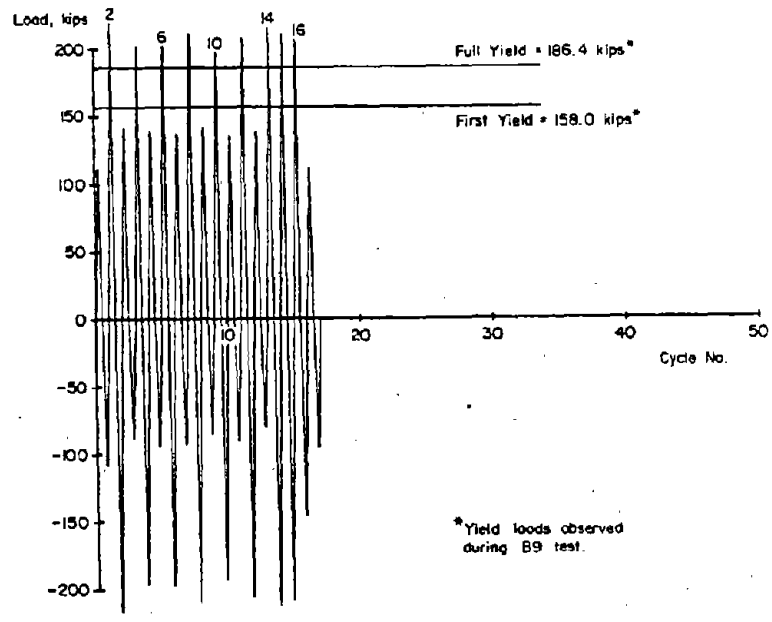

Fig. A-36 Modified Reversing Load History

may soften a structure such that the limiting value is not a "conservative" measure. He suggests that a more appropriate measure would be determined if the structure is loaded near its limiting value in the first cycle.

It was also anticipated that a load history with a large initial cycle would be more representative of actual response to earthquake ground motion. Analytical studies[17] have shown that the maximum deflection response usually occurs near the onset of base motion and that maximum deflection response is rarely preceded by large amplitude cycles. In addition, analytical studies indicate that, for isolated structural walls, the maximum number of fully reversed large-amplitude cycles of deformation corresponding to a twenty second earthquake is about six.

Therefore, to investigate the variable of reversing load history, the load history shown in Fig. A-36 was used. The first small cycle is applied to crack the specimen in both directions. The second cycle is a large inelastic cycle at some predetermined maximum rotational ductility. The load history includes two more cycles at the maximum ductility, three cycles at 80% of the maximum ductility and six small cycles at a ductility of 1.1. The cycles are applied in the sequence indicated in Fig. A-36. The loading is controlled by measured rotations at the 6 ft level.

The use of this loading history has the character of a proof test. Some measure of the limiting value of ductility must be available prior to the test. In this program, use of the modified reversing load history was intended to verify maximum ductilities measured during the incrementally increasing load history tests.

APPENDIX B - TEST RESULTS

TABLE OF CONTENT

APPENDIX B - TEST RESULTS

Introduction

In this section the methods used for analysis and presentation of data from the tests are described in general. Results from each lateral load test are then presented in detail. Specimen behavior during testing is described and resulting data discussed.

Data Presentation and Analysis

Loading History

Loads and top deflections applied to each specimen are plotted versus cycle number. In addition, rotations at the 6-ft (1.83 m) level are plotted versus cycle number for specimens B9, B9R and B10. First yield and full yield levels are indicated on these figures.

First yield load is defined as the first load at which a yield strain was measured in the boundary element tensile reinforcement. It was determined by monitoring specific strain gages during loading.

Full yield load is defined as the load at which all of the main tensile reinforcement in the boundary element had yielded. It was determined from interpolation between measured strains at load stages before and after full yield.

In the specimen loading history, an inelastic cycle is defined as a complete reversed load cycle during which both load and deflection exceeded the first yield level.

Continuous Load-Deformation Relationships

Two continuous plots of load versus top deflection figures and one plot of load versus deflection at the 6-ft (1.83 m) level are presented for each test. The first figure shows the initial cycles with first cracking indicated. The second and third figures show cycles for the entire test.

One continuous load rotation at the 6-ft (1.83 m) level figure is presented for each test except Specimen B6. This figure is not available for B6 because of a plotter malfunction.

Included on the above figures are indications of yield loads and failure modes. These are the only figures for each specimen that include all loading cycles.

Other load-deformation type figures described below include only selected cycles. For specimens subjected to an incrementally increasing load history, only the first cycle of each loading increment is shown. These cycles are numbered on the figures. For specimens subjected to the modified load history, only the large inelastic cycles are shown. This results in a discontinuity in the positive loading half of the loops for these specimens. These cycles are also numbered on the figures.

Moment-Rotation Relationships

Reversing Load. The reversing moment-rotation data are shown for each specimen at three levels. These are the base level, the 3-ft (0.91 m) level and the 6-ft (1.83 m) level. The fixed body rotation at the top of the base block is subtracted out of the data used for these figures. However, rotations caused by slip of flexural steel anchored within the base block are included in measured rotations. The moment plotted in all cases is the moment at the base level. This includes the P- moment from the applied axial load.

Monotonic Load. One of the objectives of the experimental program was to compare the behavior of specimens subjected to reversing load with the behavior under monotonic loading. Since time and cost prohibited a monotonic test for each type of specimen, a calculated "monotonic" moment-rotation relationships were used to compare monotonic and reversing load conditions.

A calculated monotonic moment-rotation relationship is presented on the figures for rotation at the 3-ft (0.91 m) and 6-ft (1.83 m) levels. These moment-rotation relationships were obtained from a moment curvature analysis based on satisfying applicable conditions of equilibrium and strain compatibility.

A linear distribution of strain over the section was assumed. Measured material properties were used. The analysis considered complete stress-strain relationships for concrete and steel, including strain hardening of the reinforcement and the effect of confinement in the concrete compression block. The Kent and Park[18] relationship was used for the confined concrete stress-strain relationship.

The maximum calculated curvature was determined by either concrete crushing or reinforcing steel fracture. A limit for web crushing was not considered in the calculation. For confined concrete, the limiting strain for the compression face was determined from an expression developed by W. G. Corley.[19]

$$\varepsilon_u = 0.003 + \left(\frac{\rho_s f_y}{15}\right)^2 \qquad \text{(B-1)}$$

where: ρ_s = the volumetric ratio of confinement reinforcement

f_y = the yield stress of confinement reinforcement in ksi.

Fracture of the reinforcing steel was assumed to occur at a strain equivalent to the measured elongation from reinforcement tension tests.

In reinforced concrete flexural members, inelastic curvature spreads over a hinge length, ℓ_p. Therefore, the theoretical curvature distribution corresponding to the actual moment distribution is not accurate. An effective curvature distribution must be determined. Rotations at a specific level can then be calculated by integrating the effective curvature distribution over the length involved.

The method used to determine an effective curvature distribution included the effect of diagonal shear cracking on the spread of the hinging region. This method is illustrated in Fig. B-1. A hinge length, ℓ_p, was determined visually from the crack pattern of each specimen. This was the height

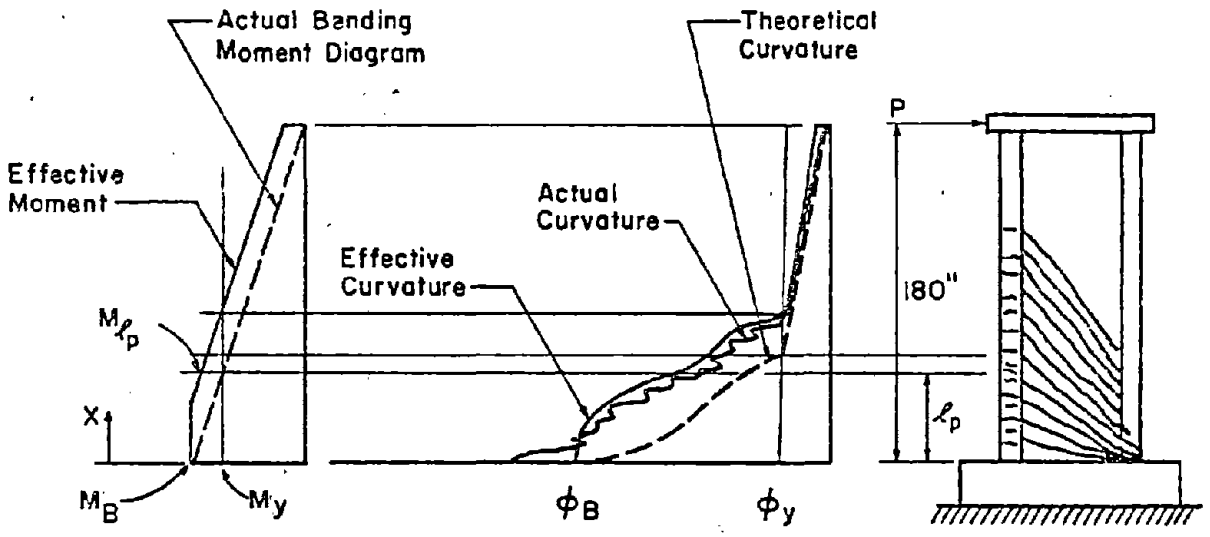

Fig. B-1 Curvature Distribution for Specimens With Inclined Cracking

at which the steepest diagonal crack extending from the base compression zone intercepted the centroid of the tension boundary element as shown in Fig. B-1. Based on equilibrium of the forces in the hinge region. Bachmann[20,21] presented a relationship for determining force in the tensile reinforcement. Using this relationship, the effective moment for flexural steel tension is:

For $0 < X \leq \ell_p$

$$M_x = M_B - \frac{X^2 \eta P}{2d} \qquad \text{(B-2)}$$

For $\ell_p < X < 180$ in.

$$M_x = M_{\ell p} - P\,(x - \ell_p) \qquad \text{(B-3)}$$

Where: M_B = Moment at the base

M_x = Effective moment at a distance X from the base

$M_{\ell p}$ = Effective moment at ℓ_p from the base

$$= M_B - \frac{(\ell_p)^2 P}{2d}$$

P = Total lateral load

η = V_s/P

V_s = Lateral load taken by stirrups across a 45 degree crack.

The calculated curvature related to this effective moment distribution was used to calculate rotations at each level.

The rotation calculations described above were performed only to obtain an estimate of monotonic rotation behavior. No attempt was made to include the effects of bond slip and variation of steel strain between cracks. Only the tensile strains are directly related to the effective moment distribution and plane sections do not remain plane. The calculated curvature is only approximately related to the effective moment at a section. Therefore, the calculated monotonic rotations should only be considered approximate values. However, the calculated monotonic strengths should be accurate estimates.

The calculated monotonic rotations for Specimen B4 from Phase I test series, are compared with the measured rotations in Fig. B-2.

The calculated maximum strength of 74.3 kips (330.5 kN) is in very close agreement with the measured strength of 75.3 kips (334.9 kN).

The calculated rotation at the base level is considerably lower than the measured. This is as expected since a major portion of the measured rotation at the base results from steel strain within the base block. This would be true in all test specimens. Therefore, no further attempt was made to compare calculated and measured rotations at the base level.

Calculated rotations at the 3-ft (0.91 m) and 6-ft (1.83 m) level overestimate the measured rotations. This is the direction of error to be expected considering the assumptions made in the calculations. However, the calculated maximum rotation is in reasonable agreement with measured at both the 3-ft and 6-ft levels. Therefore, the plots of calculated monotonic rotation at these two levels were superimposed on measured reversed load rotation plots for each specimen.

It should be noted that calculated rotations are not intended to be an estimate of rotations in specimens under reversed loading. They are intended to be an estimate of rotations under monotonic loading. They are shown on the figures to demonstrate the effects of reversed loading on strength, ductility and rotation.

Shear Distortion Relationships

Shear distortion plots are shown for each specimen over three zones as indicated in Fig. B-4. Zone 1 is from the top of he base block to the 3-ft level. Zone 2 is from the 3-ft level to the 6-ft level. The shear distortions in these two zones were calculated from measured deformations as previously described in the section on instrumentation.

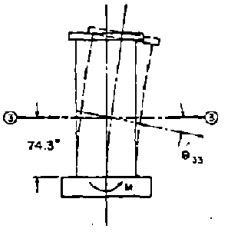

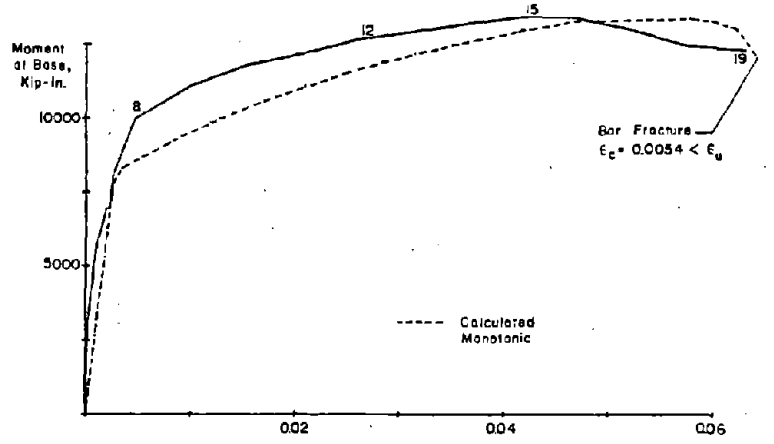

a) At 6 ft Level

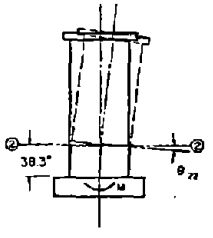

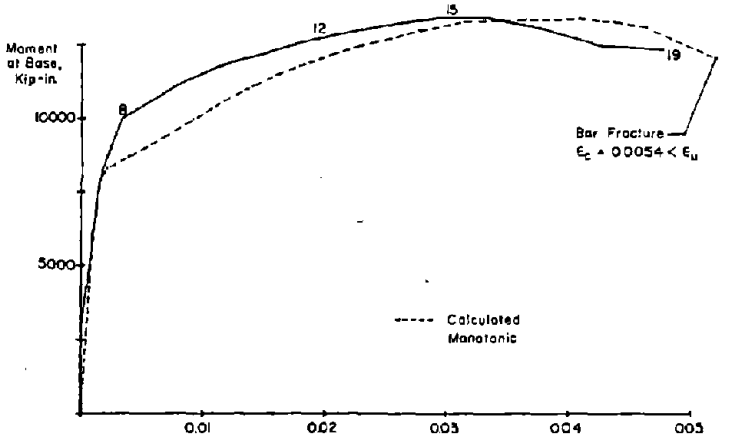

b) At 3 ft Level

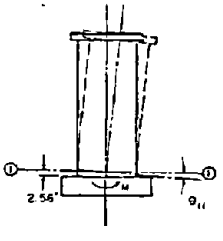

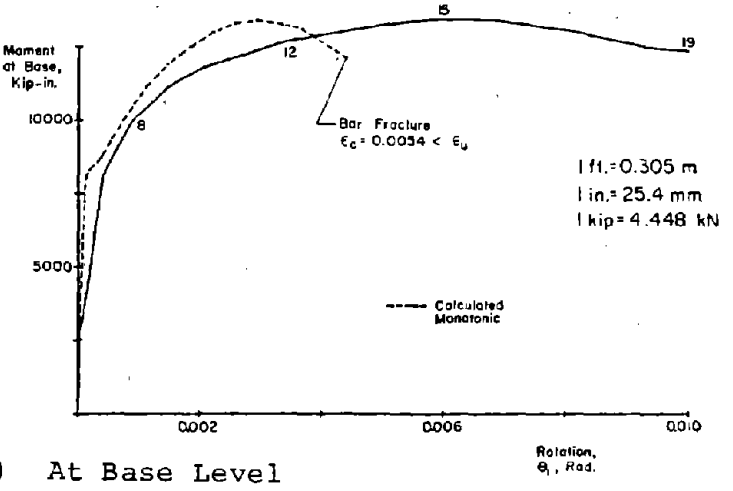

c) At Base Level

Fig. B-2 Moment at the Base Versus Rotation for Specimen B4

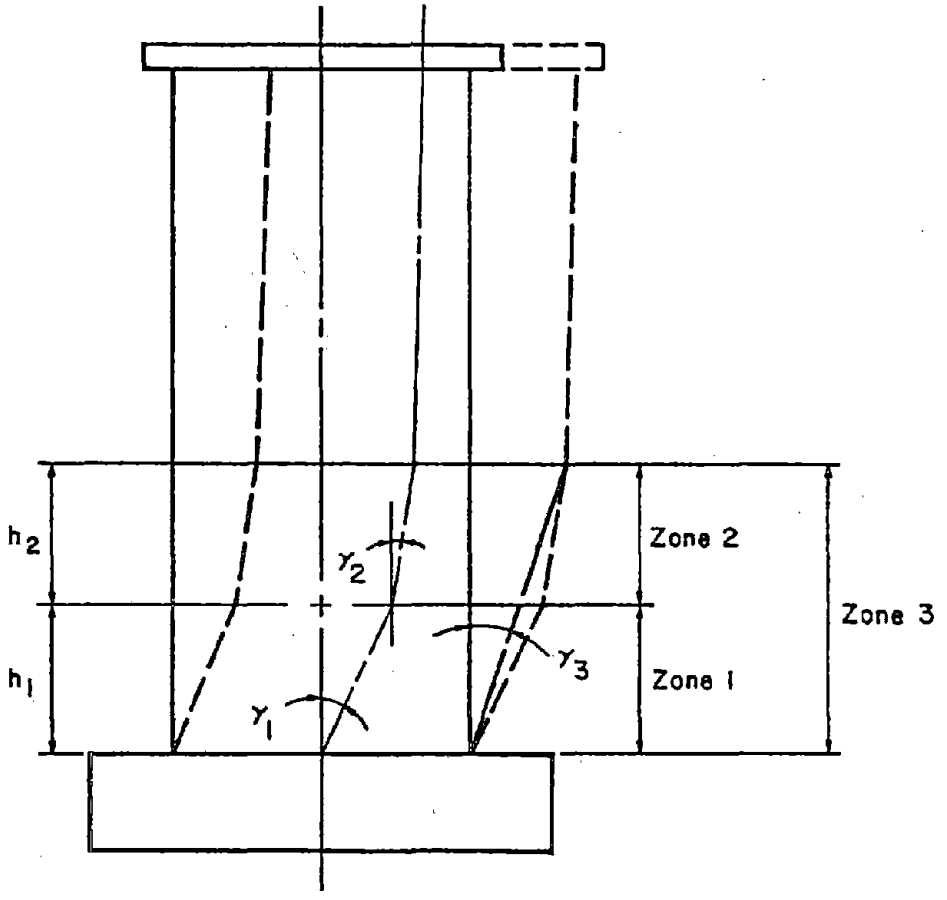

Fig. B-3 Location of Shear Distortion Measurements

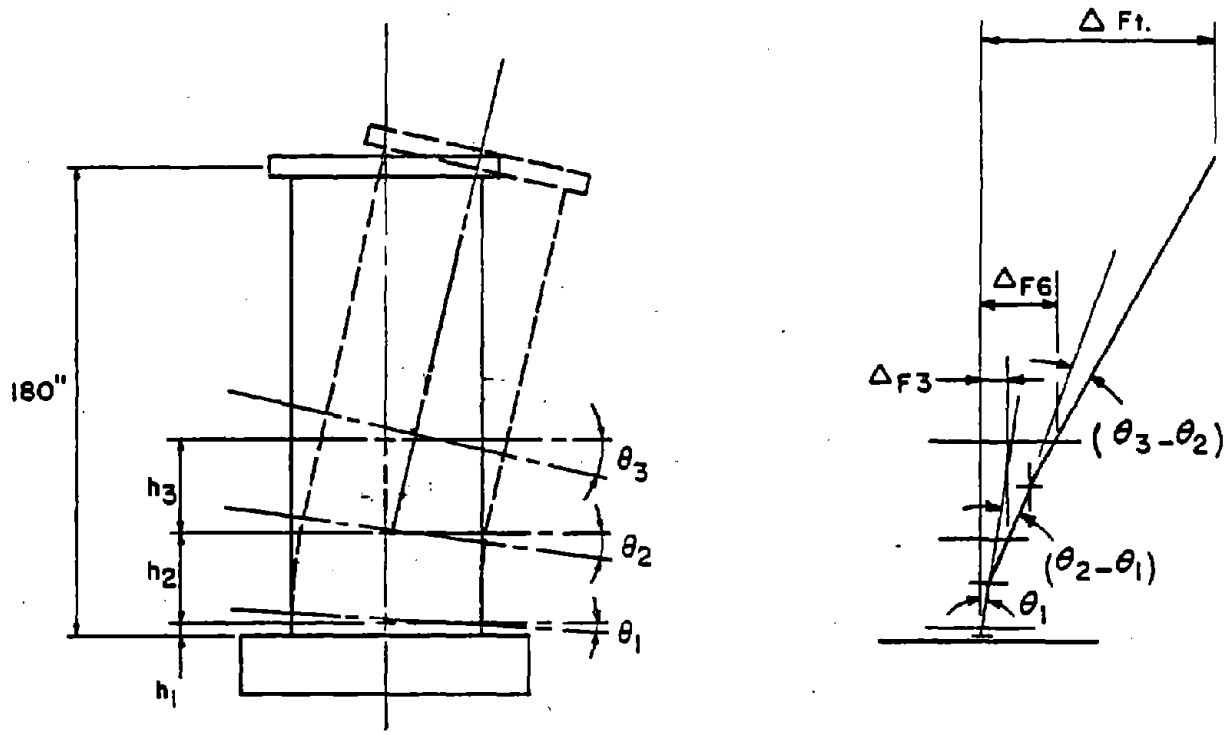

Fig. B-4 Flexural Deformations

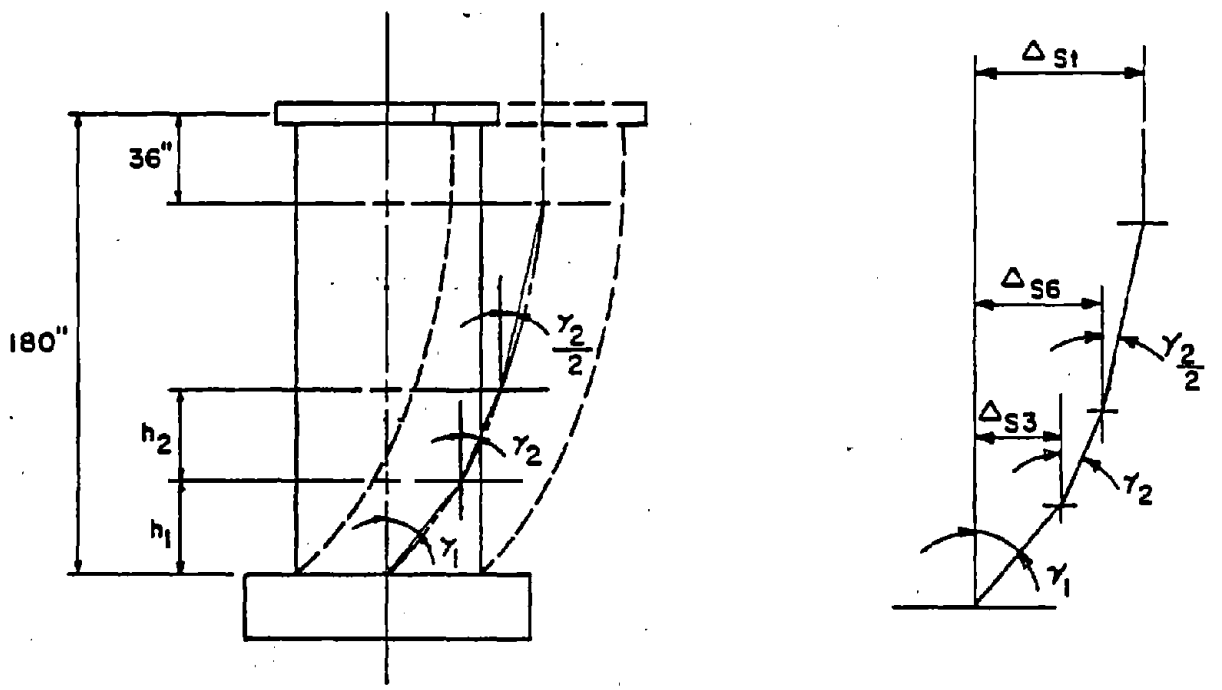

Fig. B-5 Shear Deformations

In order to present the average shear distortion over what is considered the hinging region, a third zone is defined. Zone 3 is from the top of the base block to the 6-ft level. Using the notation defined in Fig. B-4 the average shear distortion in Zone 3 was calculated from the distortions in Zones 1 and 2 by:

$$\gamma_3 = \frac{\gamma_1 \ h_1 + \gamma_2 \ h_2}{h_1 + h_2} \qquad \text{(B-5)}$$

It should be stated that the shear distortions presented here cannot be considered exact values. Because of diagonal cracking, plane sections not remaining plane, and the existence of a moment gradient across the zones, these shear distortions should only be considered as approximate values and an indication of load versus shear deformation behavior.

Slip at Construction Joints

Load versus slip plots are shown for each specimen at Construction Joints CJ1, CJ2, and CJ3. The base construction joint data is an accurate representation of slip at the base joint, CJ1. However, the measurements at CJ2 and CJ3 were often influenced by diagonal cracks passing between the gage brackets and, therefore, are not representation of construction joint slip. These measurements do indicate the horizontal component of a diagonal crack width.

Deflections

Total deflection of the specimen at the 3-ft (0.91 m), 6-ft (1.83 m) and top levels were separated into deflections attributed to base rotation, flexural rotation and shear distortion. This data is presented in two types of figures.

The first type of figure shows the separate components of deflection versus the total deflection in inches. The abscissa

is the displacement ductility ratio using the measured deflection at the full yield load as the yield deflection. Axes of these plots are proportioned so that a 45 degree line represents the total measured deflection.

For specimens subjected to the incrementally increasing load history, the first type of figure shows deflections corresponding to the maximum positive load in the first cycle of each loading increment. For specimens subjected to the modified load history, deflections are shown for the positive loading half of the first inelastic cycle, Cycle 2. A second set of figures shows the deflections for the positive loading half of an inelastic cycle during the latter part of the test. A comparison of these two sets of figures indicates changes in the components of deflection resulting from reversing loads.

The second type of figure shows the deflected shape of the wall at maximum positive and negative loads in various cycles. One plot shows the total deflected shape from measurements at five levels on the specimen. Two other plots show the deflected shape attributed to flexural and shear deformations.

Each set of figures includes the deflected shape in two inelastic cycles at equivalent top deflections that had one or several inelastic cycles between them. This demonstrates the stability of the deflected shape under cycle loading. Also included is the deflected shape immediately before and after significant strength deterioration.

For both types of figures the flexural and shear deflections were caculated from the measured rotations and distortions.

The flexural deflections were calculated assuming the measured rotations over a gage length to be concentrated at the center of that gage length. For the top deflection, the wall between the 6-ft (1.83 m) level and the top was considered rigid. Therefore, using the notation defined in Fig. B-4:

$$\Delta_{F3} = \theta_1\left(h_2 + \frac{h_1}{2}\right) + (\theta_2 - \theta_1)\ \frac{h_2}{2} \qquad \text{(B-6)}$$

$$\Delta_{F6} = \theta_1\left(h_3 + h_2 + \frac{h_1}{2}\right) + (\theta_2 - \theta_1)\left(h_3 + \frac{h_2}{2}\right) + (\theta_3 - \theta_2)\frac{h_3}{2} \quad \text{(B-7)}$$

$$\Delta_{Ft} = \theta_1\left(180 - \frac{h_1}{2}\right) + (\theta_2 - \theta_1)\left[180 - \left(h_1 + \frac{h_2}{2}\right)\right] + (\theta_3 - \theta_2)\left[180 - \left(h_1 + h_2 + \frac{h_3}{2}\right)\right] \quad \text{(B-8)}$$

The shear deflections at the 3-ft and 6-ft (0.91 m and 1.83 m) levels were calculated as described under instrumentation. In calculating the shear deflection at the top of the wall, the shear strain was assumed to be zero at a distance of 36 in. (0.91) m) (- d/2) from the top. There would actually be some elastic shear deformation in this top segment, however, the magnitude is insignificant. An average shear distortion of $\gamma_2/2$ was assumed over the distance from the 6-ft level up to 36 in. from the top of the wall. Therefore, using the notation defined in Fig. B-5:

$$\Delta_{S3} = \gamma_1 h_1 \quad \text{(B-9)}$$

$$S6 = \gamma_1 h_1 + \gamma_2 h_2 \quad \text{(B-10)}$$

$$St = \gamma_1 h_1 + \gamma_2 h_2 + \frac{\gamma_2}{2}[180 - (h_1 + h_2 + 36)] \quad \text{(B-11)}$$

The calculated flexural and shear deflections at the 3-ft and 6-ft levels are as accurate as the measured data. The deflection components calculated for the top of the wall are considered approximate values and are presented as extrapolated data.

Base Slip Versus Shear Distortions

In the deflection component analysis described above no attempt was made to separate the construction joint slip from the shear deflections because of the previously indicated limitation of the slip data. However, since the base joint slip data is considered accurate, it was separated from the

shear deflection at the 3-ft level. For each specimen, the base slip is shown on two figures as a percentage of the total shear deflection at the 3-ft (0.91 m) level. For specimens subjected to the incrementally increasing load history, the data is presented at the maximum positive and negative loads in the first cycle of each loading increment. For specimens subjected to the modified load history, the data is presented for the first inelastic cycle, Cycle 2, and for an equivalent inelastic cycle during the latter part of the test.

Reinforcing Strains

Several types of figures showing reinforcing steel strain data are presented for each specimen.

The first type shows cyclic load versus strain relationships for two vertical bars in the boundary elements, for two horizontal bars in the web and for two confinement hoops. The other types of figures show the strain gradient over the height of the wall and across horizontal sections at several locations for vertical, horizontal and confinement reinforcement.

The strain gages used on the reinforcing steel usually lost bond with the steel between a strain of 0.015 and 0.030. Therefore, on the majority of figures, the strain scale was limited to 0.0125. A dashed arrow and cycle number indicate when a strain gage stopped functioning or the gage reading went off scale.

Specimen B6

Test Description

Specimen B6 was similar to Specimen B5 in the Phase I test series[1] and B7 in Phase II test series. It had 3.67% vertical reinforcement in each column and confinement reinforcement in the lower 6-ft of the boundary elements. However, the design compressive strength of the concrete in B6 was 3,000 psi (20.7 MPa). Specimen B5 and B7 were designed for 6000 psi (41.4 MPa) concrete. Specimen B6 was loaded with a uniform axial load of 423 psi (2.92 MPa). This axial load corresponds to 10% of the axial load capacity of the wall.

The test consisted of 26 loading cycles as shown in Fig. B-6. The load versus top deflection relationship for Specimen B6 is shown in Figs. B-7 and B-8. The complete load versus deflection relationship at the 6-ft level is shown in Fig. B-9.

The first significant cracking was observed in Cycle 4 at a load of 45 kips (200 kN). First yielding occurred in Cycle 16 at a load of 144.2 kips (641.4 kN). Maximum measured crack widths at this stage were 0.005 in. (0.13 mm) in the tension column and 0.014 in. (0.36 mm) across a diagonal crack in the web.

Diagonal cracks directed toward the outer compression face at the base of the wall were at an angle of approximately 39° from vertical in Specimen B6. The crack pattern at +3 in. (76.2 mm) and -3-in. deflections is shown in Figs. B-10 and B-11.

First indication of splitting in the concrete cover of the outer compression face was noted in Cycle 16. Significant crushing of the concrete cover occurred in Cycle 22. A slight reverse curvature developed in the lower 3 ft of the boundary elements during Cycle 22.

First indication of spalling and flaking along diagonal cracks occurred in Cycle 23. A slight indication of crushing of a compression strut in the right side of the web approximately 18 in. above the base was noted in Cycle 24.

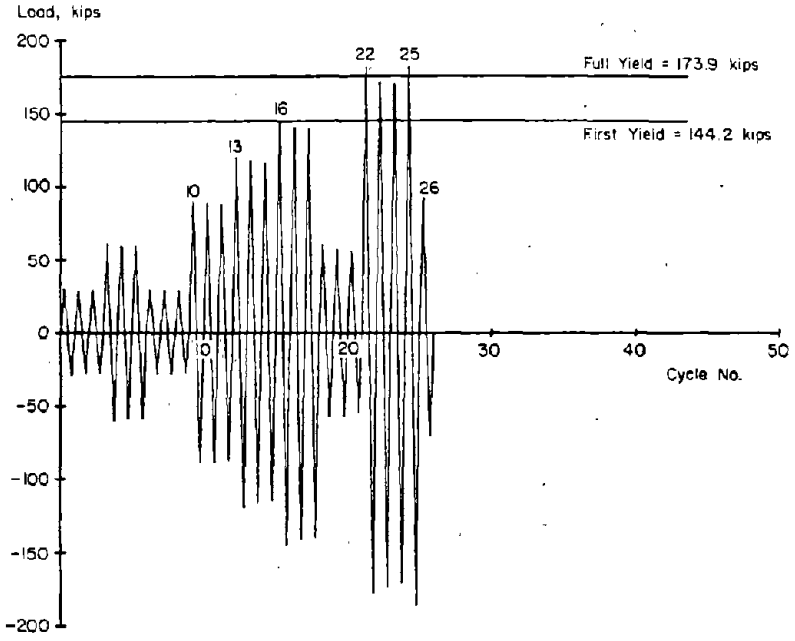

a) Load History

1 in. = 25.4 mm

1 kip = 4.448 kN

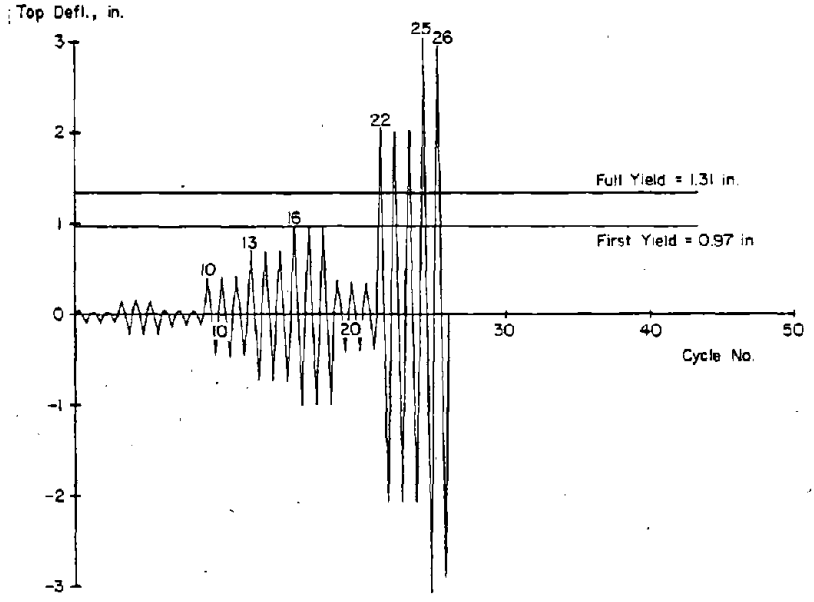

b) Deflection History

Fig. B-6 Loading History for Specimen B6

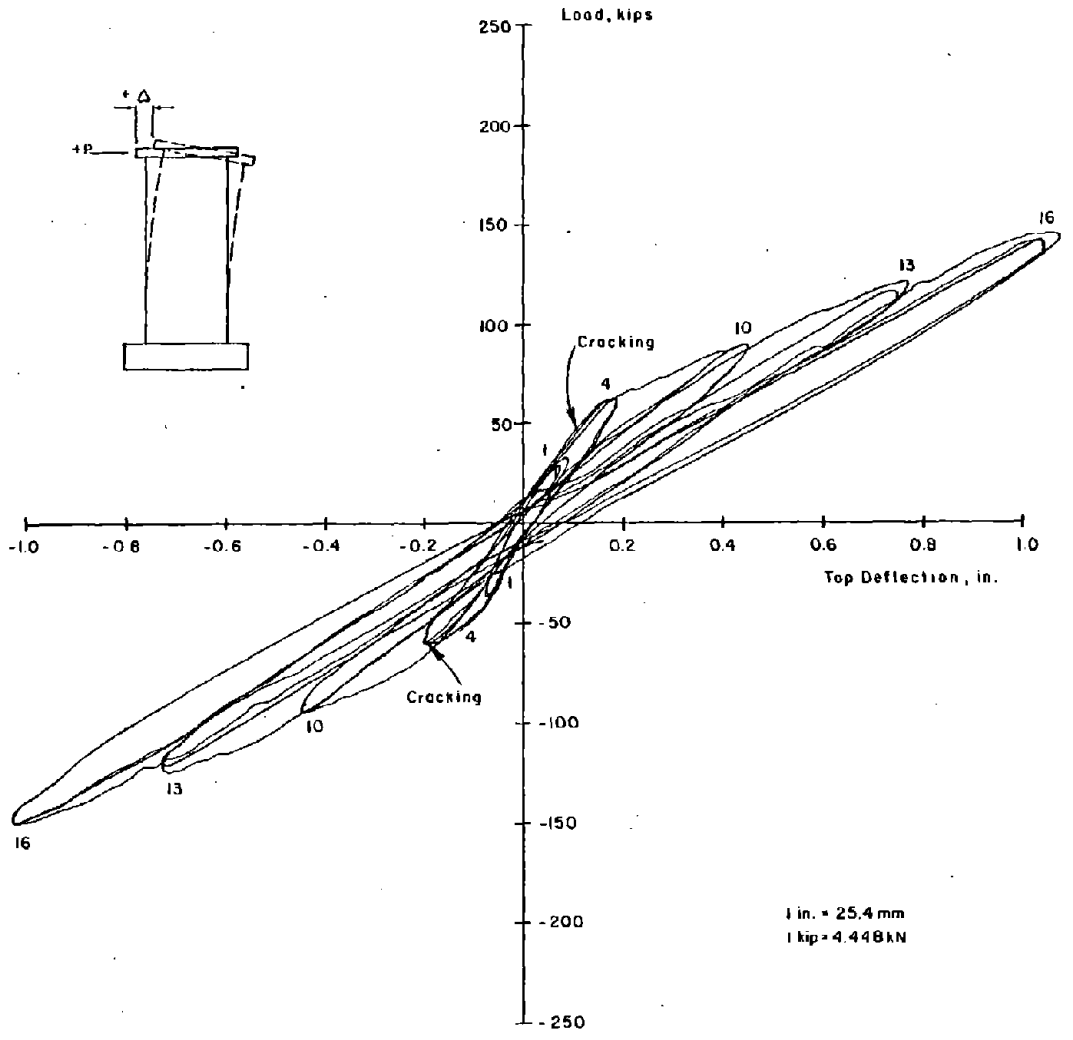

Fig. B-7 Continuous Load - Top Deflection for Initial Cycles for Specimen B6

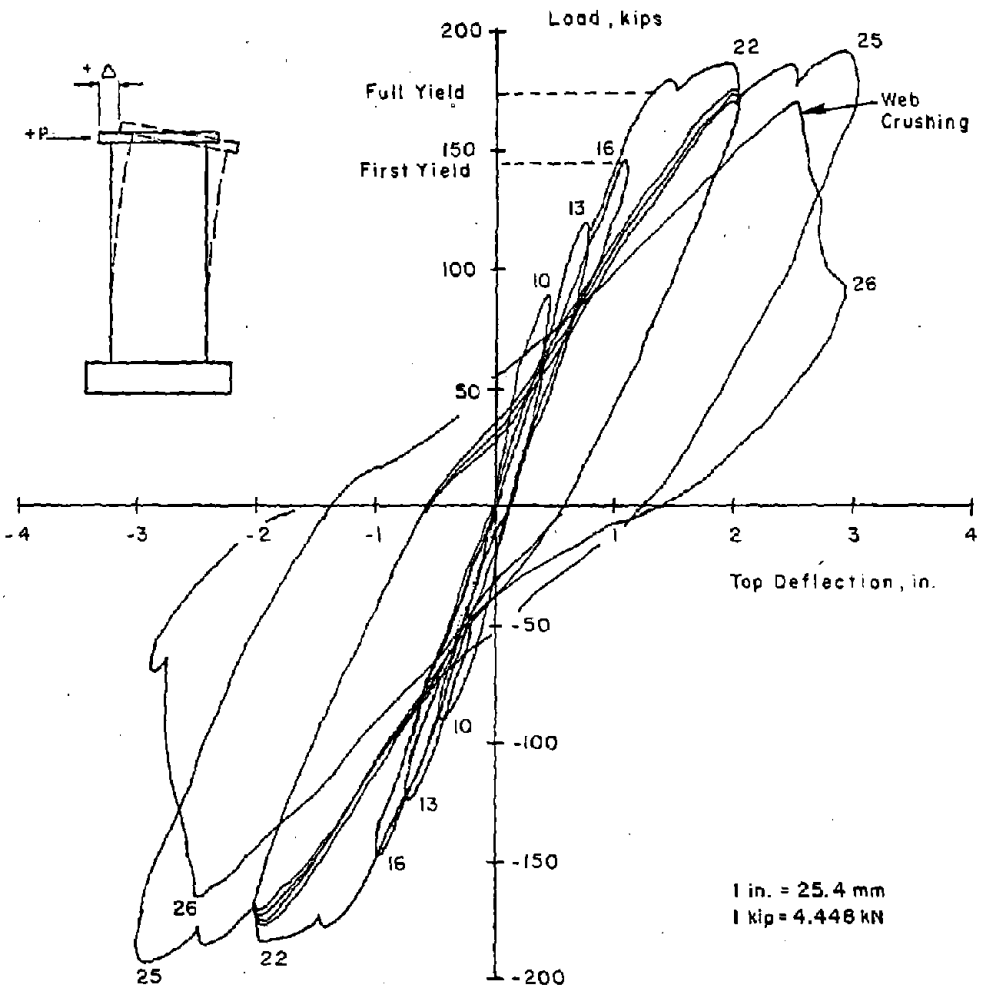

Fig. B-8 Continuous Load - Top Deflection for Specimen B6

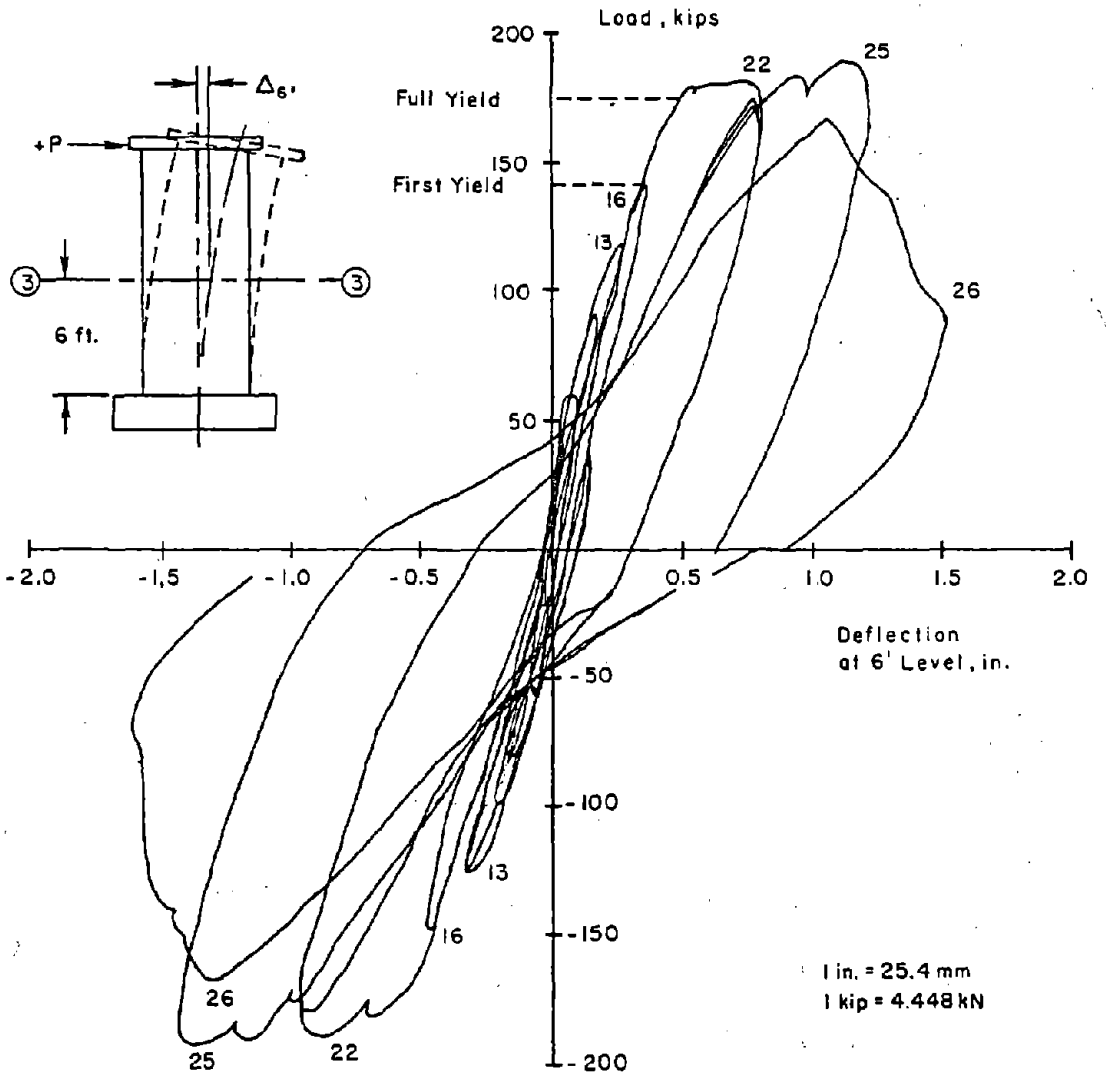

Fig. B-9 Continuous Load - Deflection at 6 ft Level for Specimen B6

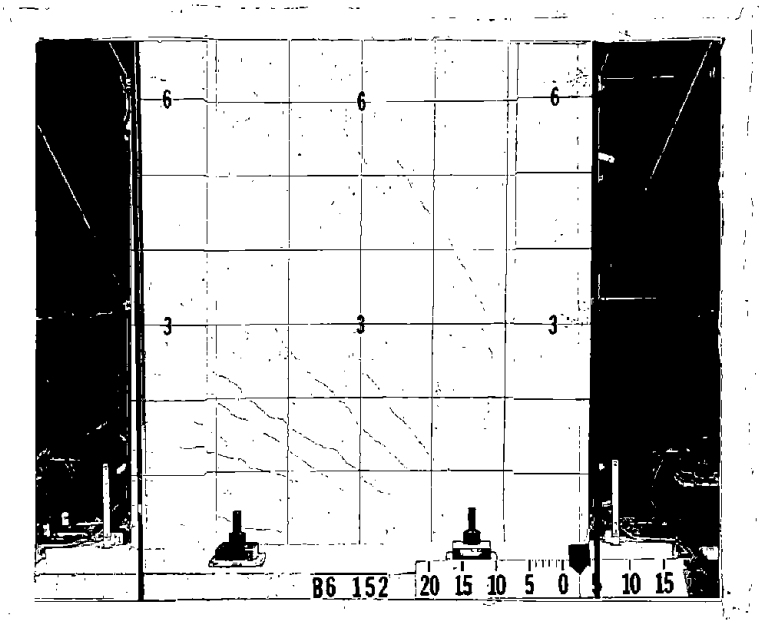

Fig. B-10 Cracking Pattern at +3 in. Deflection for Specimen B6

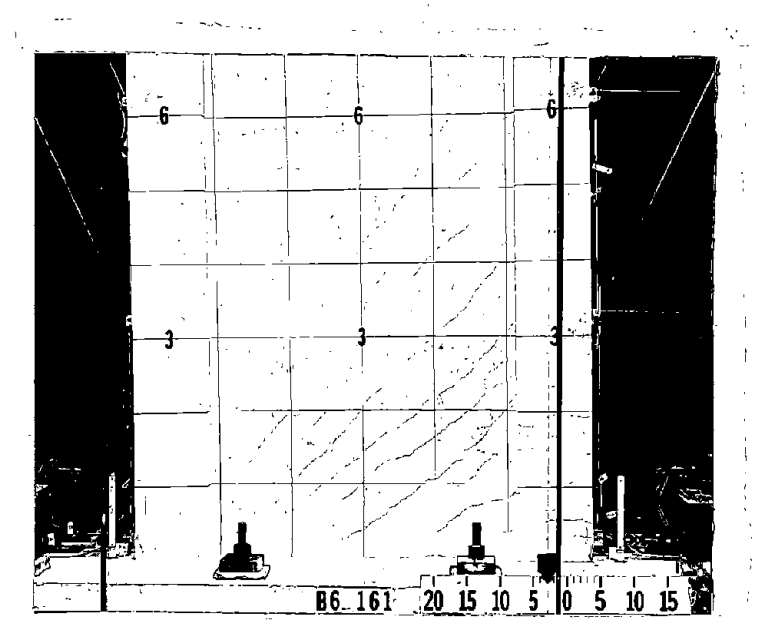

Fig. B-11 Cracking Pattern at -3 in. Deflection for Specimen B6

This crushing increased in Cycle 25 as the wall was loaded with the first 3-in. deflection cycle. However, the load capacity continued to increase.

The maximum load measured, 185.5 kips (825.1 kN), occurred in Cycle 25 at a -3-in. (76.2 mm) deflection. This load corresponds to a nominal shear stress, $v_{max} = 13.8 \sqrt{f'_c}$ ($1.15 \sqrt{f'_c}$, MPa). The design shear capacity using the 1971 ACI Building Code equations (11-13) and (11-33) was 132 kips (587.1 kN). This corresponds to a nominal shear stress of $v = 9.7 \sqrt{f'_c}$ ($0.81 \sqrt{f'_c}$ MPa). This design allowed $3.3 \sqrt{f'_c}$ ($0.27 \sqrt{f'_c}$, MPa) in the concrete with the steel taking $6.4 \sqrt{f'_c}$ ($0.53 \sqrt{f'_c}$ MPa) at 60 ksi.

As the specimen was being loaded to a +3-in. deflection in Cycle 26, several compression struts crushed simultaneously. The crushing occurred in the struts immediately above those that intercepted the base of the column. Load from crushed struts was transferred to higher and lower struts. Several lower struts then crushed. However, a complete horizontal failure plane did not form as was the case for Phase I specimens, which had no axial load. Instead, struts sheared through along a vertical plane. Figures B-12 and B-13 show the specimen prior to and after web crushing.

The fact that a horizontal failure plane did not develop is attributed to the increased stiffness of the boundary element in the presence of axial load. The vertical failure plane may not have developed if floor slabs had been present at the story levels.

As the load capacity was dropping the specimen was "caught" by closing the deflection control valve in the hydraulic system. The measured load at this stage had decreased to 49% of the maximum measured load.

The specimen sustained at least 80% of the maximum measured load capacity through 4 inelastic cycles. The last inelastic loading increment in which the load was at or above 80% of the maximum for all 3 cycles was $\pm$2 in. (50.1 mm).

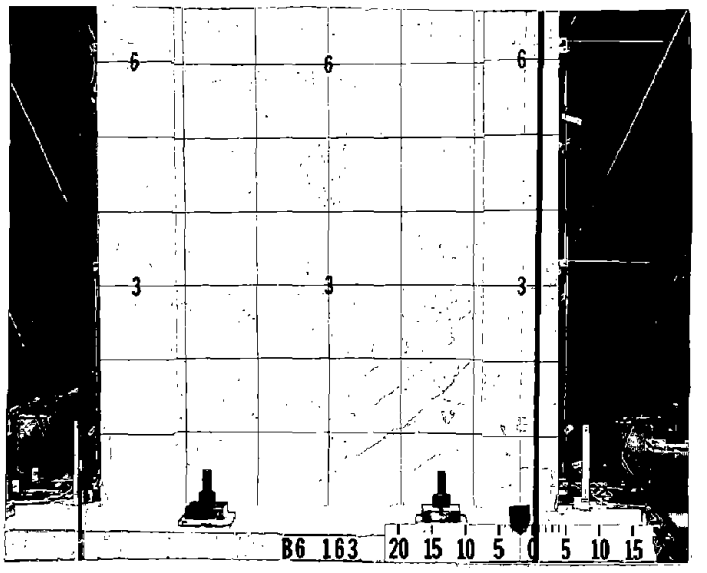

Fig. B-12 Specimen B6 Prior to Web Crushing

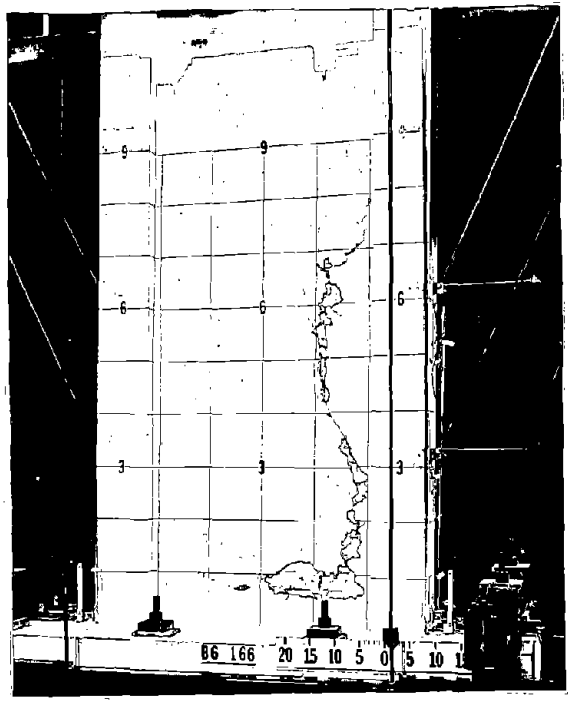

Fig. B-13 Specimen B6 After Web Crushing

Although the web was considerably damaged at the end of the test, the columns were in good condition. This wall could have been repaired by replacing the web.

Discussion of Results

Moment-Rotation. Moment-rotation data for Specimen B6 are shown in Fig. B-14. The maximum measured moment was 97% of the calculated monotonic maximum. This calculated maximum was based on attainment of an ultimate compressive strain of $\varepsilon_u = 0.0045$ in the boundary element.

The relationship between calculated monotonic and measured rotations at the 3-ft (0.91 m) and 6-ft (1.83 m) levels is similar to that observed in the previously reported tests without axial load. Rotations tended to concentrate in the lower 3 ft of the wall to a greater extent than was assumed in calculations.

Shear Distortion. The shear-distortion loops for B6 are shown in Fig. B-15. As in the previously reported tests without axial load, a shear "yielding" occurred during the same cycle in which flexural yielding occurred. However, this "yielding" is not as evident in the 3-ft to 6-ft zone. A major portion of the shear distortions occurred in the lower 3 ft (0.91 m). This differs from the shear distortion distribution observed in specimens without axial load in which shear distortions were more evenly distributed throughout the lower 6 ft (1.83 m).

For Cycle 25 pinching is evident in all three zones.

Slip at Construction Joints. The slip at construction joints in B6 is shown in Fig. B-16. The slip at CJ1 exhibits yielding similar to shear "yielding" during the same cycle that flexural yielding occurred. As shown in Fig. B-17, the slip at CJ1 was a relatively constant 10% of the total shear deflection in the lower 3 ft (0.91 m).

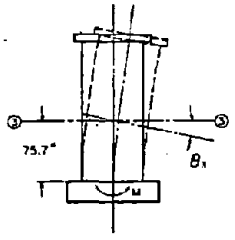

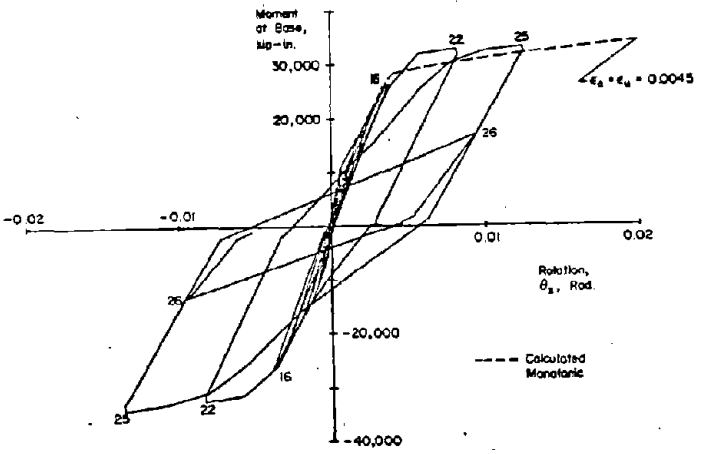

a) At 6 ft Level

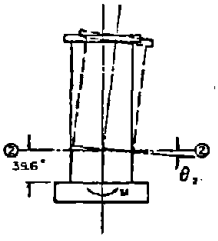

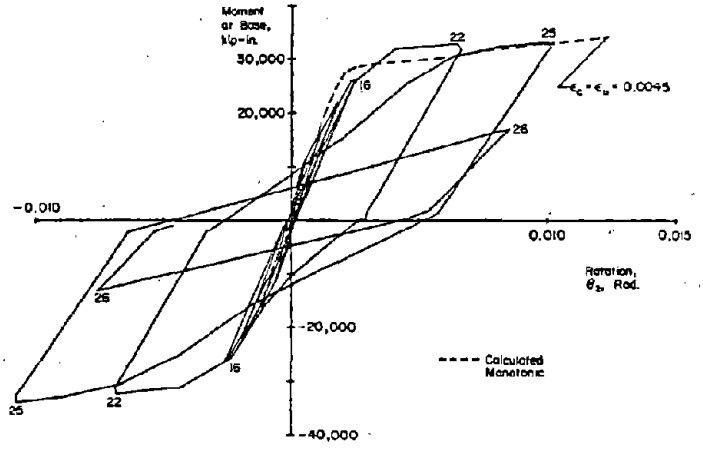

b) At 3 ft Level

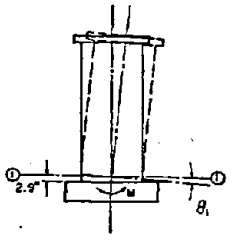

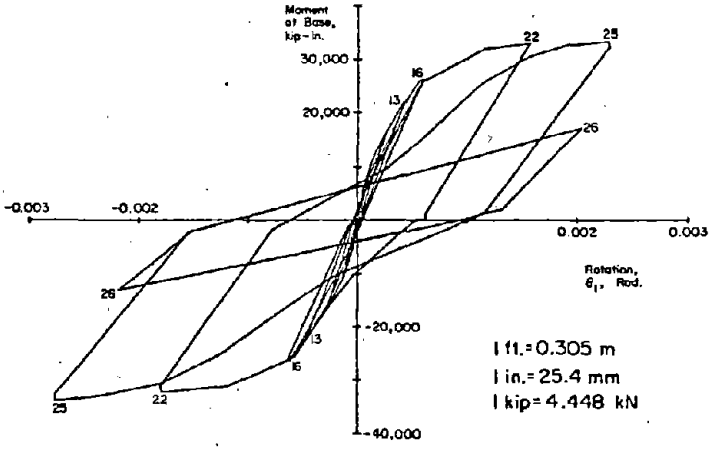

c) At Base Level

Fig. B-14 Moment at Base versus Rotation for Specimen B6

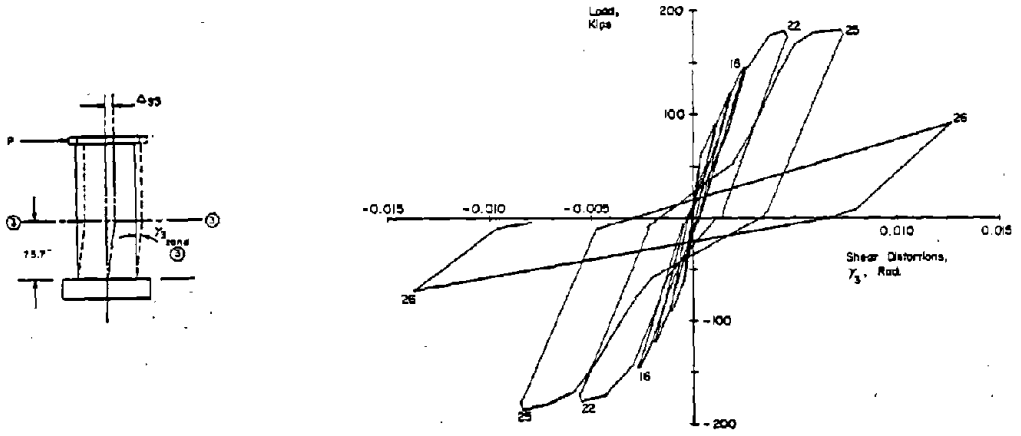

a) In Base to 6 ft Level

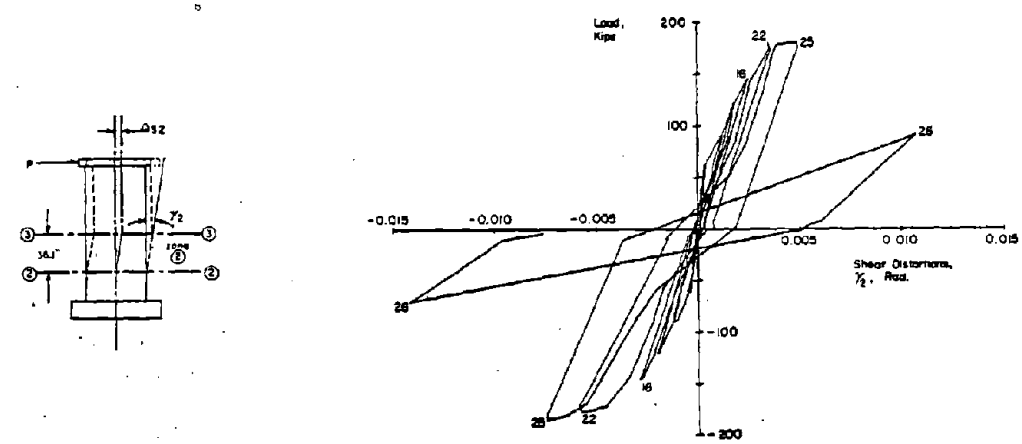

b) In 3 ft to 6 ft Level

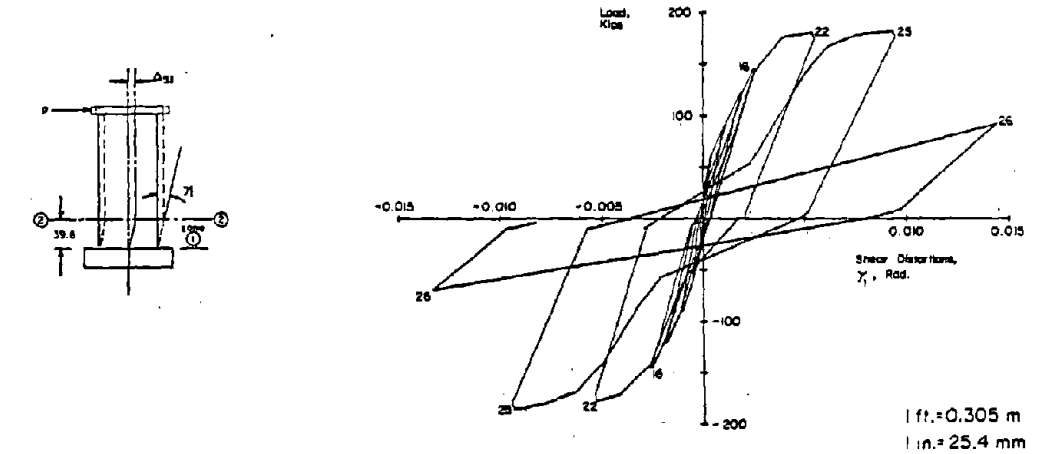

c) In Base to 3 ft Level

Fig. B-15 Load versus Shear Distortion for Specimen B-6

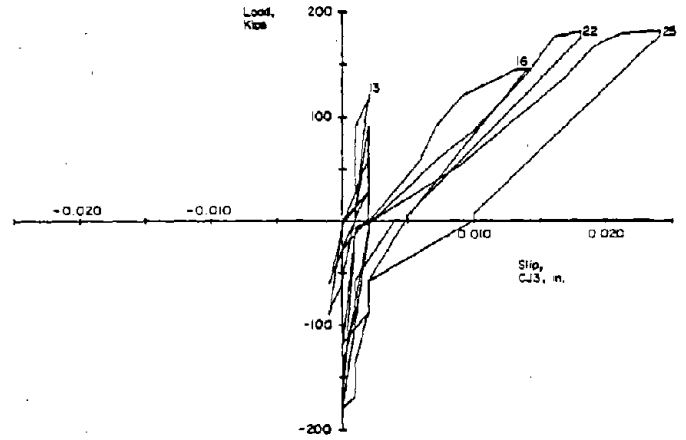

a) At 6 ft Level

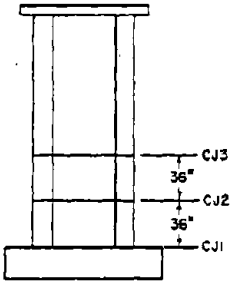

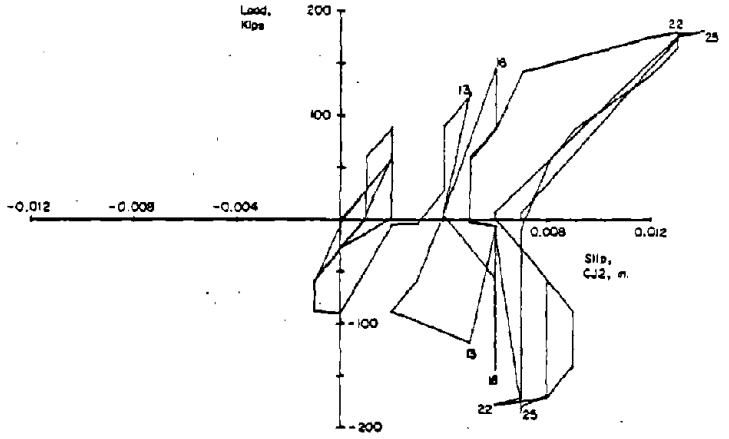

b) At 3 ft Level

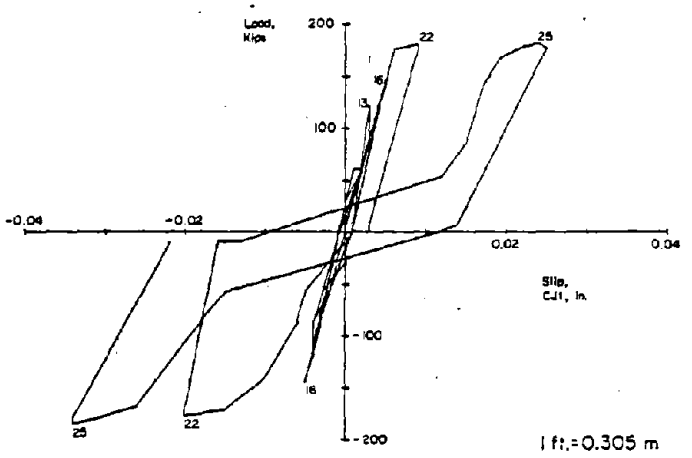

c) At Base Level

1 ft.=0.305 m
1 in.=25.4 mm
1 kip=4.448 kN

Fig. B-16 Load versus Slip at Construction Joints for Specimen B6

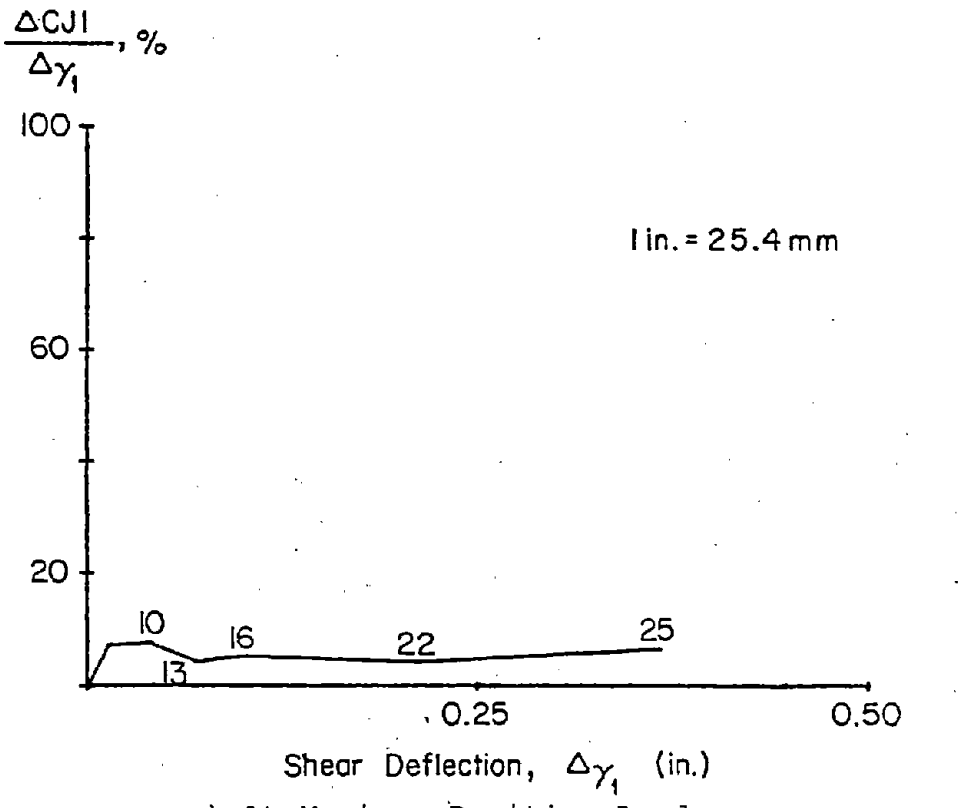

a) At Maximum Positive Loads

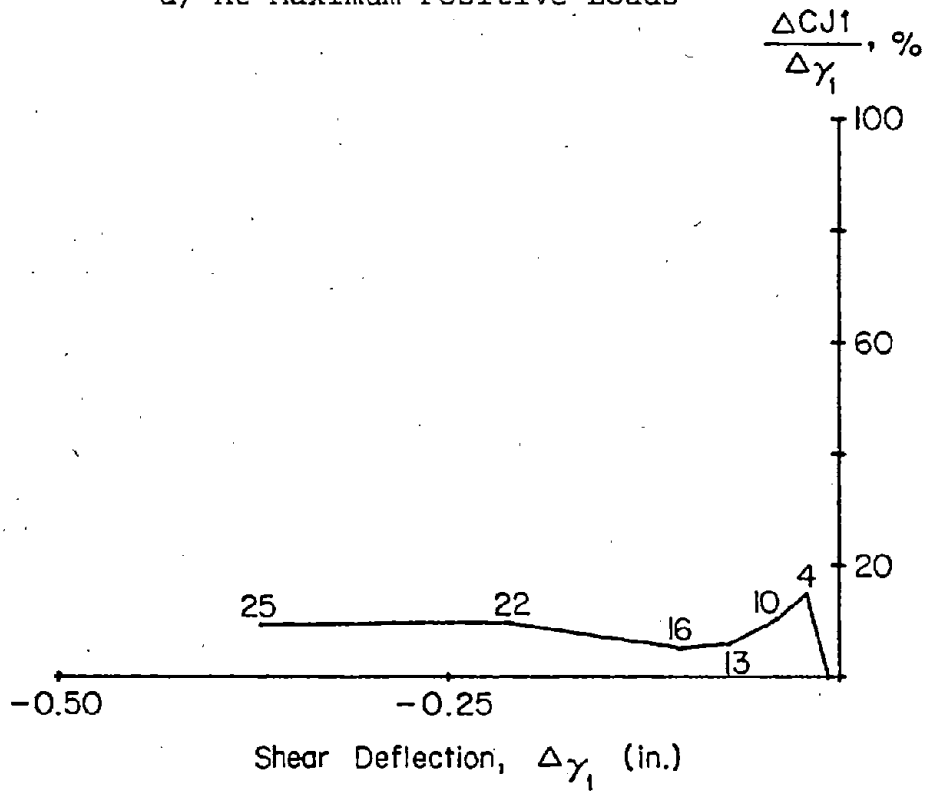

b) At Maximum Negative Loads

Fig. B-17 Slip at Base Construction Joint versus Shear Deflection in Zone 1 for Specimen B6

The plots for CJ2 and CJ3 are unsymmetrical. Measurements were affected by diagonal cracking.

Deflections. Deflection components and deflected shapes are shown in Figs. B-18 and B-19. These figures indicate that shear deflections were a relatively constant portion of the total throughout most of the test, but increased slightly near the end of the test.

Deflected shapes for Cycles 22 and 24 show only a slight decrease in shear stiffness during the 2 in. (50.8 mm) increment.

Reinforcement Strains. Figures B-20 through B-23 show reinforcement strains in the specimen at various stages.

Figure B-20 shows that outer bars in the compression elements near the base, were in compression in every cycle. Figure B-21 shows that yielding occurred up to the 6-ft (1.83 m) level in cycle 25.

Figures B-22 and B-23 show the strain gradient in the vertical reinforcement at various levels.

Figures B-24 through B-28 show the cyclic strain-load relationship and the strain gradients in the horizontal bars. These figures indicate considerable yielding between the 3-ft to 9-ft (0.91 m to 2.74 m) level. Figures B-25 and B-26 for gages HH and HA indicate that, although no yielding occurred near the end hooks, appreciable stresses were present. This was especially the case in the lower 18 in. (0.46 m), because the boundary elements act as dowels in this region.

Figures B-29 through B-30 show the cyclic strain-load relationships and the vertical strain gradient in the outer leg of the confinement hoops. These figures indicate that hoops in the lower two feet were stressed significantly although no yielding occurred. The maximum measured hoop strain occurred at a level 10 in. (0.25 m) above the base.

a) At Top of Wall

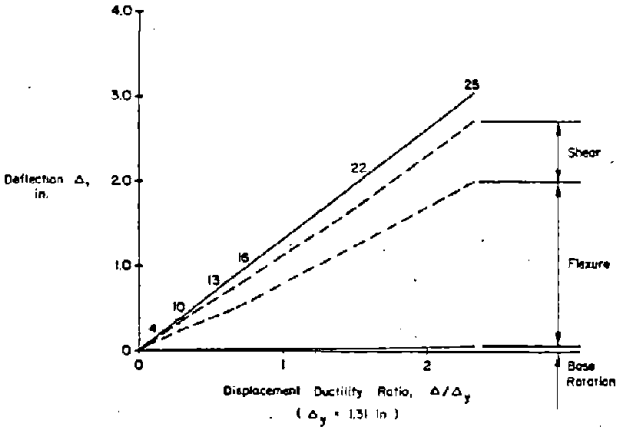

b) At 6 ft Level

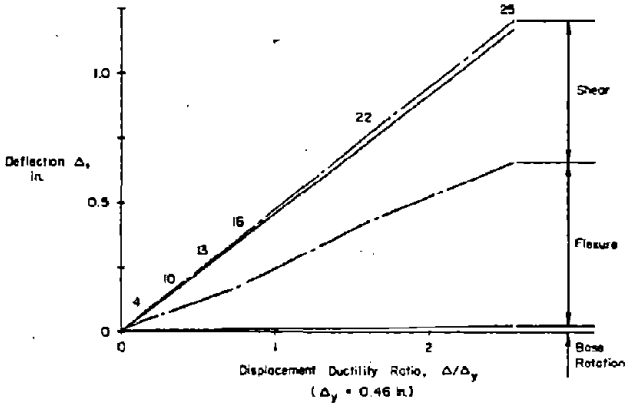

c) At 3 ft Level

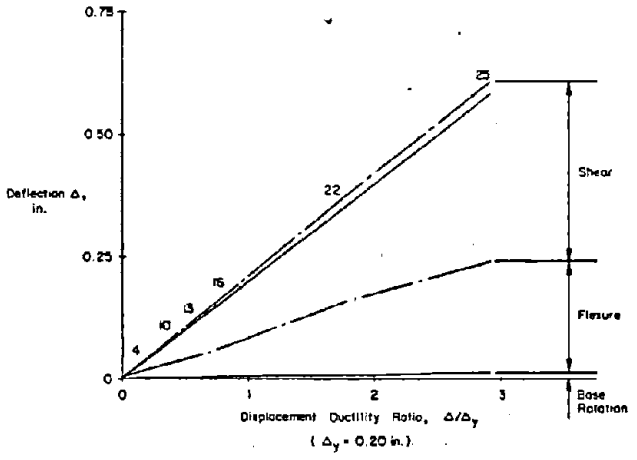

—— CALCULATED FROM MEASURED DEFOMATION
---- EXTRAPOLATED
—— MEASURED TOTAL

1 in. = 25.4 mm
1 ft. = 0.305 m

Fig. B-18 Components of Deflection for Specimen B6

a) Flexural

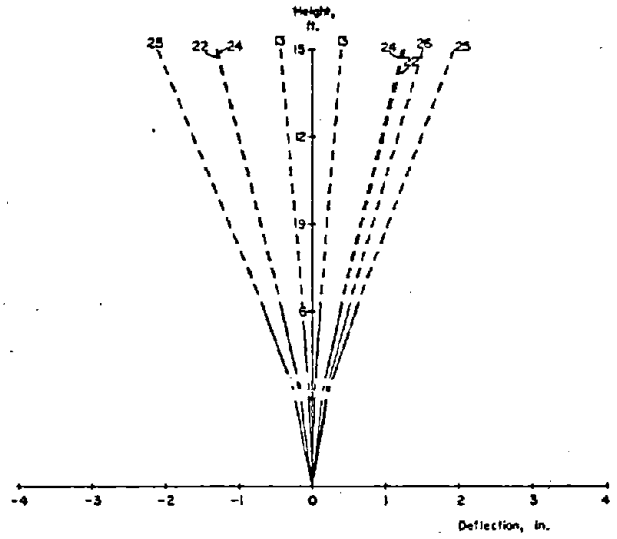

b) Shear

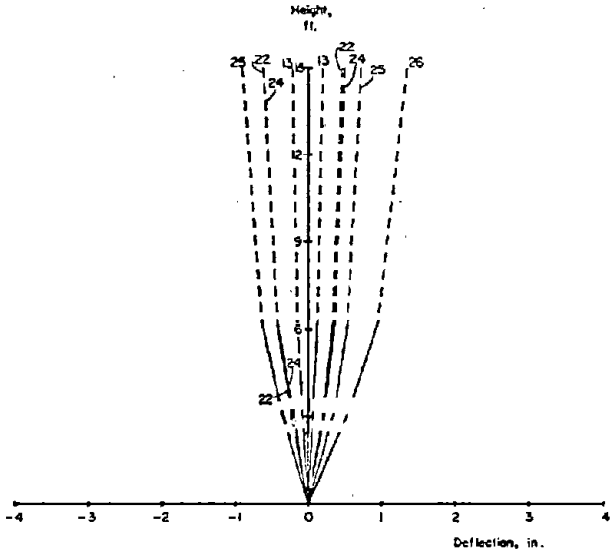

c) Total

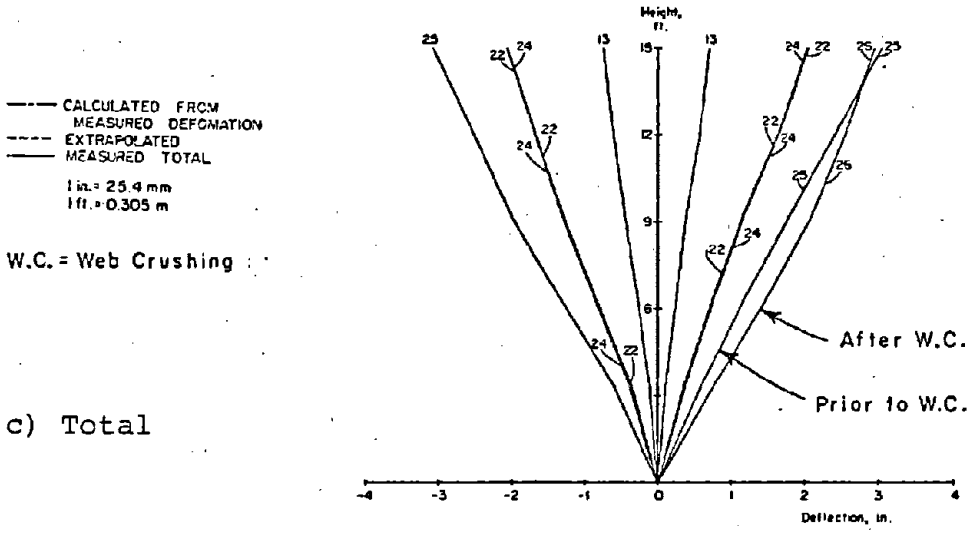

Fig. B-19 Deflected Shape for Specimen B-6

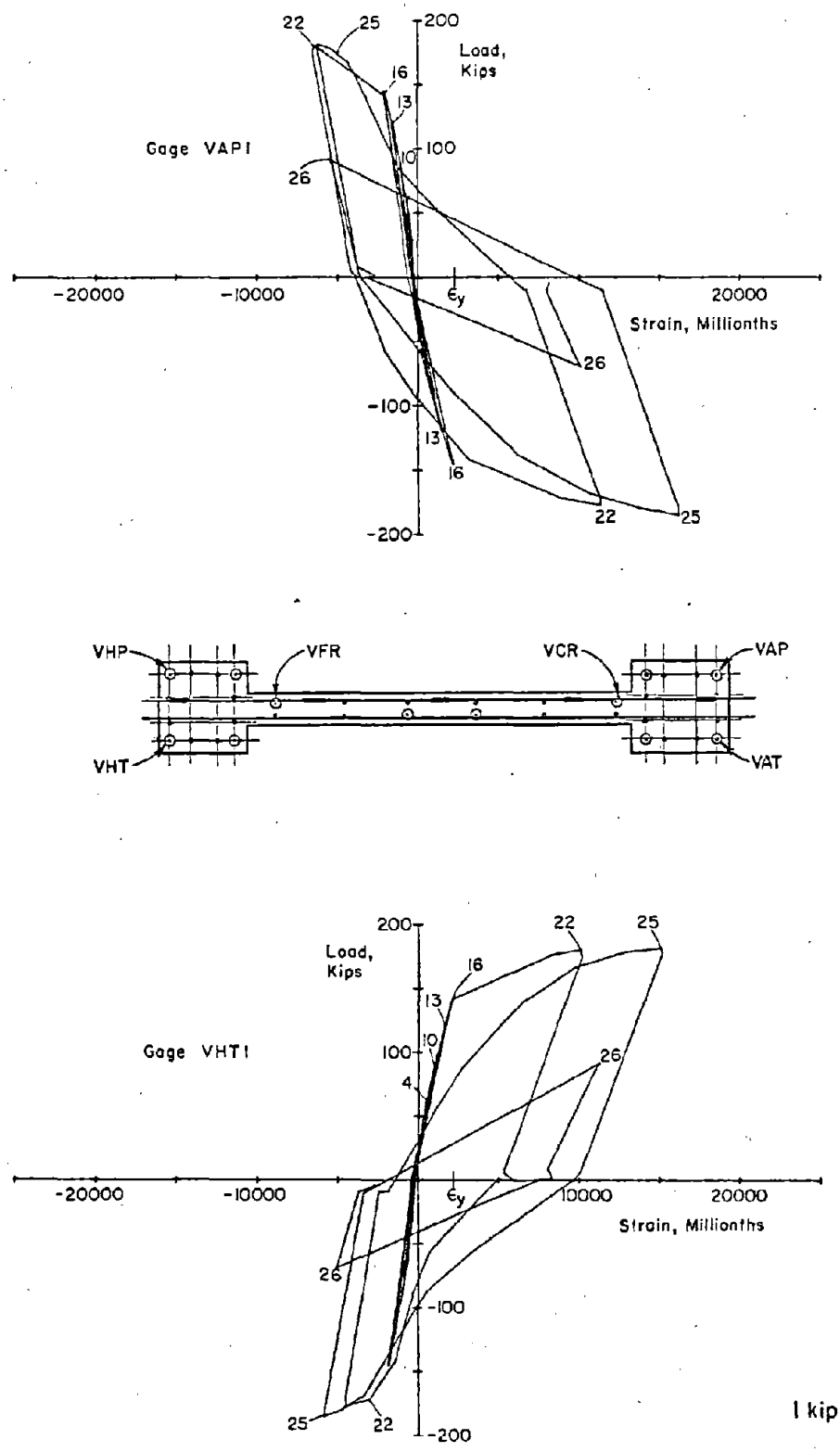

Fig. B-20 Measured Strains on Vertical Reinforcement at Base of Specimen B6

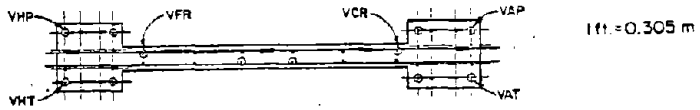

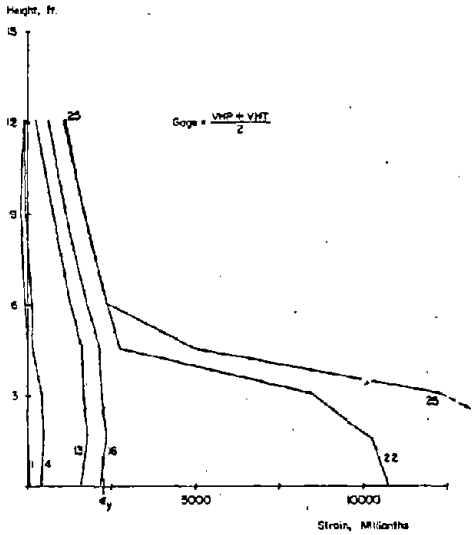

a) Average of VHP and VHT

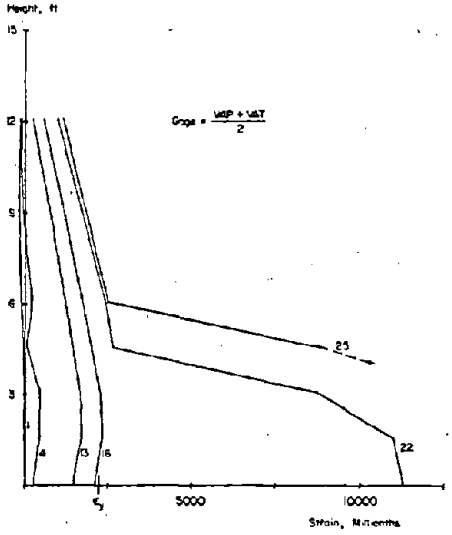

b) Average of VAP and VAT

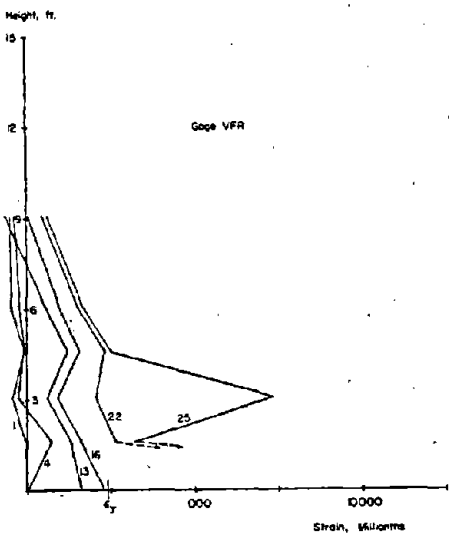

c) Strain Gage VFR

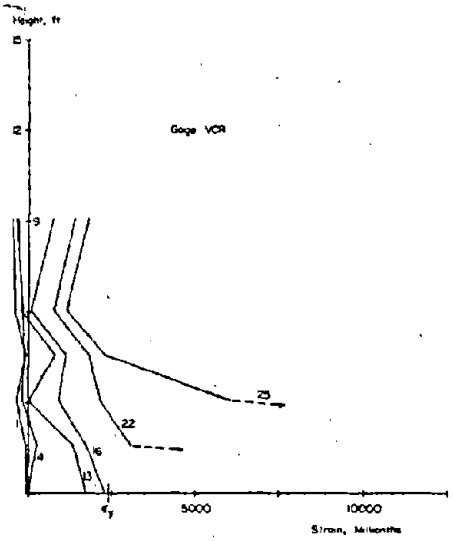

d Strain Gage VCR

Fig. B-21 Vertical Reinforcement Strains at Maximum Loads for Specimen B6

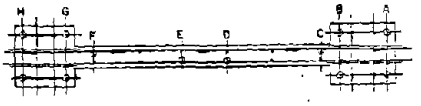

1 ft.=0.305 m

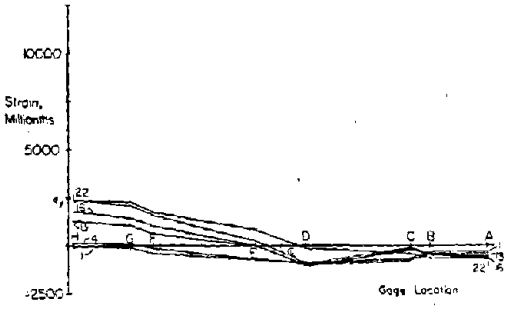

a) At 6 ft Level

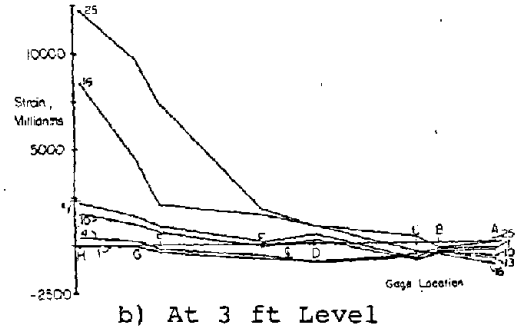

b) At 3 ft Level

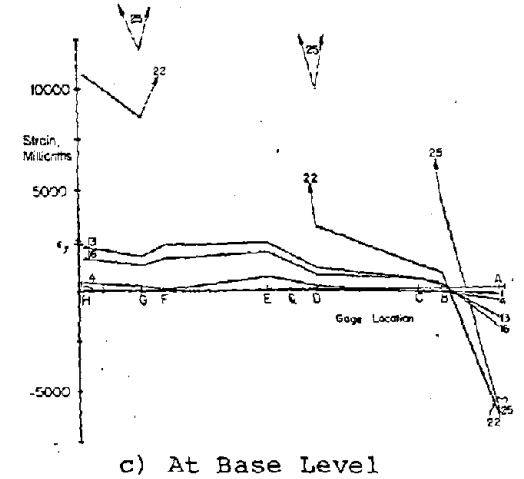

c) At Base Level

Fig. B-22 Vertical Reinforcement Strains at Maximun Positive Loads for Specimen B6

1 ft.=0.305 m

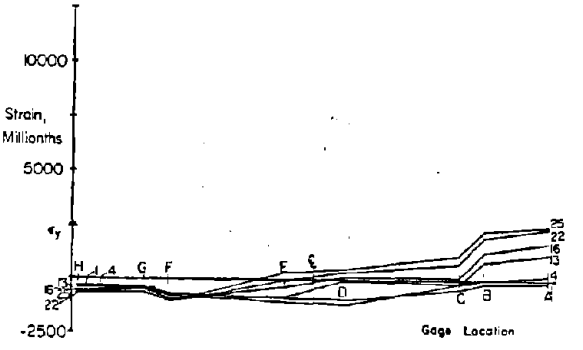

a) At 6 ft Level

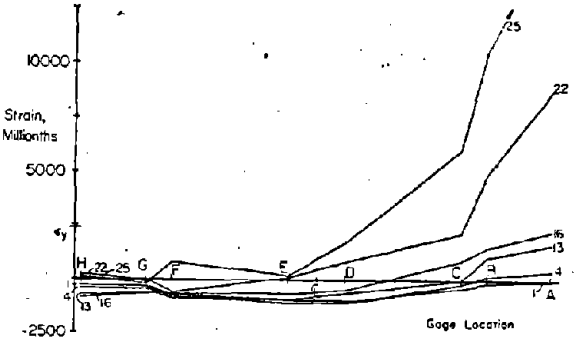

b) At 3 ft Level

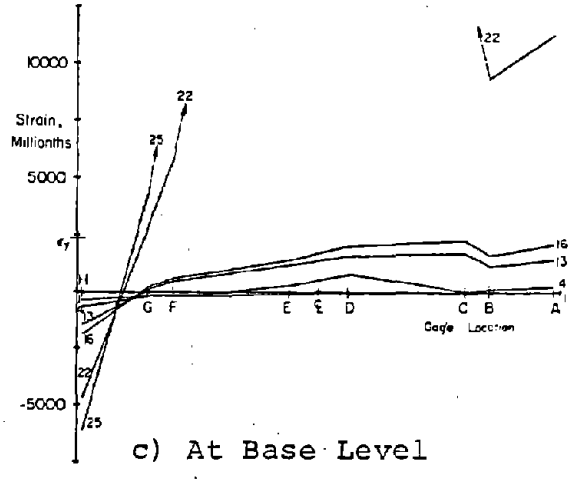

c) At Base Level

Fig. B-23 Vertical Reinforcement Strains at Maximum Negative Loads for Specimen B6

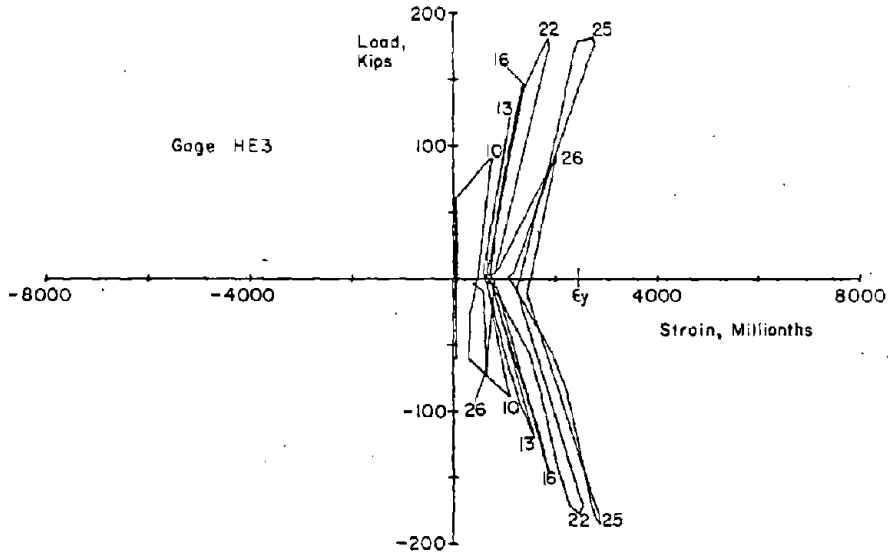

1 in. = 25.4 mm
1 kip = 4.448 kN

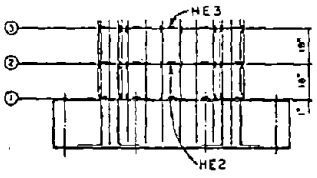

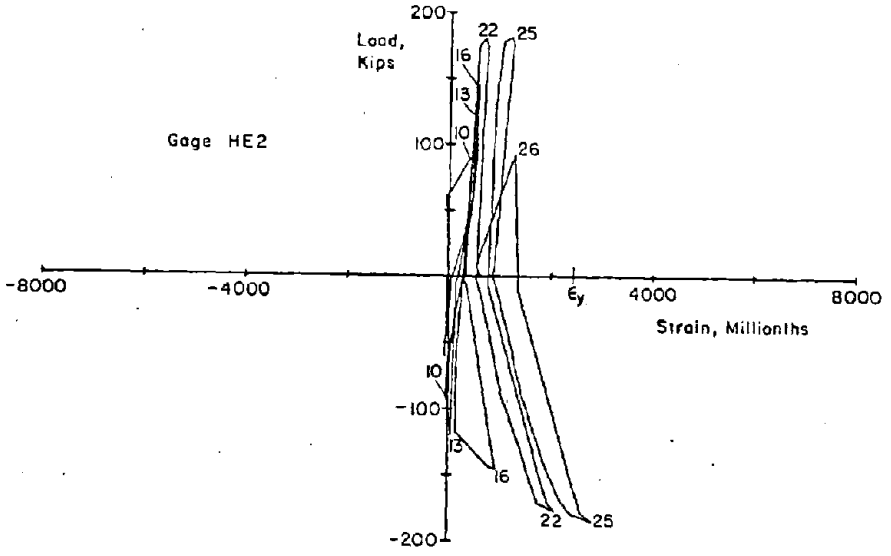

Fig. B-24 Measured Strains on Horizontal Reinforcement for Specimen B6

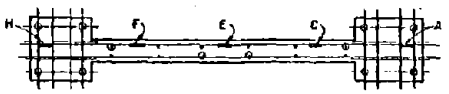

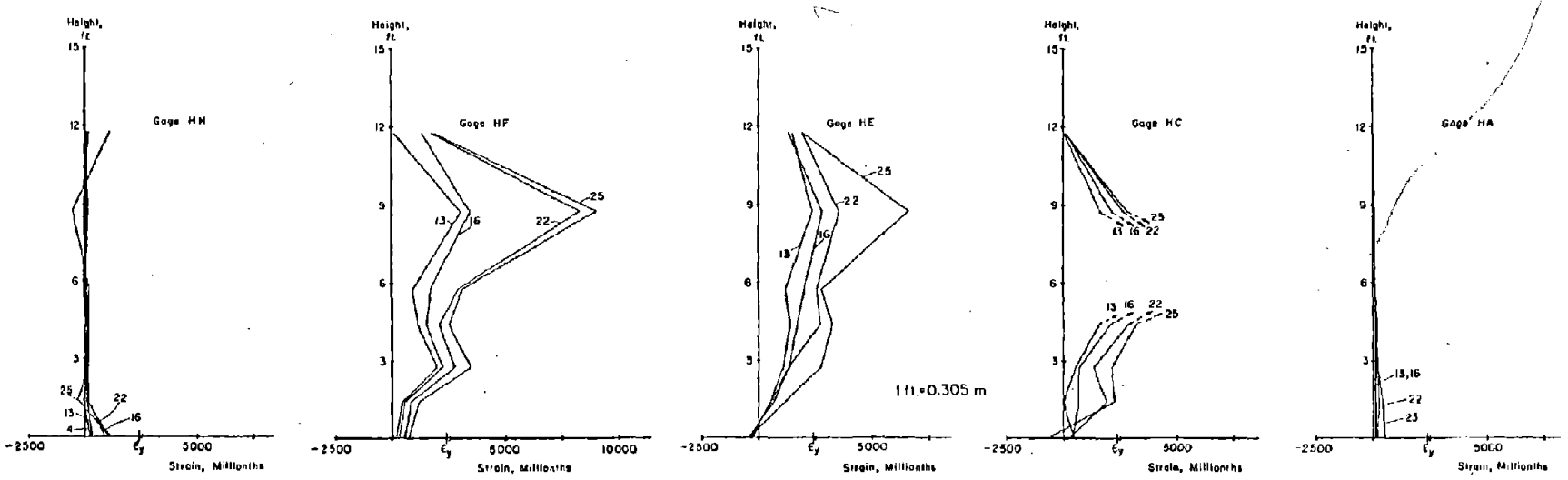

Fig. B-25 Horizontal Reinforcement Strains at Maximum Positive Loads for Specimen B6

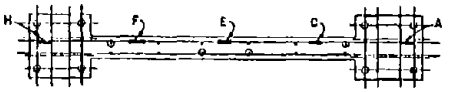

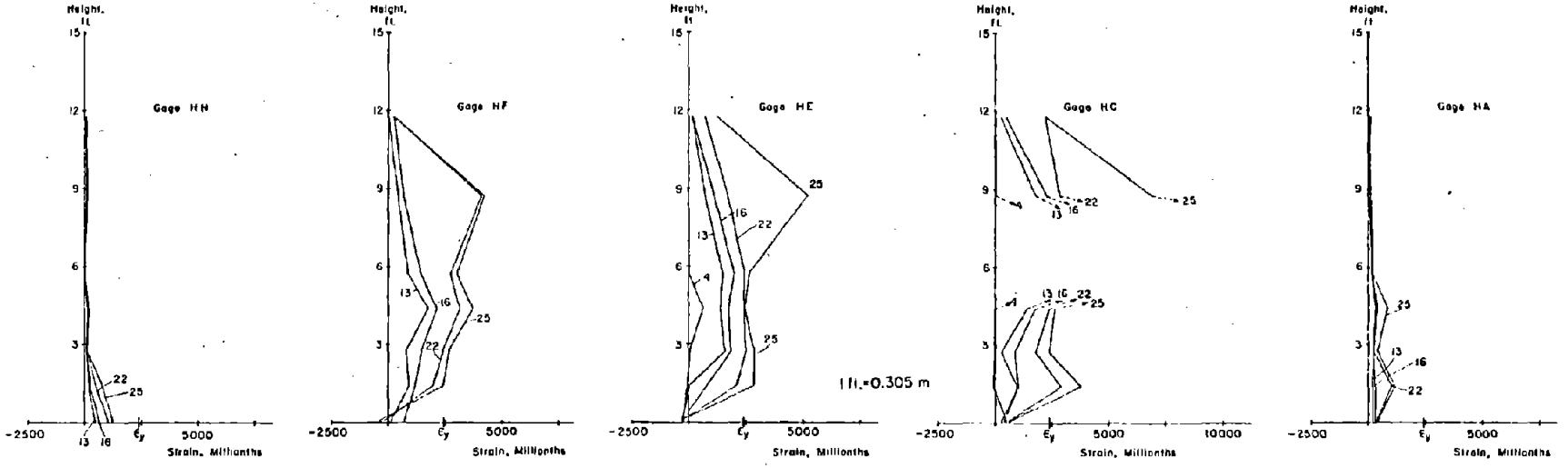

Fig. B-26 Horizontal Reinforcement Strains at Maximum Negatife Loads for Specimen B6

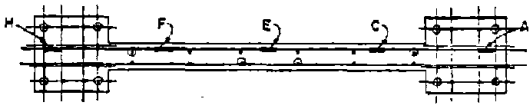

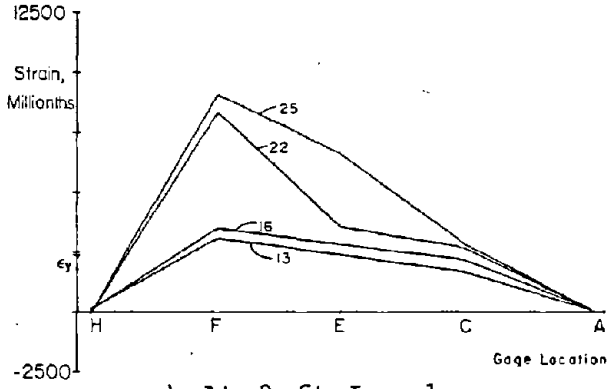

a) At 9 ft Level

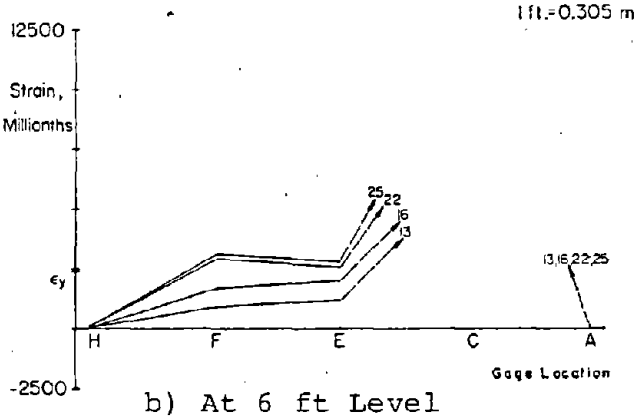

b) At 6 ft Level

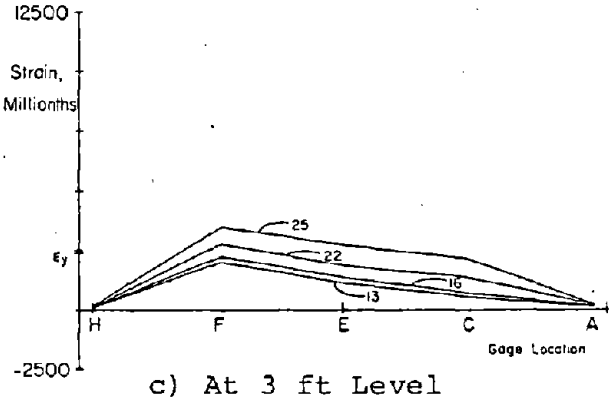

c) At 3 ft Level

Fig. B-27 Horizontal Reinforcement Strains in Web at Maximum Positive Loads for Specimen B6

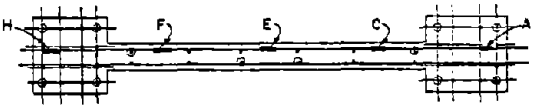

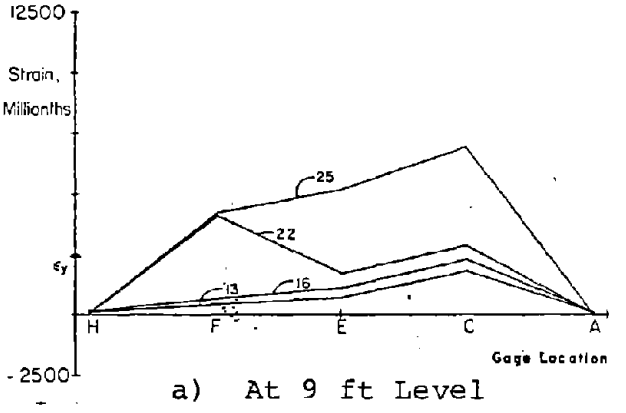

a) At 9 ft Level

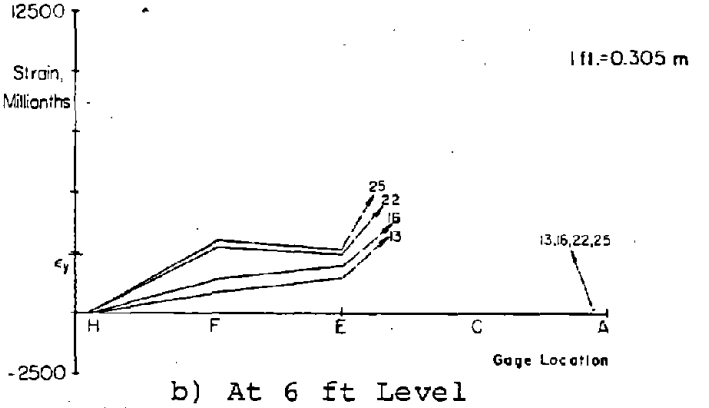

b) At 6 ft Level

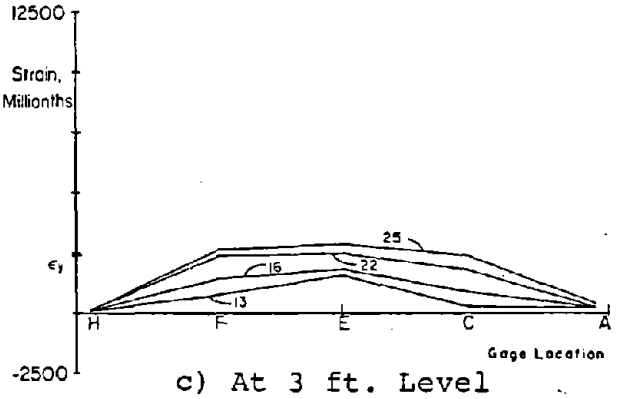

c) At 3 ft. Level

Fig. B-28 Horizontal Reinforcement Strains in Web at Maximum Negative Loads for Specimen B6

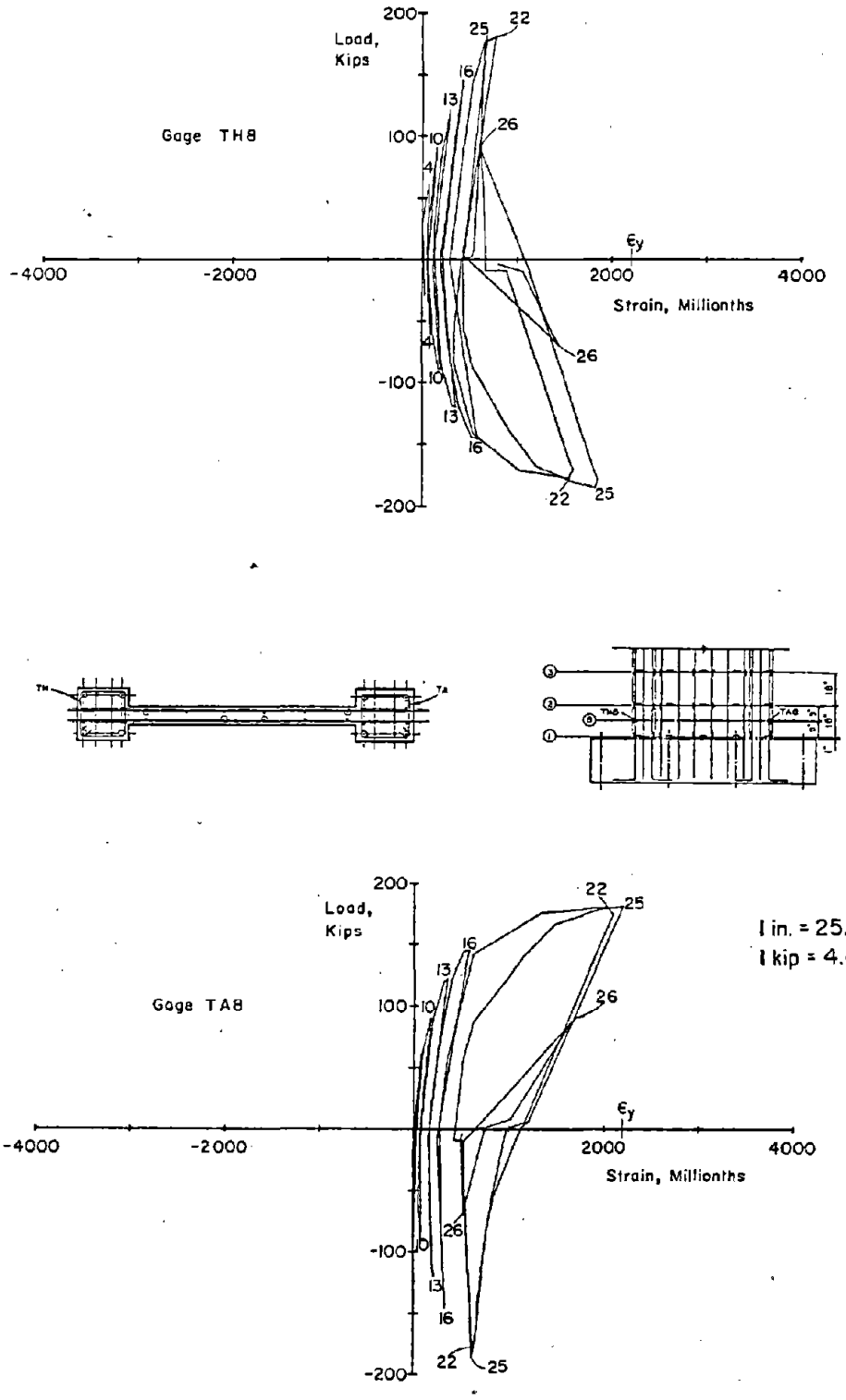

Fig. B-29 Measured Strains on Confinement Hoop Reinforcement for Specimen B6

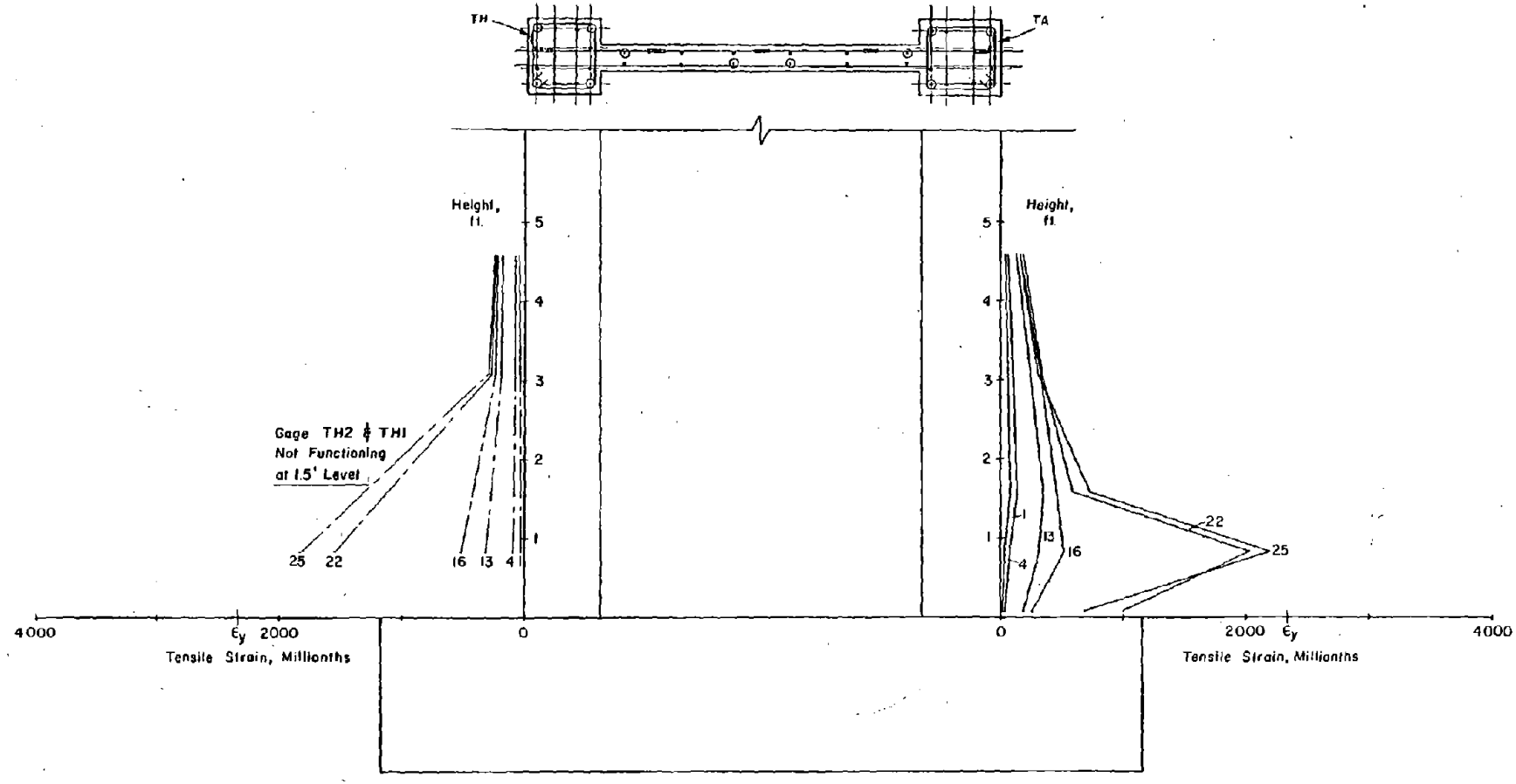

Fig. B-30 Confinement Hoop Reinforcement Strains at Maximum Loads for Specimen B6

Specimen B7

Test Description

Specimen B7 were similar to Specimen B6 with 3.67% vertical reinforcement in each column and confinement reinforcement in the lower 6 ft of the boundary elements. However, B7 had a concrete strength of 6000 psi (41.4 MPa). Specimen B7 was loaded axially to a uniform stress 545 psi (3.75 MPa). This axial load corresponds to 7% of the axial load capacity of the wall.

The test consisted of 31 loading cycles as shown in Fig. B-31. The complete load versus top deflection relationship for Specimen B7 is shown in Figs. B-32 and B-33. The complete load versus deflection and rotation relationships at the 6-ft level are shown in Figs. B-34 and B-35.

First significant cracking was observed in Cycle 10 at a load of 90 kips (400 kN). First yielding occurred in Cycle 13 at a load of 161.2 kips (717.0 kN). The maximum measured crack widths at this stage were 0.007 in. (0.18 mm) in the tension column and 0.017 in. (0.43 mm) across a diagonal crack in the web.

The crack pattern that developed was similar to the crack pattern in B6. The cracks directed toward the outer compression face at the base of the wall were at an angle of approximately 40° from vertical. Crack patterns at +3 in. (76.2 mm) and -3 in. Deflection are shown in Figs. B-36 and B-37.

At equivalent deflections measured diagonal cracks widths in B7 were less than those measured in B5 a companion wall without axial loads. As an example, with the top of the wall at 3-in. deflection, a measured diagonal crack width in the lower 3 ft of the wall was 0.051 in. (1.30 mm) in B7 versus 0.090 (2.29 mm) in B5.

First indication of crushing in the concrete cover of the outer compression faces was noted in Cycle 19. First indication of spalling and flaking along diagonal cracks occurred in Cycle 10. This spalling and flaking in the web and crushing of

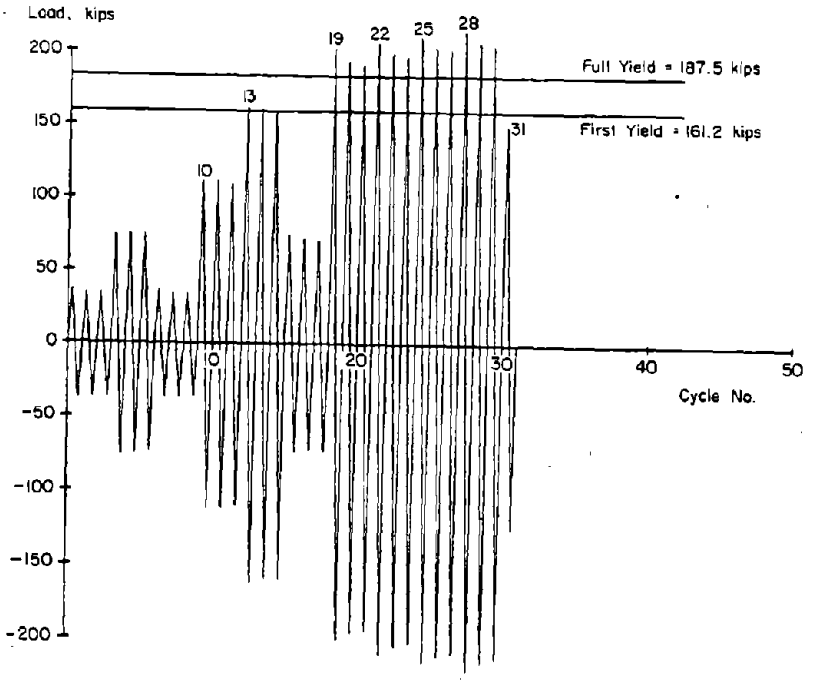

a) Load History

1 in. = 25.4 mm
1 kip = 4.448 kN

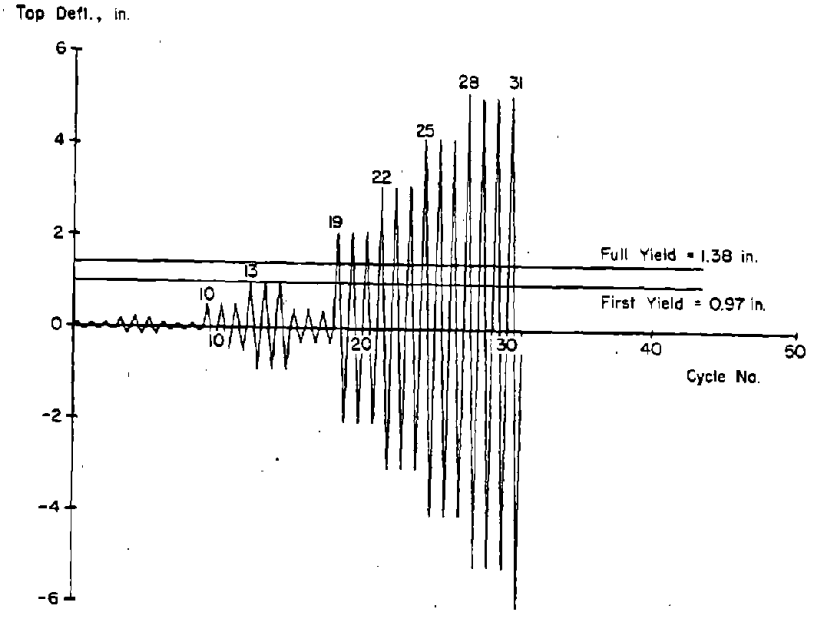

b) Deflection History

Fig. B-31 Loading History for Specimen B7

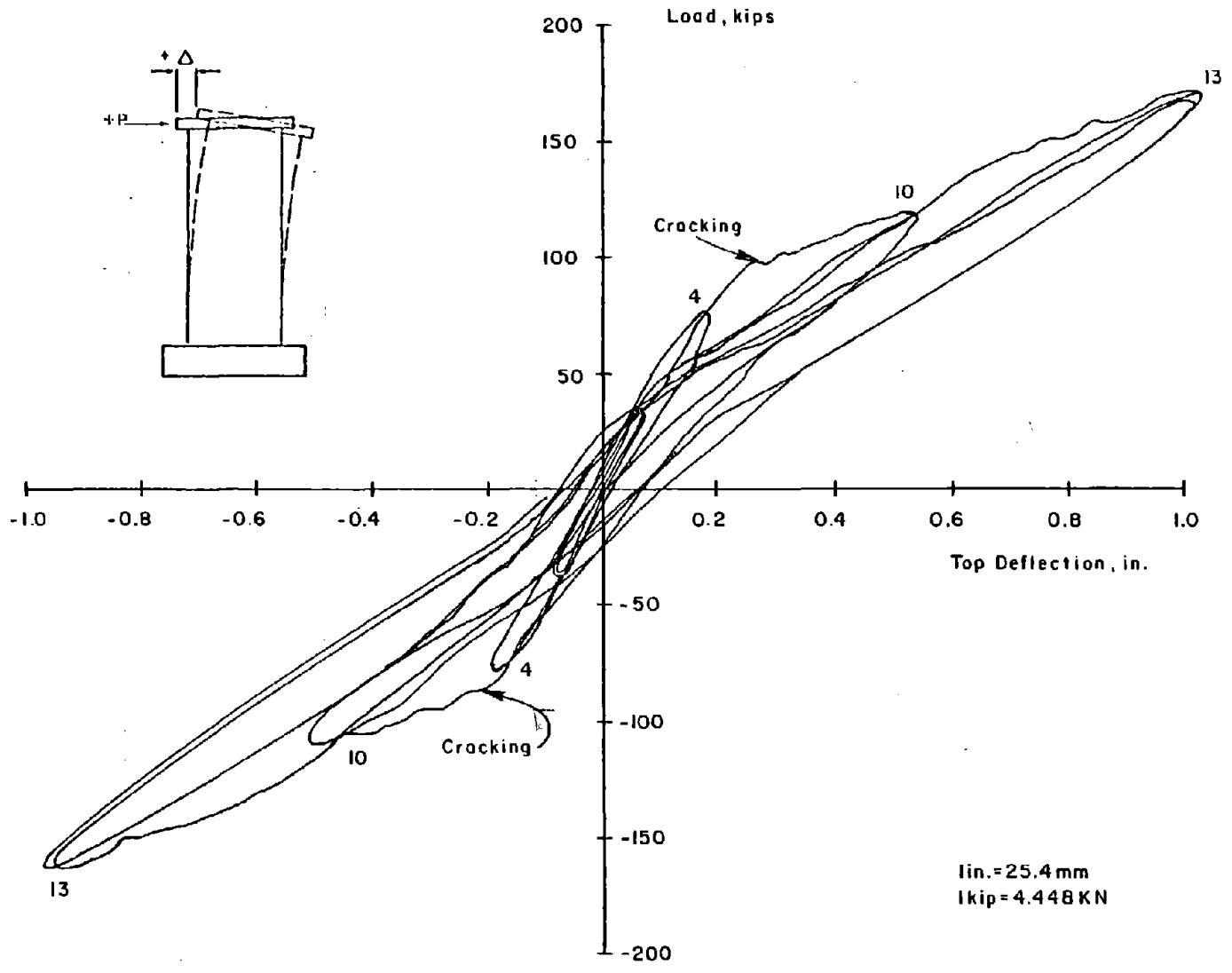

Fig. B-32 Continuous Load - Top Deflection for Initial Cycles for Specimen B7

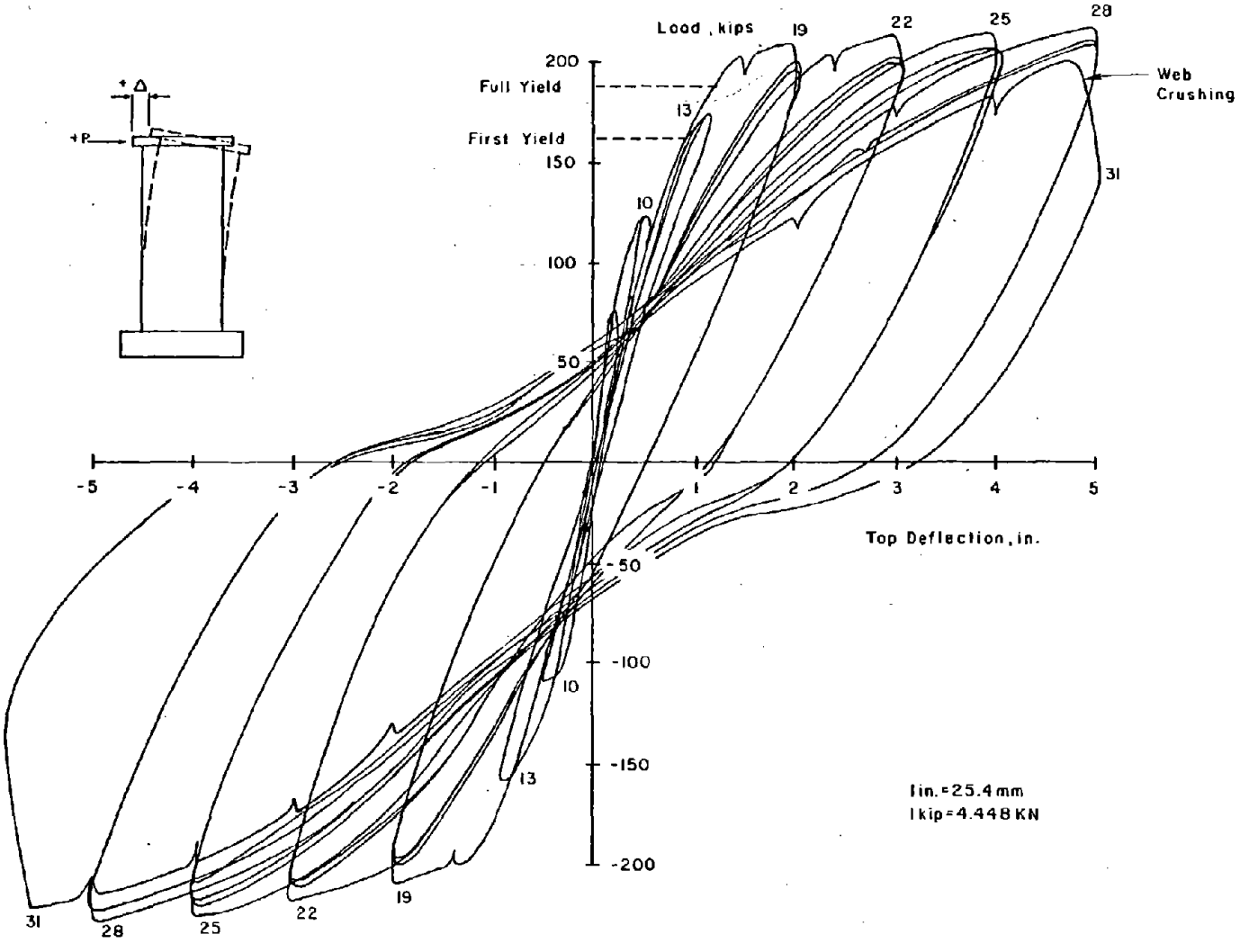

Fig. B-33 Continuous Load - Top Deflection for Specimen B7

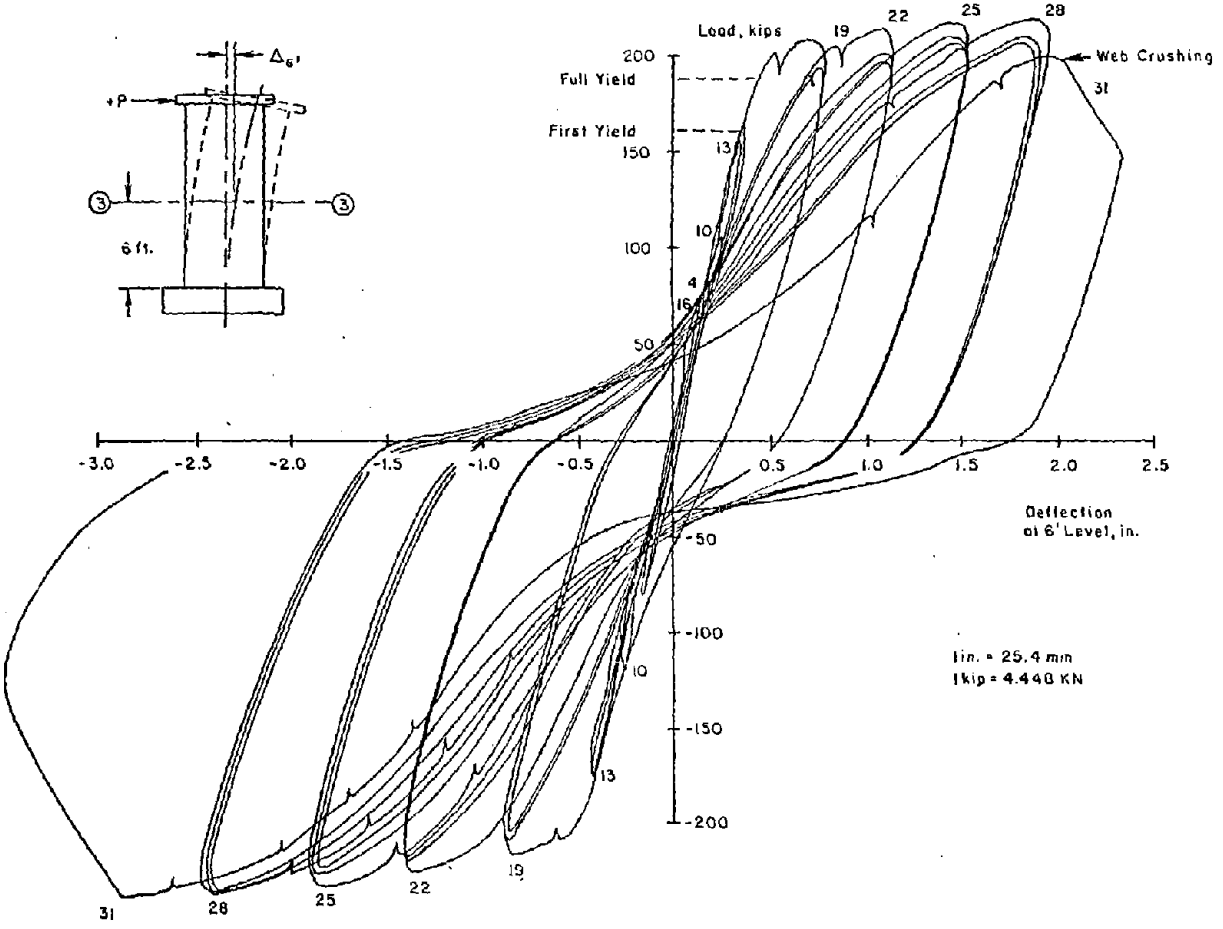

Fig. B-34 Continuous Load - Deflection at 6 ft Level for Specimen B7

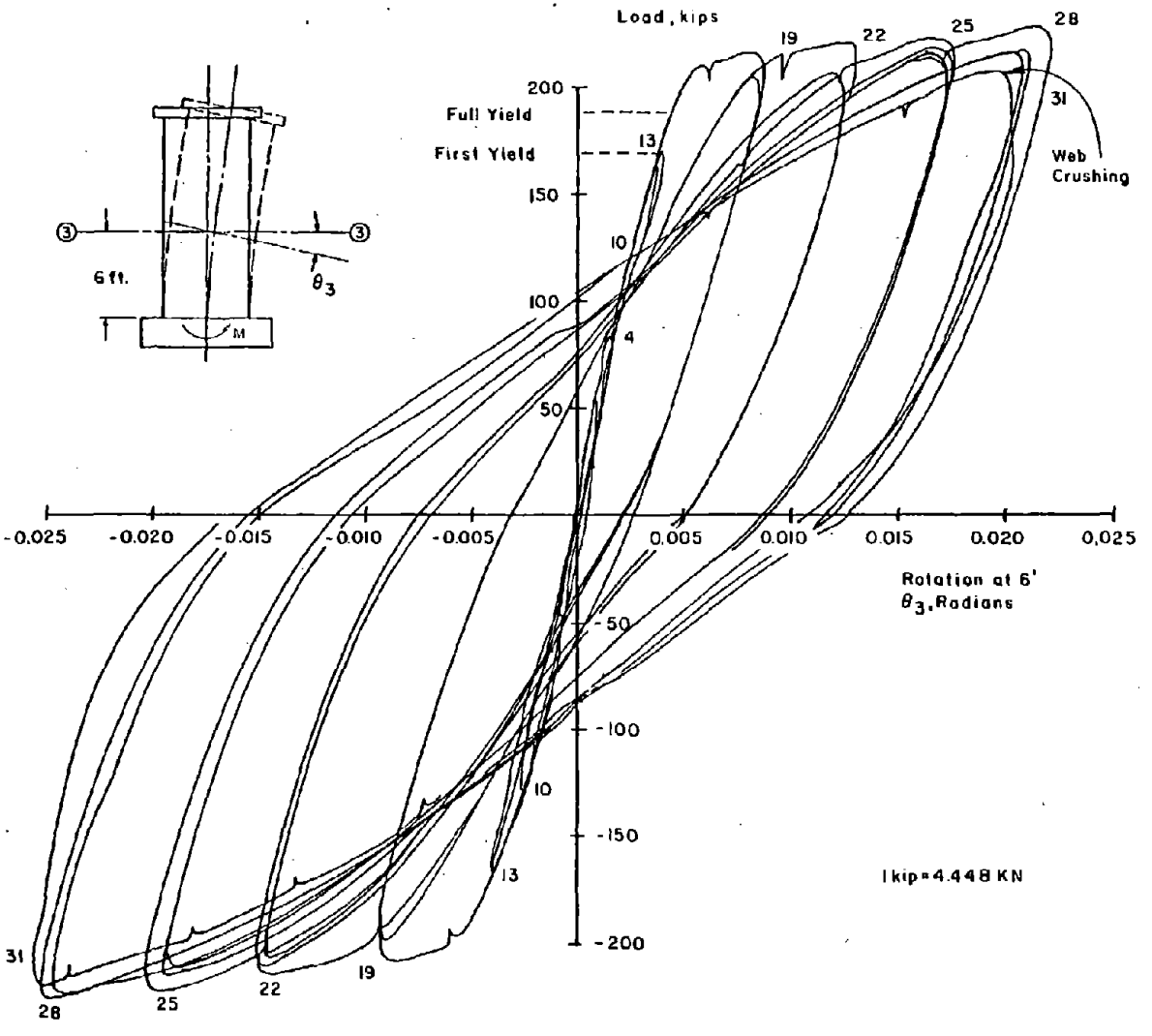

Fig. B-35 Continuous Load - Rotation at 6 ft Level for Specimen B7

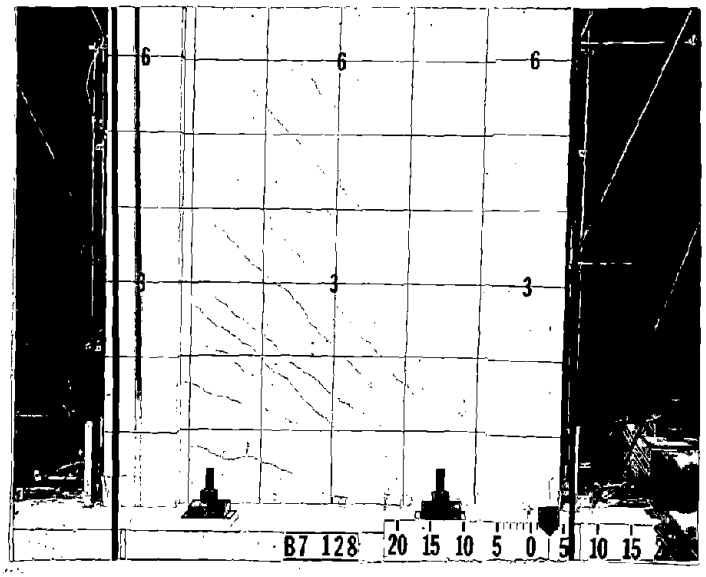

Fig. B-36 Cracking Pattern at +3 in. Deflection for Specimen B7

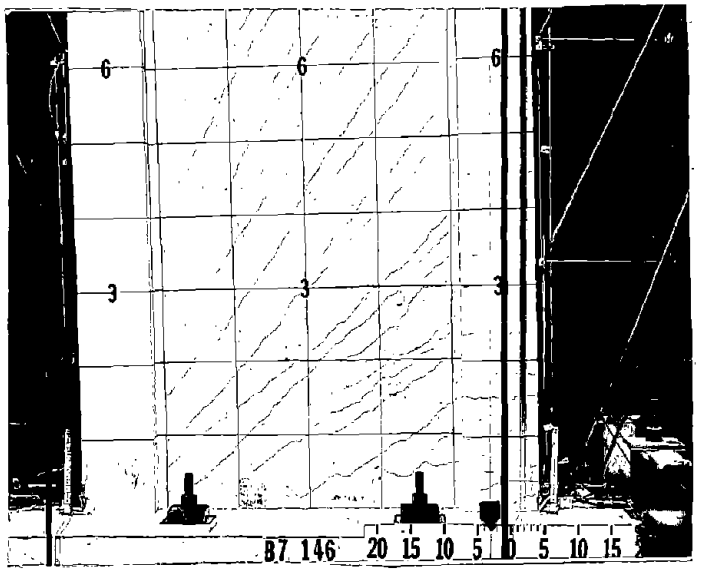

Fig. B-37 Cracking Pattern at -3 in. Deflection for Specimen B7

the outer compression faces progressively increased as more and larger load cycles were applied to the specimen.

A slight reverse curvature developed in the lower 3 ft of the boundary elements during Cycle 22.

A slight indication of crushing in the compression struts in both the right and left sides of the web approximately 18 in. above the base was noted in Cycle 25.

The maximum load measured, 220.4 kips (980.3 kN), occurred in Cycle 28 at a -5-in. (127.0 mm) deflection. This load corresponds to a nominal shear stress of $v_{max} = 10.9 \sqrt{f'_c}$ ($0.91 \sqrt{f'_c}$ MPa). The design shear capacity using the 1971 ACI Building Code Equations (11-13) and (11-33) was 148 kips (658.3 kN). This corresponds to a nominal shear stress of $v = 7.3 \sqrt{f'_c}$ ($0.61 \sqrt{f'_c}$ MPa).

As the specimen was being loaded to a +6-in. deflection in Cycle 31, several compression struts crushed simultaneously. The pattern of crushing, load redistribution and resulting shear plane were very similar to those that occurred in Specimen B6. Figures B-38 and B-39 show the specimen immediately prior to and after web crushing. As in B6, a vertical failure plane rather than a horizontal plane developed after web crushing. This is attributed to stiffness of the boundary elements in the presence of the axial load.

As the load capacity was dropping the specimen was "caught" by closing the deflection control valve in the hydraulic system. The measured load at this stage had decreased to 68% of the maximum measured load.

The specimen sustained at least 80% of the maximum measured load capacity through 12 inelastic cycles. The last inelastic loading increment in which the load was sustained at or above 80% of the maximum for all 3 cycles was at ± 5 in. (127.0 mm).

Although the web was considerably damaged at the end of the test, the columns were in good condition. This wall could have been repaired simply by replacing the web.

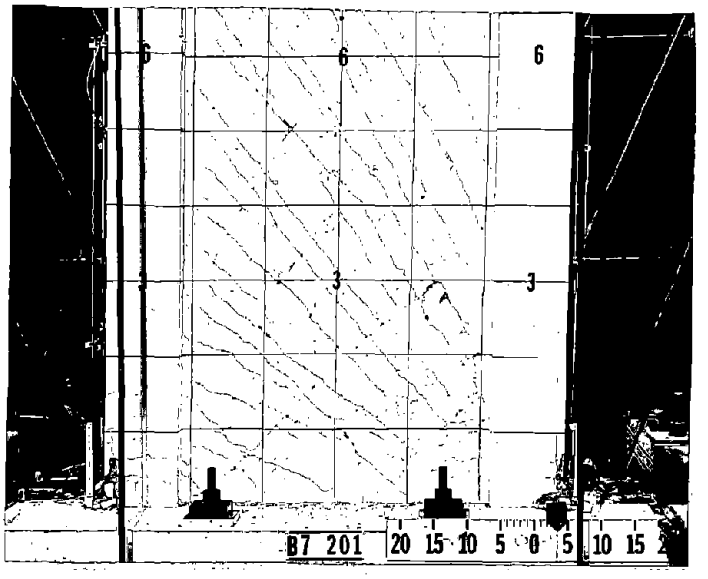

Fig. B-38 Specimen B7 Prior to Web Crushing

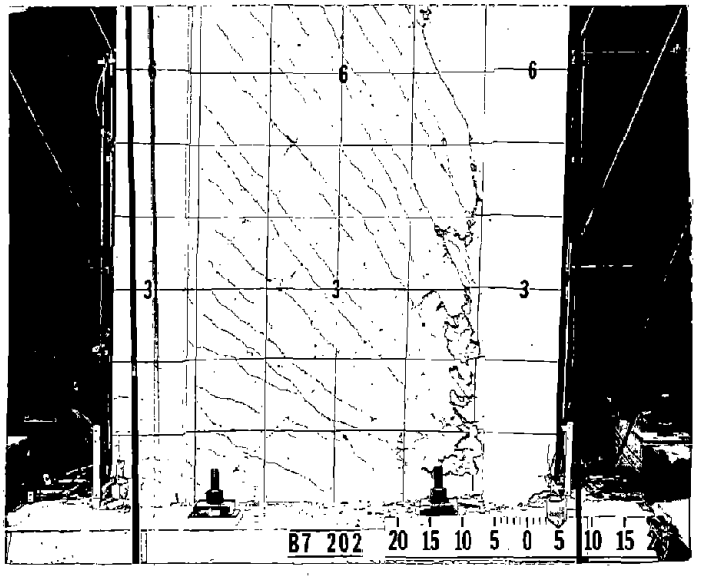

Fig. B-39 Specimen B7 After Web Crushing

Discussion of Results

Moment-Rotation. Moment-rotation data for Specimen B7 is shown in Fig. B-40. The maximum measured moment was 86% of the calculated monotonic maximum. This calculated maximum was based on attainment of the ultimate compressive strain of $\varepsilon_u = 0.0071$ in the boundary element.

The relationship between calculated monotonic and measured rotations at the 3-ft (0.91 m) and 6-ft (1.83 m) levels is similar to that observed in Specimen B6 and in specimens in the previously reported tests without axial load. Rotation tended to concentrate in the lower 3 ft of the wall to a greater extent than was assumed in calculations.

The maximum rotation measured at the 6-ft level for a stable increment was - 0.0242 rad. This corresponds to a rotational ductility of 5.2. The corresponding maximum rotation for Specimen B5 which had no axial load, was 0.0171 rad. which corresponds to a rotational ductility of 2.7. It is evident that axial load significantly incresed rotational ductility.

Shear Distortion. The shear-distortion loops for B7 are shown in Fig. B-41. As in the previously reported tests without axial load, a shear "yielding" occurred during the same cycle in which flexural yielding occurred. However, as in Specimen B6 this "yielding" is not as evident in the 3-ft to 6-ft zone. A major portion of the shear distortions occurred in the lower 3 ft (0.91 m). This differs from the shear distortion distribution observed in specimens without axial load in which shear distortions were more evenly distributed throughout the lower 6 ft (1.83 m).

The maximum shear distortion in Zone 3 attained in a stable increment was 0.0141 rad. at a 5-in. top deflection. The maximum attained in the B5 test was 0.0184 rad. at a 4-in. top deflection. A comparison of peak loads and shear distortions for these specimens indicates that axial load increased the effective shear stiffness in B7 by as much as 240%.

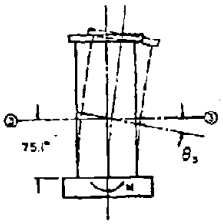

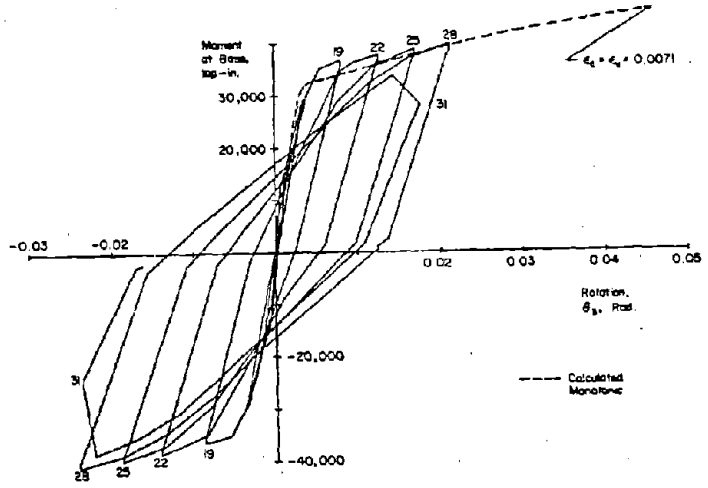

a) At 6 ft Level

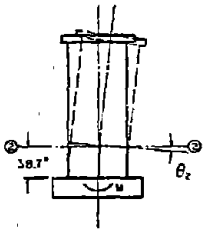

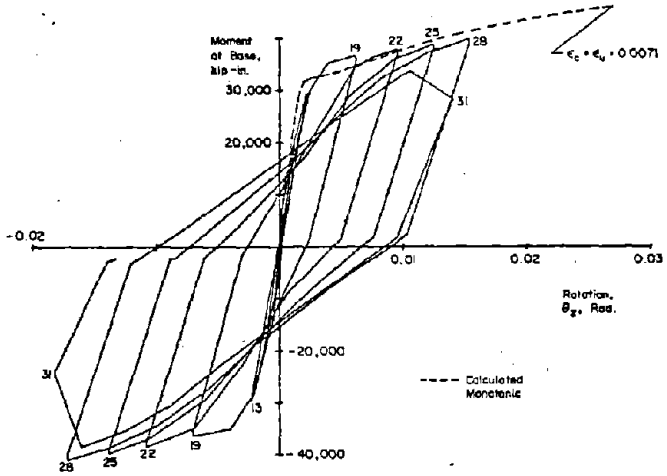

b) At 3 ft Level

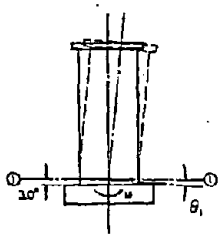

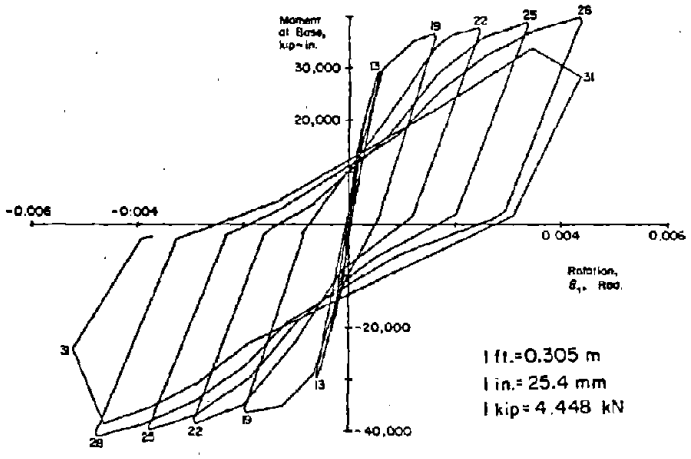

c) At Base Level

Fig. B-40 Moment at Base versus Rotation for Specimen B7

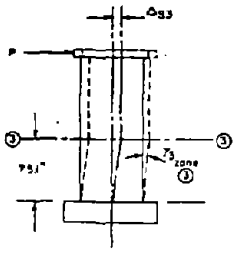

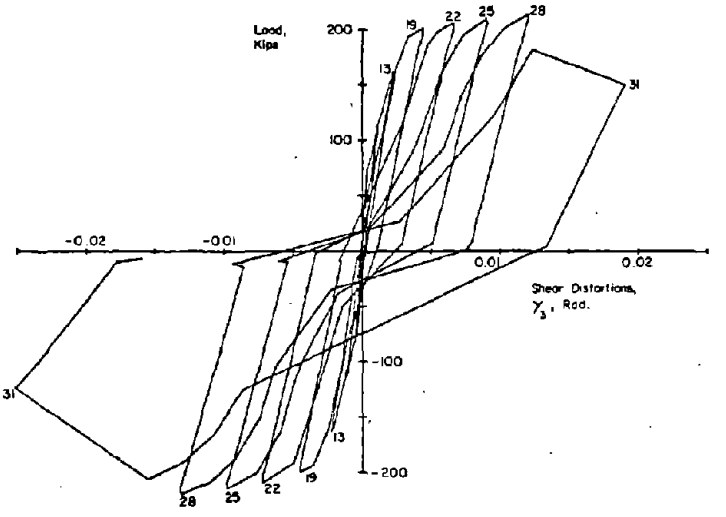

a) In Base to ft Level

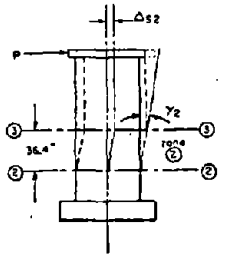

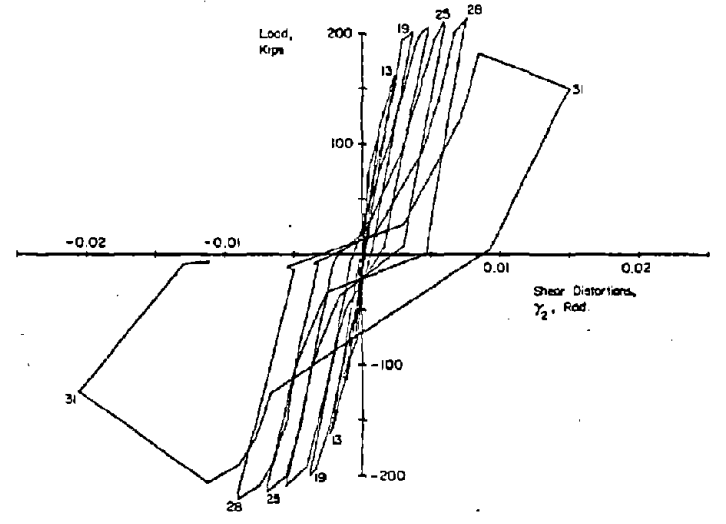

b) in 3 ft to 6 ft Level

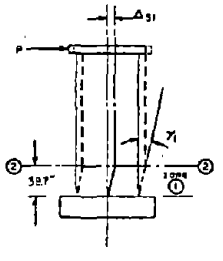

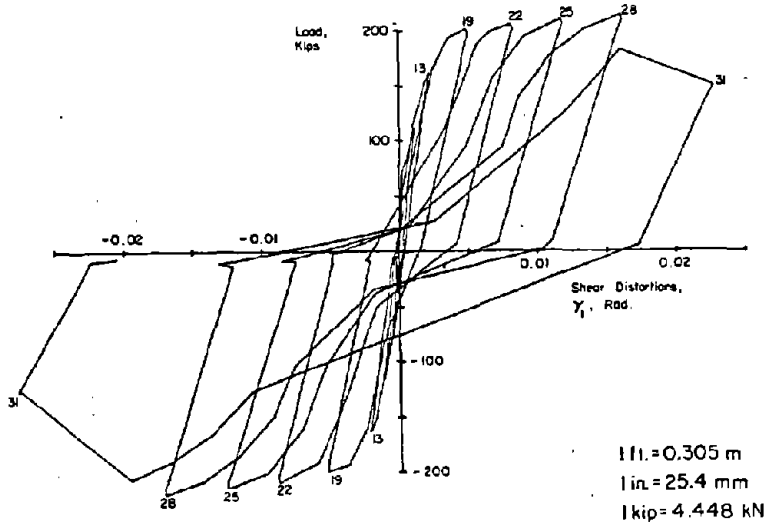

c) In Base to 3 ft Level

Fig. B-41 Load versus Shear Distortion for Specimen B7

Slip at Construction Joints. Slip at construction joints in B7 is shown in Fig. B-42. The slip at CJ1 exhibits yielding similar to shear "yielding". These were observed during the same cycle that flexural yielding occurred. As shown in Fig. B-43, the slip at CJ1 was a relatively constant 15% of the total shear deflection in the lower 3 ft (0.91 m).

The slip plots for CJ2 and CJ3 are unsymmetrical. Measured slips were affected by diagonal cracking.

A comparison of peak loads and slip at CJ1 for Specimens B5 and B7 indicates that the axial load in B7 increased the effective slip stiffness by as much as a factor of 1.8.

Deflections. The deflection components and deflected shapes are shown in Figs. B-44 and B-45. These figures show that shear deflections were a relatively constant portion of the total throughout most of the test and increased slightly near the end of the test.

The deflected shapes for Cycles 22 and 24 show only a slight decrease in shear stiffness during the 3-in. (76.2 mm) increment. A larger decrease in stiffness is indicated by the deflected shapes for Cycles 28 and 30, the first and last cycles of the 5-in. (127.0 mm) increment.

Reinforcement Strains. Figures B-46 through B-56 show reinforcement strains in the specimen at various stages.

Figure B-46 shows that outer bars in the compression elements near the base were in compression during every cycle. Figure B-47 shows that yielding occurred up to the 9-ft (2.75 m) level in Cycle 28.

Figures B-48 and B-49 show the strain gradient in the vertical reinforcement at various levels. The gradient in the compression zone near the base shows the neutral axis continued to move toward the outer compression face. This indicates that the ultimate concrete compressive stress had not yet been reached.

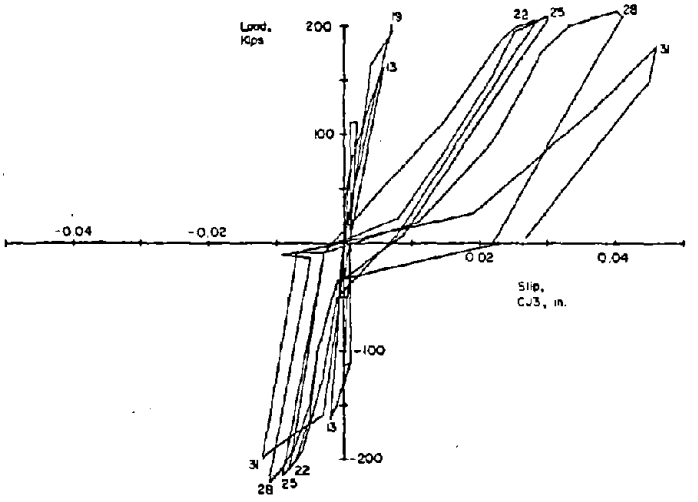

a) At 6 ft Level

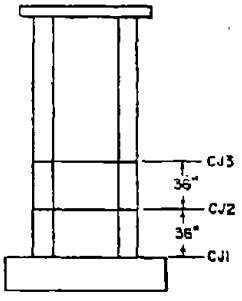

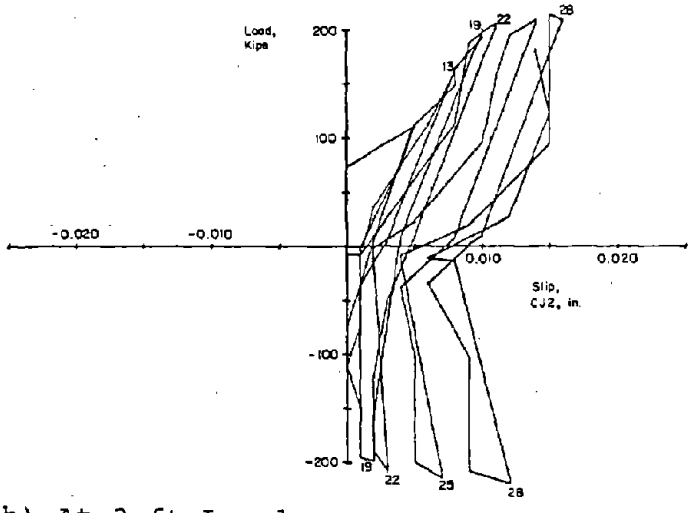

b) At 3 ft Level

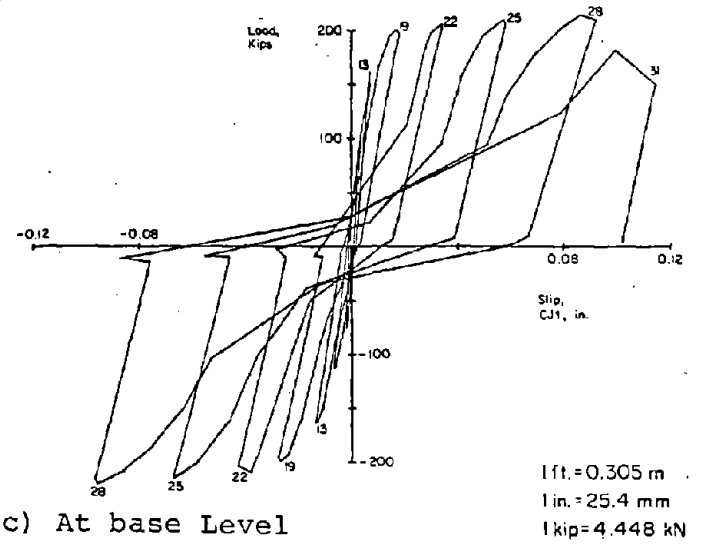

c) At base Level

Fib. B-42 Load versus Slip at Construction Joints for Specimen B7

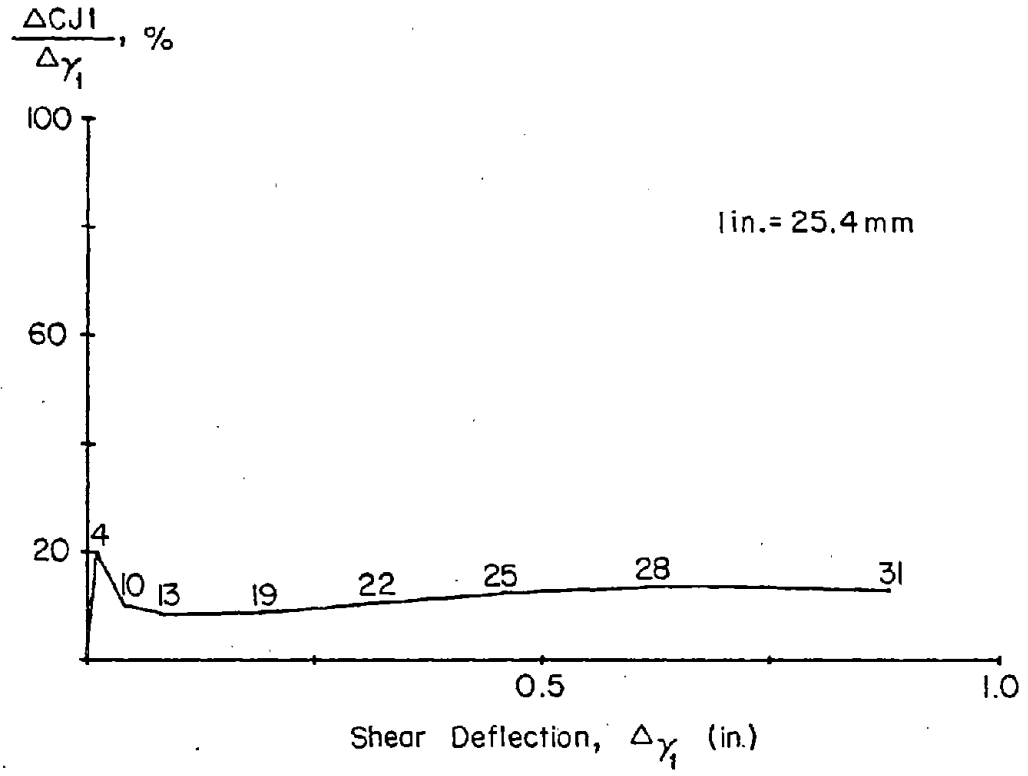

a) At Maximum Positive Loads

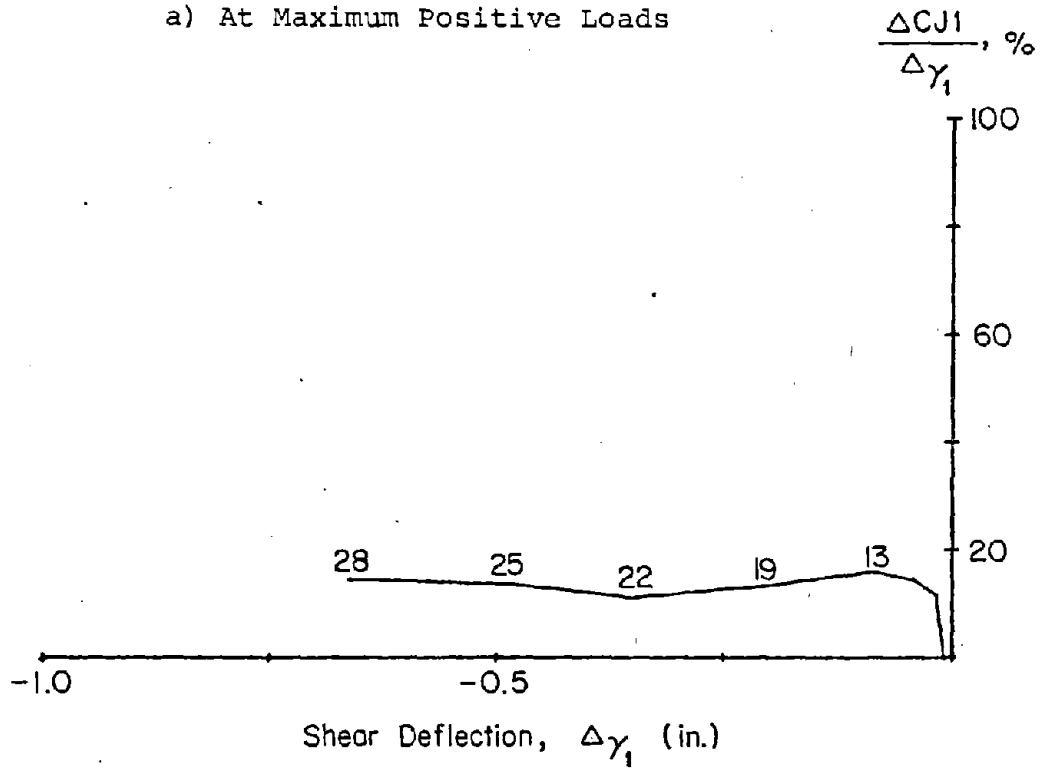

b) At Maximum Negative Loads

Fig. B-43 Slip at Base Construction Joint versus Shear Deflection in Zone 1 for Specimen B7

a) At Top of Wall

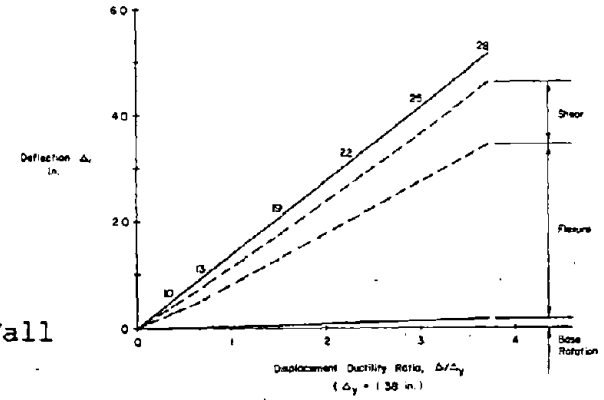

b) At 6 ft Level

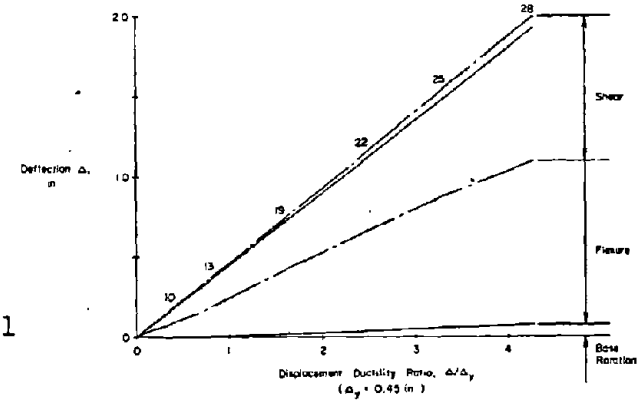

c) At 3 ft Level

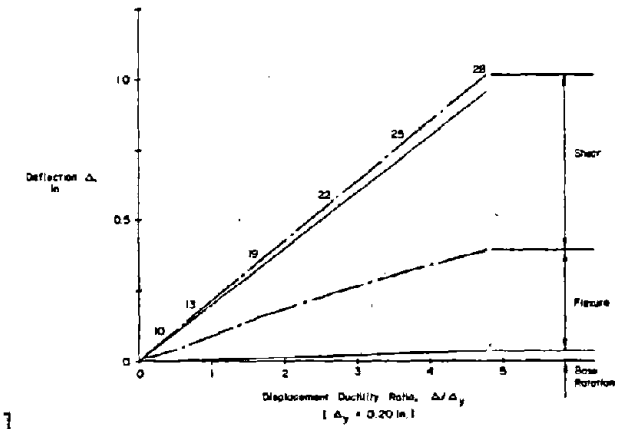

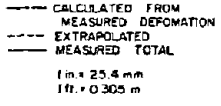

Fig. B-44 Components of Deflection for Specimen B7

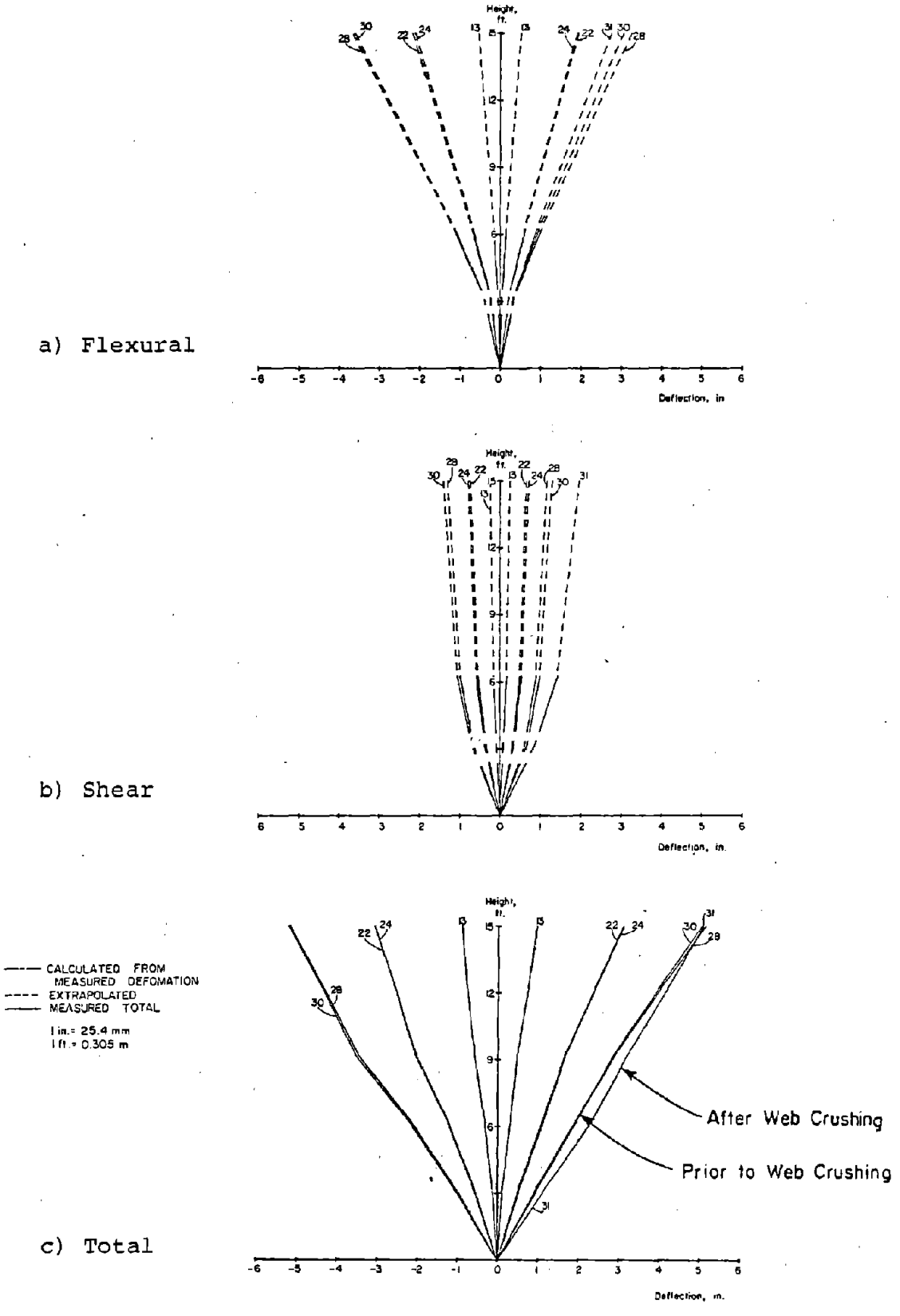

Fib. B-45 Deflected Shape for Specimen B7

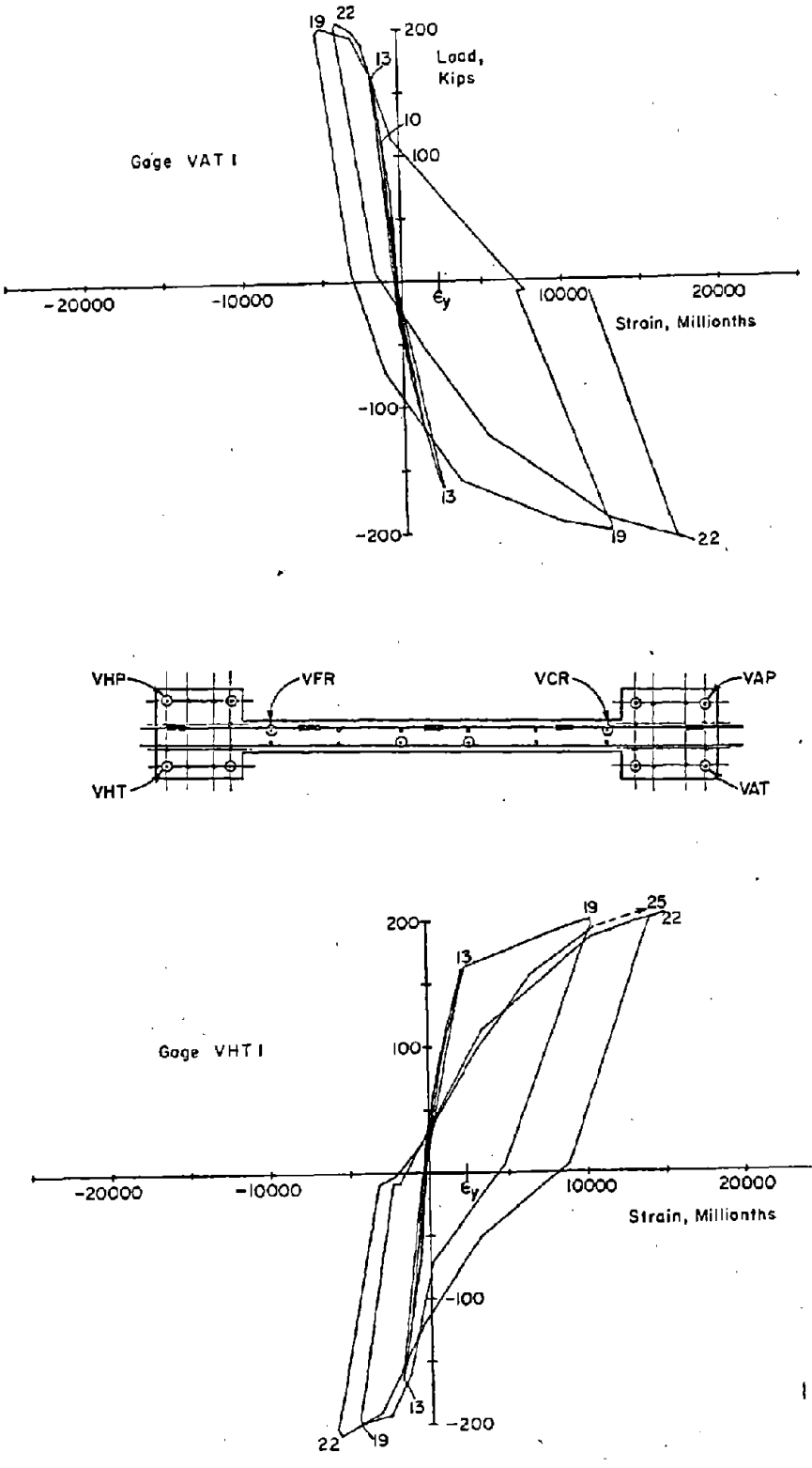

Fig. B-46 Measured Strains on Vertical Reinforcement at Base of Specimen B7

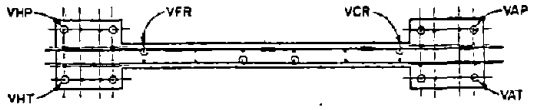

1 ft.=0.305 m

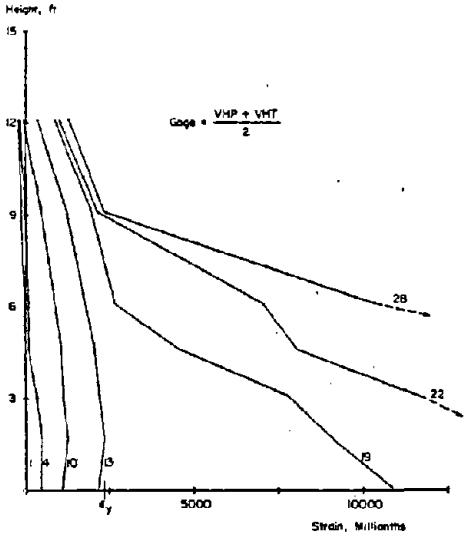

a) Average of VHP and VHT

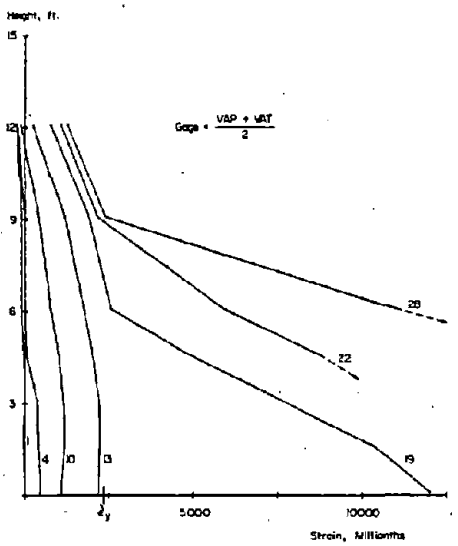

b) Average of VAP and VAT

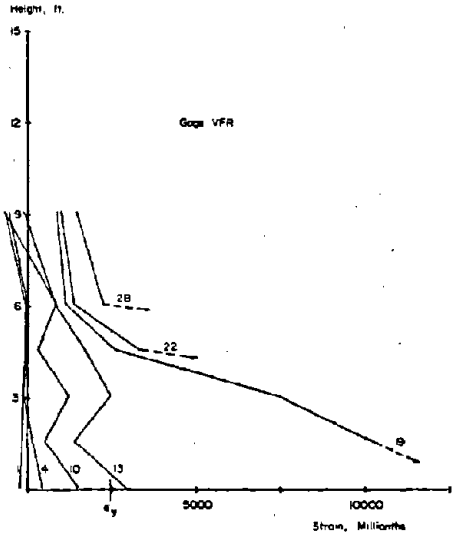

c) Strain Gage VFR

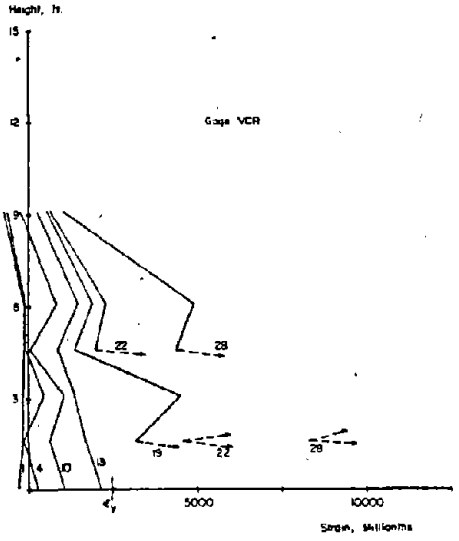

d) Strain Gage VCR

Fig. B-47 Vertical Reinforcement Strains at Maximum Loads for Specimen B7

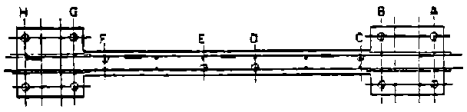

1 ft.=0.305 m

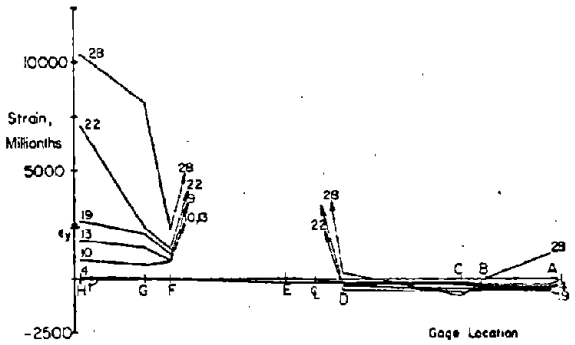

a) At 6 ft Level

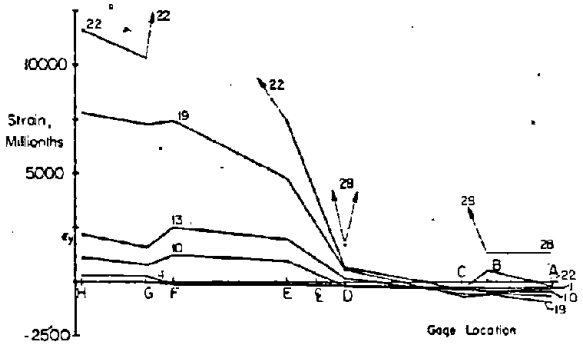

b) At 3 ft Level

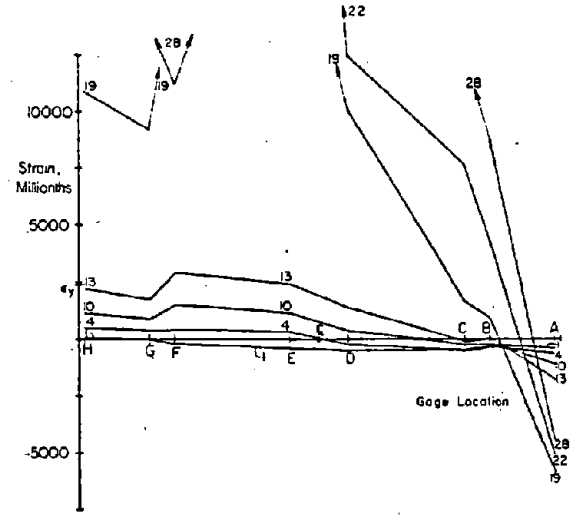

c) At Base Level

Fig. B-48 Vertical Reinforcement Strains at Maximum Positive Loads for Specimen B7

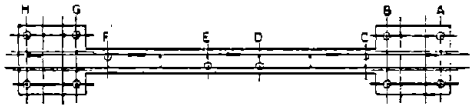

1 ft.=0.305 m

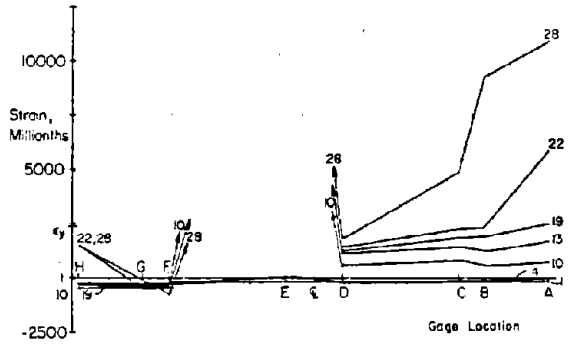

a) at 6 ft Level

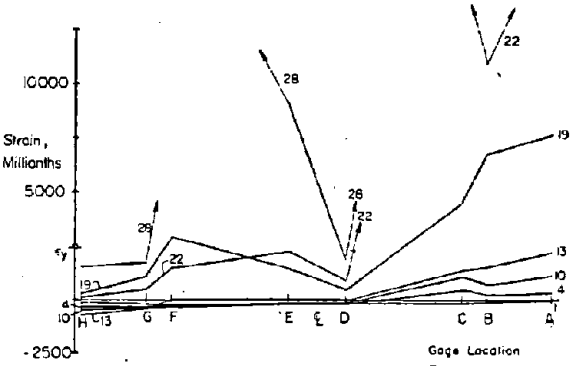

b) At 3 ft Level

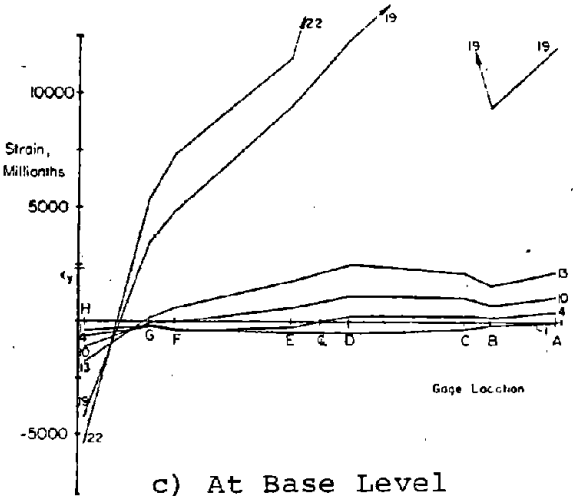

c) At Base Level

Fig. B-49 Vertical Reinforcement Strains at Maximum Negative Loads for Specimen B7

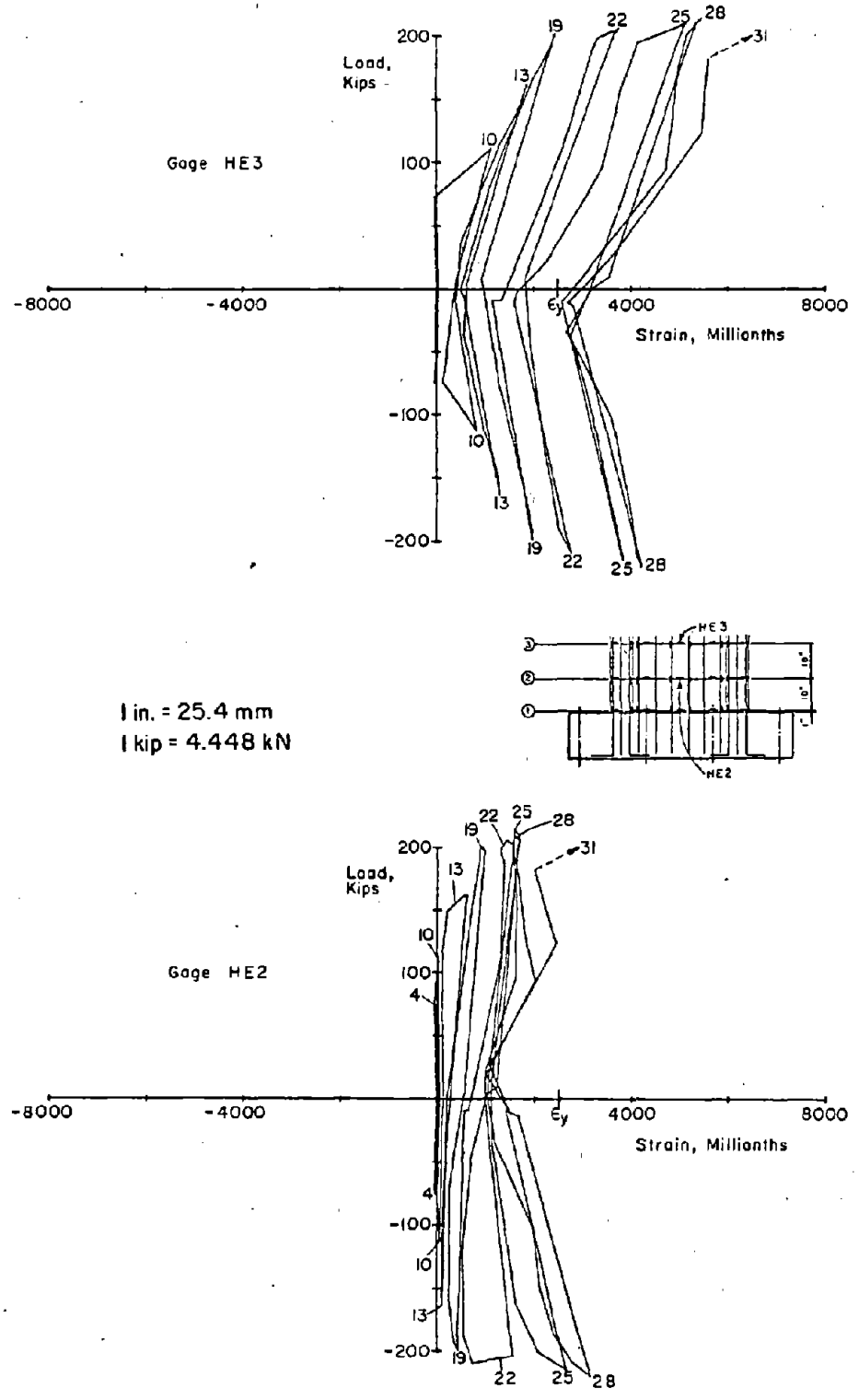

Fig. B-50 Measured Strains on Horizontal Reinforcement for Specimen B7

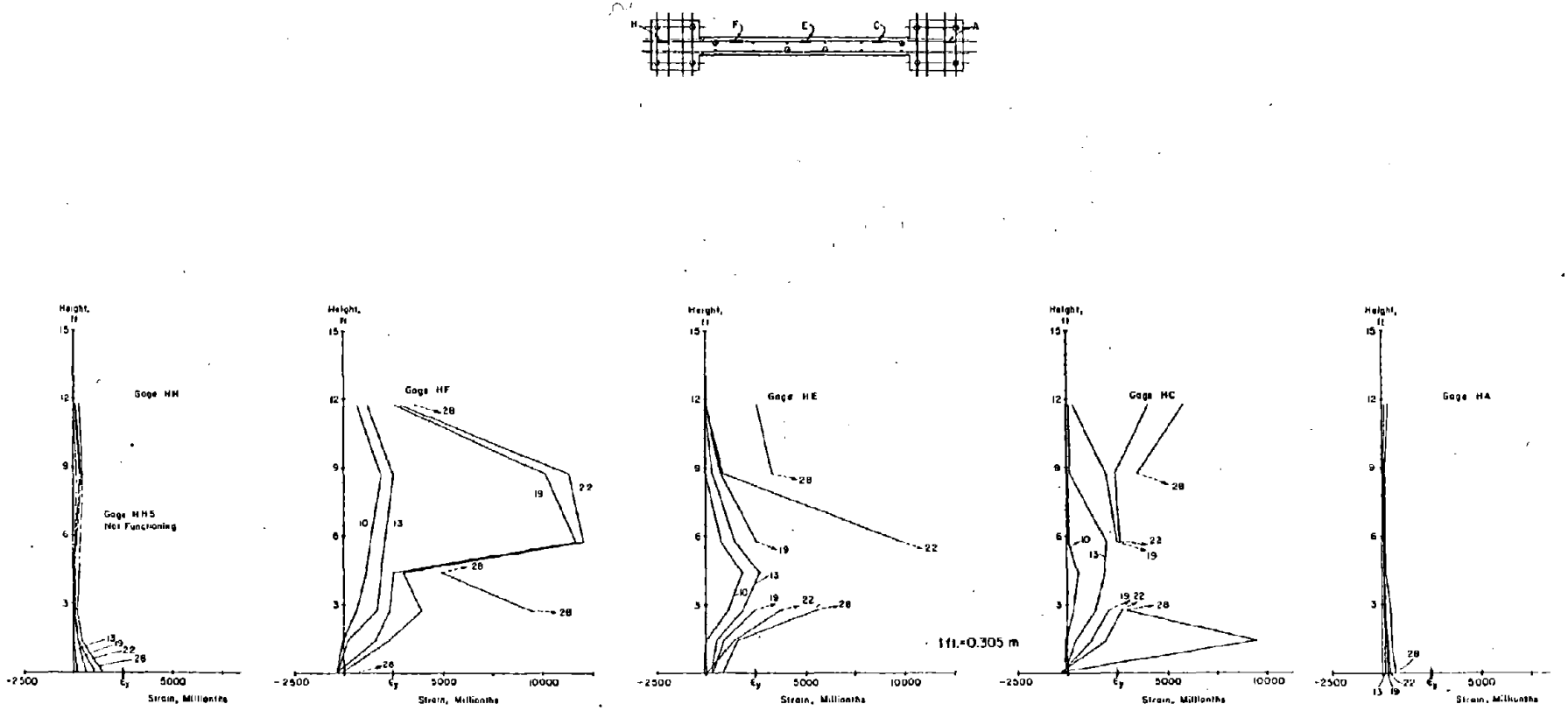

Fig. B-51 Horizontal Reinforcement Strains at Maximum Positive Loads for Specimen B7

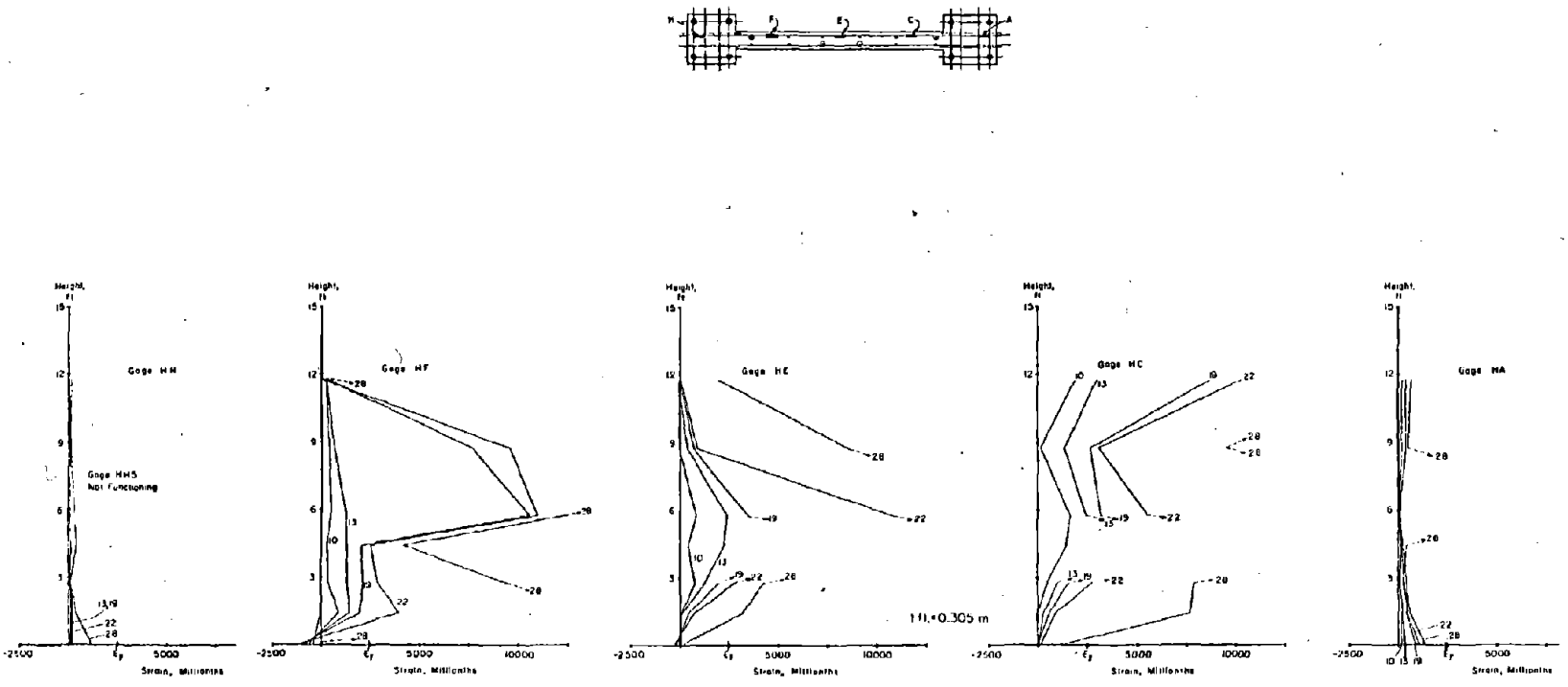

Fig. B-52 Horizontal Reinforcement Strains at Maximum Negative Loads for Specimen B7

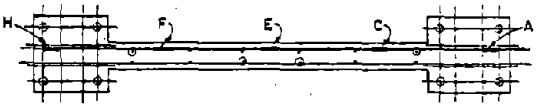

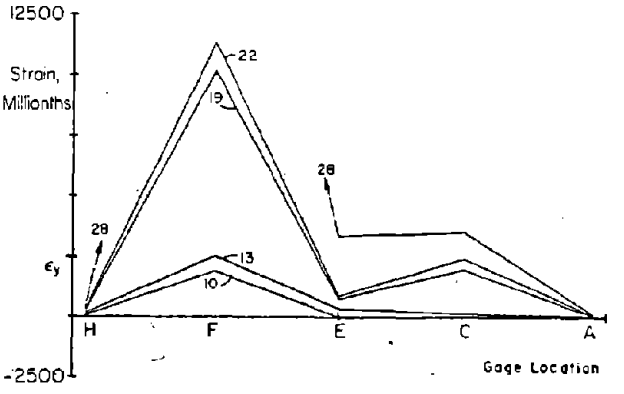

a) At 9 ft Level

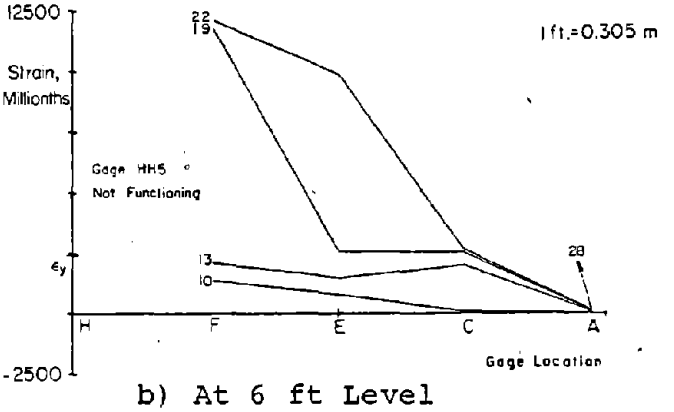

b) At 6 ft Level

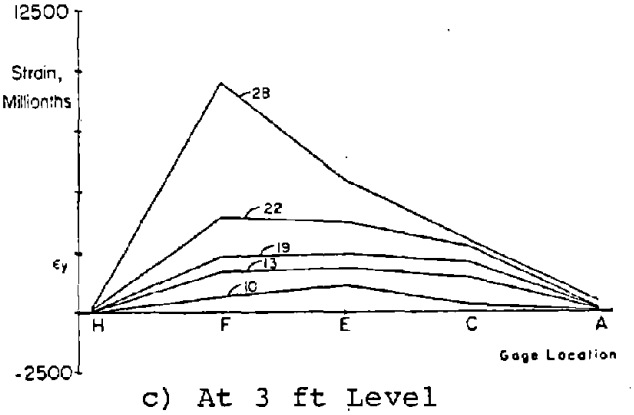

c) At 3 ft Level

Fig. B-53 Horizontal Reinforcement Strains in Web at Maximum Positive Loads for Specimen B7

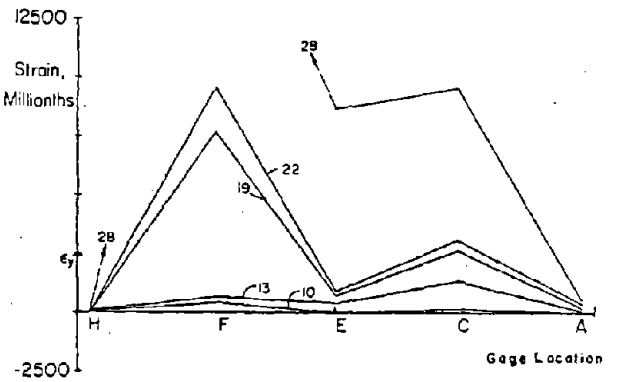

a) At 9 ft Level

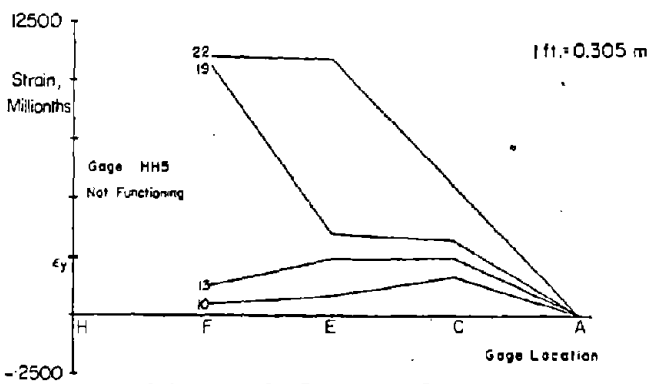

b) At 6 ft Level

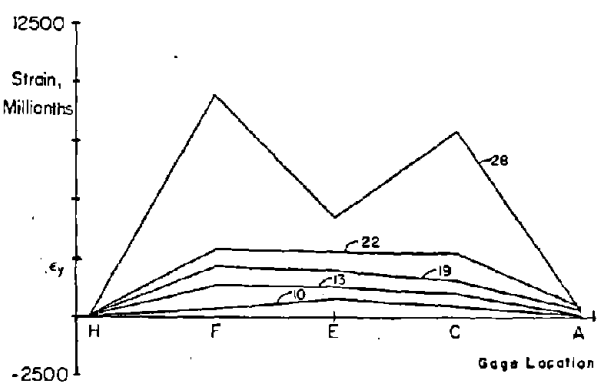

c) At 3 ft Level

Fig. B-54 Horizontal Reinforcement Strains in Web at Maximum Negative Loads for Specimen B7

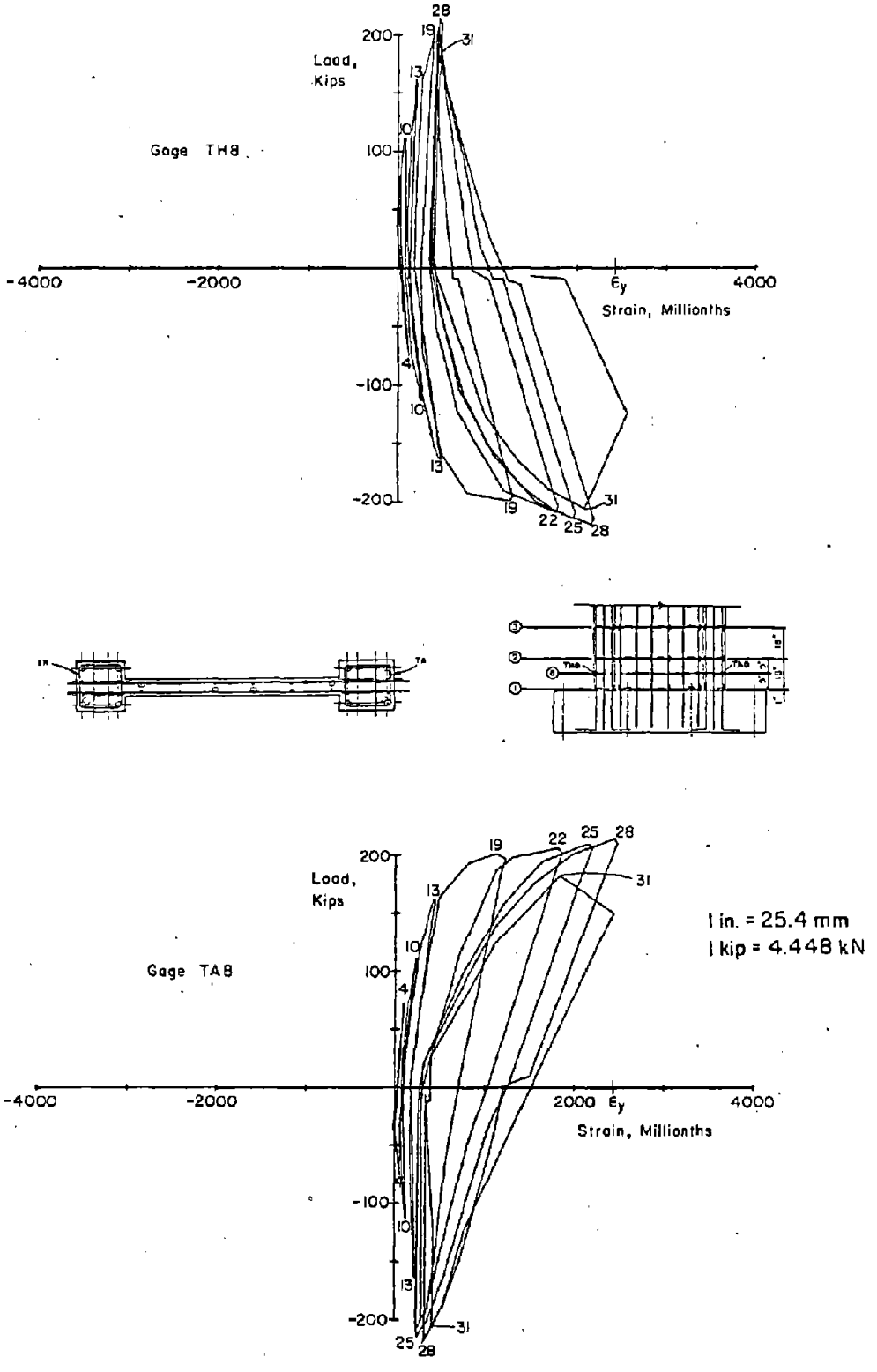

Fig. B-55 Measured Strains on Confinement Hoop Reinforcement for Specimen B7

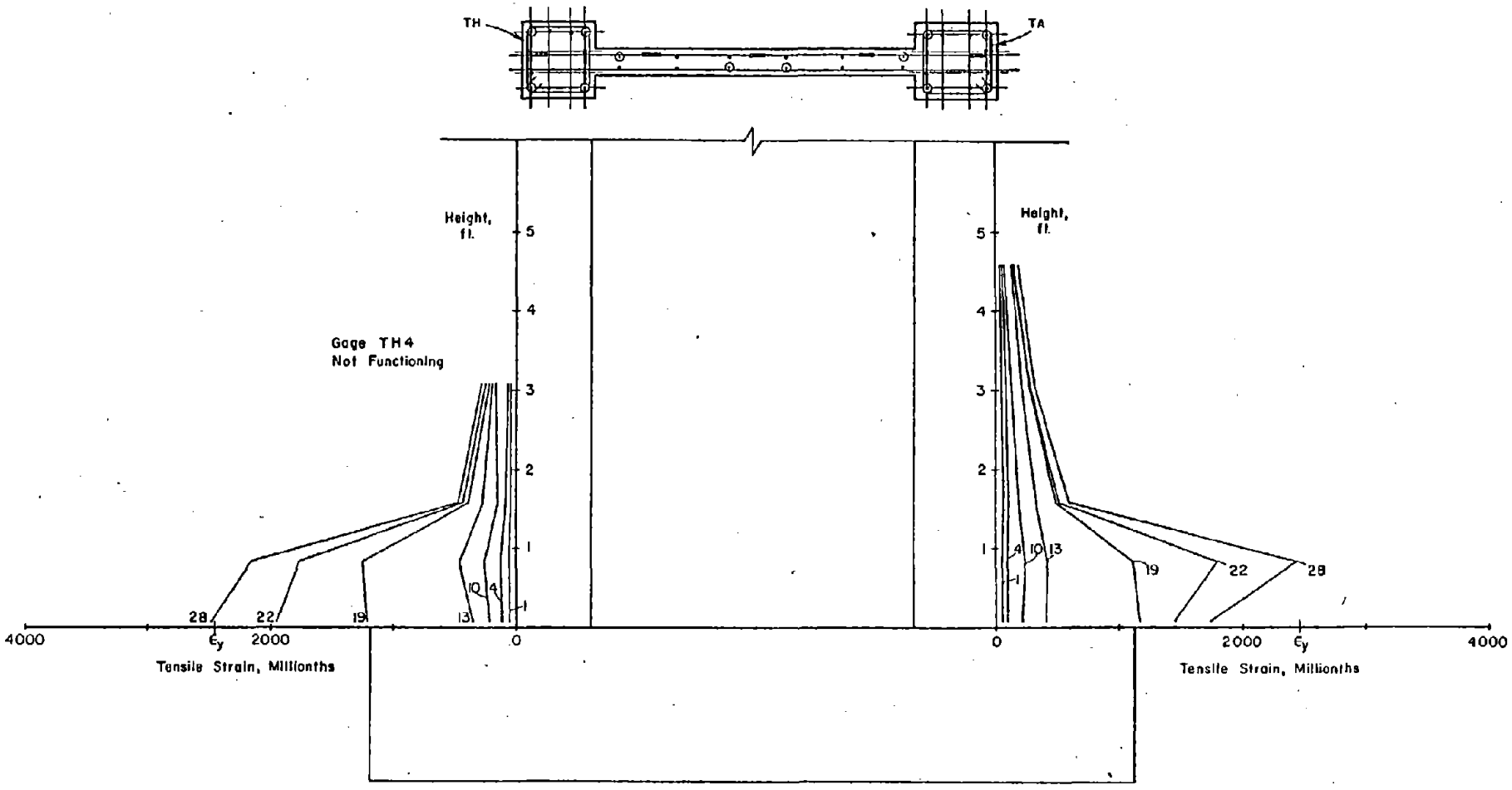

Fig. B-56 Confinement Hoop Reinforcement Strains at Maximum Loads for Specimen B7

Figures B-50 through B-54 show the cyclic strain-load relationship and the strain gradients in the horizontal bars. These figures indicate considerable yielding between the 18-in. to 9-ft (0.46 m to 2.74 m) level. Figures B-51 and B-52 for gages HH and HA indicate that, although no yielding occurred near the end hooks, appreciable stresses were present. This was particularly evident in the lower 18 in. (0.46 m) because the boundary elements act as dowels in this region.

Figures B-55 and B-56 show the cyclic strain-load relationship and the vertical strain gradient in the outer leg of the confinement hoops. These figures show that only the hoops in the lower two feet were stressed significantly. Strains near yield were observed in the hoops during the latter cycles of this test.

Specimen B8

Test Description

Specimen B8 was similar to Specimen B7 with 3.67% vertical reinforcement in each column and confinement reinforcement in the lower 6 ft of the boundary element. However, Specimen B8 contained 2.2 times the area of horizontal steel that was in Specimen B7. The design shear capacity for B8 using the 1971 ACI Building Code Equations (11-13) and (11-33), disregarding the $10\sqrt{f'_c}$ limit and assuming 60 ksi (413.7 MPa) in the horizontal steel was 256.4 kips (1140.5 kN). The calcuatled maximum flexural capacity for B8 including strain hardening of the vertical reinforcement was 241.4 kips (1073.8 kN). As with Specimen B7, Specimen B8 was loaded axially at a uniform stress of 545 psi (3.75 MPa).

The test consisted of 31 loading cycles as shown in Fig. B-57. The complete load versus top deflection relationship for Specimen B8 is shown in Figs. B-58 and B-59. The complete load versus deflection and rotation relationships at the 6-ft level are shown in Figs. B-60 and B-61.

First significant cracking was observed in Cycle 10 at a load of 85 kips (378 kN). First yielding occurred in Cycle 13 at a load of 155.4 kips (691.2 kN). The maximum measured crack widths at this stage were 0.010 in. (0.25 mm) in the tension column and 0.011 in. (0.28 mm) across a diagonal crack in the web.

The crack pattern that developed was similar to that in B7. Cracks directed toward the outer compression face at the base of the wall were at an angle of approximately 38° from vertical. The crack patterns at +3 in. (76.2 mm) and -3 in. deflection are shown in Figs. B-62 and B-63.

The major difference in the observed behavior of B8 versus B7 is the diagonal crack widths. With the top of wall at a 5-in. deflection a measured diagonal crack width in the lower 3 ft of the wall was 0.086 in. (2.18 mm) in B7 versus 0.036 in. (0.91 mm) in B8. A measured diagonal crack width in the second

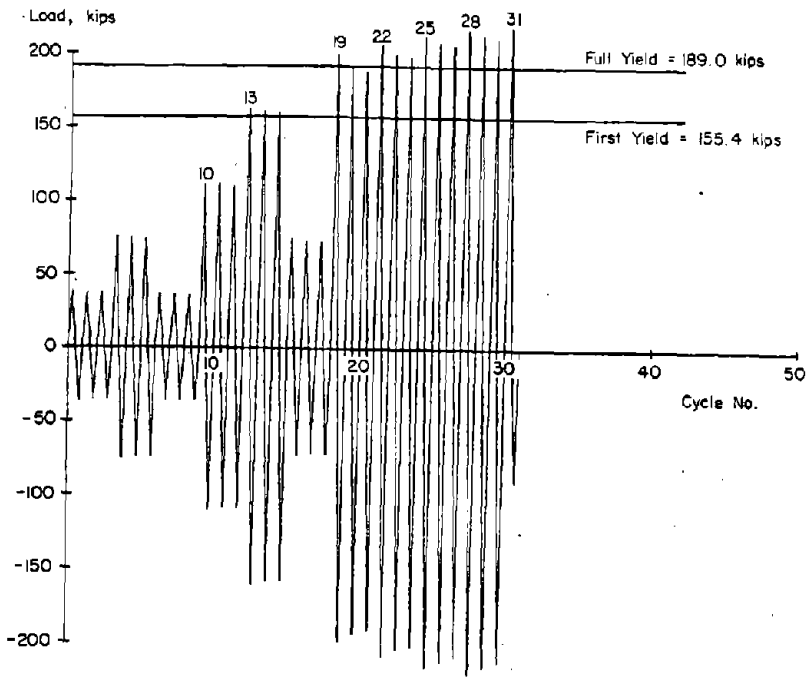

a) Load History

1 in. = 25.4 mm
1 kip = 4.448 kN

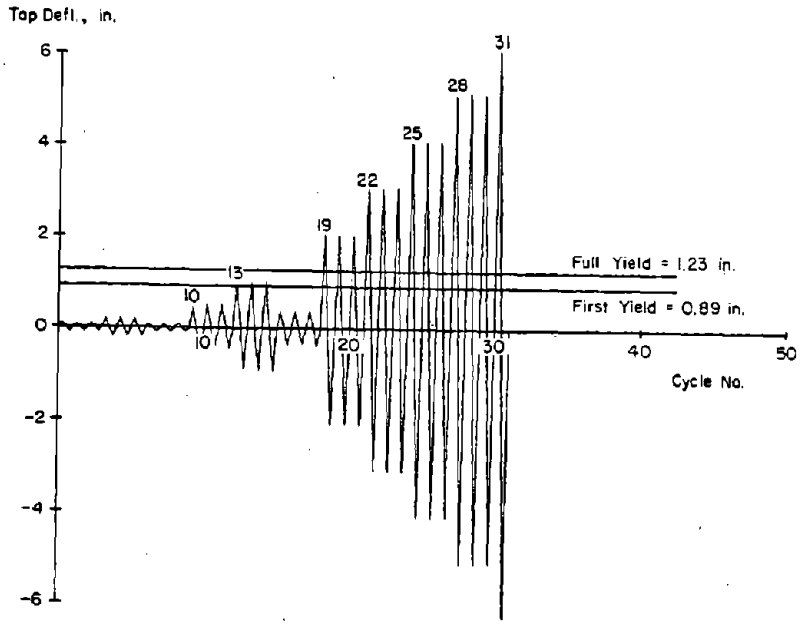

b) Deflection History

Fig. B-57 Loading History for Specimen B8

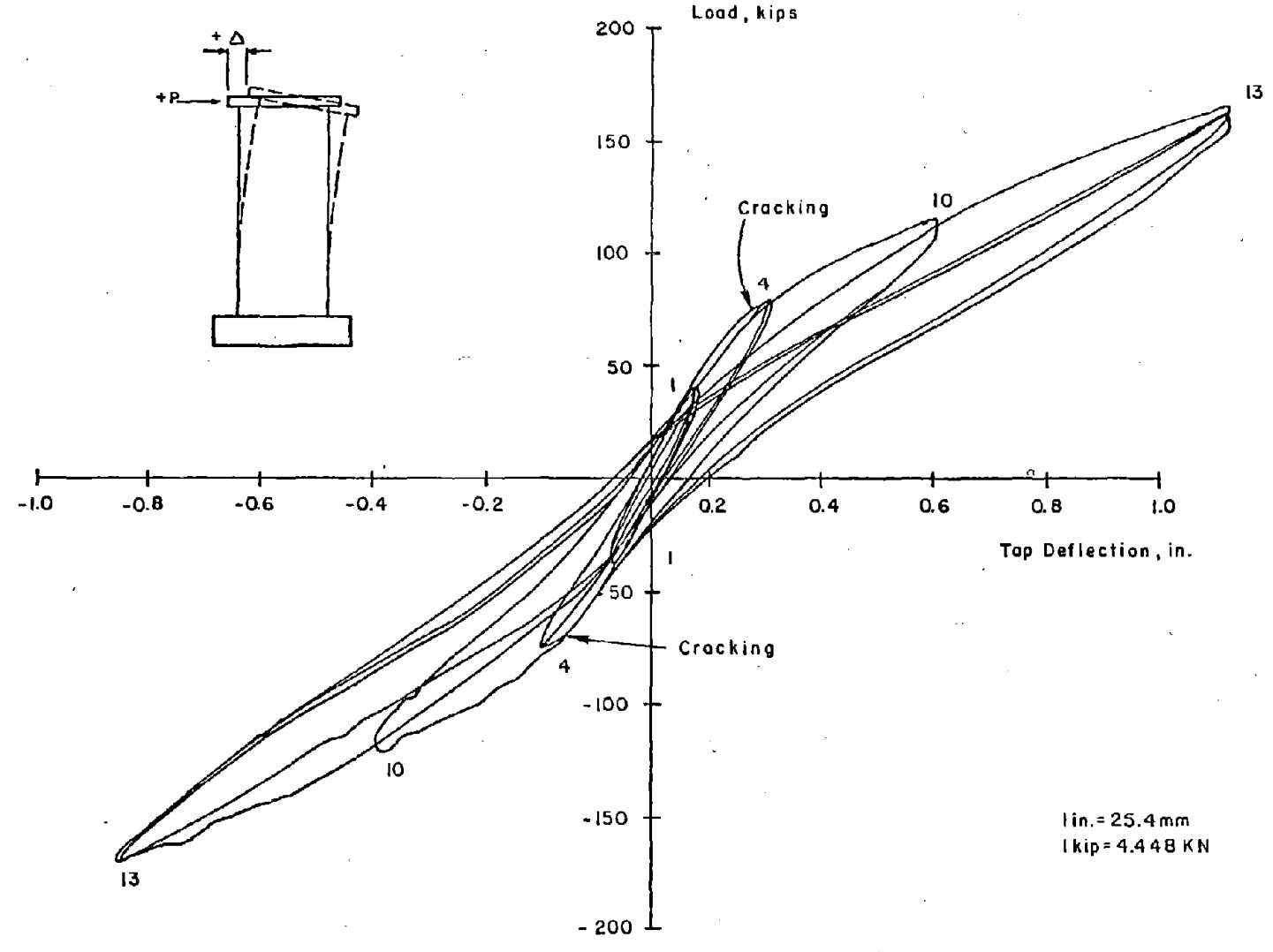

Fig. B-58 Continuous Load - Top Deflection for Initial Cycles for Specimen B8

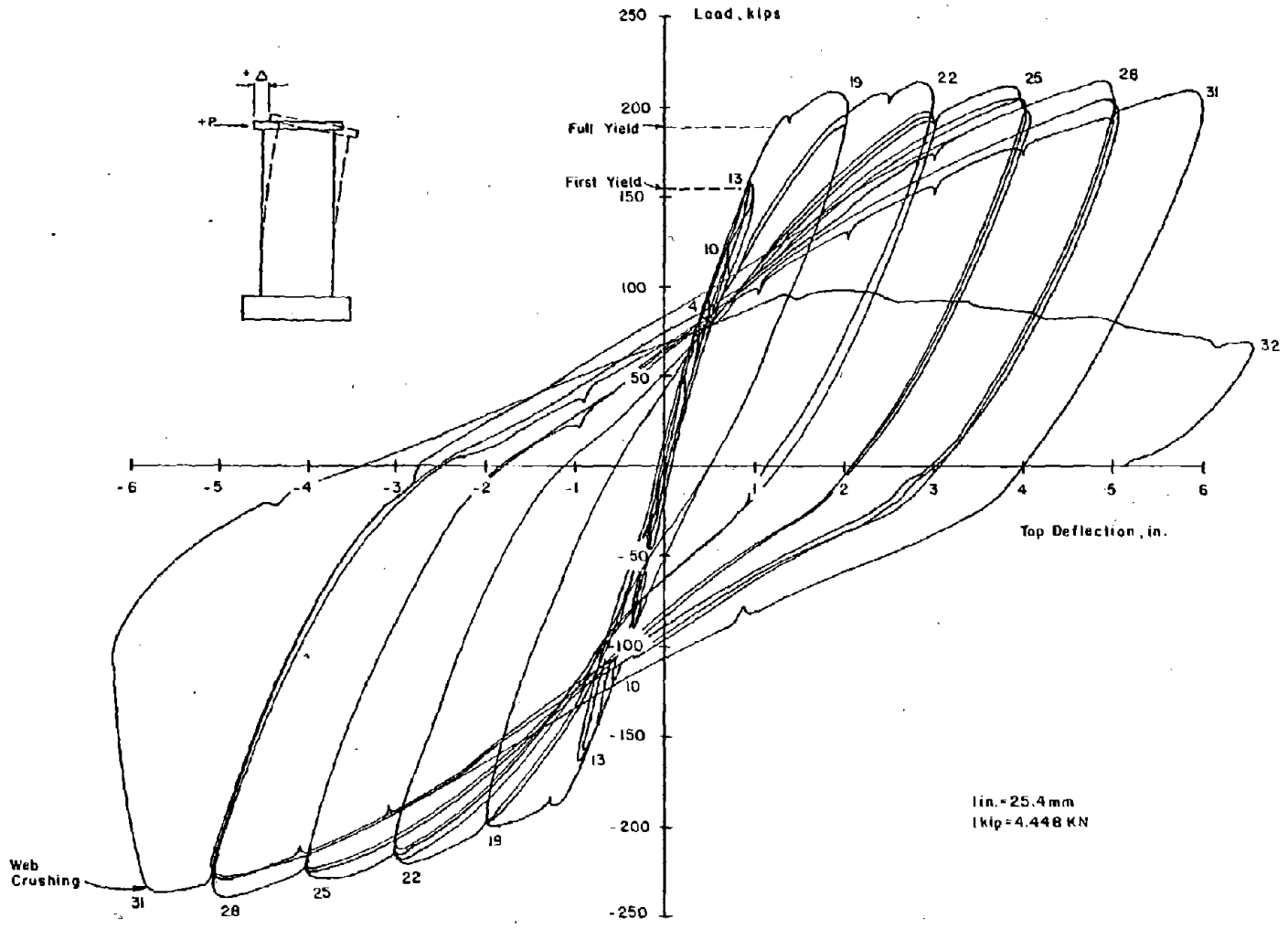

Fig. B-59 Continuous Load - Top Deflection for Specimen B8

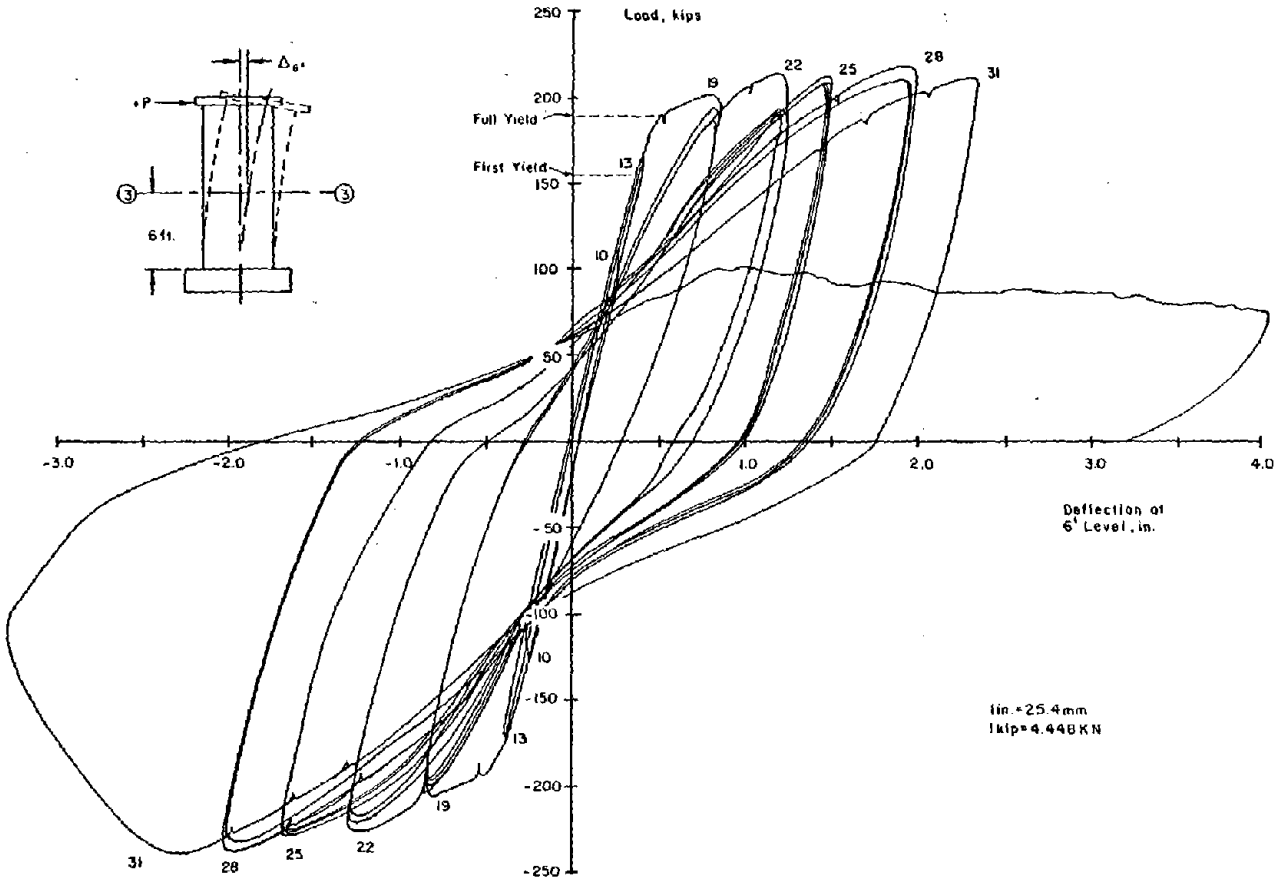

Fig. B-60 Continuous Load - Deflection at 6 ft Level for Specimen B8

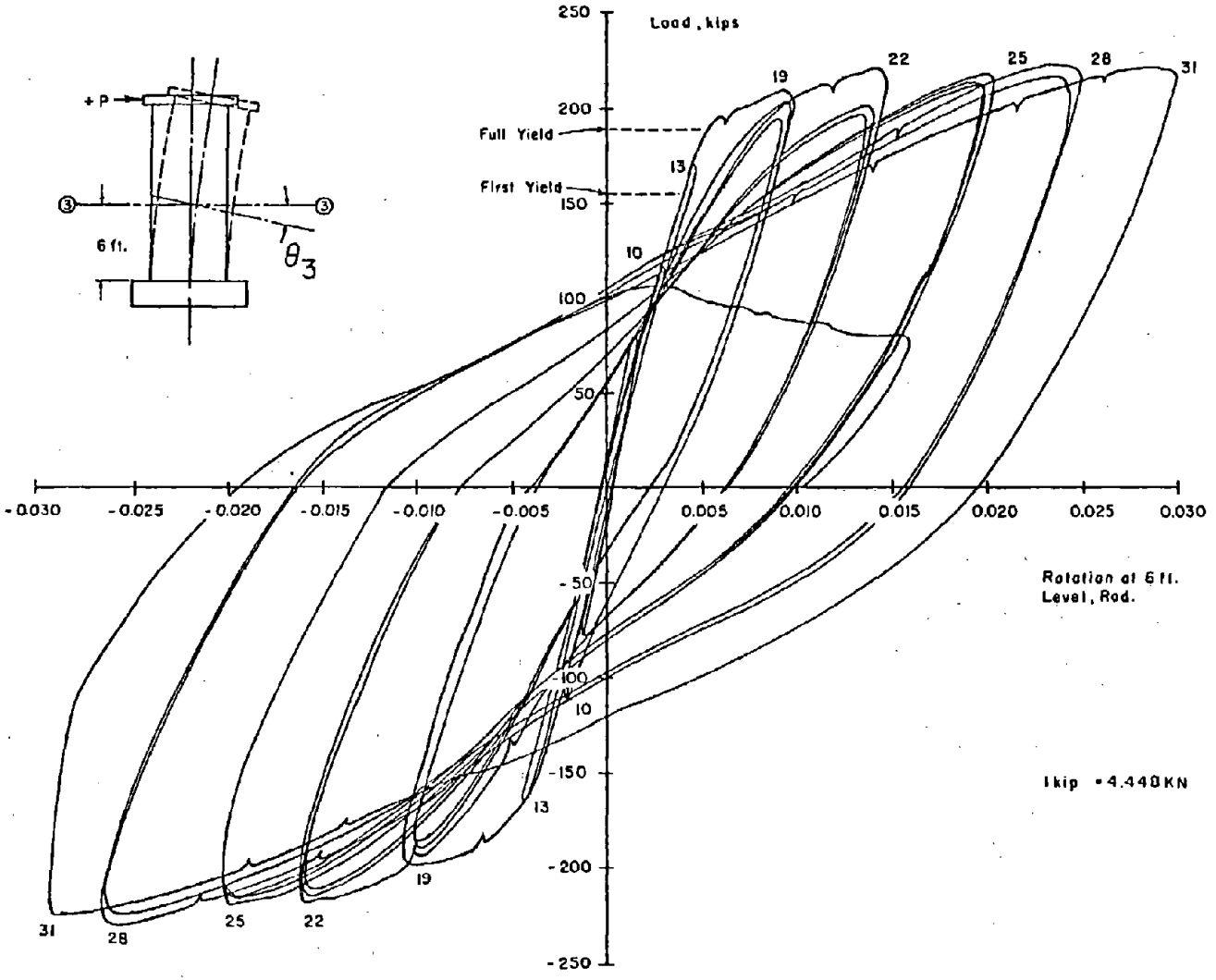

Fig. B-61 Continuous Load - Rotation at 6 ft Level for Specimen B8

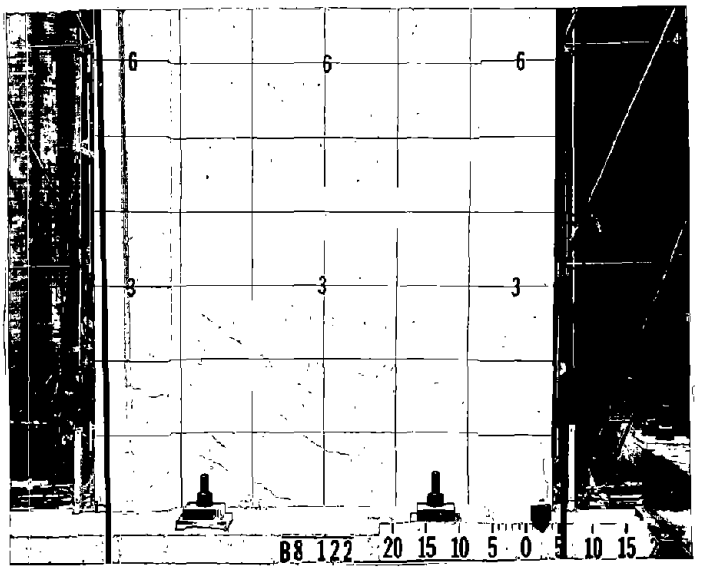

Fig. B-62 Cracking Pattern at +3 in. Deflection for Specimen B8

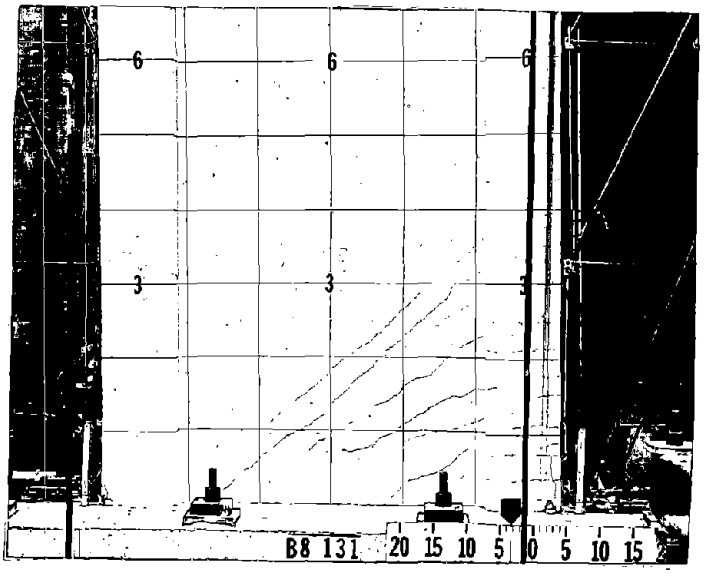

Fig. B-63 Cracking Pattern at -3 in. Deflection for Specimen B8

3-ft lift of the wall was 0.053 in. (1.35 mm) in B7 versus 0.024 (0.61 mm) in B8. Diagonal crack widths above a 45^{o} line through the base remained small throughout the test of Specimen B8. Figures B-64 and B-65 show the cracking in Specimens B7 and B8 at a -5-in. deflection.

Another significant difference in the behavior of Specimen B8 was the development of a predominantly horizontal crack across the wall during the latter part of the test. The horizontal crack was approximately 9 in. (229 mm) above the base. This crack can be seen in Fig. B-66.

For B8, first indication of crushing in the concrete cover of the outer compression faces was noted in Cycle 14. First indication of spalling and flaking along diagonal cracks occurred in Cycle 20. This spalling and flaking in the web and crushing of the outer compression faces progressively increased as more and larger load cycles were applied to the specimen.

A slight indication of crushing in the web near the right and left ends of the horizontal crack approximately 9-in. (229 mm) above the base was noted in Cycle 26.

No reverse curvature of the lower 3 ft of the boundary elements was noted in the test of Specimen B8.

The measured maximum load 219.8 kips (977.7 kN), occurred in Cycle 28 at a -5-in. (127.0 mm) deflection. This load corresponds to a nominal shear stress of $v_{max} = 11.7\sqrt{f'_c}$. This load is nearly identical to the maximum load measured in the test of B7 at an equivalent top deflecion.

A significant increase in the spalling and crushing in the lower 3 ft of the web was noted during the 5-in. deflection loading increment. As the specimen was being loaded to a +6-in. deflection in Cycle 31, a slight but noticeable increase in slip occurred along the horizontal crack about 9 in. (229 mm) above the base. However, load capacity was not affected.

As the specimen was being loaded to a -6-in. deflection in Cycle 31, several compression struts crushed simultaneously. Web crushing was immediately followed by developement of both horizontal and vertical failure planes. Figures B-66 and B-67 show the specimen immediately prior to and after web crushing.

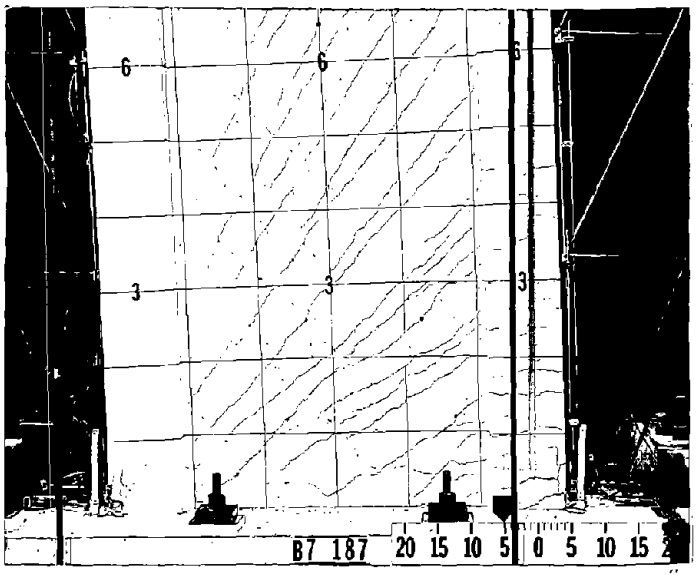

Fig. B-64 Craking Pattern at -5 in. Deflection for Specimen B7

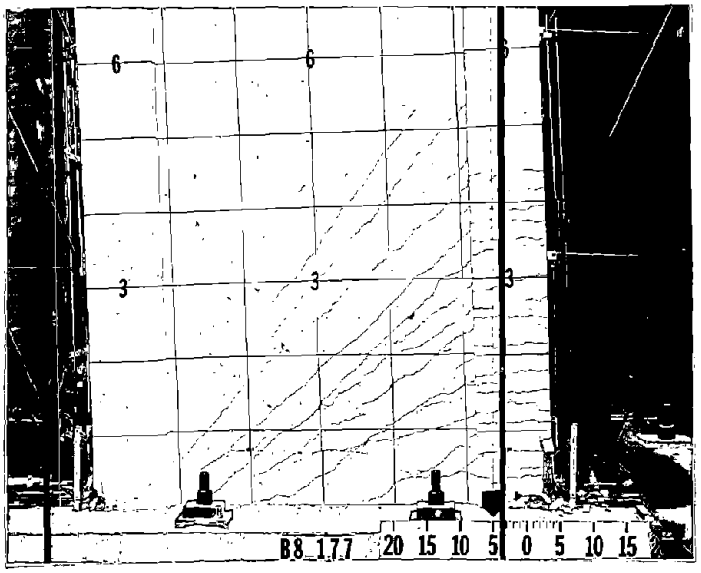

Fig. B-65 Cracking Pattern at -5 in. Deflection for Specimen B8

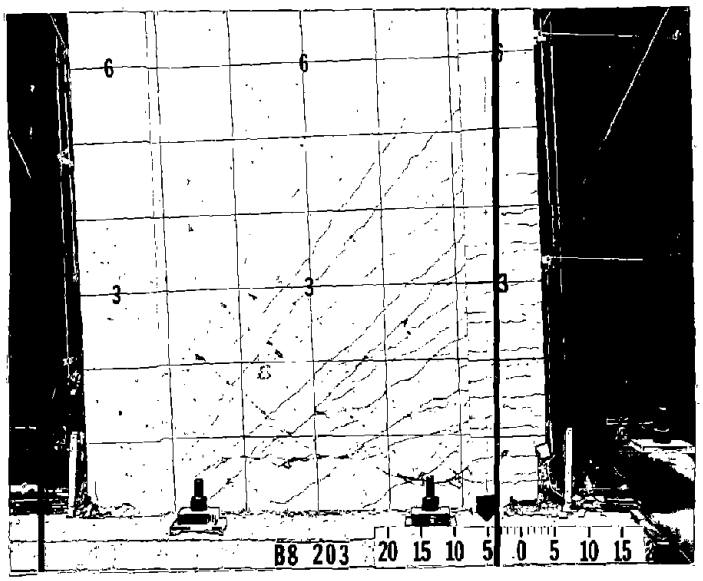

Fig. B-66 Specimen B8 Prior to Web Crushing

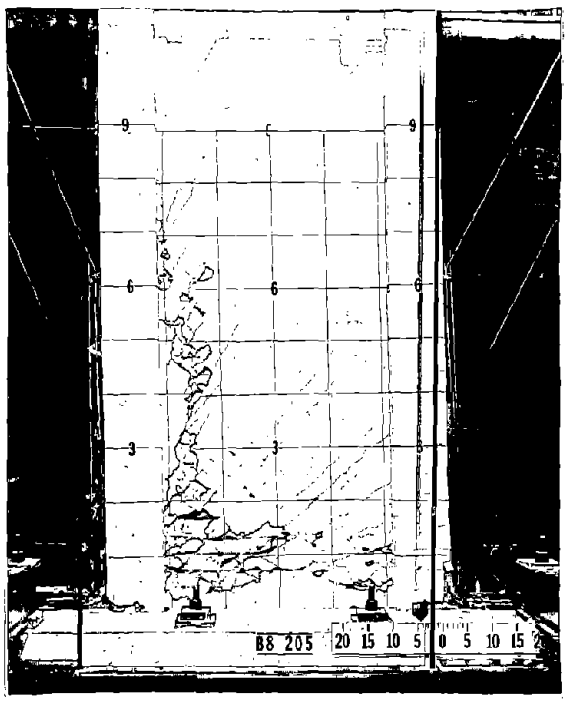

Fig. B-67 - Specimen B8 After Web Crushing

As the load capacity was dropping the specimen was "caught" by closing the deflection control valve in the hydraulic system. The measured load at this stage had decreased to 41% of the maximum measured load.

The specimen sustained at least 80% of the maximum measured load capacity through 12 inelastic cycles. The last inelastic loading increment in which the load was sustained at or above 80% of the maximum for all 3 cycles was at ±5 in. (127.0 mm). This is the same as the results of the test of Specimen B7. The observed load-top deflection envelope for B8 was nearly identical to that of Specimen B7.

Discussion of Results

Moment-Rotation. Moment-rotation data for Specimen B8 are shown in Fig. B-68. The maximum measured moment was 91% of the calculated monotonic maximum. This calculated maximum was based on attainment of an ultimate compressive strain of $\varepsilon_u = 0.0065$ in the boundary element.

The relationship between calculated monotonic and measured rotations at the 3-ft (0.91 m) and 6-ft (1.83 m) levels differed from that observed in previous tests. For B8, the relationship between calculated and measured rotations at the 3-ft (0.91 m) and 6-ft (1.83 m) levels were approximately the same. In previous specimens, rotations were concentrated in the lower 3 ft. In addition, for B8 there was no noticeable pinching in the loops at the 3-ft and 6-ft levels. This is attributed to additional capacity across diagonal cracks from the increased horizontal reinforcement.

Maximum rotations attained in Specimen B8, and corresponding rotational ductilities, were nearly identical to those in Specimen B7.

Shear Distortion. Shear-distortion loops for B8 are shown in Fig. B-69. As in the previously reported tests, a shear "yielding" occurred during the same cycle in which flexural

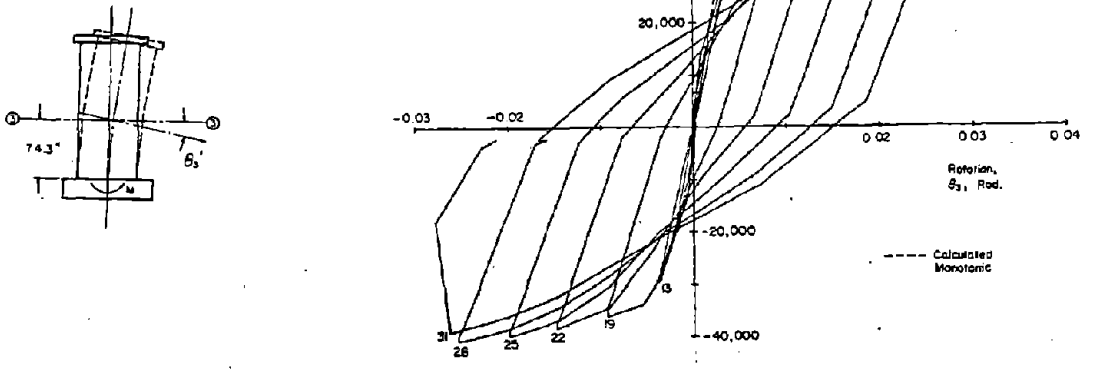

a) At 6 ft Level

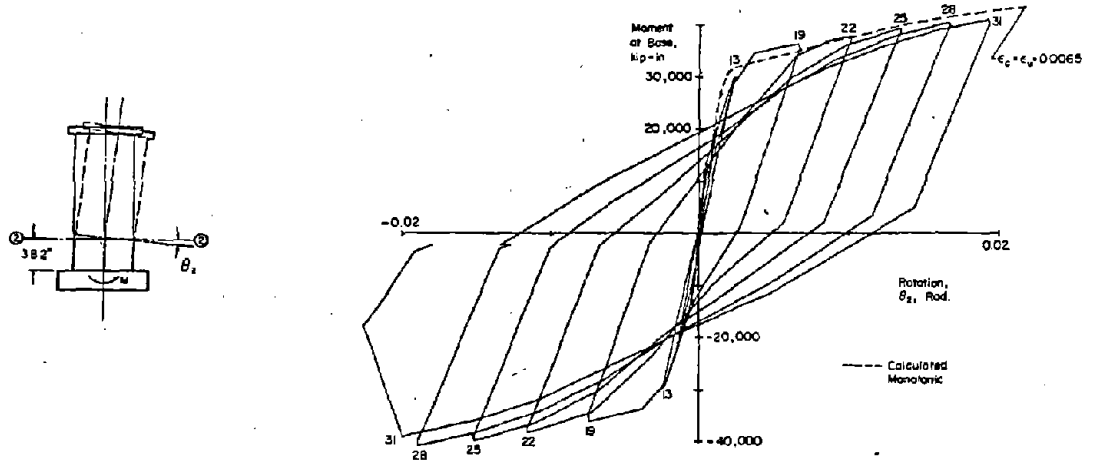

b) At 3 ft Level

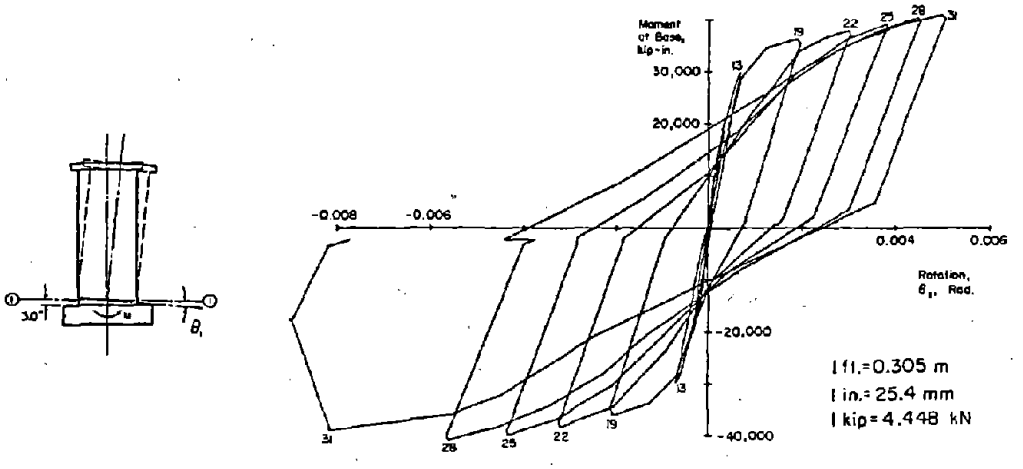

c) At Base Level

Fig. B-68 Moment at Base versus Rotation for Specimen B8

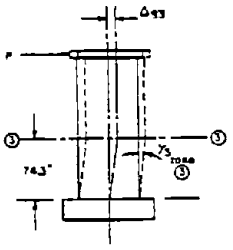

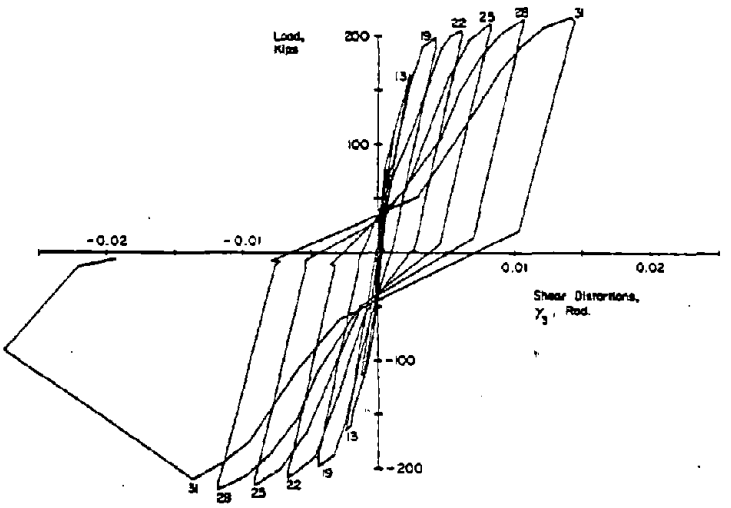

a) In Base to 6 ft Level

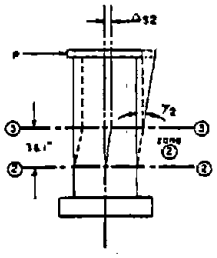

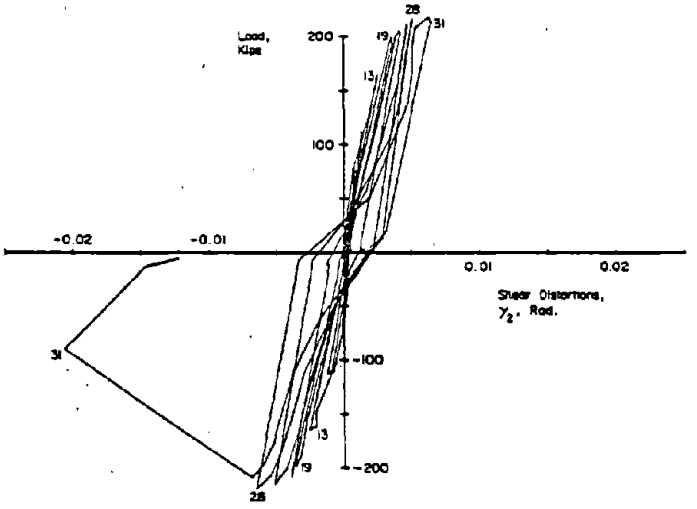

b) In 3 ft to 6 ft Level

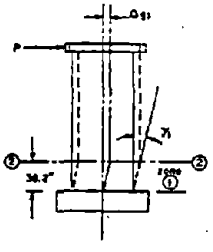

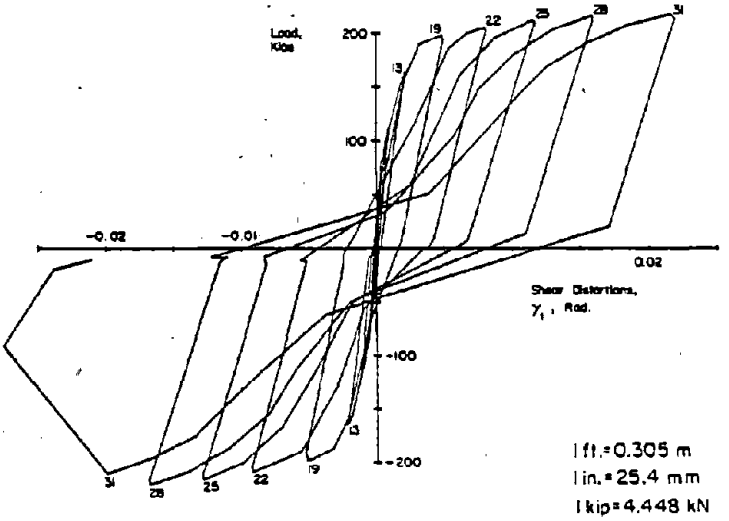

c) In Base to 3 ft Level

Fig. B-69 Load versus Shear Distortion for Specimen B8

yielding occurred. However, for B8 this "yielding" was not as evident in the 3-ft to 6-ft zone. Practically all of the inelastic shear distortions occurred in the lower 3 ft (0.91 m). This result is attributed to the additional capacity across diagonal cracks provided by the extra horizontal steel. This additional capacity decreased the "spread" of vertical steel yielding that accompanies diagonal cracking. Thus, with the extent of flexural yielding decreased in Zone 2, the "shear yielding" also decreased.

A comparison of shear distortions in B7 and B8 indicates nearly identical distortions occurred in Zone 1 which was the major zone of distortions in both specimens. However, with the reduced distortions in Zone 2 of B8, the total distortions in Zone 3 were reduced by approximately 15% over those in B7. This is a relatively insignificant increase in shear stiffness compared to the increase in amount of horizontal reinforcement.

Slip at Construction Joints. Slip at construction joints in B8 is shown in Fig. B-70. Slip at CJ1 exhibits yielding similar to shear "yielding". This occurred during the same cycle that flexural yielding occurred. As shown in Fig. B-71, the slip at CJ1 was a relatively constant 15% of the total shear deflection in the lower 3 ft (0.91 m).

The magnitude of slips at CJ1 in Specimen B8 were nearly identical to those in Specimen B7. Although the slip plots for CJ2 and CJ3 in Specimen B8 are unsymmetrical and affected by diagonal cracking, these plots show significantly less movement at these locations than was observed in Specimen B7. The horizontal components of diagonal crack widths were lower in B8.

Deflections. Deflection components and deflected shapes are shown in Figs. B-72 and B-73. These figures show that shear deflections are a relatively constant portion of the total throughout most of the test and increased slightly near the end of the test.

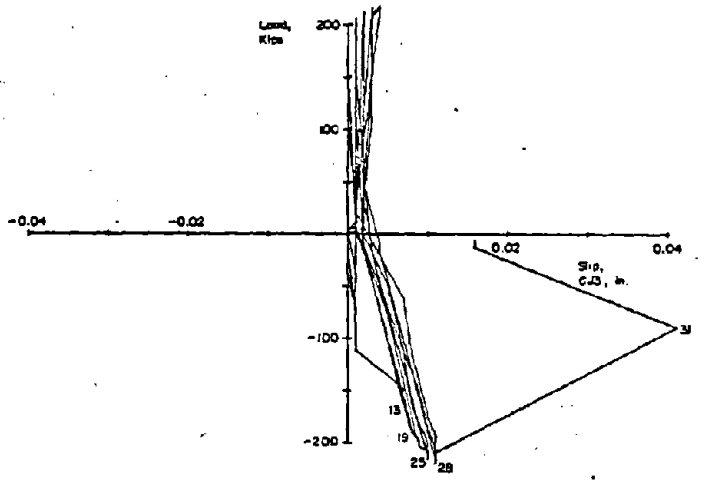

a) At 6 ft Level

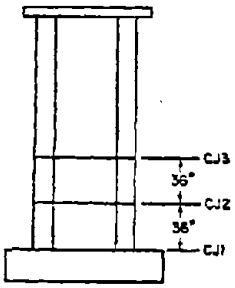

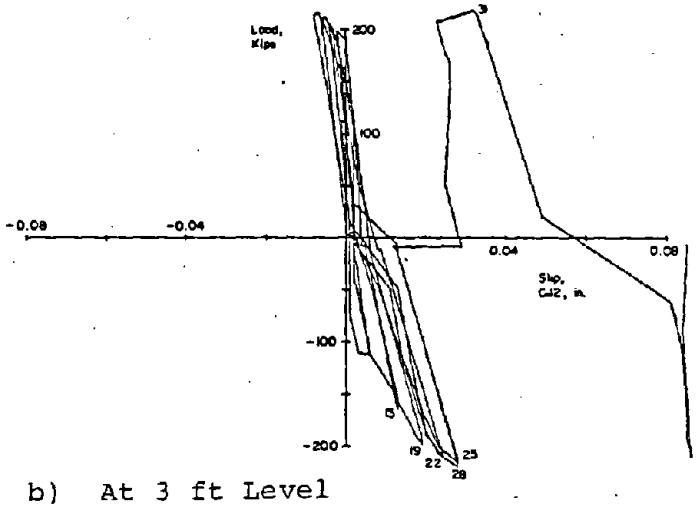

b) At 3 ft Level

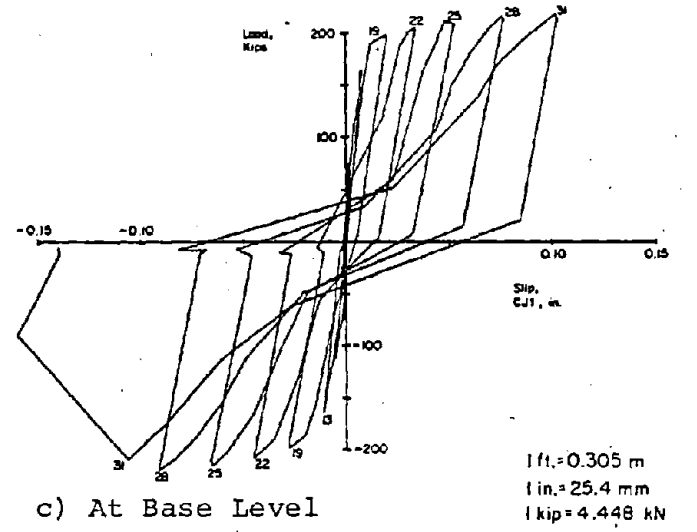

c) At Base Level

Fig. B-70 Load versus Slip at Construction Joints for Specimen B8

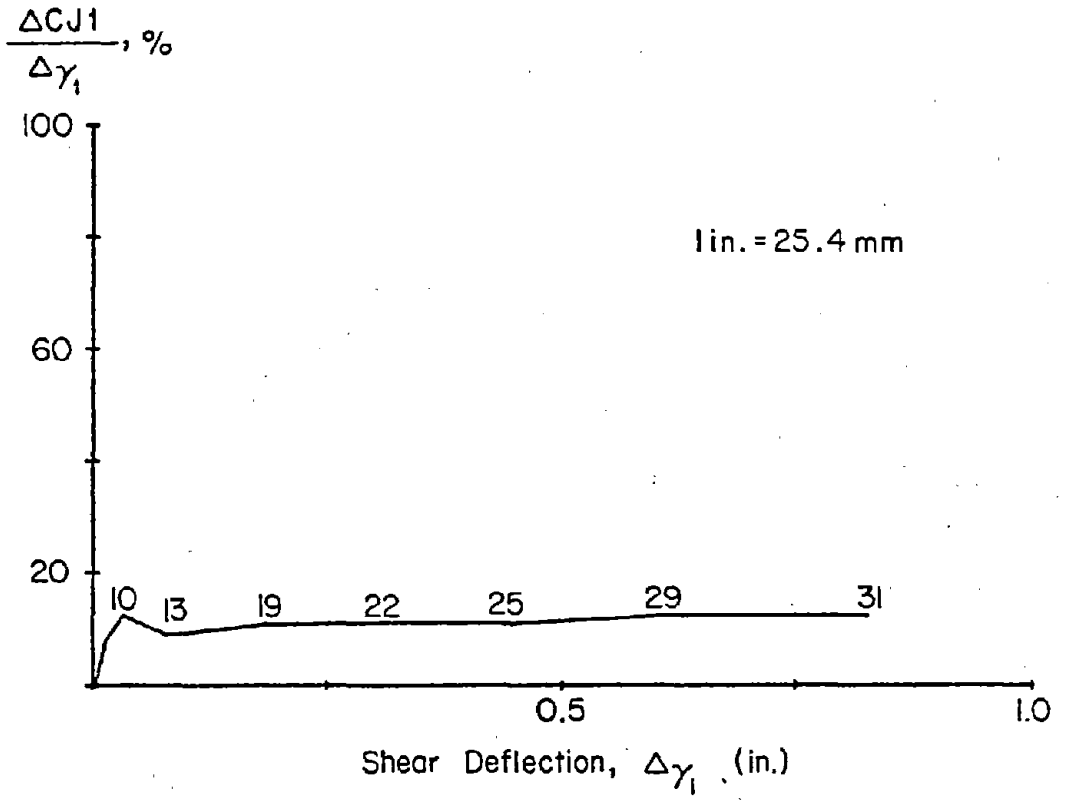

a) At Maximum Positive Loads

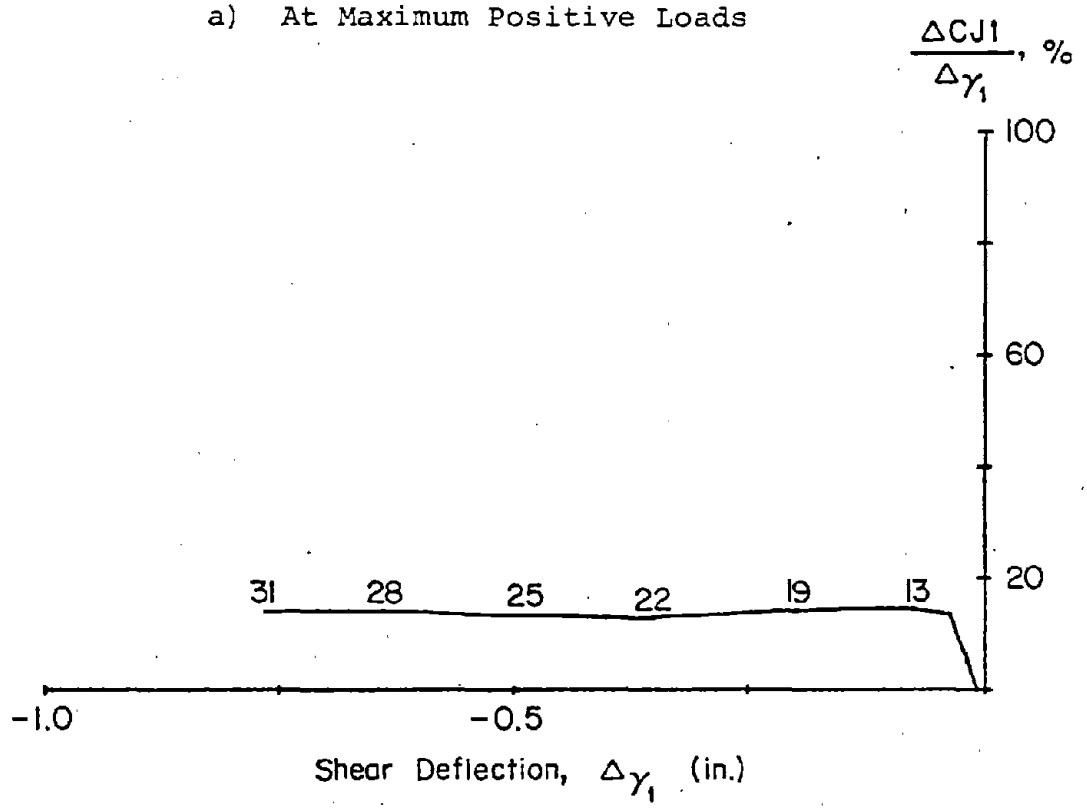

b) At Maximum Negative Loads

Fig. B-71 Slip at Base Construction Joint versus Shear Deflection in Zone 1 for Specimen B8

a) At Top of Wall

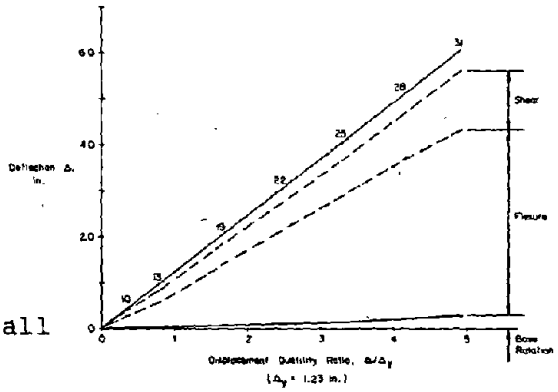

b) At 6 ft Level

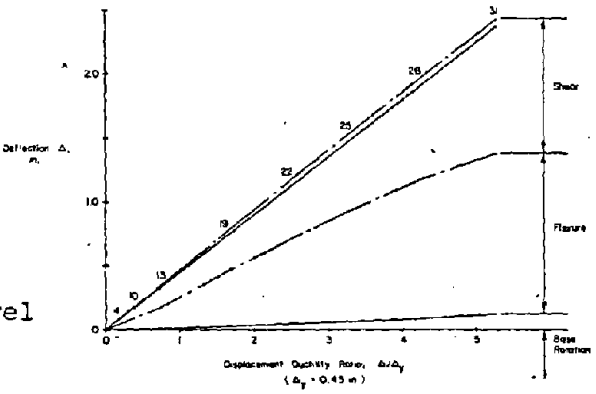

c) At 3 ft Level

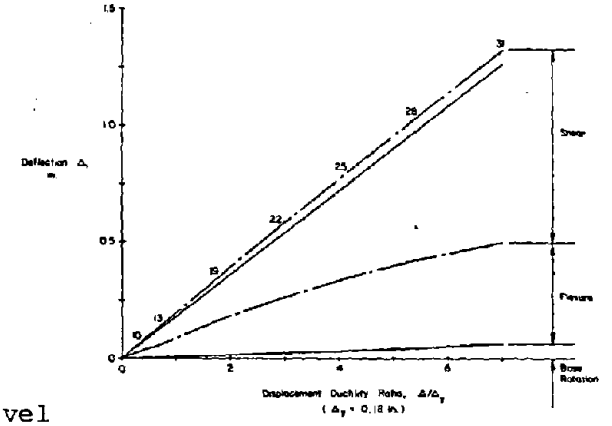

CALCULATED FROM MEASURED DEFORMATION
EXTRAPOLATED
MEASURED TOTAL

1 in. = 25.4 mm
1 ft. = 0.305 m

Fig. B-72 Components of Deflection for Specimen B8

a) Flexural

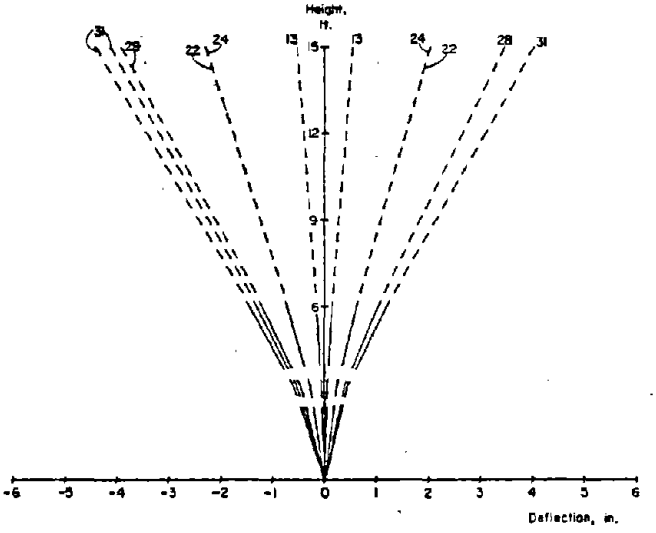

b) Shear

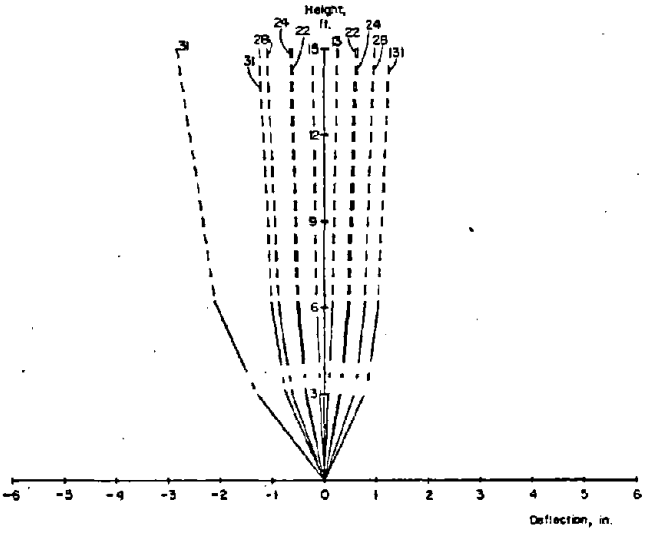

c) Total

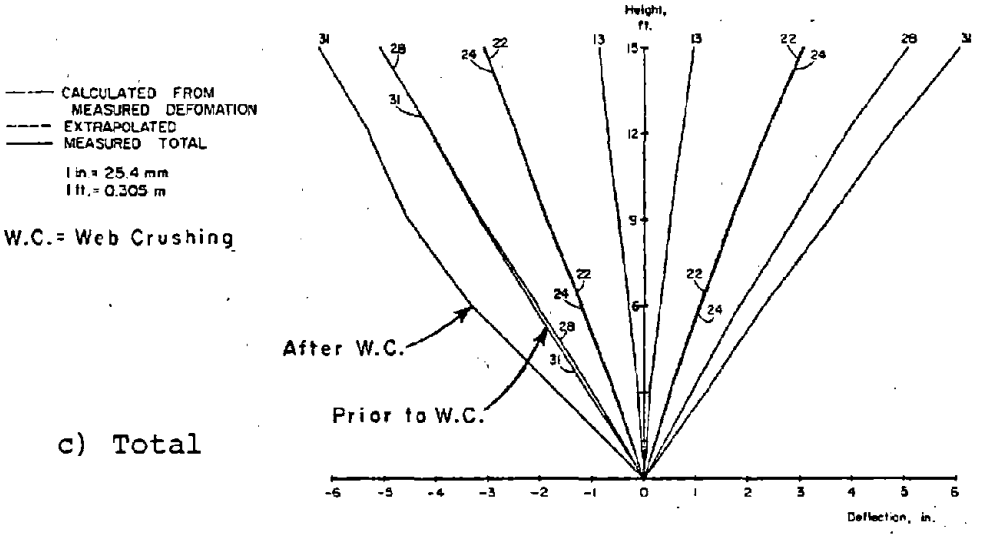

Fig. B-73 Deflected Shape for Specimen B8

The deflected shapes for Cycles 22 and 24 show only a slight decrease in shear stiffness during the 3-in. (76.2 mm) increment. A large decrease in stiffness is indicated by the deflected shapes for Cycles 28 and 31, at an equal top deflection of -5-in. (127.0 mm).

Reinforcement Strains. Figures B-74 through B-84 show reinforcement strains in the specimen at various stages.

Figure B-74 shows the cyclic load versus strain relationship for the outer reinforcing bars at the base level.

Figure B-75 shows that yielding occurred up to the 9-ft (2.75 m) level in Cycle 28. However, a comparison of data for B8 and B7 indicates that the extent of yielding up the wall was slightly lower in B8 at equivalent load stages.

Figures B-76 and B-77 show the strain gradient in the vertical reinforcement at various levels. The gradient in the compression zone near the base shows the neutral axis moving away from the outer compression face in the latter cycles indicating the ultimate concrete compressive stress had been reached in the outer fibers.

Figures B-78 through B-82 show the cyclic strain-load relationship and the strain gradients in the horizontal bars. These figures indicate that although the yield strain was approached, only gage HE 2 showed significant yielding in the last few cycles of the test. Figures B-79 and B-80 for gages HH and HA indicate that, although no yielding occurred near the end hooks, appreciable stresses were present. This was particularly evident in the lower 18 in. (0.46 m) because the boundary elements act as dowels in this region.

Figures B-83 and B-84 show the cyclic strain-load relationship and the vertical strain gradient in the outer leg of the confinement hoops. These figures show that only hoops in the lower two feet were stressed significantly. Strains near yield were observed in the hoops in the latter cycles of the test.

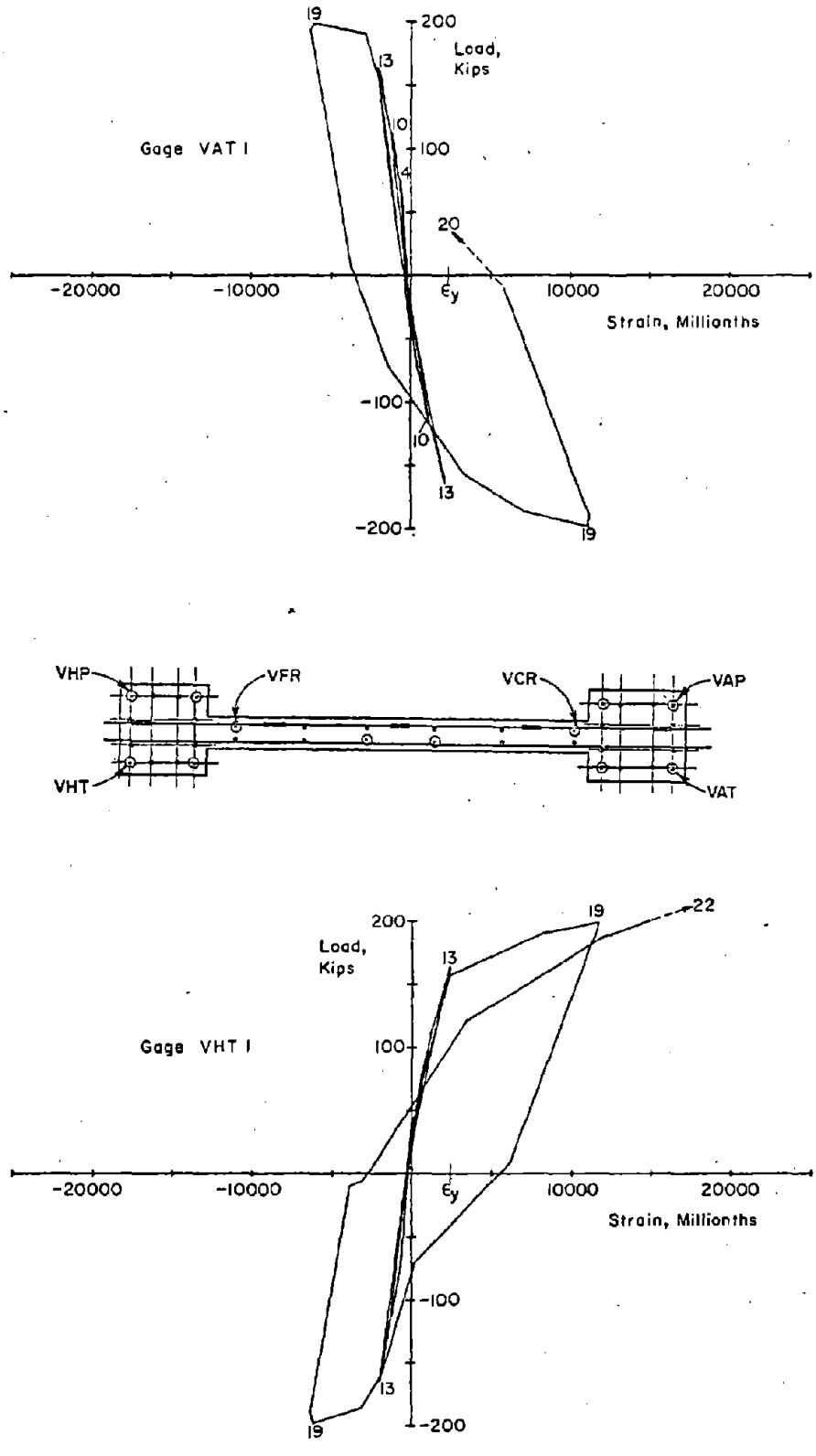

1 kip = 4.448 kN

Fig. B-74 Measured Strains on Vertical Reinforcment at Base of Specimen B8

1 ft.=0.305 m

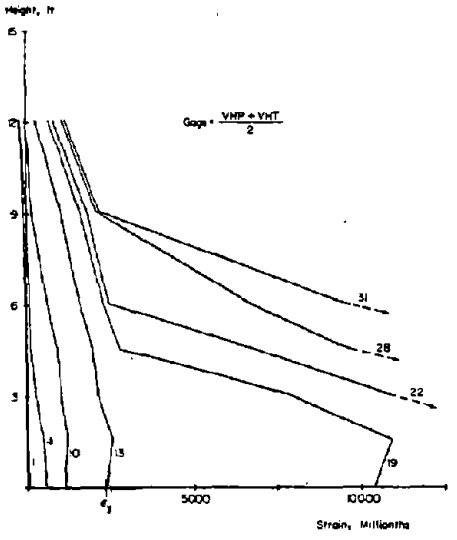

a) Average of VHP and VAT

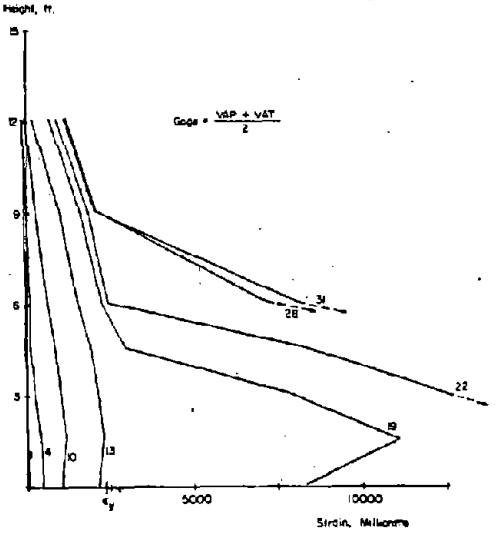

b) Average of VAP and VAT

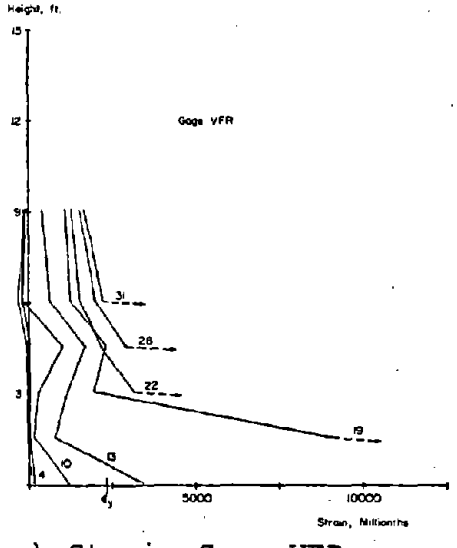

c) Strain Gage VFR

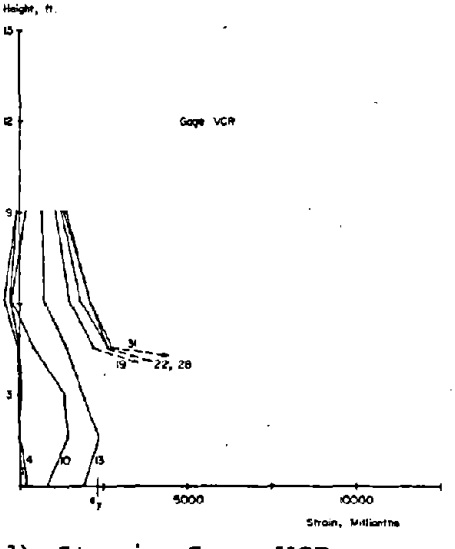

d) Strain Gage VCR

Fig. B-75 Vertical Reinforcement Strains at Maximum Loads for Specimen B8

1 ft = 0.305 m

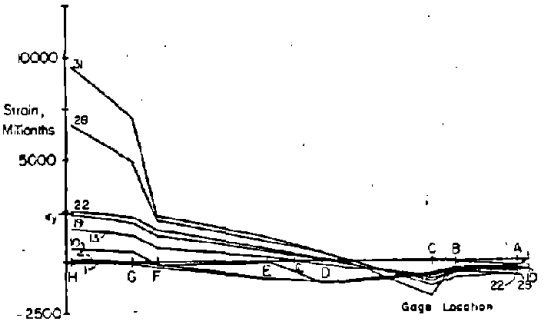

a) At 6 ft Level

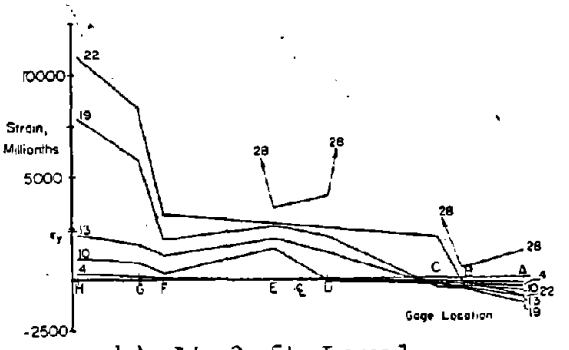

b) At 3 ft Level

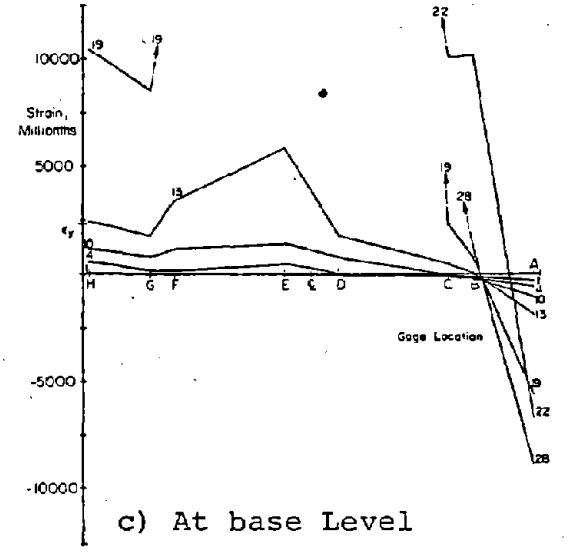

c) At base Level

Fig. B-76 Vertical Reinforcement Strains at Maximum Positive Loads for Specimen B8

1 ft. = 0.305 m

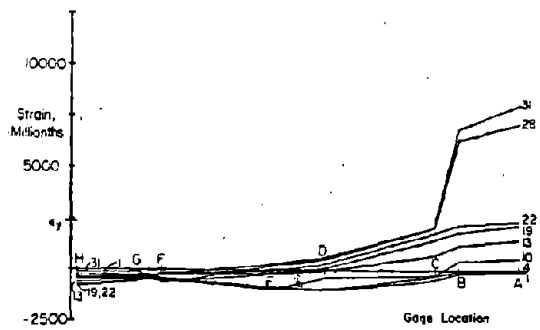

a) At 6 ft Level

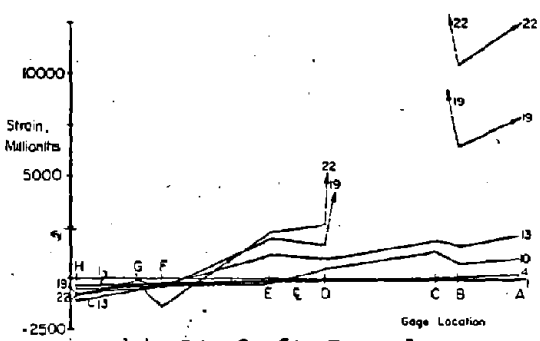

b) At 3 ft Level

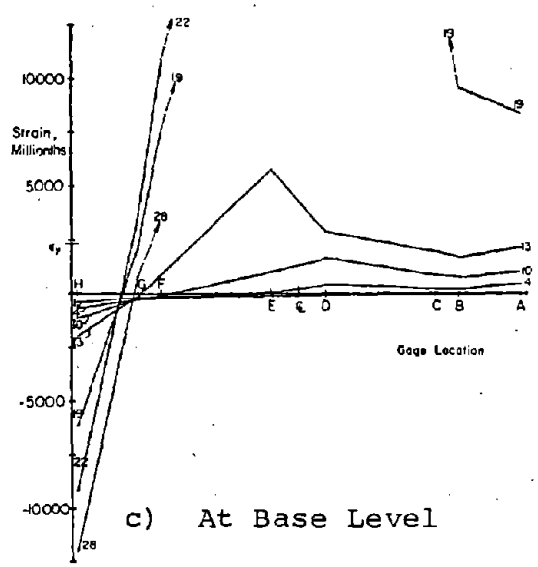

c) At Base Level

Fig. B-77 Vertical Reinforcement Strains at Maximum Negative Loads for Specimen B8

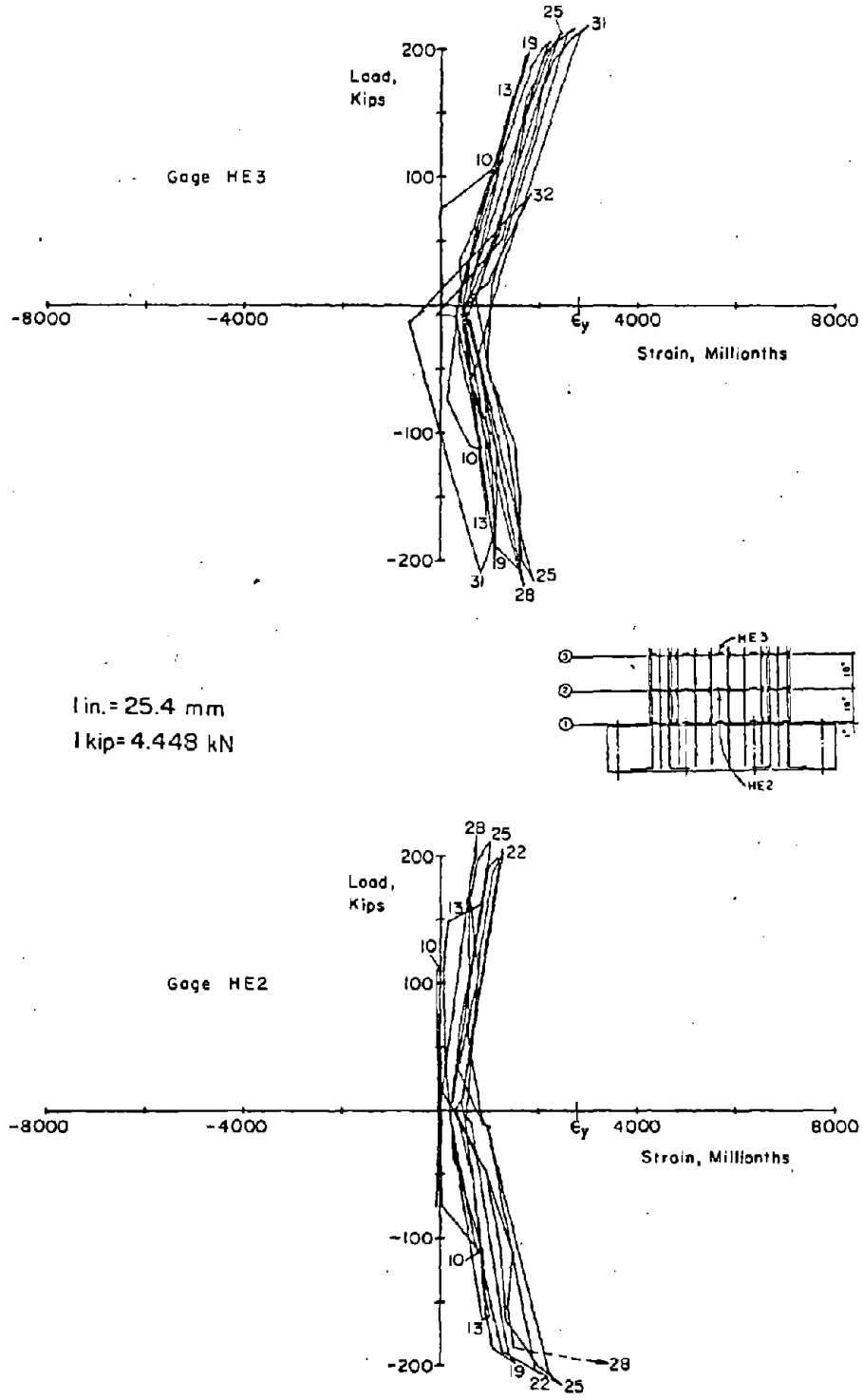

Fig. B-78 Measured Strains on Horizontal Reinforcement for Specimen B8

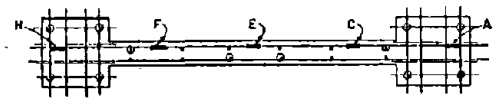

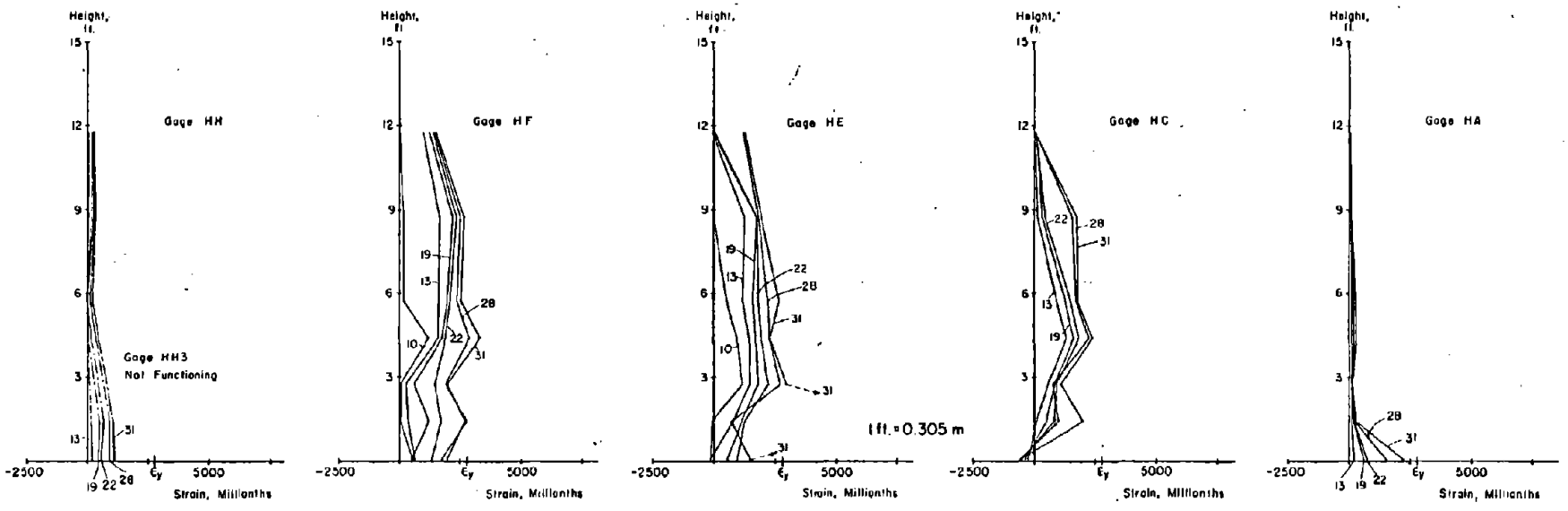

Fig. B-79 Horizontal Reinforcement Strains at Maximum Positive Loads for Specimen B8

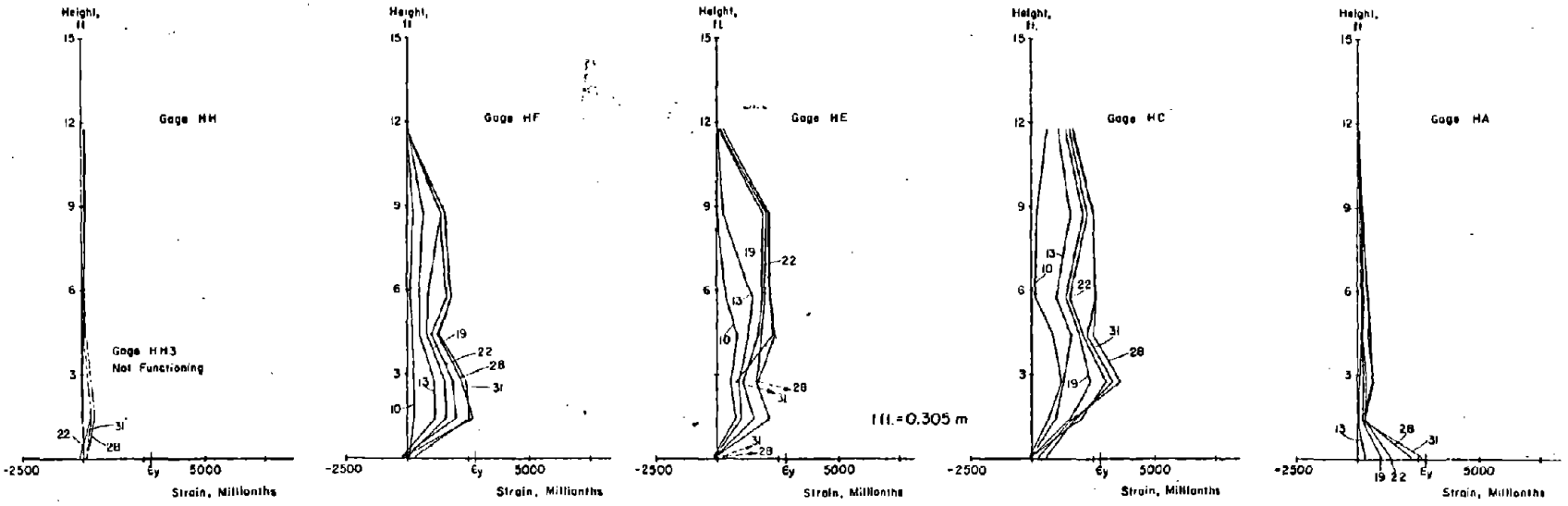

Fig. B-80 Horizontal Reinforcement Strains at Maximum Negative Loads for Specimen B8

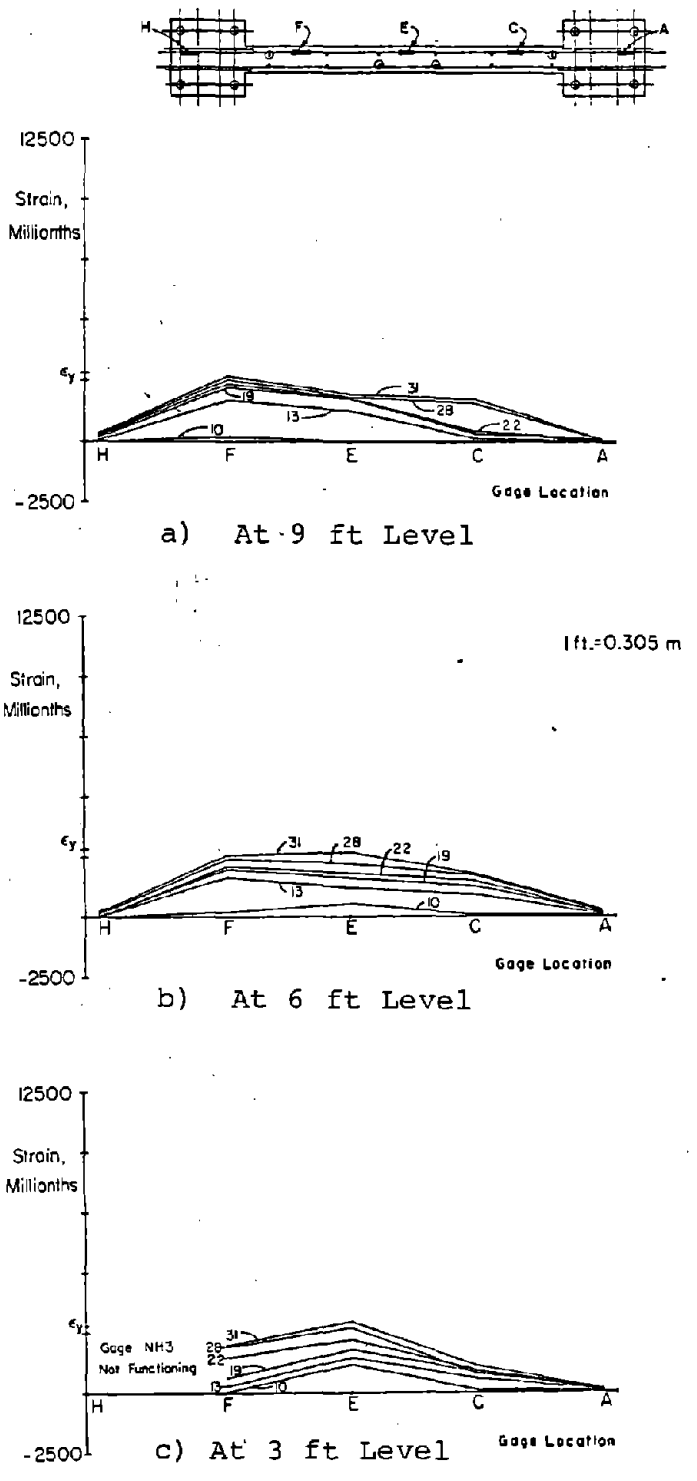

Fig. B-81 Horizontal Reinforcement Strains in Web at Maximum Positive Loads for Specimen B8

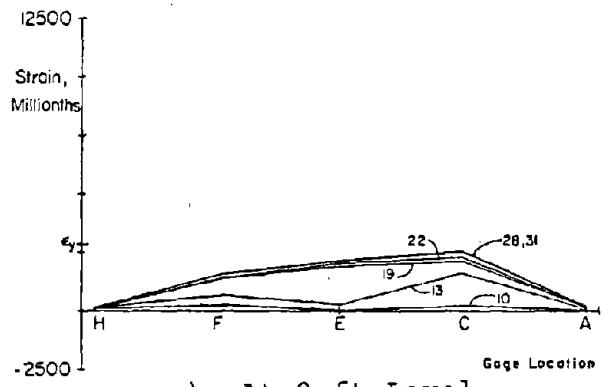

a) At 9 ft Level

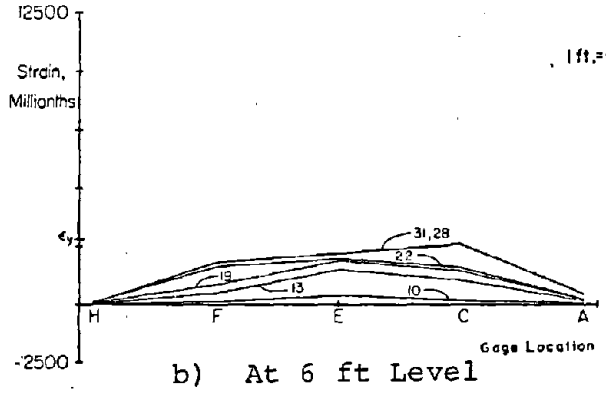

b) At 6 ft Level

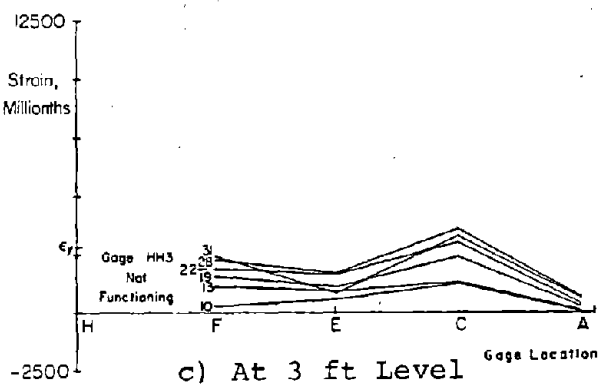

c) At 3 ft Level

Fig. B-82 Horizontal Reinforcement Strains in Web at Maximum Negative Loads for Specimen B8

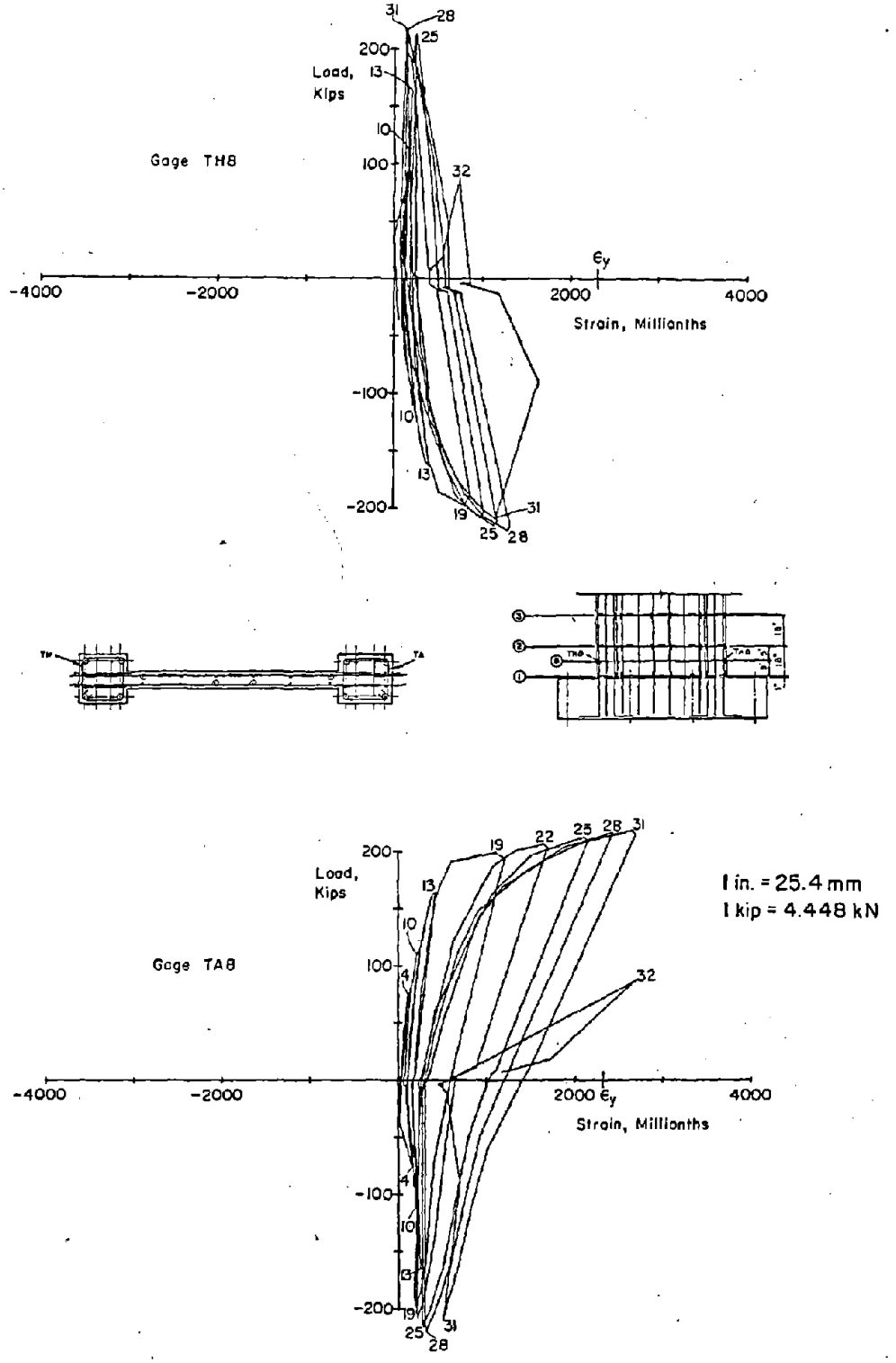

Fig. B-83 Measured Strains on Confinement Hoop Reinforcement for Specimen B8

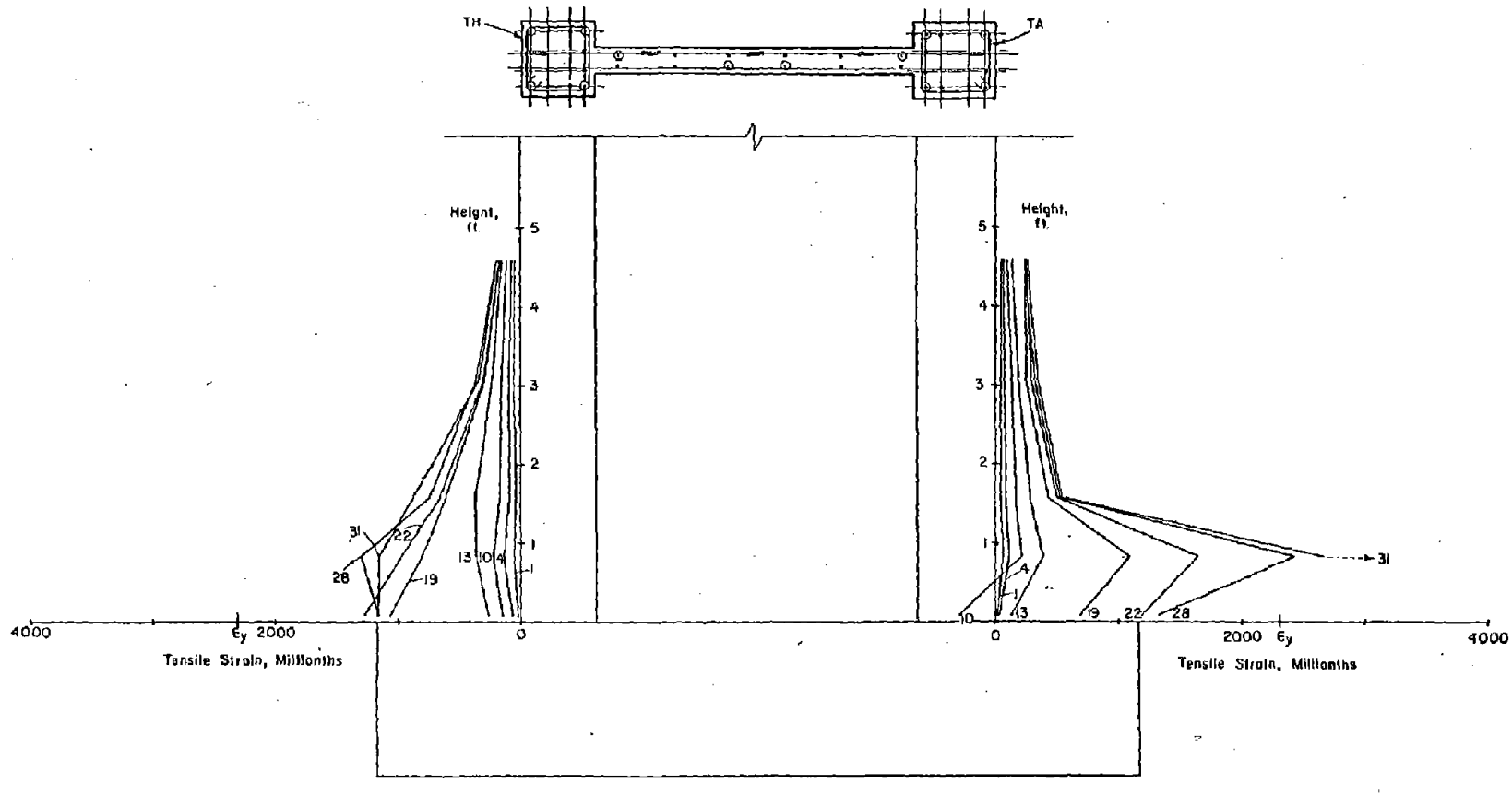

Fig. B-84 Confinement Hoop Reinforcement Strains at Maximum Loads for Specimen B8

Specimen B9

Test Description

Specimen B9 was similar to Specimen B7 with 3.67% vertical reinforcement in each column and confinement reinforcement in the lower 6 ft of the boundary element. Specimen B9 was tested to investigate the significance of loading history on the behavior of the wall.

Specimen B7 attained a maximum measured rotation at the 6-ft level of θ_{max} = 0.0242 rad. in Cycle 28. This corresponds to a rotational ductility of θ_{max} / θ_y = 5.2. The load capacity of the specimen was sustained through three full reversed cycles at this deformation level. Therefore, the available rotational ductility in Specimen B7 was taken as 5.0 for the incrementally increasing load history.

To determine if at least this ductility of 5.0 was available for the load history described in Appendix A, θ_{max} for the first inelastic cycle of Specimen B9 was taken as five times the measured full yield rotation of Specimen B7.

As in Specimen B7, Specimen B9 was loaded axially at a uniform stress 545 psi (3.75 MPa) during the lateral load test.

The test consisted of four complete loading cycles as shown in Fig. B-85. The complete load versus top deflection relationship for Specimen B9 is shown in Fig. B-86. The complete load versus deflection and rotation relationships at the 6-ft level are shown in Figs. B-87 and B-88.

The first load cycle was applied to develop cracking in both directions. First significant cracking was observed at a load of 75 kips (334 kN).

First yielding occurred in Cycle 2, Load Stage 18, at a load of 158.0 kips (703.0 kN). Full yielding occurred in Cycle 2, Load Stage 19, at a load of 186.4 kips (829.1 kN). The maximum measured crack widths at this stage were 0.011 in. (0.28 mm) in the tension column and 0.015 in. (0.38 mm) across a diagonal crack in the web.

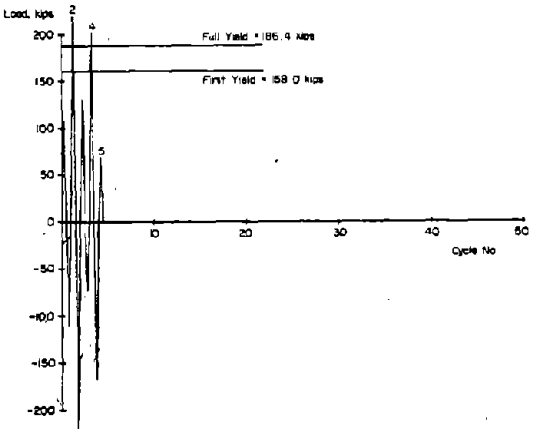

a) Load History

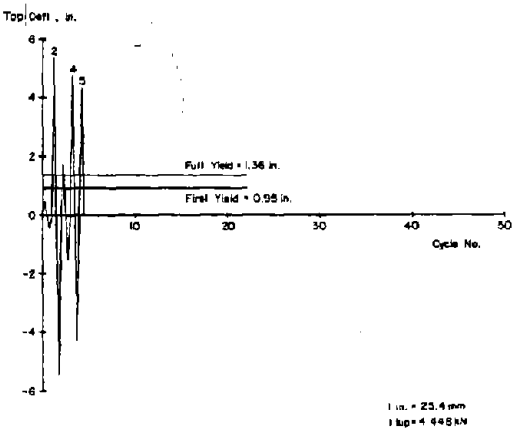

b) Deflection History

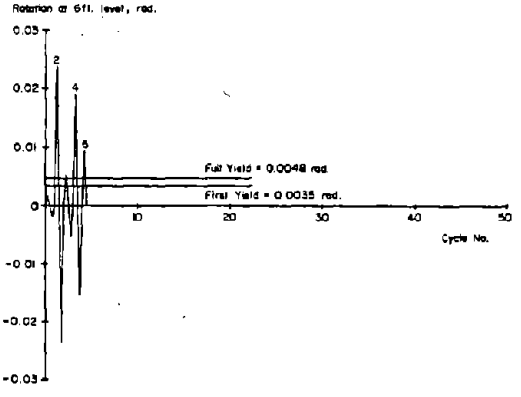

c) Rotation History

Fig. B-85 Loading History for Specimen B9

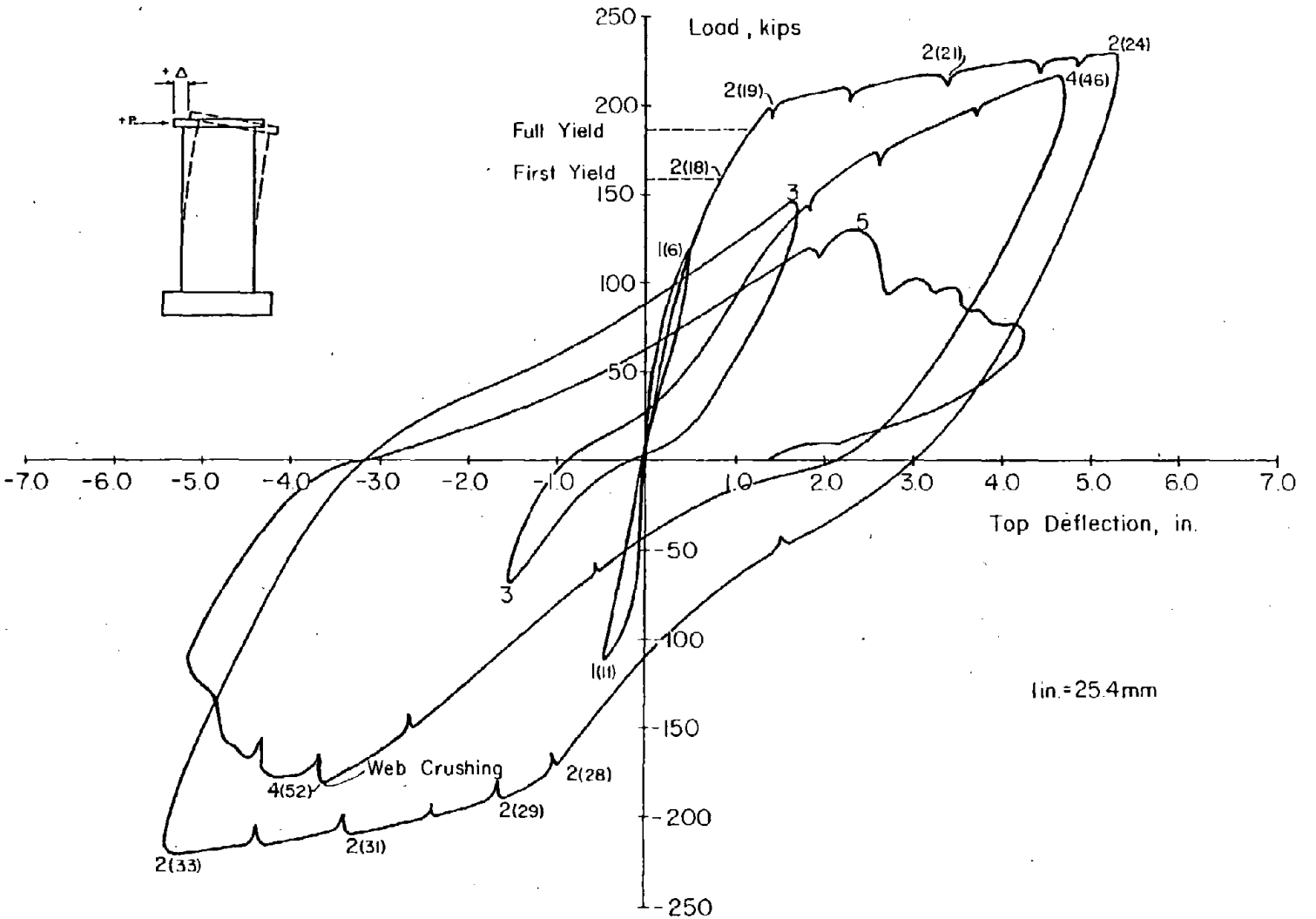

Fig. B-86 Continuous Load - Top Deflection for Specimen B9

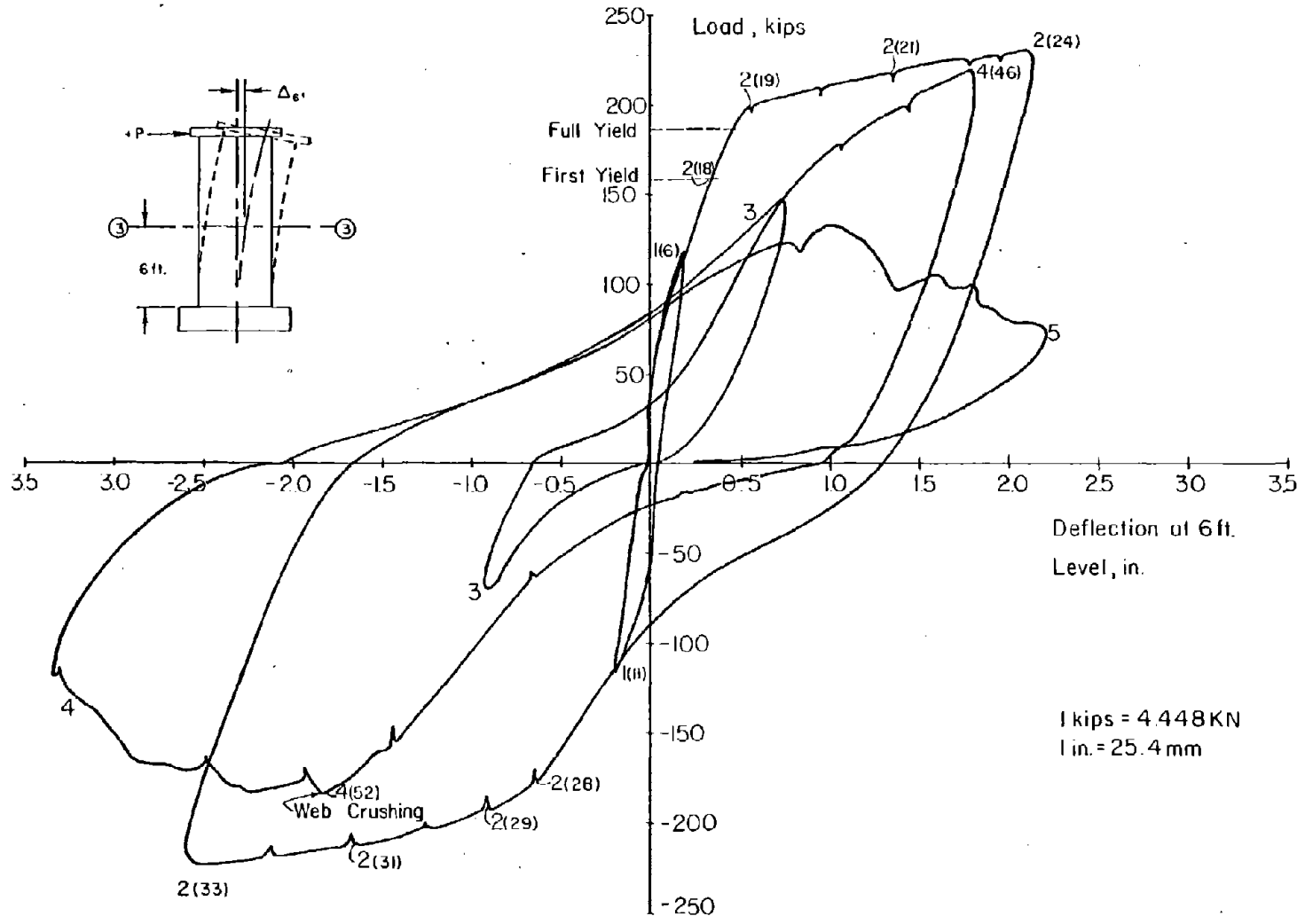

Fig. B-87 Continuous Load - Deflection at 6 ft Level for Specimen B9

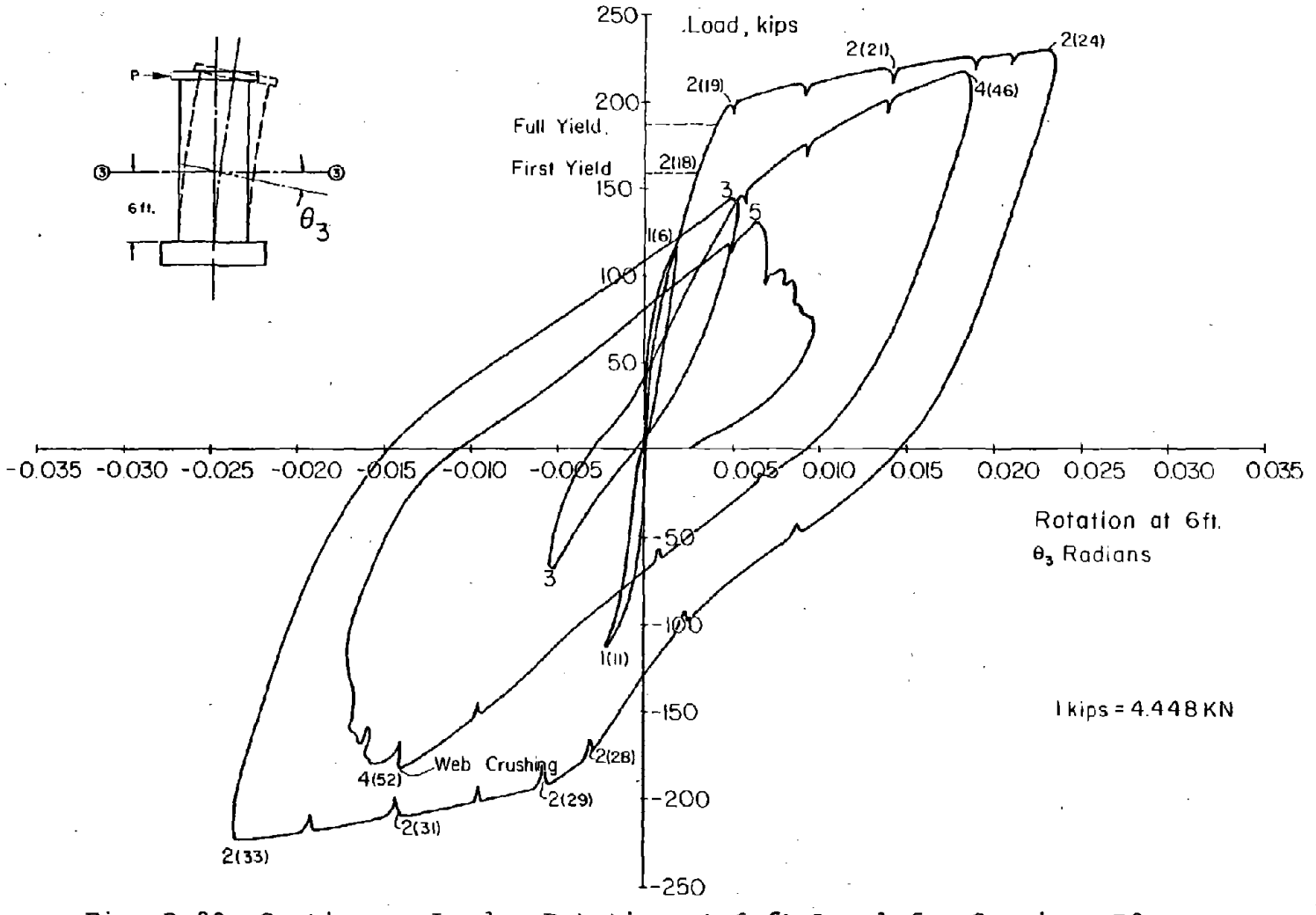

Fig. B-88 Continuous Load - Rotation at 6 ft Level for Specimen B9

First indication of crushing in the concrete cover of the outer compression face was noted at Load Stage 20. This crushing progressively increased as the wall was loaded to a top deflection of +5.37 in. and a rotation of 0.0236 rad. at the 6-ft level. However, the confined core of the column was in good condition.

The crack pattern that developed is shown in Fig. B-89. This cracking was very similar to that developed in Specimen B7. The measured crack widths in B9 were of the same order of magnitude as those measured in B7 at equivalent deformations.

Except for the crushing at the compression face, the wall exhibited no significant signs of distress at the first positive peak load. There was no indication of spalling or crushing in the compression strut system.

The maximum load measured in Cycle 2 was 219.6 kips (976.8 kN). This maximum is nearly identical to the maximums measured in B7 and B8 at equivalent deformation levels. The load corresponds to a nominal shear stress of $v_{max} = 11.4 \sqrt{f'_c}$ ($0.95 \sqrt{f'_c}$ MPa). The design shear capacity using 1971 ACI Building Code equations (11-13) and (11-33) was 148 kips (658.3 kN) which corresponds to a nominal shear stress of $v = 7.7 \sqrt{f'_c}$ psi) ($0.64 \sqrt{f'_c}$ MPa).

As the specimen was being loaded to a peak negative load in Cycle 2, an indication of crushing was noted in a compression strut on the left side of the web approximately 2 ft (0.61 m) above ther base. First spalling along diagonal cracks occurred. Also, spalling from opening of crosstie end hooks was noted in the lower 3 ft (0.91 m) of the compression face. The crack pattern at the peak negative load is shown in Fig. B-90.

No significant changes occurred in the wall during Cycle 3. A significant increase in spalling occurred along the diagonal cracks in the web as the specimen was loaded to the peak positive load of Cycle 4.

As the specimen was being loaded to the peak negative load of Cycle 4, several compression struts in the lower left region

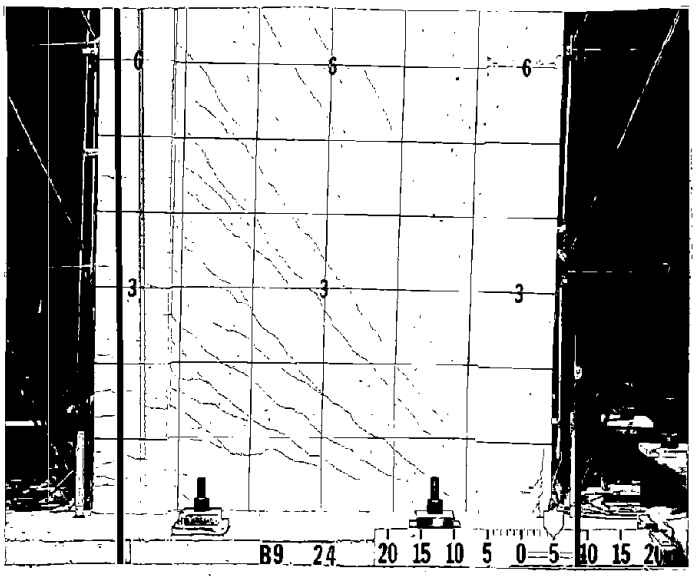

Fig. B-89 Cracking Pattern at Maximum Positive Load in Cycle 2 for Specimen B9

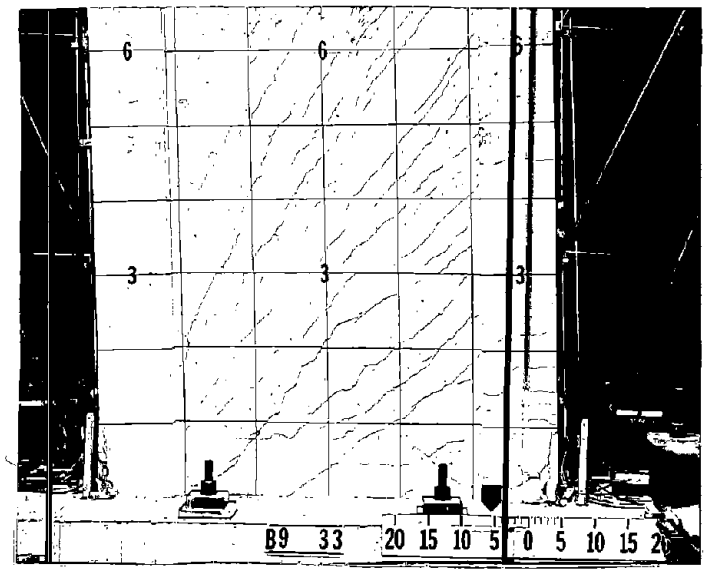

Fig. B-90 Cracking Pattern at Maximum Negative Load in Cycle 2 for Specimen B9

of the web crushed. This crushing was immediately followed by development of a failure plane along a diagonal crack extending up from the compression column approximately 2 ft above the base at about 25^{o} from vertical. Figures B-91 and B-92 show the wall immediately before and after web crushing.

Imposing further deformations on the wall develop vertical and horizontal failure planes as shown in Fig. B-93.

Specimen B9 did not sustain its load capacity through the modified load history at a maximum rotational ductility of 5.0. The load and deformations imposed on Specimen B9 were of the same magnitude as those for which Specimen B7 sustained its load capacity through three complete cycles using the incrementally increasing load history.

Discussion of Results

Moment-Rotation. Moment-rotation data for Specimen B9 are shown in Fig. B-94. The maximum measured moment was 91% of the calculated monotonic maximum. This calculated maximum was based on attainment of an ultimate compressive strain of $\varepsilon_u = 0.0066$ in the boundary element.

Since the positive load half of Cycle 2 is essentially a monotonic test up to the maximum rotation placed on B9, Fig. B-94 provides an opportunity to evaluate the calculated monotonic curve. As shown in the figures, for rotations beyond yield there is less rotation occurring at a particular load level than the calculations predict. However, the two curves tend to converge. Part of the difference is attributed to the crack distribution. The calculated rotation is based on a completely cracked section. The actual wall progresses from an uncracked section at the start of loading to a completely cracked section near maximum rotations. In general, the calculated and measured curves show good agreement.

The relationship between the calculated monotonic and measured rotations at the 3-ft (0.91 m) and 6-ft (1.83 m) levels is similar to that observed in most of the previously reported reversing load tests. Actual rotations were concentrated in

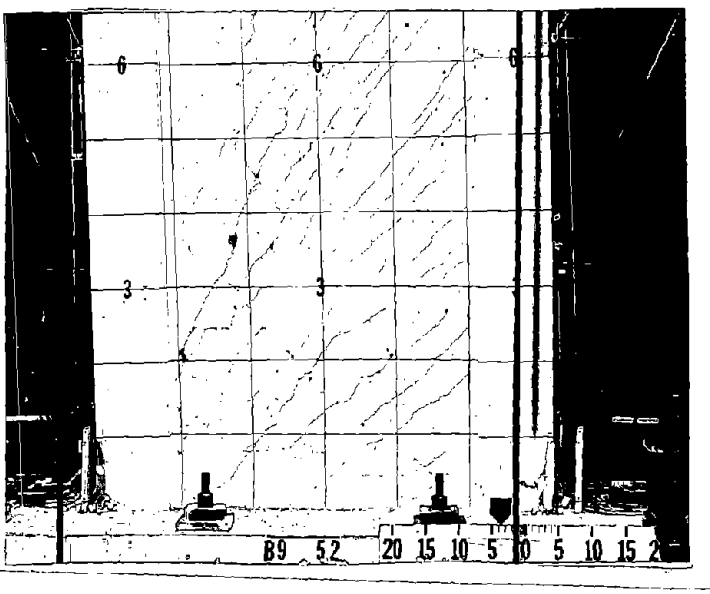

Fig. B-91 Specimen B9 Prior to Web Crushing

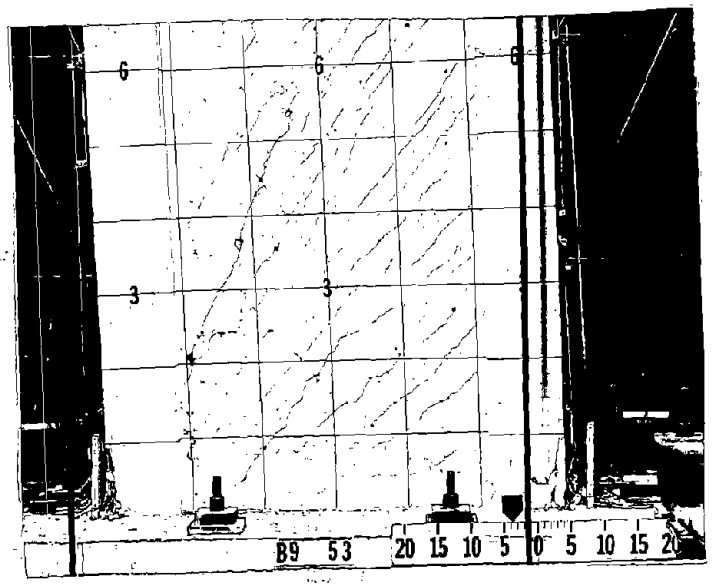

Fig. B-92 Specimen B9 After Web Crushing

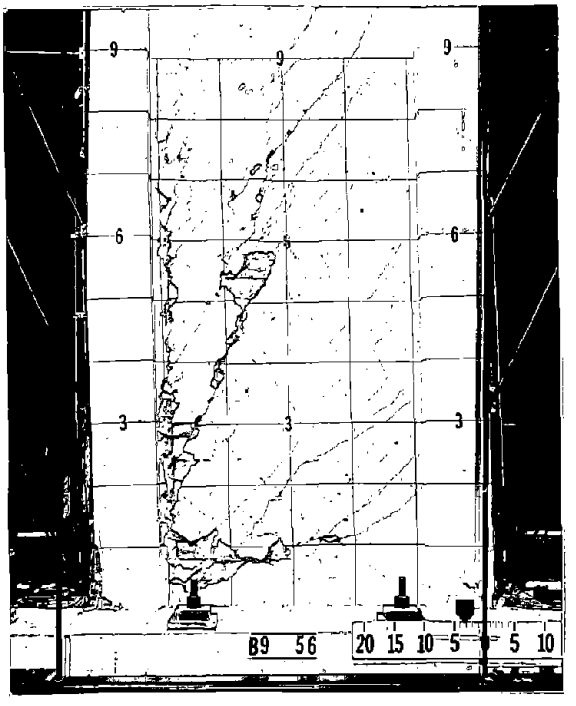

Fig. B-93 Specimen B9 at End of Test

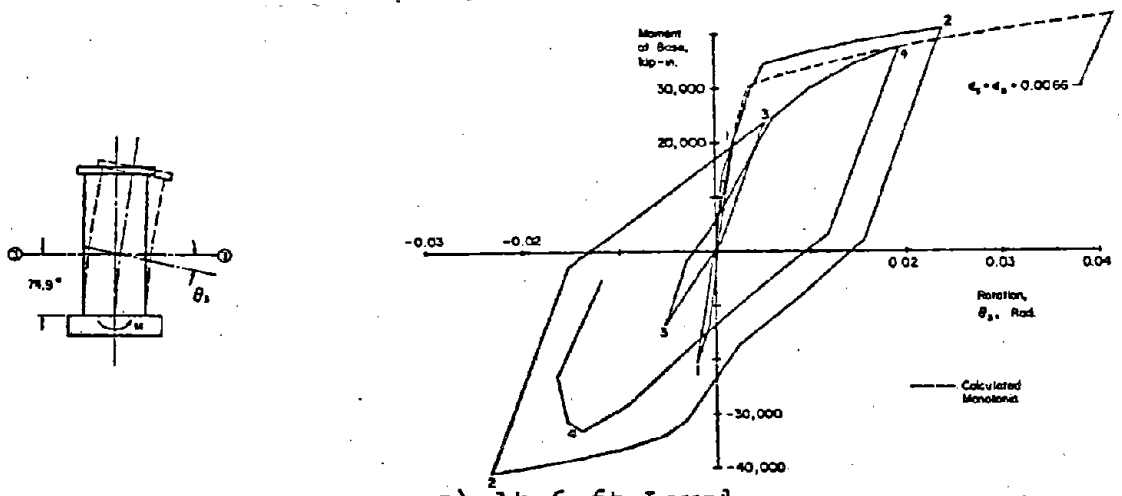

a) At 6 ft Level

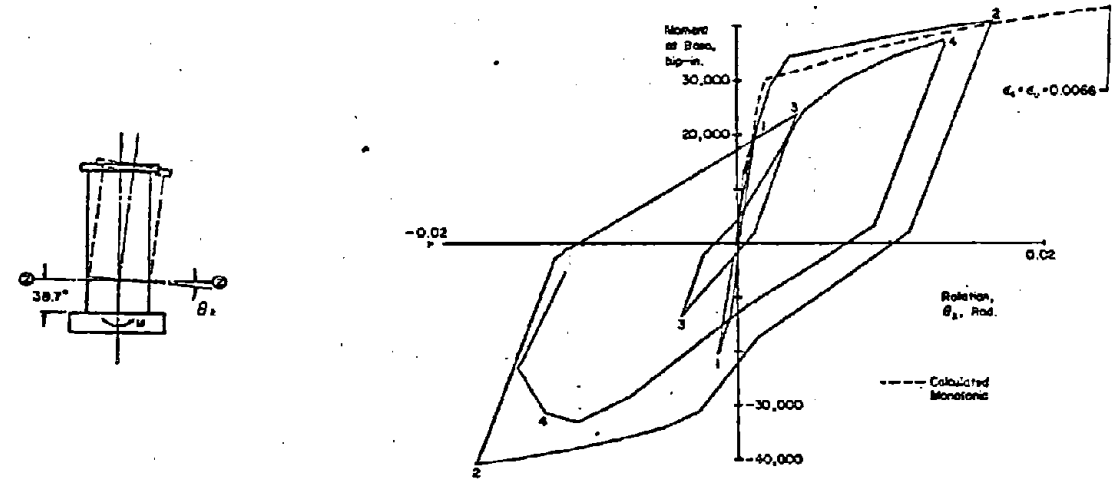

b) At 3 ft Level

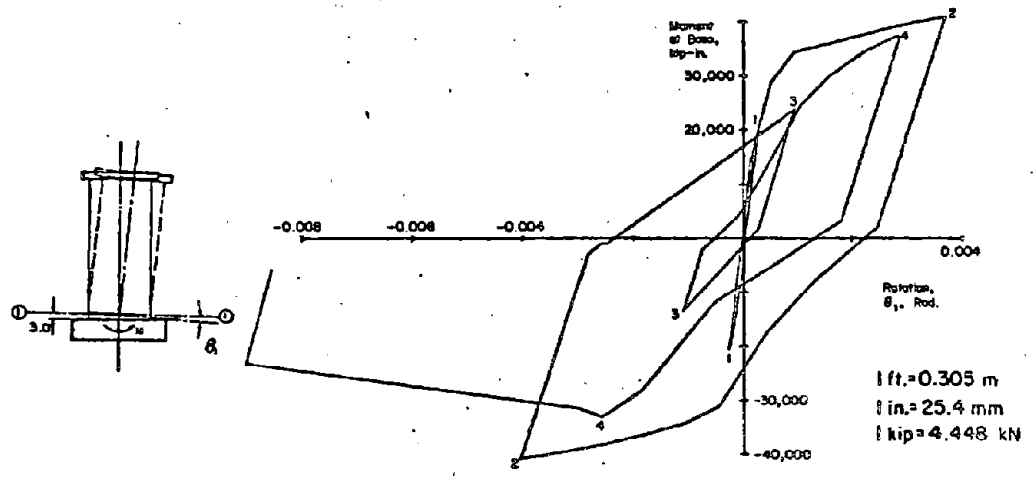

c) At Base Level

Fig. B-94 Moment at Base versus Rotation for Specimen B9

the lower 3 ft of the wall to a greater extent than was assumed in the calculations.

Shear Distortion. The shear-distortion curves for B9 are shown in Fig. B-95. As in the previously reported tests without axial load, a shear "yielding" occurred during the same cycle in which flexural yielding occurred.

Comparison of Cycles 2 and 4 indicates a significant loss of shear stiffness from just one inelastic reversal.

Comparison of the shear distortion data for Specimens B9 and B7 shows that for the positive "monotonic" half of Cycle 2 of B9, shear distortions were approximately 15% less than those in the last stable inelastic cycle of B7. However, with one reversal, shear distortions attained in the negative half of Cycle 2 were almost identical to those measured in B7 after 12 inelastic cycles. This indicates that the degredation in shear stiffness is more a function of previous maximum inelastic deformations than of abrasion and loss of material from repeated reversals.

Slip at Construction Joints. Slip at construction joints in B9 is shown in Fig. B-96. Slip at CJ1 exhibits yielding similar to shear "yielding" during the same cycle that flexural yielding occurred. As shown in Fig. B-97, the slip at CJ1 ranged from 10% to 15% of the total shear deflection in the lower 3 ft (0.91 m).

Slip plots for CJ2 and CJ3 are unsymmetrical. Measurements were affected by diagonal cracking.

Deflections. Deflection components and deflected shapes are shown in Figs. B-98 through B-100. Comparison of Figs. B-98 and B-99 shows the increase in the shear component of deflection as a result of one large inelastic reversal.

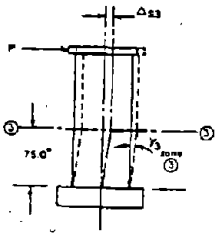

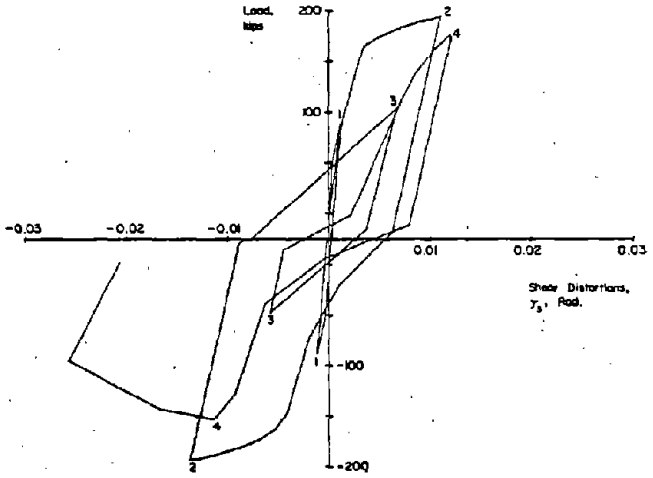

a) In Base to 6 ft Level

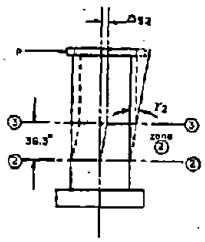

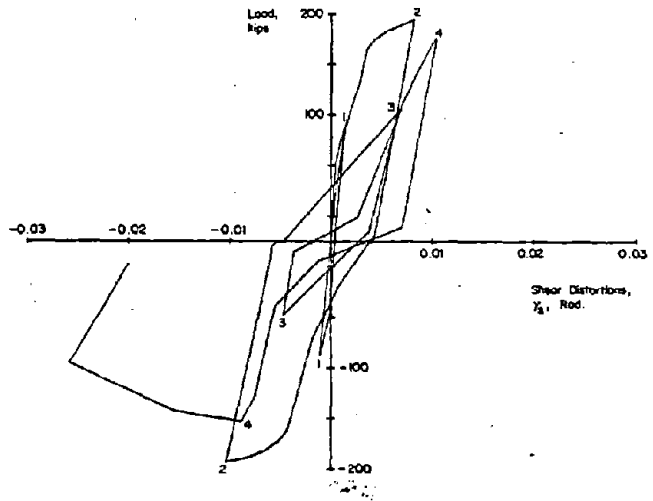

b) In 3 ft to 6 ft Level

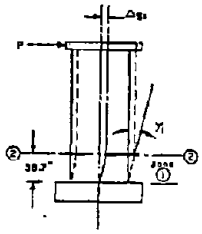

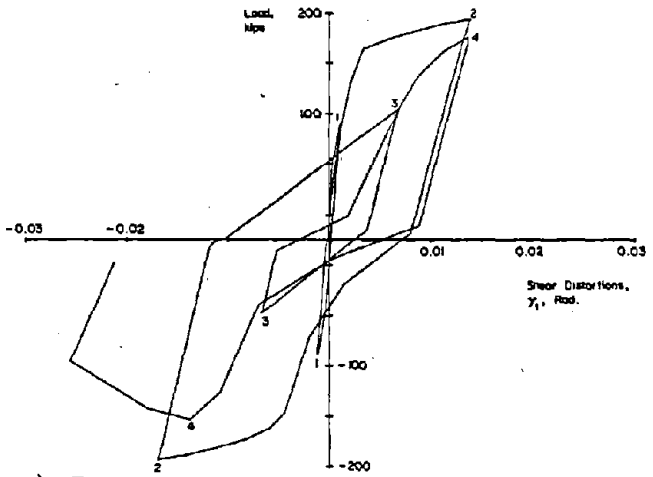

c) In Base to 3 ft Level

1 ft.=0.305 m
1 in.=25.4 mm
1 kip=4.448 kN

Fig. B-95 Load versus Shear Distortion for Specimen B9

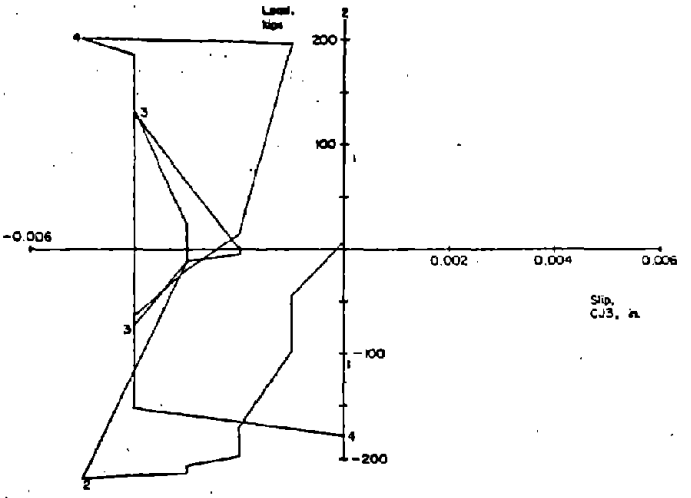

a) At 6 ft Level

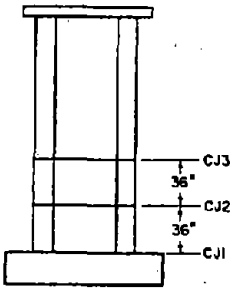

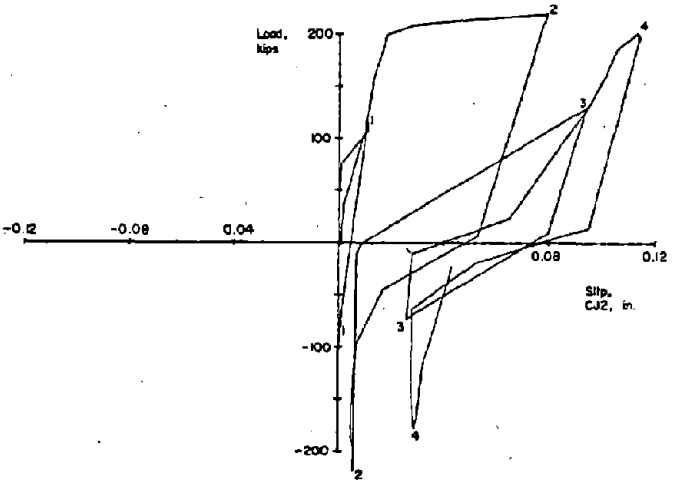

b) At 3 ft Level

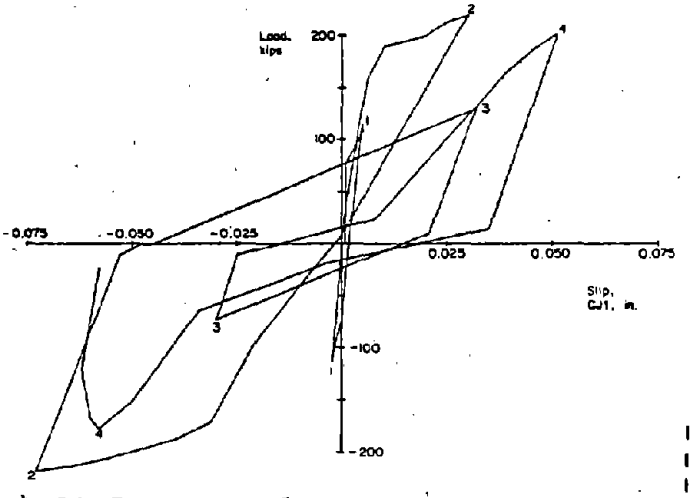

1 ft.=0.305 m
1 in.=25.4 mm
1 kip=4.448 kN

c) At Base Level

Fig. B-96 Load versus Slip at Construction Joints for Specimen B9

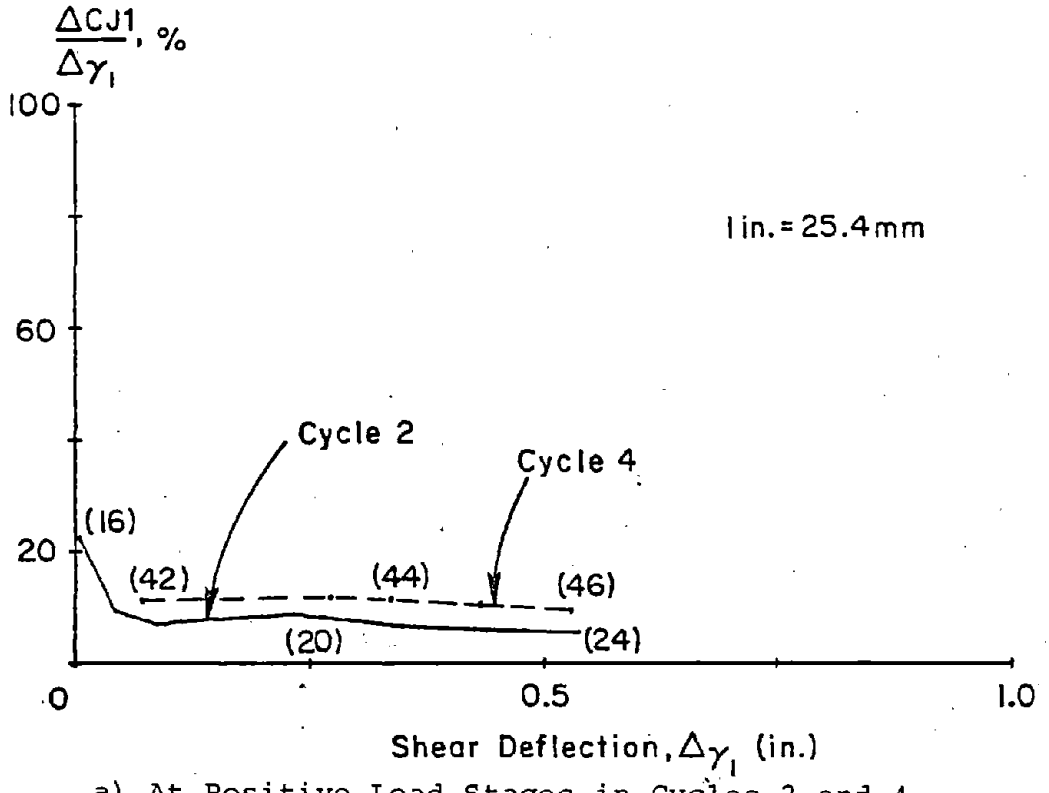

a) At Positive Load Stages in Cycles 2 and 4

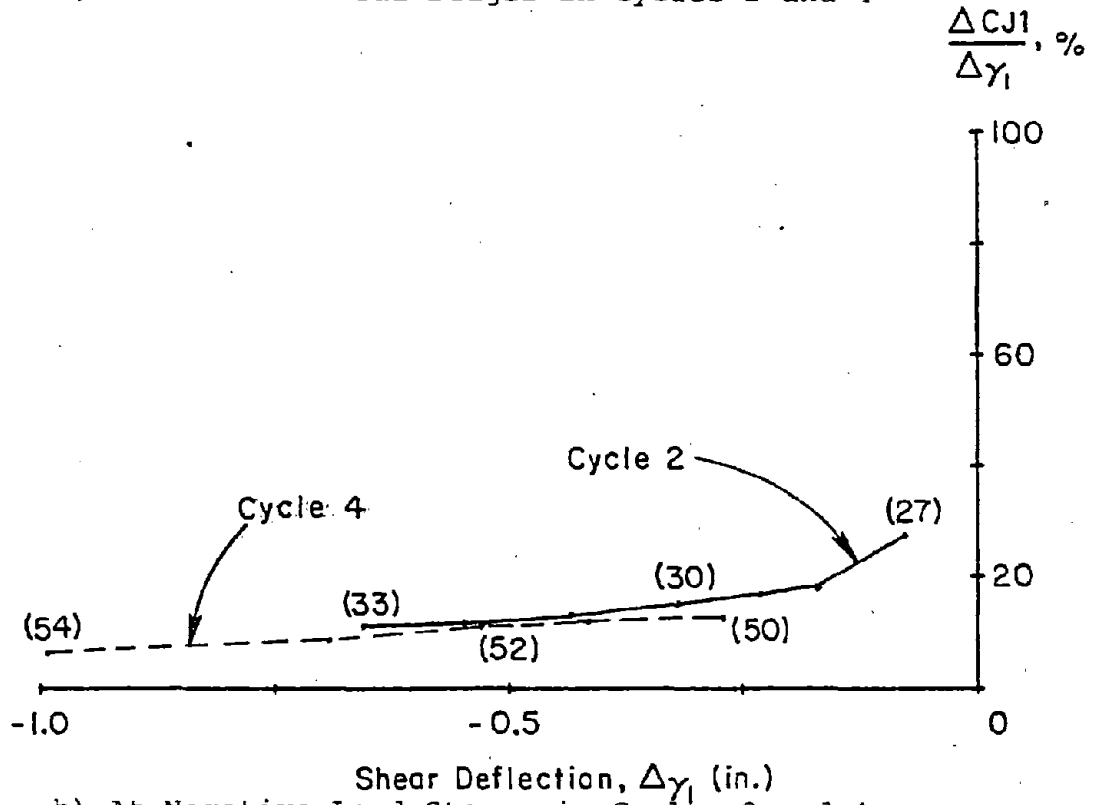

b) At Negative Load Stages in Cycles 2 and 4

Fig. B-97 Slip at Base Construction Joint versus Shear Deflection in Zone 1 for Specimen B9

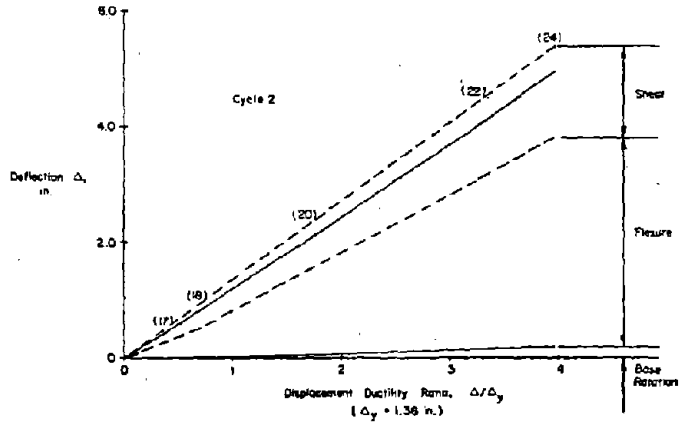

a) At Top of Wall

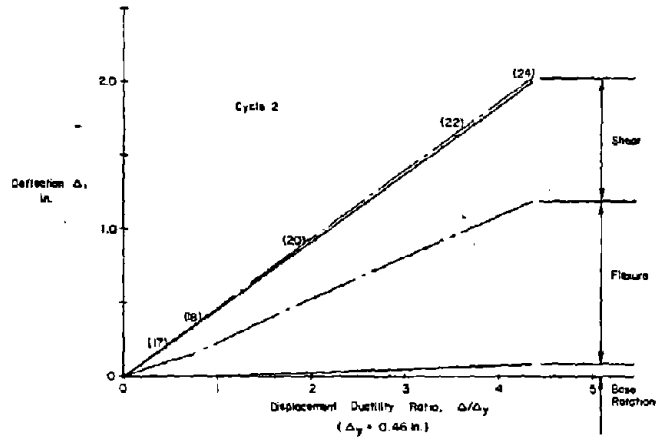

b) At 6 ft Level

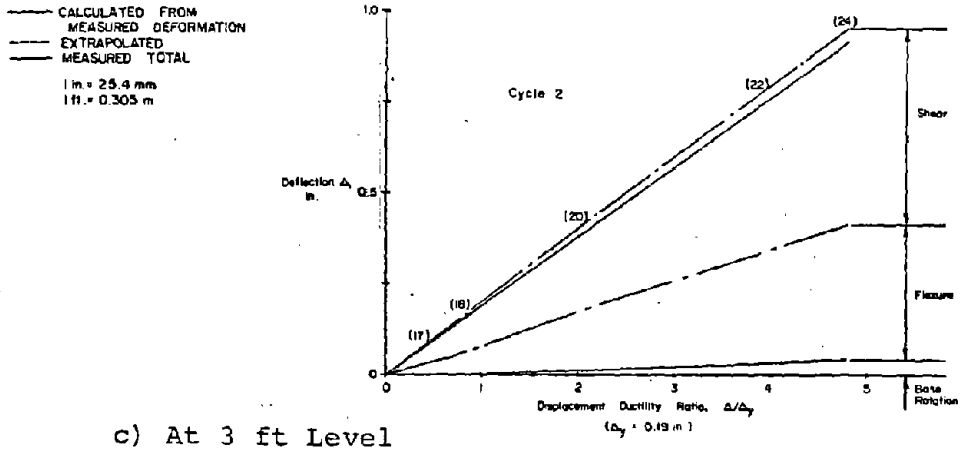

c) At 3 ft Level

Fig. B-98 Components of Deflection for Specimen B9 in the Positive Half of Cycle 2

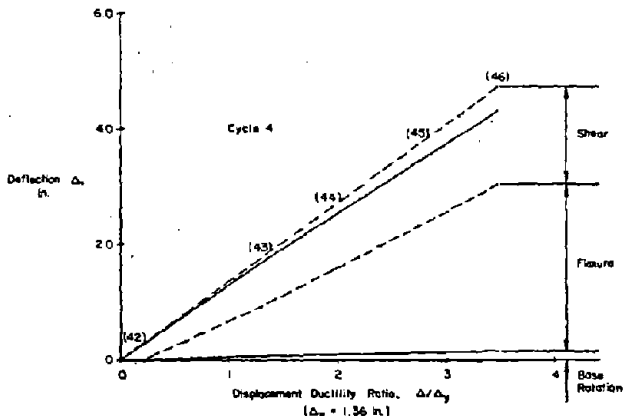

a) At Top of Wall

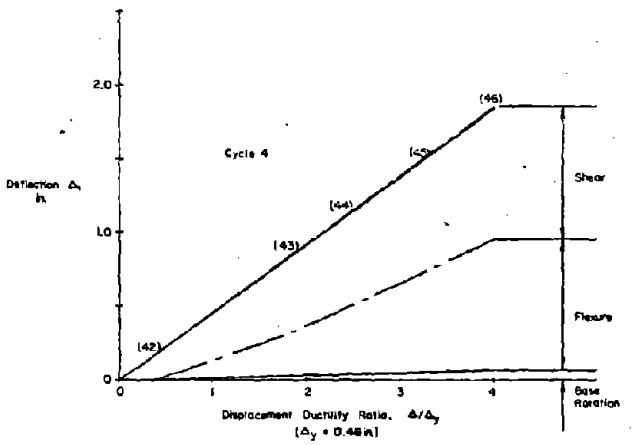

b) At 6 ft Level

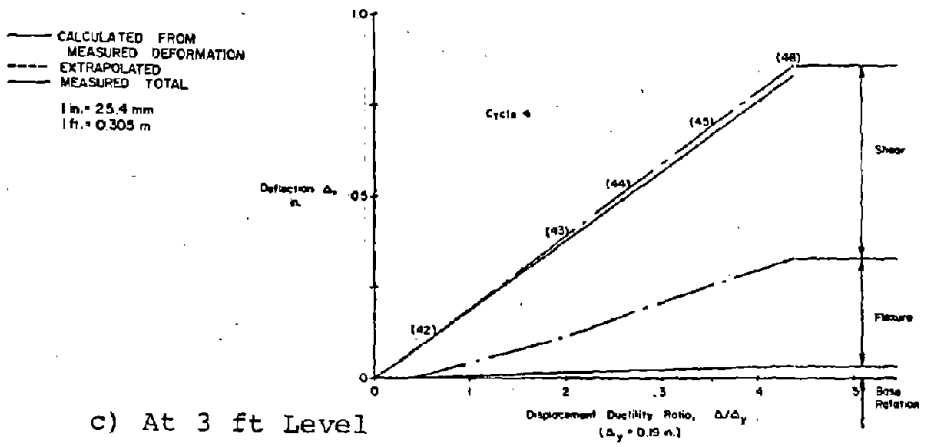

c) At 3 ft Level

Fig. B-99 Components of Deflection for Specimen B9 in the Positive Half of Cycle 4

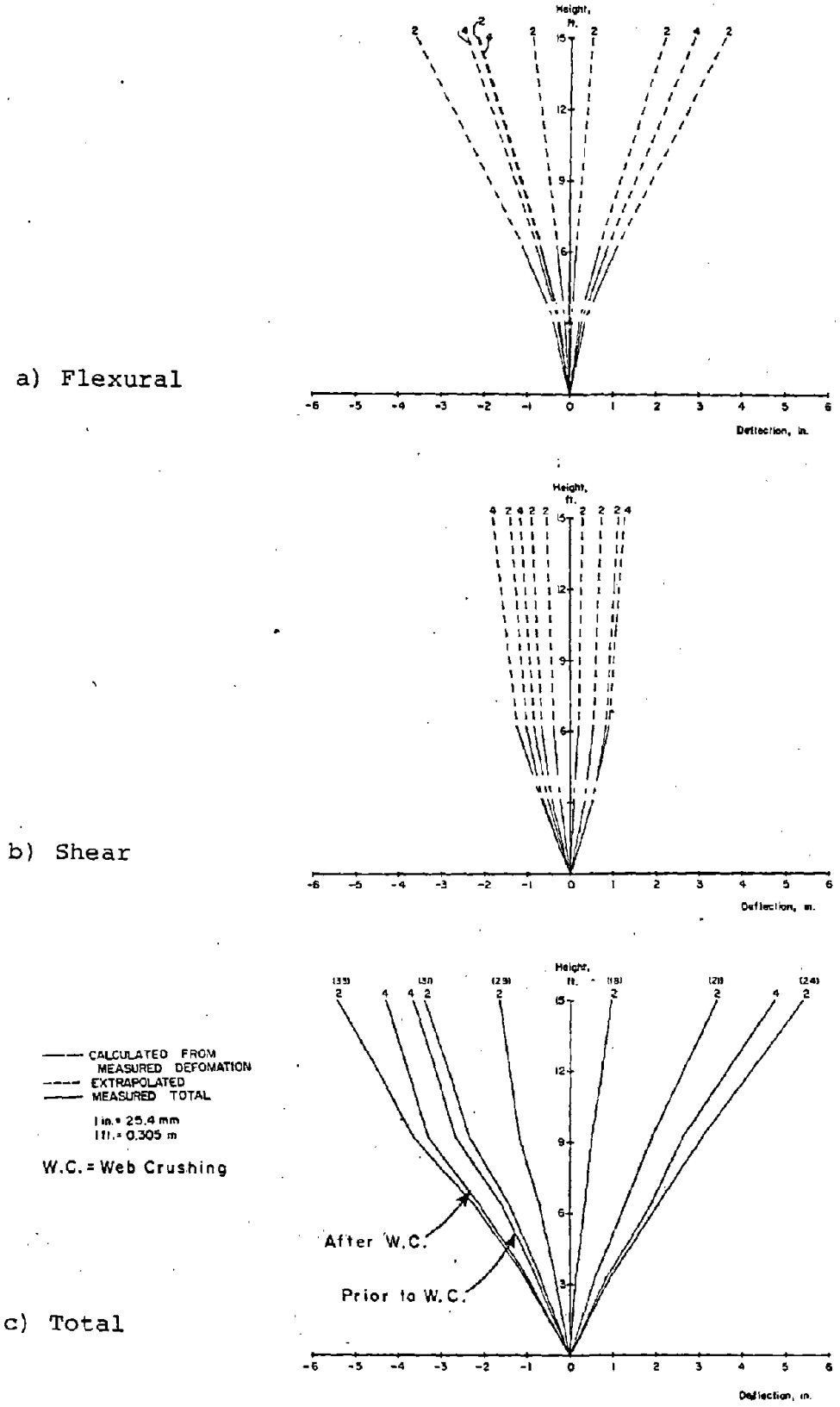

Fig. B-100 Deflected Shape for Specimen B9

Reinforcement Strains. Figures B-101 through B-111 show reinforcement strains in Specimen B9 at various stages. Many of the lines in these figures are incomplete, particularly those for negative load. This is because of the large number of gages that were strained beyond their working range in the first half of Cycle 2.

Figure B-101 shows the load versus strain relationship for the outer reinforcing bars at the base level.

Figure B-102 shows that yielding occurred up to the 9-ft (2.75 m) level in Cycle 2.

Figures B-103 and B-104 show the strain gradient in the vertical reinforcement at various levels.

Figures B-105 through B-109 show the cyclic strain-load relationship and the strain gradients in the horizontal bars. These figures indicate considerable yielding from the 18-in. to the 9-ft (0.46 m to 2.74 m) level. Figures B-105 and B-106 for gages HH and HA indicate that, although no yielding occurred near the end hooks, appreciable stresses were present. This was particularly evident in the lower 18 in. (0.46 m) because the boundary elements acting as dowels in this region.

Figures B-110 and B-111 show the cyclic strain-load relationship and the vertical strain gradient in the outer leg of the confinement hoops. These figures show that only the hoops in the lower two feet were stressed significantly. Strains beyond yield were observed in the hoops at the peak loads in Cycle 2.

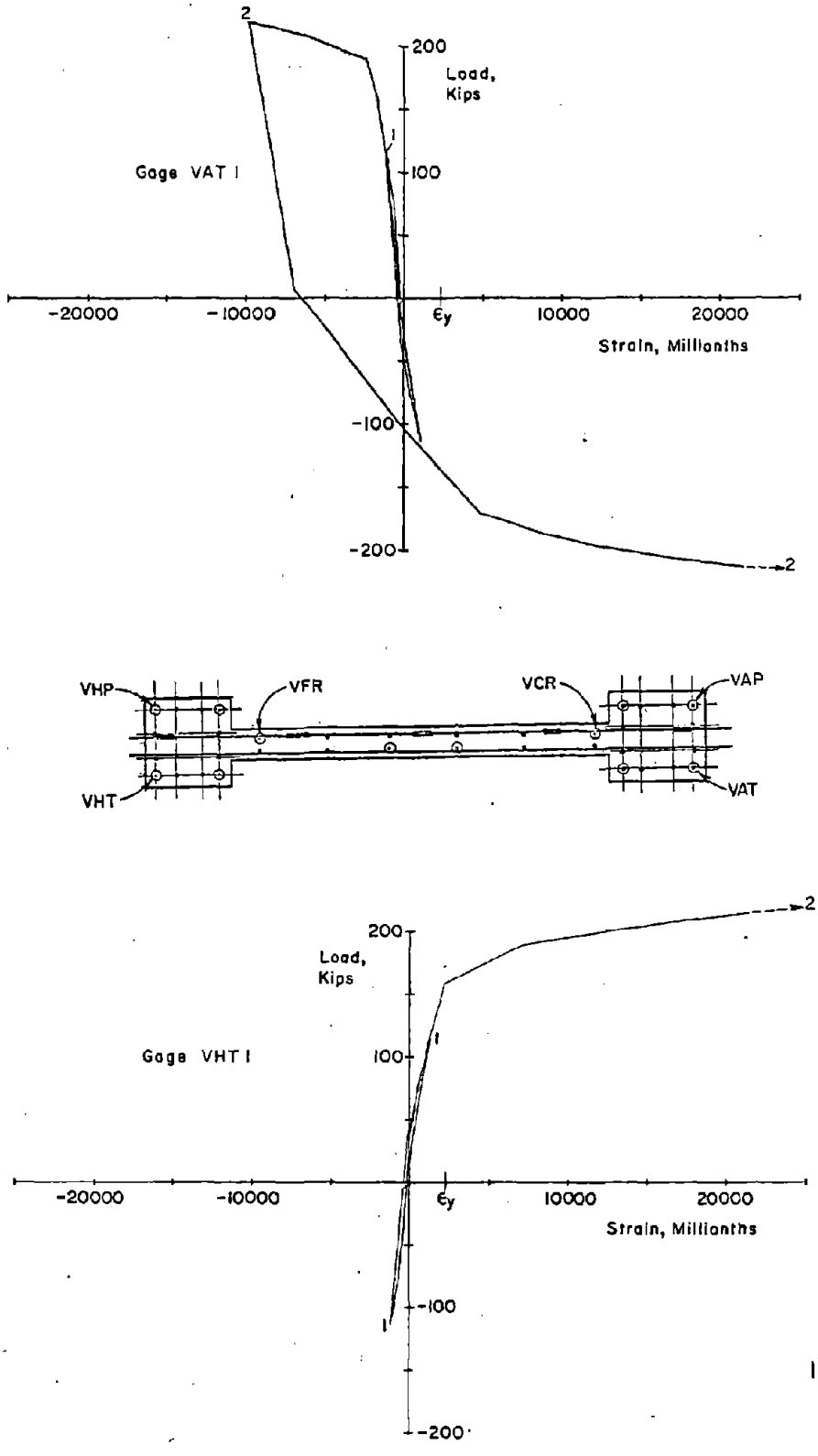

1 kip = 4.448 kN

Fig. B-101 Measured Strains on Vertical Reinforcement at Base of Specimen B9

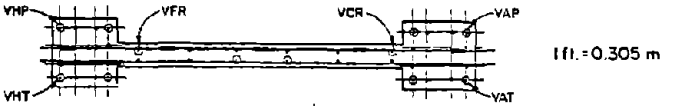

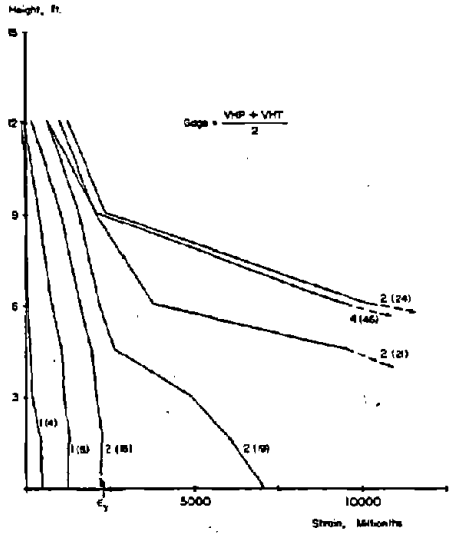

a) Average of VHP and VHT

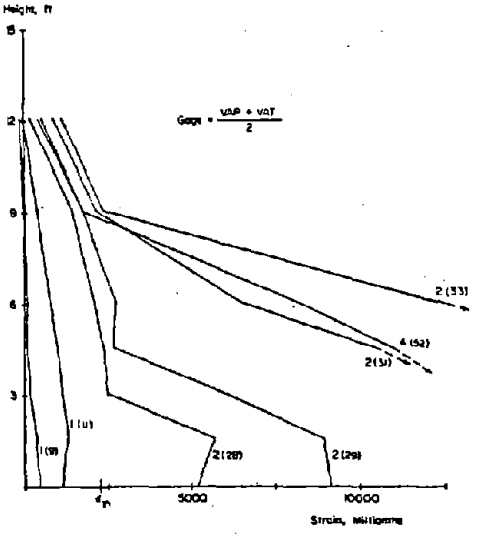

b) Average of VAP and VAT

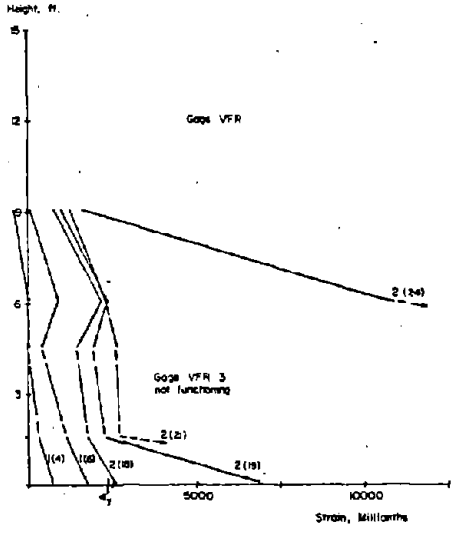

c) Strain Gage VFR

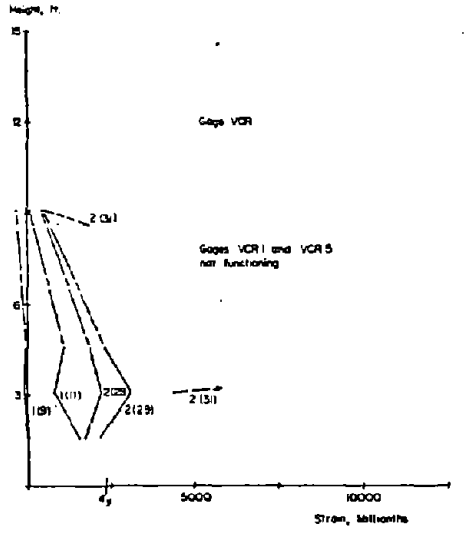

d) Strain Gage VCR

Fig. B-102 Vertical Reinforcement Strains at Maximum Loads for Specimen B9

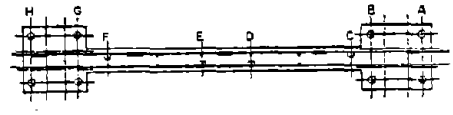

1 ft.=0.305 m

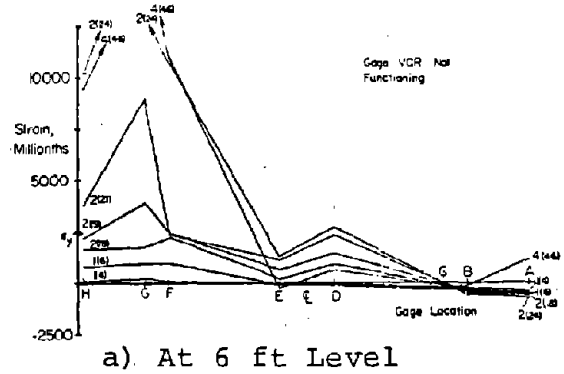

a) At 6 ft Level

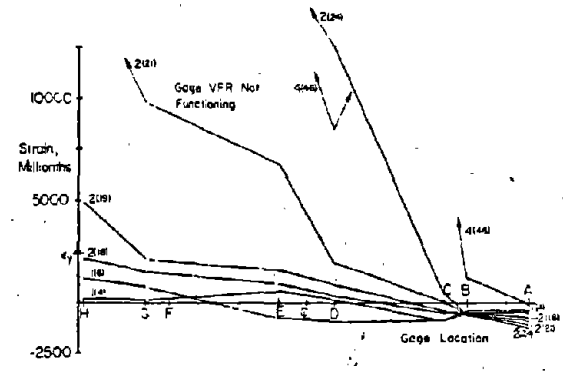

b) At 3 ft Level

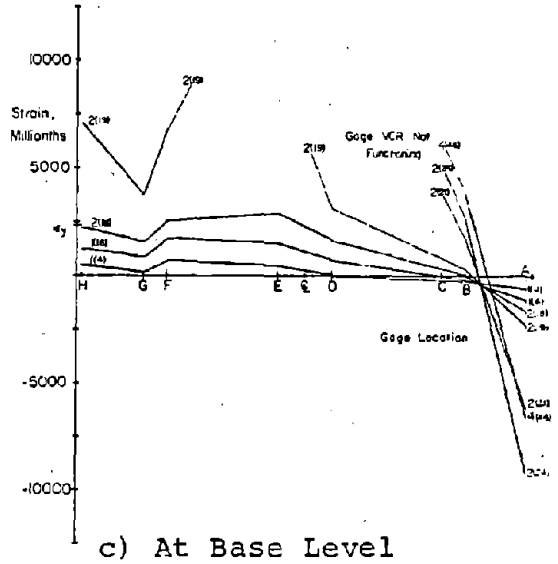

c) At Base Level

Fig. B-103 Vertical Reinforcement Strains at Maximum Positive Loads for Specimen B9

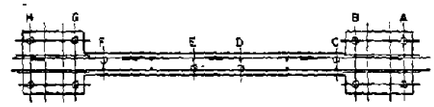

1 ft.=0.305 m

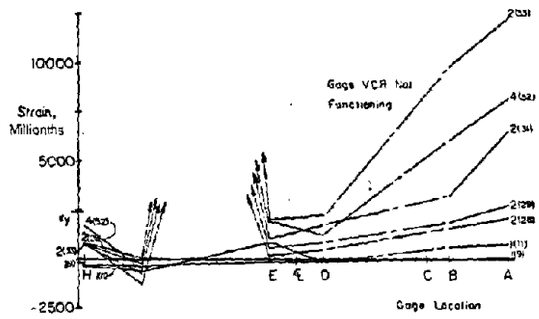

a) At 6 ft Level

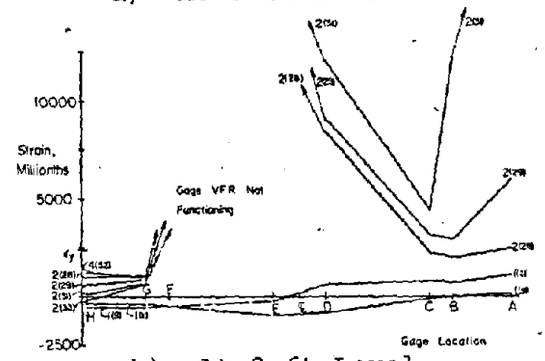

b) At 3 ft Level

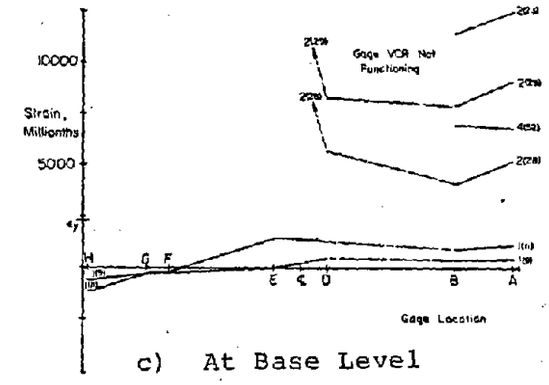

c) At Base Level

Fig. B-104 Vertical Reinforcement Strains at Maximum Negative Loads for Specimen B9

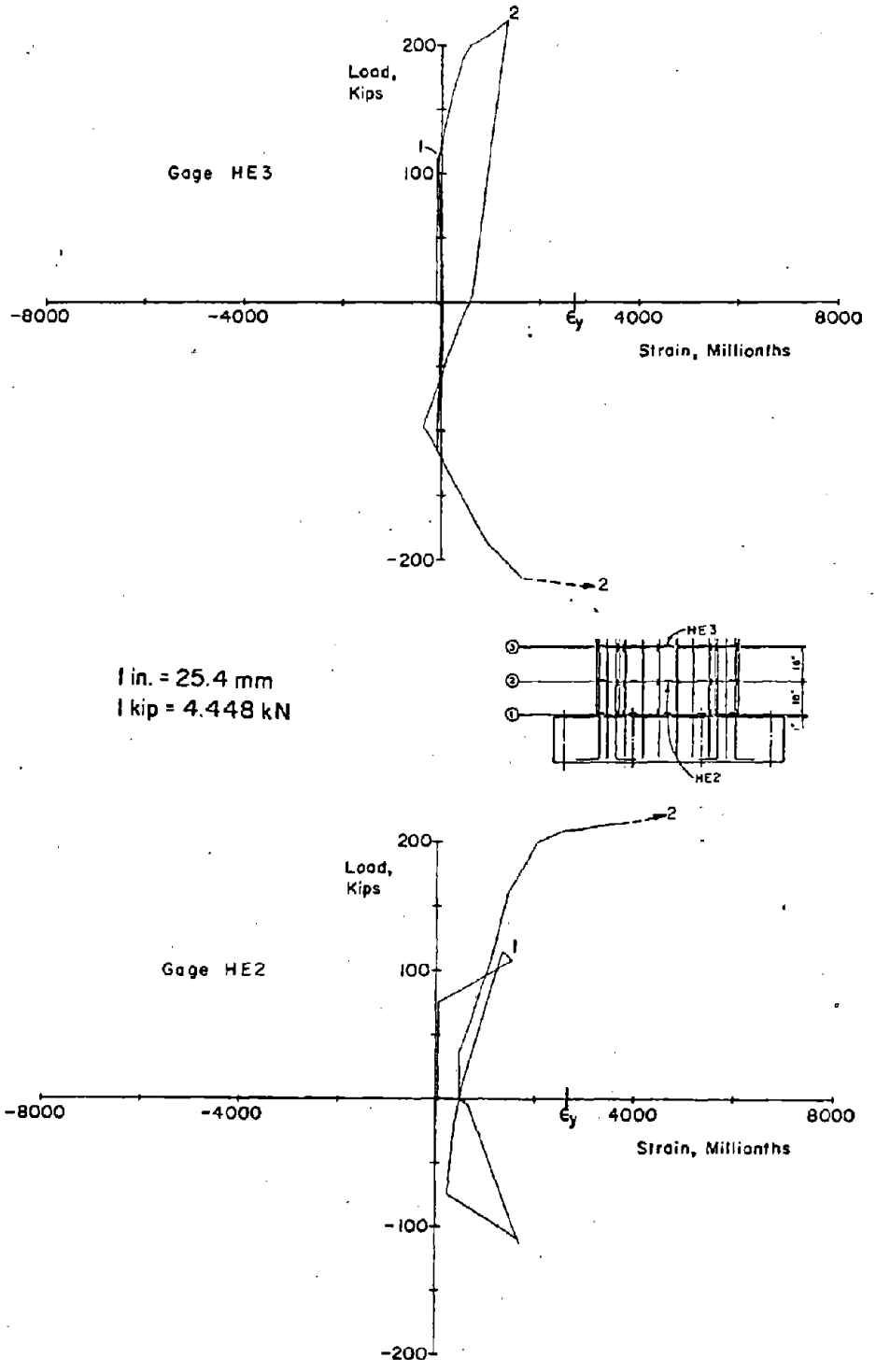

Fig. B-105 Measured Strains on Horizontal Reinforcement for Specimen B9

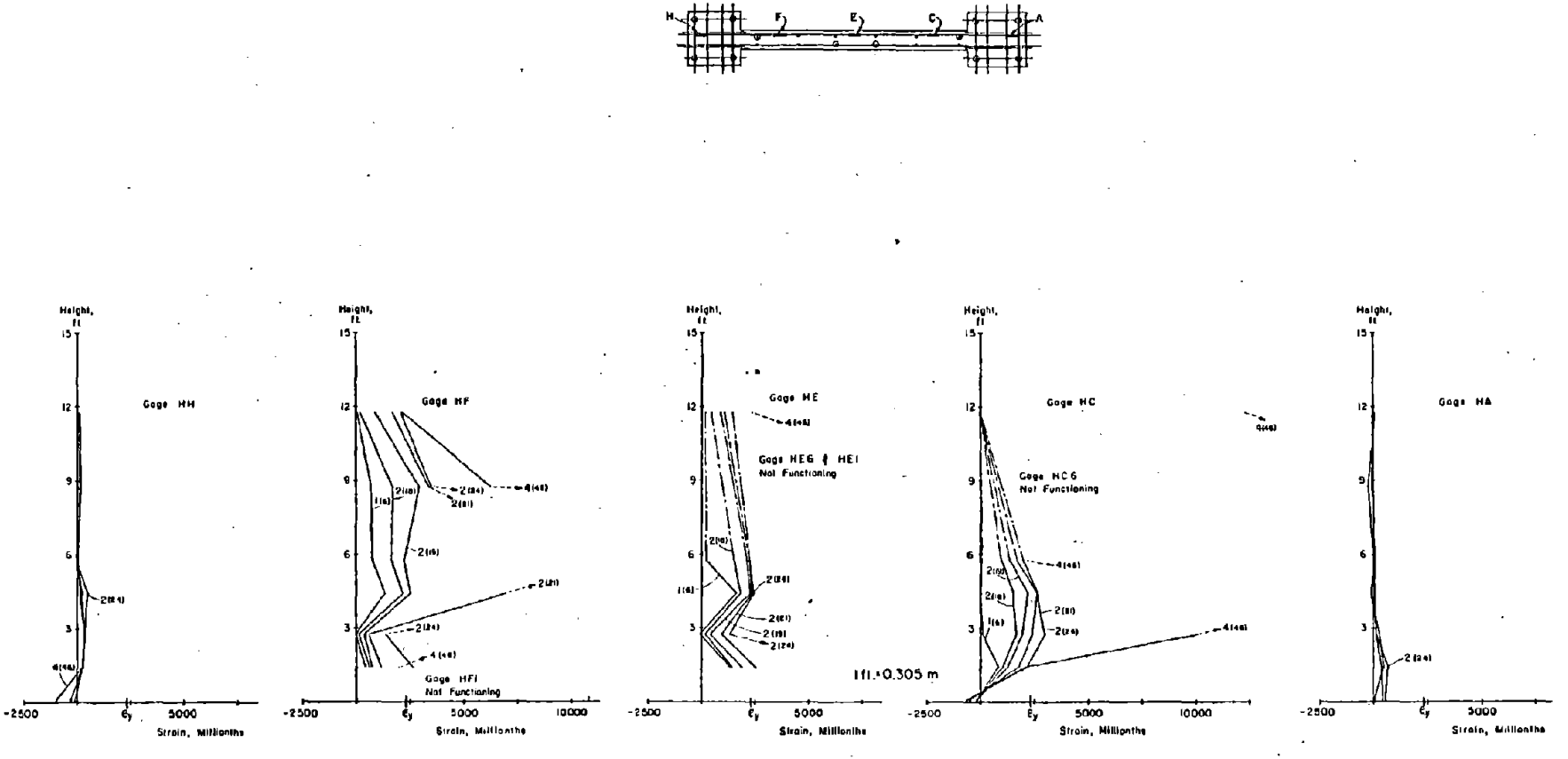

Fig. B-106 Horizontal Reinforcement Strains at Maximum Positive Loads for Specimen B9

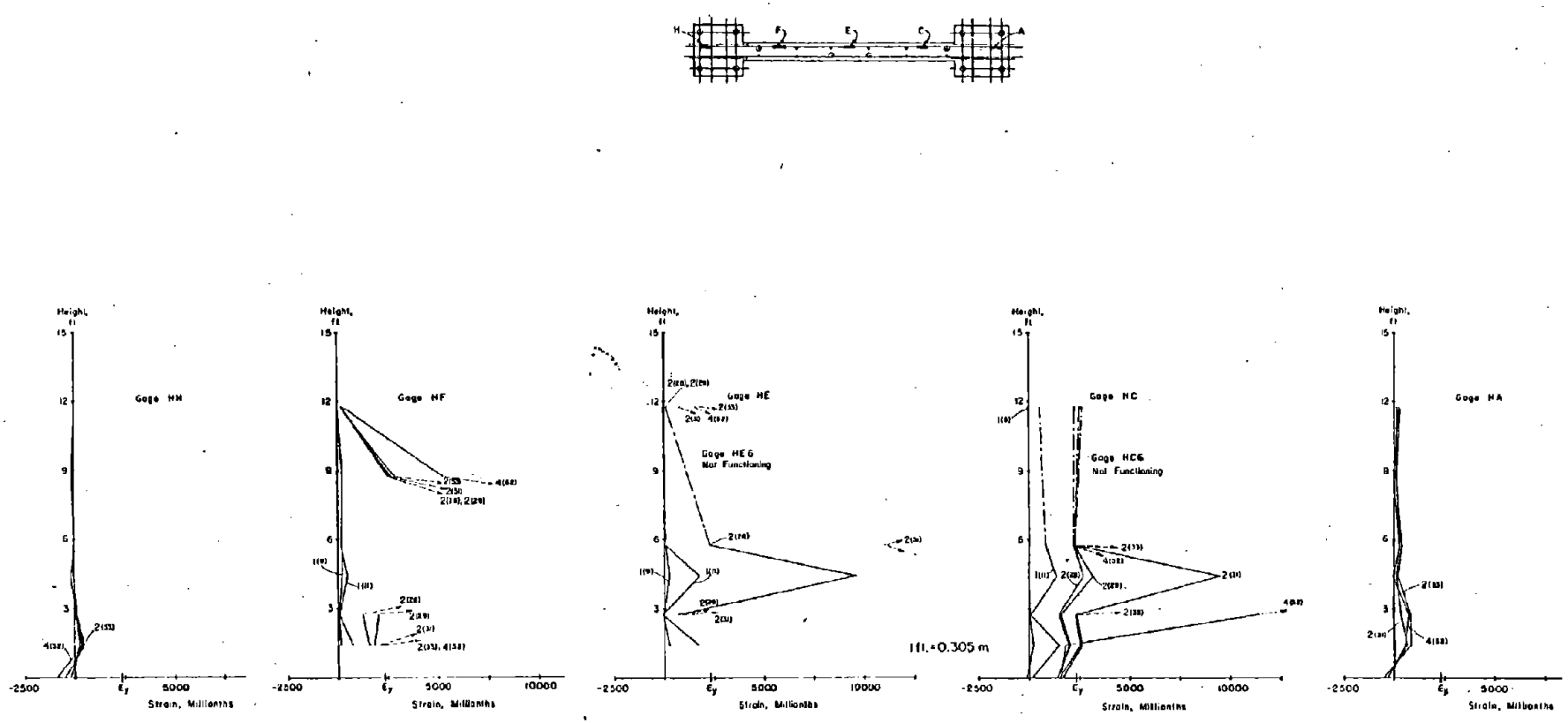

Fig. B-107 Horizontal Reinforcement Strains at Maximum Negative Loads for Specimen B9

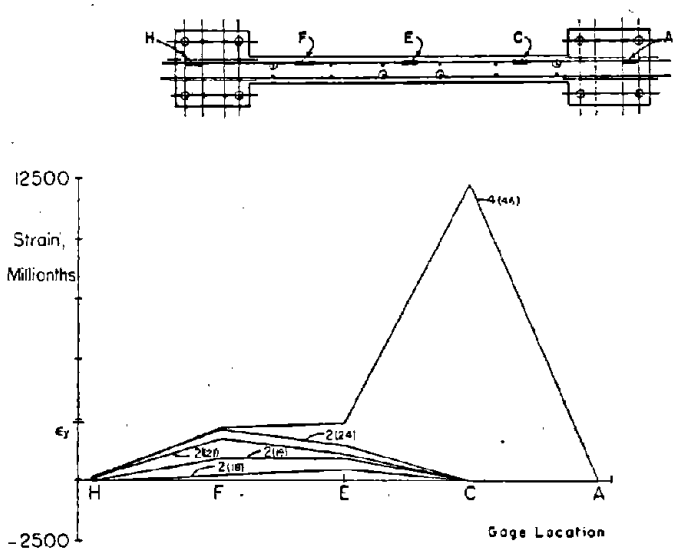

a) At 12 ft Level

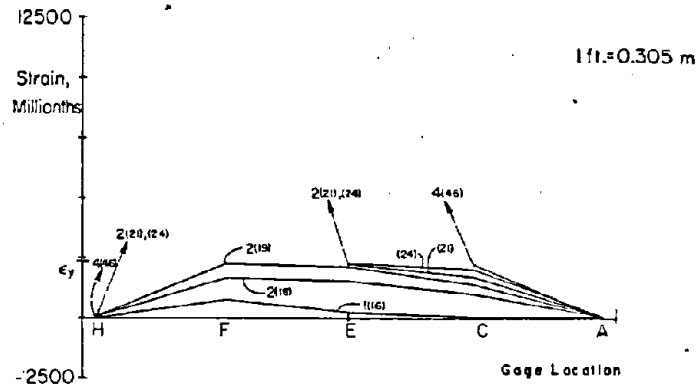

b) At 6 ft Level

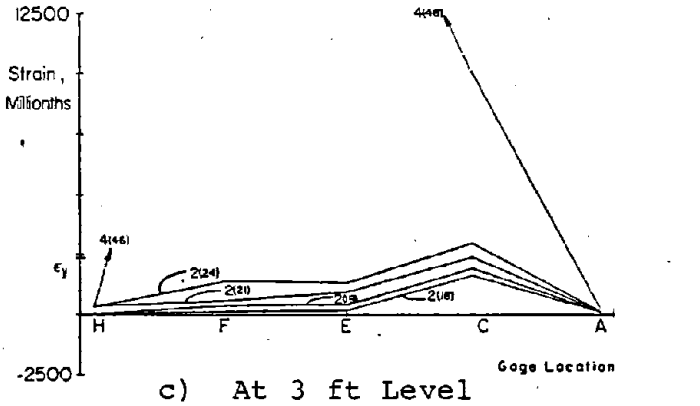

c) At 3 ft Level

Fig. B-108 Horizontal Reinforcement Strains in Web at Maximum Positive Loads for Specimen B9

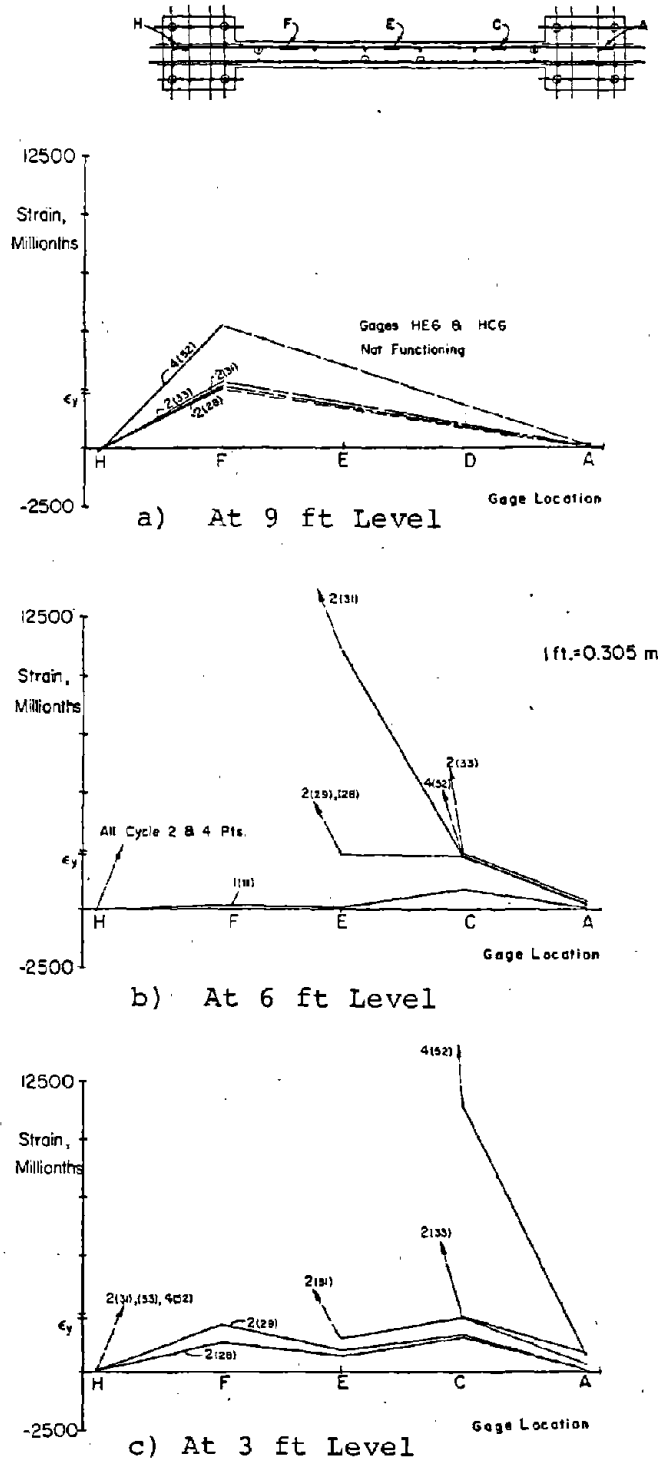

Fig. B-109 Horizontal Reinforcement Strains in Web at Maximum Negative Loads for Specimen B9

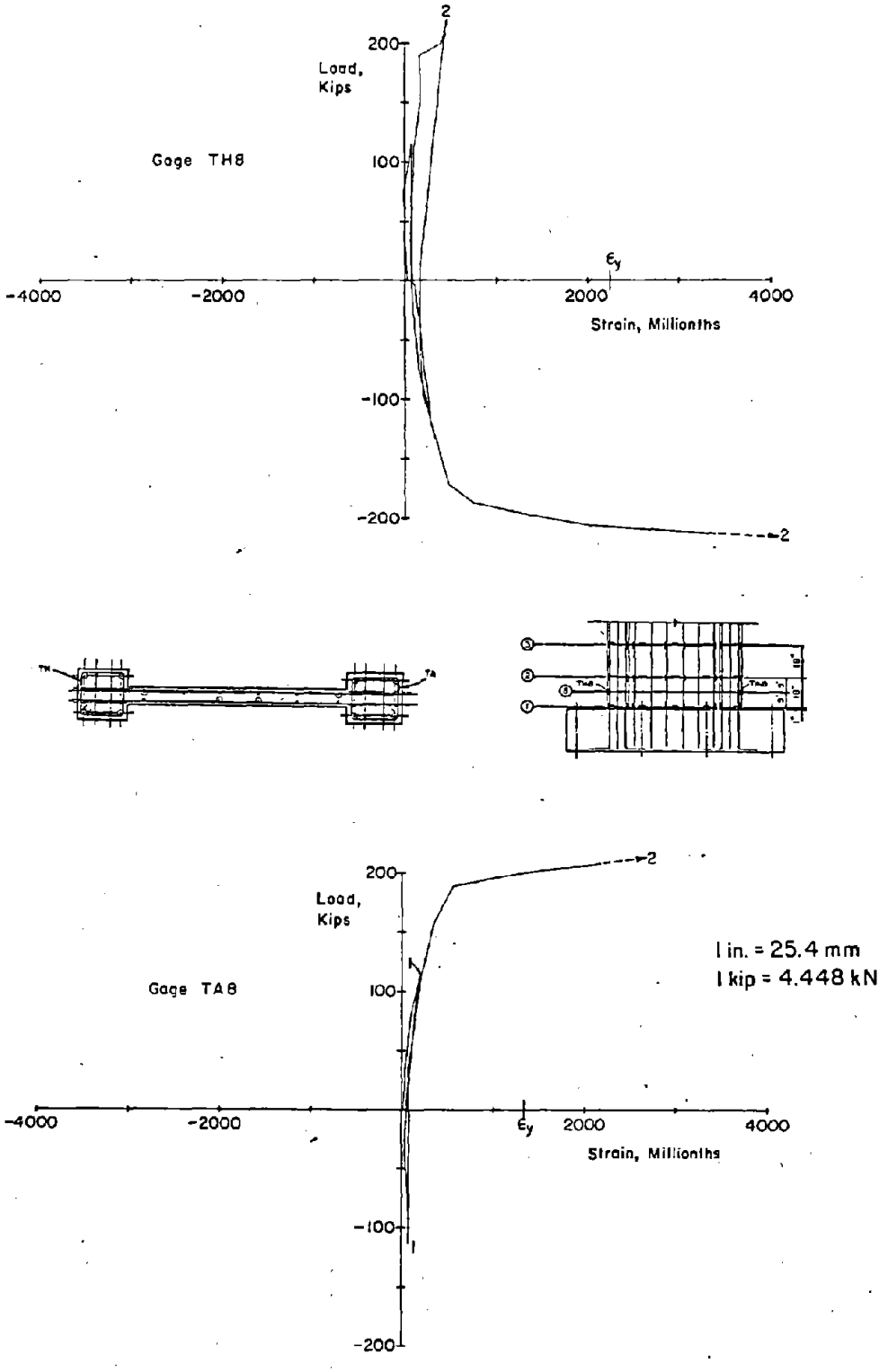

Fig. B-110 Measured Strains on Confinement Hoop Reinforcement for Specimen B9

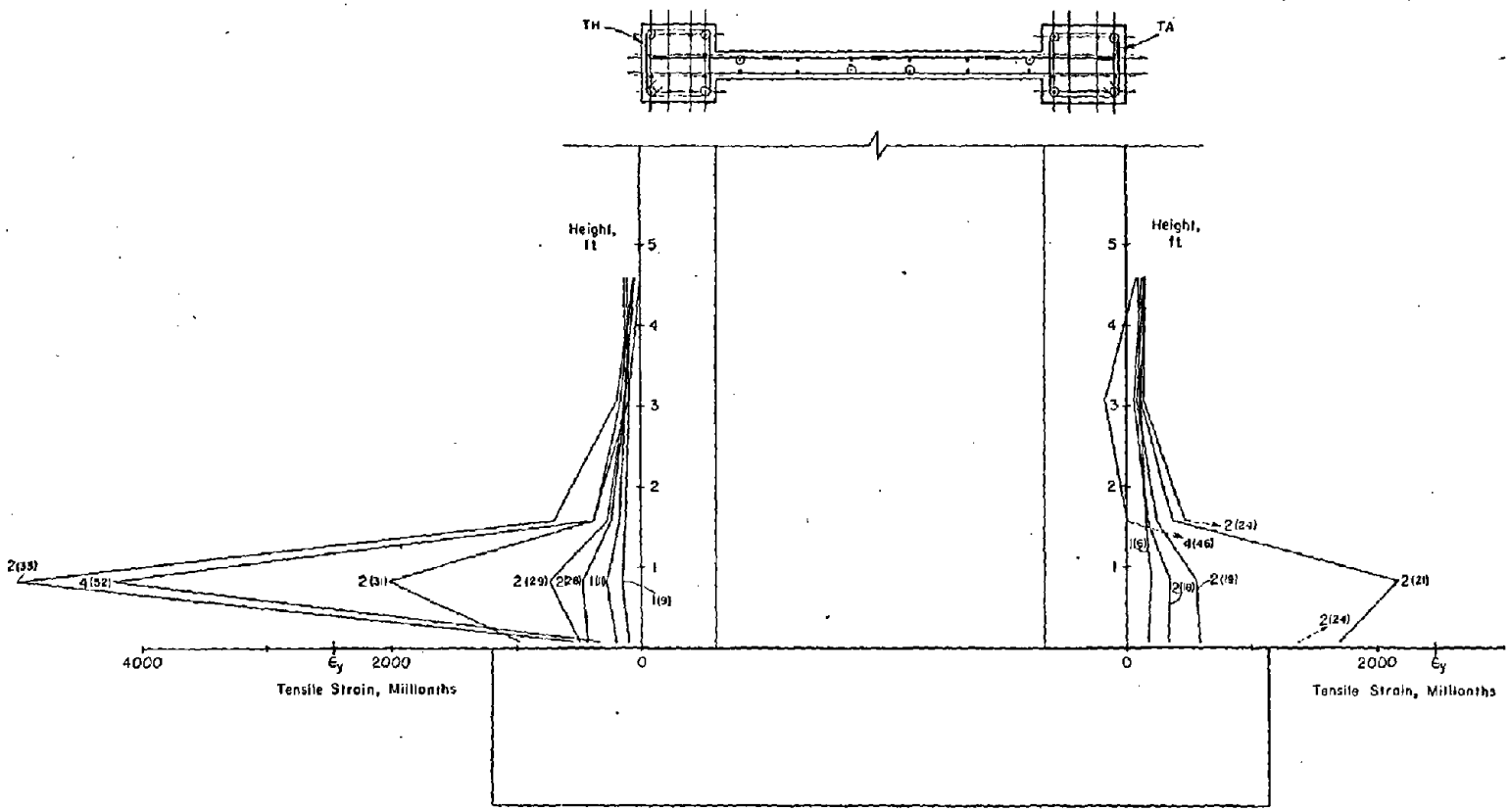

Fig. B-111 Confinement Hoop Reinforcement Strains at Maximum Loads for Specimen B9

Specimen B9R

Test Description

Specimen B9R was a repair of B9 as described in Appendix A. The repair consisted essentially of replacing the orginal 4-in. thick web with a 6-in. thick web. Therefore, the nominal shear stresses were decreased by 33%. For purposes of comparison, B9R was tested with the same modified load history as intended for use on Specimen B9. The θ_{max} for the first inelastic cycle of Specimen B9R was taken as five times the measured full yield rotation for Specimen B7. The lateral load test for B9R was conducted similar to the test of Specimen B9. An exception was that since nearly all strain gages were inoperative at the end of the B9 test, no steel strains were monitored or recorded during the test of B9R.

Specimen B9R was loaded axially during the lateral load test with the same total force as that used on B9. With the increase in web thickness, the resulting uniform axial stress was 451 psi (3.11 MPa) which was 83% of that in Specimen B9.

The test consisted of 16 complete loading cycles as shown in Fig. B-112. The complete load versus top deflection relationship for Specimen B9R is shown in Fig. B-113. The complete deflection and rotation relationships at the 6-ft level are shown in Figs. B-114 and B-115.

The first load cycle was applied to develop cracking in both directions. First significant cracking in the web was observed at a load of 75 kips (334 kN). Prior to web cracking, Specimen B9R had approximately 35% of the effective lateral stiffness measured in B9 prior to cracking. After significant cracking in the web, B9R had approximately 60% of the effective lateral stiffness measured in B9 with a comparable amount of cracking.

In the first half of Cycle 2, B9R was loaded to the maximum rotation at the 6-ft level that was measured in B9. In this cycle with the load equal to measured full yield load of B9, the effective initial lateral stiffness in B9R was 50% of that

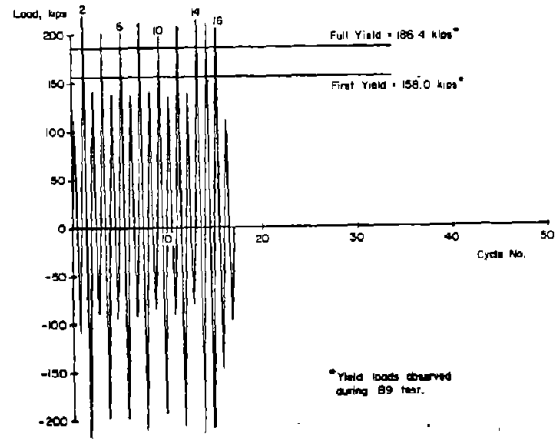

a) Load History

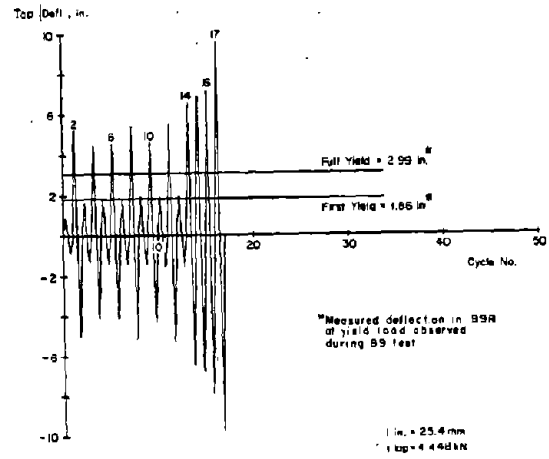

b) Deflection History

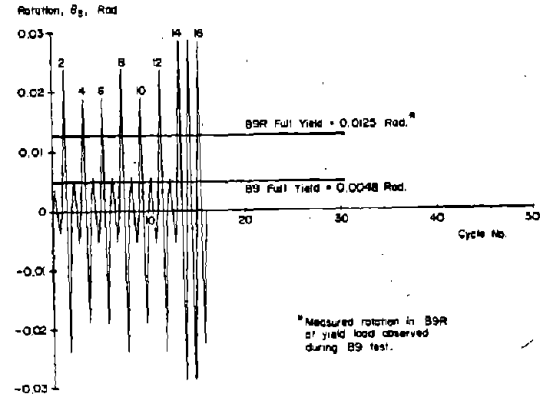

c) Rotation History

Fig. B-112 Loading History for Specimen B9R

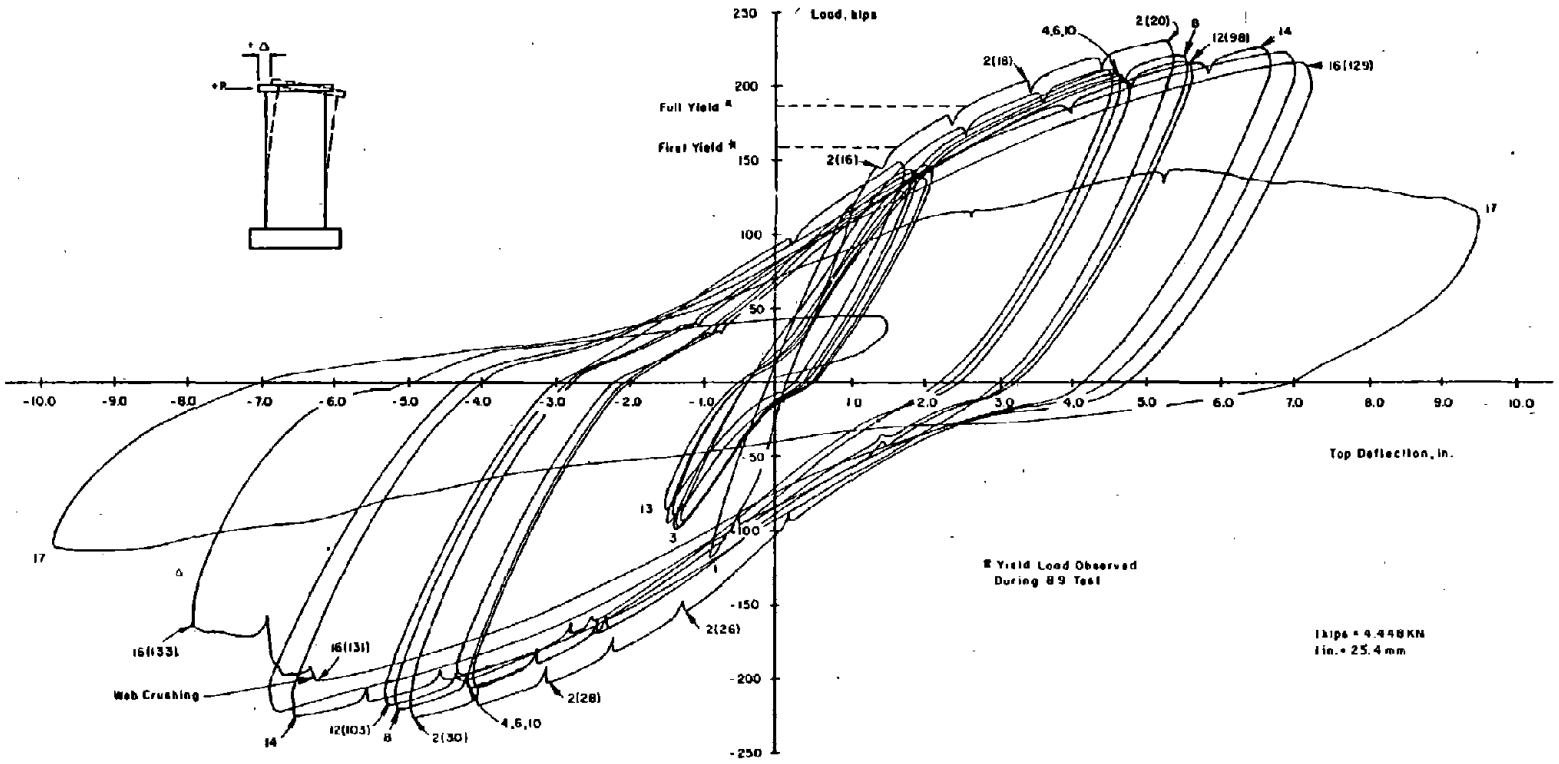

Fig. B-113 Continuous Load - Top Deflection for Specimen B9R

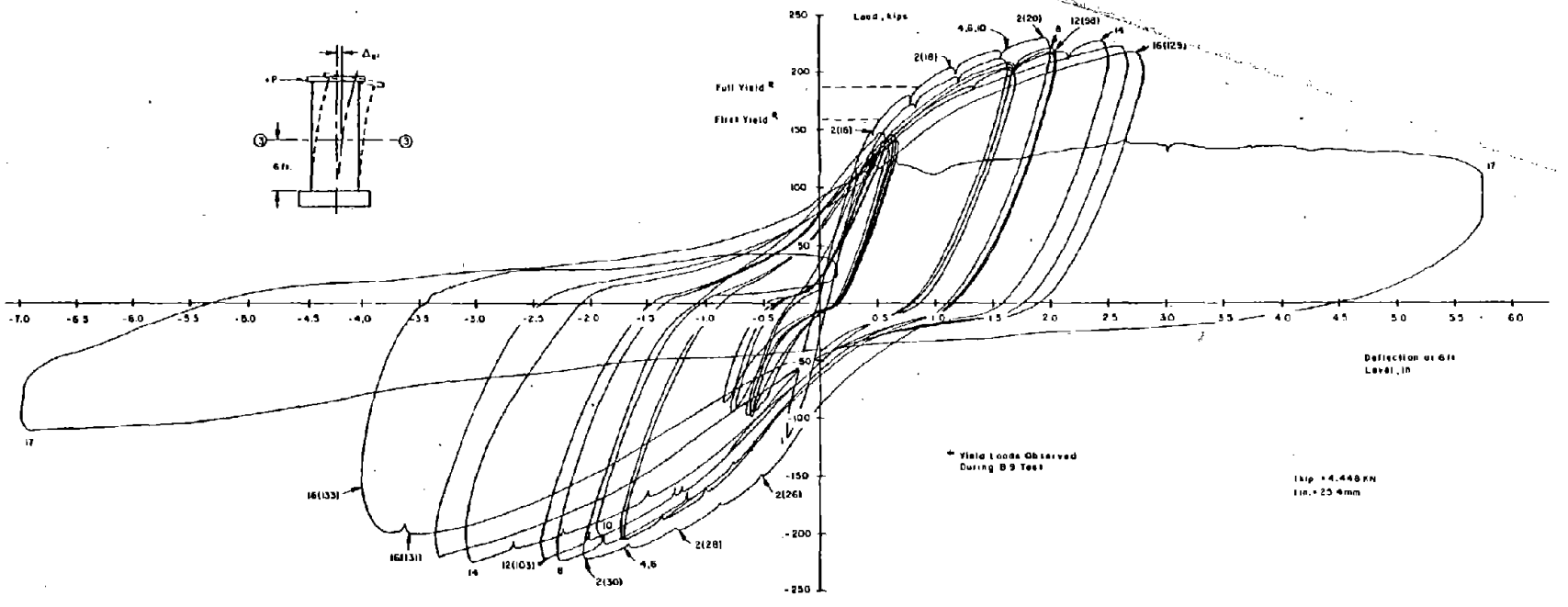

Fig. B-114 Continuous Load - Deflection at 6 ft Level for Specimen B9R

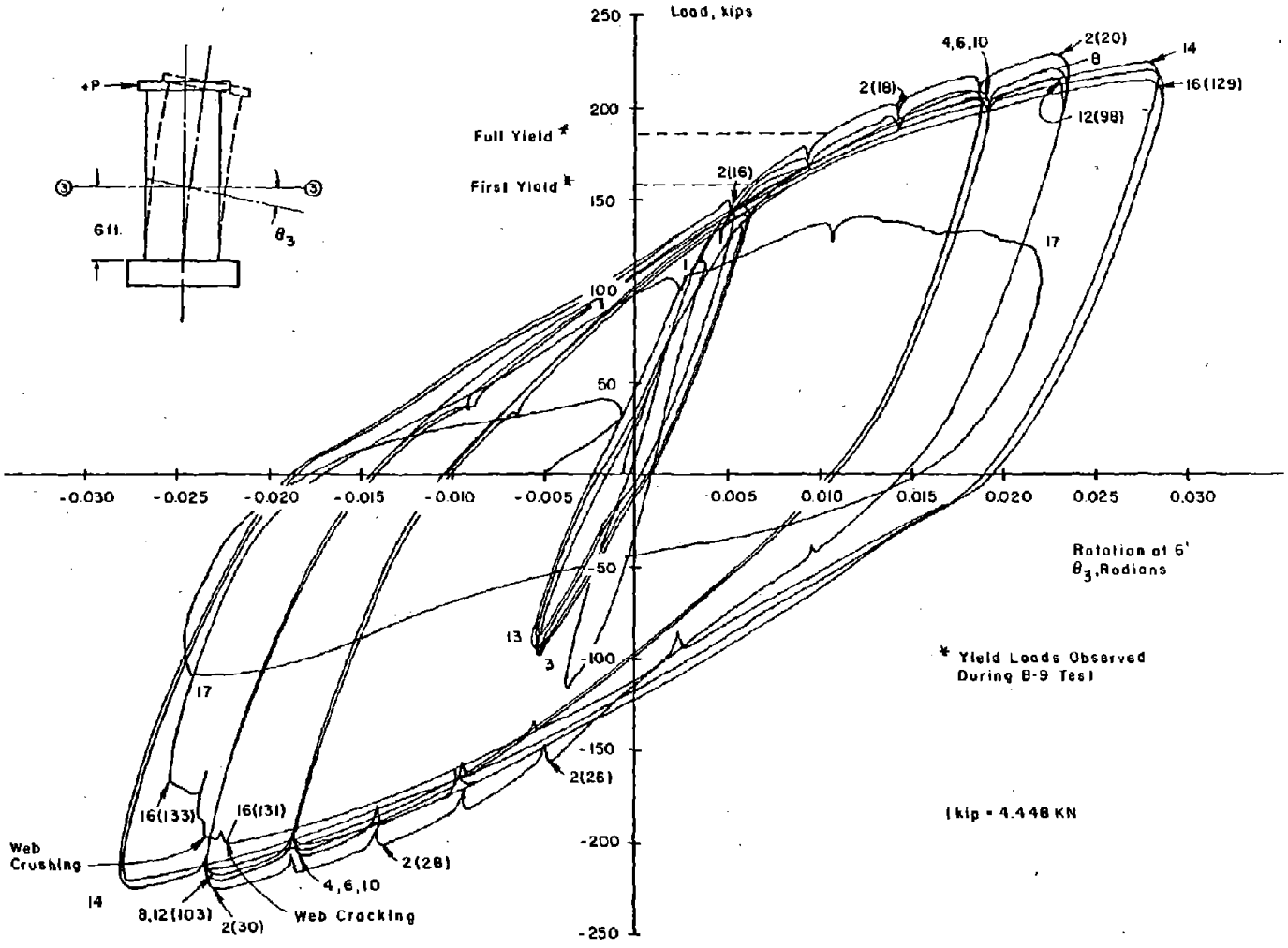

Fig. B-115 Continuous Load - Rotation at 6 ft Level for Specimen B9R

measured in B9. However, at the peak of Cycle 2, the maximum loads, rotations and deflections in B9R were nearly identical to those measured in Specimen B9.

During the positive half of Cycle 2, the patched cover of the compression column face cracked and spalled and a vertical crack formed in the lower 3 ft at the interface of the web and compression column. The maximum measured diagonal crack width was 0.25 in. (6.35 mm) at the peak load in Cycle 2. However, neither the compression strut system nor the compression column core exhibited any signs of distress.

Upon reversal of loading in the negative half of Cycle 2, Specimen B9R exhibited load-deformation relationships very similar to those measured in the second half of Cycle 2 for B9.

In this negative half cycle, the patched cover on the compression column face spalled and cracked and again a vertical crack formed in the lower 3 ft at the interface of the web and compression column. In addition, a slight amount of spalling was noted along the diagonal cracks in the lower 6 ft of the web. In addition, a horizontal crack approximately 16-in. (0.41 m) long formed along the construction joint at the 3-ft level.

Crack patterns that developed at the peak positive and negative loads in Cycle 2 are shown in Figs. B-116 and B-117. This cracking was very similar to that which developed in Specimen B9.

Except for a small increase in the spalling and flaking along diagonal web cracks, no significant changes occurred in Cycles 3, 4 or 5.

In Cycle 6 apparent crushing of one of the lower compression struts was noted approximately 10 in. (254 mm) above the base in the center of the web. There was no loss of load capacity associated with this crushing. It was determined during Cycle 12 that the crushing was initiated by buckling of a vertical bar which pushed off the concrete cover. Photographs of this crushing and buckling are shown in Figs. B-118 and B-119. Except for continually increasing spalling and flaking

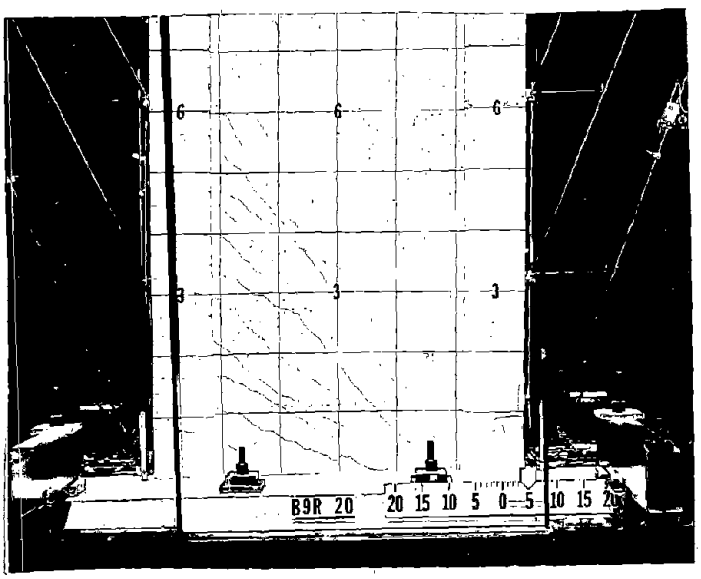

Fig. B-116 Cracking Pattern at Maximum Positive Load in Cycle 2 for Specimen B9R

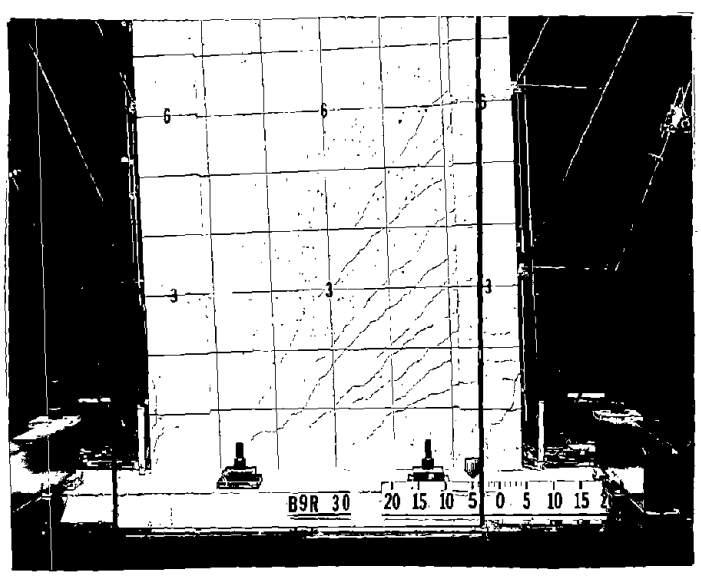

Fig. B-117 Cracking Pattern at Maximum Negative Load in Cycle 2 for Specimen B9R

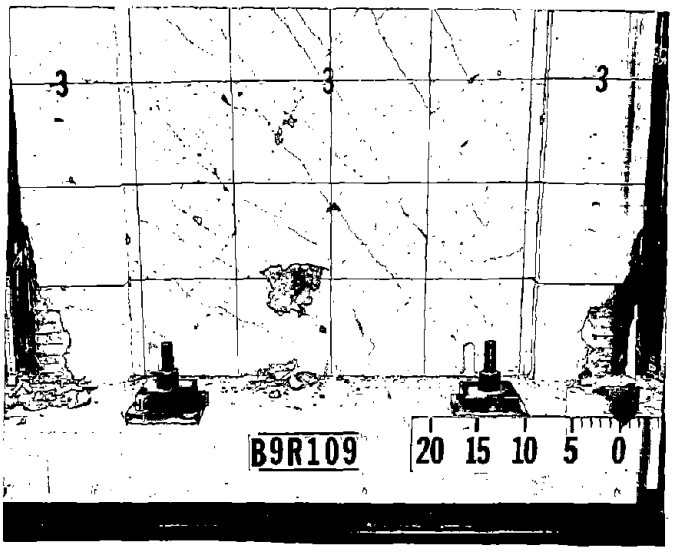

Fig. B-118 Spalling in the Web of Specimen B9R Caused by Buckling of Vertical Reinforcement

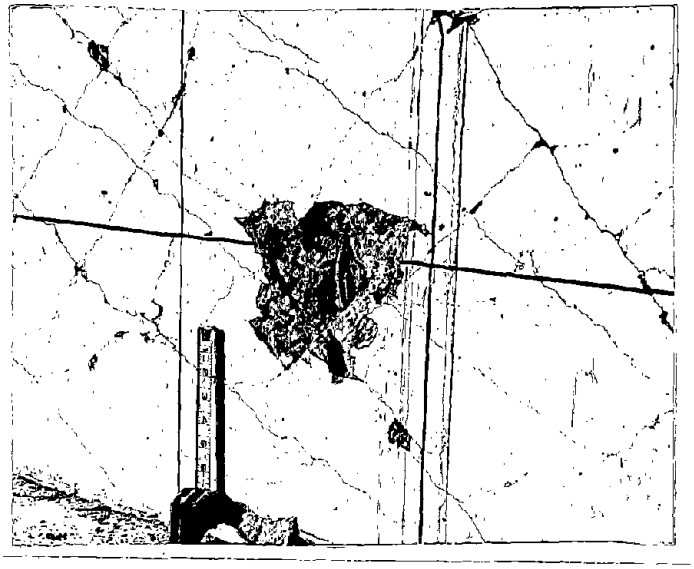

Fig. B-119 Spalling in the Web of Specimen B9R Caused by Buckling of Vertical Reinforcement

along diagonal web cracks, no other significant changes occurred in Cycles 6 through 13. This completed the planned modified load history for a maximum rotational ductility of 5.0 (based on the full yield rotation measured in B9). The lower 3 ft of the wall at this stage is shown in Fig. B-118.

Despite the spalling and crushing in the web by the end of Cycle 13, the load capacity of the wall was not impaired. It was therefore decided to use an incrementally increasing load history for the remainder of the test. The wall was to be loaded with three cycles at each increasing multiples of the B9 full yield rotation until it was destroyed. The first loading increment was at six times the B9 full yield rotation.

Except for increased spalling in the web, no significant changes occurred in Cycles 14, 15 and the positive half of 16. Upon approaching the peak load in the negative half of Cycle 16, several compression struts crushed in the lower left region of the web. Figures B-120 and B-121 show the specimen prior to and after web crushing.

The maximum load measured was 218.7 kips (972.8 kN) in Cycle 2. This maximum is nearly identical to the maximums measured in B7, B8 and B9 at equivalent deformation levels. The load corresponds to a nominal shear stress of $v_{max} = 7.0 \sqrt{f'_c}$ ($0.58 \sqrt{f'_c}$ MPa). The maximum load measured in Cycle 16 was 205.8 kips (915 kN) which was 94% of that in Cycle 2.

Specimen B9R sustained its load capacity through the complete modified load history with a maximum rotation corresponding to what would have been a ductility of 5 in Specimen B9. It also sustained two cycles at what would have been a ductility of 6.0. Therefore, lowering the nominal maximum shear stress by increasing the web thickness enhanced inelastic performance considerably.

Discussion of Results

Moment-Rotation. The moment-rotation data for Specimen B9R are shown in Fig. B-122. Envelopes for B9 data are included. At the peak load in Cycle 2, the load and rotations

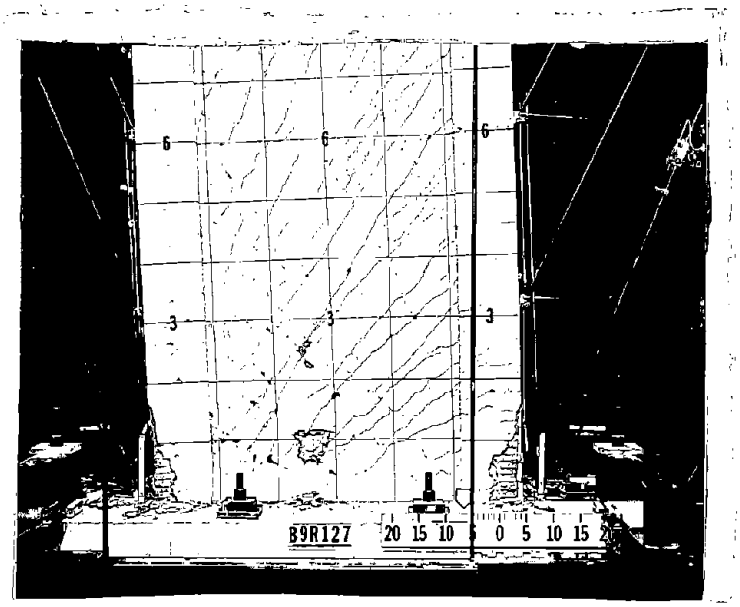

Fig. B-120 Specimen B9R Prior to Web Crushing

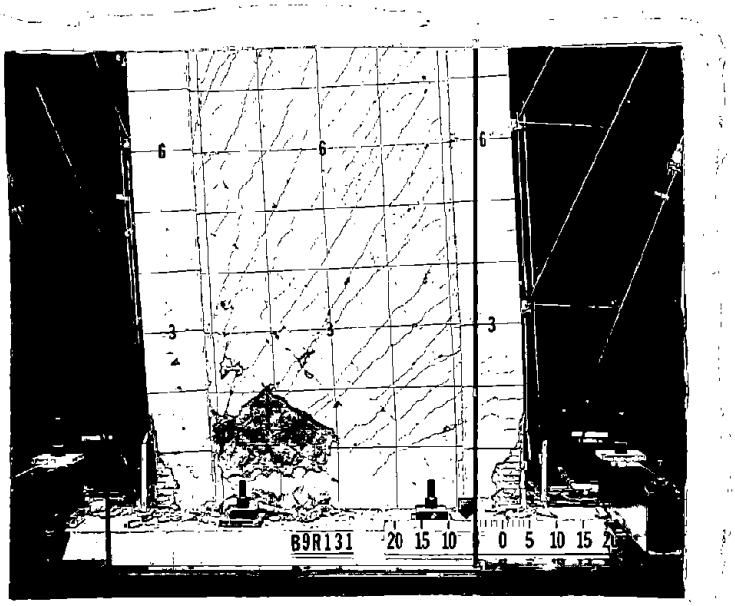

Fig B-121 Specimen B9R After Web Crushing

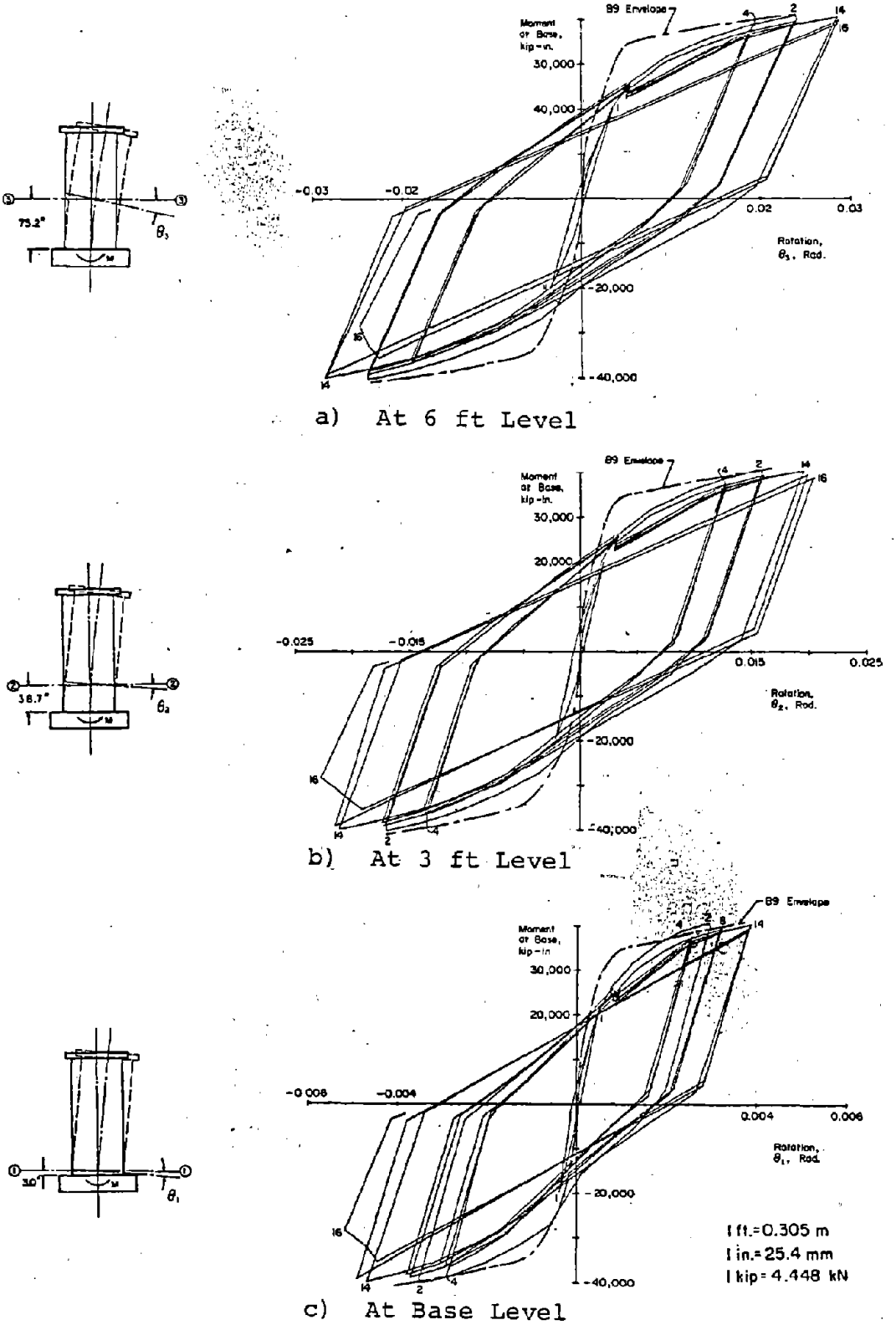

Fig. B-122 Moment at Base versus Rotation for Specimen B9R

at the 3-ft and 6-ft (0.91 m and 1.83 m) levels where very similar to those in B9. Maximum rotation at the base level was somewhat less in B9R at the peak load for Cycle 2.

Shear Distortion. Shear-distortion curves for B9R are shown in Fig. B-123. The curves do not exhibit a well defined yielding region. This was also the case for the moment-rotation curves. The continual decrease in the shear stiffness with repeated cycling can be see in Fig. B-123.

Specimen B9R had 15% and 30% less shear distortion than did B9 in the positive and negative halves of Cycle 2. This was the effect of increased web thickness. However, by Cycle 15, Specimen B9R had 40% more shear distortion than the maximum measured in B9.

Slip at Construction Joints. Slip at construction joints in B9R is shown in Fig. B-124. This slip plot for CJ1 is similar to that for shear distortions showing a continual decrease in shear-slip stiffness. The slip plots for CJ2 and CJ3 are unsymmetrical. Measured slips were affected by diagonal cracking.

Figure B-125 shows the slip at CJ1 as a percentage of shear deflections in Zone 1 for the positive and negative loading portions of Cycles 2 and 14. This figure shows that slip at CJ1 contributed a relatively large portion of the diffraction during the first load stages of a cycle, but decreased to 10% to 15% at peak loads.

Deflections. The deflection components and deflected shapes are shown in Figs. B-126 through B-128. Comparison of Figs. B-126 and B-127 shows the increase in the shear component of deflection between Cycle 2 and 14.

The deflected shapes for Cycle 2, Load Stages 20 and 30, and Cycle 12, Load Stages 98 and 103, indicate the change in stiffness during the modified load history at a maximum rotation of five times yield.

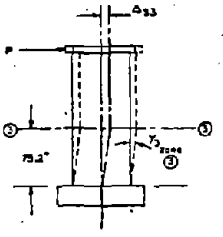

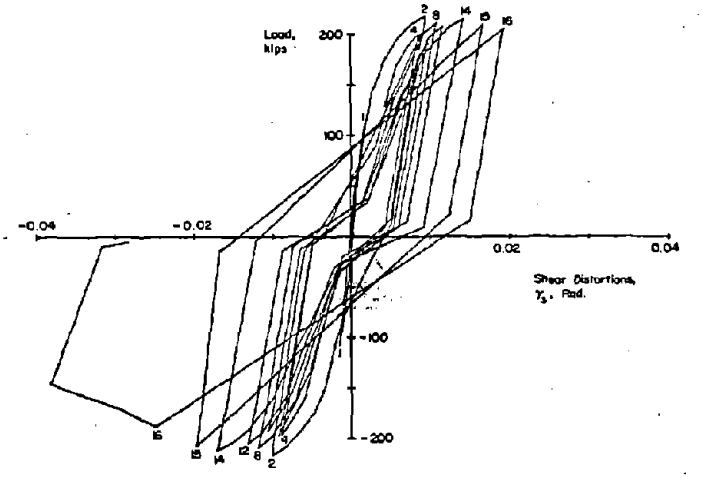

a) In Base to 6 ft Level

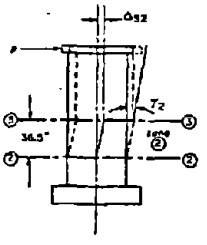

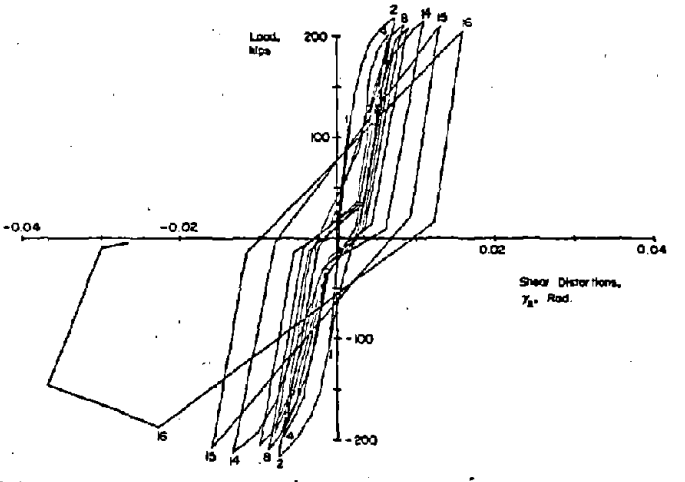

b) In 3 ft to 6 ft Level

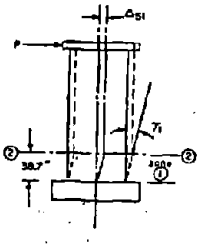

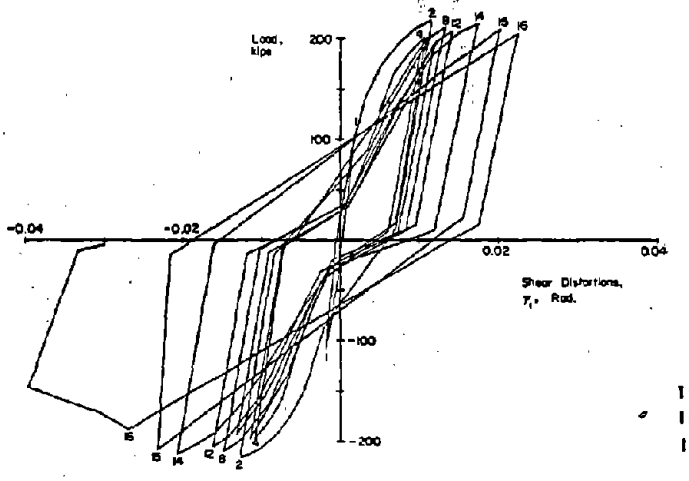

1 ft = 0.305 m
1 in. = 25.4 mm
1 kip = 4.448 kN

c) In Base to 3 ft Level

Fig. B-123 Load versus Shear Distortion for Specimen B9R

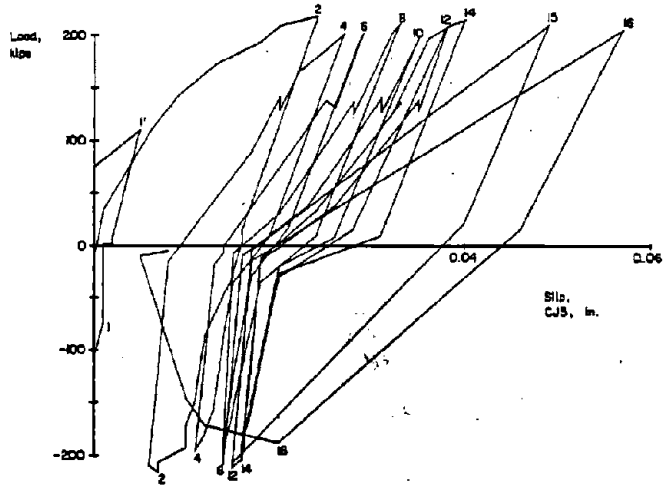

a) At 6 ft Level

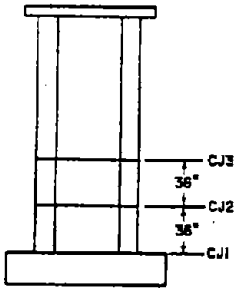

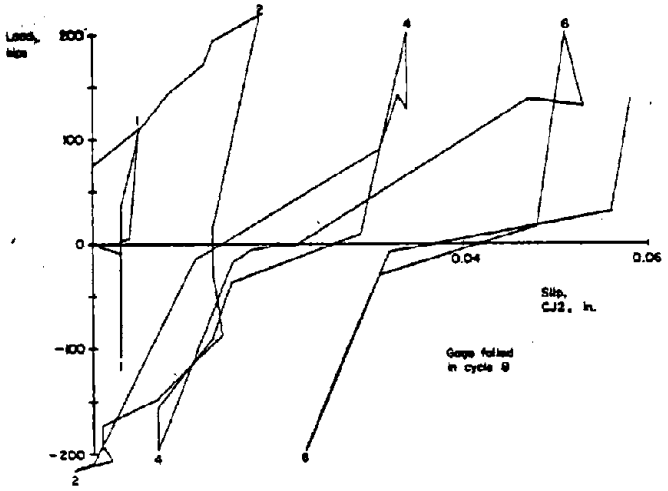

b) At 3 ft Level

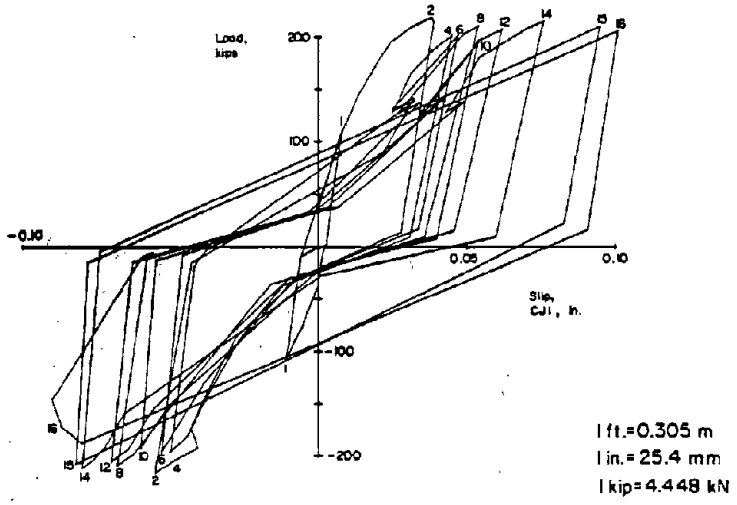

c) At Base Level

Fig. B-124 Load versus Slip at Construction Joints for Specimen B9R

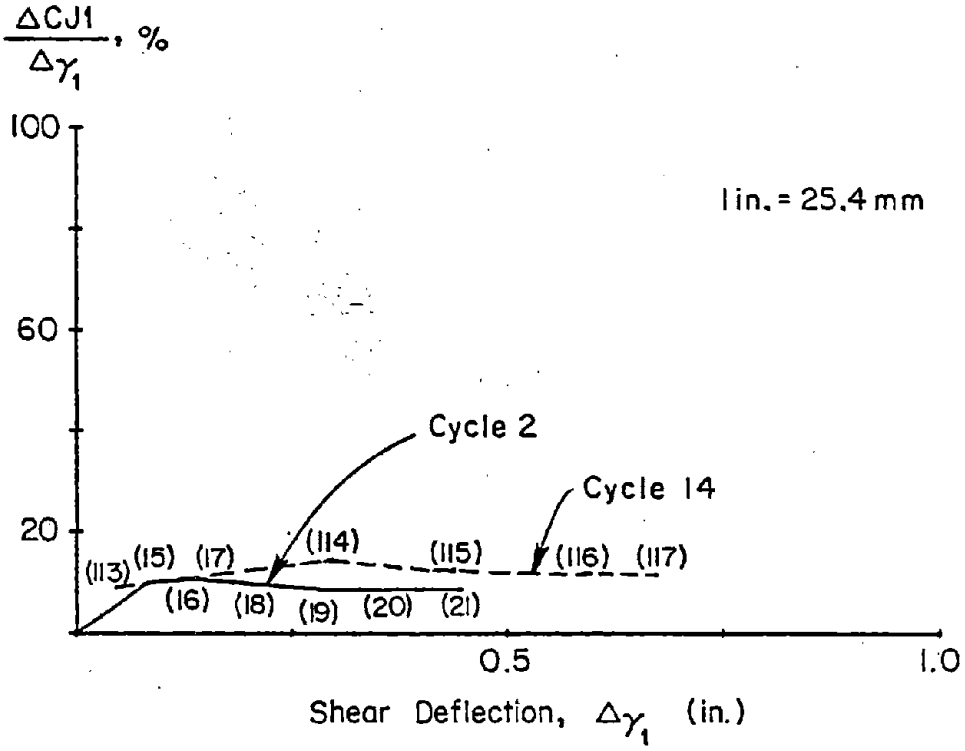

a) At Positive Load Stages in Cycle 2 and 14

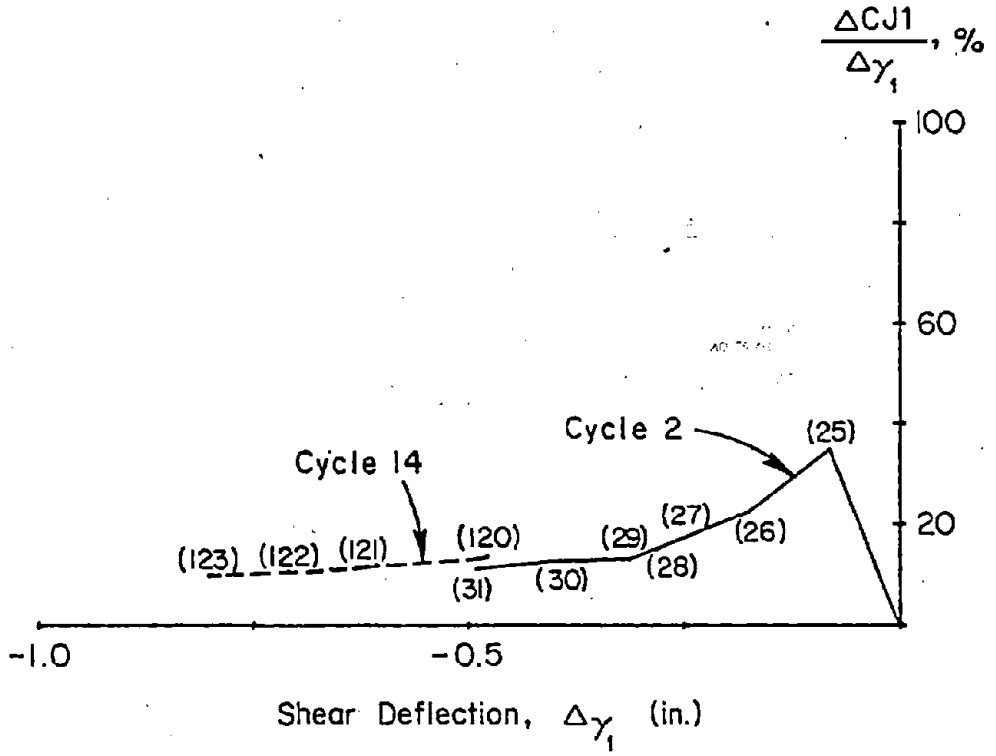

b) At Negative Load Stages in Cycle 2 and 14

Fig. B-125 Slip at Base Construction Joint versus Shear Deflection in Zone 1 for Specimen B9R

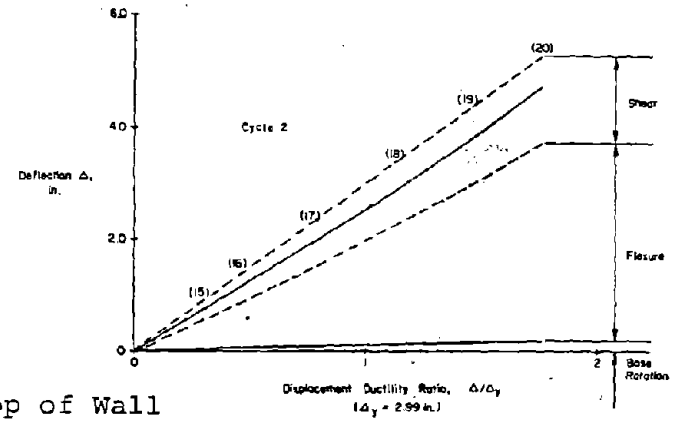

a) At Top of Wall

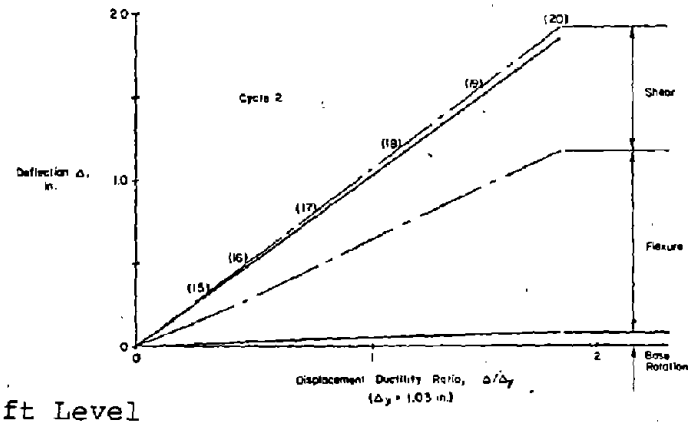

b) A 6 ft Level

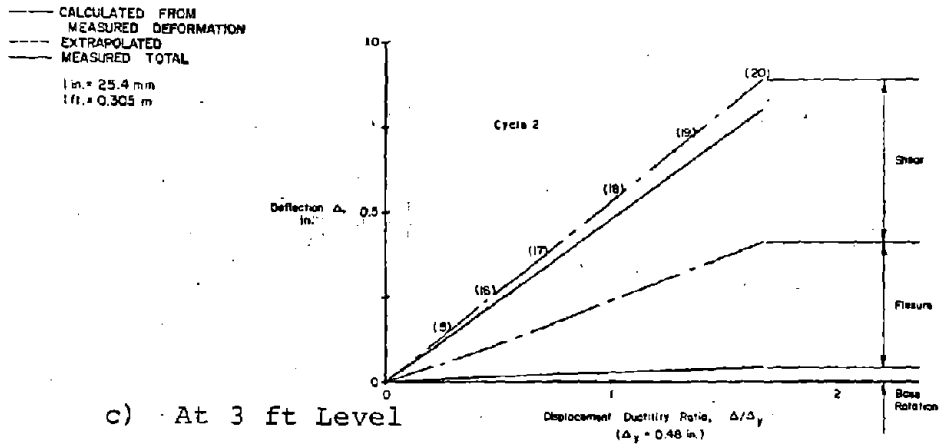

c) At 3 ft Level

Fig. B-126 Components of Deflection for Specimen B94 in the Positive Half of Cycle 2

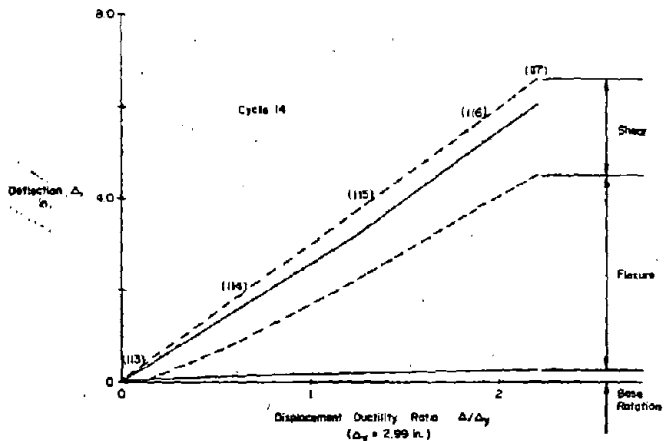

a) At Top of Wall

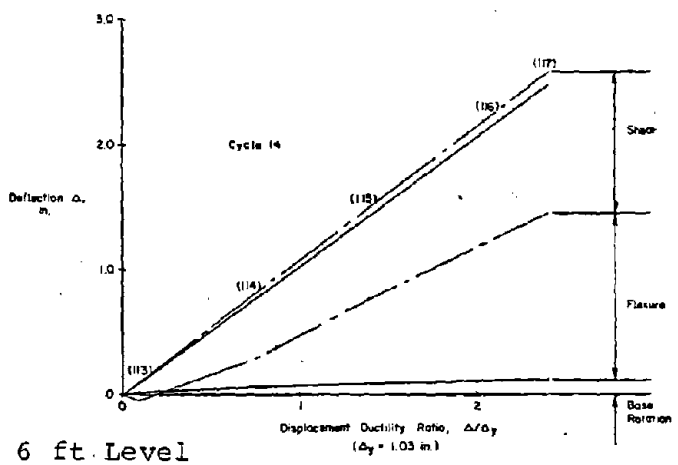

b) A 6 ft Level

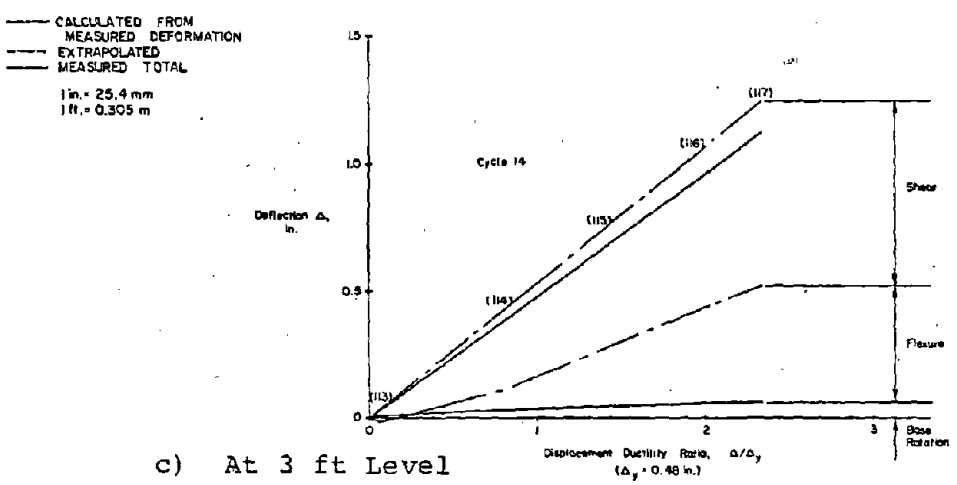

c) At 3 ft Level

Fig. B-127 Components of Deflection for Specimen B9R in the Positive Half of Cycle 14

a) Flexural

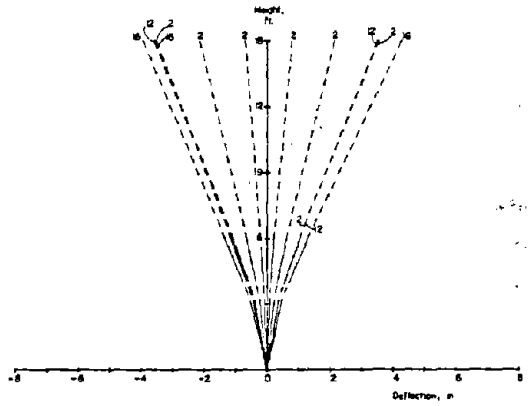

b) Shear

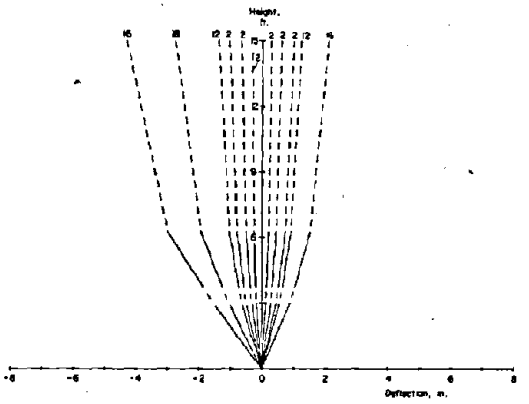

c) Total

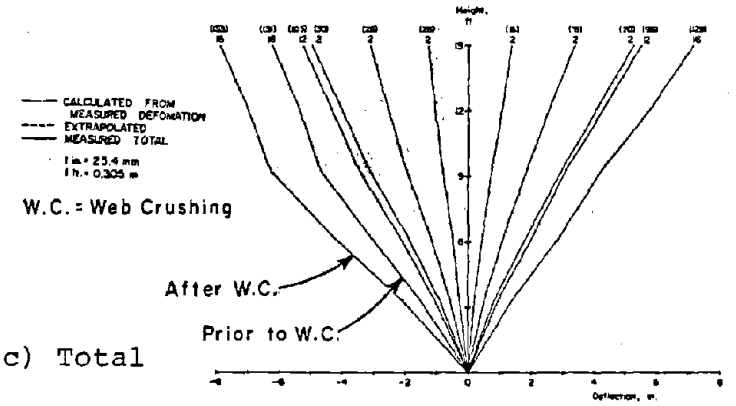

Fig. B-128 Deflected Shape for Specimen B9R

Specimen B10

Test Description

Specimen B10 was a barbell shaped wall with 1.97% vertical reinforcement in each column and confinement reinforcement in the lower 6 ft of the boundary elements. It was constructed to investigate the influence of shear stress on inelastic behavior in the mid shear range. Prior to Specimen B10, the test program had included several specimens with $v_{max} \leq 3\sqrt{f'_c}$, several with a $v_{max} \geq 7\sqrt{f'_c}$ without axial load and several with a $v_{max} \geq 10\sqrt{f'_c}$ with axial load. Two distinct types of behavior were observed depending on the level of shear.

The program included one specimen with a $v_{max} = 7\sqrt{f'_c}$ with axial load. However, this was a repaired specimen, B9R. Specimen B10 was designed to have a $v_{max} = 8\sqrt{f'_c}$ with axial load to investigate the type of behavior that would predominate. Also, Specimen B10 was designed to have a moment capacity with axial load applied equal to the measured moment capacity of Specimen B5 without axial load.

Unfortunately, a construction problem developed in Specimen B10. Figures B-129 and B-130 show honeycombing in the lower 9 in. (0.23 m) of one of the boundary elements. The honeycombing was the result of insufficient consolidation within the congested confinement reinforcement. Although the possibility of honeycombing exists in full scale structures, the problem is increased in reduced scale models.

The honeycombed cover was chipped down to what appeared to be solid core concrete and then patched with a sand cement mortar prior to the start of the lateral load test.

Since B9R had sustained the modified load history at a maximum rotation corresponding to a ductility of 5.0 it was anticipated that B10 would also sustain this load history. For purposes of comparison with B9R, the B10 test was started with the modified load history at a maximum rotational ductility of 5.0. It was anticipated that, upon completion of this modified load history, the incrementally increasing history would be used for the remainder of the test to failure.

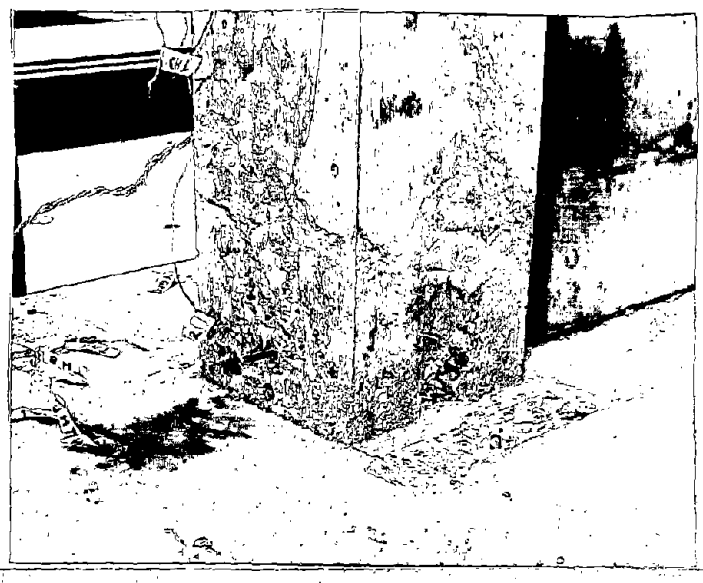

Fig. B-129 Unconsolidated Concrete in Base of Boundary Element in Specimen B10

Fig. B-130 Closeup of Unconsolidated Concrete in Base of Boundary Element in Specimen B10

The test consisted of 14 complete loading cycles as shown in Fig. B-131. The complete load versus top deflection relationship for Specimen B10 is shown in Fig. B-132. Complete load versus deflection and rotation relationships at the 6-ft level are shown in Figs. B-133 and B-134.

The first load cycle was applied to develop cracking in both directions. First significant cracking was observed at a load of 75 kips (334 kN).

First yielding occurred in Cycle 2, Load Stage 13, at a load of 120.0 kips (533.8 kN). Full yielding occurred in Cycle 2, Load Stage 14, at a load of 139.7 kips (621.4 kN). The maximum measured crack widths at this stage were 0.011 in. (0.28 mm) in the tension column and 0.019 in. (0.48 mm) across a diagonal crack in the web.

First indication of crushing in the concrete cover of the outer face of the compression column was noted at Load Stage 15, corresponding to a rotation of two times yield. The compression column for the positive half of Cycle 2 was not the column with the patched concrete. Crushing progressively increased as the wall was loaded to a top deflection of +4.91 in., a 6-ft level rotation of 0.02392 rad. and a maximum load of 159.0 kips (707.2 kN).

Except for the crushing at the compression face, the wall exhibited no signs of distress in the positive half of Cycle 2. The maximum measured crack widths at the peak were 0.036 in. (0.91 mm) in the tension column and 0.095 in. (2.41 mm) across a diagonal crack in the web.

In the negative load half of Cycle 2, the patched cover on the compression column started to spall at Load Stage 21 corresponding to a rotational ductility of one times yield. The patched cover continued to crush and spall as the load increased, however, the confined core appeared to be in good condition. The load attained was 148.3 kips (659.6 kN), which was 93% of that attained in the positive half of Cycle 2.

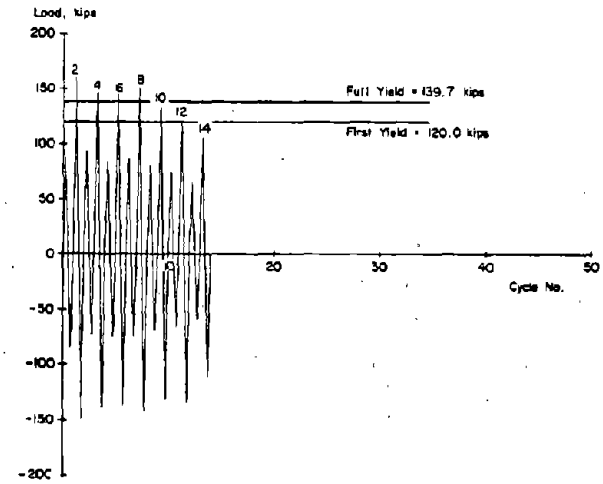

a) Load History

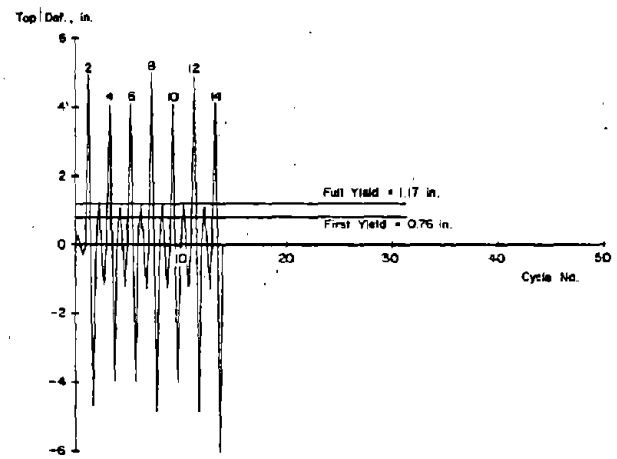

b) Deflection History

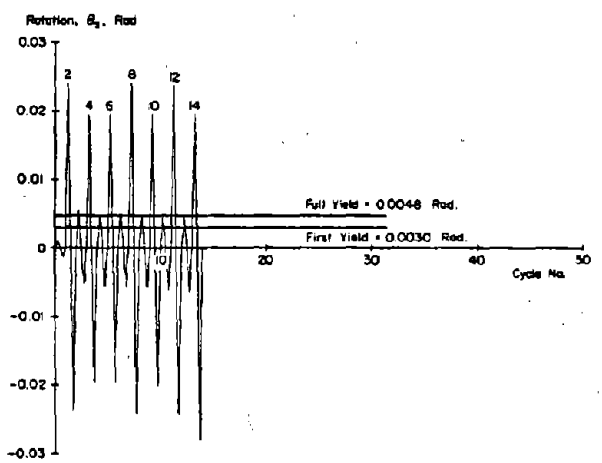

c) Rotation History

Fig. B-131 Loading History for Specimen B10

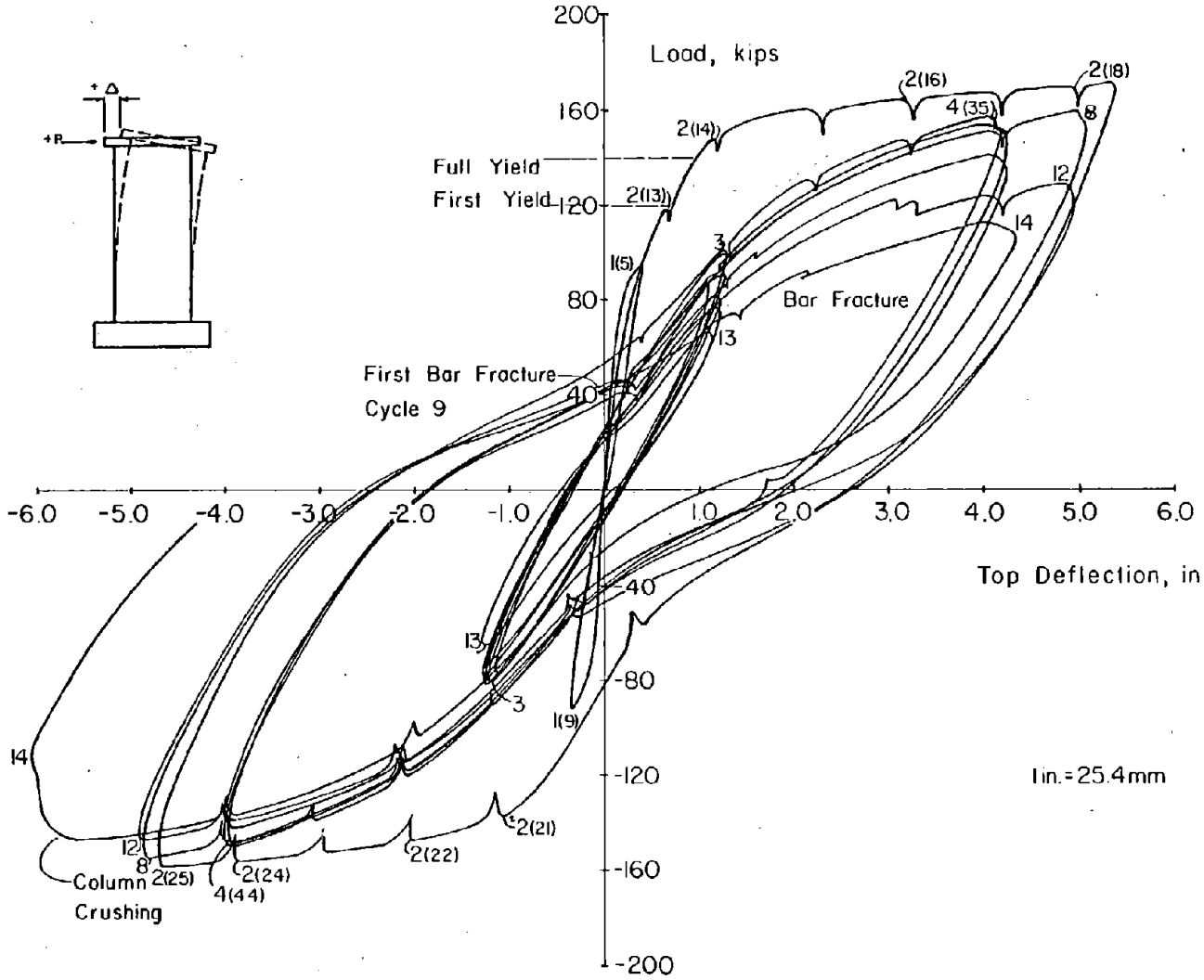

Fig. B-132 Continuous Load - Top Deflection for Specimen B10

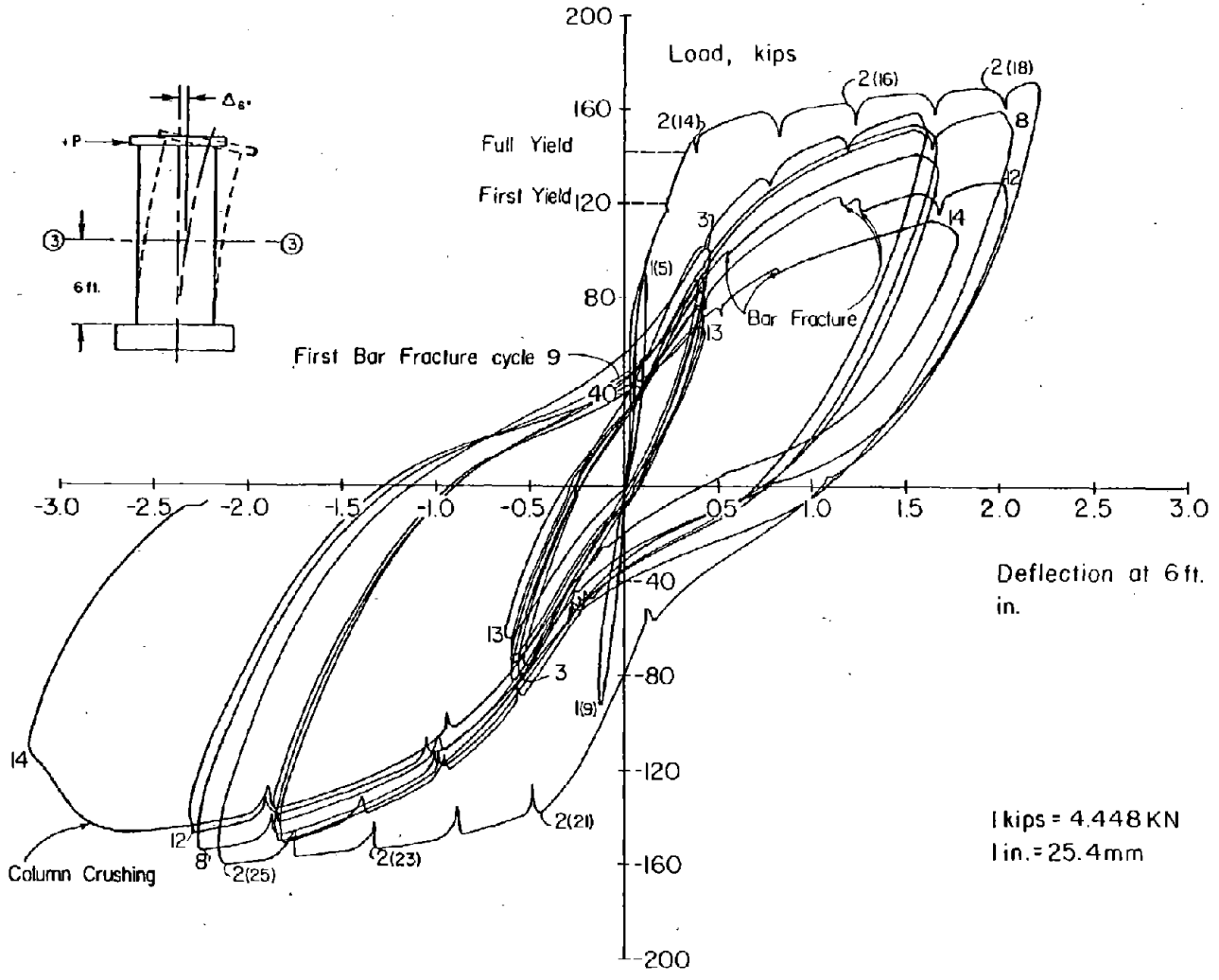

Fig. B-133 Continuous Load - Deflection at 6 ft Level for Specimen B10

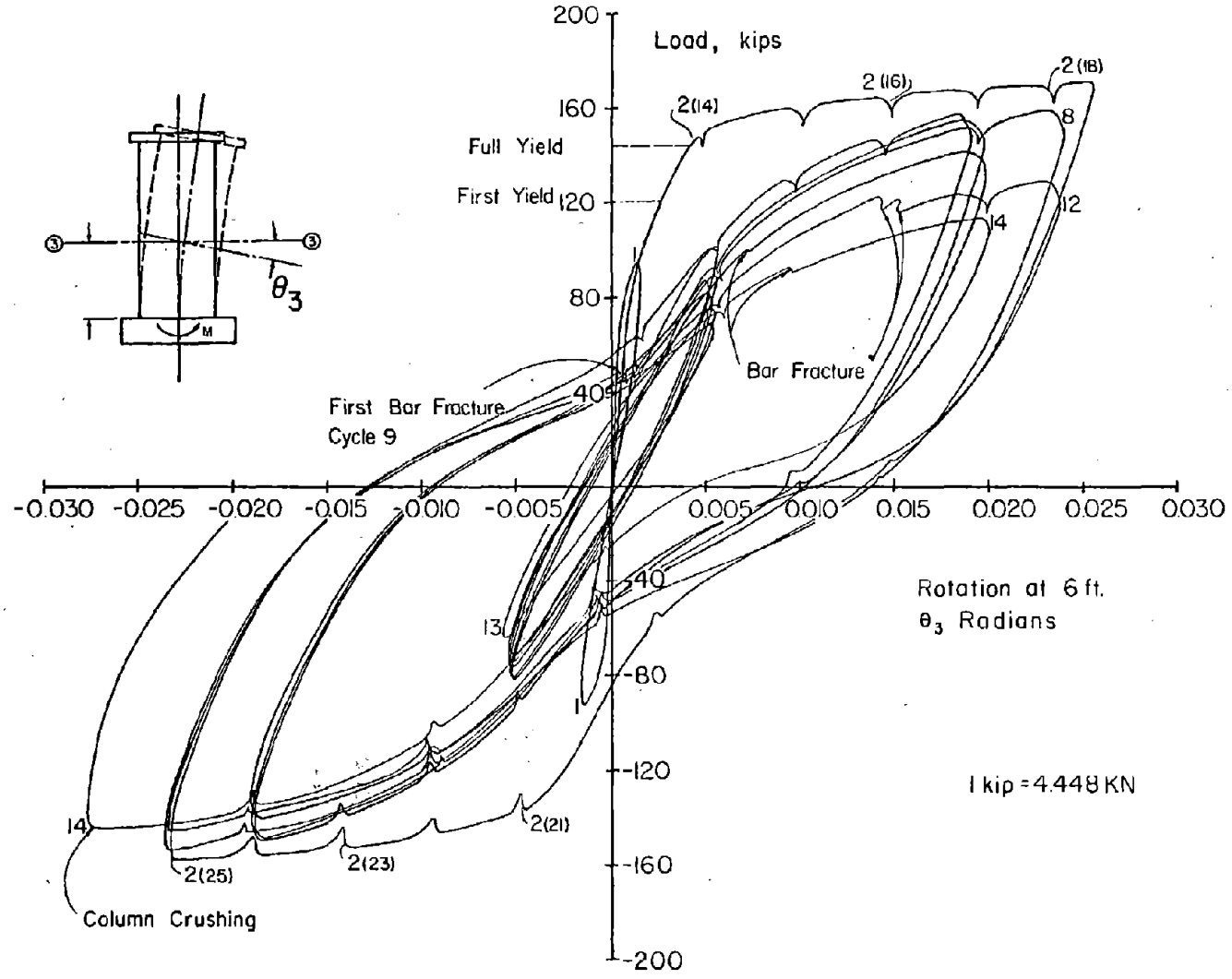

Fig. B-134 Continuous Load - Rotation at 6 ft Level for Specimen B10

The crack pattern that developed was similar to that in the specimens subjected to high shear. A complete diagonal compression strut system formed for each direction of loading. Figures B-135 and B-136 show the specimen at maximum positive and negative loading in Cycle 2.

No significant changes occurred in Cycles 3, 4, 5, or in the positive half of Cycle 6. A few 90^{o} end hooks on confinement crossties near the base of the repaired column started to open slightly when this column was in compression.

In the negative half of Cycle 6 the two corner bars in the outer pair of the compression column started to buckle between confinement hoop. The 90^{o} end hooks of horizontal shear reinforcement started to open near the base. Also, crushing of concrete was observed within the confined core. Apparently honey-combed concrete was not completely repaired.

No significant changes occurred in Cycle 7. However, in the negative half of Cycle 8, the outer two rows of compression column vertical bars buckled. Some buckled sideways within the hoop as honeycombed core concrete was lost. Others buckled outward bowing the confinement hoops.

In the positive half of Cycle 9 one of the previously buckled corner bars fractured. Another outer bar fractured in the positive half of Cycle 10. However, the load reached at the positive peak of Cycle 10 was 92% of that at the positive peak of Cycle 4.

There was increased buckling and crushing in the compression column during the negative half of Cycle 10. The load reached at the negative peak of Cycle 10 was 94% of that at the positive peak of Cycle 4.

Three more previously buckled bars fractured before the peak load in Cycle 12 was reached. The maximum load reached in the positive half of Cycle 12 was 76% of the maximum in Cycle 2.

There was no significant change during Cycle 13. This completed the modified load history at a maximum rotational ductility of 5.0 Figure B-137 shows the wall at this stage.

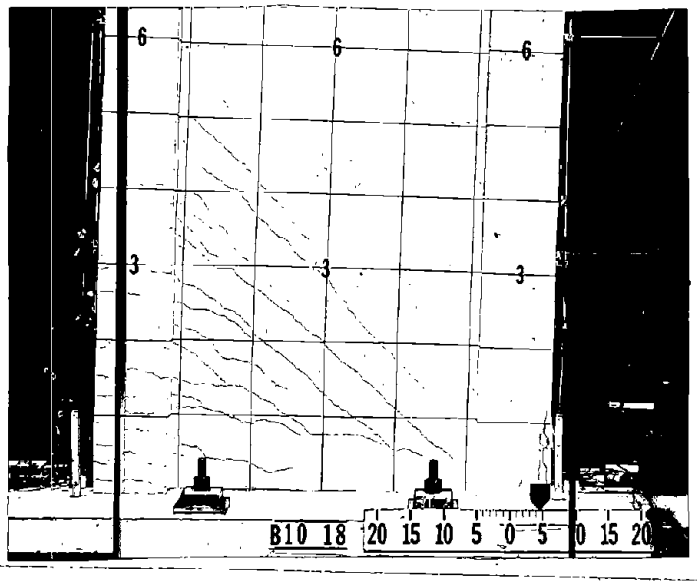

Fig. B-135 Cracking Pattern at Maximum Positive Load in Cycle 2 for Specimen B10

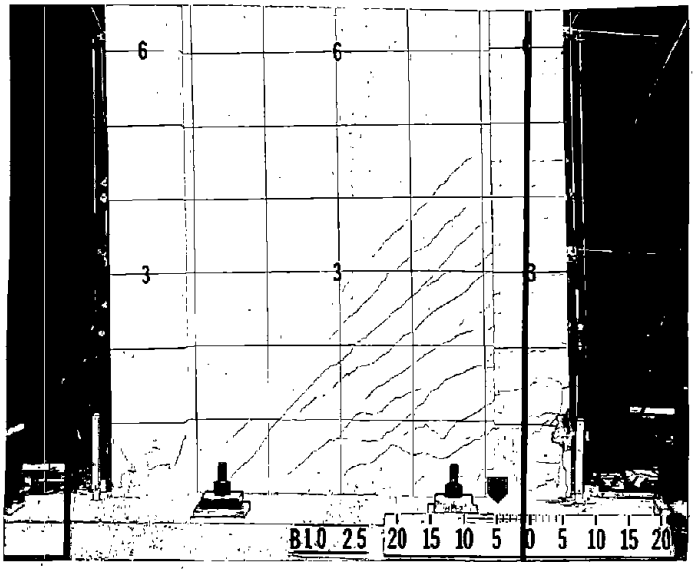

Fig. B-136 Cracking Pattern at Maximum Negative Load in Cycle 2 for Specimen B10

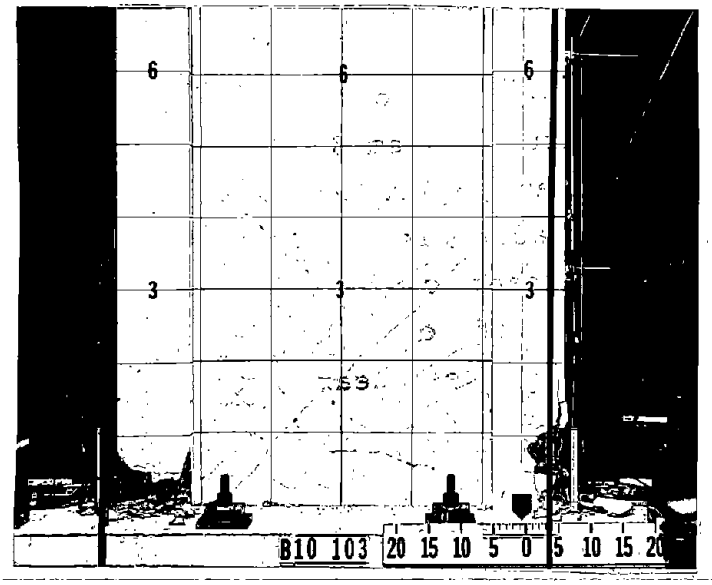

Fig. B-137 Specimen B10 After Completion of Modified Load History

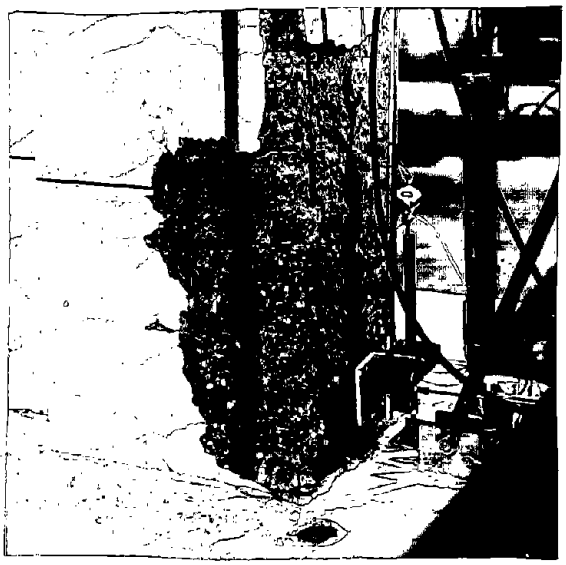

Fig. B-138 Left Column after Completion of Modified Load History

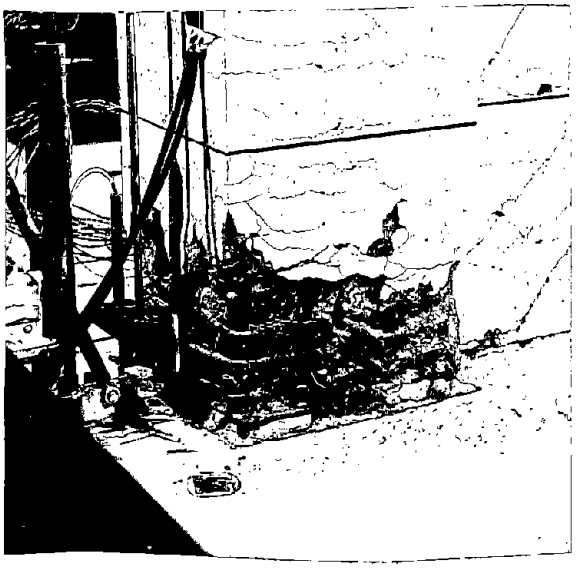

Fig. B-139 Right Column After Completion of Modified Load History

Figures B-138 and B-139 show details of the left and right columns, respectively. It should be noted that the right hand column and the wall web showed very little sign of distress at this stage. The damage in the left column was attributed to poor quality construction. However, even with the honeycombed concrete and resulting bar buckling and fracture, the specimen sustained 76% of its initial strength throughout the modified load history.

Since loading to larger positive rotations would have caused additional bar fractures, it was decided at this stage to load to a positive ductility of four then to a negative ductility of six for three cycles.

During the negative half of the first cycle of this increment, Cycle 14, the compression boundary element crushed completely and all remaining bars in this column buckled. The compression zone then moved into the web which immediately crushed. The drop in load capacity was sudden. Figures B-140 and B-141 show the wall and the left column at the end of the test.

Discussion of Results

Moment-Rotation. Moment-rotation data for Specimen B10 are shown in Fig. B-142. The maximum measured moment was 95% of the calculated monotonic maximum. This calculated maximum was based on attainment of an ultimate compressive strain of ε_u =0.0067 in the boundary element.

As in the test of Specimen B9, the positive half of Cycle 2 was essentially a monotonic test up to the maximum rotation applied. The relationship between the calculated monotonic curves and the measured curves is similar to that observed in the test of B9.

The nonsymmetry of the plot of θ_1, one occurs because of the crushing of honeycombed concrete at the base of one boundary element.

Shear Distortion. The shear-distortion loops for B10 are shown in Fig. B-143. As in the previously reported tests a shear "yielding" occurred during the same cycle in which flexural yielding occurred. Nonsymmetry of the plot for γ_1, indicates the effect of the honeycombed concrete.

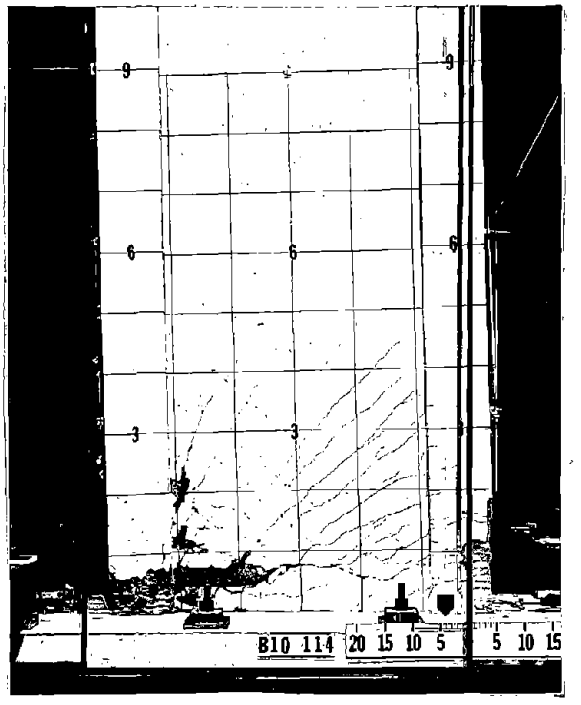

Fig. B-140 Specimen B10 at End of Test

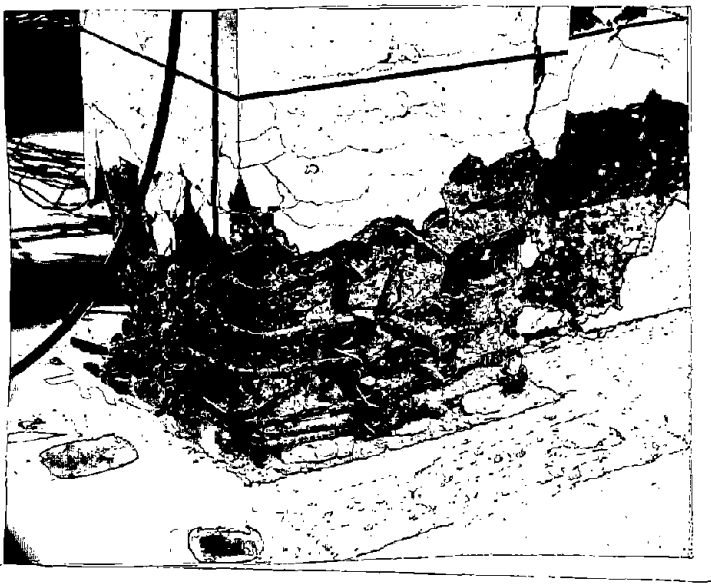

Fig. B-141 Boundary Element with Unconsolidated Concrete at End of Test

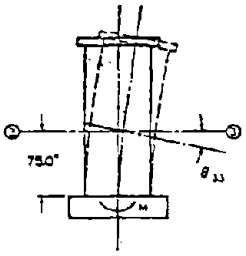

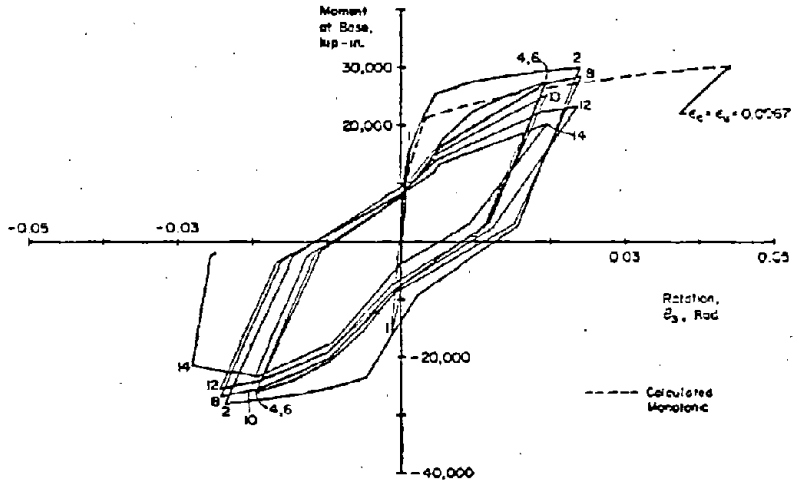

a) At 6 ft Level

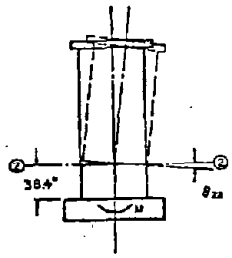

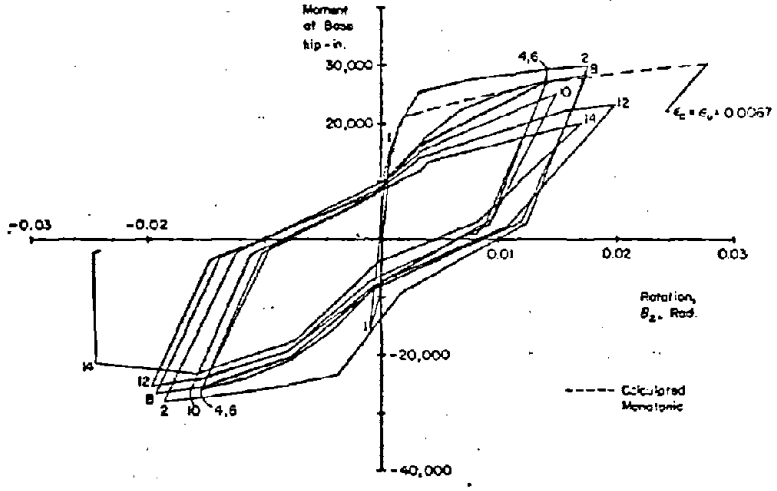

b) At 3 ft Level

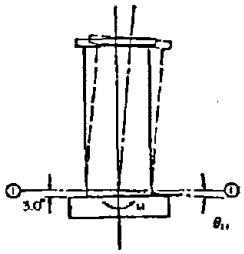

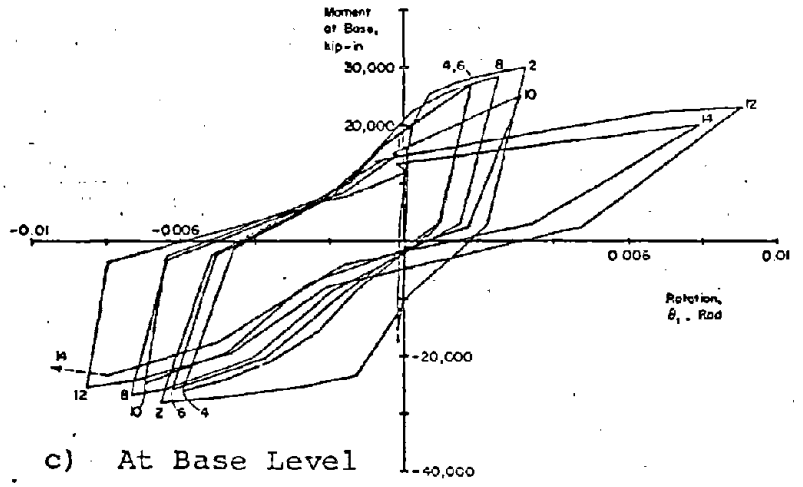

c) At Base Level

Fig. B-142 Moment at Base versus Rotation for Specimen B10

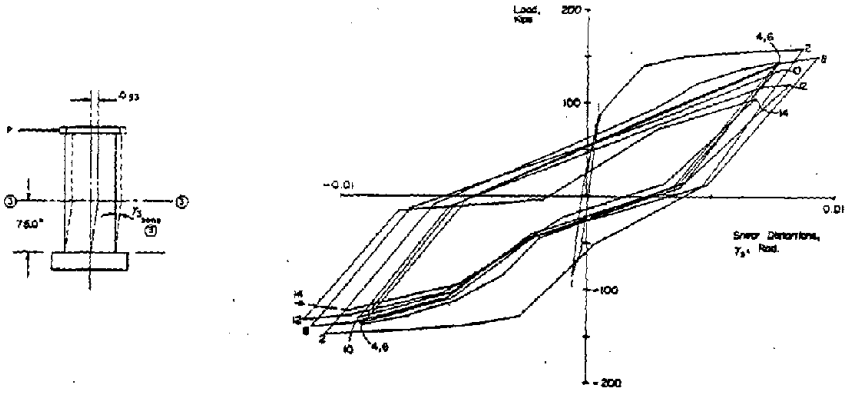

a) In Base to 6 ft Level

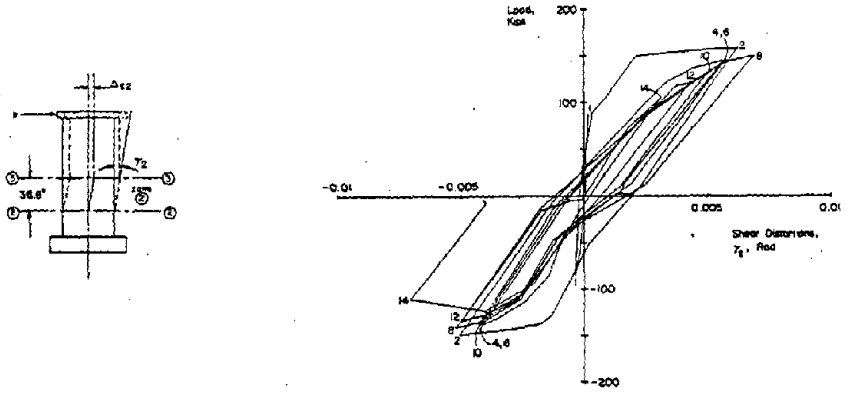

b) In 3 ft to 6 ft Level

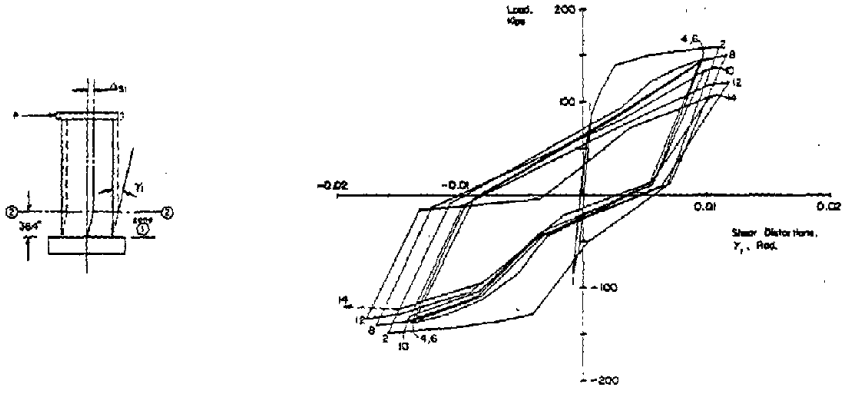

c) In Base to 3 ft Level

Fig. B-143 Load versus Shear Distortion for Specimen B10

The positive half of Cycle 2 provides data for comparing the monotonically loaded behavior of B10 with that of B9. At the peak positive load of 159.0 kips (707.23 kN), in Cycle 2 γ_3, in B10 was 0.00869 rad. At a similar point for Specimen B9, the load was 219.6 kips (976.8 kN) and γ_3 was 0.01113 rad. These peaks occurred at equivalent rotations at the 6-ft level. The load versus shear distortion ratios show that the effective shear stiffnesses were approximately equal in B9 and B10 at equal rotations.

Slip at Construction Joints. Slip at construction joints in B10 is shown in Fig. B-144. Slip at CJ1 exhibits yielding similar to shear "yielding" during the same cycle that flexural yielding occurred.

Figure B-144 also demonstrates the effect of the honeycombed concrete in that significantly larger slippage occurred under negative load. Figure B-145 shows that slip was about 5% of the positive shear deflections in the lower 3 ft (0.91 m). It was 15% of the negative shear deflections.

Deflections. Deflection components and deflected shapes are shown in Figs. B-146 through B-148. Comparison of Figs. B-146 and B-147 shows a relatively small change in the shear component of deflection between Cycle 2 and Cycle 8. This is also demonstrated by comparison of deflected shapes for Cycle 2, Load Stages 18 and 25, and the deflected shapes for Cycle 8.

Reinforcement Strains. Figures B-149 through B-159 show reinforcement strains in the specimen at various stages. Figure B-149 shows the cyclic load versus strain relationship for the outer vertical reinforcing bars at the base level.

Figure B-150 shows that yielding occurred up to the 9-ft (2.75 m) level in Cycle 2. Figures B-151 and B-152 show the strain gradient in the vertical reinforcement at various levels.

Figures B-153 through B-157 show the cyclic strain-load relationship and the strain gradients in the horizontal bars. These figures indicate that the yield strain was approached between the 18 in. (0.46 m) and 9-ft (2.74 m) levels and was exceeded at the 3-ft level (0.91 m).

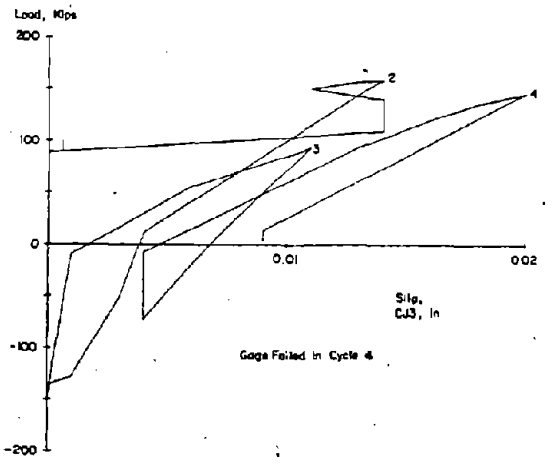

a) At 6 ft Level

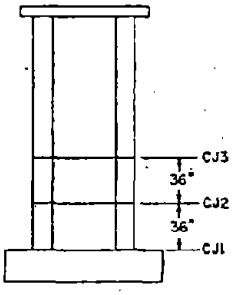

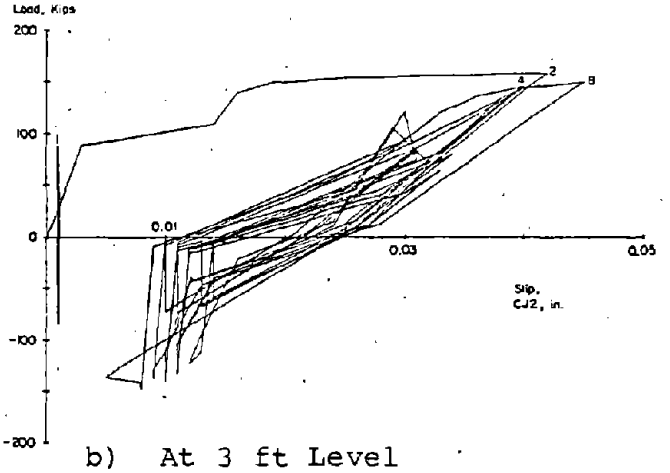

b) At 3 ft Level

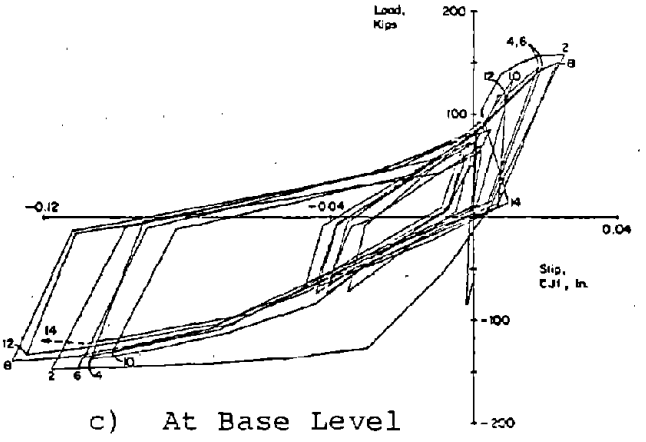

c) At Base Level

Fig. B-144 Load versus Slip at Construction Joints for Specimen B10

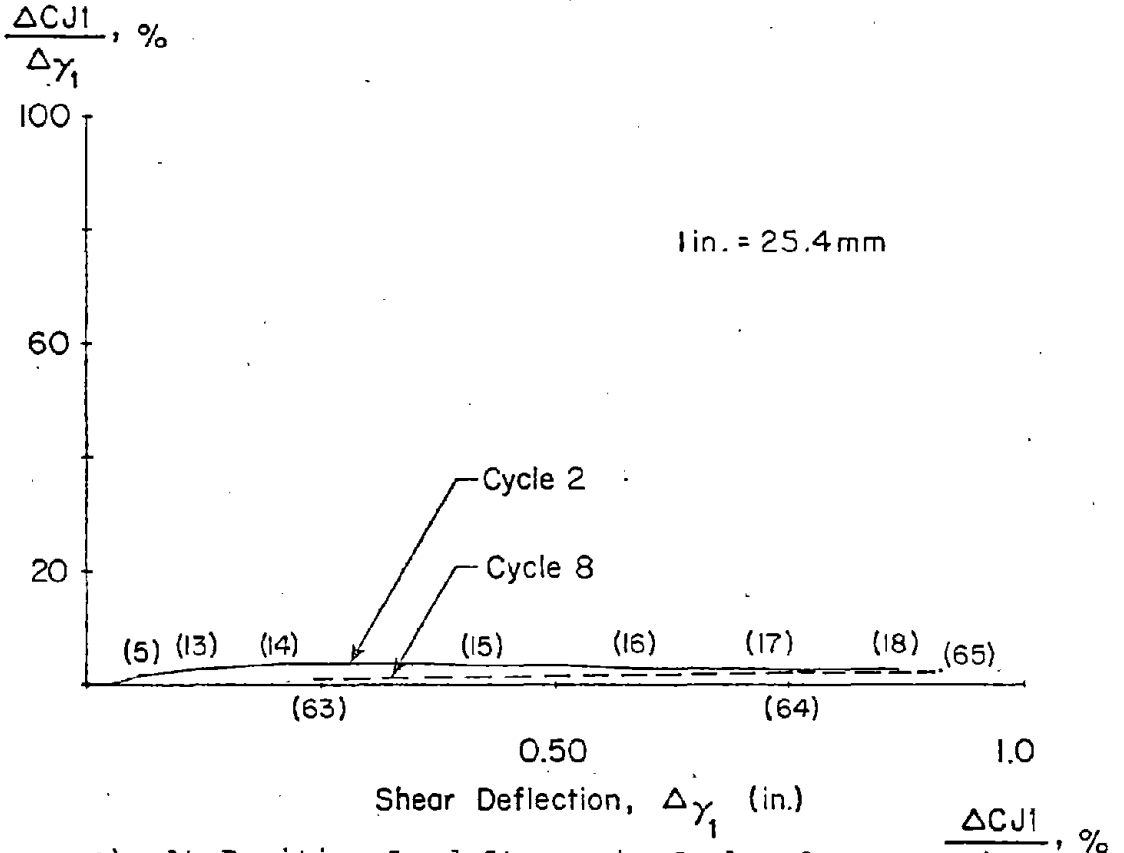

a) At Positive Load Stages in Cycles 2 and 8

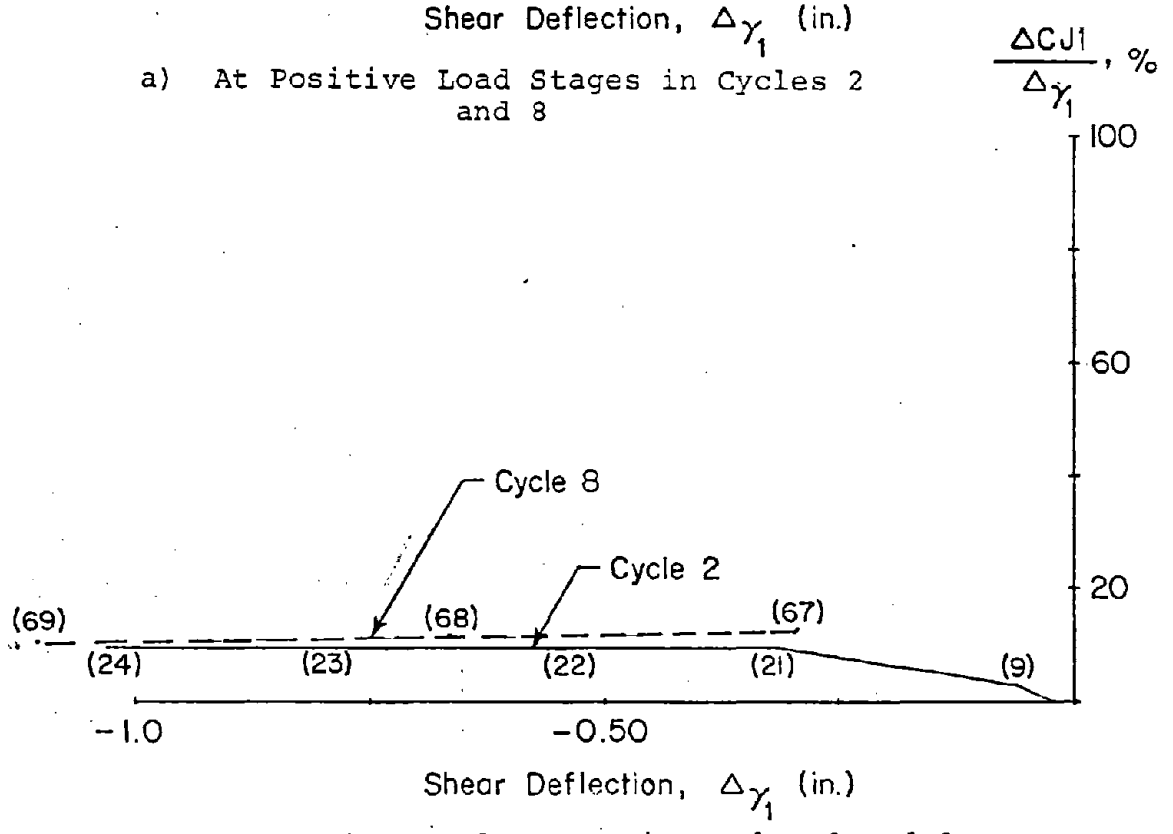

b) At Negative Load Stages in Cycles 2 and 8

Fig. B-145 Slip at Base Construction Joint versus Shear Deflection in Zone 1 for Specimen B10

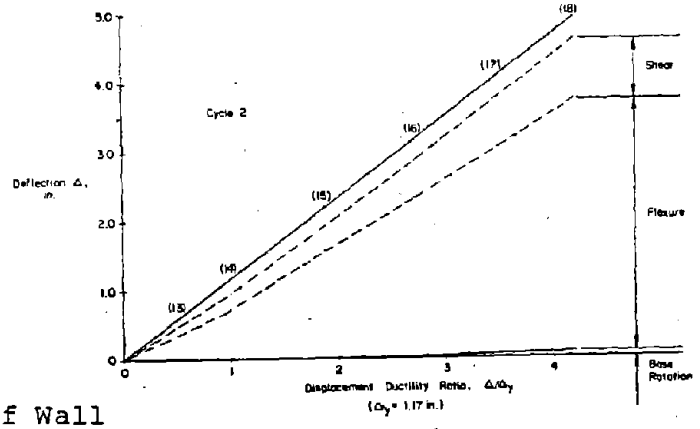

a) At Top of Wall

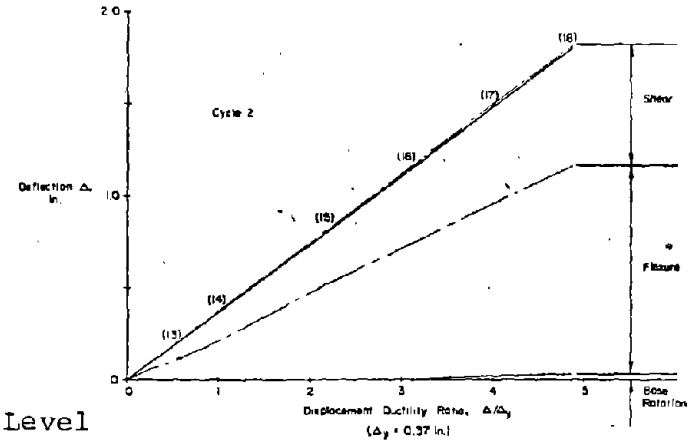

b) At 6 ft Level

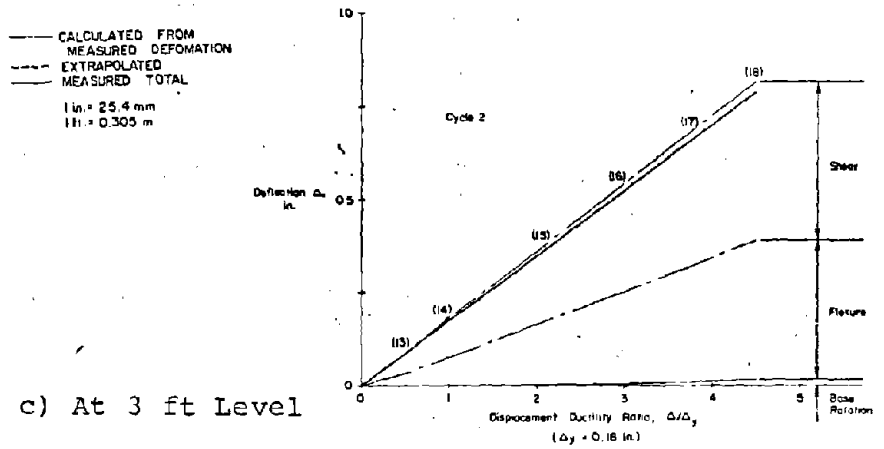

c) At 3 ft Level

Fig. B-146 Components of Deflection for Specimen B10 in the Positive Half of Cycle 2

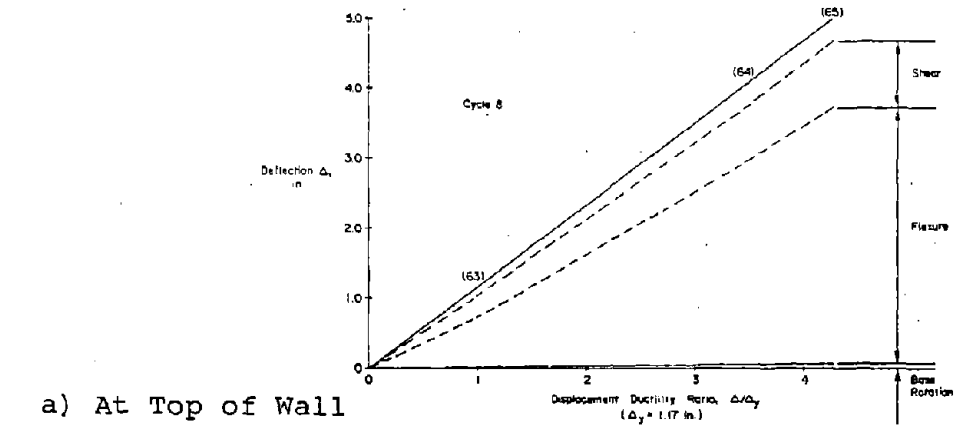

a) At Top of Wall

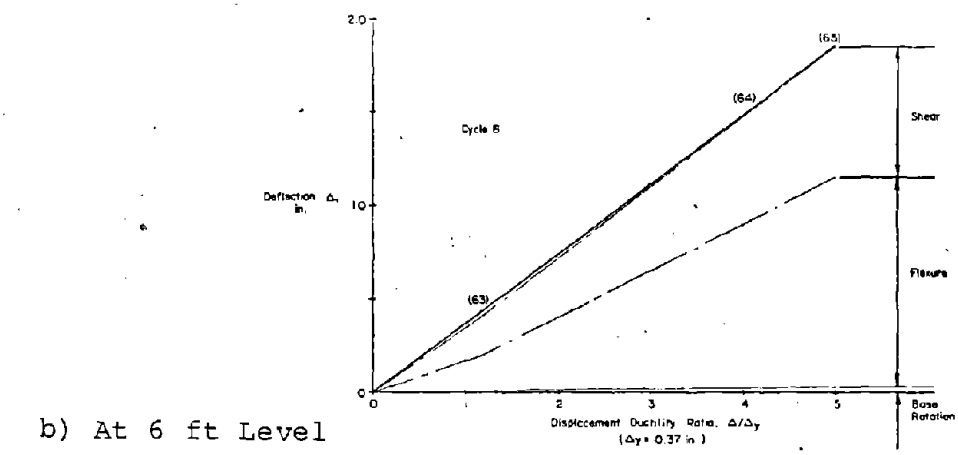

b) At 6 ft Level

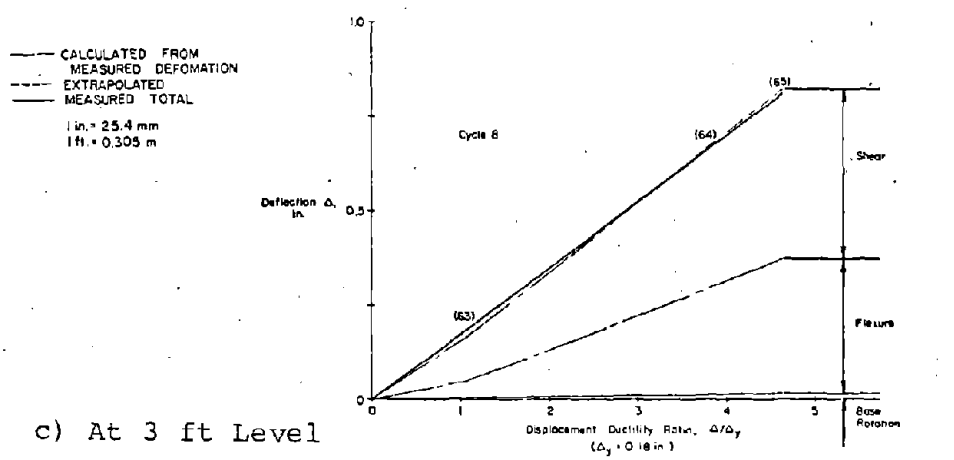

c) At 3 ft Level

Fig. B-147 Components of Deflection for Specimen B10 in the Positive Half of Cycle 8

a) Flexural

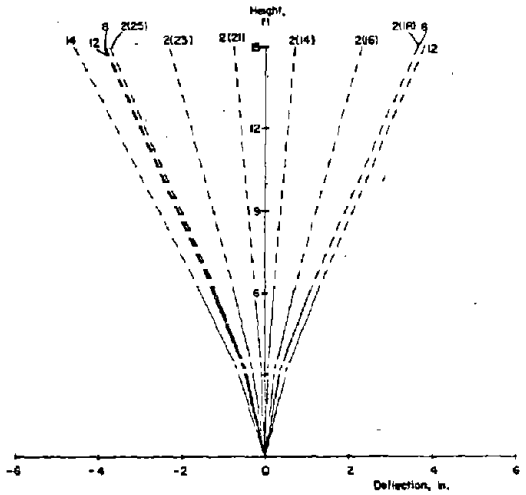

b) Shear

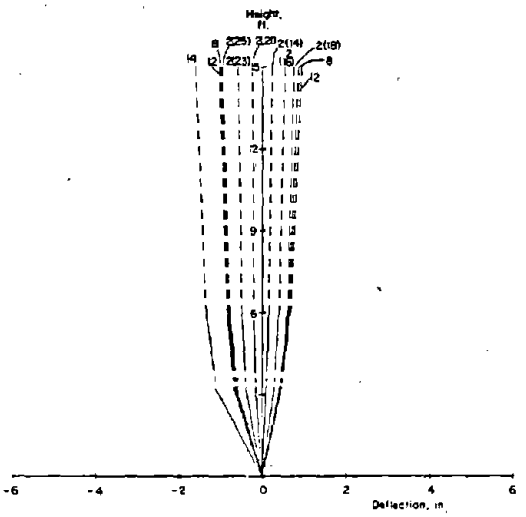

c) Total

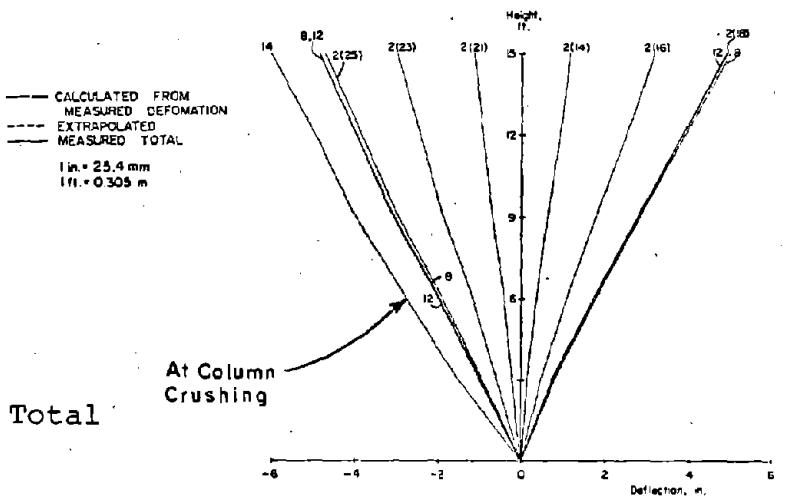

Fig. B-148 Deflected Shape for Specimen B10

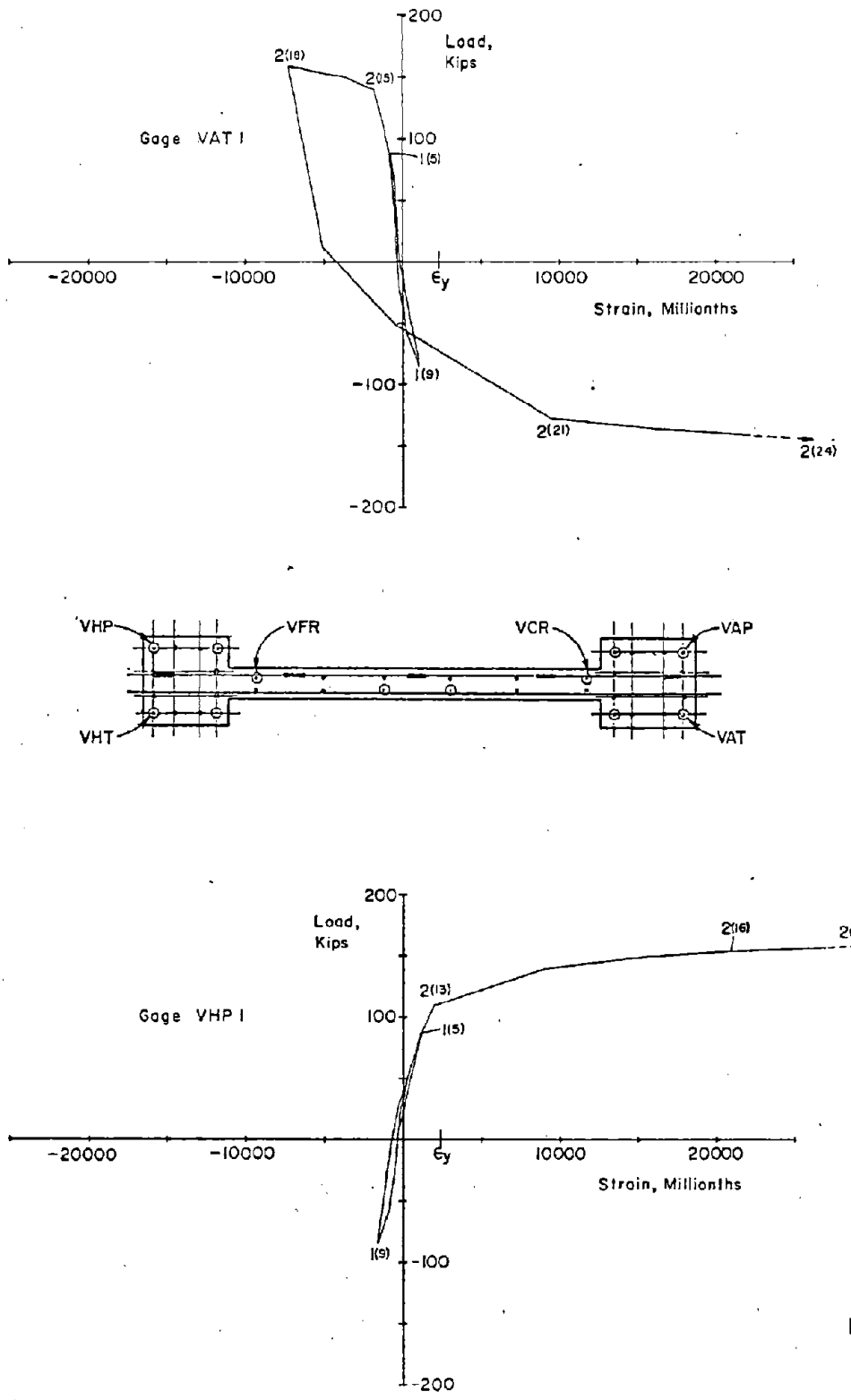

Fig. B-149 Measured Strains on Vertical Reinforcement at Base of Specimen B10

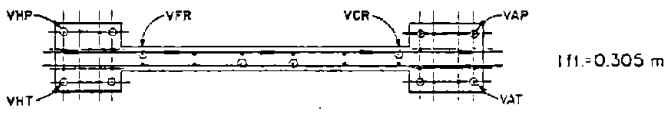

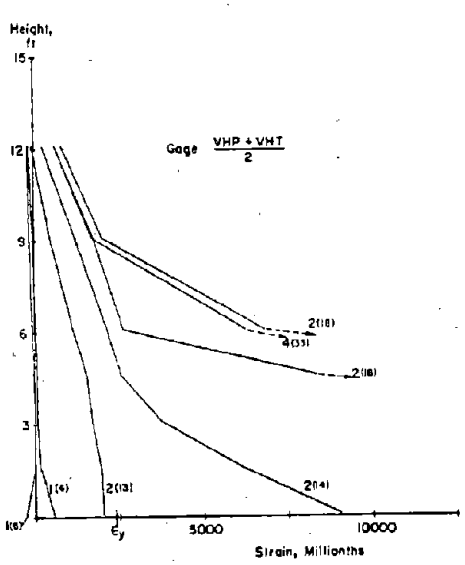

a) Average of VHP and VHT

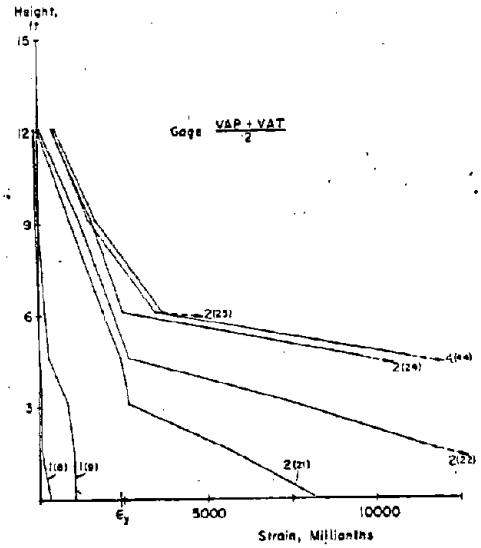

b) Average of VAP and VAT

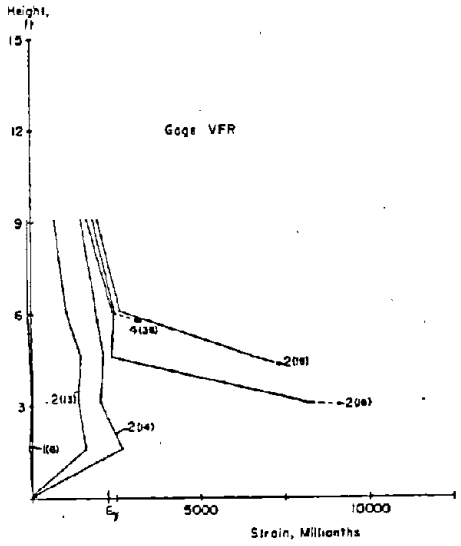

c) Strain Gage VFR

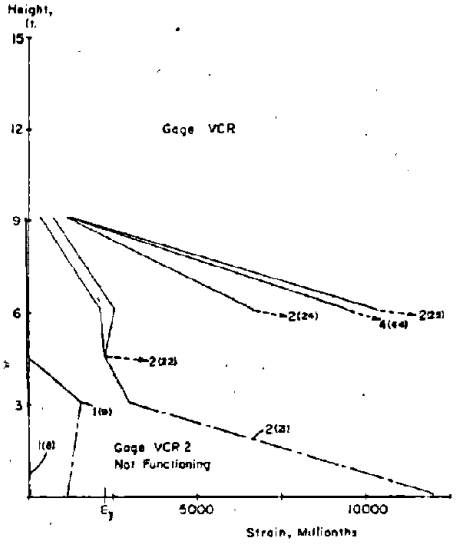

c_ Strain Gage VCR

Fig. B-150 Vertical Reinforcement Strains at Maximum Loads for Specimen B10

1 ft.=0.305 m

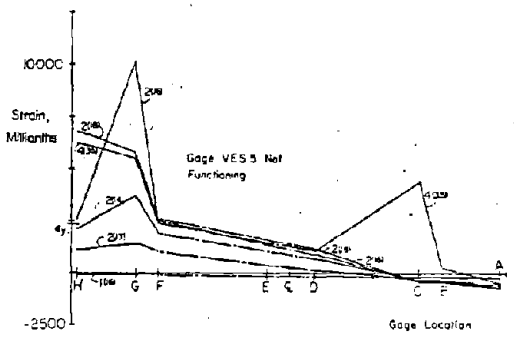

a) At 6 ft Level

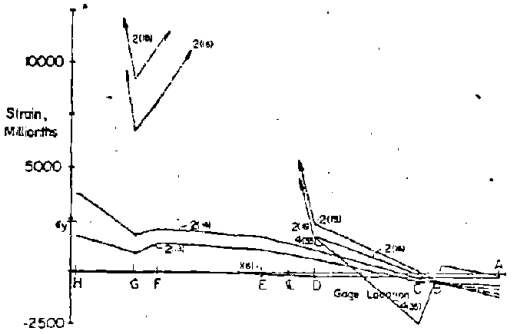

b) At 3 ft Level

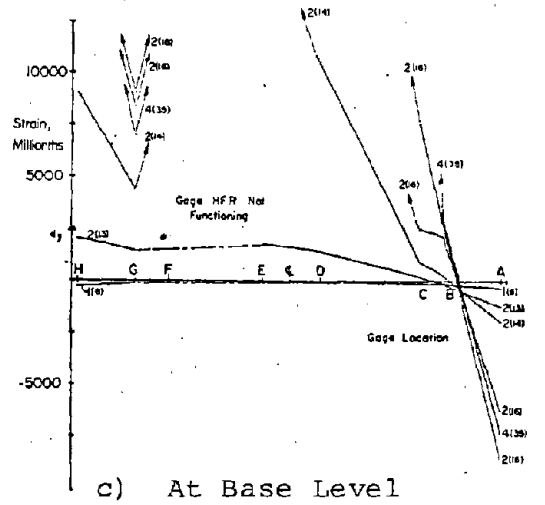

c) At Base Level

Fig. B-151 Vertical Reinforcement Strains at Maximum Positive Loads for Specimen B10

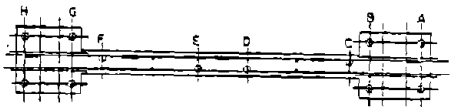

1ft.=0.305 m

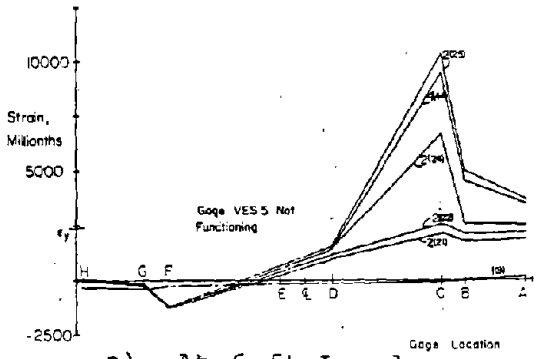

a) At 6 ft Level

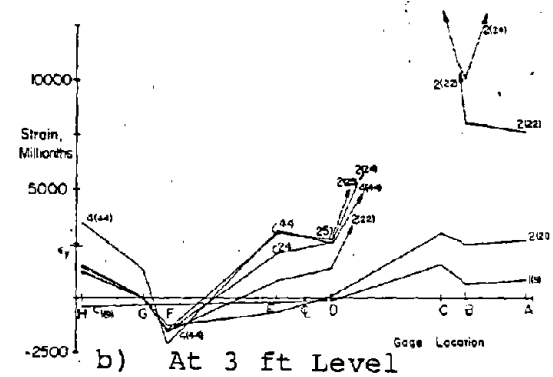

b) At 3 ft Level

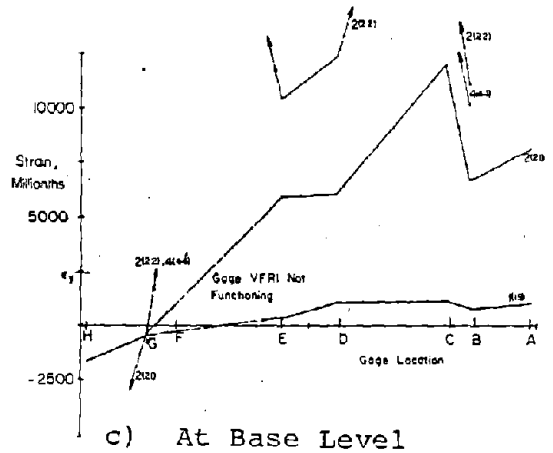

c) At Base Level

Fig. B-152 Vertical Reinforcement Strains at Maximum Negative Loads for Specimen B10

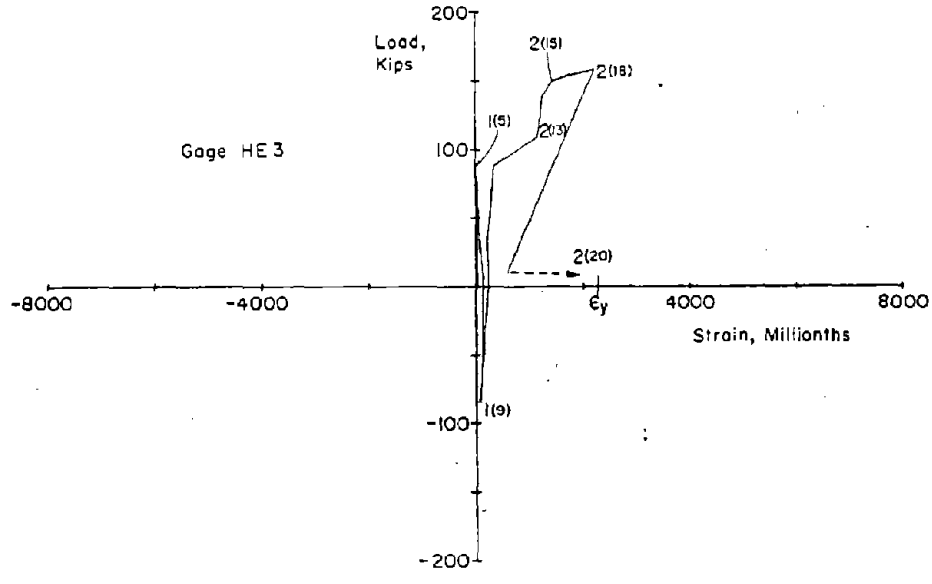

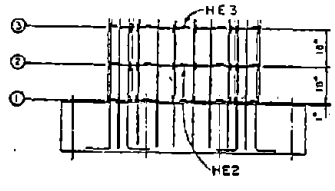

1 in. = 25.4 mm
1 kip = 4.448 kN

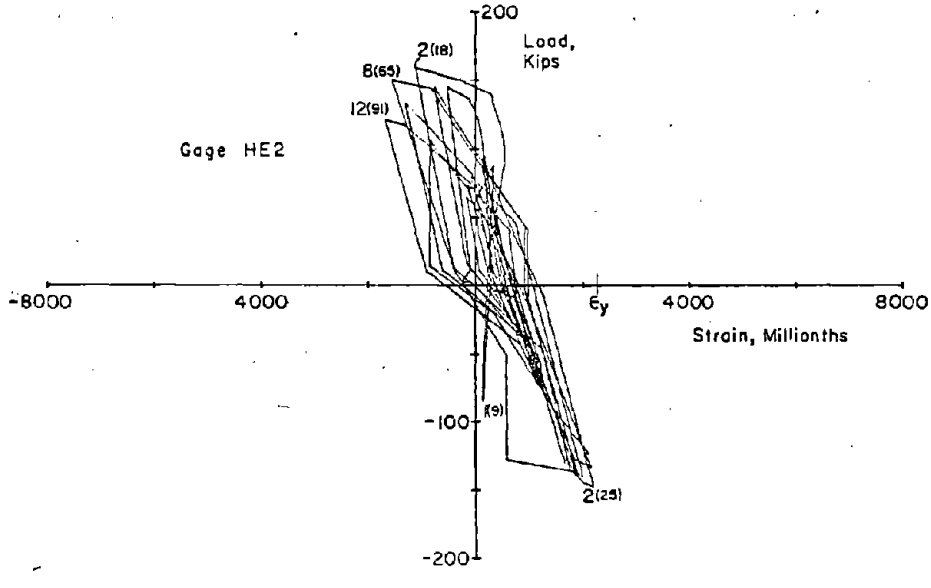

Fig. B-153 Measured Strains on Horizontal Reinforcement for Specimen B10

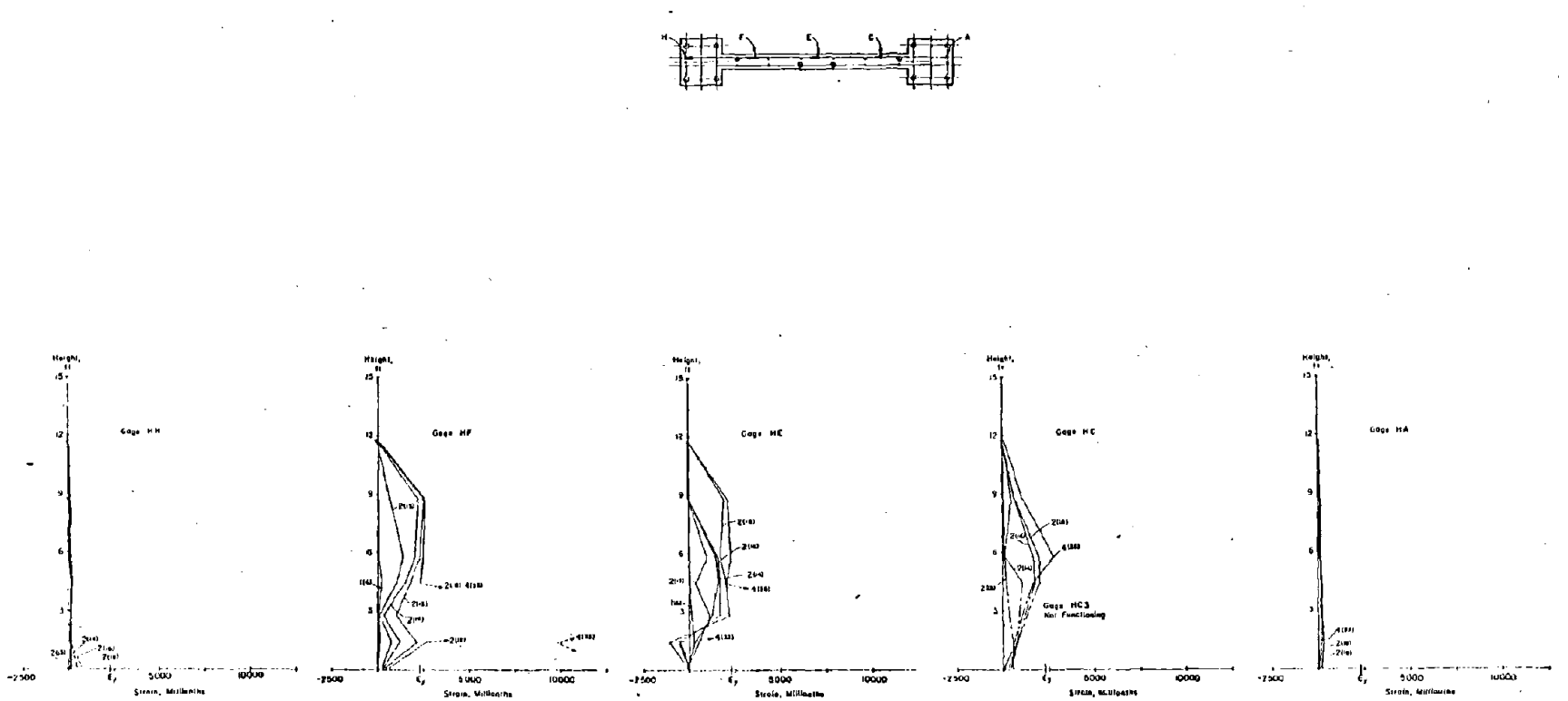

Fig. B-154 Horizontal Reinforcement Strains at Maximum Positive Loads for Specimen B10

1 in =0.305 m

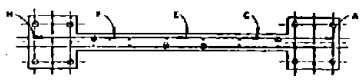

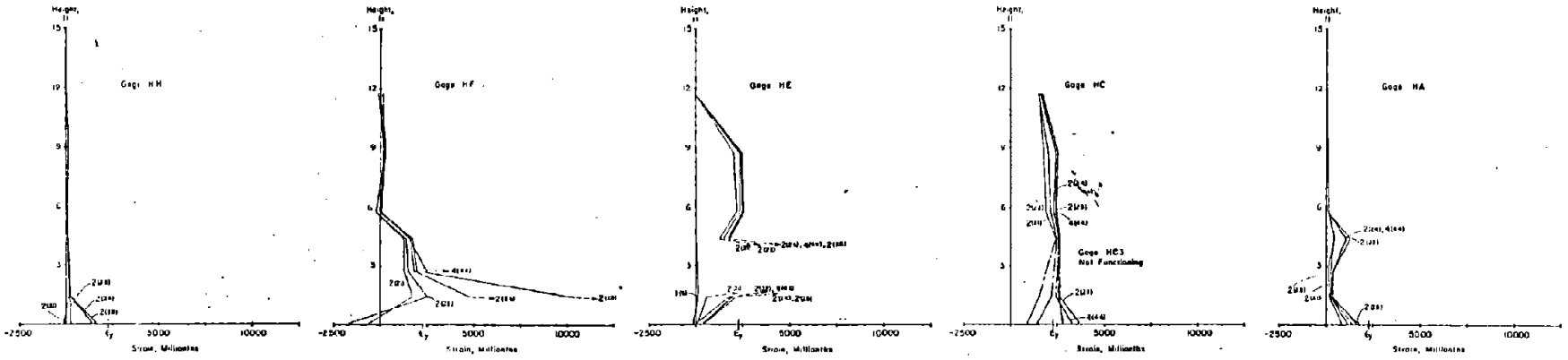

Fig. B-155 Horizontal Reinforcement Strains at Maximum Negative Loads for Specimen B10

1ft = 0.305 m

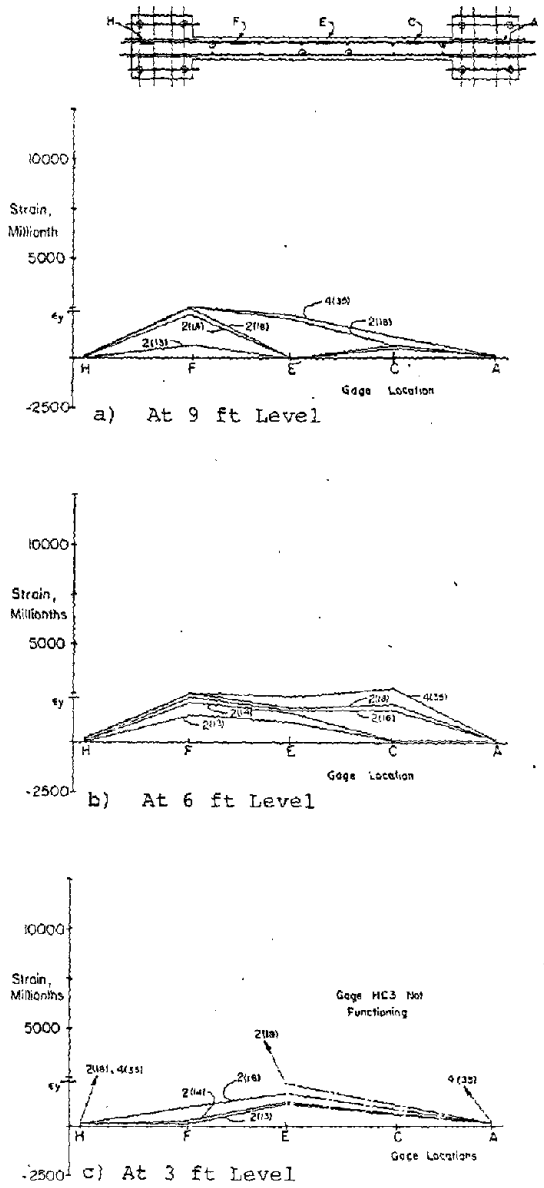

Fig. B-156 Horizontal Reinforcement Strains in Web at Maximum Positive Loads for Specimen B10

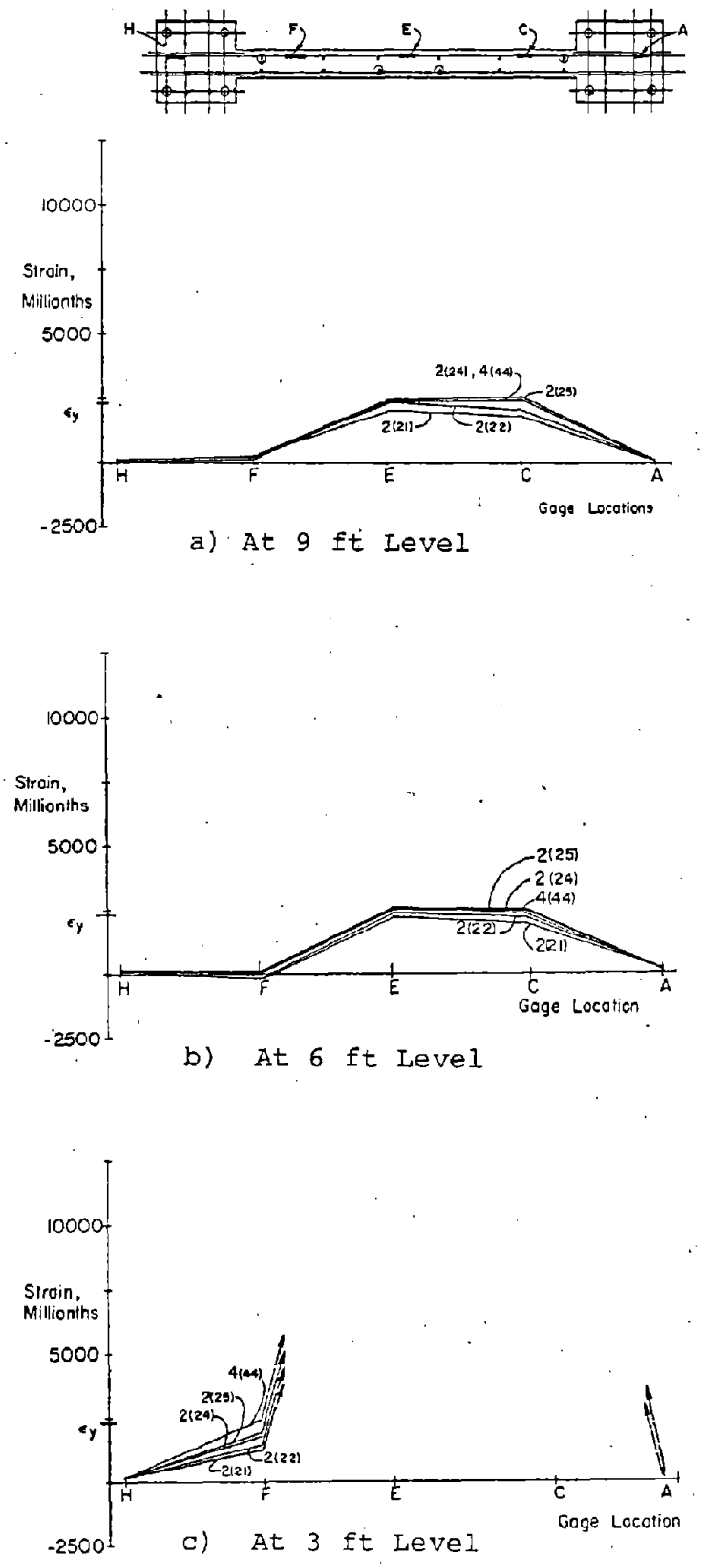

Fig. B-157 Horizontal Reinforcement Strains in Web at Maximum Negative Loads for Specimen

Figures B-158 and B-159 show the cyclic strain-load relationship and the vertical strain gradient in the outer leg of the confinement hoops. These figures show that only hoops in the lower two feet were stressed significantly. Strains near yield were observed in the hoops within the lower 1 ft (0.30 m) of the right boundary element. Plots for the left boundary element show strains when out of range in the region of the honeycombed concrete.

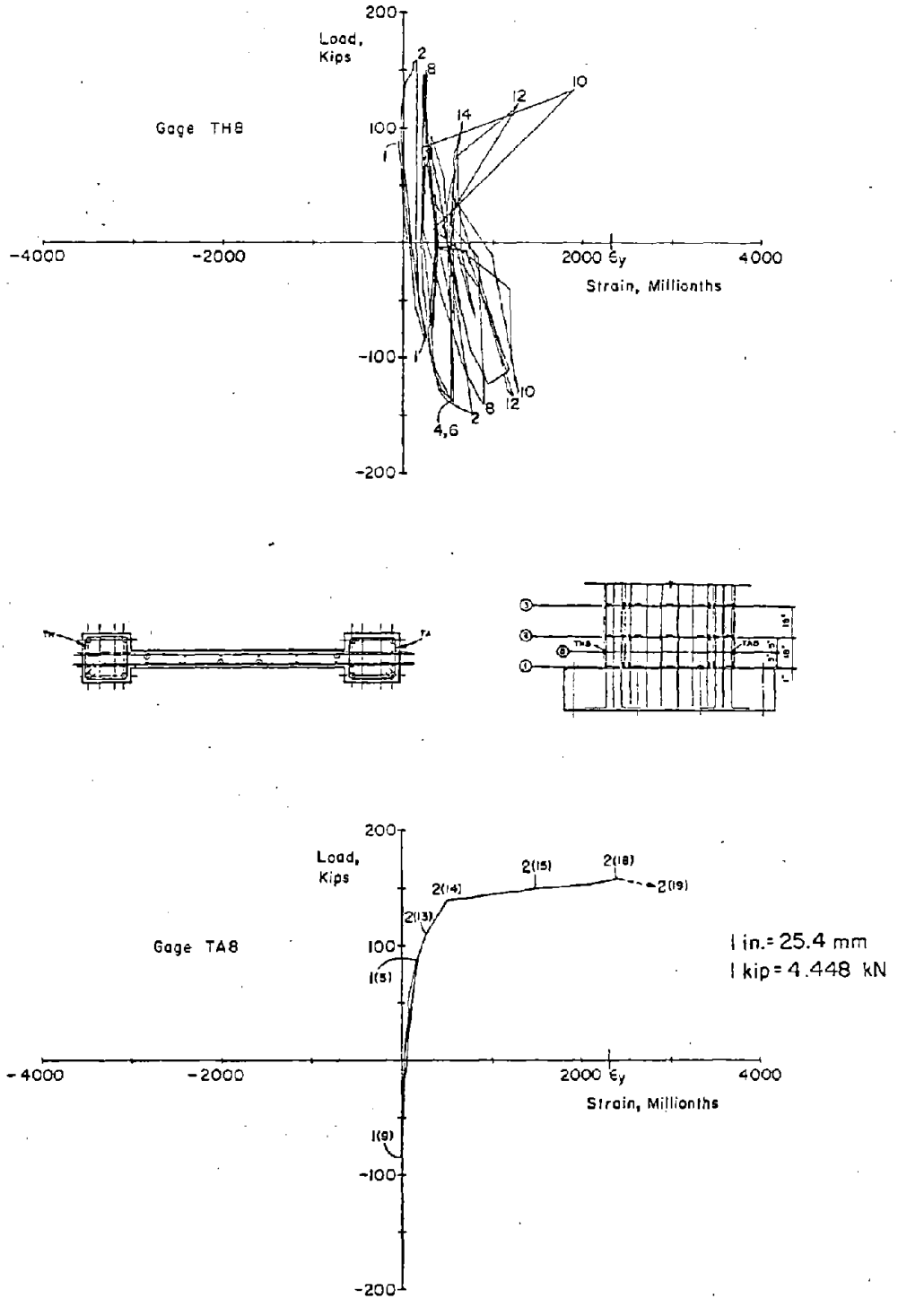

Fig. B-158 Measured Strains on Confinement Hoop Reinforcement for Specimen B10

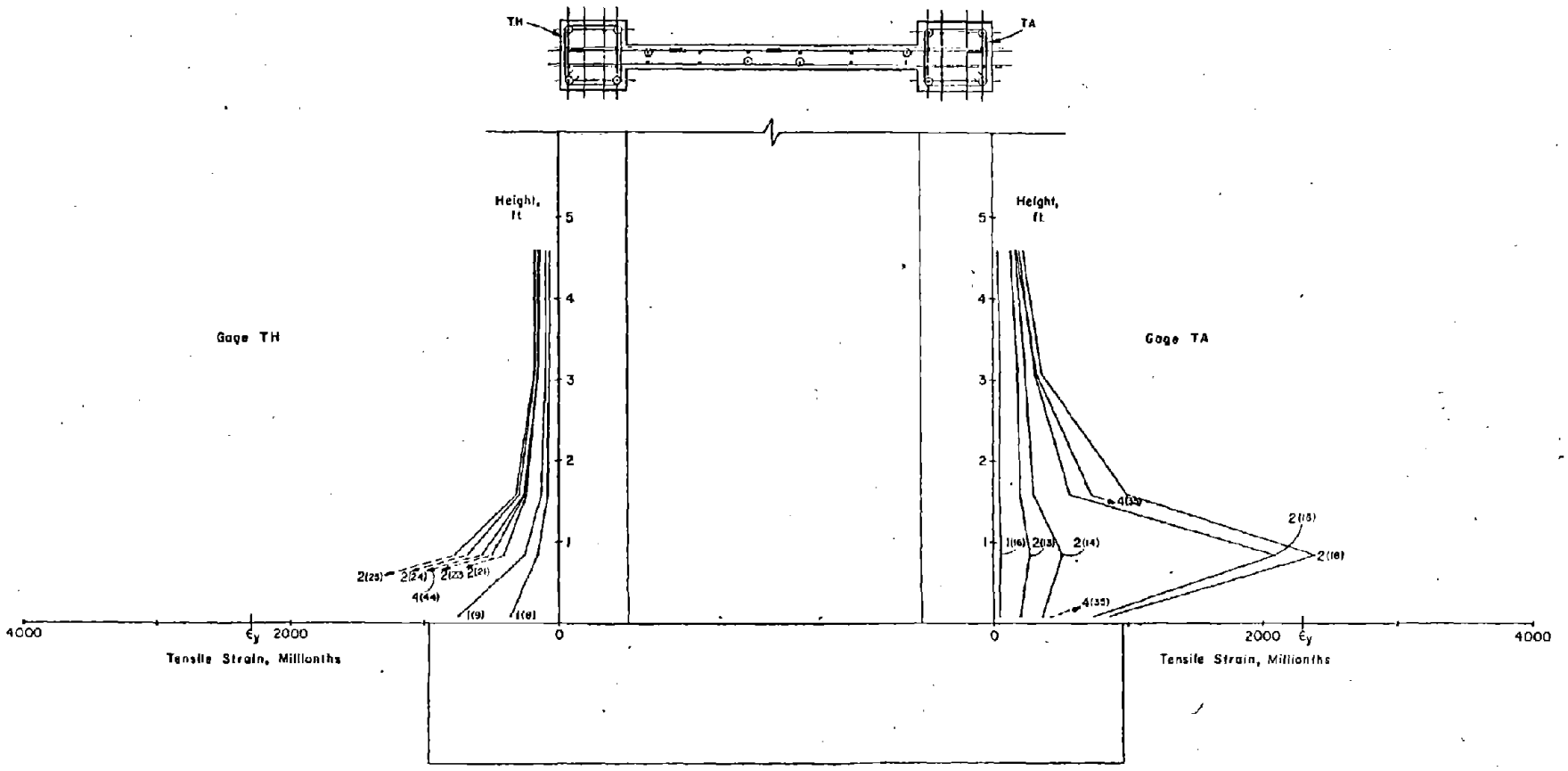

Fig. B-159 Confinement Hoop Reinforcement Strains at Maximum Loads for Specimen B10

Specimen F2

Test Description

Specimen F2 was a flanged shaped wall designed to contain confined boundary elements within the intersecting regions of the web and flanges. The objective of the test of F2 was to investigate the effectiveness of these stiffened boundary elements in dowel action as compared to the confined boundary elements of a barbell section. ACI design moment and shear, and calculated maximum moment capacities of Specimen F2 were very similar to those for Specimen B7.

Specimen F2 was loaded axially at a uniform stress of 482 psi (3.32 MPa) during the lateral load test. The axial force was equal to that applied to Specimen B7.

The test consisted of 28 loading cycles as shown in Fig. B-160. The complete load versus top deflection relationship for Specimen B7 is shown in Figs. B-161 and B-162. Complete load versus deflection and rotation relationships at the 6-ft level are shown in Figs. B-163 and B-164.

First significant cracking was observed in Cycle 10 at a load of 75 kips (334 kN). First yielding occurred in Cycle 13 at a load of 156.0 kips (693.9 kN). The maximum measured crack widths at this stage were 0.012 in. (0.30 mm) in the tension flange and 0.012 in. (0.30 mm) across a diagonal crack in the web.

The crack pattern that developed was similar to patterns in the other specimens subjected to high shear stresses. The cracks started as horizontal flexural cracks in the flanges that progressed into diagonal shear cracks in the web. These cracks were small and finely distributed in the confined boundary element regions of the flange and web. They converged into larger more coarsely distributed cracks in the unconfined portions of the web and flanges. The cracks directed toward the outer compression face at the base of the wall were at an angle of approximately 40° from vertical. The crack pattern at +3-in. (76.2 mm) and -3-in. deflections are shown in Figs. B-165 and B-166.

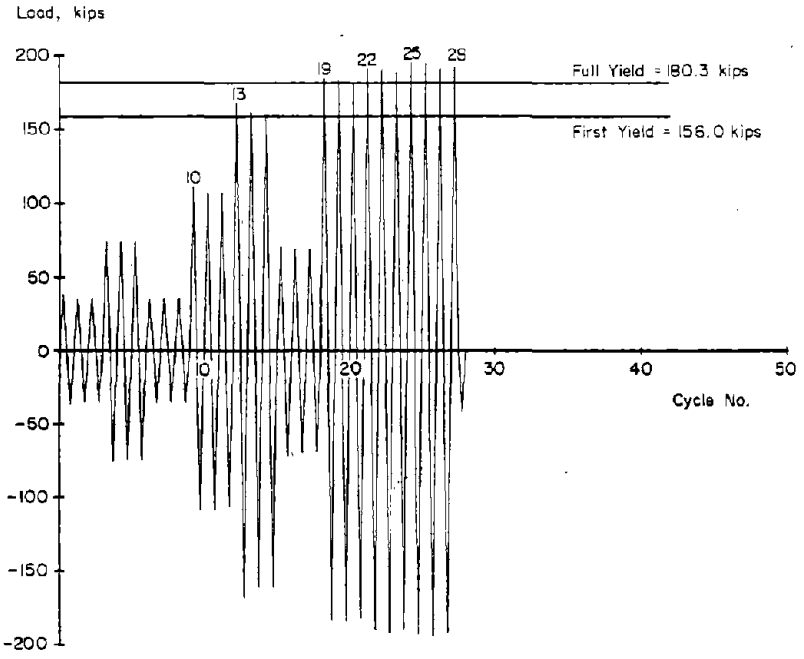

a) Load History

1 in. = 25.4 mm
1 kip = 4.448 kN

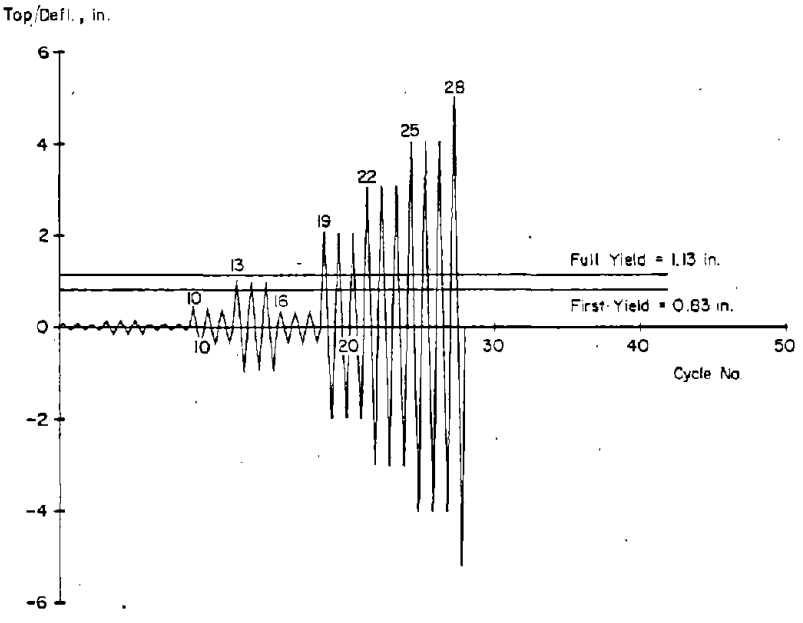

b) Deflection History

Fig. B-160 Loading History for Specimen F2

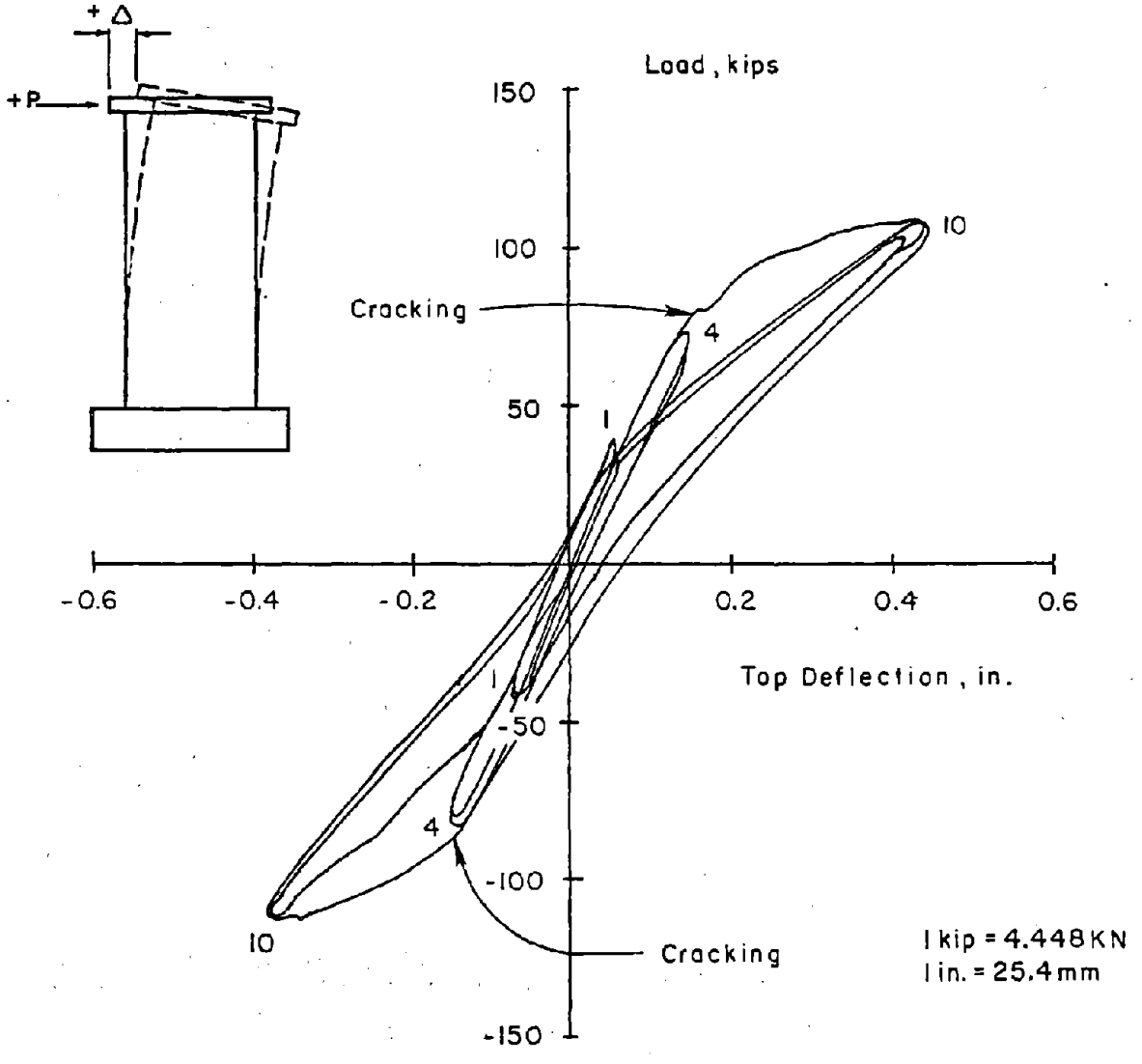

Fig. B-161 Continuous Load - Deflection for Initial Cycles for Specimen F2

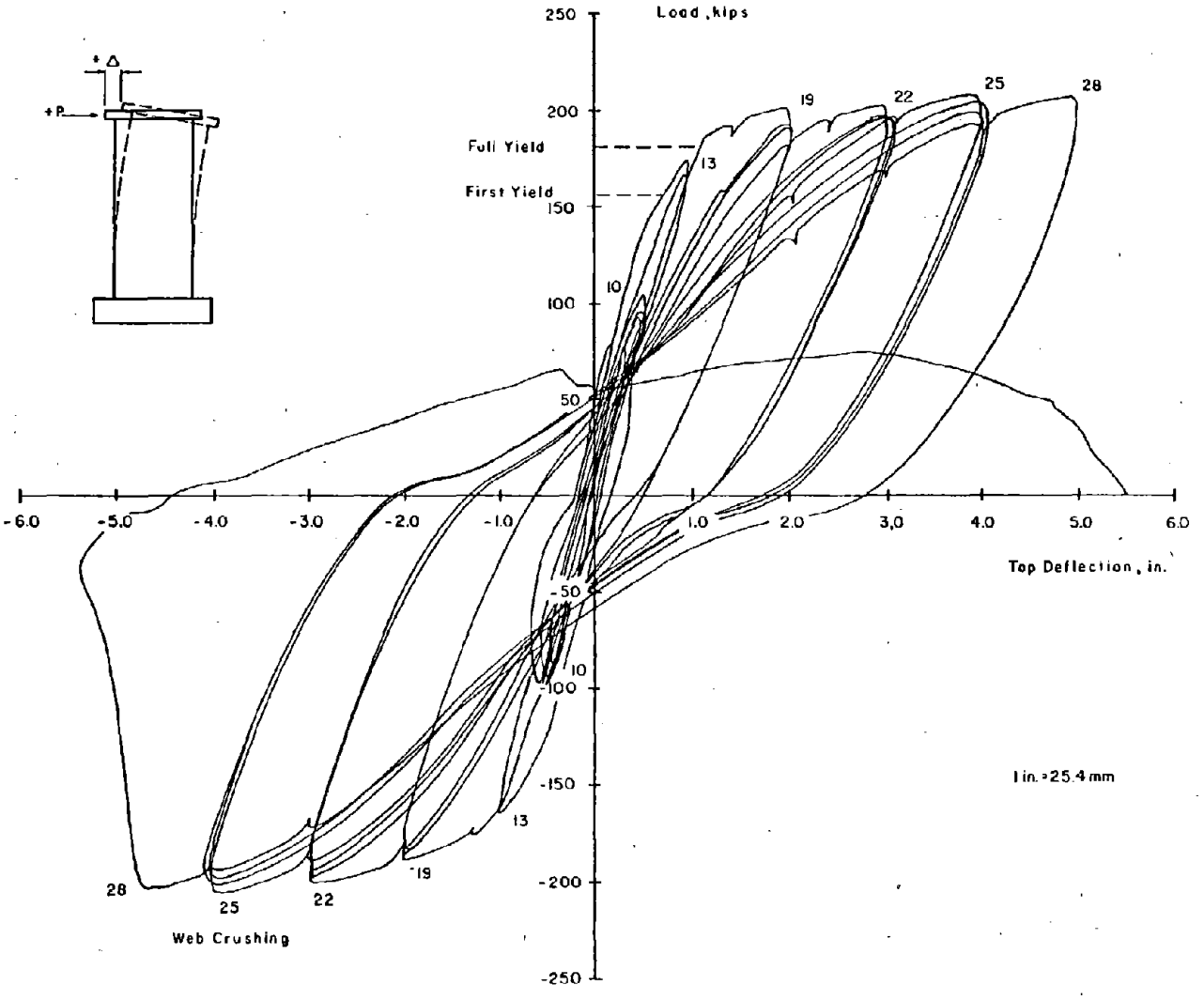

Fig. B-162 Continuous Load - Top Deflection for Specimen F2

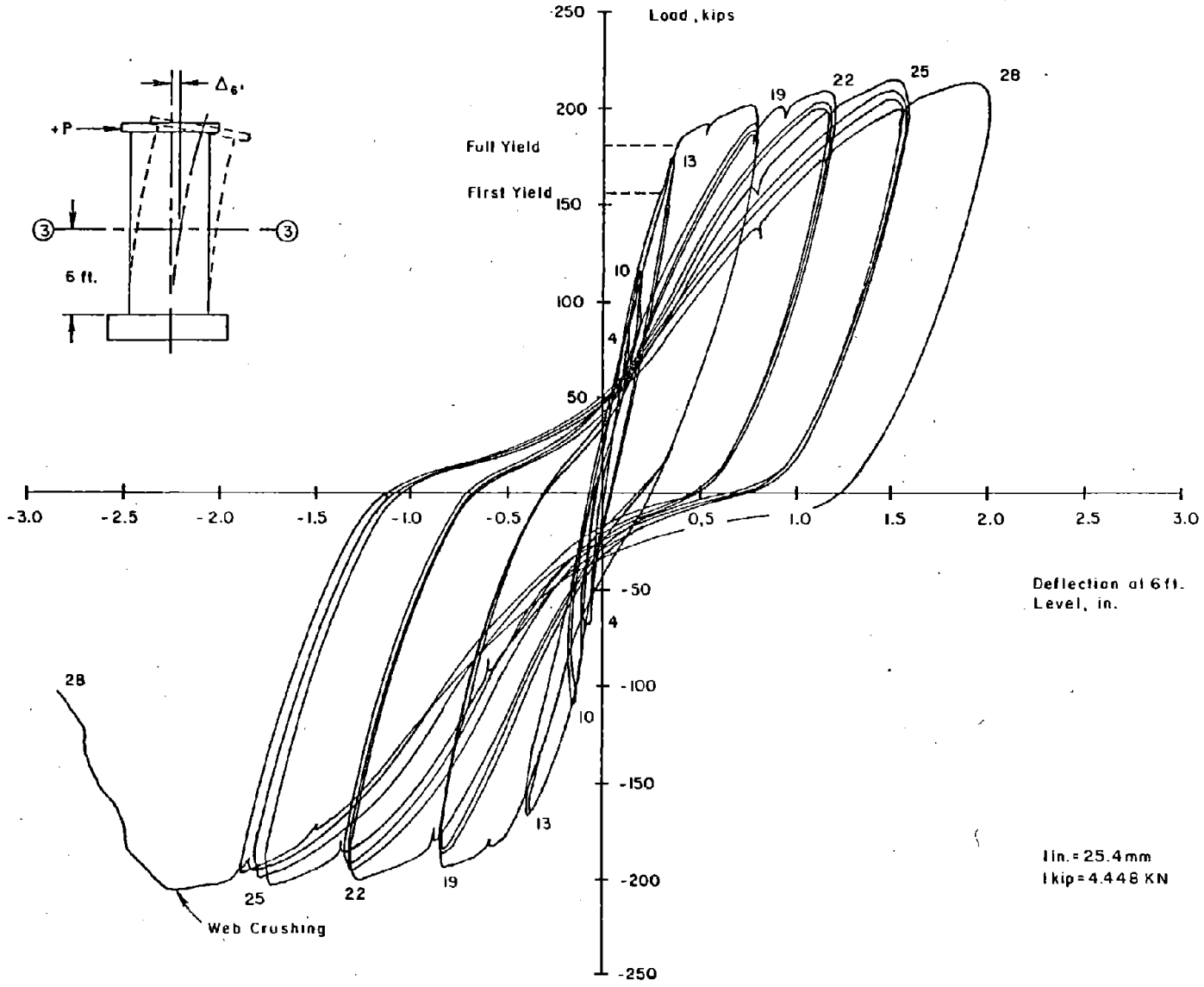

Fig. B-163 Continuous Load - Deflection at 6 ft Level for Specimen F2

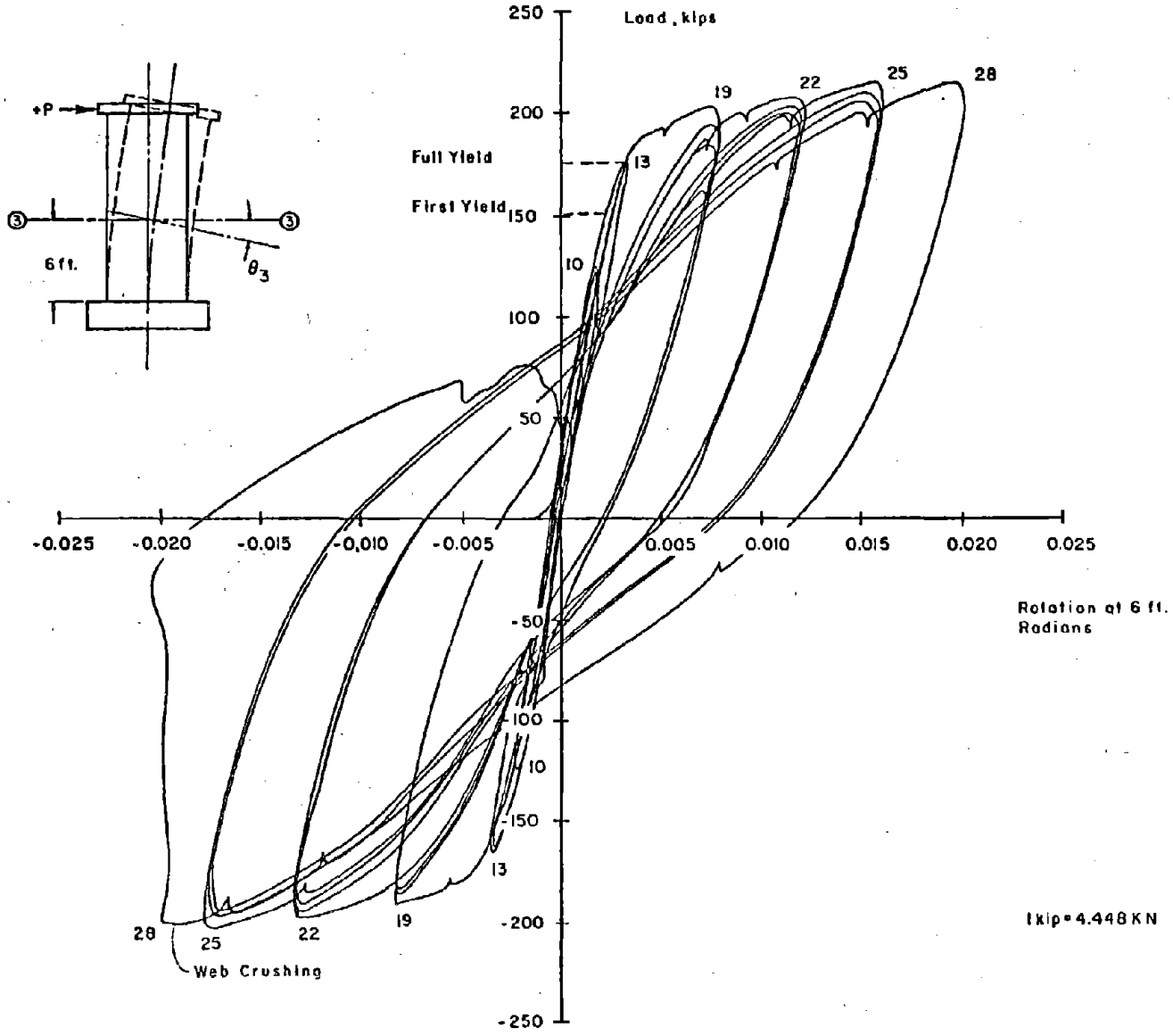

Fig. B-164 Continuous Load - Rotation at 6 ft Level for Specimen F2

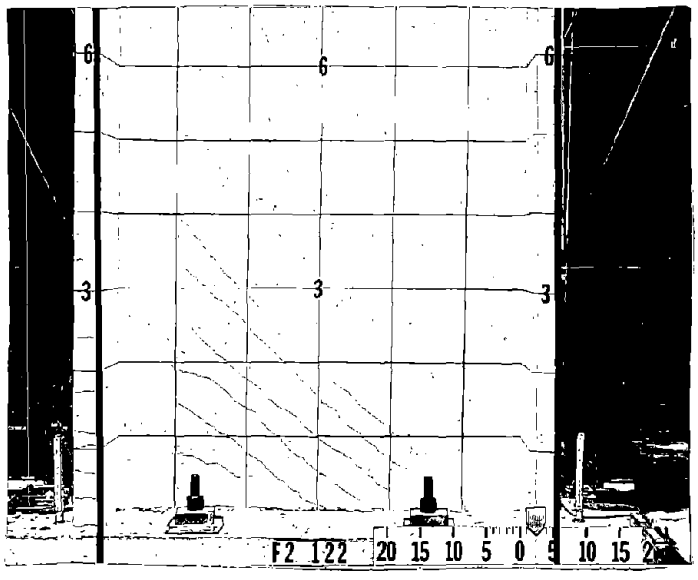

Fig. B-165 Cracking Pattern at +3 in. Deflection for Specimen F2

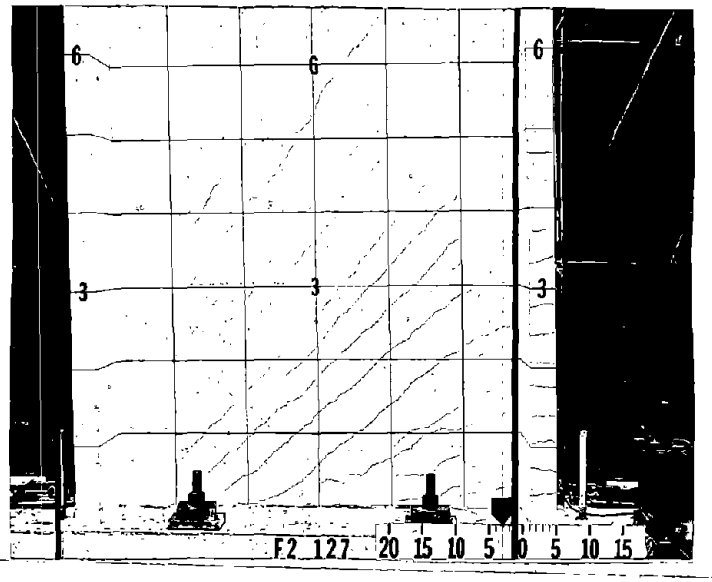

Fig. B-166 Cracking Pattern at -3 in. Deflection for Specimen F2

The behavior of Specimen F2 in the initial inelastic loading cycles did not differ significantly from that of Specimen B7. First indication of spalling and flaking along diagonal cracks was noted in Cycle 19. First indication of crushing in the unconfined portion the web occurred in Cycle 22. Also, spalling caused by opening of crosstie end hooks was noted in the confined portion of the web in Cycle 22. Crushing and spalling progressively increased as more and larger load cycles were applied to the specimen.

During Cycle 25 a predominately horizontal crack started to form in the web approximately 5 in. above the base block. Also, significant crushing was noted in lower left confined region of the web in Cycle 25. A reverse curvature in the lower 1 ft (0.3 m) level of the flanges was noted. Vertical cracks were observed in the lower 2 ft-6 in. (0.76 m) of the flange. These cracks were caused by bowing as the flanged restrained the web from slipping. Load capacity continued to increase with increased deflection.

The maximum load measured, 199.5 kips (887.4 kN) occurred in Cycle 25 at a +4-in. (101.6 mm) deflection. This load corresponds to a nominal shear stress of $v_{max} = 10.2 \sqrt{f'_c}$ ($0.85 \sqrt{f'_c}$, MPa). The design shear capacity using 1971 ACI Building Code Equations (11-13) and (11-33) was 148 kips (658.3 kN). This corresponds to a nominal shear stress of $v = 7.7 \sqrt{f'_c}$ ($0.64 \sqrt{f'_c}$ MPa).

As the specimen was being loaded to a +5-in. deflection in Cycle 28, significant crushing of the unconfined portion of the flange occurred. However, the confined portion was in good condition and the maximum load observed was 197.5 kips (878.5 kN), which was 98% of the maximum measured in Cycle 25.

As the specimen was being loaded to a -5-in. deflection in Cycle 28, several compression struts in the lower left portion of the web crushed simultaneously. Immediately after crushing the compression flange sheared, and a horizontal failure plane through the web developed. One horizontal reinforcing bar crossing this plane fractured. The failure was sudden and the load dropped to 20% of the maximum measured load before the

deflection control hydraulic valve was closed. Figures B-167 and B-168 show Specimen F2 immediately prior to and after web crushing.

The specimen sustained at least 80% of the maximum measured load capacity through nine inelastic cycles. The last inelastic loading increment in which the load was sustained at or above 80% of the maximum for all three cycles was at ±4 in. (101.6 mm). A significant difference between the behavior of F2 and B7 was the extent of damage to the boundary element. At the end of the test of B7 the columns were in good condition and the wall could have been repaired by replacing the web. At the end of the test of F2 the boundary elements were extensively damaged and repairs would have been considerably more difficult.

Discussion of Results

Moment-Rotation. Moment-rotation data for Specimen F2 is shown in Fig. B-169. The maximum measured moment was 82% of the calculated monotonic maximum. The calculated maximum was limited by an unstable equilibrium condition in balancing tension and compression forces in the section. The instability results when the strain corresponding to maximum compressive strength of the concrete is exceeded at the extreme compression face. After this stage, the neutral axis must move away from the outer face to produce equilibrium. Because of the large width available in the flange, the depth of the compression zone is very small. As the neutral axis moves into the web, the available width of the compression zone decreases drastically. Therefore, the depth of the compression zone cannot be increased sufficiently to attain enough concrete in compression to balance the tension. The instability corresponds to a sudden and complete loss of load capacity from crushing of the compression boundary element and web. This type of sudden failure can occur in specimens that have large relatively shallow boundary elements, thin webs and a high percentage of vertical reinforcement. In the test of Specimen F2, web crushing occurred before this unstable situation was reached.

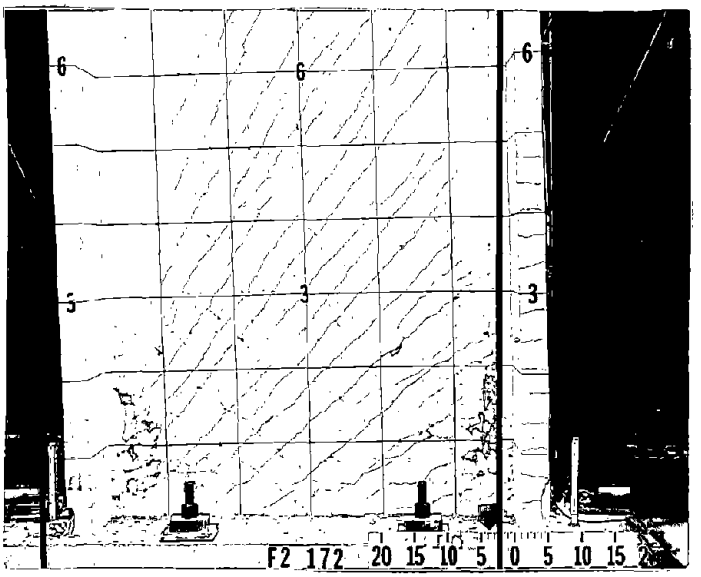

Fig. B-167 Specimen F2 Prior to Web Crushing

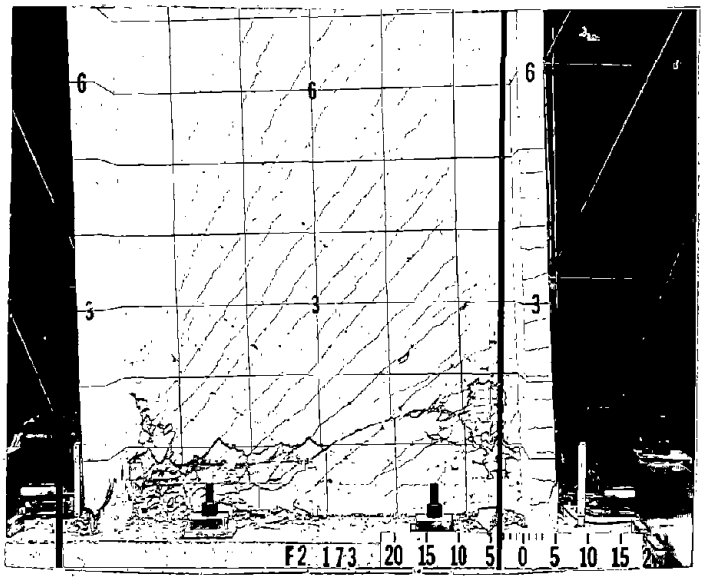

Fig. B-168 Specimen F2 After Web Crushing

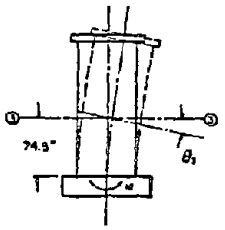

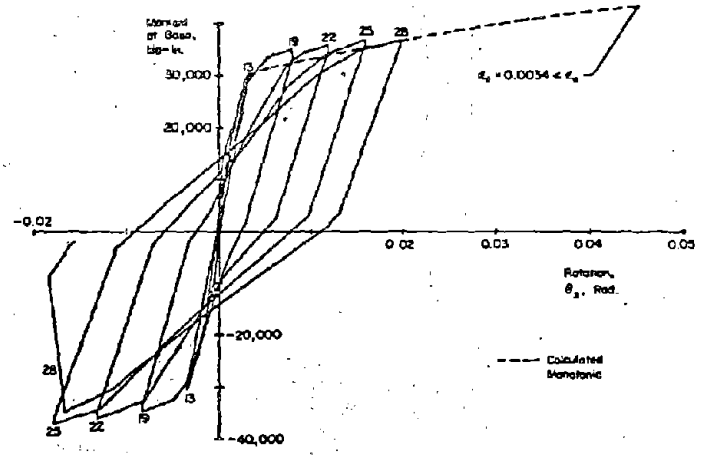

a) At 6 ft Level

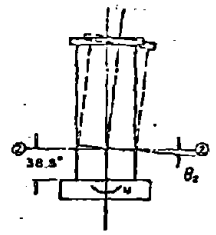

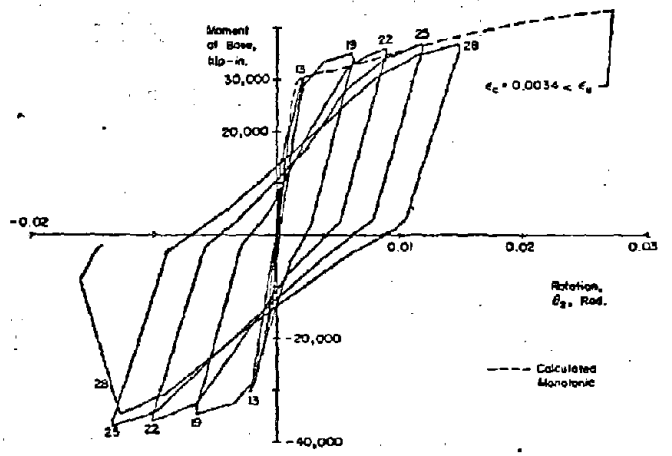

b) At 3 ft Level

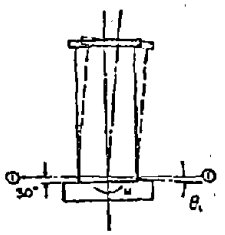

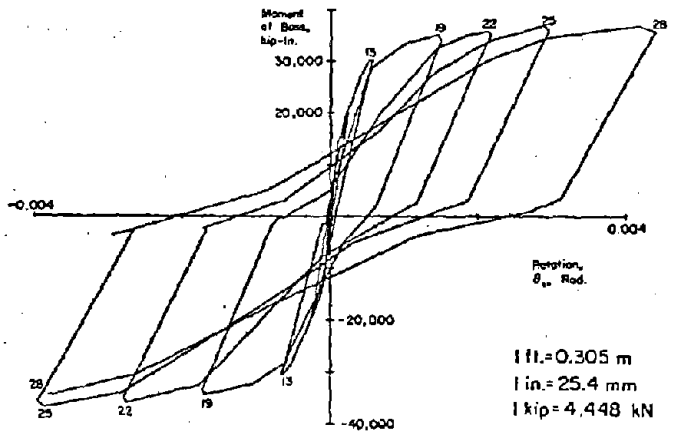

c) At Base Level

Fig. B-169 Moment at Base versus Rotation for Specimen F2

The relationship between the calculated monotonic and measured rotations at the 3-ft (0.91 m) and 6-ft (1.83 m) levels is similar to that observed in most of the previous tests. Actual rotations were concentrated in the lower 3 ft of the wall to a greater extent than was assumed in the calculations. Pinching of the loops is evident after Cycle 22.

The maximum rotation at the 6-ft level in a stable increment of the F2 test was 0.0179 rad. This corresponds to a rotational ductility of 4.9. For comparison, this maximum rotational ductility was 5.2 in Specimen B7. Therefore, the inelastic rotation of the flanged section with a special confined boundary elements nearly matched that for a barbell section.

Shear Distortion. Shear-distortion loops for F2 are shown in Fig. B-170. As in the previously reported tests, shear "yielding" occurred during the same cycle in which flexural yielding occurred. A major portion of the shear distortions occurred in the lower 3 ft (0.91 m).

A comparison of peak loads and shear distortions in Cycle 27 for Specimens F2 and B7 shows that the effective shear stiffness in F2 was 76% of the effective shear stiffness in B7.

Slip at Construction Joints. Slip at construction joints in F2 is shown in Fig. B-171. The slip at CJ1 exhibits yielding similar to shear "yielding" during the same cycle that flexural yielding occurred. As shown in Fig. B-172, slip at CJ1 was a approximate 15% of the total shear deflection in the lower 3 ft (0.91 m).

A comparison of peak loads and slip at CJ1 in Cycle 27 for Specimens F2 and B7 shows that the effective stiffness in F2 was actually 13% higher than that in B7.

Deflections. Deflection components and deflected shapes are shown in Figs. B-173 and B-174. These figures show that shear deflections were a relatively constant throughout most of the test and increased slightly near the end of the test.

A comparison of the portion of deflections attributed to shear for Specimens F2 and B7 shows that the shear deflections were a significantly higher percentage of the total in F2.

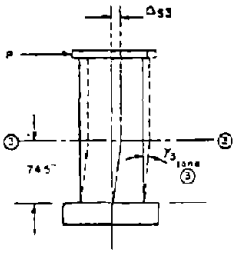

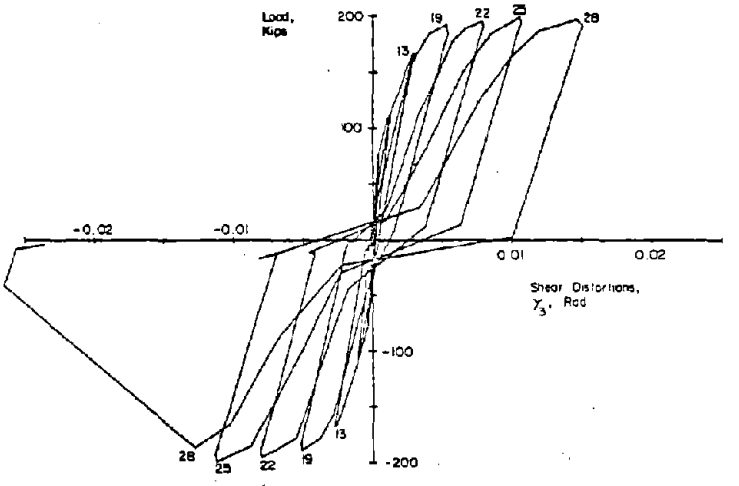

a) In Base to 6 ft Level

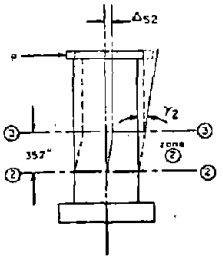

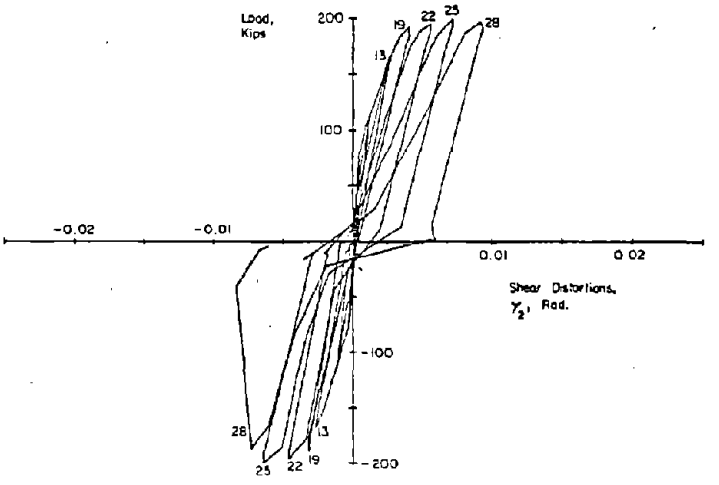

b) In 3 ft to 6 ft Level

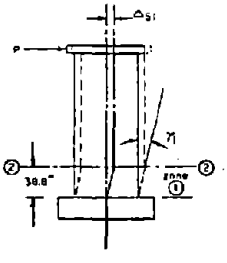

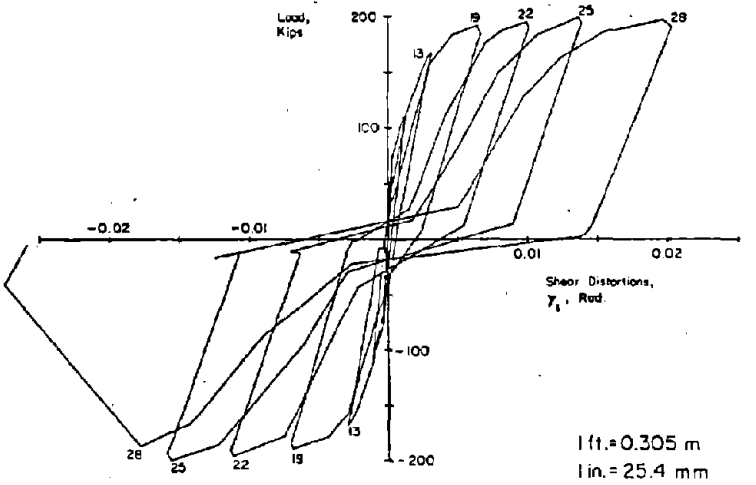

c) In Base to 3 ft Level

1 ft.=0.305 m
1 in.=25.4 mm
1 kip=4.448 kN

Fig. B-170 Load versus Shear Distortion for Specimen F2

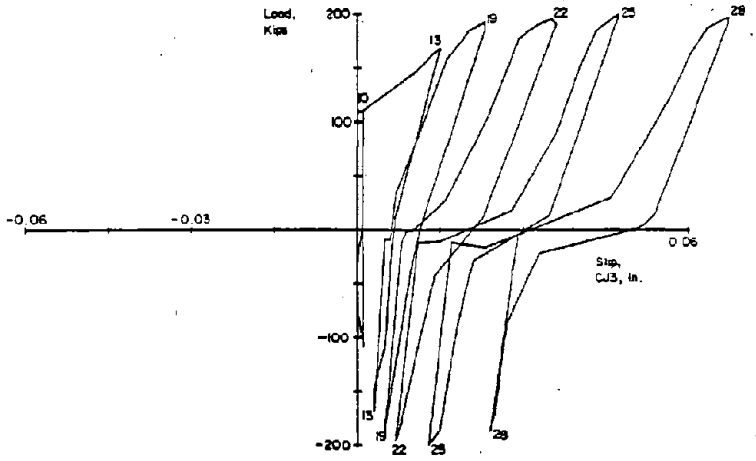

a) At 6 ft Level

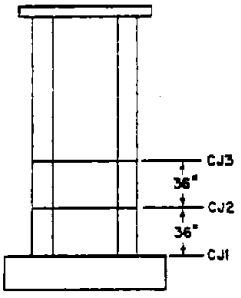

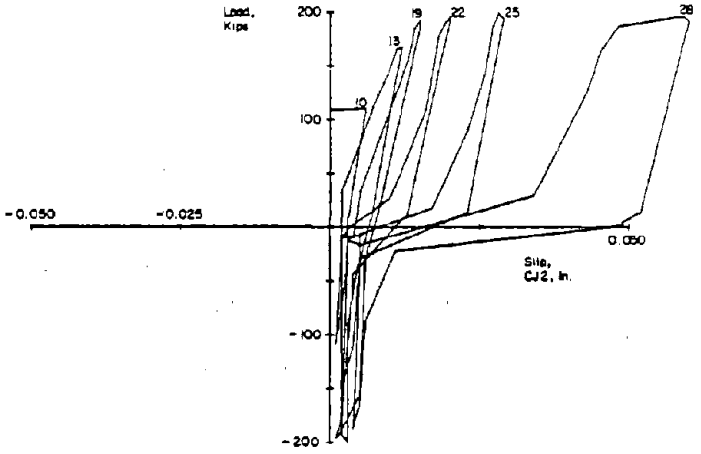

b) At 3 ft Level

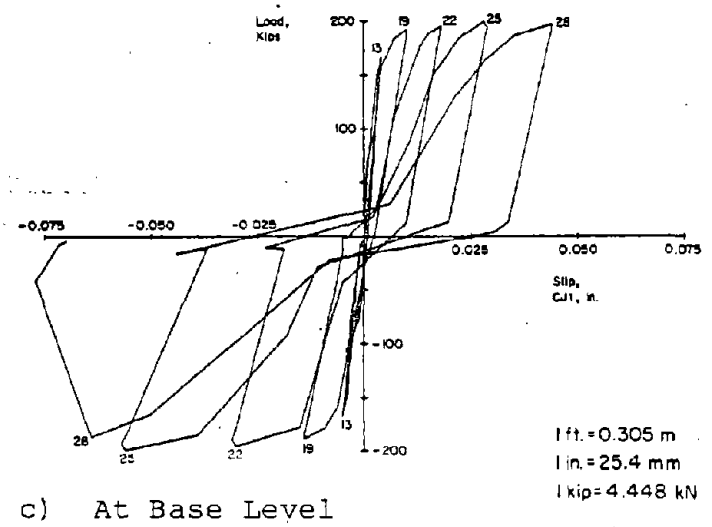

c) At Base Level

Fig. B-171 Load versus Slip at Construction Joints for Specimen F2

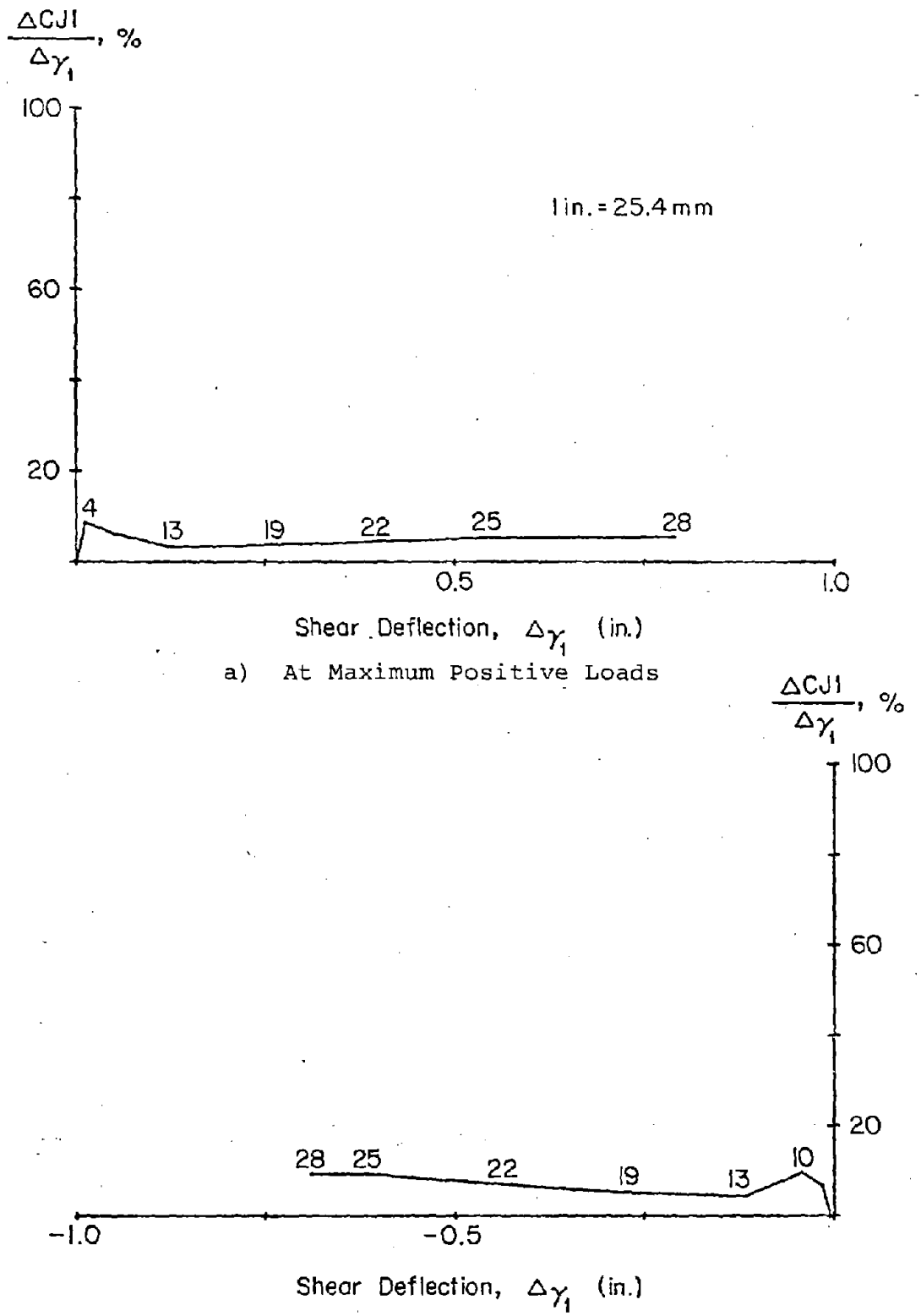

Fig. B-172 Slip at Base Construction Joint versus Shear Deflection in Zone 1 for Specimen F2

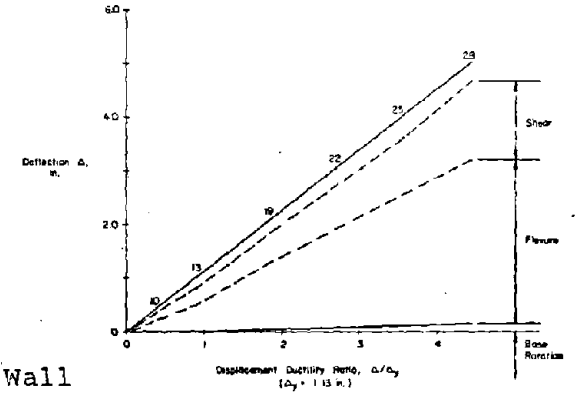

a) At Top of Wall

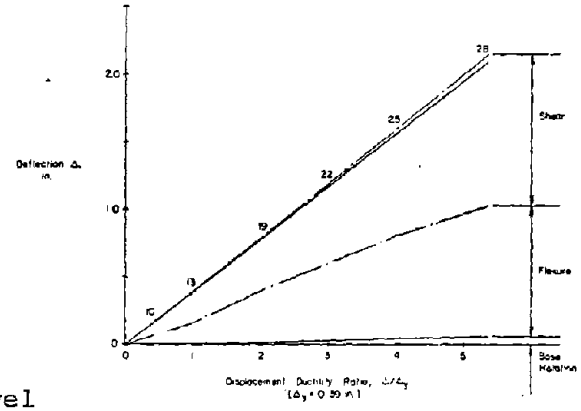

b) At 6 ft Level

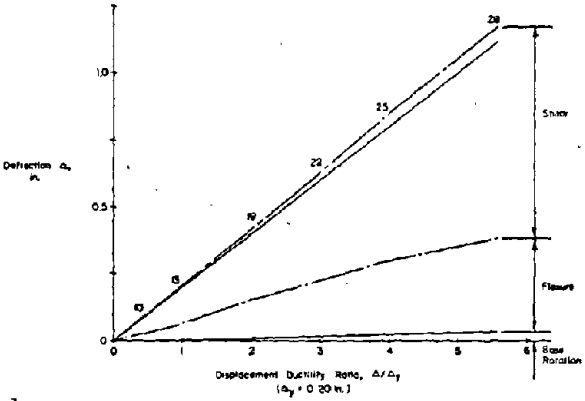

CALCULATED FROM MEASURED DEFOMATION
EXTRAPOLATED
MEASURED TOTAL

1 in = 25.4 mm
1 ft = 0.305 m

c) At 3 ft Level

Fig. B-173 Components of Deflection for Specimen F2

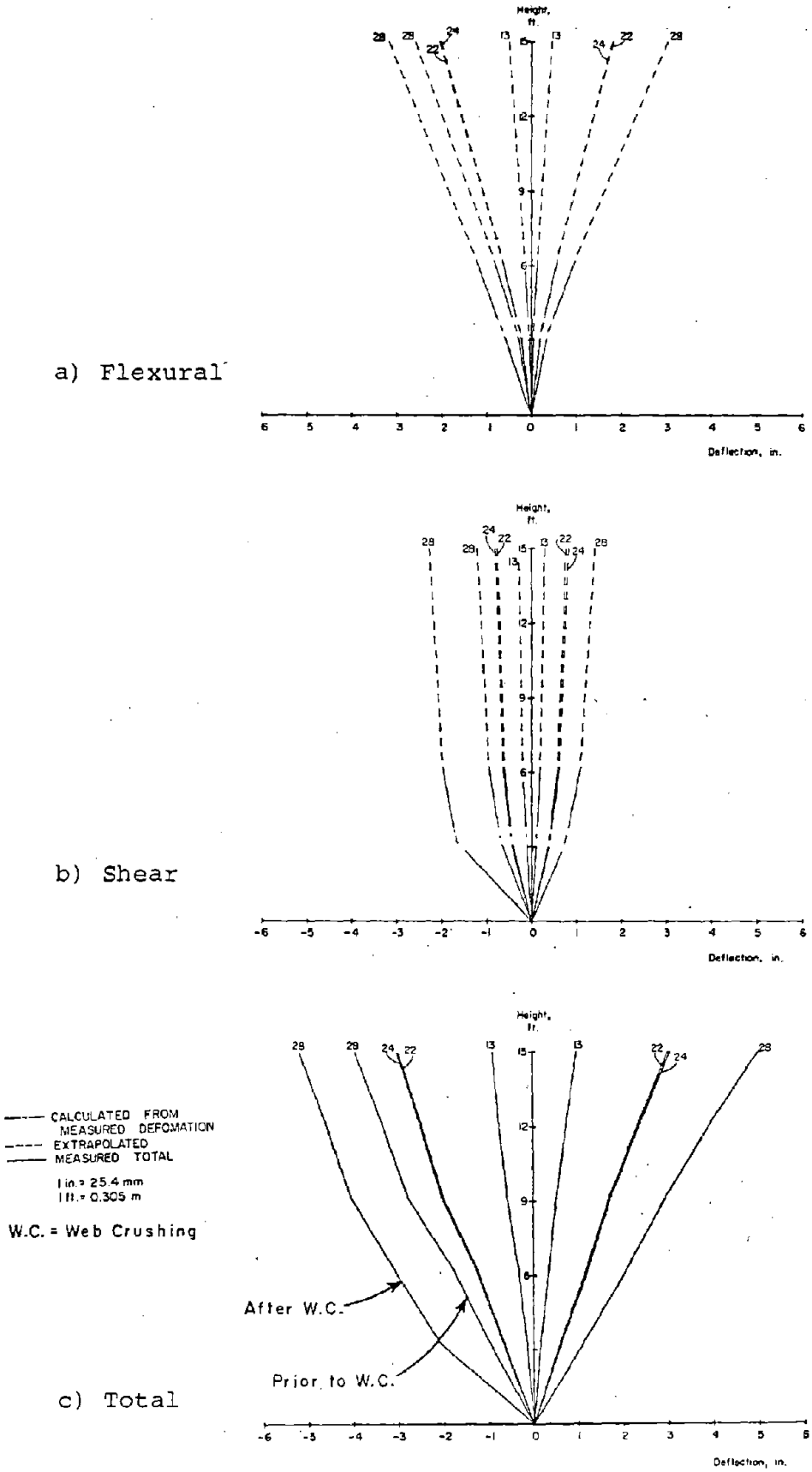

Fig. B-174 Deflected Shapes for Specimen F2

Deflected shapes for Cycles 22 and 24 show only a very slight decrease in shear stiffness during the 3-in. (76.2 mm) increment.

Reinforcement Strains. Figures B-175 through B-185 show reinforcement strains in the specimen at various stages.

Figure B-175 shows the cyclic load versus strain relationship for the outer reinforcing bars at the base level.

Figure B-176 shows that yielding occurred up to the 9-ft (2.75 m) level in Cycle 28.

Figures B-177 and B-178 show the strain gradient in the vertical reinforcement at various levels.

Figures B-179 through B-183 show the cyclic strain-load relationship and the strain gradients in the horizontal bars. These figures indicate considerable yielding between the 18-in. to 12-ft (0.46 m to 3.65 m) levels. Figures B-180 and B-181 indicate that yielding occurred near the end hooks at the 3 ft level for location HA and appreciable stresses were present in the lower 3-ft (0.91 m) for location HJ. This occurs because the boundary elements act as dowels in this region.

Figures B-184 through B-185 show the cyclic strain-load relationship and the vertical strain gradient in the confinement hoops. These figures differ from similar figures for the barbell specimens because the gages used were on a longitudinal leg of the hoops parallel to the plane of the web. Therefore, these strain are influenced significantly by shear stresses in the confined boundary element.

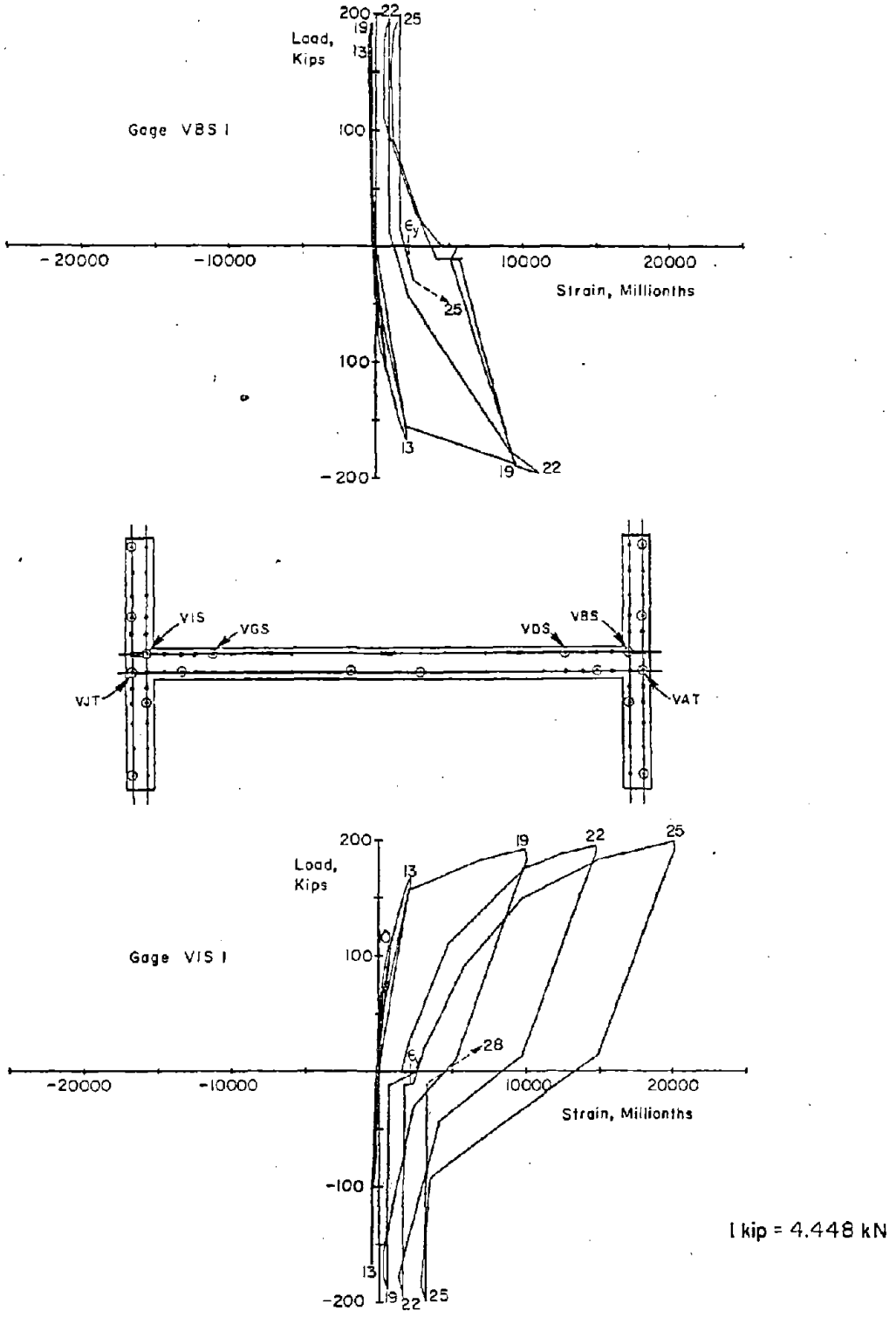

Fig. B-175 Measured Strains on Vertical Reinforcement at Base of Specimen F2

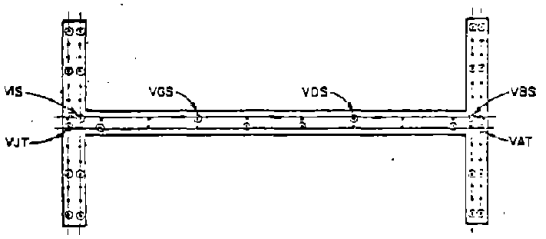

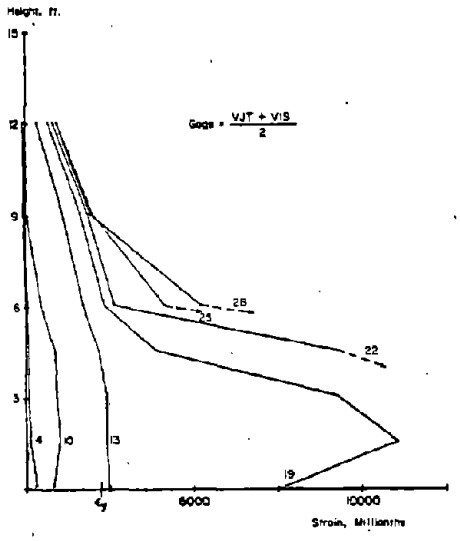

a) Average of VJT and VIS

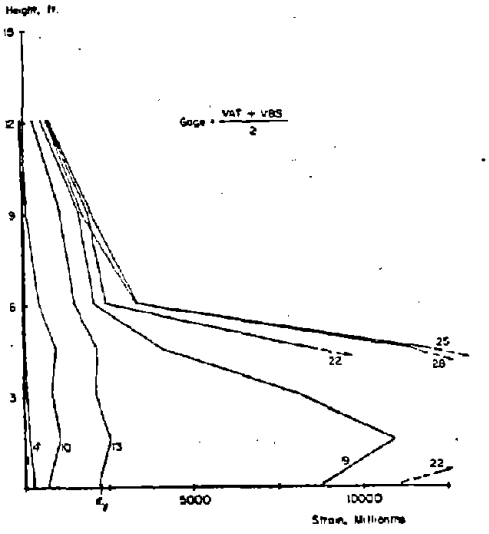

b) Average VAT and VBS

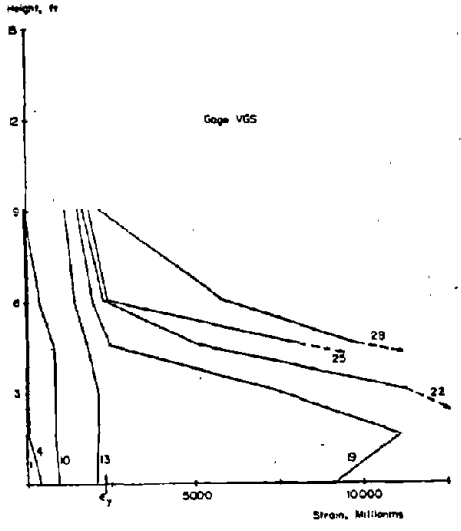

c) Strain Gage VGS

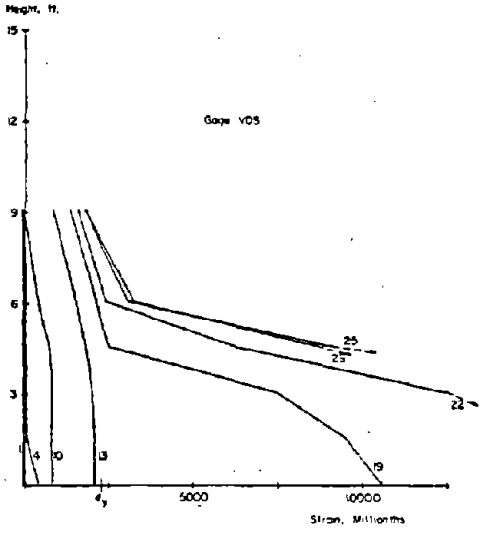

d) Strain Gage VDS

Fig. B-176 Vertical Reinforcement Strains at Maximum Loads for Specimen F2

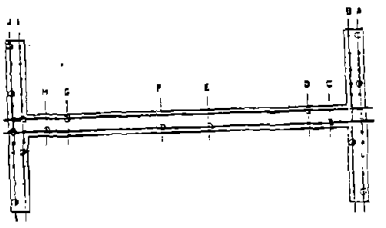

1 ft. = 0.305 m

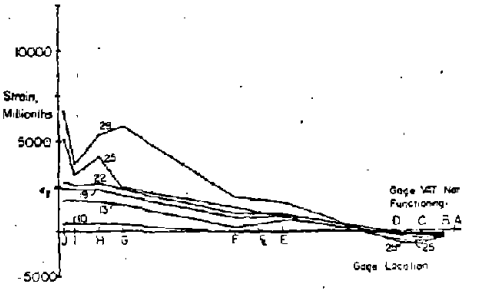

a) At 6 ft Level

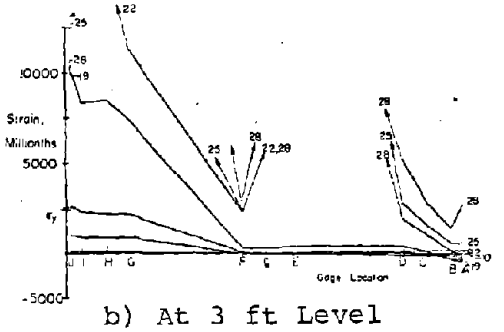

b) At 3 ft Level

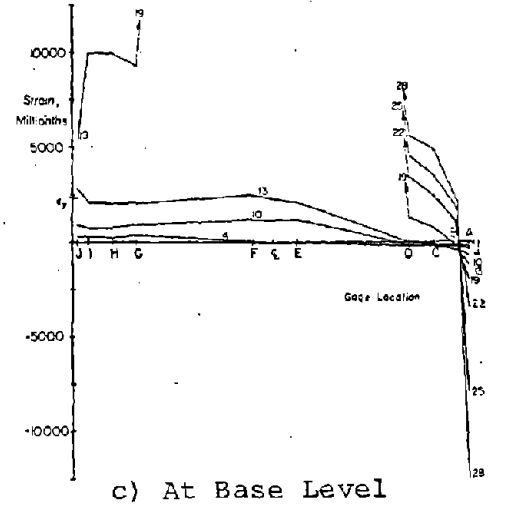

c) At Base Level

Fig. B-177 Vertical Reinforcement Strains at Maximum Positive Loads for Specimen F2

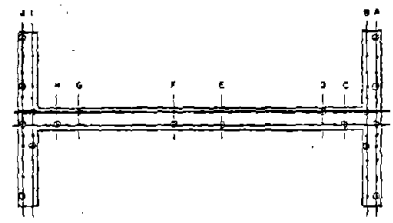

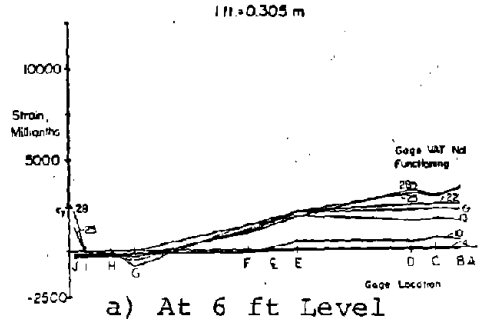

a) At 6 ft Level

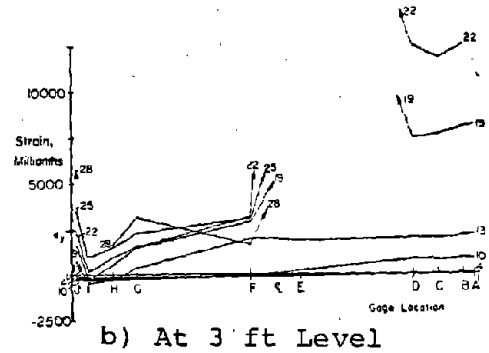

b) At 3 ft Level

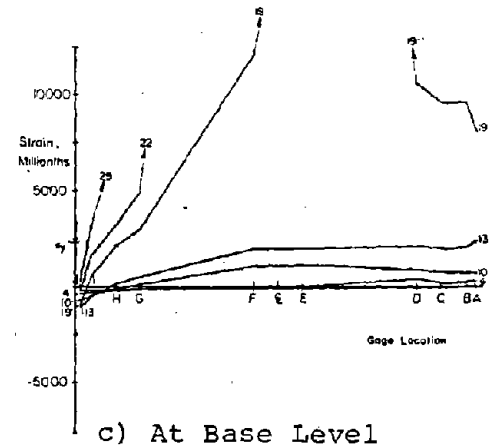

c) At Base Level

Fib. B-178 Vertical Reinforcement Strains at Maximum Negative Loads for Specimen F2

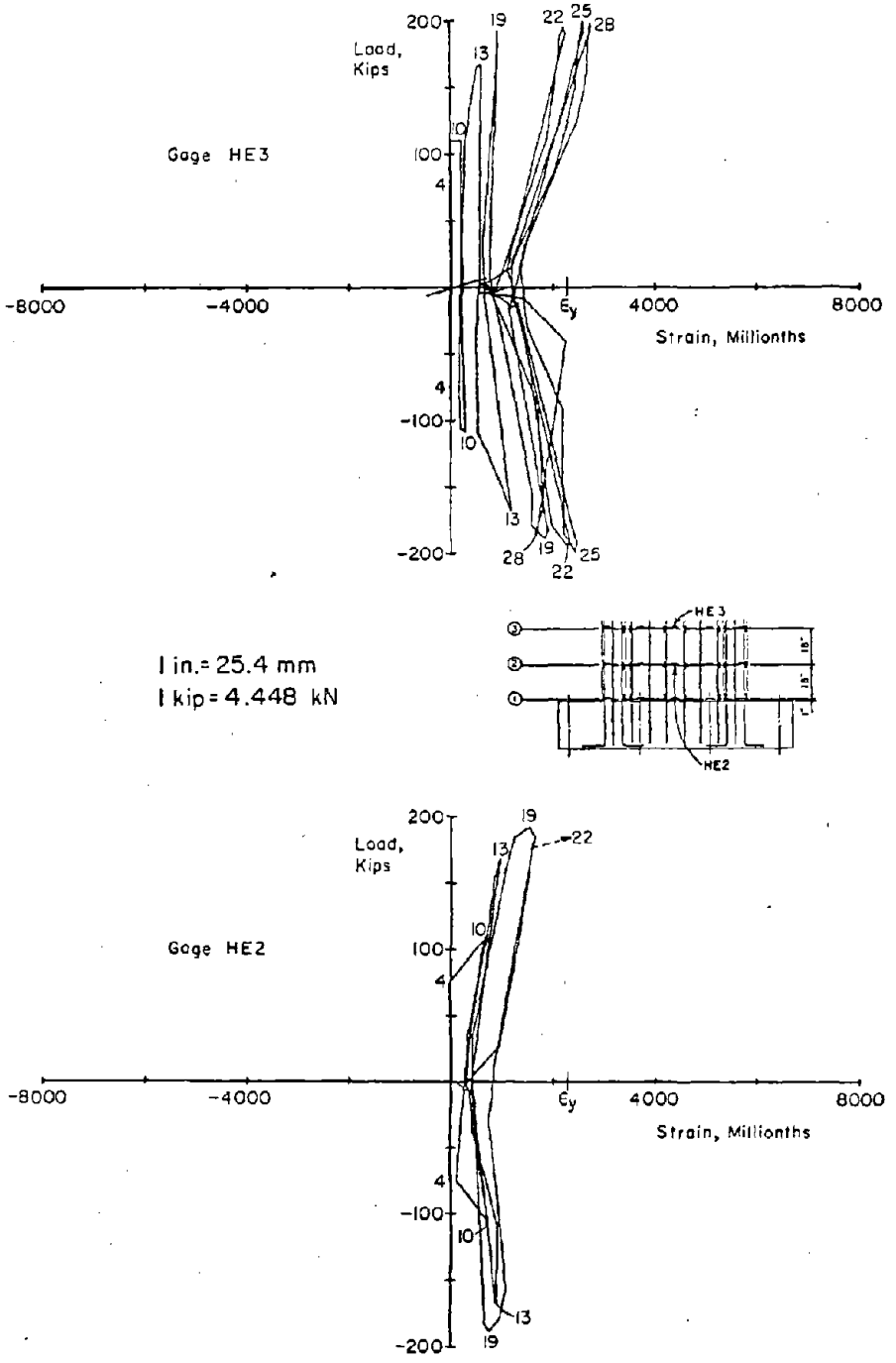

Fig. B-179 Measured Strains on Horizontal Reinforcement for Specimen F2

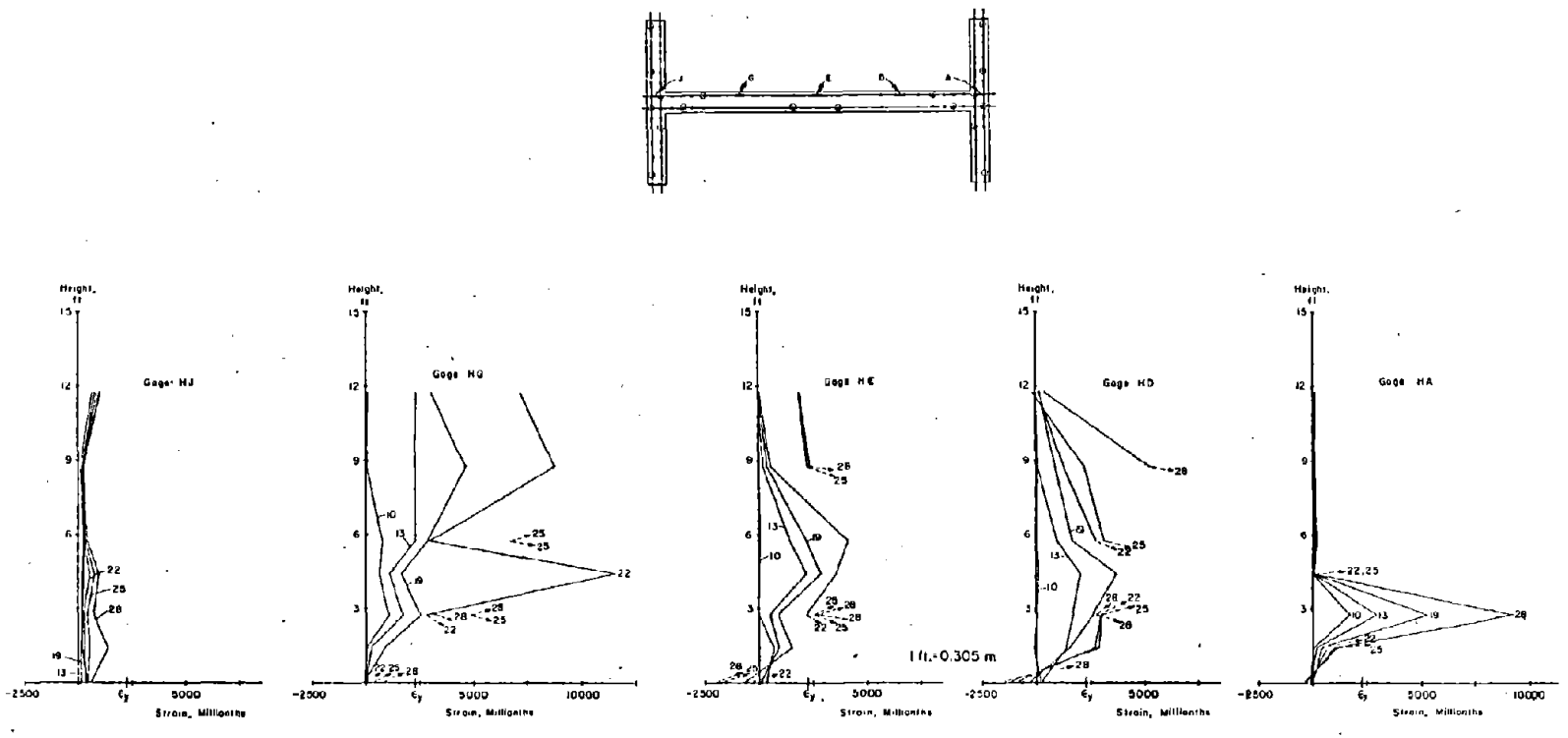

Fig. B-180 Horizontal Reinforcement Strains at Maximum Positive Loads for Specimen F2

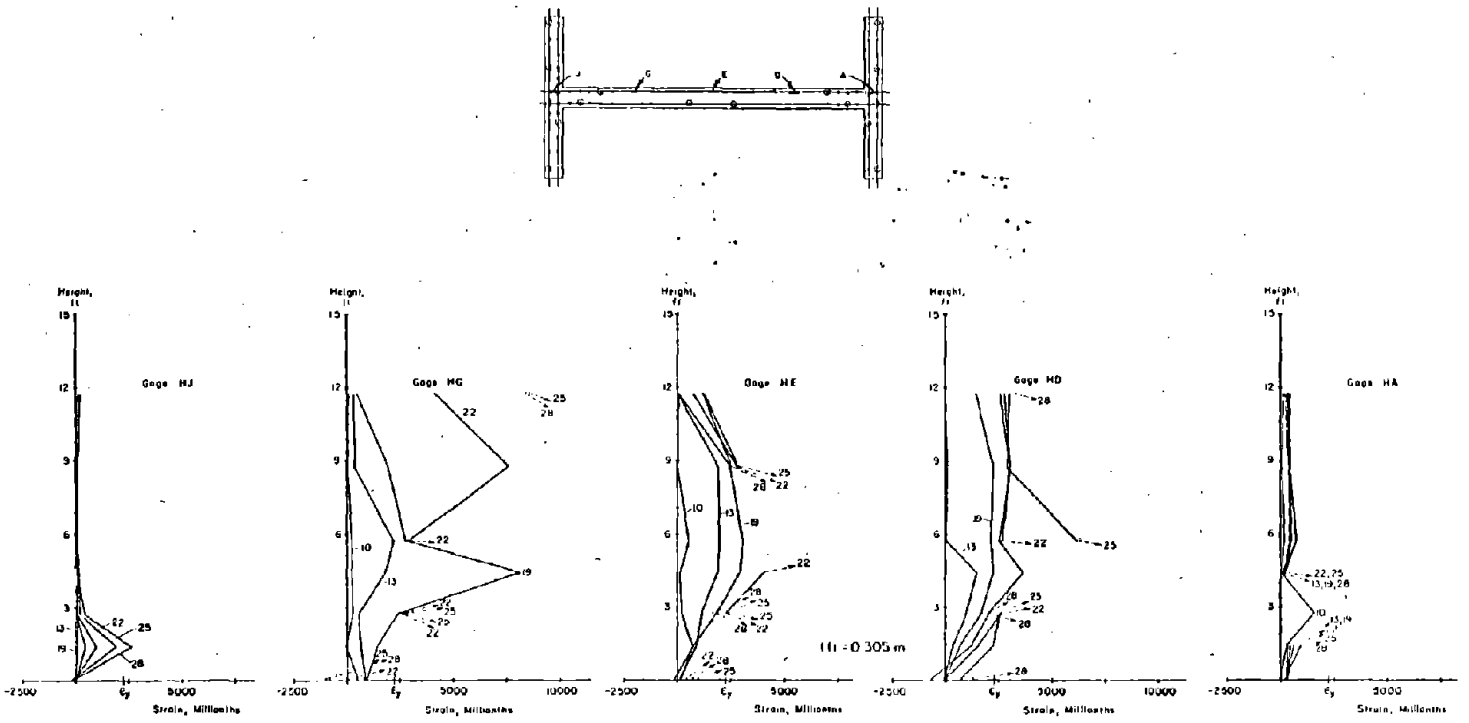

Fig. B-181 Horizontal Reinforcement Strains at Maximum Negative Loads for Specimen F2

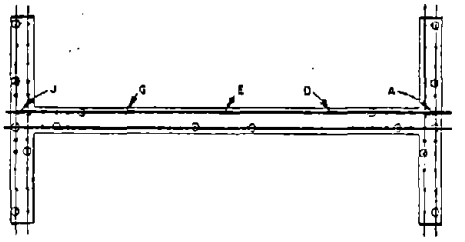

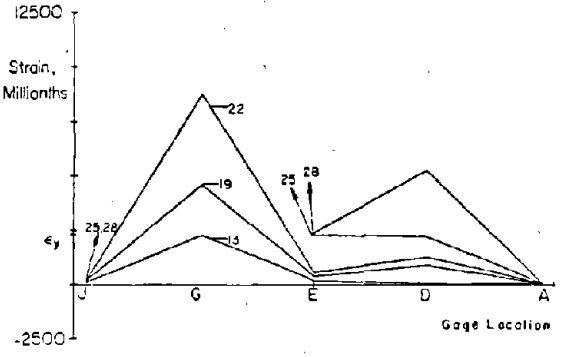

a) At 9 ft Level

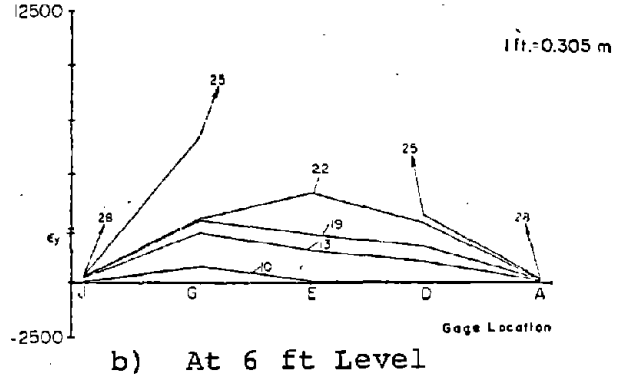

b) At 6 ft Level

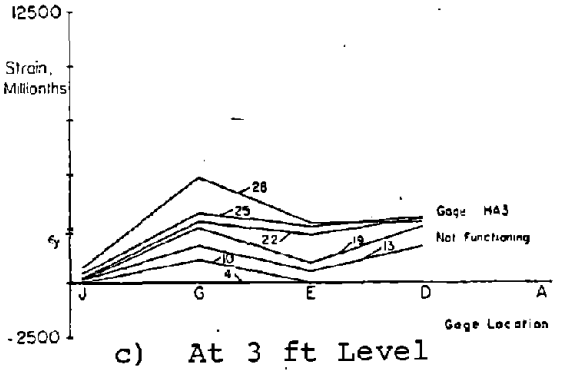

c) At 3 ft Level

Fig. B-182 Horizontal Reinforcement Strains in Web at Maximum Positive Loads for Specimen F2

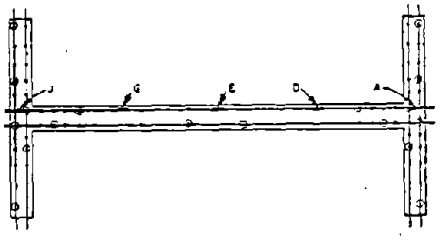

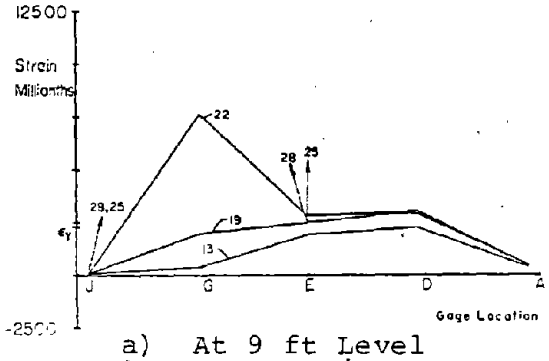

a) At 9 ft Level

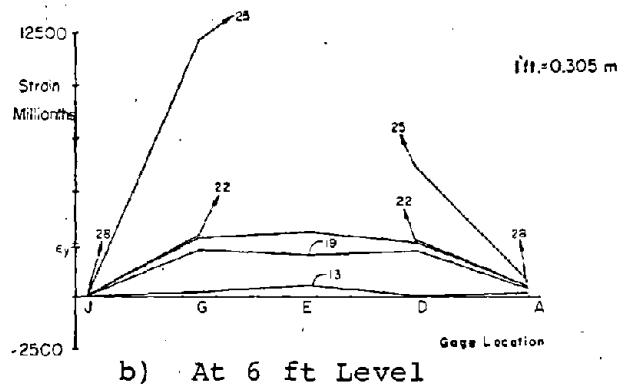

b) At 6 ft Level

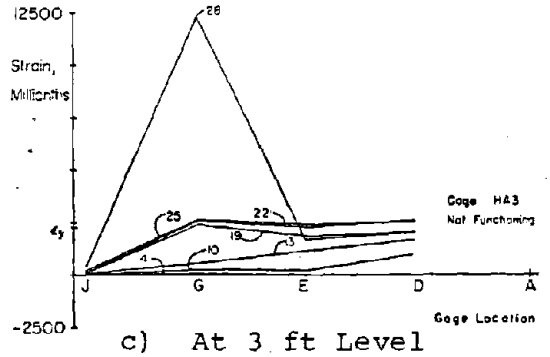

c) At 3 ft Level

Fig. B-183 Horizontal Reinforcement Strains in Web at Maximum Negative Loads for Specimen F2

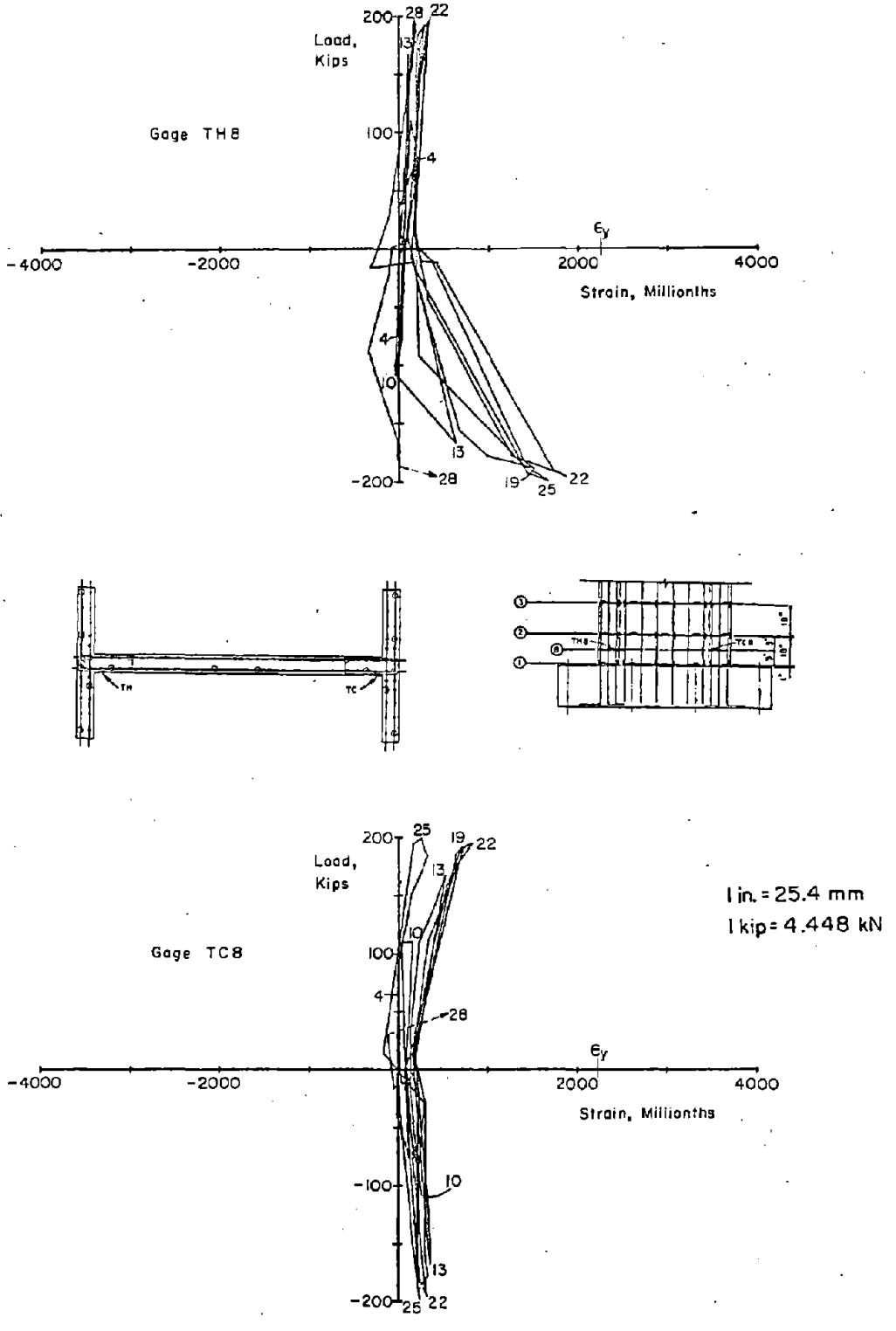

Fig. B-184 Measured Strains on Confinement Hoop Reinforcement for Specimen F2

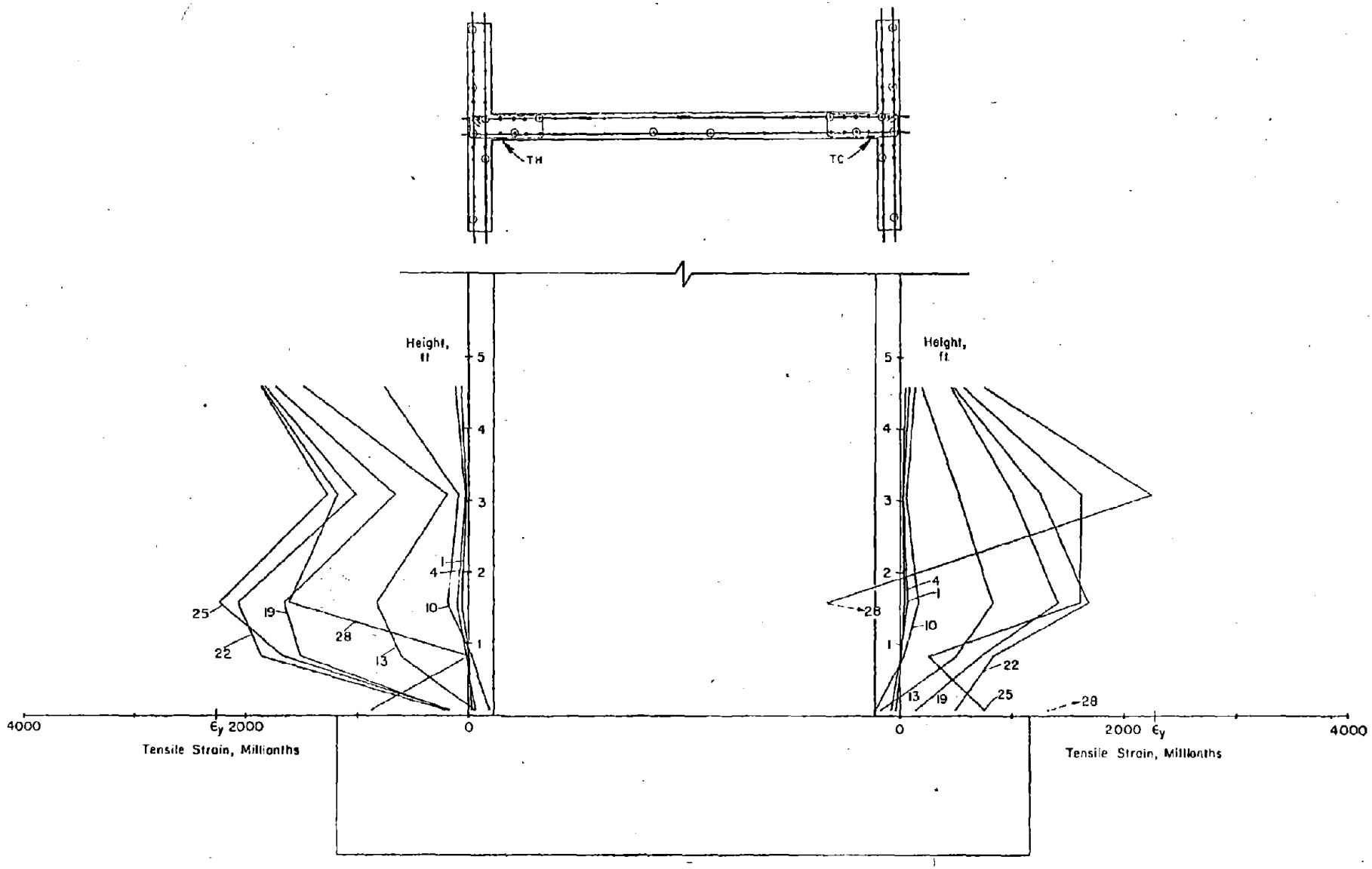

Fig. B-185 Confinement Hoop Reinforcement Strains at Maximum Loads for Specimen F2